



Technische Universität München

Fakultät für Chemie

## **Development and Preclinical Evaluation of Radiolabeled GLP-1 Receptor Ligands and PSMA Inhibitors**

**Veronika Barbara Felber**

Vollständiger Abdruck der von der Fakultät für Chemie der Technischen Universität  
München zur Erlangung des akademischen Grades einer  
**Doktorin der Naturwissenschaften (Dr. rer. nat.)**  
genehmigten Dissertation.

**Vorsitzende: Prof. Dr. Angela Casini**

Prüfer der Dissertation:

1. Prof. Dr. Hans-Jürgen Wester
2. apl. Prof. Dr. Matthias Eiber

Die Dissertation wurde am 06.07.2021 bei der Technischen Universität München eingereicht und  
durch die Fakultät für Chemie am 02.11.2021 angenommen.



# TABLE OF CONTENTS

<b>I. INTRODUCTION .....</b>	<b>11</b>
1.1. GLP-1 receptor ligand development.....	14
1.1.1. Glucagon-like peptide 1 receptor .....	14
1.1.2. Glucagon-like peptide-1.....	18
1.1.3. GLP-1R as target for molecular imaging and radiotherapy .....	23
1.1.4. GLP-1R-targeting radioligands.....	25
1.1.5. Current limitations for the diagnosis and PRRT of insulinomas.....	30
1.2. PSMA ligand development .....	33
1.2.1. Prostate-specific membrane antigen.....	33
1.2.2. PSMA as target for molecular imaging and radiotherapy .....	39
1.2.3. PSMA-targeting radioligands.....	41
1.2.4. Current limitations for radioligand therapy of prostate cancer .....	47
<b>II. OBJECTIVES .....</b>	<b>50</b>
2.1. Design of GLP-1R ligands with improved pharmacokinetics - objective I.....	50
2.2. Design of PSMA ligands with improved pharmacokinetics - objective II .....	53
<b>III. MATERIALS AND METHODS.....</b>	<b>56</b>
3.1. Materials.....	56
3.1.1. Chemicals .....	56
3.1.2. Equipment.....	57
3.2. Methods .....	59
3.2.1. Synthesis of GLP-1 receptor ligands.....	63
3.2.2. Synthesis of PSMA ligands .....	80
3.2.3. Cold metal complexation .....	123
3.3. Radiolabeling .....	128
3.3.1. <sup>125</sup> I-labeling .....	128
3.3.2. <sup>177</sup> Lu-labeling .....	131
3.4. <i>In vitro</i> experiments .....	135
3.4.1. Cell culture.....	135
3.4.2. Affinity determinations (IC <sub>50</sub> ) .....	136
3.4.3. Stability studies of PSMA substrate mimetics.....	137
3.4.4. Internalization studies.....	137
3.4.5. Lipophilicity .....	138
3.5. <i>In vivo</i> experiments.....	139
3.5.1. Biodistribution studies.....	139

## TABLE OF CONTENTS

3.5.2.	Metabolite analysis .....	143
3.5.3.	$\mu$ SPECT/CT imaging .....	144
<b>IV.</b>	<b>RESULTS AND DISCUSSION .....</b>	<b>145</b>
4.1.	GLP-1 receptor ligand development.....	145
4.1.1.	Reference ligand identification and optimization of <sup>125</sup> I-labeling.....	145
4.1.2.	Development and implementation of a cell-based assay for screening of GLP-1R-targeting compounds.....	147
4.1.2.1.	Radioligand binding studies on INS-1E cells.....	148
4.1.2.2.	Radioligand binding studies on HEK293-hGLP-1R and HEK293 cells.....	150
4.1.2.3.	Competitive binding experiments .....	152
4.1.3.	Synthesis and <i>in vitro</i> evaluation of small peptides targeting the GLP-1 receptor.....	154
4.1.3.1.	SiFA-tagged undecapeptides .....	154
4.1.3.2.	Peptides without C-terminal bulky substituents.....	156
4.1.3.3.	SiFA-tagged chimeras of A-1 and GLP-1 .....	157
4.1.3.4.	C-terminal pentadecapeptide of GLP-1 .....	160
4.1.3.5.	Lead peptide A-1.....	161
4.2.	PSMA ligand development .....	171
4.2.1.	Preliminary studies on isolated PSMA inhibitor motifs and PSMA substrate mimetics .....	171
4.2.1.1.	Investigations on isolated PSMA inhibitor motifs with modifications within the central Zn <sup>2+</sup> -binding unit.....	171
4.2.1.2.	Preliminary studies on PSMA substrate mimetics.....	173
4.2.2.	Synthesis, <i>in vitro</i> and <i>in vivo</i> evaluation of radiohybrid PSMA ligands with modifications at the inhibitor part.....	176
4.2.2.1.	Synthesis.....	177
4.2.2.2.	Cold complexation and radiolabeling.....	186
4.2.2.3.	<i>In vitro</i> evaluation.....	187
4.2.2.4.	<i>In vivo</i> evaluation .....	192
<b>V.</b>	<b>SUMMARY AND CONCLUSION .....</b>	<b>203</b>
<b>VI.</b>	<b>REFERENCES .....</b>	<b>206</b>
<b>VII.</b>	<b>APPENDIX .....</b>	<b>228</b>
7.1.	List of abbreviations.....	228
7.2.	Publications and notes on the protection of copyright.....	233
7.3.	Funding .....	233
7.4.	Aknowledgements.....	233

## ABSTRACT

### – ABSTRACT –

**AIMS AND OBJECTIVES:** Elevated kidney uptake remains a major limitation of radiometallated exendin-derived ligands of the glucagon-like peptide 1 receptor (GLP-1R). In patients with insulinomas or other GLP-1R-overexpressing tumors, close local proximity of the tumor(s) to the kidneys impairs an exact localization for surgical excision. Moreover, due to potential severe nephrotoxicity, GLP-1R-targeted tumor treatment by peptide receptor radionuclide therapy (PRRT) has not been envisaged yet. Based on the previously published potent GLP-1R-activating undecapeptide **A-1**, short-chained GLP-1R ligands were developed to investigate whether kidney uptake can be reduced by decreasing the overall ligand charge (ligand-based reduced kidney uptake) or by means of direct <sup>18</sup>F-labeling (nuclide-based decreased renal retention).

In contrast, elevated salivary gland uptake remains a major limitation during radioligand therapy (RLT) of prostate cancer (PCa) patients with radiolabeled inhibitors of the enzyme prostate-specific membrane antigen (PSMA). Thus, radiolabeled PSMA inhibitors can cause severe xerostomia. Hypothesizing that only dedicated parts of the inhibitor motif are responsible for this high non-target tissue accumulation, ligands with modifications at the urea-based inhibitor unit were synthesized and evaluated in *in vitro* and *in vivo* studies. Structural alterations were introduced based on the scaffold of the high-affinity radiohybrid (rh) PSMA ligand, rhPSMA-10 (**B-1**).

**METHODS:** <sup>125</sup>I-Labeling of glucagon-like peptide 1 (GLP-1) and [Nle<sup>14</sup>, Tyr(3-I)<sup>40</sup>]exendin-4 was performed via the Iodogen method. Radioligand binding studies were conducted with [Nle<sup>14</sup>, [<sup>125</sup>I]Tyr(3-I)<sup>40</sup>]exendin-4 using GLP-1R<sup>+</sup> INS-1E and stably transfected HEK293-hGLP-1R cells under varying conditions, such as different temperature, incubation period, cell number, radioligand concentration and incubation medium. Furthermore, [Nle<sup>14</sup>, [<sup>125</sup>I]Tyr(3-I)<sup>40</sup>]exendin-4 was used as reference radioligand in HEK293-hGLP-1R cell-based competitive binding assays. GLP-1R ligands were prepared via solid-phase peptide synthesis (SPPS) or via fragment coupling in solution.

Assembly of modified binding motifs for PSMA ligands was established on-resin and adjusted in individual cases. If not practicable, binding motifs were synthesized in solution. Peptide chain elongations were performed according to optimized standard protocols via SPPS. *In vitro* experiments were performed using PSMA<sup>+</sup> LNCaP cells. *In vivo* studies as well as  $\mu$ SPECT/CT scans were conducted with male LNCaP tumor xenograft-bearing CB17-SCID mice.

**RESULTS:** In contrast to [<sup>125</sup>I]Tyr(3-I)<sup>19</sup>-GLP-1, that showed high radiolysis already after short-term storage, [Nle<sup>14</sup>, [<sup>125</sup>I]Tyr(3-I)<sup>40</sup>]exendin-4 exhibited sufficiently high radiochemical stability over at least 16 days (RCP  $\geq$  92%) and high uptake in transfected HEK293-hGLP-1R cells and hence, was used as reference radioligand. Conversely, INS-1E cells provided only low radioligand binding and insufficient sigmoidal dose-response. Therefore, all *in vitro* experiments were conducted with HEK293-hGLP-1R cells at optimized conditions. In contrast to the three reference ligands GLP-1

## ABSTRACT

( $IC_{50} = 23.2 \pm 12.2$  nM), [Nle<sup>14</sup>, Tyr(3-I)<sup>40</sup>]exendin-4 ( $IC_{50} = 7.63 \pm 2.78$  nM) and [Nle<sup>14</sup>, Tyr<sup>40</sup>]exendin-4 ( $IC_{50} = 9.87 \pm 1.82$  nM), all GLP-1R-targeting small peptides (9 - 15 amino acids), including lead peptide **A-1**, exhibited only medium to low affinities ( $> 189$  nM). Only SiFA-tagged undecapeptide **A-5** ( $IC_{50} = 189 \pm 35$  nM) revealed a higher affinity than **A-1** ( $IC_{50} = 669 \pm 242$  nM).

PSMA inhibitors with a) modifications within the central Zn<sup>2+</sup>-binding unit, b) proinhibitor motifs and c) substituents & bioisosteres of the P1'- $\gamma$ -carboxylic acid were synthesized and evaluated. Modifications within the central Zn<sup>2+</sup>-binding unit of rhPSMA-10 (L-Glu-urea-L-Glu) provided three compounds. Thereof, only carbamate **B-13** exhibited high affinity ( $IC_{50} = 7.11 \pm 0.71$  nM), but low tumor uptake ( $5.31 \pm 0.94\%$  ID/g, 1 h p.i. and  $1.20 \pm 0.55\%$  ID/g, 24 h p.i.). All proinhibitor motif-based ligands (three in total) exhibited low binding affinities ( $> 1$   $\mu$ M), no notable internalization and very low tumor uptake ( $< 0.50\%$  ID/g). In addition, four compounds with P1'- $\gamma$ -carboxylate substituents were developed and evaluated. Thereof, only tetrazole derivative **B-21** revealed high affinity ( $IC_{50} = 16.4 \pm 3.8$  nM), but also this inhibitor showed low tumor uptake ( $3.40 \pm 0.63\%$  ID/g, 1 h p.i. and  $0.68 \pm 0.16\%$  ID/g, 24 h p.i.). Salivary gland uptake in mice remained at an equally low level for all compounds (between  $0.02 \pm 0.00\%$  ID/g and  $0.09 \pm 0.03\%$  ID/g), wherefore apparent tumor-to-submandibular gland and tumor-to-parotid gland ratios for the modified peptides were distinctly lower (factor 8 - 45) than for [<sup>177</sup>Lu]Lu-rhPSMA-10 at 24 h p.i. By contrast, differences in salivary gland uptake were detectable at 1 h p.i. Carbamate [<sup>177</sup>Lu]Lu-**B-13** exhibited a two-fold higher tumor-to-submandibular gland ratio than EuE-based inhibitor [<sup>177</sup>Lu]Lu-rhPSMA-7.3. The tumor-to-submandibular gland ratio of tetrazole derivative [<sup>177</sup>Lu]Lu-**B-21** was in the same range as for [<sup>177</sup>Lu]Lu-rhPSMA-7.3. Nevertheless, salivary gland uptake at 1 h p.i. was still at a low level (between  $0.37 \pm 0.08\%$  ID/g and  $1.44 \pm 0.25\%$  ID/g).

**CONCLUSIONS:** The novel peptides, including lead peptide **A-1**, could not compete with favorable *in vitro* characteristics of 30- and 40-residue peptides GLP-1, [Nle<sup>14</sup>, Tyr(3-I)<sup>40</sup>]exendin-4 and [Nle<sup>14</sup>, Tyr<sup>40</sup>]exendin-4. Accordingly, radiolabeling experiments were not conducted. The favorable EC<sub>50</sub> values of **A-1** provided by the literature could not be transferred to competitive binding experiments. Due to its poor IC<sub>50</sub> values, the use of **A-1** as a basic scaffold for the design of further GLP-1R-targeting radioligands cannot be recommended. Prospective investigations might include the scaffold of **A-5**, although substantial optimizations concerning affinity and lipophilicity would be required. In sum, GLP-1R-targeting radioligands with reduced kidney uptake could not be obtained in this work, which emphasizes the need for further ligands addressing this particular issue.

At 24 h p.i. none of the investigated modified PSMA ligands could compete with the *in vivo* characteristics of the EuE-based inhibitor [<sup>177</sup>Lu]Lu-rhPSMA-10. Although two derivatives (**B-13** and **B-21**) were found to exhibit high affinities, tumor uptake at 24 h p.i. was considerably low, while uptake in salivary glands remained unaffected. By contrast, at 1 h p.i. clearer distinctions between EuE- and non-EuE based inhibitors were possible concerning their salivary gland uptake and

## ABSTRACT

revealed one derivative (**B-13**) with a two-fold higher tumor-to-submandibular gland ratio compared to the EuE-based compound [<sup>177</sup>Lu]Lu-rhPSMA-7.3. However, due to the overall low salivary gland uptake also at 1 h p.i., it remains to be proven that early examination time points in this animal model will also allow for a clear identification of radiolabeled PSMA inhibitors with reduced salivary gland uptake in future studies.

## ZUSAMMENFASSUNG

### – ZUSAMMENFASSUNG –

**ZIELSETZUNGEN:** Eine wesentliche Limitation von radiometallierten Exendin-basierten Liganden des GLP-1 Rezeptors (GLP-1R) besteht in ihrer erhöhten Nierenaufnahme. Bei Patienten mit Insulinomen oder anderen GLP-1R-überexprimierenden Tumoren führt die unmittelbare Nähe des Tumors/der Tumore zu den Nieren daher zu Beeinträchtigungen in der genauen Lokalisierung, die für eine chirurgische Entfernung aber unabdingbar ist. Darüber hinaus wurde eine GLP-1R-gerichtete Tumorbehandlung durch Peptidrezeptorradiationuklidtherapie (PRRT) auf Grund von potenziell schwerer Nephrotoxizität bisher noch nicht angestrebt. Basierend auf dem zuvor veröffentlichten potenten GLP-1R-aktivierenden Undecapeptid **A-1** wurden kurzkettenige GLP-1R-Liganden entwickelt, um zu untersuchen, ob die Nierenaufnahme durch Reduktion der Gesamtladung des Liganden (Ligand-basierte reduzierte Nierenaufnahme) oder durch direkte <sup>18</sup>F-Markierung (Nuklid-basierte verminderte Nierenretention) verringert werden kann.

Im Gegensatz dazu stellt die erhöhte Aufnahme in Speicheldrüsen eine wesentliche Limitation während der Radioligandentherapie (RLT) von Prostatakrebspatienten (PCa) mit radioaktiv markierten Inhibitoren des prostataspezifischen Membranantigens (PSMA) dar. Dementsprechend können radioaktiv markierte PSMA Inhibitoren schwere Xerostomie verursachen. Unter der Hypothese, dass nur bestimmte Teile des Inhibitormotivs für diese hohe Akkumulation im Nicht-Zielgewebe verantwortlich sind, wurden Liganden mit Modifikationen an der ureabasierten Inhibitoreinheit synthetisiert und in *in vitro* und *in vivo* Studien evaluiert. Entsprechende strukturelle Veränderungen wurden an dem hochaffinen radiohybriden (rh) PSMA Liganden rhPSMA-10 (**B-1**) eingeführt.

**METHODEN:** Die <sup>125</sup>I-Markierungen von Glucagon-like peptide 1 (GLP-1) und [Nle<sup>14</sup>, Tyr(3-I)<sup>40</sup>]Exendin-4 erfolgten mittels Iodogen. Radioligand-Bindungsstudien wurden mit [Nle<sup>14</sup>, [<sup>125</sup>I]Tyr(3-I)<sup>40</sup>]Exendin-4 unter Verwendung von GLP-1R<sup>+</sup> INS-1E und stabil transfizierten HEK293-hGLP-1R Zellen unter verschiedenen Bedingungen, wie unterschiedlicher Temperatur, Inkubationszeit, Zellzahl, Radioligandkonzentration und in unterschiedlichem Inkubationsmedium durchgeführt. Darüber hinaus wurde [Nle<sup>14</sup>, [<sup>125</sup>I]Tyr(3-I)<sup>40</sup>]Exendin-4 als Referenzradioligand in HEK293-hGLP-1R-zellbasierten kompetitiven Bindungsassays verwendet. GLP-1R Liganden wurden über Festphasenpeptidsynthese (SPPS) oder über Fragmentkopplung in Lösung hergestellt.

Der Aufbau modifizierter Bindemotive für PSMA Liganden erfolgte am Harz und wurde individuell angepasst. Wenn nicht praktikabel, erfolgte die Synthese der Bindemotive in Lösung. Die Verlängerungen der Peptidketten wurden gemäß der optimierten Standardprotokolle mittels SPPS durchgeführt. *In vitro* Experimente erfolgten mit PSMA<sup>+</sup> LNCaP Zellen. *In vivo* Studien sowie  $\mu$ SPECT/CT Scans wurden mit männlichen LNCaP-Tumorxenotransplantat-tragenden CB17-SCID Mäusen durchgeführt.

## ZUSAMMENFASSUNG

ERGEBNISSE: Im Gegensatz zu [<sup>125</sup>I]Tyr(3-I)<sup>19</sup>-GLP-1, bei welchem bereits nach kurzer Zeit hohe Radiolyse zu beobachten war, zeigte [Nle<sup>14</sup>, [<sup>125</sup>I]Tyr(3-I)<sup>40</sup>]Exendin-4 eine ausreichend hohe radiochemische Stabilität (RCP ≥ 92%) über mindestens 16 Tage und eine hohe Aufnahme in transfizierte HEK293-hGLP-1R Zellen und wurde daher als Referenzradioligand verwendet. INS-1E Zellen hingegen zeigten nur eine geringe Radioligandbindung und eine unzureichende sigmoidale Dosisantwort. Daher wurden alle *in vitro* Experimente mit HEK293-hGLP-1R Zellen unter optimierten Bedingungen durchgeführt. Im Gegensatz zu den drei Referenzliganden GLP-1 (IC<sub>50</sub> = 23.2 ± 12.2 nM), [Nle<sup>14</sup>, Tyr(3-I)<sup>40</sup>]Exendin-4 (IC<sub>50</sub> = 7.63 ± 2.78 nM) und [Nle<sup>14</sup>, Tyr<sup>40</sup>]Exendin-4 (IC<sub>50</sub> = 9.87 ± 1.82 nM), zeigten alle GLP-1R-gerichteten kleinen Peptide (9 - 15 Aminosäuren), einschließlich Leitstruktur **A-1**, nur mittlere bis niedrige Affinitäten (> 189 nM). Nur das SiFA-tragende Undecapeptid **A-5** (IC<sub>50</sub> = 189 ± 35 nM) zeigte eine höhere Affinität als **A-1** (IC<sub>50</sub> = 669 ± 242 nM).

PSMA Inhibitoren mit a) Modifikationen innerhalb der zentralen Zn<sup>2+</sup>-Bindeeinheit, b) Proinhibitormotiven und c) Substituenten und Bioisosteren der P1'-γ-Carbonsäure wurden synthetisiert und evaluiert. Modifikationen innerhalb der zentralen Zn<sup>2+</sup>-Bindeeinheit von rhPSMA-10 (L-Glu-urea-L-Glu) lieferten drei Verbindungen. Davon zeigte nur Carbamat **B-13** eine hohe Affinität (IC<sub>50</sub> = 7.11 ± 0.71 nM), aber eine geringe Tumoraufnahme (5.31 ± 0.94% ID/g, 1 h p.i. und 1.20 ± 0.55% ID/g, 24 h p.i.). Alle Proinhibitormotiv-basierten Liganden (insgesamt drei) zeigten geringe Bindungsaffinitäten (> 1 μM), keine nennenswerte Internalisierung und eine sehr geringe Tumoraufnahme (< 0.50% ID/g). Zusätzlich wurden vier Verbindungen mit P1'-γ-Carboxylatsubstituenten entwickelt und evaluiert. Davon zeigte nur Tetrazolderivat **B-21** eine hohe Affinität (IC<sub>50</sub> = 16.4 ± 3.8 nM), aber auch dieser Inhibitor erreichte nur eine geringe Tumoraufnahme (3.40 ± 0.63% ID/g, 1 h p.i. und 0.68 ± 0.16% ID/g, 24 h p.i.). Die Speicheldrüsenaufnahme in Mäusen blieb für alle Verbindungen auf einem gleich niedrigen Niveau (zwischen 0.02 ± 0.00% ID/g und 0.09 ± 0.03% ID/g), weshalb die Tumor-zu-Submandibularis und Tumor-zu-Parotis Verhältnisse für die modifizierten Peptide augenscheinlich deutlich niedriger (Faktor 8 - 45) ausfielen als für [<sup>177</sup>Lu]Lu-rhPSMA-10 bei 24 h p.i. Im Gegensatz dazu waren Unterschiede in der Speicheldrüsenaufnahme bei 1 h p.i. feststellbar. Carbamat [<sup>177</sup>Lu]Lu-**B-13** zeigte ein zweifach höheres Tumor-zu-Submandibularis Verhältnis als der EuE-basierte Inhibitor [<sup>177</sup>Lu]Lu-rhPSMA-7.3. Das Tumor-zu-Submandibularis Verhältnis des Tetrazolderivats [<sup>177</sup>Lu]Lu-**B-21** lag im gleichen Bereich wie für [<sup>177</sup>Lu]Lu-rhPSMA-7.3. Nichtsdestotrotz befand sich die Speicheldrüsenaufnahme auch bei 1 h p.i. auf einem niedrigen Niveau (zwischen 0.37 ± 0.08% ID/g and 1.44 ± 0.25% ID/g).

SCHLUSSFOLGERUNGEN: Die neuen Peptide, einschließlich Leitstruktur **A-1**, zeigten nur mittlere bis niedrige Affinitäten und stellen somit keine Konkurrenz zu den 30 und 40 Aminosäuren langen Peptiden GLP-1, [Nle<sup>14</sup>, Tyr(3-I)<sup>40</sup>]Exendin-4 und [Nle<sup>14</sup>, Tyr<sup>40</sup>]Exendin-4 dar. Dementsprechend wurden keine Radiomarkierungsexperimente durchgeführt. Die in der Literatur

## ZUSAMMENFASSUNG

angegebenen vorteilhaften  $EC_{50}$  Werte von **A-1** konnten nicht auf kompetitive Bindungsexperimente übertragen werden. Auf Grund seiner schlechten  $IC_{50}$  Werte ist die Verwendung von **A-1** als Grundgerüst für das Design weiterer GLP-1R-gerichteter Radioliganden nicht zu empfehlen. Für zukünftige Untersuchungen könnte das Gerüst von **A-5** berücksichtigt werden, obwohl wesentliche Optimierungen hinsichtlich Affinität und Lipophilie erforderlich wären. Insgesamt konnten in dieser Arbeit keine GLP-1R-gerichteten Radioliganden mit verringerter Nierenaufnahme erhalten werden, was die Notwendigkeit weiterer Liganden für diese spezielle Fragestellung unterstreicht.

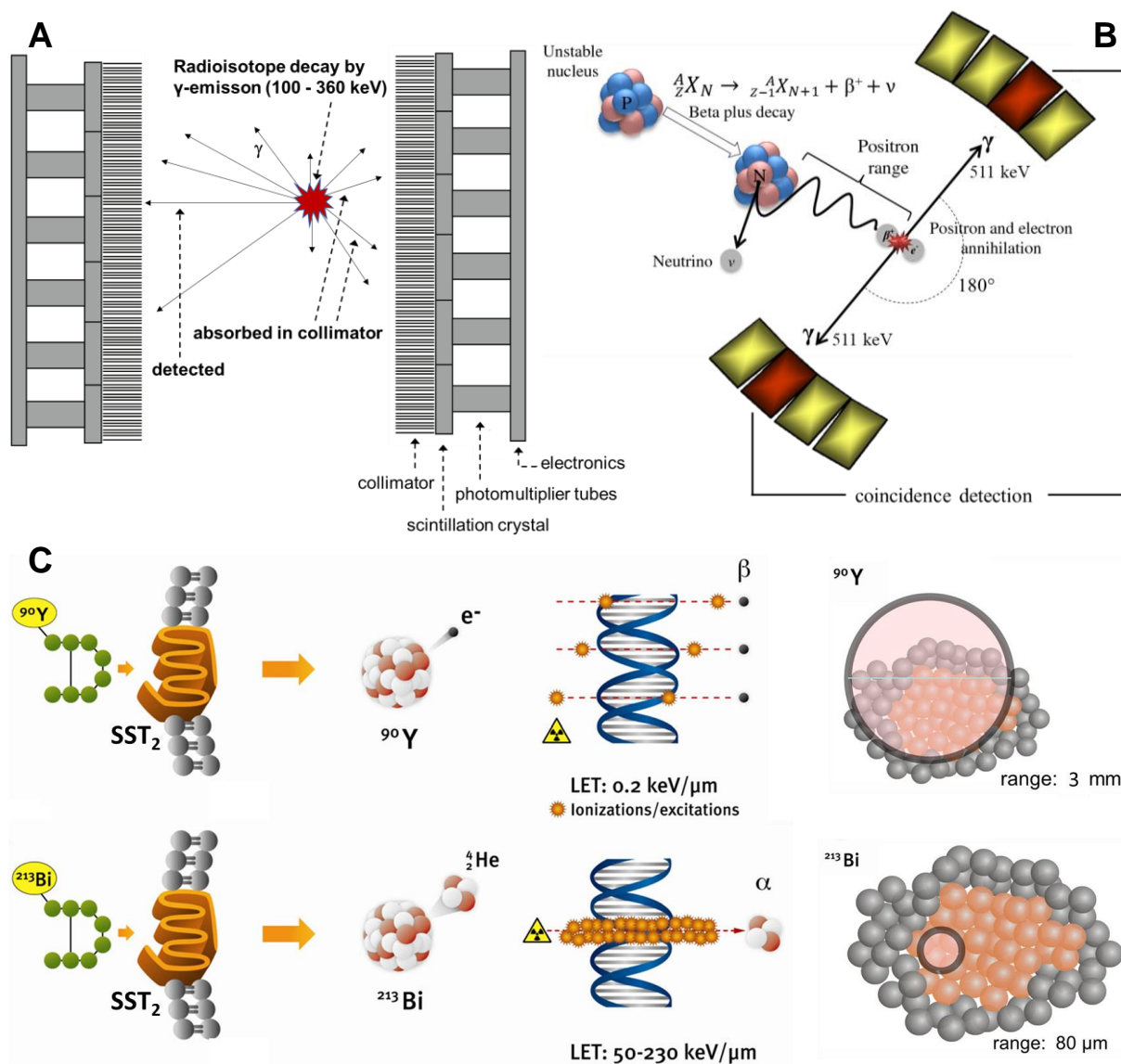
Bei 24 h p.i. erreichte keiner der modifizierten PSMA Liganden die *in vivo* Eigenschaften des EuE-basierten Inhibitors [ $^{177}\text{Lu}$ ]Lu-rhPSMA-10. Trotz hoher Affinität zweier Derivate (**B-13** und **B-21**), wiesen diese nur eine niedrige Tumoraufnahme auf, während die Aufnahme in den Speicheldrüsen unverändert blieb. Dagegen waren bei 1 h p.i. deutlichere Unterscheidungen zwischen EuE- und nicht-EuE-basierten Inhibitoren bezüglich deren Aufnahme in die Speicheldrüsen möglich und zeigten ein Derivat (**B-13**) mit einem zweifach höheren Tumor-zu-Submandibularis Verhältnis im Vergleich zu der EuE-basierten Verbindung [ $^{177}\text{Lu}$ ]Lu-rhPSMA-7.3. Aufgrund der insgesamt geringen Speicheldrüsenaufnahme auch bei 1 h p.i. bleibt jedoch zu beweisen, dass frühe Untersuchungszeitpunkte in diesem Tiermodell auch in zukünftigen Studien eine eindeutige Identifizierung radiomarkierter PSMA Inhibitoren mit reduzierter Speicheldrüsenaufnahme ermöglichen.

## I. INTRODUCTION

In numerous cancers, pathological upregulation of physiological processes allows to differentiate a tumor from healthy, non-inflamed tissue and serves as the molecular basis for *in vivo* imaging and targeted radionuclide therapy (TRT).<sup>[1-3]</sup> Positron emission tomography (PET) and single-photon emission computed tomography (SPECT) agents like 2-[<sup>18</sup>F]fluoro-2-deoxy-D-glucose [<sup>18</sup>F]FDG, 3'-deoxy-3'-[<sup>18</sup>F]fluorothymidine ([<sup>18</sup>F]FLT), [<sup>18</sup>F]NaF, [<sup>11</sup>C]methionine, <sup>99m</sup>Tc-methylene diphosphonate ([<sup>99m</sup>Tc]MDP) and <sup>99m</sup>Tc-pertechnetate [<sup>99m</sup>TcO<sub>4</sub>]<sup>-</sup> enable the visualization of altered metabolic or proliferative processes and are thus vastly applied for diagnosis in oncology.<sup>[4, 5]</sup> However, with the aim to expand the radiopharmaceutical tracer repertoire and develop even more specific and sensitive tracers, more purposive strategies are mandatory and indeed continuously under development.

Over three decades ago, the concept of addressing overexpressed peptide receptors or enzymes has been established and is now emerging to an expedient method for precise imaging and if realizable, TRT of certain tumor entities.<sup>[1, 2]</sup> Thereby, radioactivity is delivered to cancer cells via radiolabeled targeting moieties like small molecules, peptides, proteins, nanoparticles, antibodies and antibody fragments able to bind specifically to peptide receptors or other unique structural features expressed in higher frequency and density on the tumor cells than in non-tumor tissues.<sup>[2, 6]</sup> Thereof, particularly radiolabeled peptides have emerged as a valuable tool for monitoring tumor or metastasis dimensions via SPECT or PET (*Figure 1A* and *1B*) before and after patient treatment with chemotherapeutics, radiation therapy or surgery. Based on the same principle, tumors can be treated by TRT if peptides are labeled with therapeutic radionuclides (*Figure 1C*).<sup>[2, 7]</sup> As a result, several high affinity ligands, labeled either with radionuclides for PET, SPECT or therapeutic applications have successfully entered clinical trials, e.g. [<sup>18</sup>F]PSMA-1007 for PSMA (NCT04644822), [<sup>68</sup>Ga]Ga-RM2 for the gastrin-releasing peptide receptor (NCT02624518), [<sup>177</sup>Lu]Lu-PP-F11N for the cholecystikinin receptor 2 (NCT02088645) and [<sup>68</sup>Ga]Ga-Pentixafor for the C-X-C chemokine receptor type 4 (NCT03436342).<sup>[8]</sup> However, despite tremendous preclinical efforts, only few peptide tracers attained FDA and/or EMA approval to date. Acutect® (<sup>99m</sup>Tc) is used for scintigraphic imaging of acute venous thrombosis, as it binds with high affinity to α<sub>IIb</sub>β<sub>3</sub> integrins, expressed on activated platelets.<sup>[9]</sup> OctreoScan® (<sup>111</sup>In), NETSPOT™ and SomaKit TOC® (<sup>68</sup>Ga) have been approved for imaging, and Lutathera® (<sup>177</sup>Lu) for targeted radiotherapy of somatostatin receptor positive gastroenteropancreatic neuroendocrine tumors (GEP-NETs).<sup>[10]</sup> Most recently, [<sup>68</sup>Ga]Ga-PSMA-11 attained approval as PET imaging agent of PSMA positive prostate cancer lesions.<sup>[11]</sup>

## INTRODUCTION



**Figure 1:** The principles of SPECT (A), PET (B) and TRT (C). (A) SPECT detector systems are based on Anger camera(s) mounted on a rotating gantry. These cameras allow the detection of  $\gamma$ -rays in an energy window between  $\sim 100$  and  $360$  keV. Respective nuclides emit photons to all directions that can be detected if they traverse a collimator hole. Collimators are used to provide positional information for detected photons.<sup>[12-14]</sup> (B) Although optimized for detection of high-energy  $511$  keV  $\gamma$ -rays, PET detectors are built up similarly, except that collimators are not mandatory.<sup>[15]</sup> Respective nuclides emit positrons that, after traveling a certain range (proportional to the  $\beta^+$ -energy), annihilate with a surrounding electron resulting in emission of two  $511$  keV photons at  $180^\circ$  to each other. These photons are electronically detected as coincidence event when they strike opposing detectors within a specified coincidence timing window, usually  $6 - 12$  nanoseconds (parts of the detector ring are schematically depicted).<sup>[15-18]</sup> (C) Principle of TRT based on  $SST_2$ -binding peptides equipped either with a  $\beta^-$ - ( $^{90}Y$ ) or  $\alpha$ -emitting ( $^{213}Bi$ ) nuclide.  $\beta^-$ -particles mainly cause repairable single-strand DNA damage, whereas non-repairable double-strand DNA breaks can be attained by  $\alpha$ -particles. The tissue range of  $\alpha$ -emitters (about  $80 \mu m$ ) is  $\sim 2$  cell diameters. The mean tissue range of the  $\beta^-$ -emitter  $^{90}Y$  ( $3$  mm) is  $\sim 75$  cell diameters. Thus, “cross-fire” radiation to surrounding normal tissue is reduced by  $\alpha$ -emitters.<sup>[19]</sup>  $SST_2$ , somatostatin receptor subtype 2; LET, linear energy transfer; DNA, deoxyribonucleic acid. *Figure 1A* was inspired by references [12, 13], *Figure 1B* was inspired by references [16-18] and *Figure 1C* was adapted from reference [19] and slightly modified.

## INTRODUCTION

Among other potential target structures, glutamate carboxypeptidase II (also named prostate-specific membrane antigen, PSMA) as a structural feature of prostate cancer (PCa) lesions emerged and enabled promising theranostic applications in prostate cancer management.<sup>[20, 21]</sup> Besides, the overexpression of glucagon-like peptide 1 receptor (GLP-1R) was described in selected neoplasms like insulinomas (benign and malignant), pheochromocytomas and gastrinomas, emphasizing its increasing role for management of neuroendocrine tumors.<sup>[22]</sup> For these reasons, this PhD thesis was focused on the development and preclinical evaluation of radiolabeled peptide-based GLP-1 receptor ligands and PSMA inhibitors.

## 1.1. GLP-1 receptor ligand development

### 1.1.1. Glucagon-like peptide 1 receptor

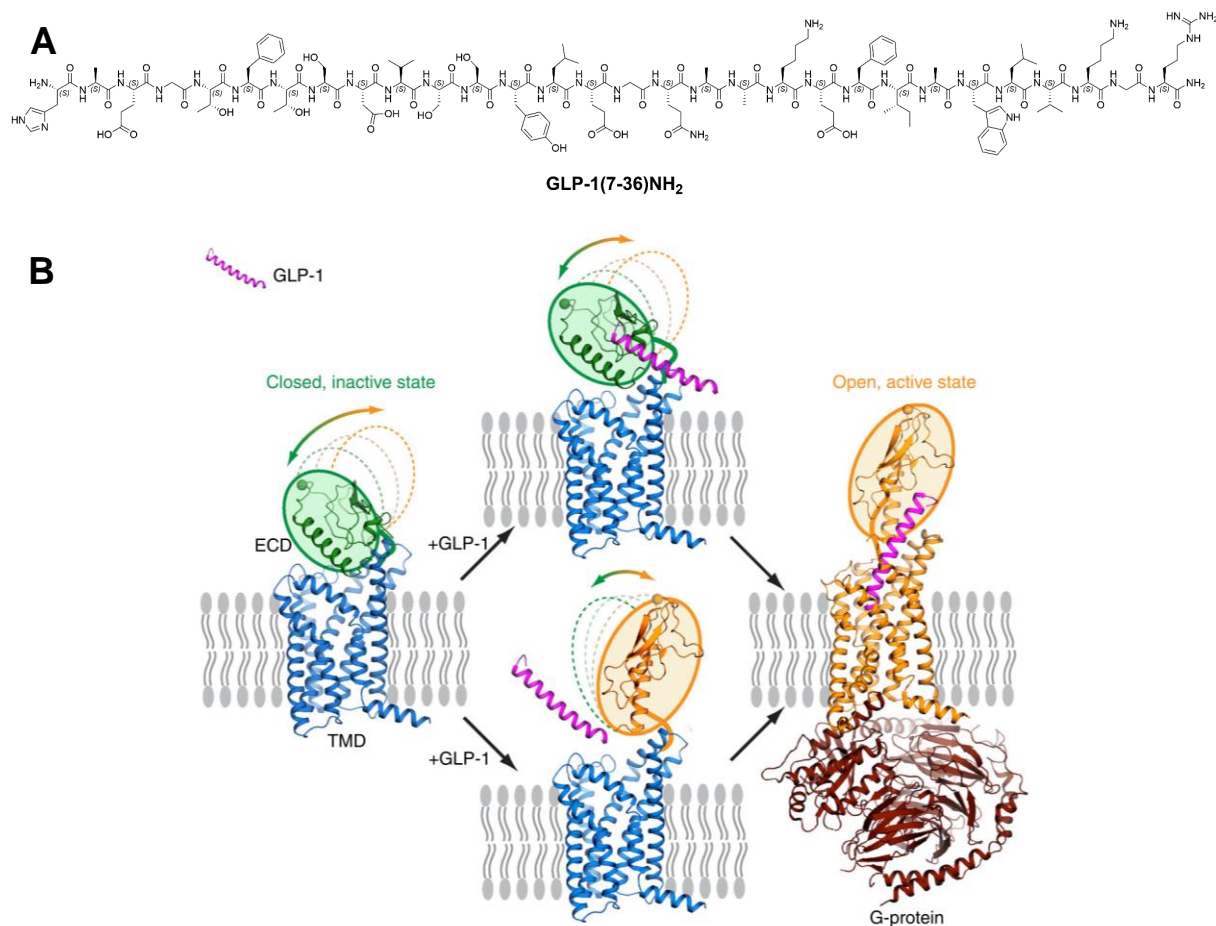
The GLP-1 receptor is a class B G protein-coupled receptor (GPCR), mainly located on  $\beta$ -cells of the pancreas in humans under normal physiological conditions. It is expressed on Brunner's glands (duodenum) and in the central nervous system (neurohypophysis and leptomeninges). A low receptor incidence was found in the gastrointestinal tract, breast, lung and kidneys.<sup>[23-25]</sup> Additionally, mRNA expression of GLP-1R was detected in the heart.<sup>[26]</sup>

GPCRs of the class B subfamily are characterized by three conserved disulfide bonds in the extracellular *N*-terminal domain. Their ligands, such as the peptide hormones glucagon-like peptide 1 and 2 (GLP-1 and GLP-2), glucagon, glucose-dependent insulinotropic polypeptide (GIP), secretin, pituitary adenylate cyclase-activating polypeptide (PACAP), vasoactive intestinal polypeptide (VIP), etc. share common structural features especially in the *N*-terminal region.<sup>[27]</sup> The glucagon receptor family, a further suborder of the class B GPCRs, consists of six members, i.e. GLP-1R, the glucagon-like peptide 2 receptor (GLP-2R), the glucagon receptor (GCGR), the glucose-dependent insulinotropic polypeptide receptor (GIPR), the growth hormone-releasing hormone receptor (GHRHR) and the secretin receptor (SCTR).<sup>[28]</sup>

Human GLP-1R is a 463-residue glycoprotein that is arranged in a classical GPCR-like manner. The extracellular *N*-terminus is connected to an  $\alpha$ -helical seven-transmembrane domain (7-TMD) that finally ends in a short intracellular *C*-terminal region.<sup>[29]</sup> The *N*-terminal domain (amino acids 1 - 128) exhibits an  $\alpha$ -helical portion at the *N*-terminus and two antiparallel  $\beta$ -strands, stabilized by three disulfide bonds (Cys<sup>46</sup> - Cys<sup>71</sup>, Cys<sup>62</sup> - Cys<sup>104</sup>, Cys<sup>85</sup> - Cys<sup>126</sup>) and a salt bridge (Arg<sup>64</sup>-Asp<sup>74</sup>).<sup>[27, 30]</sup> Moreover, this part of the receptor accommodates six tryptophan residues (Trp<sup>39</sup>, Trp<sup>72</sup>, Trp<sup>87</sup>, Trp<sup>91</sup>, Trp<sup>110</sup> and Trp<sup>120</sup>), conserved in human and rat GLP-1R (91% sequence identity). Successive mutations of the tryptophans by alanine residues in rat GLP-1R revealed almost all tryptophans to be crucial for receptor ligand interaction, with the exception of Trp<sup>87</sup>.<sup>[31]</sup>

Binding of the endogenous ligand GLP-1 (*Figure 2A*) to the intact GLP-1 receptor is supposed to proceed according to the 'two-domain' model (*Figure 2B*).<sup>[32, 33]</sup> Thereby, the *C*-terminal part of the ligand is initially bound by the extracellular *N*-terminal domain, enabling a second interaction between *N*-terminal residues of the ligand and the 7-TMD of the receptor. Besides, a small portion of GLP-1R already exists in the open conformation state to which ligand binding is readily possible without further conformational changes of the extracellular receptor part.<sup>[33]</sup> Peptide binding to the juxtamembrane domain occurs by several essential *N*-terminal residues of GLP-1, with histidine at the very *N*-terminal end being responsible for activating the receptor and stimulating intracellular signaling.<sup>[34]</sup>

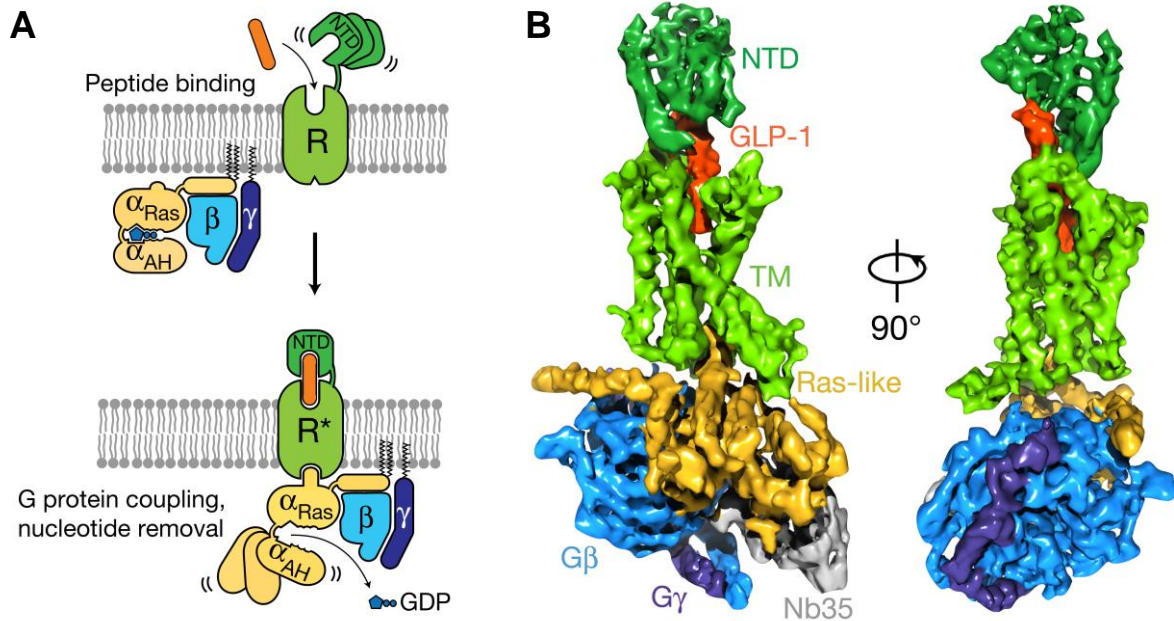
## INTRODUCTION



**Figure 2:** (A) Molecular structure of the endogenous GLP-1R ligand glucagon-like peptide 1(7-36)amide. (B) The canonical ‘two-domain’ activation pathway. Without the presence of GLP-1 (left), the receptor is dynamic and the extracellular domain (ECD) can adopt multiple conformations (dashed circles) but favors a closed inactive state (solid green circle). Subtle dynamics of the ECD allow for binding of GLP-1’s C-terminus to the ECD (upside at the middle), which triggers further dissociation of the ECD from the TMD. This enables GLP-1’s N-terminus to enter the orthosteric pocket in the TMD and activate the receptor (right). Alternatively, the pre-existing small population with open conformation (solid yellow circle) can accommodate GLP-1 smoothly (downside at the middle) and then trigger further conformational changes within the TMD that enable intracellular accommodation of the downstream G protein (right). The ECD movements are indicated with arrows, and the closed and open conformations are colored with green and yellow backgrounds, respectively. The inactive (PDB: 6LN2) and active (PDB: 5VAI) TMDs are shown as blue and yellow cartoons, respectively. The G protein from the active structure (PDB: 5VAI) is shown as brown cartoon. Cell membranes are shown as grey lipid bilayers.<sup>[33]</sup> Figure 2B was taken from reference [33].

Activation of the receptor, intracellular signaling and inactivation of GLP-1R follows the known mechanisms for G protein-coupled receptors (Figure 3A).<sup>[35, 36]</sup> GLP-1R activation enables translation of an extracellular surface signal (i.e. GLP-1 binding) to the intracellular receptor side, resulting in G protein engagement (primarily the stimulatory G protein G<sub>s</sub>) and activation of various downstream signaling cascades.<sup>[37]</sup>

## INTRODUCTION

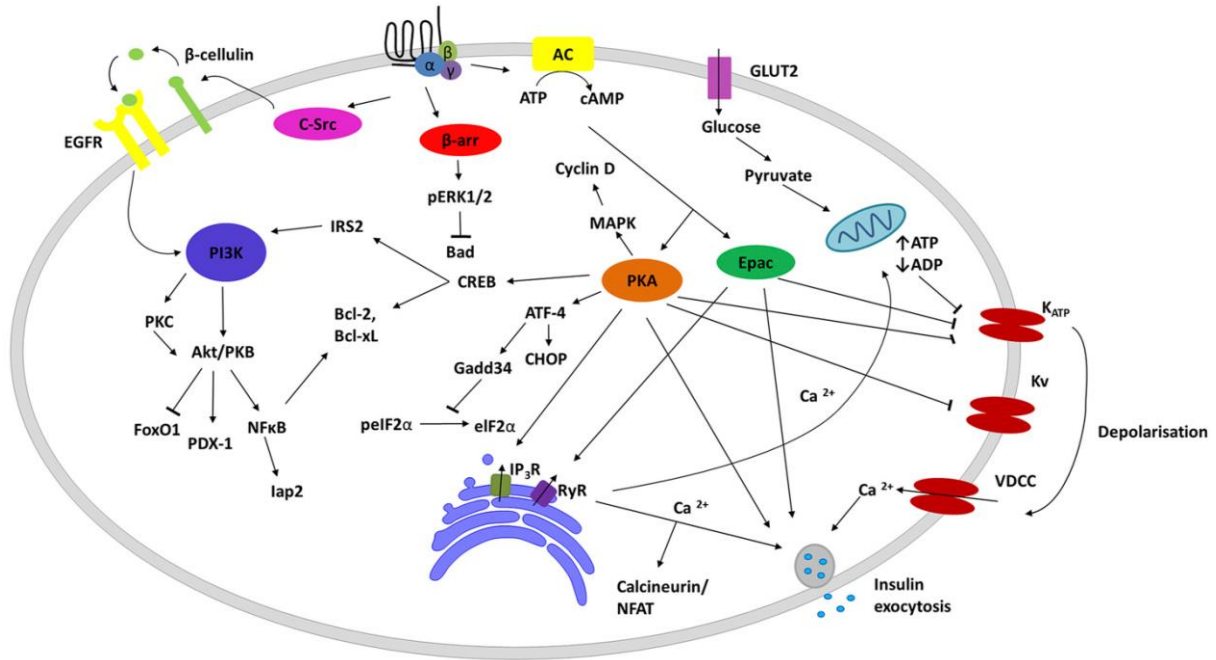


**Figure 3:** (A) Schematic representation of the activation of a class B GPCR by an extracellular peptide agonist via the 'two-domain' binding mechanism. NTD, N-terminal domain; R, receptor; AH,  $\alpha$ -helical domain; GDP, guanosine 5'-diphosphate. (B) Cryo-electron microscopy (EM) structure of a human GLP-1 - rabbit GLP-1R- $G_s$  complex. Views of the GLP-1R- $G_s$  complex cryo-EM density map, coloured by subunit (transmembrane domains in light green, N-terminal domain in dark green, GLP-1 peptide in orange,  $G_{\alpha s}$  Ras-like in gold,  $G_{\beta}$  in light blue,  $G_{\gamma}$  in dark blue and Nb35 in grey).<sup>[37]</sup>  $G_s$ , heterotrimeric G protein that stimulates cAMP-dependent pathway;  $G_{\alpha s}$ ,  $G_s$  alpha subunit; Ras, Rat sarcoma G protein;  $G_{\beta/\gamma}$ ,  $\beta/\gamma$  subunit of G protein; Nb35, nanobody 35. *Figures 3A and 3B* were taken from reference [37].

Intracellular signaling pathways have been predominantly investigated in transfected (human or murine GLP-1R) recombinant cell lines and human pancreatic  $\beta$ -cells, with the latter representing a main object of study. In these organisms, GLP-1R-based activation of G-proteins results in elevated 3', 5'-cyclic adenosine monophosphate (cAMP) levels, increased calcium mobilization and activation of two downstream effectors, protein kinase A (PKA) and exchange protein activated by cAMP (Epac). Apart from G protein-coupled mechanisms, also G protein independent pathways like  $\beta$ -arrestin protein recruitment are present. Especially in pancreatic  $\beta$ -cells, these signaling pathways lead to glucose-stimulated insulin secretion, insulin synthesis and storage as well as  $\beta$ -cell survival, proliferation, and neogenesis (*Figure 4*).<sup>[29]</sup>

Several GLP-1-mediated physiological effects have also been identified for extrapancreatic GLP-1R expression sites like in the liver, kidneys, gastrointestinal tract, brain and cardiovascular system. However, the mechanistic basis for these effects is less well characterized.<sup>[29]</sup>

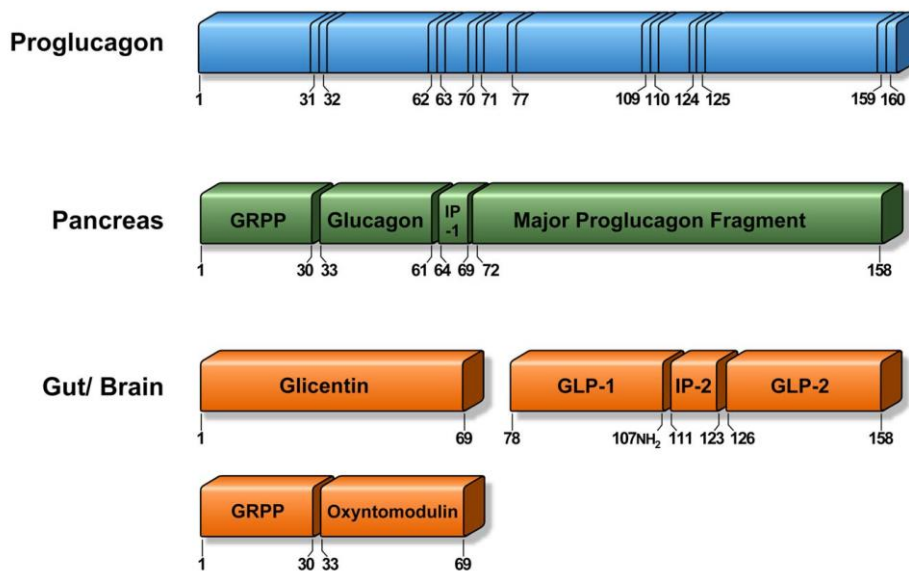
## INTRODUCTION



**Figure 4:** Summary of the main characterized pathways of glucose and GLP-1 signaling in the pancreatic  $\beta$ -cell. Increased plasma glucose levels provoke glucose uptake and metabolism by the  $\beta$ -cell.<sup>[38]</sup> Intracellular glucose stimulates mitochondrial adenosine 5'-triphosphate (ATP) synthesis. ATP indirectly promotes  $\text{Ca}^{2+}$  influx and in combination with GLP-1R-mediated activation of PKA and Epac, stimulates insulin release.<sup>[29, 38, 39]</sup> Biosynthesis of insulin is triggered by increased intracellular  $\text{Ca}^{2+}$  levels that activate calcineurin and nuclear factor of activated T cells (NFAT), which in turn promote insulin gene transcription. In addition, GLP-1 signaling pathways promote  $\beta$ -cell proliferation, neogenesis, and inhibition of apoptosis via reduction of endoplasmic reticulum stress, activation of cyclin D and elevated expression of anti-apoptotic proteins B-cell lymphoma-2 and -xL (Bcl-2, Bcl-xL). Further upregulation of anti-apoptotic Bcl-2, Bcl-xL and inhibitor of apoptosis protein-2 (Iap2) is mediated by phosphatidylinositol-3-kinase (PI3K) activation. Individual biochemical processes are described in more detail by Graaf *et al.*<sup>[29]</sup> Figure 4 was taken from reference [29].

### 1.1.2. Glucagon-like peptide-1

Glucagon-like peptide-1 is an insulinotropic incretin hormone, postprandially secreted by entero-endocrine cells (L-cells) of the small intestine and promotes glucose-dependent insulin release by interaction with its designated receptor (GLP-1R), located on pancreatic  $\beta$ -cells. The peptide hormone is generated by tissue-specific posttranslational processing of proglucagon.<sup>[29, 40]</sup> Transcription of the proglucagon gene, located on human chromosome 2, mainly occurs in the pancreas, the small intestine, and the CNS. The resulting mRNA is translated into a single protein (proglucagon) and then processed by tissue-specific prohormone convertases (*Figure 5*).<sup>[29, 39]</sup>



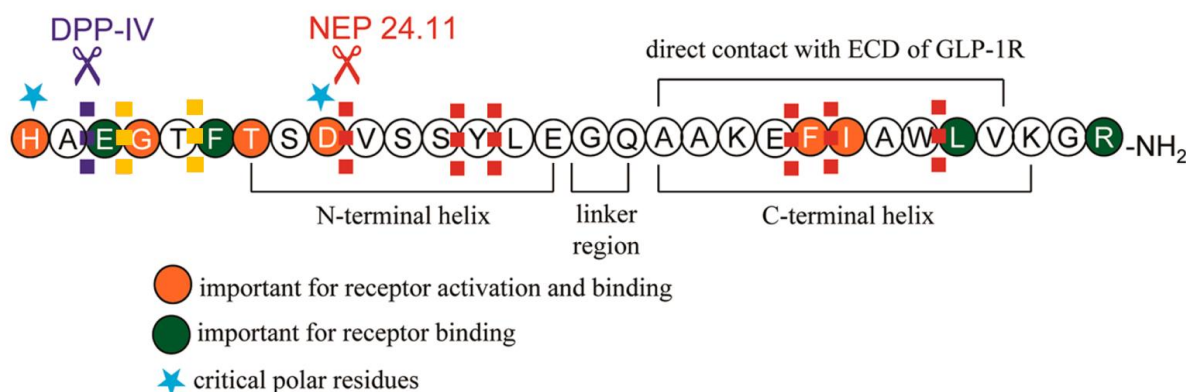
**Figure 5:** Differential posttranslational processing of proglucagon in the pancreas as well as in the gut and brain. In the pancreatic  $\alpha$ -cells, the proglucagon protein is processed by prohormone convertase 2 (PC2) into glicentin-related polypeptide (GRPP), glucagon, intervening peptide-1 (IP-1) and major proglucagon fragment which is not further cleaved. GLP-1 (78 - 107NH<sub>2</sub>), GLP-2, intervening peptide-2 (IP-2) and glicentin are generated by prohormone convertase 1/3 (PC1/3) in the brain and in the L-cells of the small intestine. Subsequent cleavage of glicentin finally results in GRPP and oxyntomodulin. The numbers indicate amino acid positions in the 160-residue proglucagon sequence. The vertical lines indicate positions of basic amino acid residues, serving as canonical cleavage sites for PC2 (pancreas) and PC1/3 (gut/brain).<sup>[29, 39]</sup> *Figure 5* was taken from reference [39].

Posttranslational processing by PC1/3 results in several forms of GLP-1, comprising different chain lengths and occasional amidation. Based on the first cloning experiments (cDNA encoding for anglerfish preproglucagon) and a presumed cleavage site after two adjacent basic residues (70 and 71, *Figure 5*), the first synthesized GLP-1 peptides supposed to effect plasma glucose and insulin levels were termed GLP-1(1-37) and GLP-1(1-36). However, since the expected insulinotropic effects could not be observed, a further processing step was assumed for creating truncated polypeptides that exhibit a closer sequence alignment with other peptide hormones of

## INTRODUCTION

the glucagon superfamily.<sup>[41]</sup> Indeed, cleavage of GLP-1(1-37) after position 6 leads to bioactive GLP-1(7-37) as well as to the equipotent GLP-1(7-36)amide, which is generated by C-terminal glycine removal of GLP-1(7-37) and subsequent amidation. The latter represents the majority of circulating GLP-1 in the small intestine (80% GLP-1(7-36)amide vs. 20% GLP-1(7-37)). In addition, plasma levels of the amidated form were observed to increase by a factor of six after food intake, whereas no significant rise of the acidic form could be observed.<sup>[42-44]</sup> Therefore, the term 'GLP-1' in this study always refers to the amidated form GLP-1(7-36)amide, unless otherwise stated.

In previous structure-activity studies, especially N-terminal residues of GLP-1 have been identified to be crucial for ligand-receptor interaction and stimulation of GLP-1R-based downstream processes (Figure 6). Site-directed single-point alanine substitutions revealed His<sup>7</sup>, Gly<sup>10</sup>, Phe<sup>12</sup>, Thr<sup>13</sup>, Asp<sup>15</sup>, Phe<sup>28</sup> and Ile<sup>29</sup> to be indispensable for maintaining high affinity towards rat GLP-1R.<sup>[40, 45]</sup> For GLP-1R activation, His<sup>7</sup>, Gly<sup>10</sup>, Asp<sup>15</sup> and Phe<sup>28</sup> were found to be of major importance. Phe<sup>28</sup> and Ile<sup>29</sup> are not directly involved in receptor activation but rather ensure a distinct conformation of GLP-1 recognized by GLP-1R.<sup>[45]</sup>



**Figure 6:** Sequence of GLP-1 and critical residues for receptor interaction. Important residues for receptor binding are colored green, those which are crucial for receptor activation and binding are colored orange. His<sup>7</sup> and Asp<sup>15</sup> as critical polar residues are additionally highlighted. Cleavage sites of dipeptidyl peptidase IV (DPP IV), neutral endopeptidase 24.11 (NEP 24.11) and further ectopeptidases are depicted in purple, red and yellow dotted lines, respectively.<sup>[34, 40, 45-51]</sup> Figure 6 was inspired by references [46, 48, 49].

Certain residues, essential for ligand-based selectivity of GLP-1 were explored by Hjorth *et al.*, who investigated alterations in binding affinity (IC<sub>50</sub>) towards GLP-1 (rat) and glucagon (porcine) receptors (~ 50% sequence identity) using GLP-1/glucagon chimeras. Substitutions in the C-terminal region of GLP-1 with the respective glucagon residues resulted in a much higher loss of affinity towards GLP-1R when compared to the analogous glucagon experiments. Even full substitution of the C-terminus of glucagon by GLP-1 residues (termed glucagon(N)-GLP-1(C)) still gave high affinities towards GCGR (47 ± 11 nM, n = 8) and GLP-1R (1.7 ± 0.8 nM, n = 8), whereas the inverted chimera (termed GLP-1(N)-glucagon(C)) showed markedly reduced affinities for both receptors (> 1000 nM, n = 5 towards GCGR and 290 ± 60 nM, n = 6 towards GLP-1R).<sup>[52]</sup>

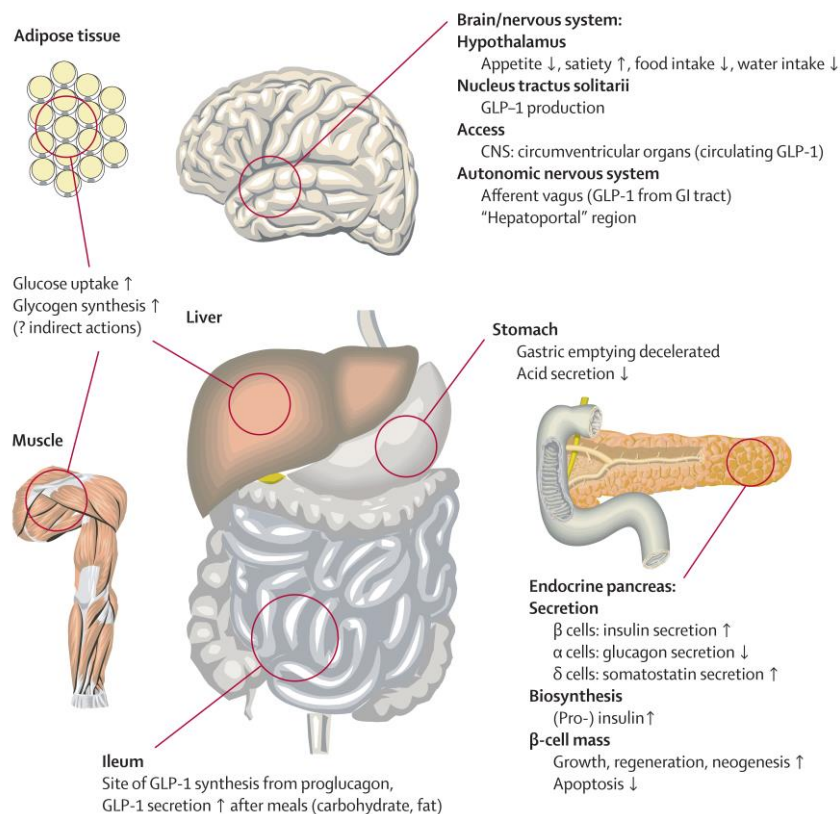
## INTRODUCTION

For this reason, it was supposed that receptor selectivity and sensitivity of GLP-1 is not only defined by distinct *N*-terminal residues (His<sup>7</sup>, Gly<sup>10</sup>, Phe<sup>12</sup>, Thr<sup>13</sup>, Asp<sup>15</sup>), but also amino acids of the *C*-terminal part are involved. In accordance with the 'two-domain' model, these results emphasize the importance of the *C*-terminus for receptor-ligand interaction.<sup>[32]</sup> Therefore, the development of high affinity short-chained peptide-based or low-molecular-weight non-peptide GLP-1R a(nta)gonists was presumed to be not realizable, since non-contiguous residues within the *N*- and *C*-terminus and also in between were essential for high affinity and potency.<sup>[53]</sup>

The most studied biological effect of GLP-1 in humans represents its glucose-dependent insulinotropic action via GLP-1R activation on pancreatic  $\beta$ -cells (*Figure 4*).<sup>[29]</sup> The risk of hypoglycemia is thereby notably reduced, as further insulin release below a blood glucose level of 3.5 mmol/L is almost completely ceased, resulting in a self-limiting process.<sup>[54]</sup> In this context it is important to note, that GLP-1 secretion (and hence insulin production) is not stimulated by elevation of plasma glucose via intravenous administration, indicating that the glucose-sensing machinery is distributed on the luminal side of the small intestine and triggered by nutrient stimuli.<sup>[55]</sup>

Beside the glucose-dependent insulinotropic action, GLP-1 also suppresses glucagon release directly via binding to GLP-1R on pancreatic  $\alpha$ -cells as well as indirectly via GLP-1-stimulated production of insulin ( $\beta$ -cells) and somatostatin ( $\delta$ -cells). Since only 20% of glucagon positive  $\alpha$ -cells were found to express GLP-1R (rat endocrine pancreas), the glucagonostatic effect was supposed to be mainly caused by insulin and somatostatin rather than by direct GLP-1-R-mediated inhibition.<sup>[29, 54, 56]</sup> Furthermore, via activation of its cognate receptor in the brain GLP-1 induces satiety, dose-dependent motility reduction of the gastrointestinal tract and deceleration of gastric emptying.<sup>[54, 57, 58]</sup> An overview of the main GLP-1-induced processes (direct and indirect) is depicted in *Figure 7*.

## INTRODUCTION



**Figure 7:** Physiology of GLP-1 secretion and action on GLP-1 receptors in different organs and tissues. GLP-1 acts directly via activation of the GLP-1R on pancreatic islets and in the brain. Activation of GLP-1R signaling pathways in the brain leads to indirect biological actions in the liver, adipose tissue, muscles and gastrointestinal tract.<sup>[58, 59]</sup> Figure 7 was taken from reference [59].

All these physiological actions of GLP-1, especially those which have beneficial effects on insulin synthesis, secretion and  $\beta$ -cell mass, have been found to be advantageous for the treatment of diabetes mellitus (type 1 as well as type 2) in humans.<sup>[39, 60]</sup> Theoretically, administration of GLP-1 would indeed normalize high blood glucose levels with simultaneous prevention of hypoglycemia. Hence, its application could provide a significant advantage over direct insulin injection. This concept is impaired, however, by the short biological half-life of endogenous GLP-1 (< 2 minutes) that mainly results from enzymatic inactivation by ectopeptidases like DPP IV and NEP 24.11 (Figure 6).<sup>[29, 47, 48]</sup>

The primary inactivating enzyme DPP IV is a serine protease with ubiquitous expression, removing *N*-terminal dipeptides not only from GLP-1 but also from other peptide hormones with Xaa-Pro and Xaa-Ala *N*-termini. In human plasma (soluble form) and surface-bound on endothelial cells, DPP IV catalyzes *N*-terminal His<sup>7</sup>-Ala<sup>8</sup> removal from GLP-1, which results in a low GLP-1R-binding metabolite (GLP-1(9-36)NH<sub>2</sub>) with almost complete loss of receptor activation, due to absent *N*-terminal His<sup>7</sup>.<sup>[34, 47, 61]</sup>

As a second inactivating enzyme, NEP 24.11 generates a number of short-chained metabolites of GLP-1, due to its known cleavage sites between Asp<sup>15</sup>-Val<sup>16</sup>, Ser<sup>18</sup>-Tyr<sup>19</sup>, Tyr<sup>19</sup>-Leu<sup>20</sup>, Glu<sup>27</sup>-Phe<sup>28</sup>,

## INTRODUCTION

Phe<sup>28</sup>-Ile<sup>29</sup> and Trp<sup>31</sup>-Leu<sup>32</sup> (*Figure 6*). NEP 24.11 is a widespread membrane-bound zinc metallopeptidase that cleaves peptides at the *N*-terminus of hydrophobic residues and metabolizes up to 50% of circulating GLP-1.<sup>[48, 62]</sup>

Fast enzymatic degradation by DPP IV, NEP 24.11 and further ectopeptidases results in only 10 - 20% of intact GLP-1 in human plasma 30 minutes after subcutaneous or intravenous injection, as determined by specific radioimmunoassays (RIAs) and a sensitive enzyme-linked immunosorbent assay (ELISA).<sup>[49, 50, 63]</sup> The degradation products in general are not able to bind or activate GLP-1R, due to loss of substantial fragments.

Therefore, peptidase-resistant GLP-1 analogs were introduced to enable treatment of type 1 and type 2 diabetes.<sup>[64, 65]</sup> Relevant approaches and results in this field were also of high importance for the development of GLP-1R-targeted tumor diagnostics and therapeutics, since the GLP-1R is of clinical interest not only due to its potential in diabetes therapy, but also because of its proven role in cancer.<sup>[22, 66]</sup> However, transfer of the GLP-1R-targeting concept indeed requires a signal/therapeutic agent, linked to the GLP-1R-binding unit. Noninvasive molecular imaging as well as targeted radiotherapy can be pursued by attachment of an appropriate PET/SPECT nuclide or an  $\alpha/\beta$ -emitting radioisotope via a connecting linker unit. These GLP-1R-targeting probes can be used either for molecular imaging of functional  $\beta$ -cell mass<sup>[67-69]</sup> or for imaging and PRRT of GLP-1R-overexpressing tumors.<sup>[22]</sup>

### 1.1.3. GLP-1R as target for molecular imaging and radiotherapy

G protein-coupled peptide hormone receptors play an increasing role as specific targets for oncological diagnosis and therapy.<sup>[2]</sup> Historically, somatostatin receptors were the first receptors found to be expressed in high frequency and at high levels in gastroenteropancreatic neuroendocrine tumors.<sup>[70]</sup> However, somatostatin receptors and in particular SST<sub>2</sub>, are insufficiently expressed in some types of neuroendocrine tumors, explaining the low rate of detection.<sup>[71-74]</sup> Somatostatin receptor scintigraphy (OctreoScan®) only reaches a sensitivity of 50 - 60% for insulinomas<sup>[75]</sup>, as the prevalent benign form was found to be characterized by a remarkable GLP-1R overexpression accompanied by a low frequency and density of somatostatin receptors.<sup>[22, 71]</sup>

Insulinomas, a type of neuroendocrine tumor derived from the  $\beta$ -cells of the pancreas, represent the most common cause of endogenous hyperinsulinemic hypoglycemia in adults.<sup>[22, 74]</sup> Although rare, insulinomas are the most frequent hormone-active tumors of the pancreas with an incidence of 4/1 000 000 per year and a slight female predominance (59%). About 90% of insulinomas are benign and occur as small, encapsulated, solitary tumors, whereas ~ 10% of insulinomas progress to malignant cancer with the formation of metastases. Insulinomas mainly occur as a single isolated tumor or can be a part of the multiple endocrine neoplasia type I (MEN I) syndrome (~ 8%), in which the tumors are always multiple, leading to a higher long-term risk of recurrent disease for patients after surgery.<sup>[76, 77]</sup> For benign insulinomas, 10-year survival is ~ 88% after complete surgical removal of the tumor. In case of malignant, metastasizing insulinomas, postoperative prognosis is poor with a 10-year survival rate of 29%.<sup>[77]</sup> Benign as well as malignant tumors are characterized by an abnormally high insulin production, even at low blood glucose concentrations (1 mmol/L).<sup>[78, 79]</sup> This results in hypoglycemia by which diplopia, blurred vision, confusion, deviant behavior or amnesia could be induced, and might progress to loss of consciousness, coma, or even permanent brain damage. Surgical resection of the tumor lesions yet represents the only curative method, traditionally accomplished by enucleation or partial pancreatic resection.<sup>[80]</sup> This treatment modality inevitably requires a precise localization of the tumor, but due to the small size (< 2 cm) of 90% of insulinomas, localization remains challenging especially with conventional imaging methods, such as magnetic resonance imaging (MRI), computed tomography (CT) as well as endoscopic (ultra)sonography.<sup>[72, 81]</sup>

Common diagnostic agents, targeting metabolic pathways or surface-exposed receptors were either suffering from low sensitivity (<sup>[18F]</sup>Fluorodopa)<sup>[66]</sup>, low glucose turnover of the neuroendocrine tumor (<sup>[18F]</sup>FDG), short half-life of the radionuclide (<sup>[11C]</sup>tryptophane) or rather low mean receptor densities (vasoactive intestinal polypeptide receptor 1 (VPAC<sub>1</sub>): 1 780 dpm/mg tissue and cholecystokinin receptor 2 (CCK<sub>2</sub>): 2 207 dpm/mg tissue), impeding a constant high rate of detection.<sup>[71, 72]</sup>

## INTRODUCTION

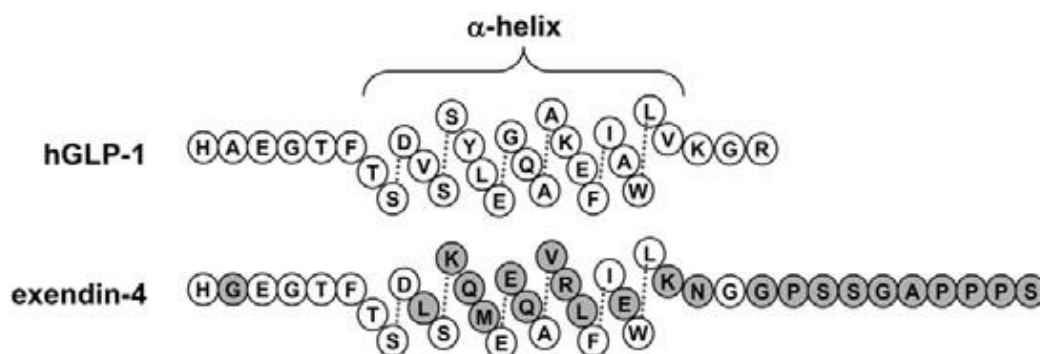
GLP-1R-targeting peptides labeled with PET or SPECT radionuclides notably surpass these imaging modalities in terms of sensitivity and selectivity. Compared to normal pancreatic islets (1 322 dpm/mg tissue), a ~ 6-fold higher receptor density was detected on insulinomas, as expressed by a radioligand binding density of 8 133 dpm/mg tissue. Furthermore, GLP-1R overexpression occurred with a notably high incidence of 93%.<sup>[22, 24]</sup> These values indicated for a high rate of unambiguously positive scans as the critical binding density value of 3 500 dpm/mg tissue (based on previous comparative data for SST<sub>2</sub>) was surpassed by more than 2-fold.<sup>[82]</sup> As a result, GLP-1R-based molecular imaging evolved for the diagnosis of insulinomas, besides targeting of GLP-1 receptors for treatment of diabetes mellitus and surveillance of  $\beta$ -cell mass. In addition, this modality enables a reliable non-invasive detection of small tumor lesions and metastases in contrast to angiography, endoscopic procedures and intraarterial calcium stimulation with venous sampling.<sup>[72, 74, 83]</sup>

For visualization of malignant insulinomas, radiolabeled GLP-1R ligands are only partially suited, since this type of tumor is more frequently characterized by elevated SST<sub>2</sub> expression (> 10 000 dpm/mg tissue, 71% incidence) than by GLP-1R overexpression (8 508 dpm/mg tissue, 36% incidence).<sup>[22, 84]</sup> Nevertheless, patients with GLP-1R positive malignant forms of insulinomas (10% malignant, thereof 36% GLP-1R positive), gastrinomas (45 - 69% malignant, in total 100% GLP-1R positive) and pheochromocytomas (10 - 40% malignant, in total 60% GLP-1R positive) might benefit from GLP-1R-based PRRT. Thereby, harmful symptoms (e.g. hypoglycemia) could be (temporary) controlled by targeting inoperable primary tumors and metastases.<sup>[22, 85-87]</sup>

Exendin-4-derived agents recently attained high relevance for the detection of benign insulinomas and other GLP-1R-overexpressing tumors, like pheochromocytomas (3 970 dpm/mg tissue, 60% incidence) and gastrinomas (2 461 dpm/mg tissue, 100% incidence).<sup>[22, 66, 88]</sup>

### 1.1.4. GLP-1R-targeting radioligands

Originally developed for the treatment of diabetes mellitus, the DPP IV-resistant GLP-1 analog exendin-4 promoted the design of radiotracers for targeting GLP-1R positive insulinomas.<sup>[65, 89]</sup> Exendin-4 shares 53% sequence homology with GLP-1 and possesses a nine-residue C-terminal extension, which is absent in the GLP-1 peptide (*Figure 8*).



**Figure 8:** Amino acid sequences of human GLP-1 and exendin-4. The central  $\alpha$ -helical regions of the peptides are indicated. Conserved amino acids are shown as open circles. Exendin-4-specific amino acids are indicated in gray.<sup>[90]</sup> *Figure 8* was adapted from reference [90].

Exendin-4 was first isolated by Eng *et al.* from the saliva of the gila monster (*heloderma suspectum*) in 1992.<sup>[91]</sup> A glycine residue at position 2 confers resistance towards enzymatic degradation by DPP IV. In combination with a low susceptibility to degradation by NEP 24.11, this leads to a notably increased biological half-life of up to four hours ( $t_{1/2}$ (GLP-1): < 2 minutes).<sup>[43, 48, 92]</sup> Compared to GLP-1, exendin-4 was found to bind with higher affinity to GLP-1R, to exhibit a similar insulinotropic potency ( $EC_{50}$ ) and an even higher efficacy (maximum response) *in vivo* (rat models).<sup>[61, 93]</sup> Exendin-3, comprising two amino acid substitutions (Ser<sup>2</sup>-Asp<sup>3</sup> in place of Gly<sup>2</sup>-Glu<sup>3</sup>) but otherwise identical to exendin-4<sup>[91]</sup>, revealed similar characteristics towards the GLP-1R and hence, also served as a basic structure for radioligand development.<sup>[94, 95]</sup> However, its agonistic behavior towards VPAC receptors at higher concentrations (greater than 100 nM) might indicate a lower receptor specificity.<sup>[91, 96, 97]</sup>

In 2002, a proof of principle for GLP-1R-based targeting of insulinomas was performed by Gotthardt *et al.* on the rat insulinoma cell line RINm5F and in a rat insulinoma animal model (NEDH rats and RINm5F cells) using [<sup>125</sup>/<sup>123</sup>I]-Tyr<sup>19</sup>-GLP-1 and [<sup>125</sup>/<sup>123</sup>I]-His<sup>1</sup>-exendin-3. Despite the metabolic instability of radioiodinated GLP-1 and the unfavorable iodination site of exendin-3, specific uptake was detected in the cell and animal models.<sup>[75]</sup> Follow-up experiments were carried out with [<sup>111</sup>In]In-DTPA-exendin-4 in a Rip1tag2 mouse model (transgenic mice that develop tumors of the pancreatic  $\beta$ -cells in a reproducible, well-defined multistage tumorigenesis pathway). This preclinical study revealed an extremely high GLP-1R density in the murine tumors (17 269 dpm/mg

## INTRODUCTION

tissue), resulting in a correspondingly high uptake of [ $^{111}\text{In}$ ]In-DTPA-exendin-4 ( $287 \pm 62\%$  IA/g) at 4 h p.i. and a clear visualization of tumors as small as 1 mm by pinhole SPECT/MRI and SPECT/CT. Additionally, tumor-to-background ratios were very high (between 13.6 for tumor-to-pancreas and 299 for tumor-to-muscle). Besides the high affinity of the unlabeled ligand towards GLP-1R ( $2.1 \pm 1.1$  nM), *in vitro* studies based on murine insulinoma-derived cells demonstrated specific internalization of [ $^{111}\text{In}$ ]In-DTPA-exendin-4. Biochemical investigations confirmed a high metabolic stability of the radiopeptide in the  $\beta$ -cell tumors as well as in human serum.<sup>[88]</sup> The latter findings substantiated the high potential of this peptide conjugate to specifically localize GLP-1R positive lesions within the pancreas and hence, [ $^{111}\text{In}$ ]In-DTPA-exendin-4 was further investigated in patients.<sup>[98]</sup>

High radioactivity accumulation in small insulinoma lesions enabled radioguided surgery with a  $\gamma$ -probe, not only by [ $^{111}\text{In}$ ]In-DTPA-exendin-4 but also in six patients preoperatively scanned with [ $^{111}\text{In}$ ]In-DOTA-exendin-4, resulting in intraoperative localization of the insulinomas and successful enucleation where possible.<sup>[74]</sup> In Switzerland, Germany and the UK, 30 adults were recruited between 2008 and 2011 during a multicenter study investigating the imaging performance of insulinomas by [ $^{111}\text{In}$ ]In-DTPA-exendin-4 SPECT/CT. Thereby, a positive predictive value of 83% was reached. Seven patients (23%) were referred to surgery solely on the basis of [ $^{111}\text{In}$ ]In-DTPA-exendin-4 imaging. For 23 assessable patients, [ $^{111}\text{In}$ ]In-DTPA-exendin-4 SPECT/CT had a higher sensitivity (95%) than CT/MRI (47%).<sup>[99]</sup>

More details about the previously mentioned patient studies and representative examples of further study outcomes in which exendin-4 derivatives have been labeled with SPECT nuclides are listed in *Table 1*.  $^{99\text{m}}\text{Tc}$  as a cost-effective alternative was chosen to reduce the relatively high  $^{111}\text{In}$ -effected radiation burden for the patients. Furthermore, PET nuclides were used for radiometallation and -halogenation, since a higher sensitivity, better spatial resolution and a more accurate quantification could be achieved with the respective exendin-4 conjugates (*Table 2*). Indirect  $^{18}\text{F}$ -labeling via prosthetic groups led to intact peptide conjugates with high affinity but resulted in prolonged and more cumbersome synthesis procedures.<sup>[89]</sup> Therefore, mainly  $^{111}\text{In}$ - and  $^{68}\text{Ga}$ -labeled derivatives entered clinical trials so far, with the latter profiting from affordable  $^{68}\text{Ga}$ -generators and no need of an on-site cyclotron.<sup>[89, 100]</sup>

## INTRODUCTION

**Table 1:** Representative clinical SPECT tracers for insulinoma imaging and study outcomes.<sup>[89]</sup>

Radio-isotope	Tracer	Patients	Peptide mass [µg]	Activity [MBq]	Results	Ref.
In-111	[Lys <sup>40</sup> (Ahx-DOTA)-NH <sub>2</sub> ]Exendin-4	6	30	82 - 97	All insulinomas correctly localized.	[74]
	[Lys <sup>40</sup> (Ahx-DTPA)-NH <sub>2</sub> ]Exendin-4	11	10 ± 2	108 - 136	Uptake in 4/11 patients.	[84]
	[Lys <sup>40</sup> (Ahx-DTPA)-NH <sub>2</sub> ]Exendin-4	30	8 - 14	80 - 128	95% sensitivity 20% specificity 83% positive predictive value	[99]
Tc-99m	[Lys <sup>40</sup> (Ahx-HYNIC/EDDA)-NH <sub>2</sub> ]Exendin-4	11	-	740	Uptake in 8/11 patients. Insulinoma confirmed in 6/8 cases after surgery.	[101]

**Table 2:** Representative clinical PET tracers for insulinoma imaging and study outcomes.<sup>[89]</sup>

Radio-isotope	Tracer	Patients	Peptide mass [µg]	Activity [MBq]	Results	Ref.
Ga-68	[Ni <sup>14</sup> , Lys <sup>40</sup> (Ahx-DOTA)-NH <sub>2</sub> ]Exendin-4	5	12 - 15.3	76 - 97	Uptake in 5/5 patients. Insulinoma confirmed in 4/4 patients after surgery.	[102]
	[Cys <sup>40</sup> (NOTA-MAL)-NH <sub>2</sub> ]Exendin-4	52	7 - 25	18.5 - 185	Surgery in 43/52 patients. Insulinoma confirmed in 42/43 patients (97.7% sensitivity)	[103]
	[Ni <sup>14</sup> , Lys <sup>40</sup> (Ahx-DOTA)-NH <sub>2</sub> ]Exendin-4	52	11.6 – 23.8	43 - 106	94.6% sensitivity 99.1% positive predictive value	[104]

## INTRODUCTION

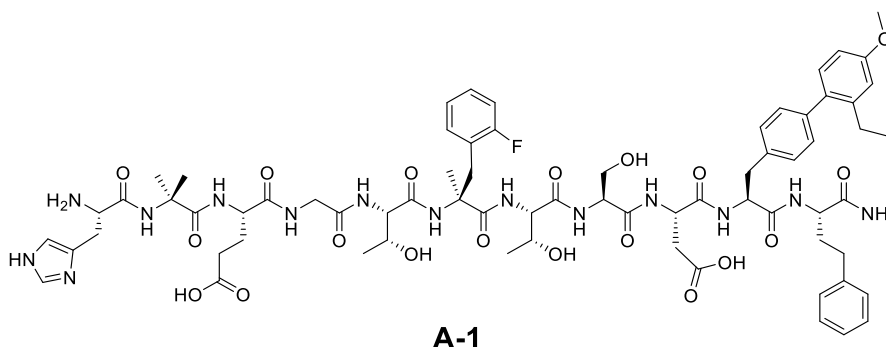
The agonistic behavior of exendin-4 towards GLP-1R decelerated gastric emptying and induced an additional release of insulin from functional insulinomas, which led to decreased blood glucose levels, nausea and vomiting in patients who underwent SPECT imaging. These side effects were also observed during PET imaging but indeed to a lesser extent, as the higher spatial resolution and sensitivity provided by PET nuclides allowed for a lower dose to apply. To reduce hypoglycemia, patients received continuous glucose infusions.<sup>[89]</sup>

Based on the finding that crucial residues for GLP-1 receptor binding and activation are located mainly at the *N*-terminal nonapeptide (*Figure 6*), radiolabels were mainly introduced at the *C*-terminal end of exendin-derived imaging agents.<sup>[46, 105]</sup> Even multichelation at this site was tolerated to a certain extent by the receptor.<sup>[95]</sup> By contrast, repositioning of the radiolabel in general provided ambiguous results, though some evidence exists for position 12 to serve as a possible conjugation site for chelator attachment.<sup>[69, 106, 107]</sup>

At present, GLP-1R-targeting radioligands that structurally clearly differ from exendin-4 are not available. Although low-molecular-weight organic molecules were developed for addressing the GLP-1R (orally available antidiabetics)<sup>[29, 108]</sup>, none of them were able to show favorable properties comparable or even superior to exendin-4/GLP-1-based polypeptide ligands.<sup>[29, 109, 110]</sup>

By contrast, short-chained undecapeptides developed in 2009 by Mapelli *et al.* were able to induce cAMP production in CHO cells, stably overexpressing the human GLP-1 receptor with similar  $EC_{50}$  values (87 pM) like GLP-1 (34 pM).<sup>[111]</sup> Indeed, these high potencies were not plausible at first sight, since downsizing of GLP-1R ligands was assumed to lead to non-binding and hence, non-signaling agonists.<sup>[52, 53]</sup> However, the bulky hydrophobic residues at the *C*-terminus (position 10 and 11) of these GLP-1 mimetics, obviously compensate for the 21-residue GLP-1(16-36)amide fragment to a certain extent. 2-Aminoisobutyric acid (Aib) instead of L-alanine was introduced at the second position to confer DPP IV resistance. For stabilization of an  $\alpha$ -helical structure presumed to be crucial, also for binding of the endogenous ligand GLP-1<sup>[112]</sup>, L-phenylalanine at position 12 (GLP-1 counting method) was substituted with L- $\alpha$ -methyl-(2-fluoro)-phenylalanine (now position 6). Additional screening experiments for alternative residues at positions 10 and 11, revealed lead peptide **A-1** which was even more potent ( $EC_{50} = 31$  pM) bearing a simple L-homophenylalanine residue at position 11 and a more bulky (2'-Et, 4'-OMe)4, 4'-L-biphenylalanine ((2'-Et, 4'-OMe)BIP) at the penultimate position (*Figure 9*).<sup>[113, 114]</sup> Unfortunately, affinity data were not presented in these studies.

## INTRODUCTION



**Figure 9:** Sequence of lead peptide **A-1**, with His<sup>1</sup>-Aib<sup>2</sup>-Glu<sup>3</sup>-Gly<sup>4</sup>-Thr<sup>5</sup>-( $\alpha$ -Me)-(2-F)-Phe<sup>6</sup>-Thr<sup>7</sup>-Ser<sup>8</sup>-Asp<sup>9</sup>-(2'-Et, 4'-OMe)BIP<sup>10</sup>-homoPhe<sup>11</sup>-NH<sub>2</sub>.<sup>[113]</sup> All amino acids are in L-configuration and given in the three-letter code. Et, ethyl; Me, methyl; BIP, 4, 4'-L-biphenylalanine.

Follow-up studies, based on these undecapeptides mainly focused on GLP-1 peptidomimetics with cyclic constraints or cyclic  $\alpha$ -conotoxin-GLP-1 chimeras.<sup>[115-117]</sup> These modifications led to a clear activity decline in cAMP signaling ( $EC_{50}$ ) in comparison to the respective non-cyclized 11-mer peptides.

Although none of these undecapeptides were converted into an imaging agent for insulinomas so far, they might potentially serve as a basis for GLP-1R radioligands with an improved pharmacokinetic profile. Despite initial positive results, the use of exendin-4-based radiometallated agents for the detection of insulinoma lesions is particularly impaired by high non-target tissue uptake in the kidneys.<sup>[89]</sup> Consequently, radioligands with improved tumor-to-kidney ratios are of major interest and might be generated via radiolabeling of a downsized GLP-1R ligand, as discussed in more detail in the following section.

### 1.1.5. Current limitations for the diagnosis and PRRT of insulinomas

Whereas radiohalogenated compounds exhibit low kidney uptake and/or fast renal excretion<sup>[106, 118]</sup>, elevated accumulation and retention in the kidneys (> 140% ID/g, 1 - 4 h p.i.) is always observable when residualizing radiometals are used for exendin-4 derivatization.<sup>[89]</sup> This non-target tissue uptake not only impairs the detection of insulinomas but could also affect the localization of other GLP-1R positive tumors like pheochromocytomas and gastrinomas, due to the close local proximity of the kidneys to the respective target organs (pancreas (insulinoma), adrenal medulla (pheochromocytoma), duodenum, pancreas and periduodenal lymph nodes (gastrinoma)).<sup>[86, 87, 119]</sup> Thereby, the intrinsically lower resolution of SPECT revealed an inferior rate of detection compared to PET.<sup>[105]</sup> Moreover, the radiation burden of the kidneys might limit the use of long-lived radioisotopes, especially in the context of PRRT approaches.<sup>[89]</sup>

Since a low amount of GLP-1R expression was detected in the kidneys and high activity accumulation by this organ could not be specifically blocked by an excess of unlabeled analog, a non-saturable, GLP-1R independent mechanism was presumed for tubular reabsorption.<sup>[94, 120, 121]</sup> Accordingly, further studies revealed that the megalin transporter system of renal proximal tubules is crucial for uptake and retention of <sup>111</sup>In-labeled exendin-4 and potential metabolites.<sup>[122-124]</sup> Kidney extracts of mice that received [<sup>18</sup>F]AIF-NOTA-exendin-4 showed a single very polar radioactive metabolite at 1 h p.i. and no detectable parent peptide. The identity of this metabolite could not be determined, but the general observation that exendin-4 peptides with C-terminal radiometal chelates exhibit very high uptake, suggests that some metabolite from the C-terminal end might be responsible for the slow egress from the kidneys.<sup>[125]</sup> By comparing the renal accumulation of the <sup>111</sup>In-labeled GPCR ligands octreotide, minigastrin, bombesin and exendin-4, Gotthardt *et al.* observed that the number of charged amino acids in these peptides correlates with their kidney uptake. Therefore, beside the radiometal chelate-induced renal retention, the high number of charged amino acids of exendin-4-based radioligands was supposed to play a critical role for tubular reabsorption, although the exact mechanism still remains unknown.<sup>[124]</sup>

A conventional method used for lowering the kidney uptake of radiotracers makes use of pre-administration of amino acids.<sup>[126]</sup> Gotthardt *et al.* applied this method for [<sup>111</sup>In]In-DTPA-exendin-4 in rats and revealed that both gelofusine (18.7% decrease) and poly-L-glutamic acid (29.4% decrease) as well as the combination of both (47.9% decrease) had a significant impact on kidney uptake, whereas the administration of L-lysine did not show any effect.<sup>[124]</sup> Besides, coinfusion of albumin-derived peptide fragments reduced the kidney uptake of [<sup>111</sup>In]In-DTPA-exendin-3 by 26% in rats.<sup>[127]</sup>

In order to circumvent any co-/pre-administration steps, modifications of the exendin-4 scaffold itself were pursued to improve the tumor-to-kidney ratio. Therefore, kidney-cleavable linkers were installed within the peptide sequence just before the radiolabeled moiety. This linker should be

## INTRODUCTION

specifically cleaved at the kidney brush-border membrane, liberating the radioactive moiety as a small fragment that can be easily excreted in the urine.<sup>[67]</sup> Yim *et al.* adapted this concept for exendin-4 by implementing the kidney-cleavable N<sup>ε</sup>-maleoyl-L-lysyl-glycine (MAL) linker. However, the kidney uptake of [<sup>64</sup>Cu]Cu-NODAGA-MAL-exendin-4 was not improved compared to the reference [<sup>64</sup>Cu]Cu-NODAGA-exendin-4.<sup>[128]</sup> Likewise, Jodal *et al.* introduced linker sequences specifically cleaved by the metalloprotease meprin β. Although cleavage was attained *in vitro*, the expected accelerated clearance from the kidneys could not be observed *in vivo* and was assigned to a slower cleavage rate of meprin β compared to the rate of peptide uptake.<sup>[123]</sup> By contrast, the insertion of a NEP 24.11-cleavable segment (L-methionyl-L-valyl-L-lysine = MVK) provided a significant reduction (~ 40% at 1 h p.i.) of renal activity accumulation in mice without impairing the tumor uptake. However, an evaluation of this concept in humans was not performed yet.<sup>[129]</sup>

Besides, preclinical studies were pursued with radiohalogenated derivatives. Läppchen *et al.* investigated the radioiodinated derivative (Nle<sup>14</sup>, [<sup>124</sup>I]-Tyr<sup>40</sup>-NH<sub>2</sub>)exendin-4 in female Balb/c nude mice, bearing rat INS-1E tumor xenografts. The tumor-to-kidney ratio was increased by a factor of ~ 32 compared to the <sup>68</sup>Ga analog [Nle<sup>14</sup>, Tyr<sup>40</sup>(Ahx-[<sup>68</sup>Ga]Ga-DOTA)-NH<sub>2</sub>]exendin-4. In contrast to radiometallated exendin-4 conjugates, the main catabolite <sup>124</sup>I-Tyr, is not retained in the lysosomes of the proximal tubular cells in the kidneys but instead freely diffuses out of the cells, wherefore radioiodine is referred to as a non-residualizing label. Upon deiodination, the released [<sup>124</sup>I]iodide rapidly accumulates in thyroid tissue and stomach via the sodium iodide symporter. Therefore, nonspecific accumulation of [<sup>124</sup>I]iodide in the thyroid and stomach remained, but could be inhibited by blocking the sodium iodide symporter with Irenat<sup>®</sup>.<sup>[118]</sup> However, residualizing labels are generally preferred, as the activity is trapped within the target tissue, resulting in a higher specificity and sensitivity *in vivo*.<sup>[120]</sup>

Studies with <sup>18</sup>F-labeled exendin-4 revealed high tracer uptake in INS-1 tumor cells and xenograft models and a rapid clearance from the kidneys compared to radiometallated analogs.<sup>[81, 106, 130, 131]</sup> Although these results suggested high potential of <sup>18</sup>F-labeled exendin-4 analogs, none of the investigated compounds were transferred into clinical application.<sup>[89, 100]</sup> Occasionally, difficulties in separating the precursor from the respective radiolabeled agent resulted in low molar activities (A<sub>m</sub>).<sup>[131, 132]</sup> As a consequence, optimal tumor uptake could not be attained, since a low peptide dose (~ 1 μg) and hence, a high molar activity (~ 200 GBq/μmol<sup>[133]</sup>) is mandatory. Moreover, dependent on the labeling methodology, a relatively high nonspecific accumulation in liver and intestines occurred in preclinical studies.<sup>[81, 106]</sup>

In order to avoid radiosynthesis via prosthetic groups, other strategies such as aluminum [<sup>18</sup>F]fluoride complexation were applied and showed high tracer uptake by the tumor. However, chelator attachment and [<sup>18</sup>F]AlF complexation again led to high kidney uptake.<sup>[125, 134]</sup>

Recently, the first direct radiofluorination of a silicon-based fluoride acceptor (SiFA)-modified exendin-4 precursor was pursued by Dialer *et al.*<sup>[135]</sup> Although kidney accumulation remained low

## INTRODUCTION

( $49 \pm 18\%$  ID/g at 1 h p.i.), this approach led to radiochemical yields (RCY) of only 1.0 - 1.5% and 6%  $^{18}\text{F}$ -incorporation for (Nle<sup>14</sup>, [ $^{18}\text{F}$ ]SiFA-Lys<sup>40</sup>)exendin-4. Azeotropic drying of [ $^{18}\text{F}$ ]fluoride as a more laborious and time-consuming drying method, in combination with harsh peptide labeling conditions (110 °C, 15 min), which were presumed to cause for degradation of the 40-residue peptide, probably accounted for this poor RCY.

In conclusion, radiolabeled exendin-3/4-based derivatives represent promising agents for molecular imaging of GLP-1R-overexpressing lesions. However, the use of the exendin-3/4 scaffold currently allows for a very limited number of peptide-radionuclide conjugates that can be only applied for insulinoma imaging in patients. Radiometallated conjugates are suffering from high renal uptake and retention. As a possible strategy to reduce kidney accumulation, radiotracers with kidney-cleavable linkers have been introduced, but a general proof-of-concept in humans is still pending. For diagnostic purposes, the use of  $^{18}\text{F}$  as an alternative label is impaired by tedious labeling methodologies and an initial attempt for direct  $^{18}\text{F}$ -labeling via a SiFA-modified precursor provided only limited success. Moreover, PRRT of GLP-1R-overexpressing tumors has not been envisaged yet. The use of radiometallated  $\alpha$ - or  $\beta$ -emitting agents potentially leads to nephrotoxicity and for  $^{131}\text{I}$ -labeled derivatives, an ingenious treatment protocol with Irenat<sup>®</sup> would be indispensable to avoid severe  $^{131}\text{I}$ -induced damage of the thyroid.

Therefore, a pharmacokinetically optimized structure (e.g. undecapeptide **A-1**, introduced in section 1.1.4) was supposed to serve as a valuable alternative by expanding the scope of possible peptide-radionuclide conjugates. More precisely, reabsorption by megalin and/or cubilin on the tubular cells and secretion of radioactive degradation products into the blood might be decreased for peptides structurally different to exendin-3/4, exhibiting fewer charged amino acid residues or an altered distribution of charges.<sup>[122-124]</sup> Accelerated clearance from the blood and kidneys would result in earlier adequate tumor-to-background and tumor-to-kidney ratios, particularly advantageous for diagnostic and therapeutic applications, which might be also combined in a theranostic approach<sup>[136]</sup>, provided that agonist-induced side effects (hypoglycemia, nausea, vomiting) are still tolerable or can be reduced by antiemetics<sup>[137]</sup> and prophylactic glucose infusions.<sup>[89]</sup>

In addition, if the respective ligands would allow for derivatization with a silicon-based fluoride acceptor moiety under improved labeling conditions in combination with the 'Munich method'<sup>[138]</sup> for  $^{18}\text{F}$ -drying, direct radiofluorination with higher RCYs might be possible, exploiting the favorable imaging characteristics of  $^{18}\text{F}$  (low  $\beta^+$  energy of max. 0.635 MeV,  $\beta^+$  decay ratio of 97%, half-life 109.8 min) and the possibility of generating GLP-1R-targeting radiohybrid ligands.<sup>[139, 140]</sup> High molar activities together with the  $^{18}\text{F}$ -derived low kidney uptake might promote the use for clinical application.

### 1.2. PSMA ligand development

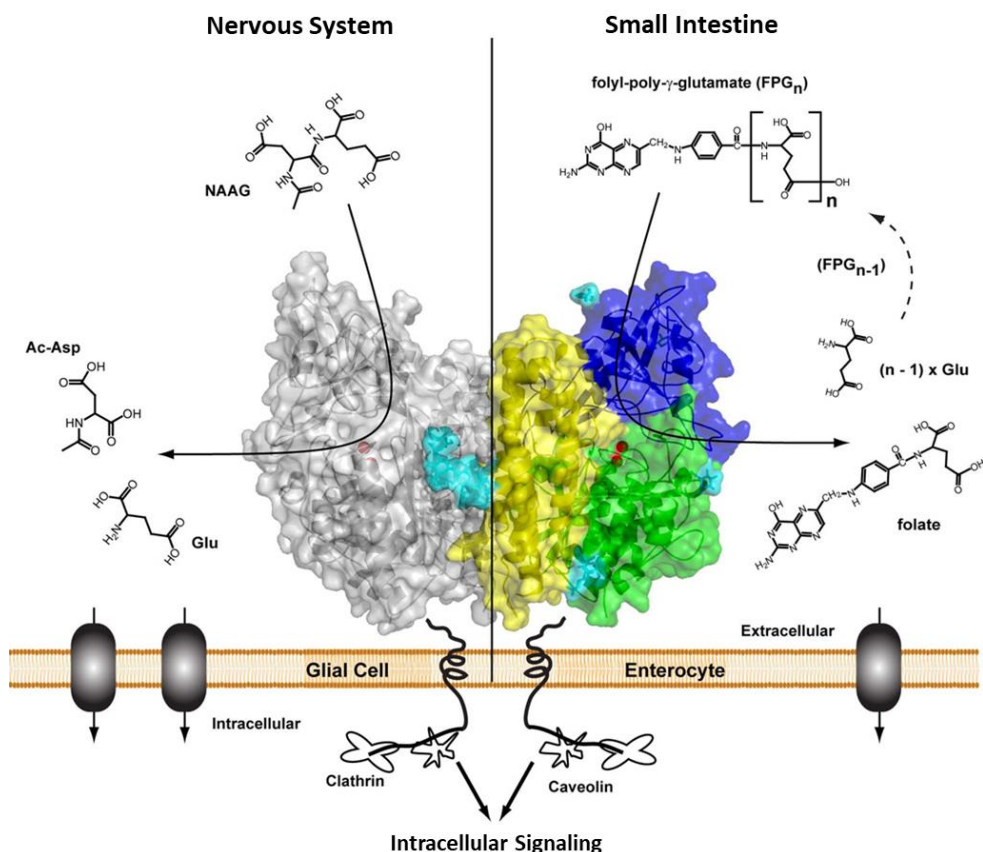
#### 1.2.1. Prostate-specific membrane antigen

The prostate-specific membrane antigen (PSMA) is a glutamate-preferring,  $Zn^{2+}$ -dependent metallopeptidase also termed glutamate carboxypeptidase II (GCP II), due to its exopeptidase activity towards substrates bearing C-terminal glutamate residues.<sup>[141-143]</sup> In healthy human tissue, physiological GCP II expression was predominantly found on the secretory-acinar epithelium of the prostate and on extraprostatic sites like the kidneys (proximal renal tubules), the brush border membrane of the small intestine and the central and peripheral nervous system (astrocytes and schwann cells).<sup>[144-147]</sup>

Depending on its site of expression and enzymatic activity, GCP II was given different names (*Figure 10*). Due to its exopeptidase activity towards the neurotransmitter *N*-acetyl-L-aspartyl-L-glutamic acid (NAAG) in the brain, GCP II was termed *N*-acetylated  $\alpha$ -linked acidic dipeptidase I (NAALADase I).<sup>[141, 148]</sup> Besides, it catalyzes the hydrolytic cleavage of  $\gamma$ -linked glutamates from polyglutamylated folate on the brush border membrane of the small intestine, where it mediates the intestinal absorption of folate (also known as vitamin B<sub>9</sub>). Thus, GCP II was named folate hydrolase 1 (FOLH1).<sup>[141, 149]</sup> Moreover, the predominant expression of GCP II on prostate epithelium and its upregulation in prostate cancer led to the term prostate-specific membrane antigen.<sup>[150-152]</sup>

PSMA is a type II transmembrane protein with a short *N*-terminal cytoplasmic domain (AA 1 - 19), a single membrane-spanning segment (AA 20 - 44) and a large *C*-terminal extracellular domain (AA 45 - 750) (*Figure 10*).<sup>[153, 154]</sup>

## INTRODUCTION

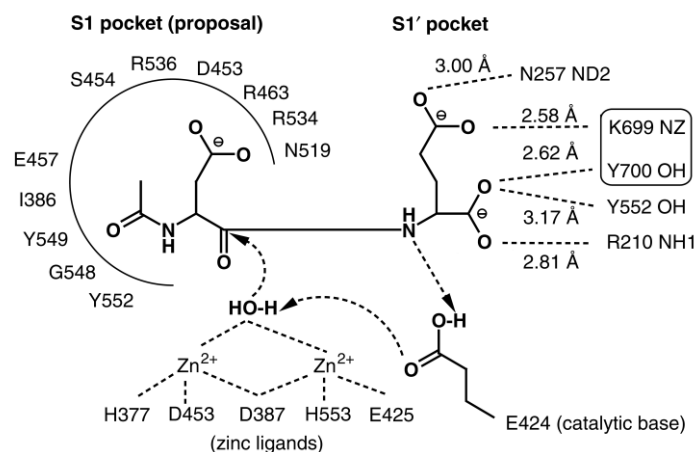


**Figure 10:** Crystal structure of the human PSMA homodimer. Right monomer shows the individual domains of the extracellular part: the protease domain, amino acids 57 - 116 and 352 - 590 (green); the apical domain, amino acids 117 - 351 (blue); and the C-terminal domain, amino acids 591 - 750 (yellow). The second monomer (left) is colored gray. N-linked sugar moieties are colored cyan, and the active-site  $Zn^{2+}$  ions are shown as red spheres. Left panel: NAAG catabolism in the mammalian nervous system. Right panel: Folate hydrolase activity at the plasma membrane of enterocytes.<sup>[142]</sup> Figure 10 was taken from reference [142].

The extracellular portion of PSMA, generally responsible for substrate recognition, can be divided into three sub-domains: the protease domain, the apical domain and the helical C-terminal domain, located at the homodimer interface. Residues of all three domains participate in formation of the binding cavity.<sup>[142, 143]</sup> The whole extracellular part is highly N-glycosylated (20 - 25% of the native molecular weight), which is indispensable for correct folding and subsequent secretion of the enzymatically active heterodimer.<sup>[155-158]</sup>

The active site of PSMA accommodates two catalytic  $Zn^{2+}$  ions, which are bridged by Asp<sup>387</sup> (Figure 11). In addition, Zn(1) is coordinated by His<sup>377</sup> and Asp<sup>453</sup>, whereas Zn(2) is ligated to His<sup>553</sup> and Glu<sup>425</sup>. In its free state, a single water molecule asymmetrically bridges both zinc ions ( $H_2O \dots Zn(1)$ , 1.79 Å;  $H_2O \dots Zn(2)$ , 2.26 Å), which in turn leads to a tetrahedral coordination of both metal ions within the binding cavity of PSMA. The bridging water molecule is also coordinated by Glu<sup>424</sup>, which further promotes its hydroxide character. Thus, it is poised to attack the peptide bond of a bound substrate, leading to a tetrahedral intermediate, hydrolysis of the peptide bond and product dissociation.<sup>[143, 154]</sup>

## INTRODUCTION



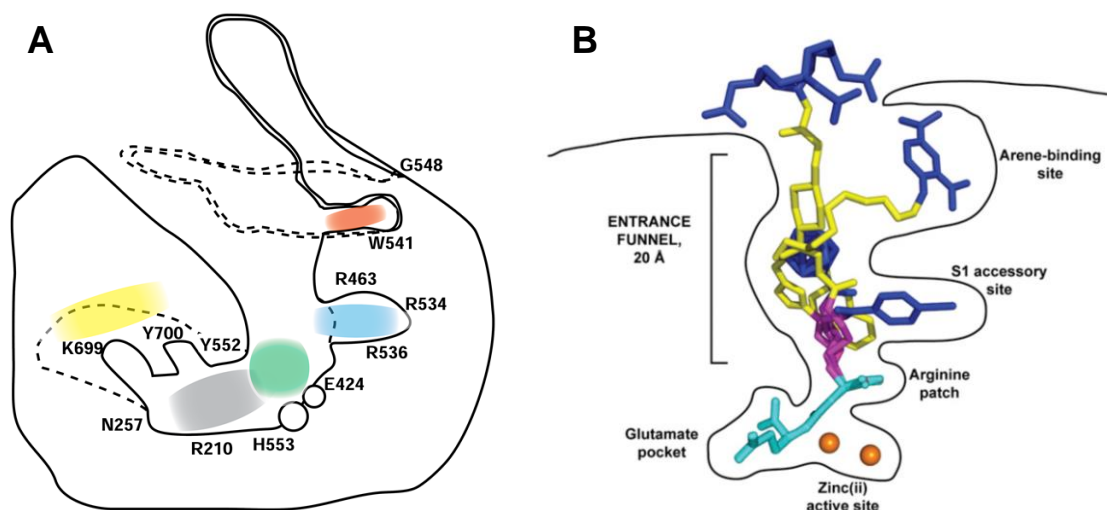
**Figure 11:** Scheme of the catalytic site of PSMA, indicating the NAAG substrate as bound to the enzyme. The binding of the *N*-acetylaspartyl portion of the substrate to the S1 pocket (left) is modeled, whereas the interactions of the glutamate residue to the S1' pocket (right) are taken from the crystal structure of the PSMA-glutamate complex (PDB: 2C6G). Residues Lys<sup>699</sup> and Tyr<sup>700</sup> of the 'glutamate sensor' are boxed. The catalytic reaction is supposed to be initiated by activation of the central nucleophile, HO–H, through the catalytic base Glu<sup>424</sup>. This is followed by nucleophilic attack of the generated hydroxyl ion onto the peptidic bond of the substrate. After cleavage, Glu<sup>424</sup> acts as a proton shuttle, that mediates transfer of the abstracted proton to the amino group of the leaving glutamate. Arrows run from nucleophile to electrophile.<sup>[154]</sup> Figure 11 was taken from reference [154].

The large binding cavity of PSMA ( $\sim 1\ 100\ \text{\AA}^2$ ) is divided by the binuclear active site into the pharmacophore S1' site and the non-pharmacophore S1 site. The S1' binding pocket is defined by an array of amino acids, including Arg<sup>210</sup>, Asn<sup>257</sup>, Glu<sup>424</sup>, Tyr<sup>552</sup> as well as Lys<sup>699</sup> and Tyr<sup>700</sup> both representing important residues of the 'glutamate sensor' (Tyr<sup>692</sup> - Ser<sup>704</sup>). All these amino acids confer specificity to L-glutamate and L-glutamate-like moieties via a complex network of ionic interactions, polar hydrogen bonds and van der Waals interactions.<sup>[143, 154, 159]</sup> Depending on the structure of the bound ligand, also further residues like Ser<sup>517</sup>, Gly<sup>518</sup>, Phe<sup>209</sup> and Leu<sup>428</sup> can be involved.<sup>[159, 160]</sup> The width of this subpocket is restricted by the side chains of Phe<sup>209</sup> and Leu<sup>428</sup>, that define a narrow channel with a diameter of approximately 8 Å. However, the  $\beta$ 15/ $\beta$ 16 hairpin, i.e. the 'glutamate sensor', represents a flexible loop (positional difference of  $\sim 4.7\ \text{\AA}$ ) by which a substantial increase of the S1' pocket and also liberation of the cleaved glutamate were supposed to be possible.<sup>[154, 159]</sup> Hence, a certain structural flexibility exists, although to a very limited degree.

More flexibility is provided by the non-pharmacophore S1 subpocket, which encompasses a  $\sim 20\ \text{\AA}$  deep funnel expanding from the binuclear active site (approximate diameter of 8 Å) towards the entrance lid (approximate diameter of 20 Å). The S1 binding site harbors a strongly positively charged region, composed by Arg<sup>463</sup>, Arg<sup>534</sup> and Arg<sup>536</sup>. This 'arginine patch', on the one hand, accounts for the strong preference of PSMA for acidic residues in the P1 position of a substrate. On the other hand, simultaneous reorientation of Arg<sup>536</sup> and Arg<sup>463</sup> unveils a 'S1 accessory hydrophobic pocket', by which bulky hydrophobic residues can be optimally coordinated.<sup>[161, 162]</sup> This ligand-dependent variability provides evidence of a unique structural plasticity, which is also

## INTRODUCTION

observed for the entrance lid of PSMA (Trp<sup>541</sup> - Gly<sup>548</sup>). Depending on the ligand dimensions, this highly flexible segment occupies a closed or open conformation, which enables processing of 'longer' substrates such as folyl-poly- $\gamma$ -glutamates.<sup>[163]</sup> Adjacent to this structural motif, parts of the entrance lid (Trp<sup>541</sup>) as well as Arg<sup>463</sup> and Arg<sup>511</sup> define a remote 'arene-binding site'.<sup>[164, 165]</sup> Addressing these structural features within the binding cavity of PSMA (*Figure 12*) proved to be a valuable tool for ligand optimization, thus, encouraging the search for further yet unknown interaction sites.<sup>[163, 166]</sup>



**Figure 12:** (A) Schematic representation of the binding cavity of PSMA. Flexible segments (the entrance lid, the arginine patch and the glutarate sensor) are depicted in two conformations by solid and dashed lines, respectively. Selected residues are shown in one-letter code. The position of the glutarate sensor for an empty S1' pocket is indicated in yellow. Polar hydrogen bonds between residues of the S1' pocket and a bound substrate are depicted in gray. Interactions in the vicinity of the active site are colored green. Formation of the arginine patch and the S1 accessory hydrophobic pocket by distinct arginine residues is indicated in blue, whereas the arene-binding site is colored in red. Zn<sup>2+</sup> ions are depicted as circles.<sup>[163]</sup> (B) Glu-ureido-based ligands within the binding cavity of PSMA for illustration of different orientations and interaction sites, depending on the ligand size. Although there is complete structural overlap of pharmacophore modules (cyan), positioning of the flexible proximal linker (magenta), functional spacer (yellow), and effector moiety (blue) is divergent within and outside the amphipathic entrance funnel. Zn<sup>2+</sup> ions are shown as orange spheres. X-ray structures of PSMA were used in complex with DCIBzL (PDB: 3D7H), ARM-P4 (PDB: 2XEG), carborane (PDB: 4OME) and PSMA-617 (unpublished data).<sup>[167]</sup> *Figure 12A* was adapted from reference [163] and *Figure 12B* was taken from reference [167].

Although PSMA was found to exhibit both NAALADase and folate hydrolase activity<sup>[168, 169]</sup>, the biological function of these enzymatic activities in normal prostate tissue remains unknown. Besides, also the impact on tumor progression and metastasis of prostate carcinomas and neovascularization in other solid tumors has not been elucidated yet.<sup>[141, 153, 170]</sup>

Rajasekaran *et al.* proposed PSMA to be a multi-functional enzyme, which could be involved in signal transduction, nutrient uptake and cell migration.<sup>[153, 171]</sup> Furthermore, PSMA is supposed to be a receptor for a yet unidentified endogenous ligand.<sup>[141, 153]</sup> Recent investigations by Barwe *et al.*

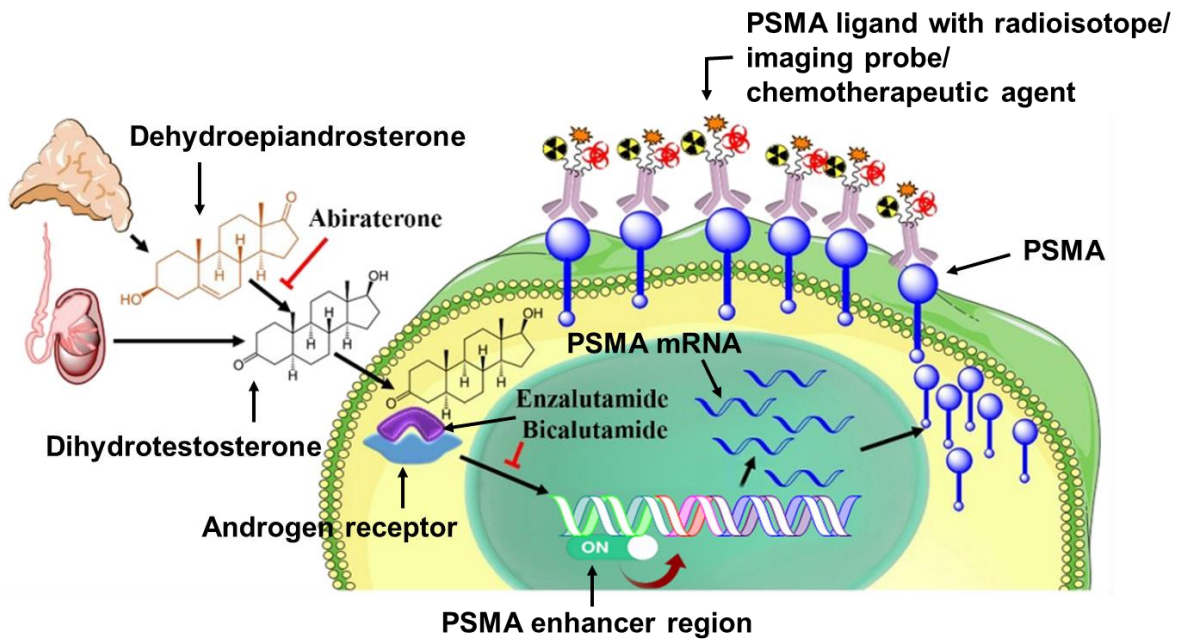
## INTRODUCTION

resulted in a direct correlation between PSMA expression on prostate cancer cells and their accumulation in human bone marrow matrix, independent of the enzymatic activity.<sup>[172]</sup> This finding has led to the assumption that PSMA expression on malignant prostate tissue could be crucial for metastasis into the bone.<sup>[172]</sup> Besides, the enzymatic activity of PSMA provides glutamate as a substrate for metabotropic glutamate receptor I (mGluR I). Upon activation, mGluR I initiates downstream pathways, critical for the pathogenesis of prostate cancer.<sup>[173]</sup>

Irrespective of the presence of a substrate and its hydrolysis, PSMA undergoes constitutive endocytosis via clathrin-coated pits in LNCaP cells. Internalization was found to be mainly mediated by the very *N*-terminal cytoplasmic pentapeptide MWNLL, whereby especially Met<sup>1</sup> and Leu<sup>5</sup> play critical roles.<sup>[171, 174, 175]</sup> Investigations on transfected PC-3 cells suggested that association of the intracellular *N*-terminus (AA 1 - 19) of PSMA with the actin-crosslinking protein filamin A is involved in its localization to the recycling endosomal compartment (REC). However, these findings remain ambiguous, since in LNCaP cells (endogenous PSMA expression) no co-immunoprecipitation of PSMA with filamin could be detected and PSMA could not be localized in the REC.<sup>[176]</sup> Nonetheless, internalization could be increased up to 3-fold upon antibody binding to the extracellular domain in a dose-dependent manner.<sup>[174]</sup> Hence, apart from its glutamate carboxypeptidase activity, PSMA was supposed to act as a receptor mediating the internalization of a putative endogenous ligand.<sup>[171, 174]</sup>

Intracellular signaling pathways have been predominantly investigated in human prostate cancer cells (primary tissue or LNCaP cells), transfected cells (human or non-human primate origin) and human astrocytes, with the latter representing a main object of study for neurological disorders.<sup>[170]</sup> Notably, androgens downregulate PSMA gene expression, reduce transcription of PSMA mRNA and consequently, inhibit PSMA expression. As a result, androgen deprivation as a therapy for advanced prostate cancer leads to an upregulated PSMA expression (*Figure 13*). This represents an important physiological process, which has to be considered for interpretation of PSMA-targeted PET as well as for defining the best time point and sequencing of diagnosis and therapy.<sup>[177-179]</sup>

## INTRODUCTION



**Figure 13:** CRPC can be managed with second generation inhibitors of the androgen receptor (AR), such as enzalutamide and bicalutamide as well as with cytochrome P450 17 $\alpha$ -hydroxylase-17,20-lyase (CYP17) inhibitor abiraterone. AR antagonists competitively inhibit androgen binding to AR, inducing activation of the PSMA enhancer region. Increased PSMA gene transcription provides a higher number of the mature protein at the surface of PCa cells, which can be targeted by PSMA ligands equipped with chemotherapeutics, imaging probes or diagnostic and therapeutic radioisotopes.<sup>[180]</sup> Figure 13 was adapted from reference [180] and slightly modified.

### 1.2.2. PSMA as target for molecular imaging and radiotherapy

Contrary to the GLP-1 receptor, PSMA does not belong to the superfamily of G protein-coupled receptors, but yet serves as a valuable target structure for molecular imaging and radiotherapy, due to its elevated expression in prostate cancer at the early and late (castration-resistant) stage of the disease as well as in metastatic lesions.<sup>[181]</sup>

The term 'prostate cancer' mainly refers to adenocarcinomas, which arise from prostatic epithelial cells and account for over 95% of all prostate cancers.<sup>[182]</sup> In 2018, this type of cancer represented the second most common cancer worldwide in men, according to data published by the International Agency of Research on Cancer. Since 2012, the number of deaths rose from a global estimated number of 307 000 to 359 000 in 2018. Thus, prostate carcinomas now represent the fourth leading cause of cancer-related death in men.<sup>[183, 184]</sup>

With prostate cancer being a global health issue, its detection and treatment was focused by many research groups in the past decades.<sup>[185]</sup> The identification of prostatic acid phosphatase (PAP) in 1938 and prostate-specific antigen (PSA) in 1980 revealed two viable serum biomarkers for prostate carcinomas.<sup>[186, 187]</sup> In 1987, PSMA was first identified by Horoszewicz *et al.* and since then evolved to a very potent biomarker for prostate cancer cells.<sup>[188-190]</sup> Despite its unsuitability as a serum-based marker, its favorable expression pattern led to intense investigations for its use as a target for imaging and treatment of PCa.<sup>[191]</sup>

Treatment options are mainly defined by the Gleason score, which still remains one of the best prognostic markers for PCa. It gives a first indication of the differentiation and invasiveness of the tumor by histopathological analysis of the glandular architecture.<sup>[192]</sup> Resultant therapeutic methods for prostate cancer range from watchful waiting to aggressive multimodal therapies depending on age, disease stage, potential side effects and other medical conditions of the patient.<sup>[189, 193]</sup> In order to determine appropriate treatment options tailored to the patient, imaging techniques should be able to accurately localize tumor lesions and determine the extent of the disease, monitor tumors over time and their response to therapy.

Conventional imaging studies of primary prostate cancer include transrectal ultrasound, CT and magnetic resonance (MR) imaging as well as bone scintigraphy (<sup>99m</sup>Tc]Tc-MDP), which is used for the detection of metastatic skeletal lesions.<sup>[194]</sup> Both CT and bone scintigraphy have limitations concerning sensitivity and specificity for the detection of early/subtle recurrence or metastasis, e.g. disease-involved lymph nodes and sclerotic bone metastases with a sub-centimeter diameter. Occasionally, also MR imaging exhibits low specificity, with benign prostatic hyperplasia at times having similar imaging characteristics to malignant tissue.<sup>[195]</sup> Positron emission tomography with <sup>11</sup>C- or <sup>18</sup>F-labeled choline has shown encouraging results for the detection of recurrent prostate cancer<sup>[196]</sup>, but has a low diagnostic accuracy for the detection of primary prostate cancer, since

## INTRODUCTION

benign pathologies in the prostate (e.g. benign prostatic hyperplasia and prostatitis) are also characterized by an increased choline uptake.<sup>[197]</sup> PET imaging with the most commonly used tracer [<sup>18</sup>F]FDG exhibits limited positivity and sensitivity for this type of malignancy, due to low glycolysis in prostate cancer cells and hence, low uptake of this diagnostic agent.<sup>[198]</sup>

High affinity radiotracers targeting PSMA were supposed to potentially address those limitations presented for diagnostic purposes.<sup>[195]</sup> Furthermore, replacement of the diagnostic nuclide with a therapeutic  $\alpha/\beta^-$ -emitter was presumed to allow for the delivery of high cytotoxic radiation doses to specific tumor sites. This concept of imaging and therapy already proved its potential as an effective modality for the management of prostate cancer.<sup>[199]</sup>

The expression of PSMA is highly upregulated in malignant prostate tissue and directly correlates with tumor grade and aggressiveness as well as with the pathological stage.<sup>[191, 200]</sup> Hence, highly elevated PSMA levels can be found in castration-resistant prostate cancer as well as in metastatic lesions located in the lymph nodes, bone, soft tissue and lungs.<sup>[153, 172]</sup> Moreover, an increased expression of PSMA was found in the neovasculature of most solid tumors, but not in normal vascular endothelium. Thus, PSMA emerged as an ideal biomarker not only for the diagnosis and treatment of prostate cancer, but also for many other forms of solid tumors.<sup>[144, 145, 201]</sup>

This involvement of PSMA in a variety of oncological diseases and especially in PCa, promoted the development of PSMA-targeted agents in recent years.

### 1.2.3. PSMA-targeting radioligands

Since the 1990's many efforts have been made to promote the development of PSMA-addressing ligands, applicable either for the treatment of neurological disorders or imaging and therapy of prostate tumors and metastases.<sup>[170, 202]</sup> Highly specific PSMA-avid monoclonal antibodies (mAb) were already available at initial studies characterizing PSMA as a target for prostate tumor cells.<sup>[148]</sup> Early promising results for the diagnosis and treatment of prostate cancer were obtained with <sup>131</sup>I, <sup>111</sup>In, <sup>90</sup>Y and <sup>177</sup>Lu-labeled antibodies mAb 7E11-C5 and mAb J591.<sup>[144, 188, 203, 204]</sup> The 7E11-C5 antibody was obtained after immunization of mice with LNCaP cells and recognizes an epitope located at the intracellular cytoplasmic domain of PSMA, with a minimal reactive peptide consisting of the first six *N*-terminal amino acids (MWNLLH).<sup>[152]</sup> As a consequence, 7E11-C5 is only able to bind to PSMA after prostate cancer cell apoptosis or necrosis.<sup>[144, 152, 204]</sup> After a decade, further efforts revealed mAb J591 that binds to viable cells by targeting an epitope located at the extracellular domain of PSMA.<sup>[205]</sup> Both antibodies have entered clinical trials and <sup>111</sup>In-labeled mAb 7E11-C5 attained FDA-approval already in 1996 and is now used for several years as diagnostic agent (ProstaScint<sup>®</sup>) in localized and metastatic prostate cancer.<sup>[206, 207]</sup>

In contrast, small molecule GCP II inhibitors were primarily synthesized for the treatment of NAALADase I-based neurological disorders and drug addiction, since antibodies are too large to pass the blood-brain barrier.<sup>[202, 208]</sup> Adaption of this approach for targeting PSMA positive peripheral tumor lesions attained more interest in recent years, since small molecules exhibit a faster rate of tumor uptake and blood clearance than antibodies as well as an increased tumor permeability.<sup>[209, 210]</sup> This leads to improved pharmacokinetics for imaging and therapy, with reduced background activity at early time points, less radiation burden on the liver and decreased myelosuppression in patients.<sup>[189, 210, 211]</sup> Moreover, SPECT imaging via radiolabeled antibodies represents a more cumbersome procedure for the patient and attending physician, as the optimal imaging time is only reached at 48 - 72 hours after injection, due to the rather slow *in vivo* pharmacokinetics of the antibodies.<sup>[189]</sup> Hence, small molecule-based imaging agents with their fast clearance from non-target tissues represent the more practicable choice, since imaging can be performed shortly after tracer administration (1 - 4 h p.i.).<sup>[189, 209, 212, 213]</sup>

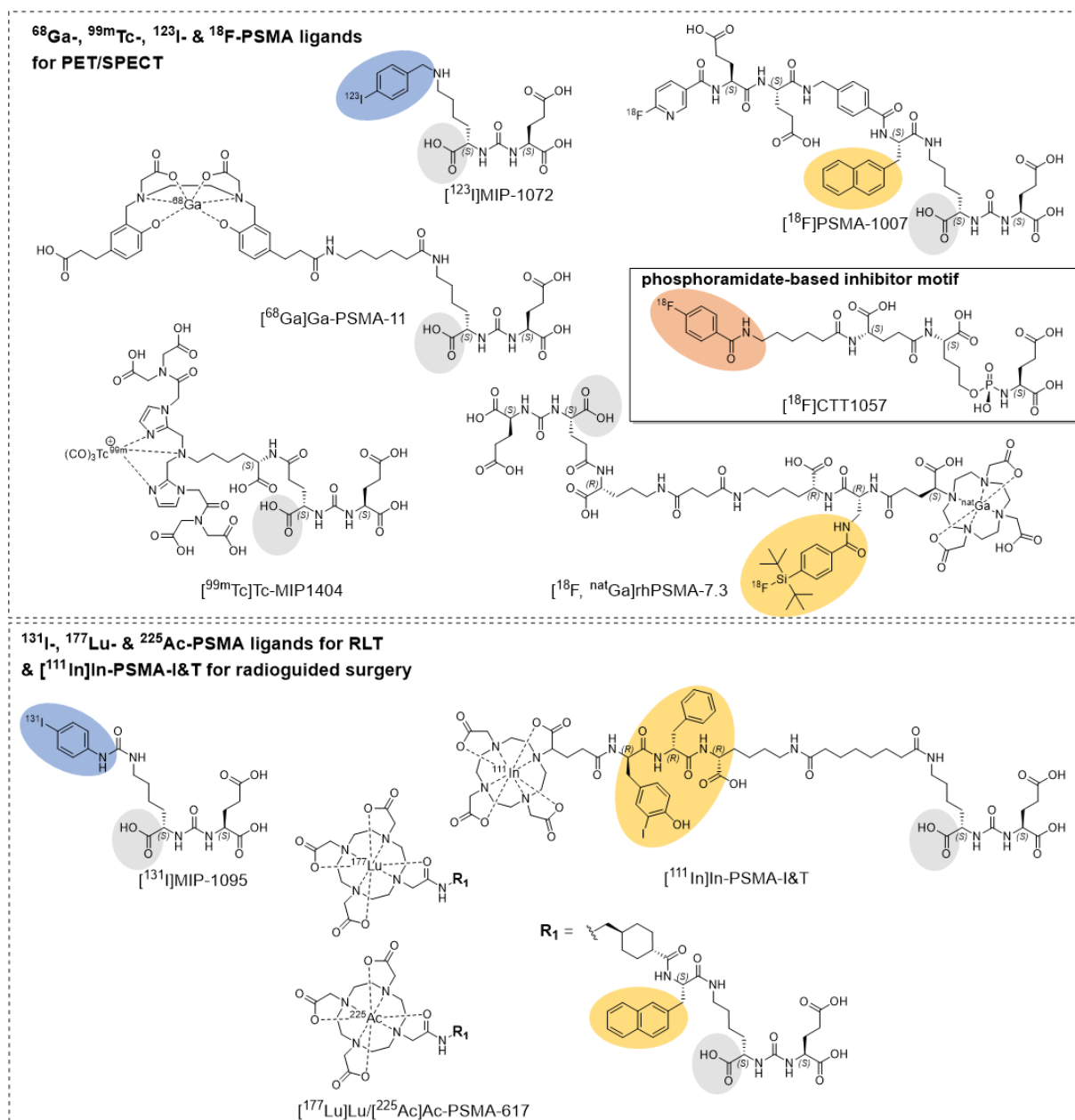
Dependent on the purpose, currently existing small molecule-based inhibitors of PSMA have been tested either in enzyme-based NAALADase assays or in live, PSMA-expressing prostate cancer cell lines. Obviously, those which are able to inhibit the NAALADase activity at very low concentrations act as promising candidates not only for the treatment of neurological disorders, but could also serve as basic structures for the diagnosis and treatment of prostate cancer.<sup>[170, 202]</sup> According to their central Zn<sup>2+</sup>-binding motif, small molecule-based PSMA inhibitors can be roughly separated into six different classes.<sup>[160, 202]</sup> The first class is constituted by phosphorous-based compounds, including phosphonic and phosphinic acid derivatives as well as phosphoramidate

## INTRODUCTION

peptidomimetics, with racemic 2-(phosphonomethyl)pentanedioic acid (2-PMPA) as the prototype PSMA inhibitor ( $K_i = 0.3 \text{ nM}$ <sup>[214]</sup>) developed in 1996 by Jackson *et al.*<sup>[160, 215]</sup> However, clinical application of initial phosphorous-based compounds was impaired by their highly polar character resulting in unsuitable pharmacokinetics for the treatment of neurological disorders (low blood-brain barrier (BBB) permeability).<sup>[216]</sup> Therefore, further small molecules which were known to act as metallopeptidase inhibitors were investigated. Examples for these classes of molecules are thiol-based derivatives and hydroxamic acids.<sup>[160, 214]</sup> In 2003, the thiol-based inhibitor 2-(3-mercaptopropyl)pentanedioic acid (2-MPPA, also known as GPI5693) was described by Majer *et al.* as the first orally bioavailable PSMA inhibitor with an  $IC_{50}$  value of 90 nM.<sup>[217]</sup> However, the relatively high oral doses required for therapy also increased the risk of thiol-induced immune reactions.<sup>[218]</sup> Despite further optimizations of the 2-MPPA scaffold<sup>[218]</sup>, this class of compounds could not reach clinical application, due to metabolic instability and insufficient selectivity.<sup>[216]</sup> Hydroxamic acid derivatives possess only moderate to low inhibitory activity against PSMA ( $\geq 220 \text{ nM}$ ), which in consequence emphasizes the need for further optimizations.<sup>[160, 219]</sup> Another group of PSMA inhibitors is constituted by conformationally restricted dipeptide mimetics, but, comparable to hydroxamic acids, their inhibitory potency towards PSMA is only moderate (100 - 900 nM).<sup>[202]</sup> Sulfonamide-based inhibitors were found to exhibit even lower affinities towards PSMA, with  $IC_{50}$  values ranging from 5  $\mu\text{M}$  to > 100  $\mu\text{M}$ .<sup>[160, 220]</sup> By contrast, urea-based compounds showed high inhibitory activity in enzyme-based NAALADase assays as well as in LNCaP cell-based competitive binding assays.<sup>[221-224]</sup>

Since high lipophilicity as for the treatment of neurological disorders represents no prerequisite for addressing peripheral tumor lesions and metastases, hydrophilic high-affinity compounds (e.g. urea-based PSMA inhibitors) have prevailed for PCa management. Early ( $[^{11}\text{C}]\text{DCMC}$ ,  $[^{125}\text{I}]\text{DCIT}$ ,  $[^{18}\text{F}]\text{DCFBC}$ ,  $[^{125}\text{I}]\text{DCIBzL}$ ,  $[^{123/124/131}\text{I}]\text{MIP-1095}$ ,  $[^{99\text{m}}\text{Tc}]\text{Tc-MIP-1404}$ ), recently ( $[^{68}\text{Ga}/^{177}\text{Lu}/^{111}\text{In}]\text{Ga/Lu/In-PSMA-I\&T}$ ,  $[^{68}\text{Ga}]\text{Ga-PSMA-11}$ ,  $[^{18}\text{F}]\text{PSMA-1007}$ ,  $[^{18}\text{F}]\text{rhPSMA-7.3}$ ,  $[^{68}\text{Ga}/^{177}\text{Lu}/^{225}\text{Ac}]\text{Ga/Lu/Ac-PSMA-617}$ ) and currently developed PSMA radioligands were/are primarily based on the Glu-urea-X motif.<sup>[136, 210, 225-232]</sup> Besides, also Glu-phosphoramidate-X-based ligands ( $[^{18}\text{F}]\text{CTT1056}$  or  $[^{18}\text{F}]\text{CTT1057}$ ) have been consistently investigated over the years, mainly due to their (pseudo-)irreversible binding to PSMA and favorable pharmacokinetics in PCa patients.<sup>[165, 233-236]</sup> Adjacent to the central  $\text{Zn}^{2+}$ -chelating group, both substance classes share a common C-terminal glutamate, addressing the pharmacophore S1' site and the inherent 'glutarate sensor' (as described in section 1.2.1). High variability of these ligands at the P1 site again corroborates the structural flexibility of the non-pharmacophore S1 pocket (*Figure 14*). Moreover, L-configuration of the binding motif was found to be indispensable for efficient binding to the active site of PSMA.<sup>[160, 237, 238]</sup>

## INTRODUCTION



**Figure 14:** Structural formulas of PSMA-targeting ligands for imaging and therapy of prostate cancer. This selection assembles Glu-urea-X and Glu-phosphoramidate-X derivatives currently investigated in clinical trials. Fragments that can be radiohalogenated ( $^{18}\text{F}$ ,  $^{123/131}\text{I}$ ) (directly or indirectly) are attached to the inhibitor motif via specifically optimized peptide linkers which were introduced for improved pharmacokinetics (yellow) and for targeting distinct sites within the non-pharmacophore S1 pocket (arginine patch: gray, S1 accessory hydrophobic pocket: blue, arene-binding site: red). Alternatively, functionalization of the linker unit with a chelator enables complexation of diagnostic ( $^{68}\text{Ga}$ ,  $^{99\text{m}}\text{Tc}$ ,  $^{111}\text{In}$ ) or therapeutic radiometals ( $^{177}\text{Lu}$ ,  $^{225}\text{Ac}$ ). Both concepts can be realized with radiohybrid ligands, such as rhPSMA-7.3, although only its radiofluorinated variant has entered clinical trials so far.<sup>[136, 165, 167, 209, 232, 239, 240]</sup>

For imaging of prostate cancer lesions, a multitude of small molecule-based PSMA ligands have been or are currently investigated in clinical trials (Figure 14).<sup>[190, 239, 240]</sup> Labeled with  $^{18}\text{F}$ ,  $^{68}\text{Ga}$ ,  $^{99\text{m}}\text{Tc}$ ,  $^{123}\text{I}$  or  $^{111}\text{In}$  these compounds show high potential for visualization of tumor lesions and

## INTRODUCTION

enable radioguided surgical excision ( $^{99m}\text{Tc}$  and  $^{111}\text{In}$ ).<sup>[209, 213, 241-244]</sup> Additionally,  $^{64}\text{Cu}$ - or  $^{44}\text{Sc}$ -labeled PSMA ligands have proved their usefulness for prolonged acquisition periods, as required for pre-therapeutic dosimetry or intraoperative applications as well as for images with higher spatial resolution.<sup>[245, 246]</sup> Thereof,  $^{68}\text{Ga}$ ]Ga-PSMA-11 recently attained FDA- and EMA-approval and thus, represents the first small molecule-based PSMA imaging agent launched on the market.<sup>[11]</sup> Since auspicious results in PCa patients were obtained with diagnostic compounds, also endoradiotherapeutic approaches were envisaged quickly (*Figure 14*).<sup>[189, 247]</sup> The use of  $\alpha$ - or  $\beta$ -emitting radioligands has been introduced as a salvage therapy for the incurable form of the disease, i.e. metastatic castration-resistant prostate cancer (mCRPC).<sup>[248]</sup> Due to their favorable *in vitro* and preclinical *in vivo* characteristics, several therapeutic agents advanced into the clinic and some of them already entered late-phase clinical trials (*Table 3*).

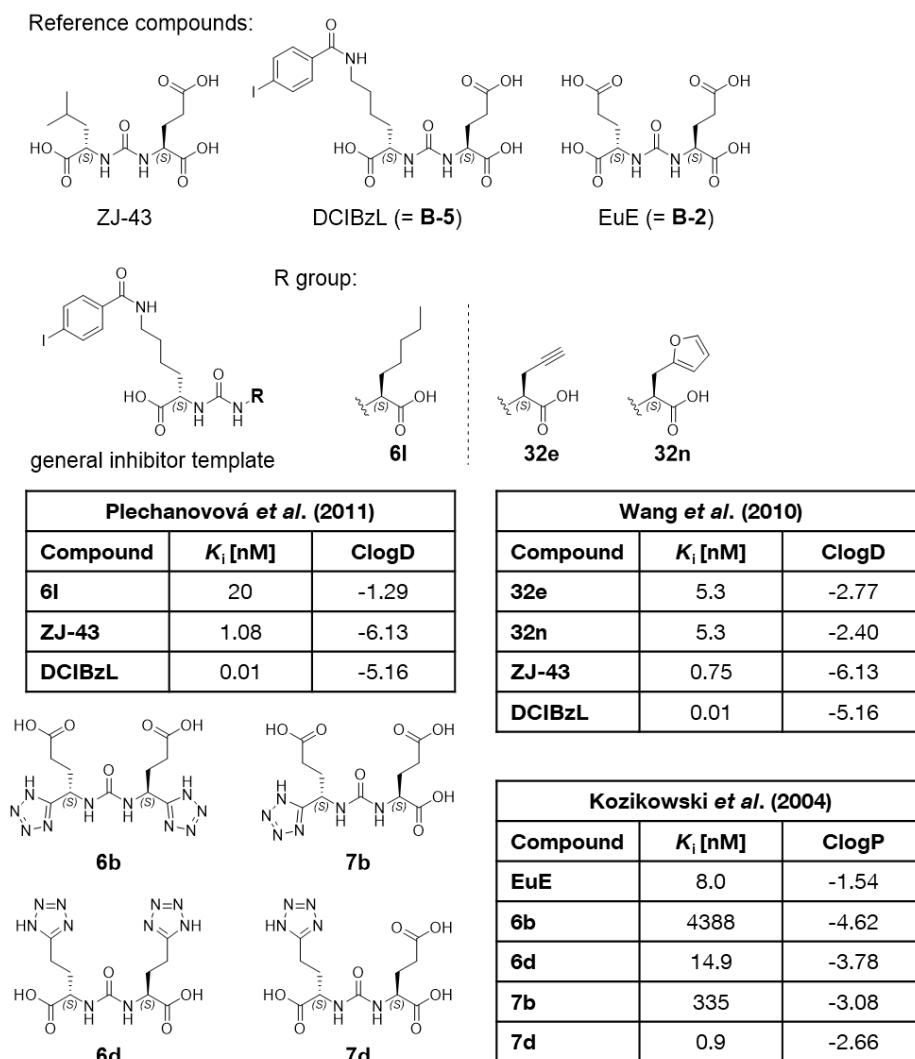
**Table 3:** *In vitro* and *in vivo* data of selected PSMA-targeting ligands, suitable for RLT of mCRPC.

Compound	Affinity ( $K_i$ ) [nM] <sup>a</sup>	Internalization <sup>b</sup>	Log D	Tumor uptake [% ID/g] <sup>c</sup>	Clinical study phase <sup>[8]</sup>	Ref.
$^{131}\text{I}$ ]MIP-1095 <sup>d</sup>	$0.24 \pm 0.14$	~ 50%	0.81 <sup>e</sup>	1 h: $20.7 \pm 5.8$ 24 h: $29.1 \pm 15.1$	II (NCT03939689)	[223, 224]
$^{177}\text{Lu}$ ]Lu-PSMA-I&T <sup>f</sup>	$7.9 \pm 2.4$ ( $\text{IC}_{50}$ )	$114 \pm 8\%$	-4.12	1 h: $7.96 \pm 1.76$ 24 h: n.d.	III (NCT04647526)	[136, 249]
$^{177}\text{Lu}$ ]Lu-PSMA-617	$6.91 \pm 1.32$	$17.51 \pm 3.99\%$ <sup>g</sup>	-2.00 <sup>h</sup>	1 h: $11.20 \pm 4.17$ 24 h: $10.58 \pm 4.50$	III (NCT03511664)	[250]
$^{225}\text{Ac}$ ]Ac-PSMA-617	$2.34 \pm 2.94$ <sup>h</sup>	n.d.	-2.00 <sup>h</sup>	n.d.	I (NCT04597411)	[250]

<sup>a</sup>Values determined with the respective non-radiolabeled compound, i.e. cold standard. Since no  $K_i$  value was available for  $^{nat}\text{Lu}$ -PSMA-I&T, the corresponding  $\text{IC}_{50}$  value is given; <sup>b</sup>Data represent specific internalization at 37 °C at 1 h for  $^{123}\text{I}$ ]MIP-1095 and  $^{177}\text{Lu}$ ]Lu-PSMA-I&T and at 45 min for  $^{177}\text{Lu}$ ]Lu-PSMA-617; <sup>c</sup>Tumor uptake in LNCaP tumor xenograft-bearing mice. For each time point: n = 5 for  $^{123}\text{I}$ ]MIP-1095, n = 4 for  $^{177}\text{Lu}$ ]Lu-PSMA-I&T and n = 3 for  $^{177}\text{Lu}$ ]Lu-PSMA-617; <sup>d</sup>Internalization and biodistribution studies were performed with  $^{123}\text{I}$ ]MIP-1095; <sup>e</sup>calculated log P; <sup>f</sup>*In vitro* data were acquired analogously to the procedures described within this work; <sup>g</sup>% applied activity/ $10^6$  LNCaP cells (n = 3); <sup>h</sup>Values determined with the compound in its free chelator form. Data for binding ( $K_i/\text{IC}_{50}$ ), internalization and tumor uptake are expressed as mean  $\pm$  SD. n.d., not determined; SD, standard deviation.

## INTRODUCTION

Hitherto, PSMA ligands with alternative residues at the P1' position, clearly differing from glutamate could not advance into the clinic. Essential experiments were conducted by Wang *et al.*, Kozikowski *et al.* and Plechanovová *et al.* who examined different substituents on their potential to irreversibly mask carboxylic acid moieties (Figure 15). However, in most cases the affinity values of the investigated compounds were found to be inferior to those obtained for their glutamate-based counterparts. Therefore, further experiments were often abandoned at an early stage and only few *in vivo* experiments in mice were conducted.<sup>[222, 251, 252]</sup>



**Figure 15:** Analysis of different carboxylic acid substituents based on known high-affinity PSMA ligands. Modifications restricted to the P1'- $\gamma$ -carboxylate were evaluated by Plechanovová *et al.*<sup>[252]</sup> and Wang *et al.*<sup>[251]</sup> Thereof, derivatives 32e and 32n showed a remarkable low  $K_i$  value, although still 7-fold and 530-fold higher than those obtained for reference compounds ZJ-43 and DCIBzL (B-5), respectively. Further positions suitable for introducing a carboxylic acid bioisostere were investigated by Kozikowski *et al.*<sup>[222]</sup> Symmetrical derivative 6d revealed a certain tolerance of the S1' pocket towards tetrazole as a P1'- $\gamma$ -carboxylic acid bioisostere, although the  $K_i$  increased by a factor of ~ 17 when compared to its glutamate-bearing counterpart 7d. By contrast, modifications at both  $\alpha$ -carboxylates (6b) resulted in a clear loss of affinity, even for compound 7b in which the crucial P1' glutamate was preserved.

## INTRODUCTION

Again, these structural modifications were introduced to attain improved pharmacokinetics (i.e. higher lipophilicity resulting in a higher BBB permeability) for the treatment of neurological disorders.<sup>[222, 251]</sup> For this purpose, also alternative substrates for PSMA were examined. Variations from the original substrate NAAG were published by Barinka *et al.* and Plechanovová *et al.* which revealed compounds bearing methionine or nonpolar aliphatic side chains at the C-terminal P1' position as potential candidates for enzymatic cleavage.<sup>[252, 253]</sup>

*N*-acetyl-L-glutamyl-L-methionine (NAGM) was cleaved by PSMA almost as fast as NAAG with a turnover number of  $0.29 \pm 0.01$  [s<sup>-1</sup>] (vs.  $0.59 \pm 0.16$  [s<sup>-1</sup>] of NAAG). However, cleavage efficiency of the enzyme was still notably higher for the original substrate NAAG ( $k_{\text{cat}}/K_{\text{m}} = 1361$  [L·s<sup>-1</sup>·mmol<sup>-1</sup>]) than for NAGM ( $k_{\text{cat}}/K_{\text{m}} = 5.5$  [L·s<sup>-1</sup>·mmol<sup>-1</sup>]), as methionine-containing peptides displayed lower  $K_{\text{m}}$  values (two to three orders of magnitude). Nonetheless, hydrolysis of NAGM after 15 h at 37 °C reached a similar extent as observed for NAAG.<sup>[253]</sup> An even more potent substrate could be identified by Plechanovová *et al.* upon investigation of substrate analogs with nonpolar aliphatic substituents at the P1' position. Among those, *N*-acetyl-L-aspartyl-L-2-aminooctanoic acid exhibited the highest turnover number ( $k_{\text{cat}} = 0.60 \pm 0.03$  [s<sup>-1</sup>]) and cleavage efficiency ( $k_{\text{cat}}/K_{\text{m}} = 75.0$  [L·s<sup>-1</sup>·mmol<sup>-1</sup>]), closest to the value for NAAG ( $930$  [L·s<sup>-1</sup>·mmol<sup>-1</sup>]).<sup>[252]</sup>

Apart from that, the glutamate carboxypeptidase activity of PSMA itself has been used for the development of poly-glutamylated prodrugs for PCa treatment either based on the methotrexate or thapsigargin scaffold.<sup>[254, 255]</sup> In both attempts, the conjugate is inactive until the PSMA-specific poly-glutamyl peptide is cleaved, thereby liberating the cytotoxic drug (methotrexate or thapsigargin) by enzymatic cleavage via PSMA. Thus, healthy tissue is spared as mainly PSMA-overexpressing tumor lesions and metastases are affected by the drug's cytotoxicity.<sup>[256]</sup> Auspicious preclinical results for poly-glutamylated thapsigargin led to further evaluation in an open label dose-escalation trial (NCT01056029).<sup>[255]</sup>

In sum, the presented options for masking the P1' glutamate, the immanent enzymatic activity of PSMA as well as its tolerance towards different Zn<sup>2+</sup>-binding groups offer the possibility to evaluate modifications of currently existing PSMA-targeting peptidomimetics with the aim to optimize their pharmacokinetic profile and to reduce their unspecific uptake.

### 1.2.4. Current limitations for radioligand therapy of prostate cancer

Conventional therapeutic modalities such as surgery, external beam radiation therapy and brachytherapy are applied for treatment of early-stage prostate cancer. Second-line treatment after failed primary surgery and radiotherapy includes androgen deprivation therapy (ADT), which can be also used in combination with chemotherapy and radiation therapy to treat the metastatic disease.<sup>[257]</sup> Progression of tumor growth can be decelerated by ADT, but only for a limited period.<sup>[258, 259]</sup> Due to loss of hormone sensitivity, castration-resistant prostate cancer (CRPC) inevitably evolves. In 10 - 20% of all PCa patients, CRPC arises within a follow-up period of approximately five years, with bone metastases already present in over 84% of these patients (i.e. metastatic CRPC). In this advanced form, containment of tumor growth by ADT is no longer possible, resulting in poor prognosis for patients, with a median survival of only 9 to 13 months.<sup>[260]</sup> Although mCRPC is incurable, it is not untreatable wherefore innovative therapeutic options available to patients have to be considered.

In particular, radioligand therapy using radiolabeled small molecule-based agents emerged as a valuable tool for the treatment of PCa lesions. Thereby, cytotoxic radiation is not only delivered to bone metastases, as for radionuclide therapy with [<sup>223</sup>Ra]RaCl<sub>2</sub><sup>[261]</sup>, but also lymph node and visceral metastases as well as recurring primary tumors are affected.<sup>[262, 263]</sup> Auspicious results obtained with highly sensitive and selective diagnostic PSMA-addressing agents paved the way for transfer of this targeted concept to RLT of mCRPC by means of  $\alpha$ - or  $\beta$ -emitting PSMA ligands.<sup>[209]</sup> Developed by Molecular Insight Pharmaceuticals Inc., [<sup>131</sup>I]MIP-1095 as the first small molecule-based endoradiotherapeutic agent, exhibited an intriguing therapy response already after a single cycle and superior dosimetric values when compared to a <sup>90</sup>Y-labeled antibody. A PSA decline of > 50% in 60.7% of patients was accompanied by a complete or moderate reduction of bone pain in 84.6% of patients.<sup>[227]</sup> However, co-emission of high-energy photons by <sup>131</sup>I requires a more elaborate radiation protection, wherefore <sup>177</sup>Lu as a more pure  $\beta$ -particle emitter was preferred for labeling of PSMA-targeting conjugates.<sup>[263-265]</sup> Thereof, [<sup>177</sup>Lu]Lu-PSMA-I&T<sup>[136]</sup> and [<sup>177</sup>Lu]Lu-PSMA-617<sup>[250]</sup> provided encouraging data from first clinical trials<sup>[263, 266]</sup> and ongoing phase III studies ([<sup>177</sup>Lu]Lu-PSMA-617, NCT03511664 and [<sup>177</sup>Lu]Lu-PSMA-I&T, NCT04647526)<sup>[8]</sup>, presuming a higher efficacy of <sup>177</sup>Lu-based RLT compared to other third-line therapies of mCRPC. For short- or non-responders (~ 30%), targeted  $\alpha$ -therapy (TAT) has been shown to be a valuable alternative treatment strategy.<sup>[267]</sup> A high linear energy transfer of  $\alpha$ -particles causes irreversible double-strand DNA breaks (*Figure 1C*), resulting in biological effects three to seven times greater than the damage produced by  $\beta$ -radiation. Moreover, less “cross-fire” radiation to surrounding normal tissue reduces hematotoxicity in patients with bone marrow involvement.<sup>[19, 268, 269]</sup> Therefore, PSMA-targeted  $\alpha$ -therapy was introduced as a further salvage therapy of end-stage mCRPC, superior to RLT with  $\beta$ -emitting ligands.<sup>[267]</sup> The first application of  $\alpha$ -emitting,

## INTRODUCTION

<sup>225</sup>Ac-labeled PSMA-617 in humans was reported in 2016 by Kratochwil *et al.* and showed complete remission in both patients.<sup>[231]</sup> Excellent treatment response could be attributed to the favorable properties of the peptide (fast tumor uptake, high internalization rate, extended tumor retention and rapid clearance of unbound ligand) and to the use of <sup>225</sup>Ac, that emits four  $\alpha$ -particles during radioactive decay.<sup>[268]</sup>

Beside kidneys (proximal tubules), the lacrimal and salivary glands have been identified as critical, dose-limiting organs.<sup>[227, 270-273]</sup> In this context it has become apparent, that <sup>177</sup>Lu-labeled PSMA inhibitors can cause xerostomia<sup>[265]</sup>, which was found to be partially irreversible when  $\alpha$ -emitter-labeled (<sup>225</sup>Ac) compounds were administered. Chronic xerostomia severely affected patients' quality of life and also led to premature termination of the therapy in some cases.<sup>[274-276]</sup> Hence, for a broader application of PSMA-targeted RLT and TAT in particular, the design of small molecule-based PSMA ligands with reduced salivary gland uptake is of high priority.

This working hypothesis presupposes a specific uptake of the aforementioned PSMA inhibitors into salivary glands, although not necessarily PSMA-specific. Whereas PSMA protein and mRNA expression in salivary glands was confirmed by Western blot and genetic analyses<sup>[150, 151, 277]</sup>, the high accumulation of radiolabeled small molecule-based ligands (e.g. [<sup>177</sup>Lu]Lu-PSMA-617 and [<sup>68</sup>Ga]Ga-PSMA-11) does not correlate with the rather low PSMA expression density detected by immunohistochemistry and low uptake of radiolabeled antibody [<sup>177</sup>Lu]Lu-J591 in patients.<sup>[188, 211, 275, 278]</sup> Indeed, unwanted non-target tissue uptake in salivary glands is markedly reduced using radiolabeled antibodies. Anyhow, therapeutic concepts using PSMA targeting antibodies are affected by slow diffusion into solid lesions and myelotoxicity due to longer blood circulation.<sup>[211, 279, 280]</sup>

Based on the fact that administration of monosodium glutamate in mice prior to [<sup>68</sup>Ga]Ga-PSMA-11 markedly reduced activity uptake in salivary glands whilst maintaining high tumor uptake, non-PSMA-specific interactions such as small molecule/anion/glutamate transporter mechanisms may be conceivable.<sup>[281]</sup> Moreover, the absorbed dose in salivary glands of PCa patients could be decreased by a factor of ~ 4 via administering a phosphoramidate-based PET agent compared to the urea-based radiotracer [<sup>68</sup>Ga]Ga-PSMA-I&T.<sup>[233]</sup> Thus, leading to the assumption that also fragments of the central Zn<sup>2+</sup>-binding ureate might serve as potential recognition sites for these transporter systems or other transporter-independent uptake mechanisms. However, the detailed mechanism of uptake into salivary and lacrimal glands and the respective target structure has not been elucidated so far.<sup>[275, 281]</sup>

This lack of knowledge led to various different approaches towards the reduction of radioactivity uptake into the salivary glands and thus corresponding unwanted side effects during radioligand therapy. After reduction of stimulus conduction by injection of botulinum toxin, a significant decrease of the SUV<sub>mean</sub> (up to 64%) in the right parotid gland compared to the left (control) was

## INTRODUCTION

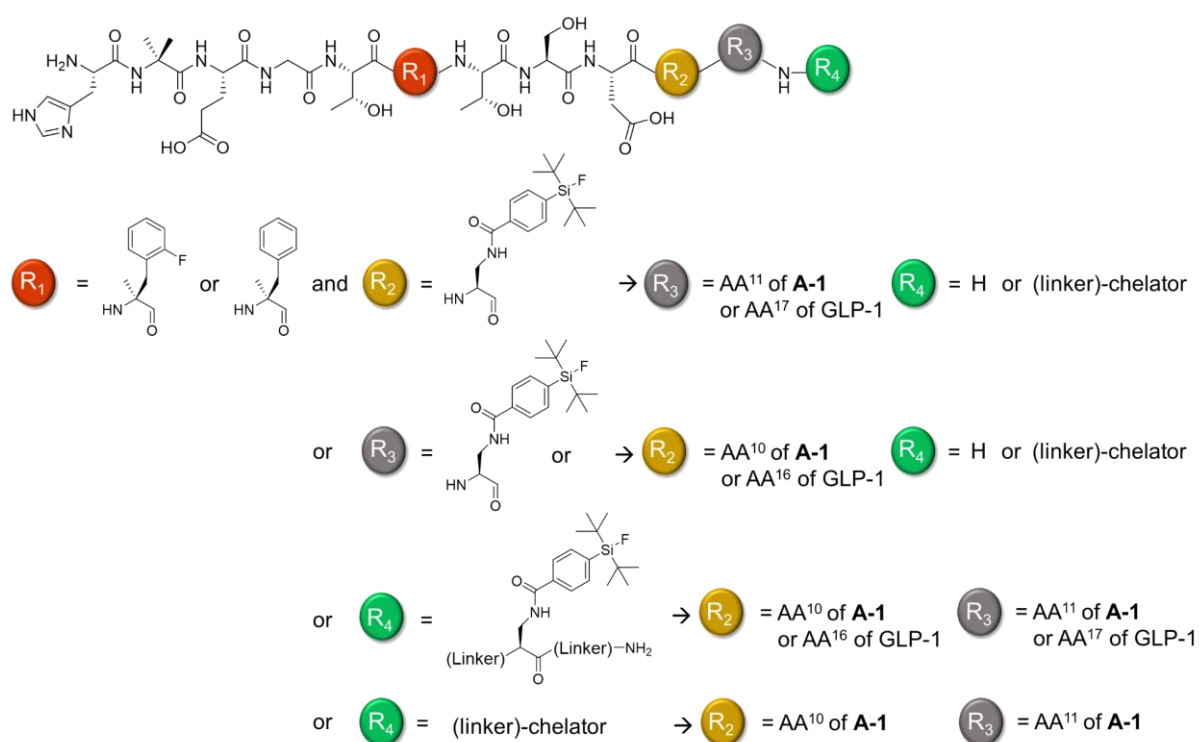
observed.<sup>[282]</sup> In contrast, external cooling with ice packs to decrease the overall blood perfusion showed no effect on ligand uptake and xerostomia when <sup>177</sup>Lu-labeled peptides were used.<sup>[283-285]</sup> Furthermore, excretion stimulus via vitamin C was investigated, but did not lead to any measurable uptake reduction of [<sup>68</sup>Ga]Ga-PSMA-11.<sup>[242]</sup> Sialendoscopy with dilatation, saline irrigation and steroid injection (prednisolone) after targeted  $\alpha$ -therapy ([<sup>225</sup>Ac]Ac-PSMA-617) showed beneficial effects on salivary gland function preservation and for patients' quality of life. However, not all radiation induced damages on the parenchyma could be avoided, as macroscopic findings during sialendoscopy revealed endothelial avascularity with the presence of stenosis.<sup>[284]</sup> All in all, those efforts did not show the desired efficacy.

In conclusion, small molecule-based PSMA radioligands represent promising agents for molecular imaging of prostate cancer or other tumors characterized by a PSMA-overexpressing neovasculature. However, high non-target tissue uptake in salivary glands affects the use of  $\alpha$ -emitter-labeled compounds for RLT. As a possible strategy to reduce activity accumulation in these organs and to allow for a more routine application of TAT, pharmacokinetically optimized peptides were supposed to serve as valuable alternative structures. Based on the findings stated above, especially those with modifications at the inhibitor part were assumed to provide suitable characteristics for targeting PSMA positive lesions with a higher tumor-to-salivary gland ratio.

## II. OBJECTIVES

### 2.1. Design of GLP-1R ligands with improved pharmacokinetics - objective I

The first aim of this thesis was to establish high-affinity GLP-1R-targeting ligands with improved pharmacokinetics. More precisely, lead peptide **A-1** (Figure 9) should be examined on its potential to act as high-affinity GLP-1R ligand and to potentially reduce non-GLP-1R-mediated uptake and retention of GLP-1R-binding radioligands in the kidneys, either by providing a peptide scaffold with a reduced overall ligand charge (ligand-based reduced kidney uptake) or by direct <sup>18</sup>F-labeling (nuclide-based decreased renal retention) (Figure 16).



,Linker' preferably composed of a varying number of amino acids

#### GLP-1:

His<sup>7</sup>-Ala-Glu-Gly<sup>10</sup>-Thr-Phe-Thr-Ser-Asp<sup>15</sup>-Val-Ser-Ser-Tyr-Leu<sup>20</sup>-Glu-Gly-Gln-Ala-Ala<sup>25</sup>-Lys-Glu-Phe-Ile-Ala<sup>30</sup>-Trp-Leu-Val-Lys-Gly-Arg<sup>36</sup>-NH<sub>2</sub>

**Figure 16:** Planned modified versions of lead peptide **A-1** (above), suitable for direct radiohalogenation and/or -metallation. The sequence of reference ligand GLP-1 (**A-2**), which should serve as a reference for all obtained *in vitro* data, is given below. AA, amino acid.

## OBJECTIVES

### Rationales for the intended ligand modifications

**A-1** as *basic scaffold*. Beside its overall short chain length (11 amino acids) and concomitant less amount of charged amino acids, the use of undecapeptide **A-1** was envisaged, due to its favorable GLP-1R-activating properties ( $EC_{50}$  (**A-1**) = 31 pM vs.  $EC_{50}$  (GLP-1) = 34 pM<sup>[111, 113]</sup>).

*Positioning of the radiolabel*. Since **A-1** and related undecapeptides have not been converted into an imaging agent for insulinomas so far, an adequate position for the radiolabel could only be roughly estimated in advance but not clearly pre-defined. As discussed in section 1.1.4, established exendin-3/4-based radiotracers are characterized by C-terminal modifications for radiolabeling, based on the finding that crucial residues for GLP-1 receptor binding and activation are located mainly at the N-terminal nonapeptide (*Figure 6*). Therefore, modifications at the C-terminus were also supposed to be preferred for **A-1**. However, for the attachment of a radiolabel to the downsized structure of **A-1**, that clearly differs from 39-residue exendin-4, previous structure-activity relationship (SAR) studies on related undecapeptides as well as on endogenous GLP-1 must be considered. For GLP-1, amino acid residues 10 to 21 (16 to 27 in GLP-1 counting method) were found to play a subordinate role in receptor binding and activation (*Figure 6*).<sup>[40, 45, 52]</sup> Accordingly, the well-tolerated bulky aromatic residues at position 10 and 11 in undecapeptide **A-1** confirm flexibility of GLP-1R towards structural modifications after position 9 and simultaneously indicate a certain preference for sterically demanding hydrophobic residues at these sites.<sup>[113, 114]</sup> Based on these SAR, placement of a bulky hydrophobic SiFA moiety at position 10 or 11 was supposed to result in a well tolerated GLP-1R ligand, suitable at the same time for direct radiofluorination. Nonetheless, a successful implementation after position 11 also remains conceivable (*Figure 16*).

In order to determine whether **A-1** possesses the ability to reduce kidney uptake also when linked to a radiometal chelate, synthesis and evaluation of the respective conjugates was planned to be conducted afterwards. Depending on the results obtained for SiFA-tagged compounds, radiohybrid concepts<sup>[140]</sup> would be envisaged or abandoned. In the latter case, lead peptide **A-1** was intended to be used as the basic scaffold for chelator attachment. The optimal position for installation of a chelator (e.g. DOTA, DOTAGA or NOTA) was more difficult to assess in advance, due to the lack of comparative data. However, it was expected to be identified via evaluation of structures with varying linker units between the known GLP-1R-binding peptide and the chelator (*Figure 16*).

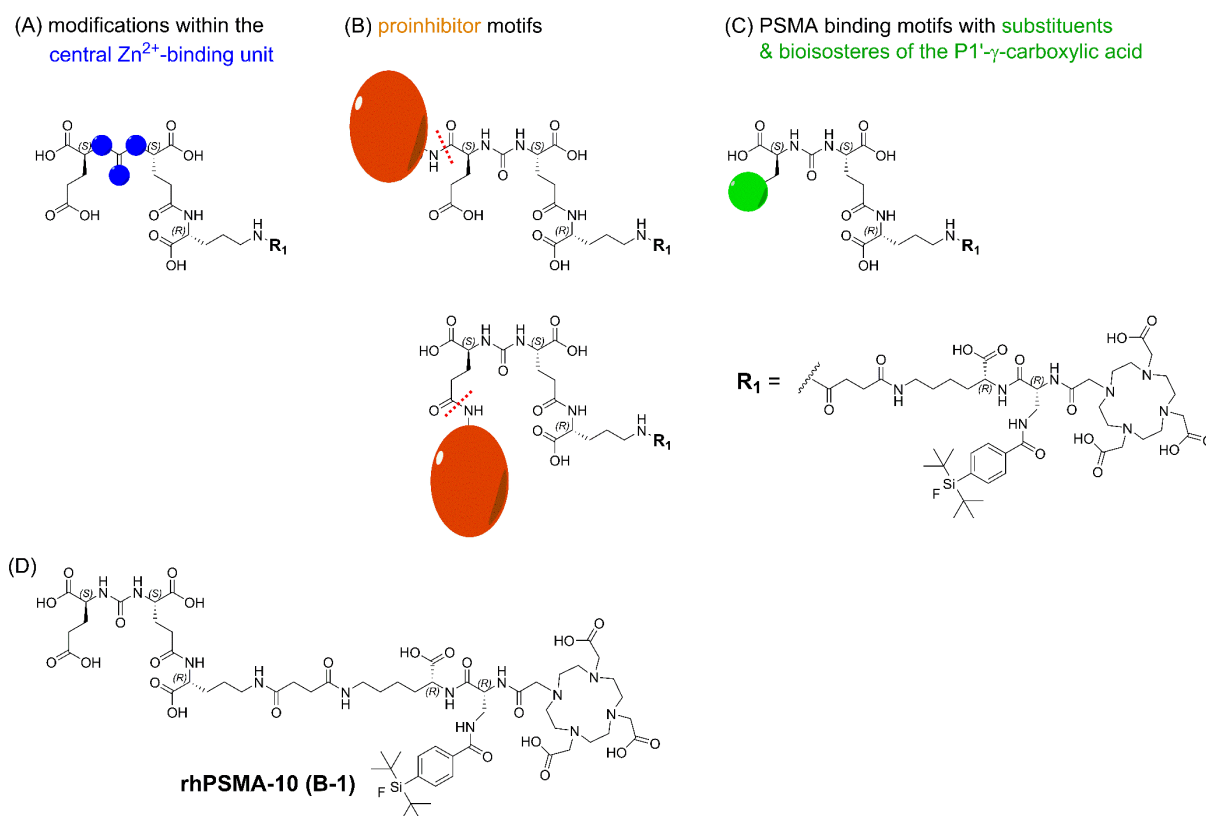
*Sites for ligand optimization*. Since position 6 represents a distinct site for ligand optimization<sup>[111]</sup>, two different residues (*Figure 16*) should be re-evaluated in order to clarify the value of this site in ligand optimization.

## OBJECTIVES

Derivatives of **A-1** suitable for direct radiolabeling (SiFA compounds) or insertion of other modifications (e.g. attachment of a chelator) were planned to be preselected by affinity determinations. As a result, the main objective of this study was to generate precursor molecules with low nanomolar  $IC_{50}$  values that preferably lie in the range of endogenous GLP-1. For this purpose, a novel cell-based assay for screening of GLP-1R-targeting compounds should be developed and implemented.

## 2.2. Design of PSMA ligands with improved pharmacokinetics - objective II

The second aim of this thesis was to establish high-affinity PSMA-targeting ligands with improved pharmacokinetics. More precisely, modifications at the urea-based inhibitor unit should be examined on their potential to reduce the non-PSMA-specific or perhaps 'transporter-mediated' uptake<sup>[271, 281]</sup> of PSMA-binding radioligands into salivary glands. Therefore, three different concepts for structural alterations were planned to be investigated (*Figure 17*).



**Figure 17:** Schematic representation of planned PSMA inhibitors containing (A) modifications within the central Zn<sup>2+</sup>-binding unit (B) proinhibitor motifs (expected cleavage sites are indicated as red dotted lines) and (C) substituents & bioisosteres of the P1'- $\gamma$ -carboxylic acid. All compounds were planned to be derived from the EuE-based ligand rhPSMA-10 (B-1) (D) which should serve as a reference for all obtained *in vitro* and *in vivo* data.

### Rationales for the intended inhibitor modifications

*Modifications within the central Zn<sup>2+</sup>-binding unit.* The C-terminal glutamate represents a common feature of both phosphoramidate- and urea based PSMA ligands. However, as stated in section 1.2.4, the absorbed dose in salivary glands of PCa patients could be decreased by a factor of ~ 4 via administering a phosphoramidate-based PET agent compared to the urea based radiotracer [<sup>68</sup>Ga]Ga-PSMA-I&T.<sup>[212, 233]</sup> Therefore, inhibitors containing modifications within the Zn<sup>2+</sup>-binding unit (i.e. thioureas and carbamates) should be synthesized, assuming that

## OBJECTIVES

fragments of the  $Zn^{2+}$ -binding group might serve as potential recognition sites for small molecule/anion/glutamate transporter systems or other transporter-independent uptake mechanisms.

Apart from this theory, the C-terminal glutamate of PSMA ligands was presumed to cause for unwanted uptake into salivary glands, based on the results of Rousseau *et al.*<sup>[281]</sup> In currently used EuE- and KuE-based PSMA inhibitors, this structural feature is set as an essential part for proper ligand binding. However, at the same time it represents the fragment which is most similar to monosodium glutamate, by which activity accumulation could be markedly reduced in salivary glands in mice if administered 15 min prior to  $[^{68}Ga]Ga$ -PSMA-11. Therefore, masking of this ligand-inherent glutamate was tried to be realized by proinhibitors (reversible masking) and PSMA ligands with substituents & bioisosteres of the P1'- $\gamma$ -carboxylic acid (irreversible masking).

*Proinhibitors.* Prodrug approaches for targeted delivery of cytotoxic agents to PCa lesions have been recently published and were further evaluated in an open label dose-escalation trial (NCT01056029).<sup>[255, 256]</sup> Hence, this prodrug principle was considered as a reasonable option for reducing non-target tissue uptake of PSMA ligands. Thereby, PSMA as hydrolytical active enzyme could act as instrument for on-site liberation of the respective inhibitor and yet serve as the target for RLT of PCa. Non-target tissue accumulation would thus be reduced to a remarkably low level, as binding of the masked inhibitor is only possible to enzymatically active sites. Variations from the original PSMA substrate *N*-acetyl-L-aspartyl-L-glutamate (NAAG), were recently published by Barinka *et al.* and Plechanovová *et al.*<sup>[252, 253]</sup> Thereof, Ac-L-Glu-L-Met and Ac-L-Asp-L-2-Aoc showed turnover numbers ( $k_{cat}$ ) and cleavage efficiencies ( $k_{cat}/K_m$ ) closest to the respective values indicated for NAAG (section 1.2.3). For this reason, both glutamate surrogates, L-Met as well as L-2-Aoc should be implemented into the existing structure of rhPSMA-10 (**B-1**). They should be linked to the  $\alpha$ - or  $\gamma$ -carboxylate of the C-terminal glutamate, as the preferred cleavage site could not be clearly specified upfront. Hydrolysis might occur between  $\alpha$ -linkages (NAALADase activity of GCP II in the central and peripheral nervous system) or between  $\gamma$ -linkages (FOLH1 activity in the gastrointestinal tract).<sup>[142]</sup> In addition, prodrug approaches focusing just on  $\gamma$ -linkages were adversely affected by metabolic instability in human plasma.<sup>[254]</sup>

*PSMA binding motifs with substituents & bioisosteres of the P1'- $\gamma$ -carboxylic acid.* Modifications at the P1'- $\gamma$ -carboxylic acid moiety were preferred, as previous studies conducted by Kozikowski *et al.* revealed substitutions at the P1' glutamate to be more tolerated at the  $\gamma$ -carboxylate than at the  $\alpha$ -carboxylate.<sup>[222]</sup> Moreover, the P1'- $\gamma$ -carboxylic acid possibly acts as the relevant recognition site for small molecule/anion/glutamate transporter systems.<sup>[281]</sup> Besides Kozikowski *et al.*, Wang *et al.* and Plechanovová *et al.* investigated the effect of carboxylic acid bioisosteres and aliphatic substituents on the affinity of urea-based inhibitors towards PSMA (Figure 15, section 1.2.3).<sup>[251, 252]</sup> On the basis of these essential studies, incorporation of the most

## OBJECTIVES

auspicious carboxylic acid substituents (i.e. L-2-aminoheptanoic acid as well as furyl, alkyne and tetrazole moieties) was pursued.

It has to be mentioned that a single atom, a group or even a whole molecule can act as a bioisostere, if it possesses a comparable volume, shape and/or physicochemical properties to the replaced structure.<sup>[286]</sup> Therefore, a similar biological effect can be assumed but is not assured. In consequence, loss of affinity was expected to a certain extent for all masking modifications but considered to be acceptable as long as tumor-to-salivary gland ratios were improving.

All these modifications were planned to be investigated based on one of our recently developed PSMA ligands, rhPSMA-10 (**B-1**).<sup>[140]</sup> Thereby, a clear distinction between the salivary gland uptake values of EuE- and non-EuE-based radioligands and higher tumor-to-salivary gland ratios at 24 h p.i. in comparison to EuE-based rhPSMA-10 (**B-1**) were of primary interest. The latter might indicate for a possible transferability to humans, despite certain species-dependent differences, i.e. a general lower uptake in mouse salivary glands.<sup>[287, 288]</sup> Preliminary studies on isolated PSMA inhibitor motifs and substrate mimetics should give a first indication, whether incorporation of the respective modifications into mature rhPSMA ligands would result in high- or low-affinity compounds.

### III. MATERIALS AND METHODS

#### 3.1. Materials

##### 3.1.1. Chemicals

All reagents were purchased from abcr GmbH (Karlsruhe, Germany), Carbolution (St. Ingbert, Germany), Fluorochem (Hadfield, United Kingdom), Iris Biotech (Marktredwitz, Germany), Merck KGaA (Darmstadt, Germany), Sigma-Aldrich Chemie GmbH (Steinheim, Germany), TCI (Eschborn, Germany) and VWR International GmbH (Darmstadt, Germany) in the quality grade "for synthesis". (Nle<sup>14</sup>, Tyr<sup>40</sup>)Exendin-4 and (Nle<sup>14</sup>, 3-iodo-Tyr<sup>40</sup>)exendin-4 were purchased from Biotrend Chemikalien GmbH (Cologne, Germany). Racemic 2-PMPA was purchased from Bio-Techne GmbH (Wiesbaden-Nordenstadt, Germany). Chematech (Dijon, France) delivered the chelator DOTA and derivatives thereof. Cell culture media and buffer solutions were purchased from Merck KGaA (Darmstadt, Germany) and Sigma Aldrich Chemie GmbH (Steinheim, Germany). [<sup>125</sup>I]Nal was purchased from Hartmann Analytic (Braunschweig, Germany) and n.c.a. [<sup>177</sup>Lu]LuCl<sub>3</sub> was delivered by ITG (Garching, Germany). Solvents were purchased from VWR International GmbH (Darmstadt, Germany) in the quality grade "HPLC grade" and used for analytical, preparative HPLC as well as column chromatography or liquid-liquid extraction. Unless otherwise stated, H<sub>2</sub>O was taken from a Barnstead™ MicroPure™ System (Thermo Fisher Scientific, Darmstadt, Germany) connected to an upstream DI 1500 ion exchange cartridge (Thermo Fisher Scientific, Darmstadt, Germany). Dry solvents were purchased from Alfa Aesar (Karlsruhe, Germany), Sigma-Aldrich Chemie GmbH (Steinheim, Germany) and VWR International GmbH (Darmstadt, Germany). Silica gel (high purity grade, 60 Å, 0.040 - 0.063 particle size) used for column chromatography was purchased from Sigma-Aldrich Chemie GmbH (Steinheim, Germany).

For SPPS on Rink amide ChemMatrix® or 2-CT resin the following *N*-terminal and side chain protection strategy was employed for standard amino acid residues (alphabetical order): Fmoc-Aib-OH, Fmoc-Ala-OH, Fmoc-L-Arg(Pbf)-OH, Fmoc-L-Asp(O*t*Bu)-OH, Fmoc-D/L-Dap(Dde)-OH, Fmoc-L-Gln(Trt)-OH, Fmoc-L-Glu-O*t*Bu, Fmoc-L-Glu(O*t*Bu)-OH\*H<sub>2</sub>O, Fmoc-Gly-OH, Boc-L-His(Boc)-OH\*DCHA, Fmoc-L-His(Trt)-OH, Fmoc-L-homoPhe-OH, Fmoc-L-Ile-OH, Fmoc-L-Leu-OH, Fmoc-D-Lys-O*t*Bu, Fmoc-L-Lys(Boc)-OH, Fmoc-D-Orn(Dde)-OH, Fmoc-L-( $\alpha$ -Me)Phe-OH, Fmoc-L-( $\alpha$ -Me)-(2-F)-Phe-OH, Fmoc-L-Phe-OH, Boc-L-Phe(4-I)-OH, Fmoc-L-Phe(4-I)-OH, Fmoc-L-Ser(*t*Bu)-OH, Fmoc-L-Thr(*t*Bu)-OH, Fmoc-L-Trp(Boc)-OH, Fmoc-L-Tyr(O*t*Bu)-OH, Fmoc-L-Tyr(3-I)-OH, Fmoc-L-Val-OH.

### 3.1.2. Equipment

*Analytical* and *preparative* RP-HPLC were performed using Shimadzu gradient systems (Shimadzu Deutschland GmbH, Neufahrn, Germany), each equipped with a SPD-20A UV/Vis detector (220 nm, 254 nm). Occasionally, a Sykam gradient HPLC system (Sykam GmbH, Eresing, Germany) equipped with a S3245 UV/Vis-Detektor (220 nm) was used for *preparative* RP-HPLC. All systems were operated by the LabSolutions software. Prior to quality control acquisitions, a control run was performed, in which only water/acetonitrile (1/1) was injected. Thereby, the system was checked for impurities in the injection port or on the column.

As different eluents and flow rates have been used for several compounds, the used methods are cited in the text and described as follows:

Method A: solvent A = water + 0.1% TFA, solvent B = acetonitrile + 2% water + 0.1% TFA

Method B: solvent A = water + 0.1% TFA, solvent B = acetonitrile + 5% water + 0.1% TFA

Method C: solvent A = water, solvent B = acetonitrile + 5% water

Method D: solvent A = water, solvent B = acetonitrile

*Analytical RP-HPLC* was performed on a Nucleosil 100 RP C18 (5  $\mu$ m, 125 mm  $\times$  4.6 mm) column (CS GmbH, Langerwehe, Germany) applying different linear solvent gradients (Method A) and a constant flow rate of 1 mL/min. Specific gradients, corresponding retention times  $t_R$  and capacity factors  $k$  are cited in the text. The capacity factor was calculated from the experimentally determined dead time ( $t_0 = 1.5$  min) of the HPLC system and the respective retention time  $t_R$ :

$$k = \frac{t_R - t_0}{t_0}$$

*Preparative RP-HPLC* was performed either on a MultoKrom 100 RP C18 (5  $\mu$ m, 125 mm  $\times$  20 mm) or a Multospher 100 RP C18 (5  $\mu$ m, 250  $\times$  20 mm) column (CS GmbH, Langerwehe, Germany) applying different linear solvent gradients (Method B or C) and different constant flow rates.

*Radio-RP-HPLC* for radiolabeling experiments of GLP-1 was performed on a Nucleosil 100 RP C18 (5  $\mu$ m, 125 mm  $\times$  4.6 mm) column (CS GmbH, Langerwehe, Germany) using a Sykam gradient system (Sykam GmbH, Eresing, Germany) with a linear solvent gradient (Method A or E) and a constant flow rate of 1 mL/min. For radioactivity detection, the outlet of the 206 PHD UV-Vis detector (Linear™ Instruments Corporation, Reno, USA) was connected to a NaI(Tl) well-type scintillation counter from EG&G Ortec (Munich, Germany).

Further acquisitions of radio-RP-HPLC chromatograms were performed on a Multospher 100 RP C18 (5  $\mu$ m, 125 mm  $\times$  4.6 mm) column (CS GmbH, Langerwehe, Germany) using a Shimadzu gradient system (Shimadzu Deutschland GmbH, Neufahrn, Germany) with a linear solvent gradient (Method A) and a constant flow rate of 1 mL/min. For radioactivity detection, the outlet of the UV

## MATERIALS AND METHODS

detector was connected to a HERM LB 500 NaI detector (Berthold Technologies, Bad Wildbad, Germany). For metabolite analysis a FlowStar<sup>2</sup> LB 514 detector (Berthold Technologies, Bad Wildbad, Germany) was additionally connected to the HERM detector.

*Flash chromatography* was performed on a Biotage flash purification system (Biotage, Uppsala, Sweden) using Biotage SNAP cartridges (KP-C18-HS, 12 g). The compounds were eluted applying different solvent gradients (Method D) and a constant flow rate of 12 mL/min.

*Mass spectra* were acquired with an Advion expression<sup>L</sup> compact mass spectrometer (Advion Ltd., Harlow, UK) with electrospray ionization (positive ion mode) and an orthogonal ion sampling from the heated capillary. The system was operated by the Mass Express software and spectra were processed using the Data Express software.

Occasionally, compounds were analyzed by a LC-MS system with a Thermo Scientific LCQ Fleet ion trap ESI mass spectrometer (Thermo Fisher Scientific, Waltham, USA) coupled to a Dionex UltiMate 3000 U-HPLC system (Thermo Fisher Scientific, Waltham, USA). For pre-analytical separation a Thermo Scientific Hypersil LCQ GOLD aQ C18 (3  $\mu$ m, 150 mm  $\times$  2.1 mm) column was used with a gradient of 10 - 90% MeCN in H<sub>2</sub>O (0.1% formic acid added to each solvent) over 20 min and a constant flow rate of 0.7 mL/min. Products were detected at 220 nm and 280 nm.

All <sup>1</sup>H- and <sup>13</sup>C-NMR spectra were measured at room temperature in either DMSO-*d*<sub>6</sub> or CDCl<sub>3</sub> on Bruker (Rheinstetten, Germany) instruments (AHV HD-300, AHV HD-400). Chemical shifts ( $\delta$ ) are reported in parts per million (ppm) and calibrated on the residual solvent signal (DMSO-*d*<sub>6</sub>: 2.50 ppm for <sup>1</sup>H and 39.5 ppm for <sup>13</sup>C, CDCl<sub>3</sub>: 7.26 ppm for <sup>1</sup>H and 77.0 ppm for <sup>13</sup>C). Multiplicities are described as follows: s = singlet, d = doublet, t = triplet, q = quartet, br = broad singlet, m = multiplet.

*Analytical thin layer chromatography* (TLC) was conducted with silica gel on aluminium support from Merck KGaA (Darmstadt, Germany) (Silica gel 60 RP-18 F<sub>254</sub>s). Substance spots were visualized either via UV illumination at 254 nm or with a 0.75% (m/v) potassium permanganate stain solution.

*Radio-thin layer chromatography* (radio-TLC) was conducted via a Scan-RAM detector (LabLogic Systems, Sheffield, United Kingdom). Cellulose strips were used for citrate-buffer (0.1 M disodium citrate sesquihydrate in H<sub>2</sub>O). Normal-phase TLC plates (Silica gel 60 F<sub>254</sub>) were used for analyses in NH<sub>4</sub>OAc buffer (1.0 M aq. NH<sub>4</sub>OAc/DMF (1/1)).

*Activity measurements* of the respective probes obtained from competitive binding assays, internalization assays, log D<sub>7.4</sub> determinations, biodistributions or metabolite analyses were measured by a 2480 WIZARD<sup>2</sup> automatic  $\gamma$ -counter (PerkinElmer, Waltham, USA) and evaluated with GraphPad PRISM.

## 3.2. Methods

### General remarks on peptide synthesis

The used equivalents of the reactants for the solid phase synthesis refer to the calculated load after attaching the first amino acid onto the resin. The specific loads are cited in the text. Syntheses were carried out at room temperature in a 10 mL syringe for peptide synthesis (Carl Roth, GmbH & Co. KG, Karlsruhe, Germany) equipped with plunger and frit (25 µm pore size). Prior to any reaction, dry resin was swelled in NMP for at least 30 min and then filtered. Unless otherwise indicated, the resin was washed with DMF (6×) after each reaction step. For storage, the resin was washed with DMF (3×) and DCM (3×) and dried in a desiccator. Solid phase synthesis of the peptides was carried out by manual operation using an Intelli-Mixer syringe shaker (Neolab, Heidelberg, Germany).

### General procedure for loading the first amino acid onto Rink amide ChemMatrix® resin and on-resin peptide bond formation (GP1)

Rink amide ChemMatrix® resin (average load: 0.50 mmol/g) was obtained as the free *N*-terminal form and hence, loading of the first amino acid and further elongation steps were performed by the same standard procedure. The (first) amino acid/SiFA-BA (1.50 eq.), TBTU (1.50 eq.) and HOBt or HOAt (1.50 eq.) were dissolved in DMF (~ 10 mL/g resin) and preactivated by addition of DIPEA (4.50 eq.) for five minutes, prior to incubation with the resin. Unless otherwise noted, the solution was added to the resin and shaken for 2 h at room temperature. Occasionally, the pH value had to be adjusted to 9 - 10 by addition of further DIPEA. In case of **A-11** and **A-12**, *sym*-collidine (9.00 eq.) was used as base for coupling of Fmoc-L-Dap(Dde)-OH.

Independent of the resin (2-CT or RACM), coupling to resin-bound bulky  $\alpha$ -quaternary amino acids like H-L-( $\alpha$ -Me)Phe and H-L-( $\alpha$ -Me)-(2-F)-Phe was performed with increased incubation periods (at least 24 h if bound to RACM or 2 × 17 - 26 h in total if bound to 2-CT resin). Moreover, HATU instead of TBTU was used as coupling reagent. Equivalents were scaled up to 3.00 eq. for the following amino acid (i.e. Fmoc-L-Thr(*t*Bu)-OH) and coupling reagents (HATU, HOBt or HOAt) as well as to 5.00 - 9.00 eq. for DIPEA (for a pH value of 9 - 10). Coupling to resin-bound H-Aib was performed also with increased incubation periods (at least 5 h if bound to RACM or 24 h if bound to 2-CT resin). Additionally, equivalents of the respective amino acid (i.e. Fmoc/Boc-L-His(Trt/Boc)-OH), TBTU, HOBt or HOAt (3.00 eq.) as well as for DIPEA (5.00 - 9.00 eq.) were scaled up.

### General procedure for loading the first amino acid onto 2-CTC resin (GP2)

The first amino acid (1.50 eq.) and DIPEA (1.33 eq.) were dissolved in DCM (5.00 mL) and stirred for 5 min at r.t. prior to addition of the dry resin (1.00 eq.). After 15 min further DIPEA (2.67 eq.)

## MATERIALS AND METHODS

was added and the reaction mixture was stirred for 75 min. Afterwards, MeOH (2 mL) was added and stirred for 15 min. The resin was washed successively with MeOH (4x), DMF (4x) and DCM (4x) and dried at least two hours or overnight in a desiccator. The load was calculated using the following formula:

$$\text{load} = \frac{(m_2 - m_1) \cdot 1000}{(M_W - M_{\text{HCl}}) \cdot m_2} \quad \left[ \frac{\text{mmol}}{\text{g}} \right]$$

$M_W$  = molecular weight of the amino acid [g/mol]

$M_{\text{HCl}}$  = molecular weight of HCl [g/mol]

$m_1$  = mass of dry 2-CTC resin before coupling [g]

$m_2$  = mass of dried resin after coupling [g]

### General procedure for on-resin peptide bond formation on 2-CT resin (GP3)

To a solution of TBTU (2.00 eq.), HOAt (2.00 eq.) and the amino acid/SiFA-BA (2.00 eq.) in DMF (~ 10 mL/g resin), DIPEA (6.00 - 9.00 eq.) was added to adjust the pH value to 9 - 10 and the mixture was allowed to preactivate for five minutes. Unless otherwise noted, the solution was added to the resin and shaken for at least 2 h at room temperature (maximum 24 h). For coupling of Fmoc-D-Dap(Dde)-OH, *sym*-collidine (6.00 - 8.00 eq.) was added instead of DIPEA. Succinic anhydride (7.00 eq.) was coupled only using DIPEA (7.00 eq.) and no further coupling reagents. For coupling of a compound with free amine (e.g. Fmoc-D-Lys-O<sup>t</sup>Bu\*HCl, 2.00 eq.), the resin-bound acid was preactivated for five minutes using TBTU (2.00 eq.), HOAt (2.00 eq.) and DIPEA (6.00 eq.). The compound was dissolved in DMF and added to the preactivated resin.

### General procedure for the on-resin Fmoc-removal (GP4)

The resin was shaken 2 × 15 min (Rink amide ChemMatrix<sup>®</sup> resin) or 5 × 5 min (2-CT resin) in 20% piperidine in DMF (v/v) to remove the Fmoc-protective group and afterwards washed with DMF (7x). If Ornithin was the first amino acid bound to the 2-CT resin, Fmoc-removal was performed 12 × 5 min in 20% piperidine.

### General procedures for the on-resin Dde-removal (GP5 & GP6)

**GP5:** If no Fmoc-group was present in the resin-bound peptide, the resin was suspended in a solution of 2% hydrazine monohydrate in DMF (10 mL), agitated for 20 min and then washed with DMF (7x).

**GP6:** If an Fmoc-group was present in the resin-bound peptide, the resin was suspended in a solution of imidazole (0.46 g/g resin) and hydroxylamine hydrochloride (0.63 g/g resin) in NMP (5.0 mL/g resin) and DMF (1.0 mL/g resin) and agitated for 2 × 3 h. Afterwards, the resin was washed with DMF (7x).

### **General procedures for monitoring the reaction progress (GP7 & GP8)**

For a test cleavage with TFA (**GP7**) a small aliquot of the resin was taken and treated with 100  $\mu$ L of TFA for 15 min at r.t. in an Eppendorf tube.

To avoid cleavage of *tert*-butyl groups or formation of other unidentifiable by-products, test cleavage was performed with HFIP/DCM (**GP8**). The resin aliquot was treated with 100  $\mu$ L of HFIP/DCM (1/4, v/v) for 30 min at r.t.

For both procedures, the respective solution (without beads!) was transferred into another Eppendorf tube and the solvent was evaporated under a stream of nitrogen. The residue was dissolved in a mixture of H<sub>2</sub>O and MeCN (1/1, v/v), now ready for RP-HPLC/MS analysis.

### **Peptide cleavage from the resin with simultaneous removal of all acid-labile protective groups (GP9)**

The resin was treated either with TFA/TIPS/H<sub>2</sub>O or TFA/TIPS/DCM (95/2.5/2.5, 10.0 mL) twice for 30 min at r.t. and washed with DCM afterwards (3 $\times$ ). The solvent was evaporated under N<sub>2</sub> flow and after lyophilization the crude product was obtained.

### **Peptide cleavage from the resin with preservation of all acid-labile protective groups (GP10 & GP 11)**

**GP10:** The resin was treated with DCM/TFE/AcOH (6/3/1, 10 - 12 mL) for 30 min at r.t. and washed with DCM afterwards (6 $\times$ ). Solvents were removed under reduced pressure and AcOH was removed by azeotropic distillation (addition of small portions of toluene, 4 $\times$ ). After removal of residual toluene and lyophilization the crude product was obtained.

**GP11:** The resin was treated with HFIP/DCM (1/4, 10 mL) for 4 h (4  $\times$  30 min, 2  $\times$  1 h) at r.t. and washed with DCM afterwards (6 $\times$ ). Solvents were evaporated under N<sub>2</sub> flow and after lyophilization the crude product was obtained.

### **General procedure for reactions under air- and moisture free conditions (GP12)**

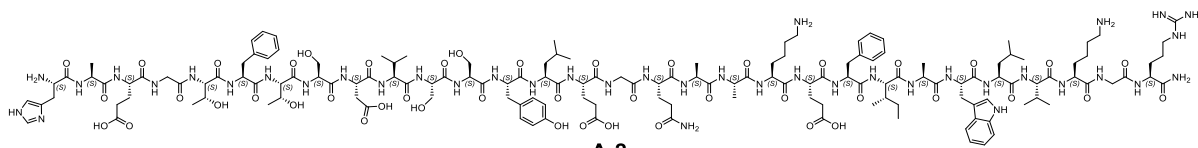
The used Schlenk flask, further glassware as well as the agitator were heated properly three times under vacuum ( $2.0 \times 10^{-3}$  -  $8.0 \times 10^{-3}$  mbar) prior to the reaction. The apparatus was flushed with argon after each heating cycle. Only dry solvents and dry reagents were used for the reactions. The addition of reagents or reactants to the reaction mixture was performed only under argon counterflow. Probes for HPLC control were also taken only under argon counterflow. If the reaction mixture was heated or evolution of gas was expected, the stop cock at the top of the apparatus was replaced by a balloon.

## MATERIALS AND METHODS

The following compounds are numbered consecutively, with GLP-1R ligands evaluated in *in vitro* experiments indicated by a prefixed '**A-**' and PSMA ligands evaluated in *in vitro* and *in vivo* experiments indicated by a prefixed '**B-**'.

### 3.2.1. Synthesis of GLP-1 receptor ligands

#### Glucagon-like peptide 1 (**A-2**)

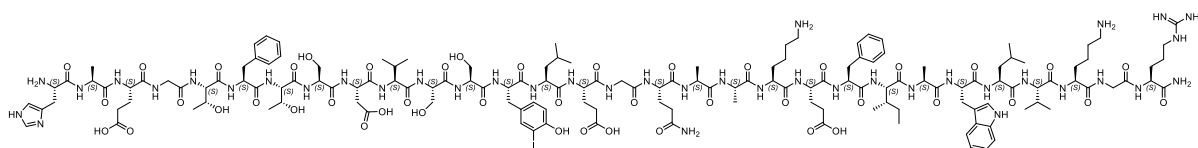


Chemical Formula:  $C_{149}H_{226}N_{40}O_{45}$   
Molecular Weight: 3297,68

GLP-1 (**A-2**) was synthesized according to standard Fmoc-SPPS on Rink amide ChemMatrix<sup>®</sup> resin (0.20 mmol, 1.00 eq.), applying the above-mentioned methods (GP1 and GP4). The reaction progress was monitored (GP7) after coupling of Fmoc-L-Leu<sup>32</sup>-OH, Fmoc-L-Glu<sup>27</sup>(*O**t*Bu)-OH, Fmoc-L-Gln<sup>23</sup>(Trt)-OH, Fmoc-L-Leu<sup>20</sup>-OH, Fmoc-L-Tyr<sup>19</sup>(*O**t*Bu)-OH, Fmoc-L-Ser<sup>14</sup>(*t*Bu)-OH, Fmoc-Gly<sup>10</sup>-OH and Fmoc-L-His<sup>7</sup>(Trt)-OH. Formation of the expected products was confirmed by RP-HPLC/MS and after removal of the Fmoc protective group from *N*-terminal histidine, the peptide was cleaved off the resin with TFA/TIPS/H<sub>2</sub>O (95/2.5/2.5, 1 × 30 min, slightly modified to GP9). The solvent was reduced in a stream of nitrogen, the peptide was precipitated in Et<sub>2</sub>O and centrifuged (3 000 rpm, ca. 1 000 g, 3 min). Purification by preparative RP-HPLC (35 - 50% B in 20 min, Method B, 5 mL/min) was performed with a small portion of the precipitate and afforded 11.7 mg of pure product **A-2**·5TFA as a colorless powder after lyophilization.

RP-HPLC (10 - 90% B in 15 min, Method A, 1 mL/min):  $t_R = 9.2$  min;  $k = 5.1$ . Calculated monoisotopic mass ( $C_{149}H_{226}N_{40}O_{45}$ ): 3295.66, found:  $m/z = 1649.0$  [ $M(\mathbf{A-2})+2H$ ]<sup>2+</sup>, 1099.7 [ $M(\mathbf{A-2})+3H$ ]<sup>3+</sup>, 825.1 [ $M(\mathbf{A-2})+4H$ ]<sup>4+</sup>.

#### Tyr(3-I)<sup>19</sup>-Glucagon-like peptide 1 (**A-3**)



Chemical Formula:  $C_{149}H_{225}I N_{40}O_{45}$   
Molecular Weight: 3423,58

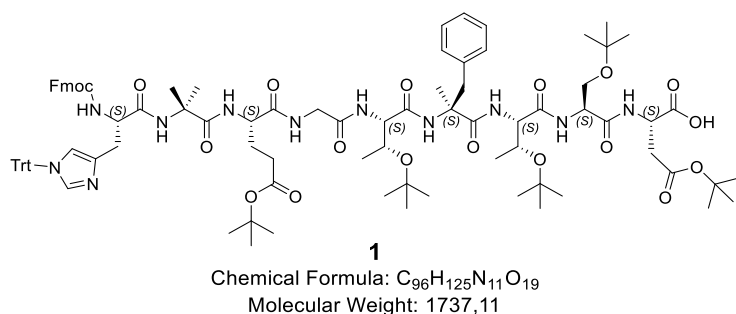
Tyr(3-I)<sup>19</sup>-GLP-1 (**A-3**) was synthesized according to standard Fmoc-SPPS on Rink amide ChemMatrix<sup>®</sup> resin (0.10 mmol, 1.00 eq.), applying the above-mentioned methods (GP1 and GP4). For coupling of Fmoc-L-Tyr-(3-I)<sup>19</sup>-OH and all following on-resin synthesis steps, 2.50 eq. were used for amino acids, TBTU and HOBt. The reaction progress was monitored (GP7) after coupling of Fmoc-L-Leu<sup>32</sup>-OH, Fmoc-L-Glu<sup>27</sup>(*O**t*Bu)-OH, Fmoc-L-Gln<sup>23</sup>(Trt)-OH, Fmoc-L-Leu<sup>20</sup>-OH, Fmoc-L-Tyr(3-I)<sup>19</sup>-OH, Fmoc-L-Ser<sup>18</sup>(*t*Bu)-OH, Fmoc-L-Ser<sup>14</sup>(*t*Bu)-OH, Fmoc-Gly<sup>10</sup>-OH and Fmoc-L-His<sup>7</sup>(Trt)-OH. Formation of the expected products was confirmed by RP-HPLC/MS and after removal of the Fmoc protective group from *N*-terminal histidine, the peptide was cleaved off the resin with TFA/TIPS/H<sub>2</sub>O (95/2.5/2.5, 1 × 30 min, slightly modified to GP9). The solvent was

## MATERIALS AND METHODS

reduced in a stream of nitrogen, the peptide was precipitated in Et<sub>2</sub>O and centrifuged (3 000 rpm, ca. 1 000 g, 3 min). Purification by preparative RP-HPLC (35 - 50% B in 20 min, Method B, 5 mL/min) was performed with a small portion of the precipitate and afforded 8.80 mg of pure product **A-3**\*5TFA as a colorless powder after lyophilization.

RP-HPLC (10 - 90% B in 15 min, Method A, 1 mL/min):  $t_R = 9.5$  min;  $k = 5.3$ . Calculated monoisotopic mass (C<sub>149</sub>H<sub>225</sub>N<sub>40</sub>O<sub>45</sub>): 3421.56, found:  $m/z = 1712.1$  [M(**A-3**)+2H]<sup>2+</sup>, 1141.6 [M(**A-3**)+3H]<sup>3+</sup>, 856.4 [M(**A-3**)+4H]<sup>4+</sup>.

### *Fmoc-L-His(Trt)-Aib-L-Glu(OtBu)-Gly-L-Thr(tBu)-L-( $\alpha$ -Me)Phe-L-Thr(tBu)-L-Ser(tBu)-L-Asp(OtBu)-OH (1)*

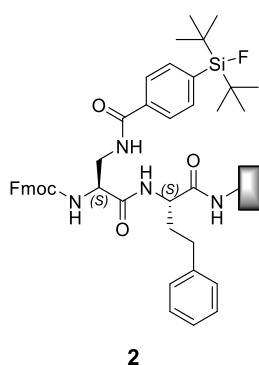


Nonapeptide **1** was synthesized on 2-CT resin according to GP2, GP3 and GP4 (load: 1.02 mmol/g, 0.31 mmol, 1.00 eq.). The peptide was cleaved off the resin according to GP10. Thereby, 545 mg of crude product **1** were obtained and used in

subsequent steps without further purification.

RP-HPLC (40 - 100% B in 15 min, Method A, 1 mL/min):  $t_R = 17.6$  min;  $k = 11$ . Calculated monoisotopic mass (C<sub>96</sub>H<sub>125</sub>N<sub>11</sub>O<sub>19</sub>): 1735.92, found:  $m/z = 868.9$  [M(**1**)+2H]<sup>2+</sup>, 1495.4 [M(**1**)-Trt+H]<sup>+</sup>, 1737.3 [M(**1**)+H]<sup>+</sup>.

### *Fmoc-L-Dap(SiFA)-L-homoPhe-RACM (2)*



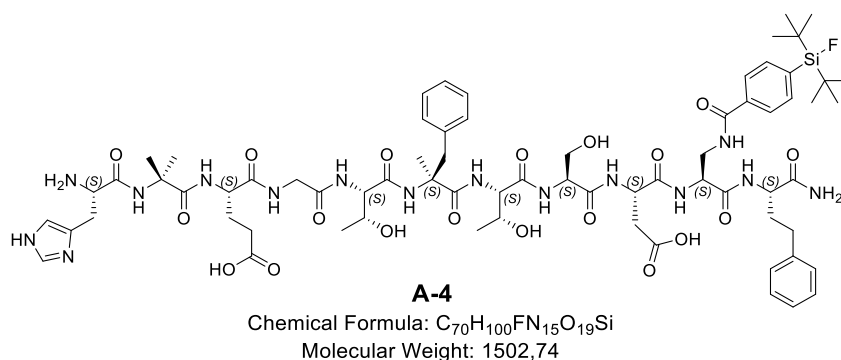
Chemical Formula: C<sub>43</sub>H<sub>51</sub>FN<sub>4</sub>O<sub>5</sub>Si  
Molecular Weight: 750,99

Dipeptide **2** was synthesized on Rink amide ChemMatrix<sup>®</sup> resin according to GP1, GP4 and GP6 (load: 0.50 mmol/g, 0.15 mmol, 1.00 eq.). A test cleavage (GP7) was performed after coupling of SiFA-BA, which revealed nearly complete conversion to product **2**.

RP-HPLC (10 - 90% B in 15 min, Method A, 1 mL/min):  $t_R = 19.5$  min;  $k = 12$ . Calculated monoisotopic mass (C<sub>43</sub>H<sub>51</sub>FN<sub>4</sub>O<sub>5</sub>Si): 750.36, found:  $m/z = 751.4$  [M(**2**)+H]<sup>+</sup>, 1501.9 [M<sub>2</sub>(**2**)+H]<sup>+</sup>.

## MATERIALS AND METHODS

### *H-L-His-Aib-L-Glu-Gly-L-Thr-L-( $\alpha$ -Me)Phe-L-Thr-L-Ser-L-Asp-L-Dap(SiFA)-L-homoPhe-NH<sub>2</sub> (A-4)*

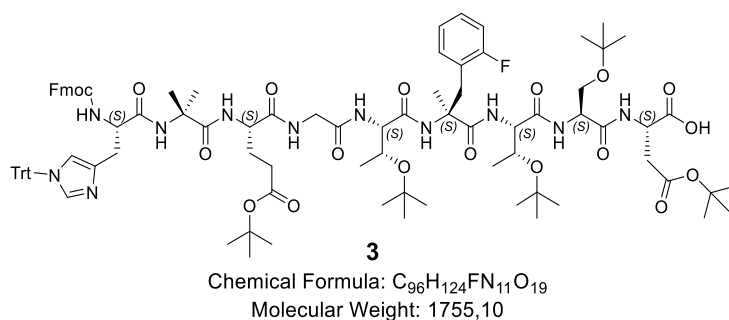


Synthesis of peptide **A-4** was conducted via fragment coupling according to GP1 and GP4. First, the Fmoc protective group was removed from **2** (37.5  $\mu$ mol, 1.00 eq.) (GP4). Afterwards, a

solution containing **1** (97.2 mg, 56.3  $\mu$ mol, 1.50 eq.), TBTU (24.1 mg, 75.0  $\mu$ mol, 2.00 eq.), HOBT (10.1 mg, 75.0  $\mu$ mol, 2.00 eq.) and DIPEA (28.7  $\mu$ L, 169  $\mu$ mol, 4.50 eq.) in DMF was added and incubated for 15 h at room temperature. Examination of the reaction progress (GP7) revealed successful coupling of **1**. Removal of the *N*-terminal Fmoc protective group (GP4), followed by cleavage of the peptide from the resin with TFA/TIPS/H<sub>2</sub>O (95/2.5/2.5, 1  $\times$  30 min, slightly modified to GP9) resulted in 2.70 mg (4.16%) of product **A-4**\*2 TFA as a colorless powder after RP-HPLC purification (35 - 50% B in 20 min, Method B, 5 mL/min) and lyophilization.

RP-HPLC (10 - 90% B in 15 min, Method A, 1 mL/min):  $t_R$  = 10.6 min;  $k$  = 6.1. Calculated monoisotopic mass (C<sub>70</sub>H<sub>100</sub>FN<sub>15</sub>O<sub>19</sub>Si): 1501.71, found:  $m/z$  = 751.9 [M(**A-4**)+2H]<sup>2+</sup>, 1502.6 [M(**A-4**)+H]<sup>+</sup>.

### *Fmoc-L-His(Trt)-Aib-L-Glu(OtBu)-Gly-L-Thr(tBu)-L-( $\alpha$ -Me)-(2-F)-Phe-L-Thr(tBu)-L-Ser(tBu)-L-Asp(OtBu)-OH (3)*



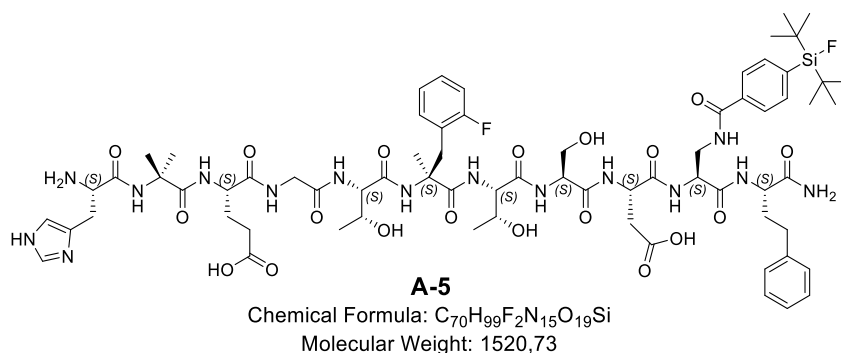
Nonapeptide **3** was synthesized on 2-CT resin according to GP2, GP3 and GP4 (load: 1.38 mmol/g, 0.21 mmol, 1.00 eq.). The peptide was cleaved off the resin according to GP10. Thereby, 162 mg of crude product **3** were obtained and used in

subsequent steps without further purification.

RP-HPLC (40 - 100% B in 15 min, Method A, 1 mL/min):  $t_R$  = 17.5 min;  $k$  = 11. Calculated monoisotopic mass (C<sub>96</sub>H<sub>124</sub>FN<sub>11</sub>O<sub>19</sub>): 1753.91, found:  $m/z$  = 878.0 [M(**3**)+2H]<sup>2+</sup>, 1513.7 [M(**3**)-Trt+H]<sup>+</sup>, 1754.6 [M(**3**)+H]<sup>+</sup>.

## MATERIALS AND METHODS

### *H-L-His-Aib-L-Glu-Gly-L-Thr-L-( $\alpha$ -Me)-(2-F)-Phe-L-Thr-L-Ser-L-Asp-L-Dap(SiFA)-L-homoPhe-NH<sub>2</sub>* (**A-5**)

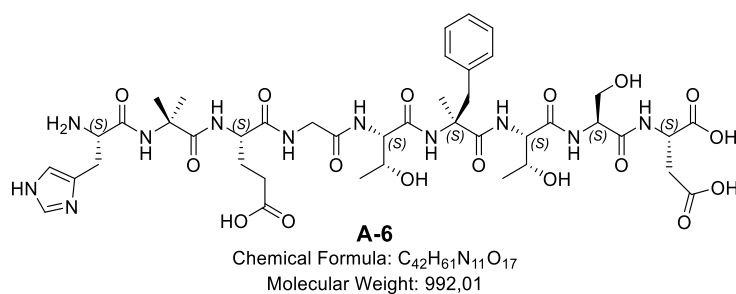


Synthesis of peptide **A-5** was conducted via fragment coupling according to GP1 and GP4. First, the Fmoc protective group was removed from **2** (37.5  $\mu$ mol, 1.00 eq.) (GP4). Afterwards, a

solution containing **3** (98.2 mg, 64.6  $\mu$ mol, 1.72 eq.), TBTU (24.1 mg, 75.0  $\mu$ mol, 2.00 eq.), HOBT (10.1 mg, 75.0  $\mu$ mol, 2.00 eq.) and DIPEA (28.7  $\mu$ L, 169  $\mu$ mol, 4.50 eq.) in DMF was added and incubated for 15 h at room temperature. Examination of the reaction progress (GP7) revealed successful coupling of **3**. Removal of the *N*-terminal Fmoc protective group (GP4), followed by cleavage of the peptide from the resin with TFA/TIPS/H<sub>2</sub>O (95/2.5/2.5, 1  $\times$  30 min, slightly modified to GP9) resulted in 5.40 mg (8.24%) of product **A-5**\*2 TFA as a colorless powder after RP-HPLC purification (35 - 50% B in 20 min, Method B, 5 mL/min) and lyophilization.

RP-HPLC (10 - 90% B in 15 min, Method A, 1 mL/min):  $t_R$  = 10.6 min;  $k$  = 6.1. Calculated monoisotopic mass (C<sub>70</sub>H<sub>99</sub>F<sub>2</sub>N<sub>15</sub>O<sub>19</sub>Si): 1519.70, found:  $m/z$  = 761.4 [M(**A-5**)+2H]<sup>2+</sup>, 1520.9 [M(**A-5**)+H]<sup>+</sup>.

### *H-L-His-Aib-L-Glu-Gly-L-Thr-L-( $\alpha$ -Me)Phe-L-Thr-L-Ser-L-Asp-OH* (**A-6**)



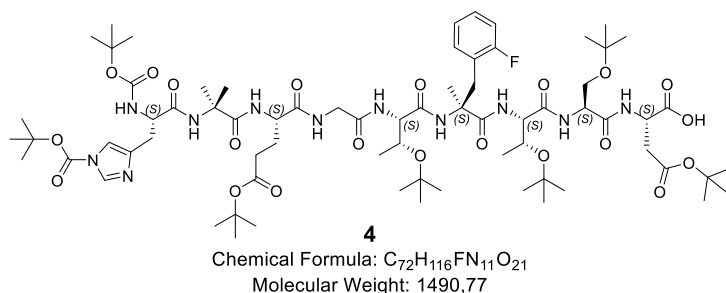
A small portion of hydrophobic nonapeptide **1** (not weighed) was partitioned by salt-induced precipitation in H<sub>2</sub>O and the lyophilized crude product was incubated with 1.10 mL TFA/TIPS (91/9) for 30 min. TFA was removed

under a stream of nitrogen prior to addition of 3.00 mL 20% piperidine in DMF (v/v). After an incubation period of 20 min, crude product **A-6** was precipitated in Et<sub>2</sub>O and centrifuged (5300 rpm, ca. 3100  $\times$  g, 4 min, 20  $^{\circ}$ C). Purification by RP-HPLC (10 - 20% B in 20 min, Method B, 5 mL/min) afforded 7.60 mg of product **A-6**\*2 TFA as a colorless powder.

RP-HPLC (10 - 90% B in 15 min, Method A, 1 mL/min):  $t_R$  = 4.25 min;  $k$  = 1.8. Calculated monoisotopic mass (C<sub>42</sub>H<sub>61</sub>N<sub>11</sub>O<sub>17</sub>): 991.42, found:  $m/z$  = 496.9 [M(**A-6**)+2H]<sup>2+</sup>, 992.4 [M(**A-6**)+H]<sup>+</sup>.

## MATERIALS AND METHODS

### *Boc-L-His(Boc)-Aib-L-Glu(OtBu)-Gly-L-Thr(tBu)-L-( $\alpha$ -Me)-(2-F)-Phe-L-Thr(tBu)-L-Ser(tBu)-L-Asp(OtBu)-OH (4)*

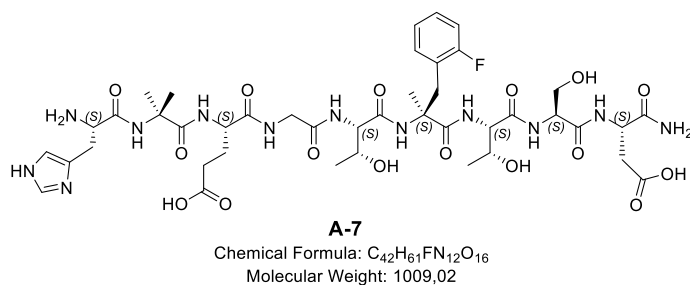


Nonapeptide **4** was synthesized on 2-CT resin according to GP2, GP3 and GP4 (load: 1.05 mmol/g, 1.73 mmol, 1.00 eq.). The peptide was cleaved off the resin according to GP10. This afforded 2.72 g of crude product **4** as a slightly yellow solid,

which was used in subsequent steps without further purification.

RP-HPLC (10 - 90% B in 15 min, Method A, 1 mL/min):  $t_R$  = 19.7 min;  $k$  = 12. Calculated monoisotopic mass (C<sub>72</sub>H<sub>116</sub>FN<sub>11</sub>O<sub>21</sub>): 1489.83, found:  $m/z$  = 1391.0 [M(**4**)-Boc+H]<sup>+</sup>, 1491.1 [M(**4**)+H]<sup>+</sup>.

### *H-L-His-Aib-L-Glu-Gly-L-Thr-L-( $\alpha$ -Me)-(2-F)-Phe-L-Thr-L-Ser-L-Asp-NH<sub>2</sub> (A-7)*

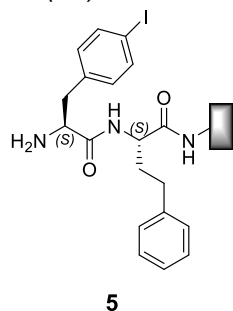


Crude product **4** (10.0 mg, ~ 6.71  $\mu$ mol, 1.00 eq.) was coupled to Rink amide ChemMatrix<sup>®</sup> resin according to GP1. After incubation for 2 h at room temperature, formation of the expected product was confirmed by RP-HPLC/MS

(GP7) and hence, the now amidated peptide was cleaved off by TFA/TIPS/H<sub>2</sub>O (GP9). TFA was removed under a stream of nitrogen, H<sub>2</sub>O was added to the crude product, frozen (-80 °C) and lyophilized. Purification by RP-HPLC (10 - 60% B in 15 min, Method B, 1 mL/min) afforded 0.40 mg (4.82%) of product **A-7**\*2 TFA as a colorless powder.

RP-HPLC (10 - 60% B in 15 min, Method A, 1 mL/min):  $t_R$  = 8.38 min;  $k$  = 4.6. Calculated monoisotopic mass (C<sub>42</sub>H<sub>61</sub>FN<sub>12</sub>O<sub>16</sub>): 1008.43, found:  $m/z$  = 505.5 [M(**A-7**)+2H]<sup>2+</sup>.

### *H-L-Phe(4-I)-L-homoPhe-RACM (5)*



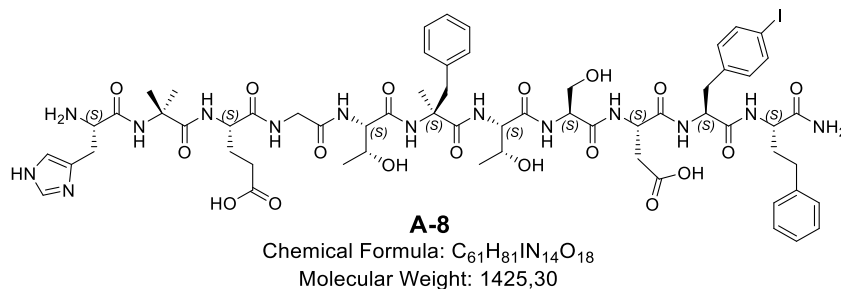
Chemical Formula: C<sub>19</sub>H<sub>22</sub>IN<sub>3</sub>O<sub>2</sub>  
Molecular Weight: 451,31

Dipeptide **5** was synthesized on Rink amide ChemMatrix<sup>®</sup> resin according to GP1 and GP4 (load: 0.50 mmol/g, 0.30 mmol, 1.00 eq.). After coupling of Fmoc-L-Phe(4-I)-OH (GP1) and removal of the N-terminal Fmoc protective group, formation of the expected product was confirmed by RP-HPLC/MS analysis (GP7), which revealed nearly complete conversion to product **5**.

RP-HPLC (40 - 100% B in 15 min, Method A, 1 mL/min):  $t_R$  = 4.76 min;  $k$  = 2.2. Calculated monoisotopic mass (C<sub>19</sub>H<sub>22</sub>IN<sub>3</sub>O<sub>2</sub>): 451.08, found:  $m/z$  = 452.4 [M(**5**)+H]<sup>+</sup>.

## MATERIALS AND METHODS

### *H-L-His-Aib-L-Glu-Gly-L-Thr-L-( $\alpha$ -Me)Phe-L-Thr-L-Ser-L-Asp-L-Phe(4-I)-L-homoPhe-NH<sub>2</sub> (A-8)*

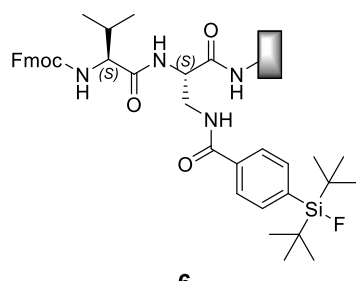


Synthesis of peptide **A-8** was conducted via fragment coupling according to GP1. A solution containing **1** (617 mg, 0.35 mmol, 1.18 eq.), TBTU (193 mg,

0.60 mmol, 2.00 eq.), HOBt (81.1 mg, 0.60 mmol, 2.00 eq.) and DIPEA (230  $\mu$ L, 1.35 mmol, 4.50 eq.) in DMF was added to C-terminal dipeptide **5** (0.30 mmol, 1.00 eq.) and incubated for 22 h at room temperature. Examination of the reaction progress (GP7) revealed successful coupling of **1**. Removal of the N-terminal Fmoc protective group (GP4), followed by cleavage of the peptide from the resin with TFA/TIPS/H<sub>2</sub>O (95/2.5/2.5, 1  $\times$  30 min, slightly modified to GP9) resulted in 4.47 mg (0.90%) of product **A-8**\*2 TFA as a colorless powder after RP-HPLC purification (35 - 38% B in 20 min, Method B, 5 mL/min) and lyophilization.

RP-HPLC (10 - 90% B in 15 min, Method A, 1 mL/min):  $t_R$  = 8.25 min;  $k$  = 4.5. Calculated monoisotopic mass (C<sub>61</sub>H<sub>81</sub>IN<sub>14</sub>O<sub>18</sub>): 1424.49, found:  $m/z$  = 713.5 [M(**A-8**)+2H]<sup>2+</sup>, 1425.8 [M(**A-8**)+H]<sup>+</sup>.

### *Fmoc-L-Val-L-Dap(SiFA)-RACM (6)*



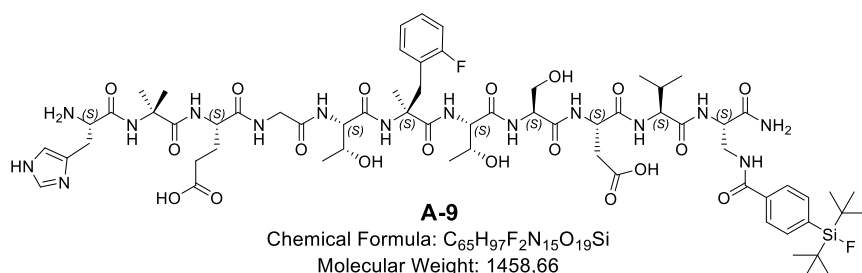
Chemical Formula: C<sub>38</sub>H<sub>49</sub>FN<sub>4</sub>O<sub>5</sub>Si  
Molecular Weight: 688,92

Dipeptide **6** was synthesized on Rink amide ChemMatrix<sup>®</sup> resin according to GP1, GP4 and GP6 (load: 0.50 mmol/g, 51.0  $\mu$ mol, 1.00 eq.). After coupling of Fmoc-L-Val-OH, formation of the expected product was confirmed by RP-HPLC/MS analysis (GP7), which revealed nearly complete conversion to product **6**.

RP-HPLC (40 - 100% B in 15 min, Method A, 1 mL/min):  $t_R$  = 16.7 min;  $k$  = 10. Calculated monoisotopic mass (C<sub>38</sub>H<sub>49</sub>FN<sub>4</sub>O<sub>5</sub>Si): 688.35, found:  $m/z$  = 689.3 [M(**6**)+H]<sup>+</sup>.

## MATERIALS AND METHODS

### *H*-L-His-Aib-L-Glu-Gly-L-Thr-L-( $\alpha$ -Me)-(2-F)-Phe-L-Thr-L-Ser-L-Asp-L-Val-L-Dap(SiFA)-NH<sub>2</sub> (**A-9**)

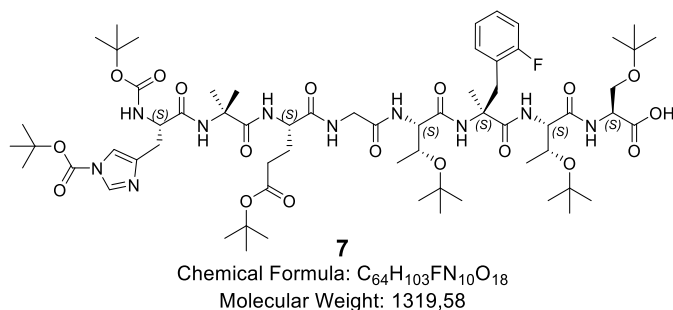


Synthesis of peptide **A-9** was conducted via fragment coupling according to GP1 and GP4. First, the Fmoc protective group was

removed from **6** (25.5  $\mu$ mol, 1.00 eq.) (GP4). Afterwards, a solution containing **3** (40.3 mg, 23.0  $\mu$ mol, 0.90 eq.), TBTU (16.4 mg, 51.0  $\mu$ mol, 2.00 eq.), HOBt (6.89 mg, 51.0  $\mu$ mol, 2.00 eq.) and DIPEA (19.6  $\mu$ L, 115  $\mu$ mol, 4.50 eq.) in DMF was added and incubated for 24 h at room temperature. Examination of the reaction progress (GP7) revealed successful coupling of **3**. Removal of the *N*-terminal Fmoc protective group (GP4), followed by cleavage of the peptide from the resin with TFA/TIPS/H<sub>2</sub>O (95/2.5/2.5, 1  $\times$  30 min, slightly modified to GP9) resulted in 8.40 mg (21.7%) of product **A-9**\*2 TFA as a colorless powder after RP-HPLC purification (30 - 80% B in 20 min, Method B, 5 mL/min) and lyophilization.

RP-HPLC (10 - 90% B in 15 min, Method A, 1 mL/min):  $t_R$  = 9.59 min;  $k$  = 5.4. Calculated monoisotopic mass (C<sub>65</sub>H<sub>97</sub>F<sub>2</sub>N<sub>15</sub>O<sub>19</sub>Si): 1457.68, found:  $m/z$  = 730.2 [M(**A-9**)+2H]<sup>2+</sup>, 1458.9 [M(**A-9**)+H]<sup>+</sup>.

### *Boc*-L-His(*Boc*)-Aib-L-Glu(*OtBu*)-Gly-L-Thr(*tBu*)-L-( $\alpha$ -Me)-(2-F)-Phe-L-Thr(*tBu*)-L-Ser(*tBu*)-OH (**7**)



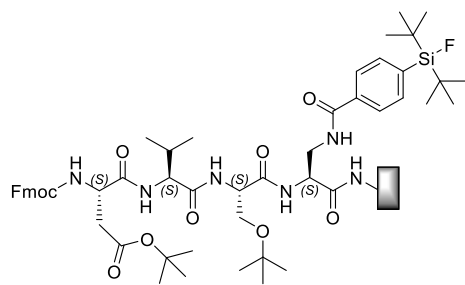
Octapeptide **7** was synthesized on 2-CT resin according to GP2, GP3 and GP4 (load: 1.31 mmol/g, 0.99 mmol, 1.00 eq.). The peptide was cleaved off the resin according to GP10. This afforded 531 mg of crude product **7** as a slightly yellow solid, which was used in subsequent

steps without further purification.

RP-HPLC (20 - 80% B in 15 min, Method A, 1 mL/min):  $t_R$  = 18.6 min;  $k$  = 11. Calculated monoisotopic mass (C<sub>64</sub>H<sub>103</sub>FN<sub>10</sub>O<sub>18</sub>): 1318.74, found:  $m/z$  = 1219.3 [M(**7**)-Boc+H]<sup>+</sup>, 1319.5 [M(**7**)+H]<sup>+</sup>.

## MATERIALS AND METHODS

### *Fmoc-L-Asp(OtBu)-L-Val-L-Ser(tBu)-L-Dap(SiFA)-RACM (8)*



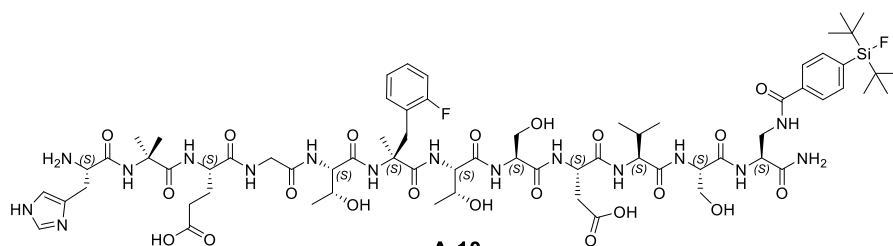
**8**

Chemical Formula:  $C_{53}H_{75}FN_6O_{10}Si$   
Molecular Weight: 1003,30

Tetrapeptide **8** was synthesized on Rink amide ChemMatrix® resin according to GP1, GP4 and GP6 (load: 0.50 mmol/g, 24.7  $\mu$ mol, 1.00 eq.). After coupling of Fmoc-L-Asp(OtBu)-OH, formation of the expected product was confirmed by RP-HPLC/MS analysis (GP7), which revealed nearly complete conversion to product **8** and an unidentifiable by-product at 12.2 min ( $m/z = 323.1$ ).

RP-HPLC (40 - 100% B in 15 min, Method A, 1 mL/min) for **8(-2tBu)**:  $t_R = 12.7$  min;  $k = 7.5$ . Calculated monoisotopic mass for **8(-2tBu)** ( $C_{45}H_{59}FN_6O_{10}Si$ ): 890.40, found:  $m/z = 891.0$  [ $M(\mathbf{8})-2tBu+H$ ]<sup>+</sup>.

### *H-L-His-Aib-L-Glu-Gly-L-Thr-L-( $\alpha$ -Me)-(2-F)-Phe-L-Thr-L-Ser-L-Asp-L-Val-L-Ser-L-Dap(SiFA)-NH<sub>2</sub> (A-10)*



**A-10**

Chemical Formula:  $C_{68}H_{102}F_2N_{16}O_{21}Si$   
Molecular Weight: 1545,74

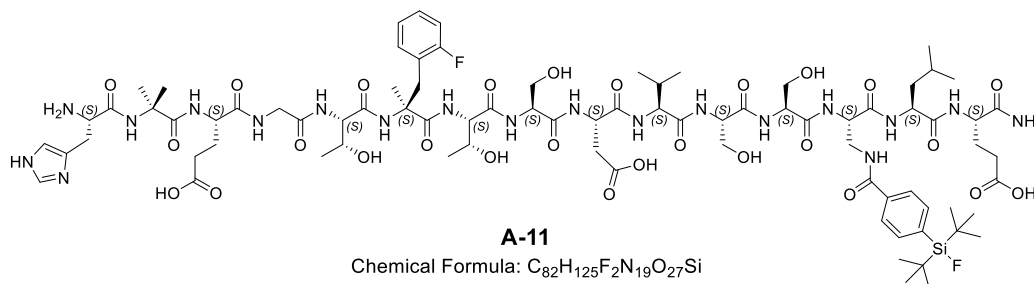
Synthesis of peptide **A-10** was conducted via fragment coupling according to GP1 and GP4. First, the Fmoc protective group was removed from **8**

(24.7  $\mu$ mol, 1.00 eq.) (GP4). Afterwards, a solution containing **7** (97.7 mg, 74.0  $\mu$ mol, 3.00 eq.), TBTU (34.4 mg, 107  $\mu$ mol, 4.34 eq.), HOBt (15.0 mg, 111  $\mu$ mol, 4.49 eq.) and DIPEA (56.6  $\mu$ L, 333  $\mu$ mol, 13.5 eq.) in DMF was added and incubated for 18.5 h at room temperature. Examination of the reaction progress (GP7) revealed successful coupling of **7**. Cleavage of the peptide from the resin with TFA/TIPS/H<sub>2</sub>O (95/2.5/2.5, 1  $\times$  30 min, slightly modified to GP9) resulted in 4.40 mg (10.7%) of product **A-10**\*2 TFA as a colorless powder after RP-HPLC purification (42 - 45% B in 20 min, Method B, 5 mL/min) and lyophilization. Chemical purity only reached 68% for this peptide, due to an unidentifiable and hardly separable by-product ( $m/z = 277.4$ , 352.0 & 392.7) at 7.99 min which covered  $\sim$  30% of the total peak area. Since only one major by-product occurred, affinity studies were performed yet for a first assessment of the IC<sub>50</sub> and to determine whether a second purification step would be reasonable.

RP-HPLC (30 - 70% B in 15 min, Method A, 1 mL/min):  $t_R = 7.71$  min;  $k = 4.1$ . Calculated monoisotopic mass ( $C_{68}H_{102}F_2N_{16}O_{21}Si$ ): 1544.71, found:  $m/z = 773.9$  [ $M(\mathbf{A-10})+2H$ ]<sup>2+</sup>.

## MATERIALS AND METHODS

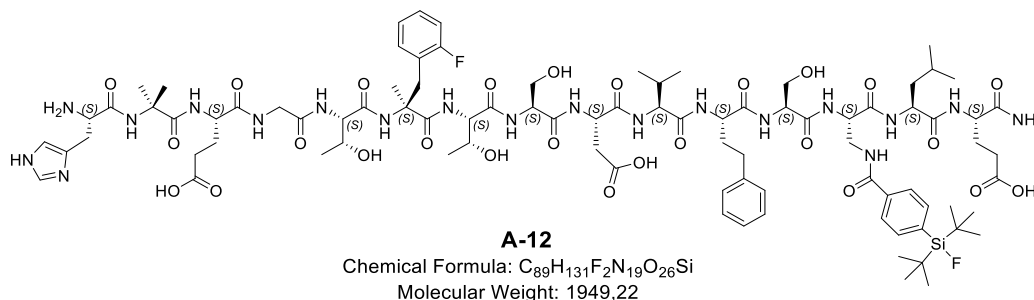
### *H-L-His-Aib-L-Glu-Gly-L-Thr-L-( $\alpha$ -Me)-(2-F)-Phe-L-Thr-L-Ser-L-Asp-L-Val-L-Ser-L-Ser-L-Dap(SiFA)-L-Leu-L-Glu-NH<sub>2</sub> (A-11)*



Preparation of pentadecapeptide **A-11** was conducted via linear synthesis on Rink amide ChemMatrix<sup>®</sup> resin according to GP1, GP4 and GP6 (load: 0.50 mmol/g, 0.13 mmol, 1.00 eq.). After coupling of Boc-L-His(Boc)-OH, formation of the expected product was confirmed by RP-HPLC/MS analysis (GP7). Cleavage of the peptide from the resin with TFA/TIPS/DCM (GP9) resulted in 22.2 mg (8.12%) of pure product **A-11**\*2 TFA as a colorless powder after RP-HPLC purification (40 - 70% B in 20 min, Method B, 5 mL/min) and lyophilization.

RP-HPLC (10 - 90% B in 15 min, Method A, 1 mL/min):  $t_R = 10.2$  min;  $k = 5.8$ . Calculated monoisotopic mass (C<sub>82</sub>H<sub>125</sub>F<sub>2</sub>N<sub>19</sub>O<sub>27</sub>Si): 1873.87, found:  $m/z = 937.8$  [M(**A-11**)+2H]<sup>2+</sup>, 1250.4 [M<sub>2</sub>(**A-11**)+3H]<sup>3+</sup>, 1875.2 [M(**A-11**)+H]<sup>+</sup>.

### *H-L-His-Aib-L-Glu-Gly-L-Thr-L-( $\alpha$ -Me)-(2-F)-Phe-L-Thr-L-Ser-L-Asp-L-Val-L-homoPhe-L-Ser-L-Dap(SiFA)-L-Leu-L-Glu-NH<sub>2</sub> (A-12)*

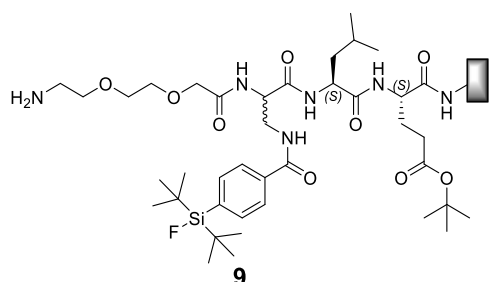


Preparation of pentadecapeptide **A-12** was conducted via linear synthesis on Rink amide ChemMatrix<sup>®</sup> resin according to GP1, GP4 and GP6 (load: 0.50 mmol/g, 0.13 mmol, 1.00 eq.). After coupling of Boc-L-His(Boc)-OH, formation of the expected product was confirmed by RP-HPLC/MS analysis (GP7). Cleavage of the peptide from the resin with TFA/TIPS/DCM (GP9) resulted in 17.2 mg (6.08%) of pure product **A-12**\*2 TFA as a colorless powder after RP-HPLC purification (40 - 70% B in 20 min, Method B, 5 mL/min) and lyophilization.

RP-HPLC (10 - 90% B in 15 min, Method A, 1 mL/min):  $t_R = 11.9$  min;  $k = 6.9$ . Calculated monoisotopic mass (C<sub>89</sub>H<sub>131</sub>F<sub>2</sub>N<sub>19</sub>O<sub>26</sub>Si): 1947.92, found:  $m/z = 974.7$  [M(**A-12**)+2H]<sup>2+</sup>, 1299.6 [M<sub>2</sub>(**A-12**)+3H]<sup>3+</sup>, 1949.1 [M(**A-12**)+H]<sup>+</sup>.

## MATERIALS AND METHODS

### *H*-O<sub>2</sub>C-*L*/*D*-Dap(SiFA)-*L*-Leu-*L*-Glu(OtBu)-RACM (**9**)

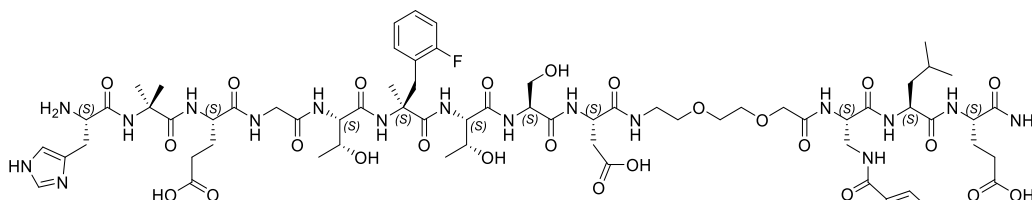


Chemical Formula: C<sub>39</sub>H<sub>67</sub>FN<sub>6</sub>O<sub>9</sub>Si  
Molecular Weight: 811,08

Peptide **9** was synthesized on Rink amide ChemMatrix<sup>®</sup> resin according to GP1, GP4 and GP6 (load: 0.50 mmol/g, 0.13 mmol, 1.00 eq.). After coupling of 8-(9-Fmoc)amino-3,6-dioxaoctanoic acid and removal of the *N*-terminal Fmoc protective group, the expected product was confirmed by RP-HPLC/MS analysis (GP7), which revealed nearly complete conversion to product **9**.

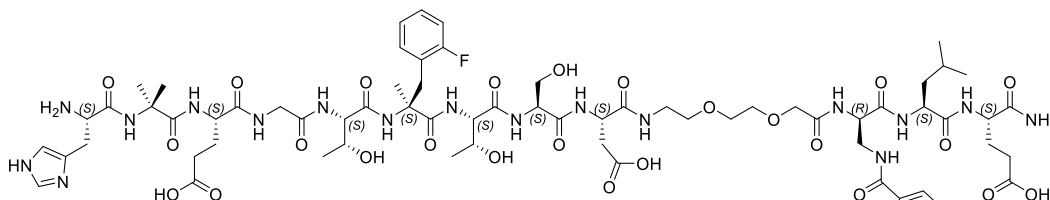
RP-HPLC (10 - 90% B in 15 min, Method A, 1 mL/min) for **9(-tBu)**: *t<sub>R</sub>* = 15.5 min; *k* = 9.3. Calculated monoisotopic mass for **9(-tBu)** (C<sub>35</sub>H<sub>59</sub>FN<sub>6</sub>O<sub>9</sub>Si): 754.41, found: *m/z* = 797.6 [M(**9**)-tBu+MeCN+H]<sup>+</sup>, 1595.4 [M<sub>2</sub>(**9**-tBu+MeCN)+H]<sup>+</sup>.

### *H*-*L*-His-*Aib*-*L*-Glu-*Gly*-*L*-Thr-*L*-(*α*-Me)-(2-*F*)-*Phe*-*L*-Thr-*L*-Ser-*L*-Asp-O<sub>2</sub>C-*L*/*D*-Dap(SiFA)-*L*-Leu-*L*-Glu-NH<sub>2</sub> (**A-13/A-14**)



**A-13**

Chemical Formula: C<sub>77</sub>H<sub>117</sub>F<sub>2</sub>N<sub>17</sub>O<sub>25</sub>Si  
Molecular Weight: 1746,96



**A-14**

Chemical Formula: C<sub>77</sub>H<sub>117</sub>F<sub>2</sub>N<sub>17</sub>O<sub>25</sub>Si  
Molecular Weight: 1746,96

Synthesis of peptides **A-13** and **A-14** was conducted via fragment coupling of the *N*-terminal fragment **4** with the resin-bound *C*-terminal peptide **9** according to GP1. A solution containing **4** (99.3 mg, 66.7 μmol, 1.00 eq.), TBTU (32.1 mg, 66.7 μmol, 1.00 eq.), HOAt (13.6 mg, 66.7 μmol, 1.00 eq.) and DIPEA (51.0 μL, 300 μmol, 4.50 eq.) in DMF was added and incubated for 3 h at room temperature. Examination of the reaction progress (GP7) revealed only very low conversion, hence **4** and all further reagents were again weighed, added and coupling was conducted for 29 h. After this period RP-HPLC/MS analysis (GP7) revealed sufficient conversion. Cleavage of the peptide from one half of the resin was conducted with pure TFA (1 × 30 min, slightly modified to GP9). Purification by RP-HPLC (40 - 90% B in 30 min, Method B, 5 mL/min and 80 - 100% B in 15 min, Method B, 1 mL/min) and lyophilization resulted in 1.41 mg (2.14%) of pure product **A-13**\*2 TFA and 2.38 mg (3.62%) of pure product **A-14**\*2 TFA, both as colorless powder.

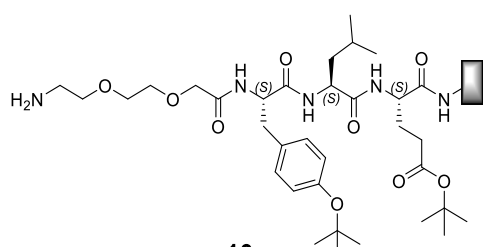
## MATERIALS AND METHODS

Racemization occurred during the coupling of Fmoc-L-Dap(Dde)-OH for synthesis of **9** and led to an enantiomeric ratio (*er*) of ~ 3/7 for **A-13/A-14**. The identity of the respective enantiomers was determined retrospectively by IC<sub>50</sub> studies of **A-13** and **A-14**.

**A-13**: RP-HPLC (80 - 100% B in 15 min, Method B, 1 mL/min):  $t_R = 6.81$  min;  $k = 3.5$ . Calculated monoisotopic mass (C<sub>77</sub>H<sub>117</sub>F<sub>2</sub>N<sub>17</sub>O<sub>25</sub>Si): 1745.81, found:  $m/z = 875.1$  [M(**A-13**)+2H]<sup>2+</sup>, 1747.8 [M(**A-13**)+H]<sup>+</sup>.

**A-14**: RP-HPLC (80 - 100% B in 15 min, Method B, 1 mL/min):  $t_R = 9.39$  min;  $k = 5.3$ . Calculated monoisotopic mass (C<sub>77</sub>H<sub>117</sub>F<sub>2</sub>N<sub>17</sub>O<sub>25</sub>Si): 1745.81, found:  $m/z = 874.6$  [M(**A-14**)+2H]<sup>2+</sup>, 1748.7 [M(**A-14**)+H]<sup>+</sup>.

### *H*-O<sub>2</sub>C-L-Tyr(*t*Bu)-L-Leu-L-Glu(*Ot*Bu)-RACM (**10**)



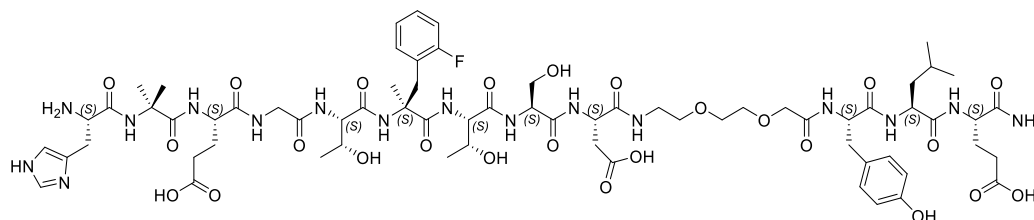
**10**  
Chemical Formula: C<sub>34</sub>H<sub>57</sub>N<sub>5</sub>O<sub>9</sub>  
Molecular Weight: 679,86

Peptide **10** was synthesized on Rink amide ChemMatrix<sup>®</sup> resin according to GP1 and GP4, starting from Fmoc-L-Glu(*Ot*Bu)-RACM (load: 0.50 mmol/g, 0.27 mmol, 1.00 eq.). After coupling of 8-(9-Fmoc)amino-3,6-dioxaoctanoic acid and removal of the *N*-terminal Fmoc protective group, formation of the expected product was confirmed by RP-HPLC/MS analysis (GP7),

which revealed nearly complete conversion to product **10**.

RP-HPLC (20 - 80% B in 15 min, Method A, 1 mL/min) for **10(-2*t*Bu)**:  $t_R = 7.05$  min;  $k = 3.7$ . Calculated monoisotopic mass for **10(-2*t*Bu)** (C<sub>26</sub>H<sub>41</sub>N<sub>5</sub>O<sub>9</sub>): 567.29, found:  $m/z = 568.3$  [M(**10**)-2*t*Bu+H]<sup>+</sup>.

### *H*-L-His-Aib-L-Glu-Gly-L-Thr-L-( $\alpha$ -Me)-(2-F)-Phe-L-Thr-L-Ser-L-Asp-O<sub>2</sub>C-L-Tyr-L-Leu-L-Glu-NH<sub>2</sub> (**A-15**)



**A-15**  
Chemical Formula: C<sub>68</sub>H<sub>99</sub>FN<sub>16</sub>O<sub>25</sub>  
Molecular Weight: 1559,63

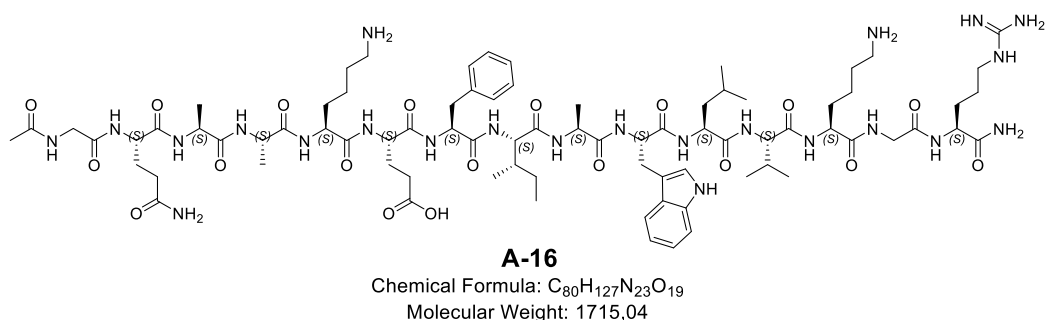
Synthesis of peptide **A-15** was conducted via fragment coupling of the *N*-terminal fragment **4** with the resin-bound *C*-terminal tetrapeptide according to GP1. A solution containing **4** (10.0 mg, 6.71  $\mu$ mol, 1.00 eq.), TBTU (4.30 mg, 13.4  $\mu$ mol, 2.00 eq.), HOAt (1.82 mg, 13.4  $\mu$ mol, 2.00 eq.) and DIPEA (41.1  $\mu$ L, 242  $\mu$ mol, 36.0 eq.) in DMF was added to **10** (6.71  $\mu$ mol, 1.00 eq.) and incubated for 18 h at room temperature. Examination of the reaction progress (GP7) revealed successful coupling of **4**. Cleavage of the peptide from the resin with TFA/TIPS/H<sub>2</sub>O (95/2.5/2.5,

## MATERIALS AND METHODS

1 × 30 min, slightly modified to GP9) resulted in 0.44 mg (3.92%) of product **A-15**\*2 TFA as a colorless powder after RP-HPLC purification (20 - 60% B in 15 min, Method B, 1 mL/min) and lyophilization. Chemical purity only reached 75.0% for this peptide, due to several unidentifiable by-products at 7.52, 9.02 and 9.94 min which covered ~ 25% of the total integrated area. In addition, two product peaks (identical *m/z*-ratio at 8.62 min (38%) and 8.76 min (62%)) occurred. Since no Fmoc-L-Dap(Dde)-OH was coupled for synthesis of **10**, it was assumed that no racemization but rather different protonation states or conformations of the peptide caused peak splitting. Hence, affinity studies were performed yet for a first assessment of the IC<sub>50</sub> and to determine whether a second purification step would be reasonable.

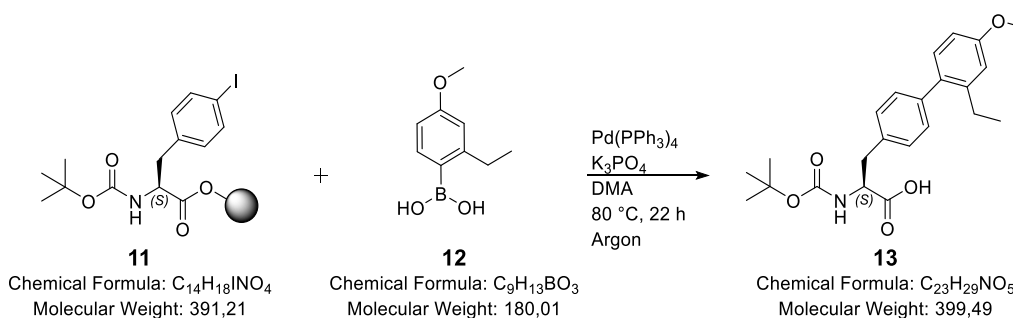
RP-HPLC (20 - 60% B in 15 min, Method B, 1 mL/min): *t<sub>R</sub>* = 8.76 min; *k* = 4.8. Calculated monoisotopic mass (C<sub>68</sub>H<sub>99</sub>FN<sub>16</sub>O<sub>25</sub>): 1558.70, found: *m/z* = 780.6 [M(**A-15**)+2H]<sup>2+</sup>, 1040.4 [M<sub>2</sub>(**A-15**)+3H]<sup>3+</sup>, 1559.8 [M(**A-15**)+H]<sup>+</sup>.

*Acetyl-Gly-L-Gln-L-Ala-L-Ala-L-Lys-L-Glu-L-Phe-L-Ile-L-Ala-L-Trp-L-Leu-L-Val-L-Lys-Gly-L-Arg-NH<sub>2</sub>*  
**(A-16)**



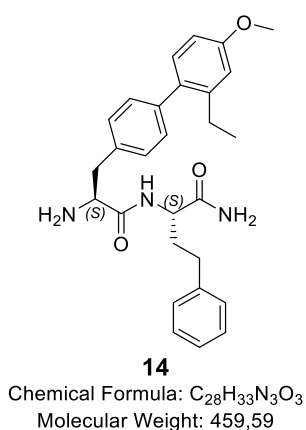
Preparation of pentadecapeptide **A-16** was conducted via linear synthesis on Rink amide ChemMatrix<sup>®</sup> resin according to GP1 and GP4 (load: 0.50 mmol/g, 93.3 μmol, 1.00 eq.). After coupling of Ac-Gly-OH, formation of the expected product was confirmed by RP-HPLC/MS analysis (GP7). Cleavage of the peptide from the resin with TFA/TIPS/H<sub>2</sub>O (95/2.5/2.5, 1 × 30 min, slightly modified to GP9) resulted in 10.2 mg (5.32%) of pure product **A-16**\*3 TFA as a colorless powder after RP-HPLC purification (40 - 55% B in 20 min, Method B, 10 mL/min) and lyophilization.

RP-HPLC (10 - 90% B in 15 min, Method A, 1 mL/min): *t<sub>R</sub>* = 11.2 min; *k* = 6.5. Calculated monoisotopic mass (C<sub>80</sub>H<sub>127</sub>N<sub>23</sub>O<sub>19</sub>): 1713.97, found: *m/z* = 573.1 [M<sub>3</sub>(**A-16**)+9H]<sup>9+</sup>, 858.6 [M(**A-16**)+2H]<sup>2+</sup>, 1144.0 [M<sub>2</sub>(**A-16**)+3H]<sup>3+</sup>, 1716.0 [M(**A-16**)+H]<sup>+</sup>.

**Boc-L-(2'-Et, 4'-OMe)BIP-L-homoPhe-NH<sub>2</sub> (13)**


Compound **13** was synthesized in analogy to a previously published procedure by Haque *et al.*<sup>[114]</sup> with some minor modifications. Resin-bound Boc-L-Phe(4-I)-2-CT (**11**) (load: 0.92 mmol/g, 0.56 mmol, 1.00 eq.) was transferred to a round-bottom flask. Boronic acid **12** (400 mg, 2.22 mmol, 4.00 eq.) dissolved in 4.77 mL DMA, Pd(PPh<sub>3</sub>)<sub>4</sub> (64.7 mg, 56.0 μmol, 0.10 eq.) dissolved in 1.60 mL DMA (6.37 mL DMA in total) and 2.24 mL of an aqueous 2 M K<sub>3</sub>PO<sub>4</sub> solution (4.48 mmol, 8.00 eq.) were added to the resin. The yellow-orange solution was heated to 80 °C and stirred under argon for 22 h. Afterwards, the resin was transferred to a syringe equipped with a frit, pore size 25 μm) and washed once with DMF. This fraction was kept together with the reaction solution. The resin was washed alternating with 10 mL of 0.5% (w/v) DDTC in DMF (3×) and 10 mL of 0.5% (v/v) DIPEA in DMF (3×) to remove palladium catalyst and other cross-coupling reagents from the resin. After final washing steps with DMF (3×) and DCM (3×) formation of product **13** could be confirmed on the resin by RP-HPLC/MS analysis (GP7). Besides, the major part of product **13** was found in the reaction solution. Therefore, it was either directly purified by flash chromatography (20 - 80% B in 10 min, Method D, 12 mL/min) or by preparative RP-HPLC (20 - 80% B in 20 min, Method B, 5 mL/min) after incubation of the resin with HFIP/DCM (GP11). In this case, the latter yielded 1.36 mg (0.61%) of purified product **13** as a brown-orange viscous oil.

RP-HPLC (20 - 80% B in 15 min, Method A, 1 mL/min):  $t_R = 17.7$  min;  $k = 11$ . Calculated monoisotopic mass (C<sub>23</sub>H<sub>29</sub>NO<sub>5</sub>): 399.20, found:  $m/z = 300.2$  [M(**13**)-Boc+H]<sup>+</sup>, 341.2 [M(**13**)-Boc+MeCN+H]<sup>+</sup>, 344.2 [M(**13**)-tBu+H]<sup>+</sup>, 385.2 [M(**13**)-tBu+MeCN]<sup>+</sup>.

**H-L-(2'-Et, 4'-OMe)BIP-L-homoPhe-NH<sub>2</sub> (14)**


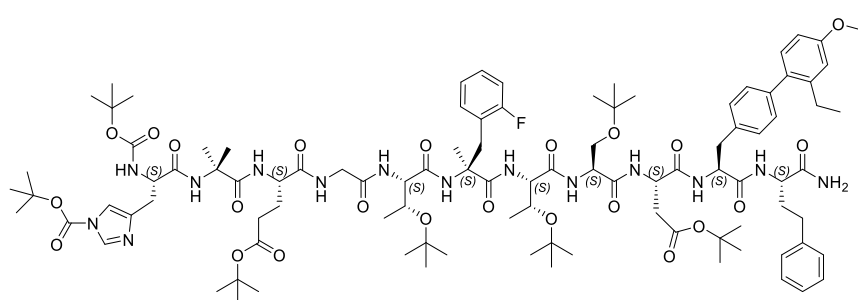
Compound **14** was synthesized in analogy to a previously published procedure by Haque *et al.*<sup>[113]</sup> with some minor modifications. Resin-bound H-L-homoPhe-RACM (load: 0.39 mmol/g, 56.4 μmol, 1.00 eq.) was swelled in NMP for 15 min. Meanwhile, **13** (28.9 mg, 73.3 μmol, 1.30 eq.) was dissolved in 3 mL DMF/DCM (2/1) and added to PyBOP (38.1 mg, 73.3 μmol, 1.30 eq.) and HOAt (10.0 mg, 73.3 μmol 1.30 eq.). DIPEA (72.3 μL, 0.43 mmol, 7.54 eq.) was added and the reaction mixture was incubated with H-L-homoPhe-RACM for 24 h. Examination of the reaction progress (GP7) revealed successful

## MATERIALS AND METHODS

conversion to product **14**, which led to cleavage of the dipeptide from the resin with TFA/TIPS/H<sub>2</sub>O (95/2.5/2.5, 1 × 30 min, slightly modified to GP9). After removal of TFA under a stream of nitrogen, H<sub>2</sub>O was added to the crude product, frozen (-80 °C) and lyophilized. Purification by RP-HPLC (30 - 90% B in 20 min, Method B, 5 mL/min) afforded 2.94 mg (9.09%) of product **14**\*TFA as a colorless powder.

RP-HPLC (40 - 100% B in 15 min, Method A, 1 mL/min):  $t_R = 8.27$  min;  $k = 4.5$ . Calculated monoisotopic mass (C<sub>28</sub>H<sub>33</sub>N<sub>3</sub>O<sub>3</sub>): 459.25, found:  $m/z = 460.4$  [M(**14**)+H]<sup>+</sup>, 482.4 [M(**14**)+Na]<sup>+</sup>, 498.4 [M(**14**)+K]<sup>+</sup>.

*Boc-L-His(Boc)-Aib-L-Glu(OtBu)-Gly-L-Thr(tBu)-L-( $\alpha$ -Me)-(2-F)-Phe-L-Thr(tBu)-L-Ser(tBu)-L-Asp(OtBu)-L-(2'-Et, 4'-OMe)BIP-L-homoPhe-NH<sub>2</sub> (**15**)*



**15**

Chemical Formula: C<sub>100</sub>H<sub>147</sub>FN<sub>14</sub>O<sub>23</sub>  
Molecular Weight: 1932.35

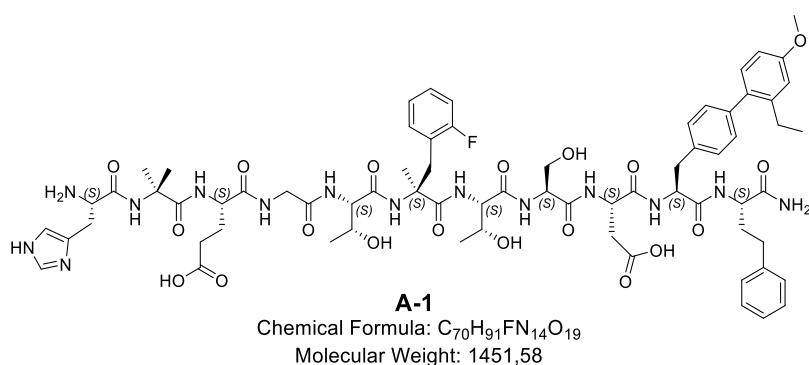
Compound **15** was synthesized in analogy to a previously published procedure by Haque *et al.*<sup>[113]</sup> with some minor modifications. First, the counterion TFA was removed from **14**

(1.42 mg, 2.48  $\mu$ mol, 1.00 eq.) by tetraalkylammonium carbonate (macroporous, polymer-bound, 18 - 50 mesh, average load = 3.00 mmol/g). Therefore, **14**\*TFA was dissolved in 300  $\mu$ L THF (supplemented with 0.5% DIPEA (v/v)), the anion exchange resin (2.48 mg, 7.43  $\mu$ mol, 3.00 eq.) was added and the mixture was stirred in a sealed glass vial for 2 h at room temperature. The reaction solution was separated from the resin and the solvent was removed *in vacuo*. Nonapeptide **4** (3.69 mg, 2.48  $\mu$ mol, 1.00 eq.), HOAt (0.67 mg, 4.95  $\mu$ mol, 2.00 eq.) and DIC (3.07  $\mu$ L, 19.7  $\mu$ mol, 8.00 eq.) were dissolved in 510  $\mu$ L DCM/DMF (9/1) and added to **14**. If necessary, DIPEA was added to adjust the pH to 9 - 10 and the mixture was stirred for 16 h at room temperature. Purification by RP-HPLC (40 -100% B in 20 min, Method B, 5 mL/min) afforded pure product **15**. MeCN was removed *in vacuo*, residual solvents (H<sub>2</sub>O) were reduced but not completely removed for the next step.

RP-HPLC (40 - 100% B in 15 min, Method A, 1 mL/min):  $t_R = 28.7$  min;  $k = 18$ . Calculated monoisotopic mass (C<sub>100</sub>H<sub>147</sub>FN<sub>14</sub>O<sub>23</sub>): 1931.07, found:  $m/z = 967.0$  [M(**15**)+2H]<sup>2+</sup>, 1932.2 [M(**15**)+H]<sup>+</sup>, 1954.2 [M(**15**)+Na]<sup>+</sup>, 1970.4 [M(**15**)+K]<sup>+</sup>.

## MATERIALS AND METHODS

### *H*-L-His-Aib-L-Glu-Gly-L-Thr-L-( $\alpha$ -Me)-(2-F)-Phe-L-Thr-L-Ser-L-Asp-L-(2'-Et, 4'-OMe)BIP-L-homoPhe-NH<sub>2</sub> (**A-1**)

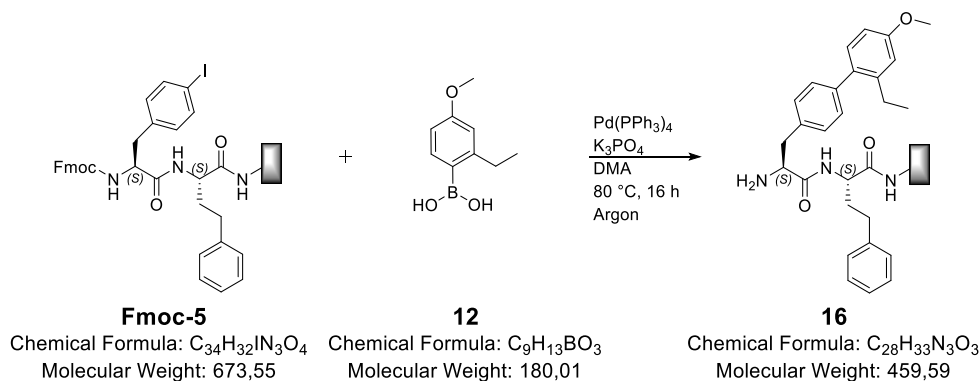


Peptide **15** in residual H<sub>2</sub>O was dissolved in 500  $\mu$ L TFA/TIPS/H<sub>2</sub>O (95/2.5/2.5) and stirred for 1 h at room temperature. TFA was removed under a stream of nitrogen, the crude product was frozen (-80 °C) and

lyophilized. Purification by preparative RP-HPLC (40 - 55% B in 20 min, Method B, 5 mL/min) afforded 2.05 mg (16.1% referred to **14**) of pure product **A-1**\*2TFA as colorless powder.

RP-HPLC (20 - 80% B in 15 min, Method A, 1 mL/min):  $t_R$  = 11.6 min;  $k$  = 6.7. Calculated monoisotopic mass (C<sub>70</sub>H<sub>91</sub>FN<sub>14</sub>O<sub>19</sub>): 1450.66, found:  $m/z$  = 726.7 [M(**A-1**)+2H]<sup>2+</sup>, 1452.1 [M(**A-1**)+H]<sup>+</sup>.

### *H*-L-(2'-Et, 4'-OMe)BIP-L-homoPhe-RACM (**16**)

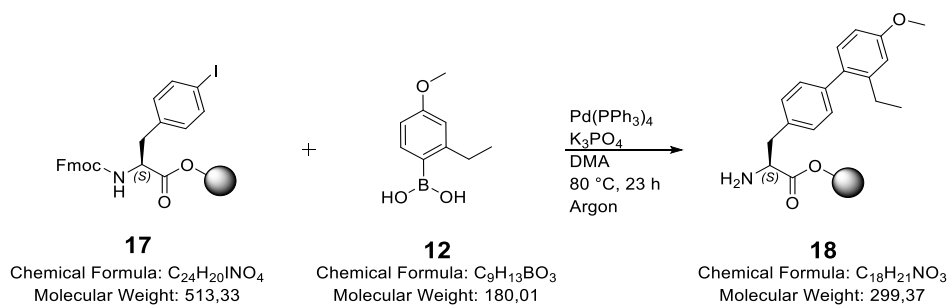


Compound **16** was synthesized in analogy to a previously published procedure by Haque *et al.*<sup>[114]</sup> with some minor modifications. Resin-bound Fmoc-L-Phe(4-I)-homoPhe-RACM (**Fmoc-5**) (load: 0.50 mmol/g, 14.0  $\mu$ mol, 1.00 eq.) was transferred to a round-bottom flask. Boronic acid **12** (10.1 mg, 56.0  $\mu$ mol, 4.00 eq.) dissolved in 120  $\mu$ L DMA, Pd(PPh<sub>3</sub>)<sub>4</sub> (1.62 mg, 1.40  $\mu$ mol, 0.10 eq.) dissolved in 40  $\mu$ L DMA (160  $\mu$ L DMA in total) and 56.0  $\mu$ L of an aqueous 2 M K<sub>3</sub>PO<sub>4</sub> solution (112  $\mu$ mol, 8.00 eq.) were added to the resin. The yellow-orange suspension was heated to 80 °C and stirred under argon for 16 h. Afterwards, the resin was transferred to a syringe equipped with a frit, pore size 25  $\mu$ m) and washed DMF (3 $\times$ ) and DCM (3 $\times$ ). Formation of product **16** on the resin could be confirmed by RP-HPLC/MS analysis (GP7).

RP-HPLC (10 - 90% B in 15 min, Method A, 1 mL/min):  $t_R$  = 13.6 min;  $k$  = 8.1. Calculated monoisotopic mass (C<sub>28</sub>H<sub>33</sub>N<sub>3</sub>O<sub>3</sub>): 459.25, found:  $m/z$  = 460.3 [M(**16**)+H]<sup>+</sup>.

## MATERIALS AND METHODS

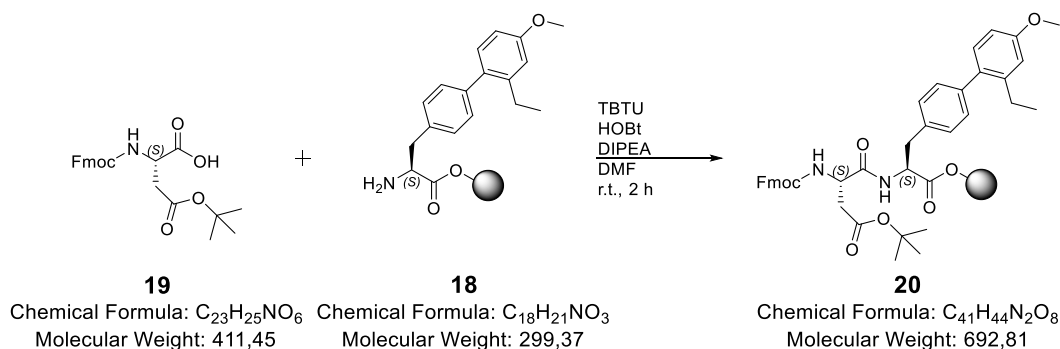
### *H*-L-(2'-Et, 4'-OMe)BIP-2-CT (**18**)



Compound **18** was synthesized in analogy to a previously published procedure by Haque *et al.*<sup>[114]</sup> with some minor modifications. Resin-bound Fmoc-L-Phe(4-I)-2-CT (**17**) (load: 0.50 mmol/g, 19.0  $\mu$ mol, 1.00 eq.) was transferred to a round-bottom flask. Boronic acid **12** (13.7 mg, 76.5  $\mu$ mol, 4.00 eq.) dissolved in 162  $\mu$ L DMA, Pd(PPh<sub>3</sub>)<sub>4</sub> (2.20 mg, 1.90  $\mu$ mol, 0.10 eq.) dissolved in 54  $\mu$ L DMA (217  $\mu$ L DMA in total) and 76.5  $\mu$ L of an aqueous 2 M K<sub>3</sub>PO<sub>4</sub> solution (153  $\mu$ mol, 8.00 eq.) were added to the resin. The yellow-orange suspension was heated to 80 °C and stirred under argon for 23 h. Afterwards, the resin was transferred to a syringe equipped with a frit, pore size 25  $\mu$ m) and washed alternating with 10 mL of 0.5% (w/v) DDTC in DMF (3 $\times$ ) and 10 mL of 0.5% (v/v) DIPEA in DMF (3 $\times$ ) to remove palladium catalyst and other cross-coupling reagents from the resin. After final washing steps with DMF (3 $\times$ ) and DCM (3 $\times$ ) formation of product **18** could be confirmed on the resin by RP-HPLC/MS analysis (GP7).

RP-HPLC (40 - 100% B in 15 min, Method A, 1 mL/min):  $t_R$  = 6.16 min;  $k$  = 3.1. Calculated monoisotopic mass (C<sub>18</sub>H<sub>21</sub>NO<sub>3</sub>): 299.15, found:  $m/z$  = 300.1 [M(**18**)+H]<sup>+</sup>, 341.1 [M(**18**)+MeCN+H]<sup>+</sup>.

### Fmoc-L-Asp(OtBu)-L-(2'-Et, 4'-OMe)BIP-2-CT (**20**)



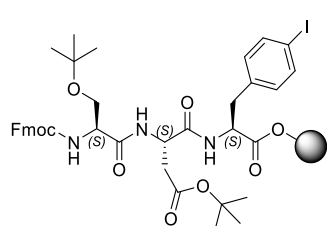
Dipeptide **20** was synthesized on 2-CT resin according to GP3, starting from *H*-L-(2'-Et, 4'-OMe)BIP-2-CT (**18**) (load: 0.50 mmol/g, 19.0  $\mu$ mol, 1.00 eq.). In brief, Fmoc-L-Asp(OtBu)-OH (**19**) (15.7 mg, 38.0  $\mu$ mol, 2.00 eq.), TBTU (12.3 mg, 38.0  $\mu$ mol, 2.00 eq.) and HOBt (5.17 mg, 38.0  $\mu$ mol, 2.00 eq.) were dissolved in DMF and DIPEA (14.6  $\mu$ L, 86.0  $\mu$ mol, 4.50 eq.) was added as base. Incubation with **18** at room temperature for 2 h revealed formation of product **20** to a proportion of 27% (59% conversion based on **18**) confirmed by RP-HPLC/MS

## MATERIALS AND METHODS

analysis (GP7). As described in section 4.1.3, this conversion was not further improvable and also not reproducible on a higher molar scale of 42.0  $\mu\text{mol}$ .

RP-HPLC (20 - 80% B in 15 min, Method A, 1 mL/min) for **20(-tBu)**:  $t_R = 17.1$  min;  $k = 10$ . Calculated monoisotopic mass for **20(-tBu)** ( $\text{C}_{37}\text{H}_{36}\text{N}_2\text{O}_8$ ): 636.25, found:  $m/z = 637.4$   $[\text{M}(\mathbf{20})\text{-tBu}+\text{H}]^+$ , 1273.7  $[\text{M}_2(\mathbf{20})\text{-tBu}+\text{H}]^+$ .

### Fmoc-L-Ser(tBu)-L-Asp(OtBu)-L-Phe(4-I)-2-CT (**21**)



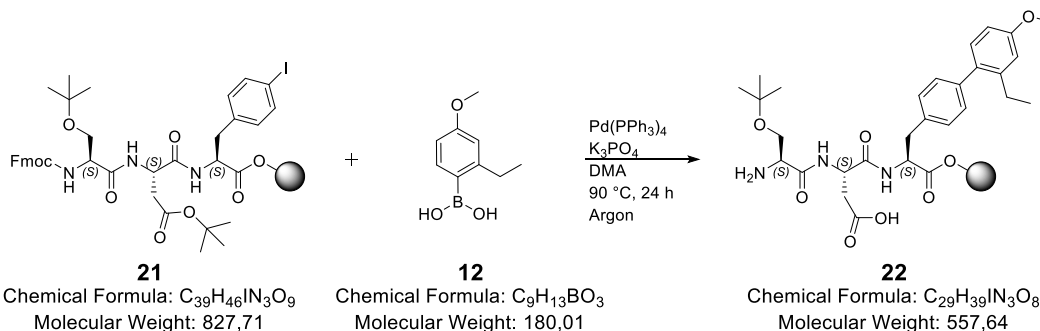
**21**

Chemical Formula:  $\text{C}_{39}\text{H}_{46}\text{I}\text{N}_3\text{O}_9$   
Molecular Weight: 827,71

Tripeptide **21** was synthesized on 2-CT resin according to GP2, GP3 and GP4 (load: 0.84 mmol/g, 0.42 mmol, 1.00 eq.). After coupling of Fmoc-L-Ser(tBu)-OH, the expected product was confirmed by RP-HPLC/MS analysis (GP8), which revealed nearly complete conversion to product **21**.

RP-HPLC (40 - 100% B in 15 min, Method A, 1 mL/min):  $t_R = 16.8$  min;  $k = 10$ . Calculated monoisotopic mass ( $\text{C}_{39}\text{H}_{46}\text{I}\text{N}_3\text{O}_9$ ): 827.23, found:  $m/z = 828.5$   $[\text{M}(\mathbf{21})+\text{H}]^+$ , 772.1  $[\text{M}(\mathbf{21})\text{-tBu}+\text{H}]^+$ , 716.0  $[\text{M}(\mathbf{21})\text{-2tBu}+\text{H}]^+$ .

### Fmoc-L-Ser(tBu)-L-Asp-L-(2'-Et, 4'-OMe)BIP-2-CT (**22**)



**21**

Chemical Formula:  $\text{C}_{39}\text{H}_{46}\text{I}\text{N}_3\text{O}_9$   
Molecular Weight: 827,71

**12**

Chemical Formula:  $\text{C}_9\text{H}_{13}\text{BO}_3$   
Molecular Weight: 180,01

**22**

Chemical Formula:  $\text{C}_{29}\text{H}_{39}\text{I}\text{N}_3\text{O}_8$   
Molecular Weight: 557,64

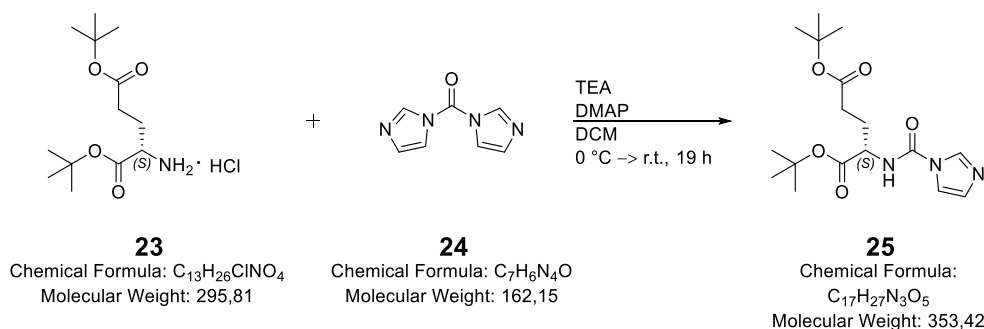
Compound **22** was synthesized in analogy to a previously published procedure by Haque *et al.*<sup>[114]</sup> with some minor modifications. Resin-bound tripeptide **21** (load: 0.84 mmol/g, 0.14 mmol, 1.00 eq.) was transferred to a round-bottom flask. Boronic acid **12** (100 mg, 0.56 mmol, 4.00 eq.) dissolved in 1.20 mL DMA,  $\text{Pd}(\text{PPh}_3)_4$  (16.2 mg, 14.0  $\mu\text{mol}$ , 0.10 eq.) dissolved in 398  $\mu\text{L}$  DMA (1.60 mL DMA in total) and 555  $\mu\text{L}$  of an aqueous 2 M  $\text{K}_3\text{PO}_4$  solution (1.11 mmol, 8.00 eq.) were added to the resin. The yellow-orange suspension was heated to 90  $^\circ\text{C}$  and stirred under argon for 24 h. Afterwards, the resin was transferred to a syringe equipped with a frit, pore size 25  $\mu\text{m}$ ) and washed alternating with 10 mL of 0.5% (w/v) DDTC in DMF (3 $\times$ ) and 10 mL of 0.5% (v/v) DIPEA in DMF (3 $\times$ ) to remove palladium catalyst and other cross-coupling reagents from the resin. After final washing steps with DMF (3 $\times$ ) and DCM (3 $\times$ ) formation of product **22** on the resin could be confirmed by RP-HPLC/MS analysis (GP8).

RP-HPLC (40 - 100% B in 15 min, Method A, 1 mL/min):  $t_R = 8.16$  min;  $k = 4.4$ . Calculated monoisotopic mass ( $\text{C}_{29}\text{H}_{39}\text{N}_3\text{O}_8$ ): 557.27, found:  $m/z = 558.0$   $[\text{M}(\mathbf{22})+\text{H}]^+$ , 502.0  $[\text{M}(\mathbf{22})\text{-tBu}+\text{H}]^+$ .

### 3.2.2. Synthesis of PSMA ligands

Reference compounds rhPSMA-10 (**B-1**) and rhPSMA-7.3 in their free chelator forms were synthesized according to previously published protocols.<sup>[140, 232]</sup> Preparation of <sup>nat</sup>Lu-**B-1** and [<sup>177</sup>Lu]Lu-**B-1** followed similar procedures to those conducted within this study.<sup>[289]</sup> Hence, their analytical data can be found elsewhere and are not again listed. IC<sub>50</sub> data of <sup>nat</sup>Lu-**B-1** as well as internalization, log D, biodistribution and  $\mu$ SPECT/CT data of [<sup>177</sup>Lu]Lu-**B-1** were not adopted from previously published studies. Instead, they were again determined to ensure a valid comparability of the obtained results and to investigate salivary gland uptake of the reference [<sup>177</sup>Lu]Lu-**B-1** at 24 h p.i. Likewise, also IC<sub>50</sub> and internalization data of [<sup>nat/177</sup>Lu]Lu-rhPSMA-7.3 were again determined. Log D data were kindly provided by Dr. Alexander Wurzer. Biodistribution data of [<sup>177</sup>Lu]Lu-rhPSMA-7.3 were taken from Yusufi *et al.*<sup>[290]</sup> and original data for calculation of tumor-to-tissue ratios at 1 h were kindly provided by Dr. Nahid Yusufi.

#### *Di-tert-butyl (1H-imidazole-1-carbonyl)-L-glutamate (25)*



Compound **25** was synthesized in analogy to a previously published procedure, with slight modifications.<sup>[223]</sup> Reactant **23** (3.00 g, 10.1 mmol, 1.00 eq.) was dissolved in dry DCM (29.7 mL) and cooled to 0 °C. Triethylamine (3.57 mL, 25.6 mmol, 2.53 eq.) and DMAP on polystyrene (load: 1.6 mmol/g, 250 mg resin, 0.40 mmol, 0.04 eq.) were added and stirred for five minutes. Afterwards, 1,1'-carbonyldiimidazole (**24**) (2.47 g, 15.2 mmol, 1.50 eq.) was added, the solution was allowed to warm to room temperature and stirred overnight. Afterwards, DMAP on polystyrene was filtered off, the mixture was dissolved with ~ 10 mL DCM and washed with NaHCO<sub>3</sub> (1x), H<sub>2</sub>O (1x) and brine (1x). The organic layer was dried over Na<sub>2</sub>SO<sub>4</sub>, filtered and the solvent removed under reduced pressure. This afforded 4.86 g of crude product **25** as a yellow viscous oil, which was used without further purification in the next step.

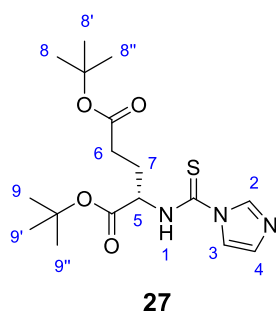
RP-HPLC (10 - 90% B in 15 min, Method A, 1 mL/min):  $t_R = 11.5$  min;  $k = 6.7$ . Calculated monoisotopic mass (C<sub>17</sub>H<sub>27</sub>N<sub>3</sub>O<sub>5</sub>): 353.20, found:  $m/z = 354.2$  [M(**25**)+H]<sup>+</sup>, 395.2 [M(**25**)+MeCN+H]<sup>+</sup>.



## MATERIALS AND METHODS

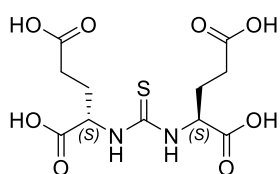
7.61 mmol, 1.50 eq.) was added, the solution was allowed to warm to room temperature and stirred overnight. The mixture was dissolved with ~ 15 mL DCM and washed with NaHCO<sub>3</sub> (1×), H<sub>2</sub>O (1×) and brine (1×). The organic layer was dried over Na<sub>2</sub>SO<sub>4</sub>, filtered and the solvent removed under reduced pressure. This afforded 1.67 g of crude product **27** as a orange-yellow oil, which was used without further purification in the next step.

RP-HPLC (10 - 90% B in 15 min, Method A, 1 mL/min):  $t_R = 13.0$  min;  $k = 6.2$ . Calculated monoisotopic mass (C<sub>17</sub>H<sub>27</sub>N<sub>3</sub>O<sub>4</sub>S): 369.17, found:  $m/z = 370.2$  [M(**27**)+H]<sup>+</sup>, 411.2 [M(**27**)+MeCN+H]<sup>+</sup>;



<sup>1</sup>H-NMR (300 MHz, CDCl<sub>3</sub>) δ(ppm): 8.45 (*virt. d*, 1H, H(1)), 7.65 (*virt. t* 1H, H(2)), 7.23 (s, 1H, H(3)), 7.18 – 7.01 (m, 1H, H(4)), 4.83 (t, <sup>3</sup>J = 5.7 Hz, 1H, H(5)), 2.56 – 2.44 (m, 2H, H(6)), 2.30 – 2.20 (m, 2H, H(7)), 1.48 (s, 9H, H(8, 8', 8'')), 1.45 (s, 9H, H(9, 9', 9'')).

### (2S,2'S)-2,2'-(thiocarbonylbis(azanediyl))diglutamic acid (**B-3**)



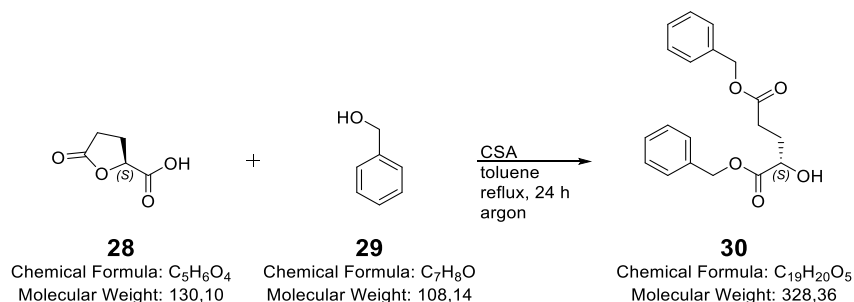
Chemical Formula: C<sub>11</sub>H<sub>16</sub>N<sub>2</sub>O<sub>8</sub>S  
Molecular Weight: 336,32

Compound **B-3** was synthesized in analogy to a previously published procedure by Weineisen *et al.*<sup>[199]</sup> with some minor modifications. Di-*tert*-butyl (1*H*-imidazole-1-carbonothioyl)-L-glutamate (**27**) (500 mg, 1.35 mmol, 1.00 eq.) was dissolved in 6.43 mL DCE and cooled to 0 °C. H-L-Glu(*t*Bu)-OtBu\*HCl (**23**) (599 mg, 2.03 mmol, 1.50 eq.) and triethylamine (46.9 μL, 3.38 mmol, 2.50 eq.) were added and stirred for further five minutes at 0 °C. The reaction mixture was warmed to 40 °C and stirred for 45 h under argon atmosphere. DCM was added for dilution of the reaction mixture and washed once with H<sub>2</sub>O (+ 1 mL brine). The aqueous phase was extracted two times with DCM, the combined organic layers were dried over Na<sub>2</sub>SO<sub>4</sub>, filtered and the solvent was removed under reduced pressure. The obtained crude product was purified by column chromatography (PE/EtOAc = 3/2,  $R_f = 1.00$ ), which gave 839 mg (> 99%) of fully *t*Bu-protected compound **B-3** ( $m/z = 561.3$ ) as a slightly yellowish solid. 100 mg (0.18 mmol, 1.00 eq.) thereof were dissolved in 100 μL DCM, incubated with TFA (100 μL, 1.31 mmol, 7.34 eq.) and stirred for 34 h at room temperature. TFA was removed in a stream of nitrogen and further purification by preparative RP-HPLC (10% B isocratic in 20 min, Method B, 5 mL/min and 2 - 10% B in 15 min, Method A, 1 mL/min) afforded 7.90 mg (13%) of pure product **B-3** as colorless solid.

RP-HPLC (2 - 10% B in 15 min, Method A, 1 mL/min):  $t_R = 9.01$  min;  $k = 5.0$ . Calculated monoisotopic mass (C<sub>11</sub>H<sub>16</sub>N<sub>2</sub>O<sub>8</sub>S): 336.06, found:  $m/z = 337.3$  [M(**B-3**)+H]<sup>+</sup>.

## MATERIALS AND METHODS

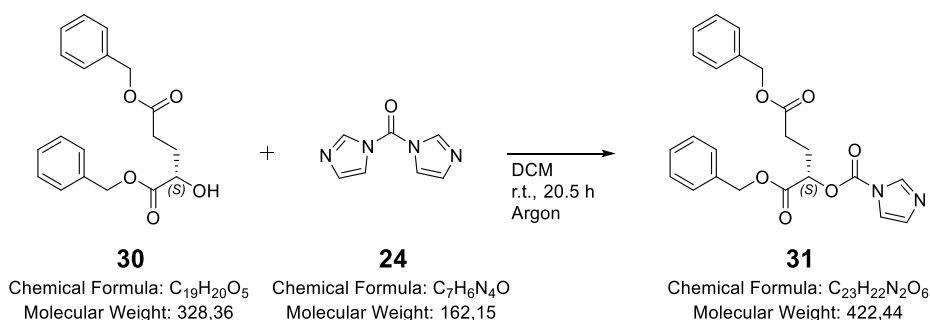
### Dibenzyl (S)-2-hydroxypentanedioate (**30**)



Compound **30** was synthesized in analogy to previously published procedures by Clark *et al.*<sup>[291]</sup> and Ravid *et al.*<sup>[292]</sup> with some minor modifications. The used glassware was pretreated as described in GP12 (air- and moisture-free conditions) and also handling of reactants proceeded by the described methods. (S)-5-Oxotetrahydrofuran-2-carboxylic acid (**28**) (500 mg, 3.85 mmol, 1.00 eq.) was dissolved in 3.50 mL dry toluene. Benzyl alcohol (1.60 mL, 15.4 mmol, 4.00 eq.) and camphor-10-sulfonic acid (14.0 mg, 60.4  $\mu$ mol, 15.7 mol%) were added and the slightly yellow reaction solution was stirred under reflux (~ 128 °C) for 24 h. Toluene was added for dilution of the reaction mixture and washed with H<sub>2</sub>O, saturated NaHCO<sub>3</sub> and again H<sub>2</sub>O. The combined organic layers were dried over Na<sub>2</sub>SO<sub>4</sub>, filtered and the solvent was removed under reduced pressure. The obtained crude product was purified by preparative RP-HPLC (40 - 80% B in 20 min, Method C, 5 mL/min), which gave 270 mg (21.3%) pure product **30** as a colorless oil.

RP-HPLC (10 - 90% B in 15 min, Method A, 1 mL/min):  $t_R$  = 14.5 min;  $k$  = 8.7. Calculated monoisotopic mass (C<sub>19</sub>H<sub>20</sub>O<sub>5</sub>): 328.13, found:  $m/z$  = 329.1 [M(**30**)+H]<sup>+</sup>, 351.1 [M(**30**)+Na]<sup>+</sup>, 367.1 [M(**30**)+K]<sup>+</sup>, 392.1 [M(**30**)+MeCN+Na]<sup>+</sup>.

### Dibenzyl (S)-2-((1H-imidazole-1-carbonyl)oxy)pentanedioate (**31**)

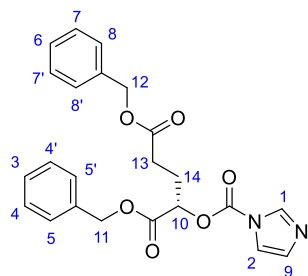


Compound **31** was synthesized in analogy to a previously published procedure by Yang *et al.*<sup>[293]</sup> with some minor modifications. Dibenzyl (S)-2-hydroxypentanedioate (**30**) (50.0 mg, 0.15 mmol, 1.00 eq.) was dissolved in 2.20 mL dry DCM and stirred at room temperature. 1,1'-Carbonyldiimidazole (**24**) (47.0 mg, 0.29 mmol, 1.93 eq.) was dissolved in 1 mL dry DCM and added to the solution, which was stirred under argon atmosphere for 20.5 h at room temperature. The reaction mixture was diluted with DCM and washed once with H<sub>2</sub>O (+ 1 mL brine). The aqueous phase was extracted two times with DCM, the combined organic phases were dried over

## MATERIALS AND METHODS

$\text{Na}_2\text{SO}_4$ , filtered and the solvent was evaporated *in vacuo*. This afforded 61.8 mg (~ 98%) of crude product **31** as colorless solid, which was used in the next step without further purification.

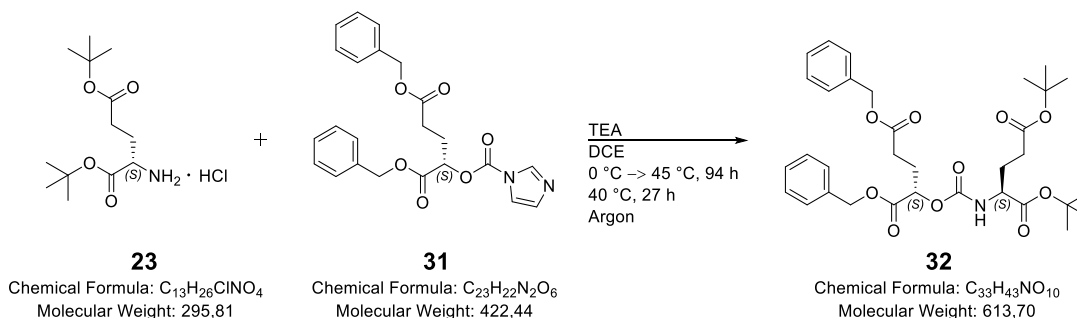
RP-HPLC (10 - 90% B in 15 min, Method A, 1 mL/min):  $t_R = 14.1$  min;  $k = 8.4$ . Calculated monoisotopic mass ( $\text{C}_{23}\text{H}_{22}\text{N}_2\text{O}_6$ ): 422.15, found:  $m/z = 423.2$  [ $\text{M}(\mathbf{31})+\text{H}$ ] $^+$ .



**31**

$^1\text{H-NMR}$  (300 MHz,  $\text{CDCl}_3$ )  $\delta$ (ppm): 8.14 (*virt. d*, 1H, H(1)), 7.41 (s, 1H, H(2)), 7.33 (*virt. d*, 10H, H(3, 4, 4', 5, 5', 6, 7, 7', 8, 8')), 7.08 (d,  $^3J = 1.6$  Hz, 1H, H(9)), 5.36 (dd,  $^3J = 7.6, 4.6$  Hz, 1H, H(10)), 5.22 (s, 2H, H(11)), 5.11 (s, 2H, H(12)), 2.58 – 2.48 (m, 2H, H(13)), 2.47 – 2.28 (m, 2H, H(14)).

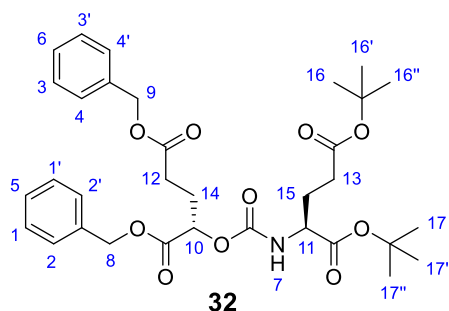
### Dibenzyl (S)-2-(((S)-1,5-di-tert-butoxy-1,5-dioxopentan-2-yl)carbamoyl)oxy)pentanedioate (**32**)



Compound **32** was synthesized in analogy to a previously published procedure by Weineisen *et al.*<sup>[199]</sup> with some minor modifications. Dibenzyl (S)-2-((1*H*-imidazole-1-carbonyl)oxy)pentanedioate (**31**) (63.3 mg, 0.15 mmol, 1.00 eq.) was dissolved in 2.00 mL DCE and cooled to 0 °C. H-L-Glu(O*t*Bu)-O*t*Bu\*HCl (**23**) (94.7 mg, 0.32 mmol, 2.13 eq.) and triethylamine (51.9  $\mu\text{L}$ , 0.38 mmol, 2.50 eq.) were added and stirred for further five minutes at 0 °C. The reaction mixture was warmed to 45 °C and stirred for 94 h under argon atmosphere. As RP-HPLC/MS analysis revealed low conversion (29% **31**, 37% **32**), again triethylamine (51.9  $\mu\text{L}$ , 0.38 mmol, 2.50 eq.) was added. The temperature was decreased to 40 °C, in order to suppress further formation of an unidentifiable by-product ( $m/z = 528.5$  & 544.5). Sufficient consumption of educt **31** (9.7% **31**, 86% **32**) was observed after another 27 h at 40 °C under argon atmosphere. DCM was added for dilution of the reaction mixture and once washed with  $\text{H}_2\text{O}$  (+ 1 mL brine). The aqueous phase was extracted two times with DCM, the combined organic layers were dried over  $\text{Na}_2\text{SO}_4$ , filtered and the solvent was removed under reduced pressure. The obtained crude product was purified by preparative RP-HPLC (70 - 90% B in 20 min, Method C, 5 mL/min), which gave 30.7 mg (33.3%) of compound **32** as a colorless oil.

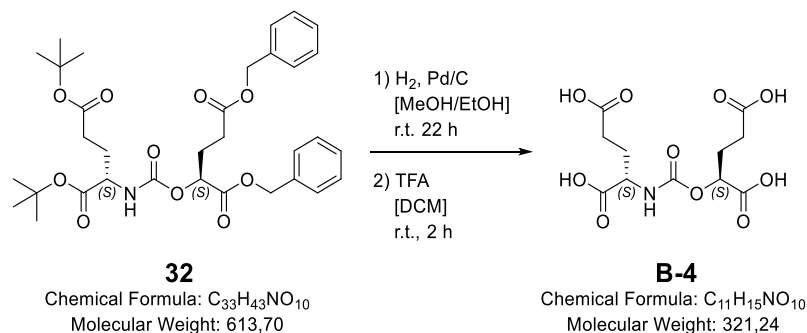
## MATERIALS AND METHODS

RP-HPLC (40 - 100% B in 15 min, Method A, 1 mL/min):  $t_R = 15.4$  min;  $k = 8.4$ . Calculated monoisotopic mass ( $C_{33}H_{43}NO_{10}$ ): 613.29, found:  $m/z = 502.4$  [ $M(\mathbf{32})-2tBu+H$ ] $^+$ , 558.5 [ $M(\mathbf{32})-tBu+H$ ] $^+$ , 614.7 [ $M(\mathbf{32})+H$ ] $^+$ , 636.6 [ $M(\mathbf{32})+Na$ ] $^+$ .



$^1H$ -NMR (300 MHz,  $CDCl_3$ )  $\delta$ (ppm): 7.34 (*virt.* dq, 10H, H(1, 1', 2, 2', 3, 3', 4, 4', 5, 6)), 5.48 (d,  $^3J = 8.4$  Hz, 1H, H(7)), 5.17 (*virt.* d, 2H, H(8)), 5.10 (s, 2H, H(9)), 5.06 (dd,  $^3J = 7.9, 4.6$  Hz, 1H, H(10)), 4.22 (td,  $^3J = 8.4, 4.7$  Hz, 1H, H(11)), 2.54 – 2.01 (m, 8H, H(12, 13, 14, 15)), 1.45 (s, 9H, H(16, 16', 16'')), 1.43 (s, 9H, H(17, 17', 17'')).

((*S*)-1,3-dicarboxypropoxy)carbonyl)-L-glutamic acid (**B-4**)

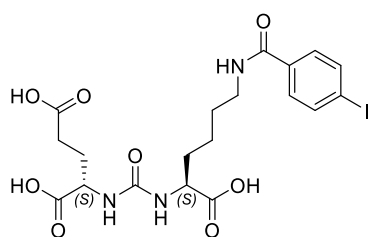


Compound **32** (30.5 mg, 0.05 mmol, 1.00 eq.) was dissolved in 2.50 mL MeOH/EtOH (4/1) and the solution was flushed 5 minutes with argon to remove dissolved oxygen. 5.30 mg of palladium on carbon (10% wt) (corresponds to 0.53 mg palladium, 5.00  $\mu$ mol, 0.10 eq.) were added and the flask was sealed with a rubber septum. Remaining air was displaced with argon and subsequently replaced by hydrogen gas. The mixture was stirred under hydrogen atmosphere at room temperature for 22 h. Palladium on carbon was filtered off, and the solvent was evaporated *in vacuo*. This afforded 22.9 mg of a ~ 1/1 mixture of crude product **32**(-2Bn) ( $m/z = 434.4$ ) and **32**(-2Bn)OMe ( $m/z = 448.6$ ) as a colorless clear oil, which was used in the next step without further purification. The transesterified by-product was not partitioned off, as the methyl ester was assumed to be either also cleaved by incubation with TFA or separated by RP-HPLC afterwards. Hence, the crude product (22.9 mg, 52.1  $\mu$ mol, 1.00 eq.) was dissolved in 200  $\mu$ L DCM, TFA (200  $\mu$ L, 2.61 mmol, 50.1 eq.) was added and the reaction mixture was stirred for 2 h at room temperature. TFA and DCM were removed under a stream of nitrogen,  $H_2O$  was added, the crude product was frozen at  $-80$   $^{\circ}C$  and lyophilized. Purification by preparative RP-HPLC (2 - 10% B in 20 min, Method B, 5 mL/min and 2 - 10% B in 15 min, Method A, 1 mL/min) afforded 0.90 mg (5.61%) of pure product **B-4** as colorless solid.

RP-HPLC (2 - 10% B in 15 min, Method A, 1 mL/min):  $t_R = 2.43$  min;  $k = 0.6$ . Calculated monoisotopic mass ( $C_{11}H_{15}NO_{10}$ ): 321.07, found:  $m/z = 304.2$  [ $M(\mathbf{B-4})-H_2O+H$ ] $^+$ , 322.4 [ $M(\mathbf{B-4})+H$ ] $^+$ , 344.4 [ $M(\mathbf{B-4})+Na$ ] $^+$ , 360.3 [ $M(\mathbf{B-4})+K$ ] $^+$ .

## MATERIALS AND METHODS

### (((S)-1-carboxy-5-(4-iodobenzamido)pentyl)carbamoyl)-L-glutamic acid (= (I-BA)KuE) (**B-5**)



**B-5**

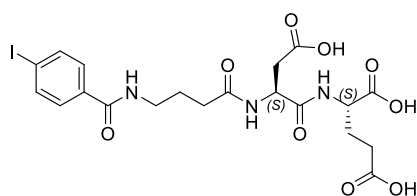
Chemical Formula: C<sub>19</sub>H<sub>24</sub>I<sub>N</sub><sub>3</sub>O<sub>8</sub>  
Molecular Weight: 549,32

Compound **B-5** was synthesized in analogy to a previously published procedure by Weineisen *et al.*<sup>[199]</sup> with some minor modifications. Already existing L-Lys-O $\text{tBu}$ -carbonyl-L-Glu(O $\text{tBu}$ )-O $\text{tBu}$  (100 mg, 0.21 mmol, 1.00 eq.) was dissolved in 13.2 mL DMF and 4-iodobenzoic acid (79.4 mg, 0.32 mmol, 1.50 eq.), HOAt (43.6 mg, 0.32 mmol, 1.50 eq.), EDC\*HCl (61.3 mg, 0.32 mmol, 1.50 eq.) and DIPEA (161  $\mu\text{L}$ , 0.95 mmol, 4.50 eq.) were added. The reaction mixture was stirred at room

temperature for 24 h. EtOAc was added for dilution of and the solution was once washed with H<sub>2</sub>O (+ 1 mL brine). The aqueous phase was extracted once with EtOAc, the combined organic layers were dried over Na<sub>2</sub>SO<sub>4</sub>, filtered and the solvent was removed under reduced pressure. The obtained crude product **B-5**(O $\text{tBu}$ )<sub>3</sub> ( $m/z$  = 718.5) was used in the next step without further purification. Thereof, 171 mg (~ 0.21 mmol pure product, 1.00 eq.) were incubated with 4.00 mL TFA (52.3 mmol, 249 eq.) and stirred for 30 min at room temperature. TFA was removed under a stream of nitrogen and further purification by preparative RP-HPLC (20 - 80% B in 20 min, Method B, 5 mL/min) afforded 72.6 mg (63%) of pure product **B-5** as colorless solid.

RP-HPLC (20 - 80% B in 15 min, Method A, 1 mL/min):  $t_R$  = 9.21 min;  $k$  = 5.1. Calculated monoisotopic mass (C<sub>19</sub>H<sub>24</sub>I<sub>N</sub><sub>3</sub>O<sub>8</sub>): 549.06, found:  $m/z$  = 550.1 [M(**B-5**)+H]<sup>+</sup>.

### (4-(4-iodobenzamido)butanoyl)-L-aspartyl-L-glutamic acid (**B-6**)



**B-6**

Chemical Formula: C<sub>20</sub>H<sub>24</sub>I<sub>N</sub><sub>3</sub>O<sub>9</sub>  
Molecular Weight: 577,33

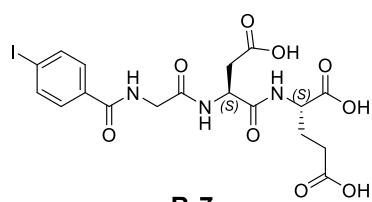
Preparation of **B-6** was conducted via linear synthesis on 2-CT resin according to GP2, GP3 and GP4 (load: 1.03 mmol/g, 0.19 mmol, 1.00 eq.). After coupling of Fmoc-L-Glu(O $\text{tBu}$ )-OH, Fmoc-L-Asp(O $\text{tBu}$ )-OH and Fmoc- $\gamma$ -Abu-OH, 4-iodobenzoic acid (91.8 mg, 0.37 mmol, 2.00 eq.) was coupled according to GP3. Formation of the

expected product was confirmed by RP-HPLC/MS analysis (GP7), which revealed successful on-resin synthesis of **B-6**. Cleavage of the peptide from the resin with TFA/TIPS/H<sub>2</sub>O (95/2.5/2.5, 1  $\times$  30 min, slightly modified to GP9) resulted in 84.8 mg (77.3%) of pure product **B-6** as a colorless solid after RP-HPLC purification (20 - 50% B in 20 min, Method B, 5 mL/min) and lyophilization.

RP-HPLC (10 - 90% B in 15 min, Method A, 1 mL/min):  $t_R$  = 6.29 min;  $k$  = 3.2. Calculated monoisotopic mass (C<sub>20</sub>H<sub>24</sub>I<sub>N</sub><sub>3</sub>O<sub>9</sub>): 577.06, found:  $m/z$  = 578.0 [M(**B-6**)+H]<sup>+</sup>.

## MATERIALS AND METHODS

### (4-iodobenzoyl)glycyl-L-aspartyl-L-glutamic acid (**B-7**)



**B-7**

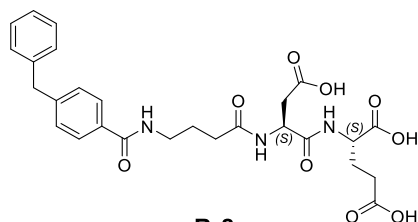
Chemical Formula:  $C_{18}H_{20}IN_3O_9$

Molecular Weight: 549,27

Preparation of **B-7** was conducted via linear synthesis on 2-CT resin according to GP2, GP3 and GP4 (load: 1.03 mmol/g, 0.19 mmol, 1.00 eq.). After coupling of Fmoc-L-Glu(OtBu)-OH, Fmoc-L-Asp(OtBu)-OH and Fmoc-Gly-OH, 4-iodobenzoic acid (91.8 mg, 0.37 mmol, 2.00 eq.) was coupled according to GP3. Formation of the expected product was confirmed by RP-HPLC/MS analysis (GP7), which revealed successful on-resin synthesis of **B-7**. Cleavage of the peptide from the resin with TFA/TIPS/H<sub>2</sub>O (95/2.5/2.5, 1 × 30 min, slightly modified to GP9) resulted in 44.1 mg (42.3%) of pure product **B-7** as a colorless solid after RP-HPLC purification (30 - 50% B in 20 min, Method B, 5 mL/min) and lyophilization.

RP-HPLC (10 - 90% B in 15 min, Method A, 1 mL/min):  $t_R = 5.89$  min;  $k = 2.9$ . Calculated monoisotopic mass ( $C_{18}H_{20}IN_3O_9$ ): 549.02, found:  $m/z = 550.1$  [ $M(\mathbf{B-7})+H$ ]<sup>+</sup>.

### (4-(4-benzylbenzamido)butanoyl-L-aspartyl-L-glutamic acid (**B-8**)



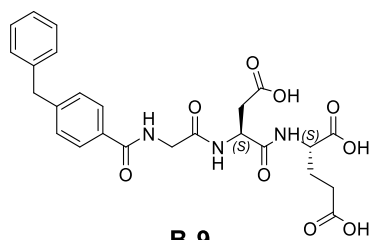
**B-8**

Chemical Formula:  $C_{27}H_{31}N_3O_9$

Molecular Weight: 541,56

Preparation of **B-8** started with linear synthesis on 2-CT resin according to GP3 and GP4 on 2-CT resin preloaded with Fmoc-L-Glu(OBzl) (load: 0.60 mmol/g, 0.09 mmol, 1.00 eq.). After coupling of Fmoc-L-Asp(OtBu)-OH and Fmoc-γ-Abu-OH, 4-iodobenzoic acid (44.6 mg, 0.18 mmol, 2.00 eq.) was coupled according to GP3. Formation of the expected iodinated product was confirmed by RP-HPLC/MS analysis (GP7). Cleavage of the peptide from the resin with TFA/TIPS/H<sub>2</sub>O (95/2.5/2.5, 1 × 30 min, slightly modified to GP9) resulted in the iodinated and still benzyl protected intermediate ( $m/z = 668.2$ ). After removal of TFA under a stream of nitrogen and subsequent lyophilization, this crude product (60.0 mg, 0.09 mmol, 1.00 eq.) was dissolved in 5.00 mL MeOH and stirred with 9.60 mg of palladium on carbon (10% wt) (corresponds to 0.96 mg palladium, 9.00 μmol, 0.10 eq.) under hydrogen atmosphere at room temperature for 26 h. Besides the expected benzyl ester cleavage, *in situ* reaction of the toluene-Pd(II)-H complex with R-[metal(II)]-I, similar to a palladium-catalyzed cross-coupling reaction, led to formation of **B-8**. Palladium on carbon was filtered off and the solvent was evaporated *in vacuo*. Purification by RP-HPLC (30 - 60% B in 20 min, Method B, 5 mL/min) afforded 2.70 mg (5.54%) of pure product **B-8** as a colorless solid.

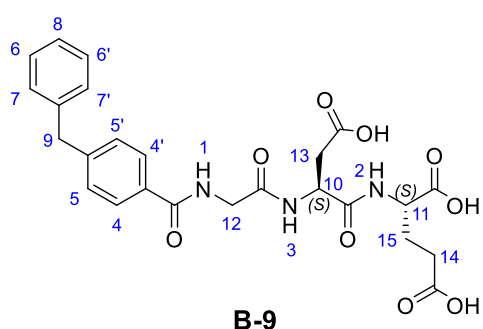
RP-HPLC (10 - 90% B in 15 min, Method A, 1 mL/min):  $t_R = 8.32$  min;  $k = 4.5$ . Calculated monoisotopic mass ( $C_{27}H_{31}N_3O_9$ ): 541.21, found:  $m/z = 542.1$  [ $M(\mathbf{B-8})+H$ ]<sup>+</sup>.

*(4-benzylbenzoyl)glycyl-L-aspartyl-L-glutamic acid (B-9)***B-9**Chemical Formula: C<sub>25</sub>H<sub>27</sub>N<sub>3</sub>O<sub>9</sub>

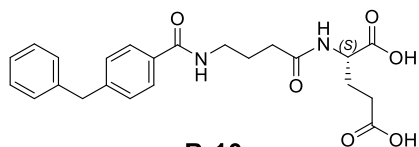
Molecular Weight: 513,50

Preparation of **B-9** started with linear synthesis on 2-CT resin according to GP3 and GP4 on 2-CT resin preloaded with Fmoc-L-Glu(OBzl) (load: 0.60 mmol/g, 0.09 mmol, 1.00 eq.). After coupling of Fmoc-L-Asp(OtBu)-OH and Fmoc-Gly-OH, 4-iodobenzoic acid (44.6 mg, 0.18 mmol, 2.00 eq.) was coupled according to GP3. Formation of the expected iodinated product was confirmed by RP-HPLC/MS analysis (GP7). Cleavage of the peptide from the resin with TFA/TIPS/H<sub>2</sub>O (95/2.5/2.5, 1 × 30 min, slightly modified to GP9) resulted in the iodinated and still benzyl protected intermediate (*m/z* = 640.2). After removal of TFA under a stream of nitrogen and subsequent lyophilization, this crude product (57.5 mg, 0.09 mmol, 1.00 eq.) was dissolved in 5.00 mL MeOH and stirred with 9.60 mg of palladium on carbon (10% wt) (corresponds to 0.96 mg palladium, 9.00 μmol, 0.10 eq.) under hydrogen atmosphere at room temperature for 2 h. Besides the expected benzyl ester cleavage, *in situ* reaction of the toluene-Pd(II)-H complex with R-[metal(II)]-I, similar to a palladium-catalyzed cross-coupling reaction, led to formation of **B-9**. Palladium on carbon was filtered off and the solvent was evaporated *in vacuo*. Purification by RP-HPLC (30 - 50% B in 20 min, Method B, 5 mL/min) afforded 10.5 mg (22.7%) of pure product **B-9** as a colorless solid.

RP-HPLC (10 - 90% B in 15 min, Method A, 1 mL/min): *t<sub>R</sub>* = 8.24 min; *k* = 4.5. Calculated monoisotopic mass (C<sub>25</sub>H<sub>27</sub>N<sub>3</sub>O<sub>9</sub>): 513.17, found: *m/z* = 514.0 [M(**B-9**)+H]<sup>+</sup>, 536.0 [M(**B-9**)+Na]<sup>+</sup>, 551.9 [M(**B-9**)+K]<sup>+</sup>.

**B-9**

<sup>1</sup>H-NMR (300 MHz, DMSO-*d*<sub>6</sub>) δ(ppm): 8.82 (t, <sup>3</sup>*J* = 5.7 Hz, 1H, H(1)), 8.31 (d, <sup>3</sup>*J* = 8.2 Hz, 1H, H(2)), 7.96 (d, <sup>3</sup>*J* = 7.9 Hz, 1H, H(3)), 7.91 – 7.81 (m, 2H, H(4, 4')), 7.34 (s, 7H, H(5, 5', 6, 6', 7, 7', 8)), 5.07 (s, 2H, H(9)), 4.65 (td, <sup>3</sup>*J* = 8.1, 5.0 Hz, 1H, H(10)), 4.23 (td, <sup>3</sup>*J* = 8.7, 4.8 Hz, 1H, H(11)), 4.00 – 3.75 (m, 2H, H(12)), 2.81 – 2.37 (m, 4H, H(13, 14)), 2.16 – 1.80 (m, 2H, H(15)).

*(4-(4-benzylbenzamido)butanoyl)-L-glutamic acid (B-10)***B-10**Chemical Formula: C<sub>23</sub>H<sub>26</sub>N<sub>2</sub>O<sub>6</sub>

Molecular Weight: 426,47

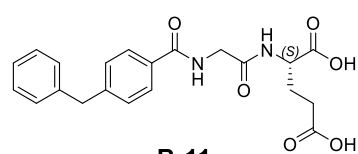
Preparation of **B-10** started with linear synthesis on 2-CT resin according to GP3 and GP4 on 2-CT resin preloaded with Fmoc-L-Glu(OBzl) (load: 0.60 mmol/g, 0.09 mmol, 1.00 eq.). After coupling of Fmoc-γ-Abu-OH, 4-iodobenzoic acid (44.6 mg, 0.18 mmol, 2.00 eq.) was coupled according to GP3. Formation of the expected iodinated product was confirmed by RP-HPLC/MS analysis (GP7). Cleavage of the peptide from the resin with TFA/TIPS/H<sub>2</sub>O (95/2.5/2.5, 1 × 30 min, slightly modified

## MATERIALS AND METHODS

to GP9) resulted in the iodinated and still benzyl protected intermediate ( $m/z = 553.1$ ). After removal of TFA under a stream of nitrogen and subsequent lyophilization, this crude product (49.7 mg, 0.09 mmol, 1.00 eq.) was dissolved in 5.00 mL MeOH and stirred with 9.60 mg of palladium on carbon (10% wt) (corresponds to 0.96 mg palladium, 9.00  $\mu\text{mol}$ , 0.10 eq.) under hydrogen atmosphere at room temperature for 26 h. Besides the expected benzyl ester cleavage, *in situ* reaction of the toluene-Pd(II)-H complex with R-[metal(II)]-I, similar to a palladium-catalyzed cross-coupling reaction, led to formation of **B-10**. Palladium on carbon was filtered off and the solvent was evaporated *in vacuo*. Purification by RP-HPLC (30 - 50% B in 20 min, Method B, 5 mL/min) afforded 2.40 mg (6.26%) of pure product **B-10** as a colorless solid.

RP-HPLC (10 - 90% B in 15 min, Method A, 1 mL/min):  $t_R = 9.05$  min;  $k = 5.0$ . Calculated monoisotopic mass ( $\text{C}_{23}\text{H}_{26}\text{N}_2\text{O}_6$ ): 426.18, found:  $m/z = 427.0$  [ $\text{M}(\text{B-10})+\text{H}$ ] $^+$ .

### (4-benzylbenzoyl)glycyl-L-glutamic acid (**B-11**)

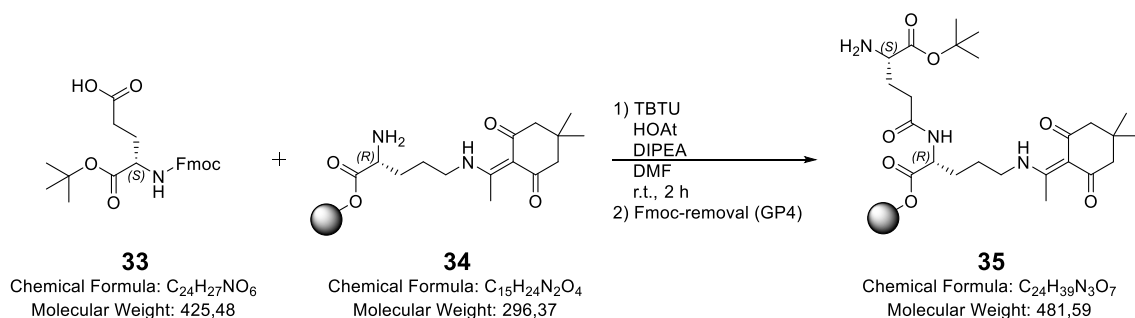


Chemical Formula:  $\text{C}_{21}\text{H}_{22}\text{N}_2\text{O}_6$   
Molecular Weight: 398,42

Preparation of **B-11** started with linear synthesis on 2-CT resin according to GP3 and GP4 on 2-CT resin preloaded with Fmoc-L-Glu(OBzl) (load: 0.60 mmol/g, 0.09 mmol, 1.00 eq.). After coupling of Fmoc-Gly-OH, 4-iodobenzoic acid (44.6 mg, 0.18 mmol, 2.00 eq.) was coupled according to GP3. Formation of the expected iodinated product was confirmed by RP-HPLC/MS analysis (GP7).

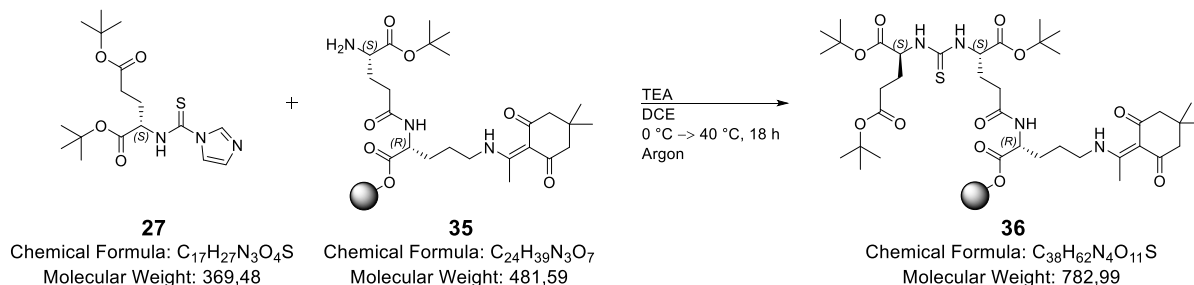
Cleavage of the peptide from the resin with TFA/TIPS/ $\text{H}_2\text{O}$  (95/2.5/2.5, 1  $\times$  30 min, slightly modified to GP9) resulted in the iodinated and still benzyl protected intermediate ( $m/z = 525.1$ ). After removal of TFA under a stream of nitrogen and subsequent lyophilization, this crude product (57.5 mg, 0.09 mmol, 1.00 eq.) was dissolved in 5.00 mL MeOH and stirred with 9.60 mg of palladium on carbon (10% wt) (corresponds to 0.96 mg palladium, 9.00  $\mu\text{mol}$ , 0.10 eq.) under hydrogen atmosphere at room temperature for 2 h. Besides the expected benzyl ester cleavage, *in situ* reaction of the toluene-Pd(II)-H complex with R-[metal(II)]-I, similar to a palladium-catalyzed cross-coupling reaction, led to formation of **B-11**. Palladium on carbon was filtered off and the solvent was evaporated *in vacuo*. Purification by RP-HPLC (30 - 50% B in 20 min, Method B, 5 mL/min) afforded 3.59 mg (10.0%) of pure product **B-11** as a colorless solid.

RP-HPLC (10 - 90% B in 15 min, Method A, 1 mL/min):  $t_R = 8.80$  min;  $k = 4.9$ . Calculated monoisotopic mass ( $\text{C}_{21}\text{H}_{22}\text{N}_2\text{O}_6$ ): 398.15, found:  $m/z = 399.0$  [ $\text{M}(\text{B-11})+\text{H}$ ] $^+$ .

*L*-Glu-[*D*-Orn(*Dde*)-2-CT]-*O*tBu (**35**)


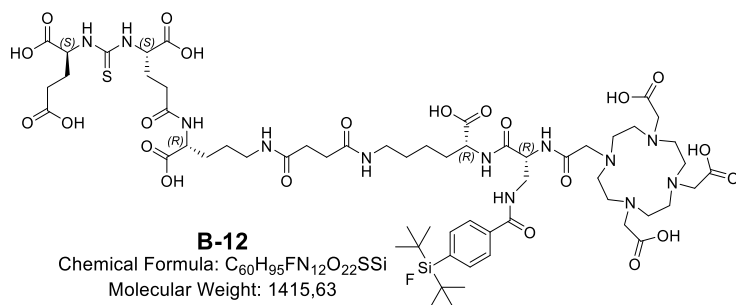
Fmoc-*D*-Orn(*Dde*)-OH was coupled to 2-CTC resin according to GP2 (load: 0.71 mmol/g, 0.34 mmol, 1.00 eq.). After removal of the Fmoc protective group (GP4), Fmoc-*L*-Glu-*O*tBu (**33**) (294 mg, 0.69 mmol, 2.00 eq.) was coupled to **34** according to GP3. After two hours, the Fmoc group of the resin-bound dipeptide was cleaved off, again according to GP4. Some resin beads were taken according to GP7 and analyzed via RP-HPLC, which indicated nearly complete conversion to **35**.

RP-HPLC (10 - 90% B in 15 min, Method A, 1 mL/min) for **35(-tBu)**:  $t_R = 8.47$  min;  $k = 4.6$ . Calculated monoisotopic mass for **35(-tBu)** (C<sub>20</sub>H<sub>31</sub>N<sub>3</sub>O<sub>7</sub>): 425.22, found:  $m/z = 426.0$  [M(**35**)-tBu+H]<sup>+</sup>.

*L*-Glu(*O*tBu)<sub>2</sub>-(thiocarbonyl)-*L*-Glu-[*D*-Orn(*Dde*)-2-CT]-*O*tBu (**36**)


Reactant **27** (160 mg of crude product, contain ~ 60% of **27** (RP-HPLC), 0.26 mmol, 1.50 eq.) was dissolved in 2 mL DCM and cooled to 0 °C. Triethylamine (59.6 μL, 0.43 mmol, 2.50 eq.) and the resin-bound dipeptide **35** (0.17 mmol, 1.00 eq.) were added and stirred for five minutes at 0 °C. The reaction mixture was heated to 40 °C and stirred for 18 h under argon atmosphere. The resin was transferred to a syringe for peptide synthesis (equipped with a frit, pore size 25 μm) and washed with DCM (4×). Some resin beads were taken according to GP8 and analyzed via RP-HPLC, which indicated nearly complete conversion to **36**.

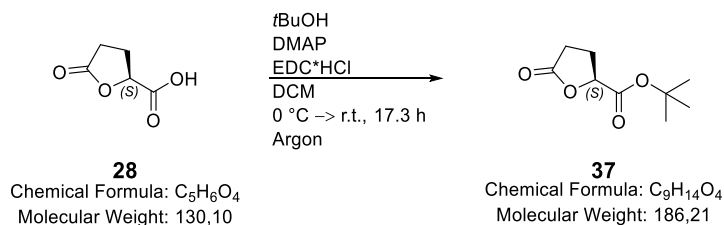
RP-HPLC (40 - 100% B in 15 min, Method A, 1 mL/min):  $t_R = 12.7$  min;  $k = 7.5$ . Calculated monoisotopic mass (C<sub>38</sub>H<sub>62</sub>N<sub>4</sub>O<sub>11</sub>S): 782.41, found:  $m/z = 783.2$  [M(**36**)+H]<sup>+</sup>, 805.4 [M(**36**)+Na]<sup>+</sup>, 822.1 [M(**36**)+K]<sup>+</sup>.

**Thioureate B-12**

Further reactions on resin-bound compound **36** (85.0  $\mu$ mol, 1.20 eq.) were performed according to standard Fmoc-SPPS on 2-CT resin, applying the above-mentioned methods (GP3 - GP8). For chelator attachment DOTA\*6 H<sub>2</sub>O (43.6 mg,

85.0  $\mu$ mol, 1.20 eq.), TBTU (22.8 mg, 71.0  $\mu$ mol, 1.00 eq.), HOAt (9.66 mg, 71.0  $\mu$ mol, 1.00 eq.) and *sym*-collidine (66.3  $\mu$ L, 0.50 mmol, 7.00 eq.) were dissolved in a mixture of DMF/DMSO (5/1, v/v) and incubated with the resin-bound amine for 23 h. As RP-HPLC/MS analysis (GP7) revealed successful coupling, the peptide was cleaved off the resin with TFA/TIPS/H<sub>2</sub>O (GP9) and purified afterwards by preparative RP-HPLC (30 - 50% B in 20 min, Method B, 5 mL/min). Subsequent lyophilization afforded 1.99 mg (1.98%) of pure product **B-12** as a colorless powder.

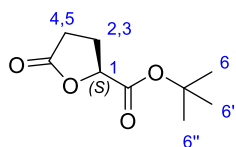
RP-HPLC (40 - 100% B in 15 min, Method A, 1 mL/min):  $t_R = 7.82$  min;  $k = 4.2$ . Calculated monoisotopic mass ( $C_{60}H_{95}FN_{12}O_{22}SSi$ ): 1414.62, found:  $m/z = 708.6$  [ $M(\mathbf{B-12})+2H$ ]<sup>2+</sup>, 1415.8 [ $M(\mathbf{B-12})+H$ ]<sup>+</sup>.

**Tert-butyl (S)-5-oxotetrahydrofuran-2-carboxylate (37)**

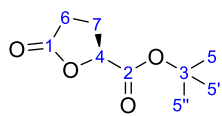
According to a previously published procedure by Zhang *et al.*<sup>[294]</sup> with slight modifications, (S)-5-oxotetrahydrofuran-2-carboxylic acid (**28**) (1.50 g, 11.5 mmol, 1.00 eq.) was weighed in a 100 mL round bottom flask and dissolved in 36 mL dry DCM. DMAP on polystyrene (1.60 mmol/g, 718 mg, 1.15 mmol, 0.10 eq.) and dry *t*BuOH (1.40 mL, 15.0 mmol, 1.30 eq.) were added and the reaction mixture was cooled to 0 °C. EDC·HCl (2.87 g, 15.0 mmol, 1.30 eq.) in 12 mL dry DCM was added slowly, the ice bath was removed, the solution was allowed to warm to room temperature and stirred under argon atmosphere for 17.3 h. DMAP on polystyrene was filtered off, the organic layer was washed once with H<sub>2</sub>O (spiked with some drops of brine), dried over Na<sub>2</sub>SO<sub>4</sub> and the solvent was removed under reduced pressure. The crude product was purified by column chromatography (toluene/EtOAc = 3/2) to afford 928 mg (43%) of compound **37** as a colorless, crystalline solid.

$t_R$  (RP-HPLC): not detectable at 220/254 nm.  $m/z$  by MS not determined.  $R_f$ -value: 0.58 (toluene/EtOAc = 3/2).

## MATERIALS AND METHODS



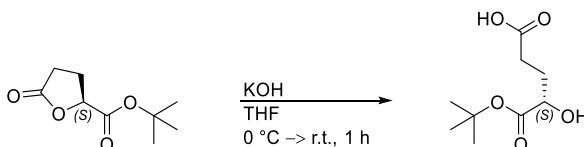
$^1\text{H-NMR}$  (300 MHz,  $\text{CDCl}_3$ )  $\delta$ (ppm): 4.83 – 4.76 (m, 1H, H(1)), 2.68 – 2.39 (m, 3H, H(2, 3, 4)), 2.32 – 2.14 (m, 1H, H(5)), 1.48 (s, 9H, H(6, 6', 6'')).



$^{13}\text{C-NMR}$  (75 MHz,  $\text{CDCl}_3$ )  $\delta$ (ppm): 176.32 (s, 1C, C(1)), 169.12 ((s, 1C, C(2)), 83.23 (s, 1C, C(3)), 76.40 (s, 1C, C(4)), 28.03 (s, 3C, C(5, 5', 5'')), 26.90 (s, 1C, C(6)), 26.00 (s, 1C, C(7)).

**37**

(*S*)-5-(*tert*-butoxy)-4-Hydroxy-5-oxopentanoic acid (**38**)



**37**

Chemical Formula:  $\text{C}_9\text{H}_{14}\text{O}_4$   
Molecular Weight: 186,21

**38**

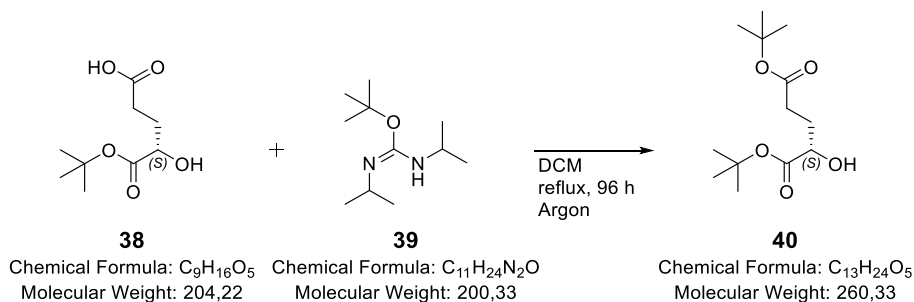
Chemical Formula:  $\text{C}_9\text{H}_{16}\text{O}_5$   
Molecular Weight: 204,22

According to a previously published procedure by Zhang *et al.*<sup>[294]</sup> with slight modifications, *tert*-butyl (*S*)-5-oxotetrahydrofuran-2-carboxylate (**37**) (425 mg, 2.28 mmol, 1.00 eq.) was dissolved in 2.40 mL THF. At 0 °C, a 1 M aqueous KOH solution (2.64 mL, 2.64 mmol, 1.16 eq.) was added dropwise over five minutes. The solution was allowed to warm to room temperature and stirred for one hour. As reaction control via TLC revealed almost complete consumption of educt **37**, THF was removed under reduced pressure and the pH value of the remaining aqueous layer was adjusted to 3 by adding 2 M HCl. The aqueous residue was extracted with EtOAc (3 $\times$ ), the combined organic phases dried over  $\text{Na}_2\text{SO}_4$ , filtered and the solvent removed under reduced pressure. This afforded 381 mg of crude product **38** as a colorless solid, which was used in the next step without further purification.

$t_R$  (RP-HPLC): not detectable at 220/254 nm. Calculated monoisotopic mass ( $\text{C}_9\text{H}_{16}\text{O}_5$ ): 204.10,  $m/z$  by MS not determined.  $R_f$ -value: 0.0 (toluene/EtOAc = 3/2).

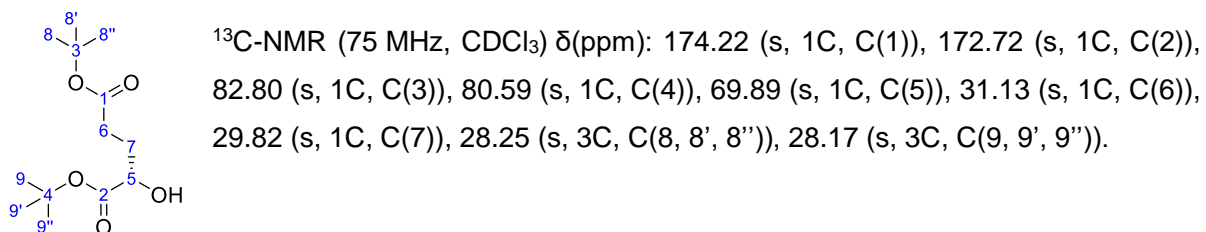
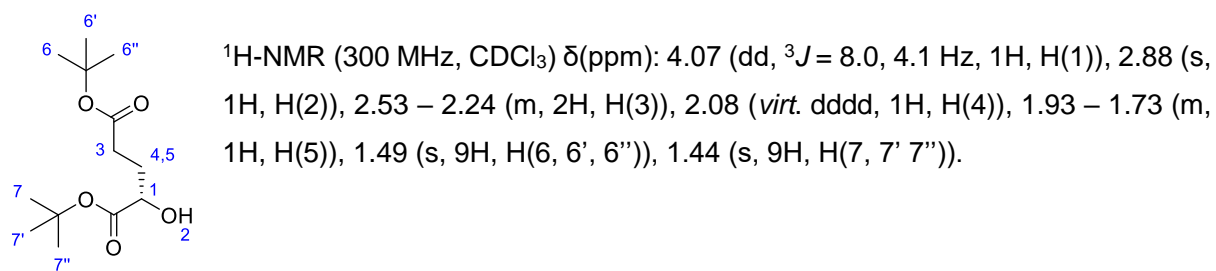
## MATERIALS AND METHODS

### Di-*tert*-butyl (*S*)-2-hydroxypentanedioate (**40**)



Compound **40** was synthesized in analogy to previously published procedures by Mathias *et al.*<sup>[295]</sup> and Bergmeier *et al.*<sup>[296]</sup> with some minor modifications. Glassware and reagents were handled under air- and moisture-free conditions (GP12). Lyophilized educt **38** (crude product, ~ 100 mg, 0.49 mmol, 1.00 eq.) was dissolved in 5 mL dry DCM and the first portion of *O*-*tert*-butyl-*N,N'*-diisopropylisourea (**39**) (162  $\mu$ L, 0.73 mmol, 1.50 eq.) was added. The reaction mixture was stirred under reflux (~ 42 °C) and argon atmosphere for 24 h. A second portion of **39** (162  $\mu$ L, 0.73 mmol, 1.50 eq.) was added and also DCM, in order to keep the solvent amount constantly between 3 and 5 mL. After stirring for further 72 h at reflux temperature and under argon atmosphere, the reaction was terminated by diluting the suspension with DCM. Solid by-products were removed by filtration and the solvent was removed under reduced pressure. Purification by column chromatography (PE/EtOAc = 9/1) provided 24.6 mg (19%) of compound **40** as a colorless liquid.

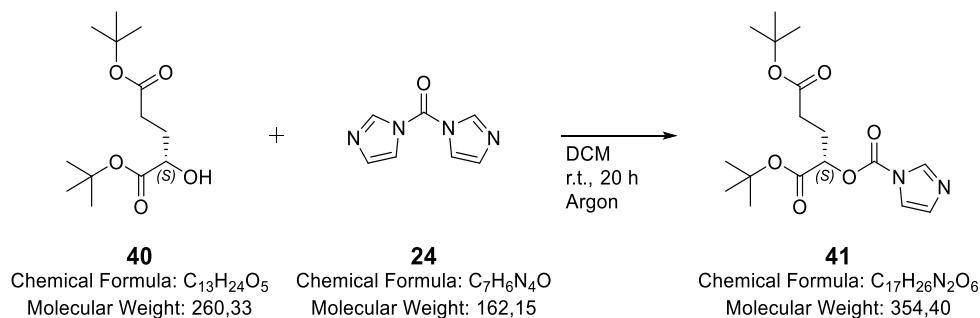
$t_R$  (RP-HPLC): not detectable at 220/254 nm.  $m/z$  by MS not determined.  $R_f$ -value: 0.65 (PE/EtOAc = 9/1).



**40**

## MATERIALS AND METHODS

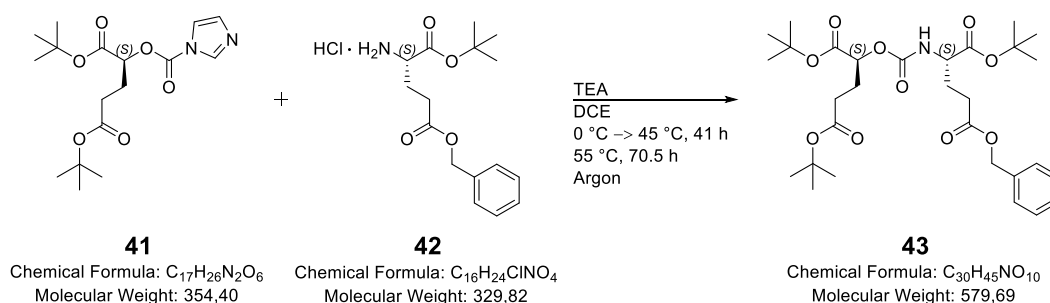
### Di-*tert*-butyl (*S*)-2-((1*H*-imidazole-1-carbonyl)oxy)pentanedioate (**41**)



Compound **41** was synthesized in analogy to a previously published procedure by Yang *et al.*<sup>[293]</sup> with some minor modifications. Di-*tert*-butyl (*S*)-2-hydroxypentanedioate (**40**) (398 mg, 1.53 mmol, 1.00 eq.) was dissolved in 25 mL dry DCM and stirred at room temperature. 1,1'-Carbonyldiimidazole (**24**) (478 mg, 2.95 mmol, 1.93 eq.) was added to the solution, which was then stirred under argon atmosphere for 20 h at room temperature. The reaction mixture was diluted with DCM and washed once with H<sub>2</sub>O. The aqueous layer was extracted two times with DCM, the combined organic phases were dried over Na<sub>2</sub>SO<sub>4</sub>, filtered and the solvent evaporated *in vacuo*. This afforded 615 mg (> 99%) of crude product as slightly yellow solid. RP-HPLC/MS control revealed nearly complete conversion to product **41**, which was used in the next step without further purification.

RP-HPLC (40 - 100% B in 15 min, Method A, 1 mL/min):  $t_R = 10.2$  min;  $k = 5.8$ . Calculated monoisotopic mass (C<sub>17</sub>H<sub>26</sub>N<sub>2</sub>O<sub>6</sub>): 354.18, found:  $m/z = 355.2$  [M(**41**)+H]<sup>+</sup>, 396.2 [M(**41**)+MeCN+H]<sup>+</sup>.

### 5-Benzyl 1-(*tert*-butyl) (((*S*)-1,5-di-*tert*-butoxy-1,5-dioxopentan-2-yl)oxy)carbonyl)-L-glutamate (**43**)

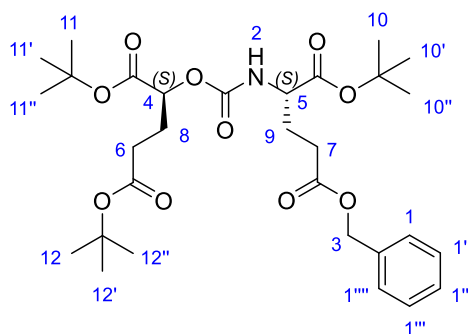


Compound **43** was synthesized in analogy to a previously published procedure by Weineisen *et al.*<sup>[199]</sup> with some minor modifications. Di-*tert*-butyl (*S*)-2-((1*H*-imidazole-1-carbonyl)oxy)pentanedioate (**41**) (542 mg, 1.53 mmol, 1.00 eq.) was dissolved in 7.29 mL DCE and cooled to 0 °C. H-L-Glu(OBzl)-OfBu\*HCl (**42**) (1.01 g, 3.06 mmol, 2.00 eq.) and triethylamine (531  $\mu$ L, 3.83 mmol, 2.50 eq.) were added and stirred for further five minutes at 0 °C. The reaction mixture was warmed to 45 °C and stirred for 41 h under argon atmosphere. As RP-HPLC/MS analysis revealed very low conversion (4.4% **43**, 44% **41**), again, H-L-Glu(OBzl)-OfBu\*HCl (**42**)

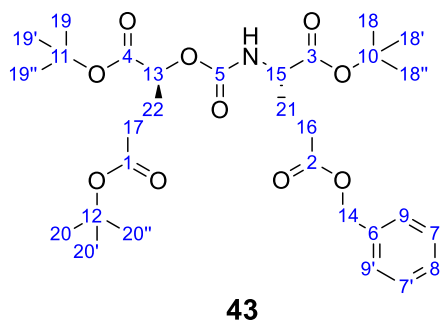
## MATERIALS AND METHODS

(1.01 g, 3.06 mmol, 2.00 eq.) and triethylamine (531  $\mu$ L, 3.83 mmol, 2.50 eq.) were added and the temperature was increased to 55  $^{\circ}$ C. Complete consumption of educt **41** was observed after 70.5 h at 55  $^{\circ}$ C under argon atmosphere. DCM was added for dilution of the reaction mixture and washed once with H<sub>2</sub>O (+ 1 mL brine). The aqueous phase was extracted two times with DCM, the combined organic layers were dried over Na<sub>2</sub>SO<sub>4</sub>, filtered and the solvent was removed under reduced pressure. The obtained crude product was purified by preparative RP-HPLC (70 - 80% B in 20 min, Method B, 5 mL/min), which gave 277 mg (31.3%) of compound **43** as a colorless oil.

RP-HPLC (40 - 95% B in 15 min, Method A, 1 mL/min):  $t_R$  = 12.6 min;  $k$  = 7.4. Calculated monoisotopic mass (C<sub>30</sub>H<sub>45</sub>NO<sub>10</sub>): 579.30, found:  $m/z$  = 412.3 [M(**43**)-3*t*Bu+H]<sup>+</sup>, 468.3 [M(**43**)-2*t*Bu+H]<sup>+</sup>, 524.4 [M(**43**)-*t*Bu+H]<sup>+</sup>, 580.5 [M(**43**)+H]<sup>+</sup>, 597.5 [M(**43**)+H<sub>2</sub>O+H]<sup>+</sup>, 602.5 [M(**43**)+Na]<sup>+</sup>, 618.5 [M(**43**)+K]<sup>+</sup>.



<sup>1</sup>H-NMR (300 MHz, CDCl<sub>3</sub>)  $\delta$ (ppm): 7.44 – 7.30 (m, 5H, H(1, 1', 1'', 1''', 1''')), 5.44 (d, <sup>3</sup> $J$  = 8.3 Hz, 1H, H(2)), 5.12 (s, 2H, H(3)), 4.84 (dd, <sup>3</sup> $J$  = 8.1, 4.6 Hz, 1H, H(4)), 4.27 (td, <sup>3</sup> $J$  = 8.2, 4.9 Hz, 1H, H(5)), 2.60 – 2.41 (m, 2H, H(6)), 2.41 – 2.28 (m, 2H, H(7)), 2.28 – 1.82 (m, 4H, H(8, 9)), 1.46 (s, 9H, H(10, 10', 10'')), 1.44 (s, 9H, H(11, 11', 11'')), 1.44 (s, 9H, H(12, 12', 12'')).

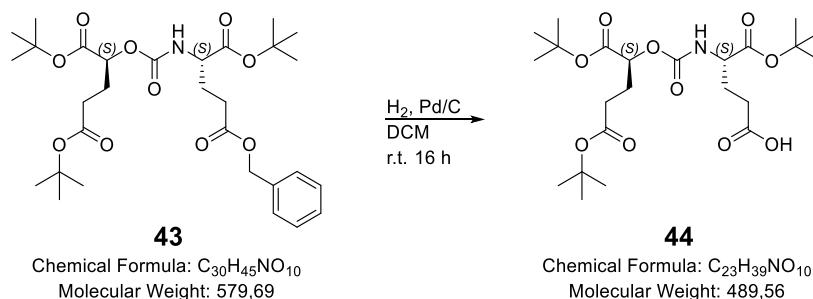


**43**

<sup>13</sup>C-NMR (75 MHz, CDCl<sub>3</sub>)  $\delta$ (ppm): 172.69 (s, 2C, C(1, 2)), 171.94 (s, 1C, C(3)), 170.95 (s, 1C, C(4)), 155.22 (s, 1C, C(5)), 136.02 (s, 1C, C(6)), 128.67 (s, 2C, C(7, 7')), 128.34 (s, 3C, C(8, 9, 9')), 82.71 (s, 1C, C(10)), 82.31 (s, 2C, C(11, 12)), 80.75 (s, 1C, C(13)), 66.57 (s, 1C, C(14)), 53.82 (s, 1C, C(15)), 31.24 (s, 1C, C(16)), 30.24 (s, 1C, C(17)), 28.23 (s, 3C, C(18, 18', 18'')), 28.12 (s, 3C, C(19, 19', 19'')), 28.09 (s, 3C, C(20, 20', 20'')), 26.80 (s, 2C, C(21, 22)).

## MATERIALS AND METHODS

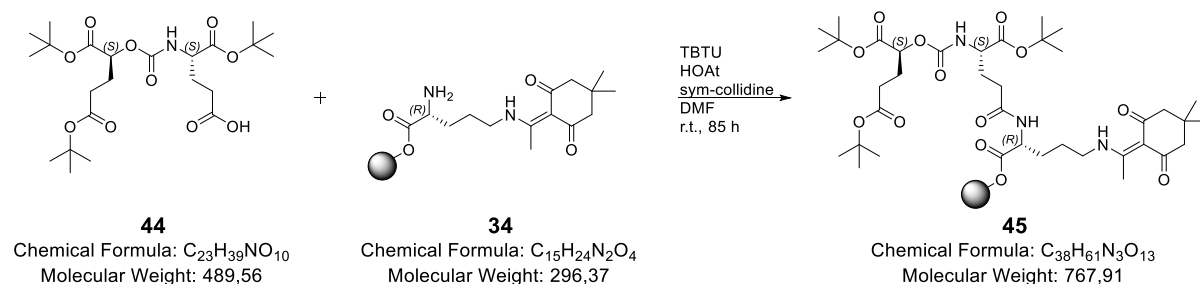
(*S*)-5-(*tert*-butoxy)-4-((((*S*)-1,5-di-*tert*-butoxy-1,5-dioxopentan-2-yl)oxy)carbonyl)amino)-5-oxopentanoic acid (**44**)



Compound **43** (139 mg, 0.24 mmol, 1.00eq.) was dissolved in 12 mL DCM and the solution was flushed 5 minutes with argon to remove dissolved oxygen. 25.5 mg of palladium on carbon (10% wt) (corresponds to 2.55 mg palladium, 24.0  $\mu$ mol, 0.10 eq.) were added and the flask was sealed with a rubber septum. Remaining air was displaced with argon and subsequently replaced by hydrogen gas. The mixture was stirred under hydrogen atmosphere at room temperature for 16 h. Palladium on carbon was filtered off, and the solvent was evaporated *in vacuo*. This afforded 59.2 mg (50.4%) of compound **44** as a colorless clear oil, which was used in the next step without further purification.

RP-HPLC (40 - 95% B in 15 min, Method A, 1 mL/min):  $t_R$  = 8.80 min;  $k$  = 4.9. Calculated monoisotopic mass (C<sub>23</sub>H<sub>39</sub>NO<sub>10</sub>): 489.26, found:  $m/z$  = 304.2 [M(**44**)-3*t*Bu-OH]<sup>+</sup>, 322.3 [M(**44**)-3*t*Bu+H]<sup>+</sup>, 378.3 [M(**44**)-2*t*Bu+H]<sup>+</sup>, 434.3 [M(**44**)-*t*Bu+H]<sup>+</sup>, 490.5 [M(**44**)+H]<sup>+</sup>, 507.5 [M(**44**)+H<sub>2</sub>O+H]<sup>+</sup>, 512.5 [M(**44**)+Na]<sup>+</sup>, 528.4 [M(**44**)+K]<sup>+</sup>.

[*S*-2-oxopentanedioic acid(O*t*Bu)<sub>2</sub>]-carbonyl-L-Glu-[*D*-Orn(Dde)-2-CT]-O*t*Bu (**45**)

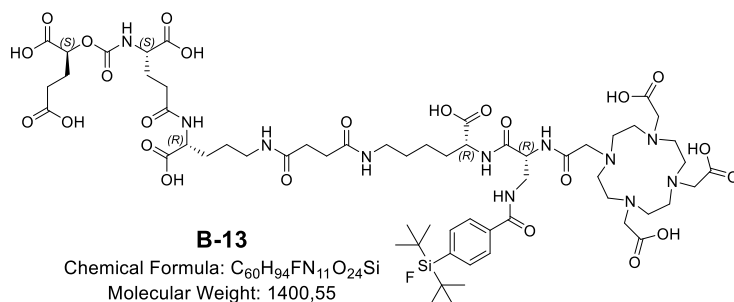


According to GP3, fragment **44** (59.2 mg, 0.12 mmol, 1.10 eq.) was coupled to resin-bound H-D-Orn(Dde) (**34**) (0.11 mmol 1.00 eq.), with TBTU (70.6 mg, 0.22 mmol, 2.00 eq.) and HOAt (29.9 mg, 0.22 mmol, 2.00 eq.) as coupling reagents and *sym*-collidine (131  $\mu$ L, 0.99 mmol, 9.00 eq.) as base. After shaking for 85 h at room temperature, formation of product **45** could be confirmed (GP7). Additionally, some resin beads were taken, treated for 20 minutes with 2% hydrazin/DMF (v/v) and analyzed via RP-HPLC/MS after a test cleavage according to GP8. Thus, stability of the carbamate moiety towards Dde-removal conditions was confirmed, as only one major peak (besides DMF) with the expected  $m/z$ -ratio of 604.6 occurred.

## MATERIALS AND METHODS

RP-HPLC (40 - 95% B in 15 min, Method A, 1 mL/min):  $t_R = 9.21$  min;  $k = 5.1$ . Calculated monoisotopic mass ( $C_{38}H_{61}N_3O_{13}$ ): 767.42, found:  $m/z = 768.7$  [ $M(\mathbf{45})+H$ ] $^+$ , 790.6 [ $M(\mathbf{45})+Na$ ] $^+$ , 806.6 [ $M(\mathbf{45})+K$ ] $^+$ .

### Carbamate **B-13**

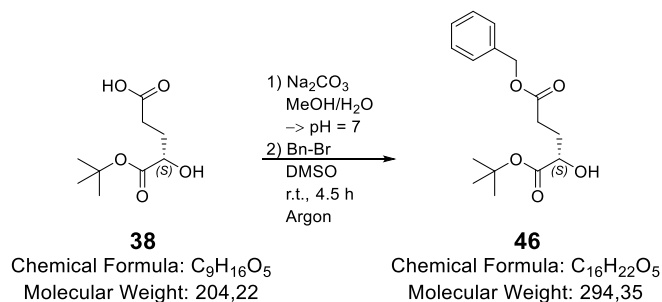


Further reactions on resin-bound compound **45** (0.11 mmol, 1.00 eq.) were performed according to standard Fmoc-SPPS on 2-CT resin, applying the above-mentioned methods (GP3 - GP8). For chelator attachment, DOTA\*6 H<sub>2</sub>O (56.4 mg, 0.11 mmol, 1.00 eq.), TBTU (29.3 mg, 91.7  $\mu$ mol, 0.83 eq.), HOAt (12.4 mg, 91.7  $\mu$ mol, 0.83 eq.) and *sym*-collidine (102  $\mu$ L, 0.77 mmol, 7.00 eq.) were dissolved in a mixture of DMF/DMSO (5/1, v/v) and incubated with the resin-bound amine for 28.5 h. As RP-HPLC/MS analysis (GP7) revealed no sufficient coupling, the resin was divided into two equivalent portions. One portion was again incubated with a freshly prepared DOTA-coupling mixture for 20 h. An only low rise in turnover led to a further DOTA-coupling step, now with DIPEA (101  $\mu$ L, 0.59 mmol, 10.7 eq.) instead of *sym*-collidine, in order to monitor and adjust the pH value to 9 - 10. After incubation for 68 h an adequate conversion was achieved and the peptide was cleaved off the resin with TFA/TIPS/H<sub>2</sub>O (GP9) and purified afterwards by preparative RP-HPLC (20 - 70% B in 20 min, Method B, 5 mL/min). Subsequent lyophilization afforded 6.30 mg (8.18%) of pure product **B-13** as a colorless powder. The second portion was cleaved off the resin with HFIP/DCM (GP11). Thereby, all acid-labile protective groups were retained. Crude product (48.0 mg, 39.0  $\mu$ mol, 1.00 eq.) was dissolved in 3.00 mL DMF and DOTA-NHS (32.5 mg, 43.0  $\mu$ mol, 1.10 eq.) as well as DIPEA (39.7  $\mu$ L, 0.23 mmol, 6.00 eq.) were added. The mixture was stirred at room temperature for 18 h. Preparative RP-HPLC (35 - 95% B in 15min, Method B, 1 mL/min) and subsequent lyophilization afforded 23.7 mg of the *tert*-butyl-functionalized peptide. Incubation with TFA/TIPS/DCM at 0 °C (slightly modified to GP9) for 1 h in total revealed 11.8 mg (21.5%) of pure product **B-13** after RP-HPLC purification (30 - 50% B in 15 min, Method B, 1 mL/min) and lyophilization. This resulted in an overall yield of 18.1 mg (13.8% yield, chemical purity > 98%) of carbamate **B-13**.

RP-HPLC (10 - 90% B in 15 min, Method A, 1 mL/min):  $t_R = 8.58$  min;  $k = 4.7$ . Calculated monoisotopic mass ( $C_{60}H_{94}FN_{11}O_{24}Si$ ): 1399.62, found:  $m/z = 701.0$  [ $M(\mathbf{B-13})+2H$ ] $^{2+}$ , 1400.9 [ $M(\mathbf{B-13})+H$ ] $^+$ , 1868.1 [ $M_4(\mathbf{B-13})+3H$ ] $^{3+}$ .

## MATERIALS AND METHODS

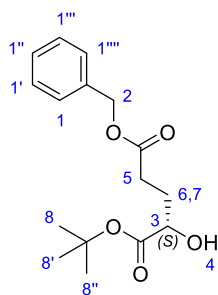
### 5-Benzyl 1-(*tert*-butyl) (*S*)-2-hydroxypentanedioate (**46**)



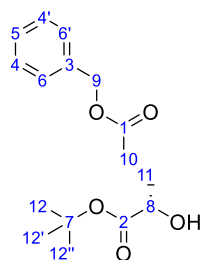
According to a previously published procedure by Shin *et al.*<sup>[297]</sup> with slight modifications, (*S*)-5-(*tert*-butoxy)-4-hydroxy-5-oxopentanoic acid (**38**) (crude product, 381 mg, 2.28 mmol, 1.00 eq.) was dissolved in 20.7 mL MeOH/H<sub>2</sub>O (10/1, v/v). The solution was stirred during continuous addition of aqueous 10% Na<sub>2</sub>CO<sub>3</sub>, which was terminated as soon as a pH value of 7 was reached (1.10 mL of 10% Na<sub>2</sub>CO<sub>3</sub> in total). All solvents were removed *in vacuo*, and the remaining residue was further dried by lyophilization, which afforded a slightly yellow solid. For the subsequent step, the used glassware was pretreated as described in GP12 (air- and moisture-free conditions) and also handling of reactants proceeded by the described methods (GP12). Lyophilized reactant **38** was dissolved in 11.4 mL dry DMSO and 5.70 mL thereof (1.14 mmol, 1.00 eq.) were transferred into a Schlenk flask. Benzyl bromide (203  $\mu\text{L}$ , 1.71 mmol, 1.50 eq.) was added and the reaction mixture was stirred at room temperature for 4.5 h under argon atmosphere. Afterwards, the reaction was quenched with H<sub>2</sub>O, the mixture was extracted with Et<sub>2</sub>O (3 $\times$ ). The organic phase was washed once with H<sub>2</sub>O, dried over Na<sub>2</sub>SO<sub>4</sub>, filtered and the solvent removed under reduced pressure. The obtained crude product was purified by preparative RP-HPLC (20 - 80% B in 20 min, Method C, 5 mL/min). Subsequent lyophilization afforded 178 mg (53.2%) of pure product **46** as a colorless solid.

RP-HPLC (10 - 90% B in 15 min, Method A, 1 mL/min):  $t_R = 15.7$  min;  $k = 9.5$ . Calculated monoisotopic mass (C<sub>16</sub>H<sub>22</sub>O<sub>5</sub>): 294.15, found:  $m/z = 239.1$  [M(**46**)-*t*Bu+H]<sup>+</sup>, 262.2 [M(**46**)-*t*Bu+Na]<sup>+</sup>, 280.2 [M(**46**)-*t*Bu+MeCN+H]<sup>+</sup>, 295.2 [M(**46**)+H]<sup>+</sup>, 317.2 [M(**46**)+Na]<sup>+</sup>, 333.2 [M(**46**)+K]<sup>+</sup>, 358.3 [M(**46**)+MeCN+Na]<sup>+</sup>.

## MATERIALS AND METHODS



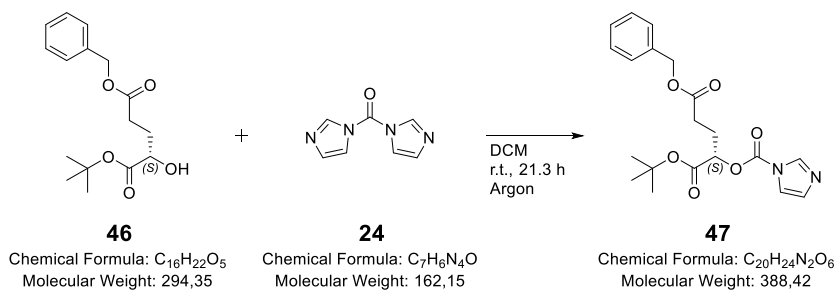
$^1\text{H-NMR}$  (300 MHz,  $\text{CDCl}_3$ )  $\delta$ (ppm): 7.38 – 7.32 (m, 5H, H(1, 1', 1'', 1''', 1''')), 5.13 (s, 2H, H(2)), 4.09 (dd,  $^3J = 7.9, 4.1$  Hz, 1H, H(3)), 2.87 (s, 1H, H(4)), 2.63 – 2.39 (m, 2H, H(5)), 2.16 (*virt.* dddd, 1H, H(6)), 1.98 – 1.81 (m, 1H, H(7)), 1.48 (s, 9H, H(8, 8', 8'')).



$^{13}\text{C-NMR}$  (75 MHz,  $\text{CDCl}_3$ )  $\delta$ (ppm): 174.04 (s, 1C, C(1)), 173.16 (s, 1C, C(2)), 136.06 (s, 1C, C(3)), 128.69 (s, 2C, C(4, 4')), 128.36 (s, 1C, C(5)), 128.32 (s, 2C, C(6, 6')), 82.96 (s, 1C, C(7)), 69.73 (s, 1C, C(8)), 66.49 (s, 1C, C(9)), 29.91 (s, 1C, C(10)), 29.63 (s, 1C, C(11)), 28.15 (s, 3C, C(12, 12', 12'')).

**46**

### 5-benzyl 1-(*tert*-butyl) (*S*)-2-((1*H*-imidazole-1-carbonyl)oxy)pentanedioate (**47**)

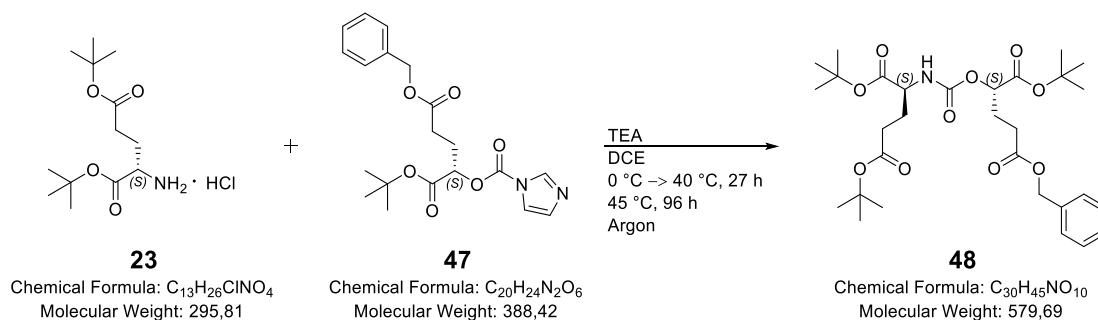


Compound **47** was synthesized in analogy to a previously published procedure by Yang *et al.*<sup>[293]</sup> with some minor modifications. 5-benzyl 1-(*tert*-butyl) (*S*)-2-hydroxypentanedioate (**46**) (71.6 mg, 0.24 mmol, 1.00 eq.) was dissolved in 4 mL dry DCM and stirred at room temperature. 1,1'-Carbonyldiimidazole (**24**) (74.5 mg, 0.46 mmol, 1.92 eq.) was dissolved in 1 mL dry DCM and added to the solution, which was stirred under argon atmosphere for 21.3 h at room temperature. The reaction mixture was diluted with DCM and washed once with  $\text{H}_2\text{O}$  (+ 1 mL brine). The aqueous phase was extracted two times with DCM, the combined organic phases were dried over  $\text{Na}_2\text{SO}_4$ , filtered and the solvent evaporated *in vacuo*. This afforded 112 mg (> 99%) of crude product as slightly yellowish oil. RP-HPLC/MS control revealed nearly complete conversion to product **47**, which was used in the next step without further purification.

RP-HPLC (40 - 100% B in 15 min, Method A, 1 mL/min):  $t_R = 10.1$  min;  $k = 5.7$ . Calculated monoisotopic mass ( $\text{C}_{20}\text{H}_{24}\text{N}_2\text{O}_6$ ): 388.16, found:  $m/z = 389.2$  [ $\text{M}(\mathbf{47})+\text{H}$ ] $^+$ , 839.5 [ $\text{M}_2(\mathbf{47})+\text{MeCN}+\text{Na}$ ] $^+$ .

## MATERIALS AND METHODS

### 5-benzyl 1-(*tert*-butyl) (*S*)-2-(((*S*)-1,5-di-*tert*-butoxy-1,5-dioxopentan-2-yl)carbamoyl)oxy)pentane-dioate (**48**)

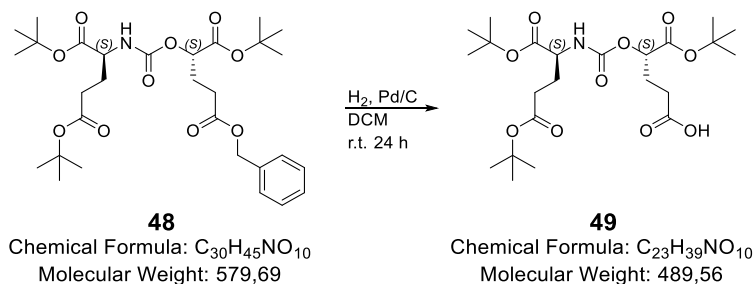


Compound **48** was synthesized in analogy to a previously published procedure by Weineisen *et al.*<sup>[199]</sup> with some minor modifications. 5-benzyl 1-(*tert*-butyl) (*S*)-2-((1*H*-imidazole-1-carbonyl)oxy)pentanedioate (**47**) (93.2 mg, 0.24 mmol, 1.00 eq.) was dissolved in 2.50 mL DCE and cooled to 0 °C. H-L-Glu(*O**t*Bu)-*O**t*Bu\*HCl (**23**) (142 mg, 0.48 mmol, 2.00 eq.) and triethylamine (83.2 μL, 0.60 mmol, 2.50 eq.) were added and stirred for further five minutes at 0 °C. The reaction mixture was warmed to 40 °C and stirred for 27 h under argon atmosphere. As RP-HPLC/MS analysis revealed very low conversion (7% **48**, 90.7% **47**), again, H-L-Glu(*O**t*Bu)-*O**t*Bu\*HCl (**23**) (284 mg, 0.96 mmol, 4.00 eq.) and triethylamine (166 μL, 1.20 mmol, 5.00 eq.) were added and the temperature was increased to 45 °C. Complete consumption of educt **47** was observed after 96 h at 45 °C under argon atmosphere. DCM was added for dilution of the reaction mixture, which was once washed with H<sub>2</sub>O (+ 1 mL brine). The aqueous phase was extracted two times with DCM, the combined organic layers were dried over Na<sub>2</sub>SO<sub>4</sub>, filtered and the solvent was removed under reduced pressure. The obtained crude product was purified by flash chromatography (65 - 98% B in 10 min, Method D, 12 mL/min), which gave 84.1 mg (60.5%) of compound **48** as a colorless viscous oil.

RP-HPLC (40 - 100% B in 15 min, Method A, 1 mL/min):  $t_R = 16.9$  min;  $k = 10$ . Calculated monoisotopic mass (C<sub>30</sub>H<sub>45</sub>NO<sub>10</sub>): 579.30, found:  $m/z = 602.1$  [M(**48**)+Na]<sup>+</sup>, 618.2 [M<sub>2</sub>(**48**)+K]<sup>+</sup>.

## MATERIALS AND METHODS

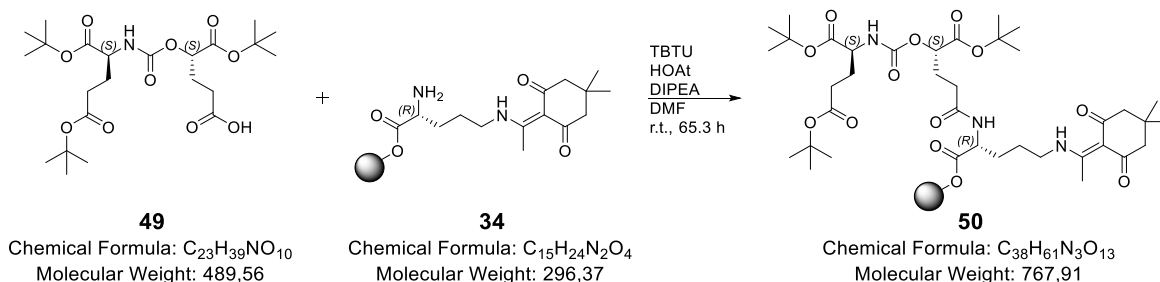
### (S)-5-(tert-butoxy)-4-(((S)-1,5-di-tert-butoxy-1,5-dioxopentan-2-yl)carbamoyl)oxy)-5-oxopentanoic acid (**49**)



Compound **48** (84.1 mg, 0.15 mmol, 1.00eq.) was dissolved in 6.20 mL DCM and the solution was flushed 5 minutes with argon to remove dissolved oxygen. 16.0 mg of palladium on carbon (10% wt) (corresponds to 1.60 mg palladium, 15.0  $\mu$ mol, 0.10 eq.) were added and the flask was sealed with a rubber septum. Remaining air was displaced with argon and subsequently replaced by hydrogen gas. The mixture was stirred under hydrogen atmosphere at room temperature for 24 h. Palladium on carbon was filtered off, and the solvent was evaporated *in vacuo*. This afforded 85.5 mg (> 99%) of compound **49** as a colorless clear oil, which was used in the next step without further purification.

RP-HPLC (40 - 100% B in 15 min, Method A, 1 mL/min):  $t_R$  = 11.6 min;  $k$  = 6.7. Calculated monoisotopic mass (C<sub>23</sub>H<sub>39</sub>NO<sub>10</sub>): 489.26, found:  $m/z$  = 304.1 [M(**49**)-3*t*Bu-OH]<sup>+</sup>, 322.1 [M(**49**)-3*t*Bu+H]<sup>+</sup>, 378.2 [M(**49**)-2*t*Bu+H]<sup>+</sup>, 434.2 [M(**49**)-*t*Bu+H]<sup>+</sup>, 490.4 [M(**49**)+H]<sup>+</sup>, 512.3 [M(**49**)+Na]<sup>+</sup>, 528.4 [M(**49**)+K]<sup>+</sup>.

### L-Glu(O*t*Bu)<sub>2</sub>-carbonyl-[(S)-2-oxopentanedioic acid-(D-Orn(Dde)-2-CT)-O*t*Bu] (**50**)

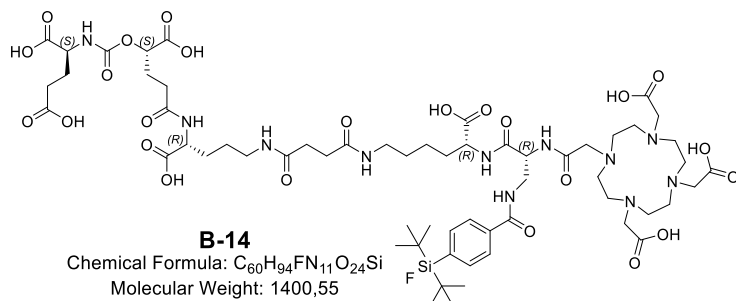


According to GP3, fragment **49** (73.4 mg, 0.15 mmol, 1.00 eq.) was coupled to resin bound H-D-Orn(Dde) (**34**) with TBTU (110 mg, 0.34 mmol, 2.29 eq.) and HOAt (46.8 mg, 0.34 mmol, 2.29 eq.) as coupling reagents and DIPEA (264  $\mu$ L, 1.55 mmol, 10.3 eq.) as base. After shaking for 65.3 h at room temperature, formation of product **50** could be confirmed (GP7). Additionally, some resin beads were taken, treated for 20 minutes with 2% hydrazin/DMF (v/v) and analyzed via RP-HPLC/MS after a test cleavage according to GP7. Thus, stability of the carbamate moiety towards Dde-removal conditions was confirmed, as only one major peak (besides DMF) with the expected  $m/z$ -ratio of 604 occurred.

## MATERIALS AND METHODS

RP-HPLC (10 - 90% B in 15 min, Method A, 1 mL/min) for **50(-3fBu)**:  $t_R = 10.1$  min;  $k = 5.7$ . Calculated monoisotopic mass for **50(-3fBu)** ( $C_{26}H_{37}N_3O_{13}$ ): 599.23, found:  $m/z = 600.5$   $[M(\mathbf{50})-3fBu+H]^+$ , 662.3  $[M(\mathbf{50})-3fBu+MeCN+Na]^+$ .

### Carbamate **B-14**

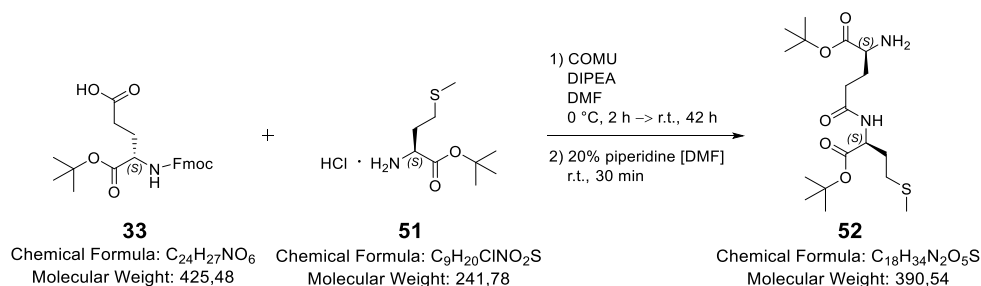


Further reactions on resin-bound compound **50** (0.15 mmol, 1.00 eq.) were performed according to standard Fmoc-SPPS on 2-CT resin, applying the above-mentioned methods (GP3 - GP8). For chelator attachment, DOTA\*6  $H_2O$  (87.1 mg,

0.17 mmol, 1.13 eq.), TBTU (45.0 mg, 0.15 mmol, 1.00 eq.), HOAt (19.1 mg, 0.15 mmol, 1.00 eq.) and *sym*-collidine (160  $\mu$ L, 1.20 mmol, 8.00 eq.) were dissolved in a mixture of DMF/DMSO (5/1, v/v) and incubated with the resin-bound amine for 19.5 h. As RP-HPLC/MS analysis (GP7) revealed successful coupling, the peptide was cleaved off the resin with TFA/TIPS/DCM (GP9) and purified afterwards by preparative RP-HPLC (35 - 45% B in 20 min, Method B, 5 mL/min). Subsequent lyophilization afforded 8.35 mg (3.98%) of pure product **B-14** as a colorless powder.

RP-HPLC (10 - 90% B in 15 min, Method A, 1 mL/min):  $t_R = 13.7$  min;  $k = 8.1$ . Calculated monoisotopic mass ( $C_{60}H_{94}FN_{11}O_{24}Si$ ): 1399.62, found:  $m/z = 701.1$   $[M(\mathbf{B-14})+2H]^{2+}$ , 1400.6  $[M(\mathbf{B-14})+H]^+$ .

### *H-L-Glu(L-Met-OtBu)-OtBu* (**52**)



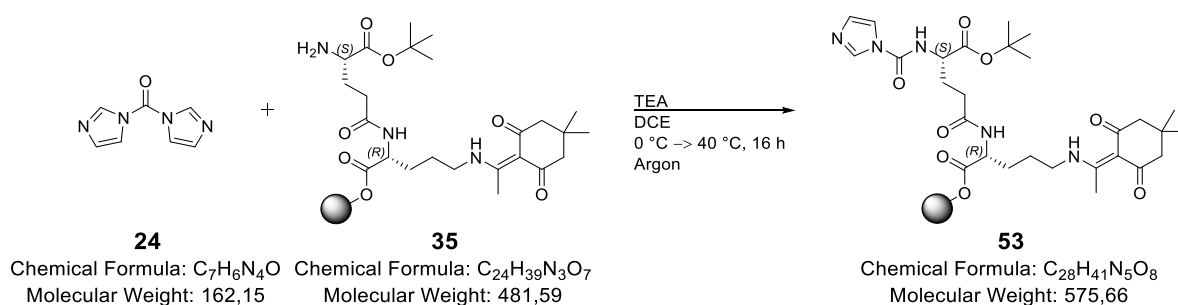
Fmoc-L-Glu-OtBu (**33**) (3.00 g, 7.05 mmol, 1.10 eq.) was dissolved in 40.1 mL DMF and cooled to 0 °C. COMU (3.02 g, 7.05 mmol, 1.10 eq) and DIPEA (5.27 mL, 31.0 mmol, 4.84 eq.) were added to reach a basic pH of 10. H-L-Met-OtBu\*HCl (**51**) (1.55 g, 6.41 mmol, 1.00 eq.) was added and the reaction mixture was stirred for further 2 h at 0 °C. The ice bath was removed and the solution was stirred at room temperature for 42 h. The reaction was terminated by addition of  $H_2O$  and diluted with  $Et_2O$ . The aqueous phase was extracted three times with  $Et_2O$  and the combined organic phases were then washed once with saturated  $NaHCO_3$  and brine. The organic layer was dried over  $Na_2SO_4$ , filtered and the solvent was removed under reduced pressure. As RP-HPLC/MS analysis revealed dipeptide Fmoc-**52** to be the main portion of the crude product,

## MATERIALS AND METHODS

5 mL of 20% piperidine (DMF) were added and stirred for 30 min at room temperature. As the dibenzofulvene-piperidine by-product could not be removed sufficiently by preparative RP-HPLC (35 - 60% B in 20 min, Method B), it was removed by column chromatography (n-Hex/EtOAc = 3/2). Afterwards, the solvent was changed (DCM/MeOH/acetone = 5/1/1) by which an adequate separation of product **52** from all remaining by-products was possible. This afforded 287 mg (11.5%) of pure product **52** as a clear, yellow oil.

RP-HPLC (10 - 90% B in 15 min, Method A, 1 mL/min):  $t_R = 9.37$  min;  $k = 5.2$ . Calculated monoisotopic mass ( $C_{18}H_{34}N_2O_5S$ ): 390.22, found:  $m/z = 391.5$  [ $M(\mathbf{52})+H$ ] $^+$ , 782.0 [ $M_2(\mathbf{52})+H$ ] $^+$ .  $R_f$ -value: 0.64 (DCM/MeOH/acetone = 5/1/1).

### 1-Carbonylimidazole-L-Glu[D-Orn(Dde)-2-CT]-OtBu (**53**)

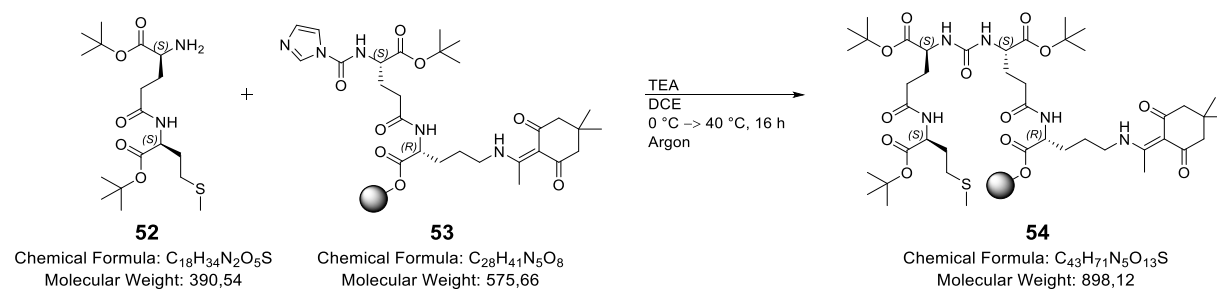


Compound **35** was transferred into a round bottom flask, where it was dissolved in 3.81 mL DCE. At 0 °C triethylamine (146  $\mu$ L, 1.05 mmol, 2.50 eq.) and 1,1'-carbonyldiimidazole (**24**) (68.1 mg, 0.42 mmol, 1.00 eq.) were added and the mixture was stirred for further 5 min at 0 °C. Afterwards, it was warmed to 40 °C and stirred for 16 h under argon atmosphere. The resin was washed with DCM (4x) and again dried in a desiccator for 30 min. Some resin beads were taken and treated with HFIP/DCM (1/4) according to GP8. RP-HPLC/MS analysis revealed nearly complete conversion to product **53**.

RP-HPLC (10 - 90% B in 15 min, Method A, 1 mL/min):  $t_R = 8.24$  min;  $k = 4.5$ . Calculated monoisotopic mass ( $C_{28}H_{41}N_5O_8$ ): 575.30, found:  $m/z = 452.4$  [ $M(\mathbf{53})$ -imidazole-*t*Bu+H] $^+$ , 508.5 [ $M(\mathbf{53})$ -imidazole] $^{++}$ , 576.6 [ $M(\mathbf{53})+H$ ] $^+$ .

## MATERIALS AND METHODS

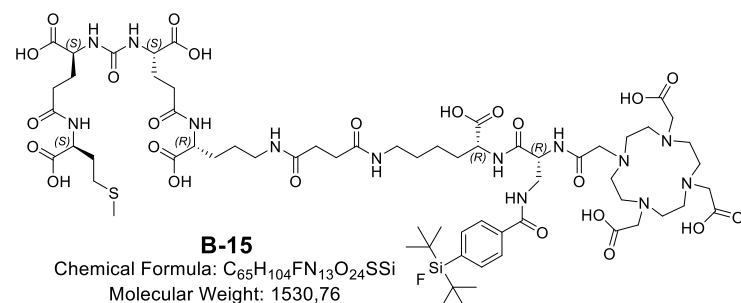
### *L*-Glu(*L*-Met-*O*tBu)-*O*tBu-carbonyl-*L*-Glu[*D*-Orn(*Dde*)-2-CT]-*O*tBu (**54**)



Compound **54** was synthesized in analogy to a previously published procedure by Weineisen *et al.*<sup>[199]</sup> with some minor modifications. The H-*L*-Glu(*L*-Met-*O*tBu)-*O*tBu dipeptide **52** (246 mg, 0.63 mmol, 1.50 eq.) was dissolved in 3.81 mL DCE and added to compound **53** (0.42 mmol, 1.00 eq.). At 0 °C triethylamine (146  $\mu$ L, 1.05 mmol, 2.50 eq.) was added and the mixture was stirred for further five minutes at 0 °C. The solution was warmed to 40 °C and stirred for 16 h under argon atmosphere. The resin was transferred to a syringe for peptide synthesis (equipped with a frit, pore size 25  $\mu$ m) and washed with DCM (4 $\times$ ). Some resin beads were taken according to GP8 and analyzed via RP-HPLC/MS, which indicated nearly complete conversion to **54**.

RP-HPLC (10 - 90% B in 15 min, Method A, 1 mL/min):  $t_R = 13.2$  min;  $k = 7.8$ . Calculated monoisotopic mass ( $C_{43}H_{71}N_5O_{13}S$ ): 897.48, found:  $m/z = 450.2$  [ $M(\mathbf{54})+2H$ ] $^{2+}$ , 470.7 [ $M(\mathbf{54})+MeCN+2H$ ] $^{2+}$ , 899.2 [ $M(\mathbf{54})+H$ ] $^+$ .

### Proinhibitor **B-15**



Further reactions on resin-bound compound **54** (0.42 mmol, 1.00 eq.) were performed according to standard Fmoc-SPPS on 2-CT resin, applying the above-mentioned methods (GP3 - GP8). Due to extensive oxidation and other side

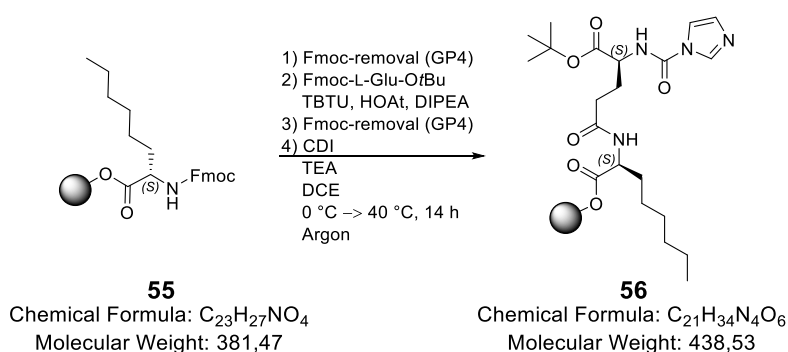
reactions, some test reactions were performed with a minor part (0.09 mmol) of the resin for optimization of SiFA-BA and DOTA coupling. Hence, further reactions were conducted on the remaining part (0.33 mmol) and all following equivalents refer to this amount of substance. The SiFA-BA moiety was attached via the Pfp-ester, which was generated previously by preactivation of SiFA-BA (93.1 mg, 0.33 mmol, 1.00 eq.) with pentafluorophenol (104  $\mu$ L, 0.99 mmol, 3.00 eq.), DIC (153  $\mu$ L, 0.99 mmol, 3.00 eq.) and pyridine (214  $\mu$ L, 2.64 mmol, 8.00 eq.) in DMF for 1.5 h. The solution was added to the resin-bound peptide and incubated for 22 h prior to Fmoc protective group removal (GP4). For chelator attachment, DOTA-NHS (276 mg, 0.36 mmol, 1.10 eq.) and DIPEA (437  $\mu$ L, 2.57 mmol, 7.79 eq.) were each dissolved in DMF. First, DIPEA in DMF was added to the resin for preactivation. After five minutes, DOTA-NHS in DMF was added and incubated with

## MATERIALS AND METHODS

the resin-bound amine for 21 h. An adequate conversion (RP-HPLC/MS after GP8) was achieved and the peptide was cleaved off the resin under argon atmosphere with TFA/TIPS/DCM/dithiothreitol (95/2.5/2.5/0.5% wt, slightly modified to GP9) (3 × 30 min) and purified afterwards by preparative RP-HPLC (30 - 60% B in 20 min, Method B and 33 - 40% B in 15 min, Method A). Subsequent lyophilization afforded 0.39 mg (0.08%) of pure product **B-15** as a colorless powder.

RP-HPLC (10 - 90% B in 15 min, Method A, 1 mL/min):  $t_R = 8.62$  min;  $k = 4.7$ . Calculated monoisotopic mass ( $C_{65}H_{104}FN_{13}O_{24}SSi$ ): 1529.68, found:  $m/z = 765.8$   $[M(\mathbf{B-15})+2H]^{2+}$ , 1531.5  $[M(\mathbf{B-15})+H]^+$ .

### 1-Carbonylimidazole-L-Glu(L-2-Aoc-2-CT)-OtBu (**56**)

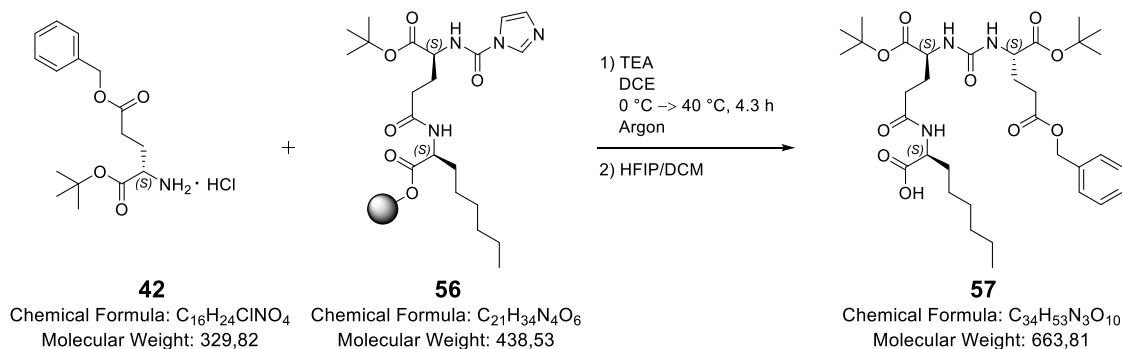


Fmoc-L-2-Aminooctanoic acid was coupled to 2-CTC resin according to GP2. Further reactions on resin-bound compound **55** (load: 0.72 mmol/g, 0.86 mmol, 1.00 eq.) were performed according to standard Fmoc-SPPS on 2-CT resin, applying the above-mentioned methods (GP3 & GP4). In brief, the Fmoc protective group was removed (GP4) and Fmoc-L-Glu-OtBu (549 mg, 1.29 mmol, 1.50 eq.) was coupled (GP3) over a period of 16 h using TBTU (552 mg, 1.72 mmol, 2.00 eq.), HOAt (234 mg, 1.72 mmol, 2.00 eq.) and DIPEA (658  $\mu$ L, 3.87 mmol, 4.50 eq.). After removal of the Fmoc protective group (GP4), the resin was dried in a desiccator for 30 min and transferred into a round bottom flask, where it was dissolved in 7.81 mL DCE. At 0 °C, triethylamine (298  $\mu$ L, 2.15 mmol, 2.50 eq.) and 1,1'-carbonyldiimidazole (154 mg, 0.95 mmol, 1.10 eq.) were added and the mixture was stirred for further 5 min at 0 °C. Afterwards, it was warmed to 40 °C and stirred for 14 h under argon atmosphere. The resin was washed with DCM (4×) and again dried in a desiccator for 30 min. Some resin beads were taken and treated with TFA according to GP7. RP-HPLC/MS revealed nearly complete conversion to product **56**.

RP-HPLC (10 - 90% B in 15 min, Method A, 1 mL/min):  $t_R = 9.61$  min;  $k = 5.4$ . Calculated monoisotopic mass ( $C_{21}H_{34}N_4O_6$ ): 438.25, found:  $m/z = 439.3$   $[M(\mathbf{56})+H]^+$ , 480.4  $[M(\mathbf{56})+MeCN+H]^+$ .

## MATERIALS AND METHODS

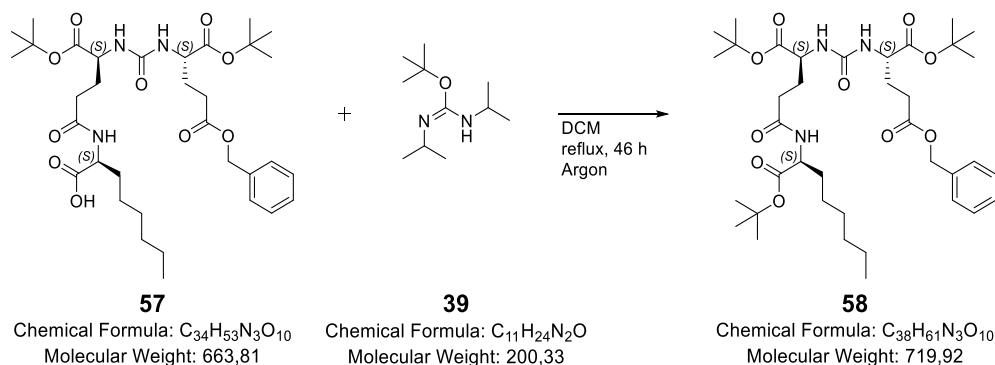
### (6*S*,10*S*,15*S*)-6,10-bis(*tert*-butoxycarbonyl)-15-hexyl-3,8,13-trioxo-1-phenyl-2-oxa-7,9,14-triazahexadecan-16-oic acid (**57**)



Compound **57** was synthesized in analogy to a previously published procedure by Weisen et al.<sup>[199]</sup> with some minor modifications. Resin-bound **56** (0.86 mmol, 1.00 eq.) was dissolved in 7.81 mL DCE and cooled to 0 °C. H-L-Glu(OBzl)-OtBu·HCl (**42**) (425 mg, 1.29 mmol, 1.50 eq.) and triethylamine (298  $\mu$ L, 2.15 mmol, 2.50 eq.) were added and stirred for further five minutes at 0 °C. The reaction mixture was warmed to 40 °C and stirred for 4.3 h under argon atmosphere. The resin was transferred to a syringe for peptide synthesis (equipped with a frit, pore size 25  $\mu$ m) and washed with DCM (4x). Some resin beads were taken according to GP8 and analyzed via RP-HPLC, which indicated nearly complete conversion to **57**. The dried resin was treated with a mixture of HFIP/DCM (GP11). The resulting yellow oil was used in the next step without further purification (81.8 mg, 14.3%).

RP-HPLC (10 - 90% B in 15 min, Method A, 1 mL/min):  $t_R$  = 15.7 min;  $k$  = 9.5. Calculated monoisotopic mass (C<sub>34</sub>H<sub>53</sub>N<sub>3</sub>O<sub>10</sub>): 663.37, found:  $m/z$  = 552.4 [M(**57**)-2*t*Bu+H]<sup>+</sup>, 608.5 [M(**57**)-*t*Bu+H]<sup>+</sup>, 664.6 [M(**57**)+H]<sup>+</sup>.

### 5-benzyl 1-(*tert*-butyl) (((*S*)-1-(*tert*-butoxy)-5-(((*S*)-1-(*tert*-butoxy)-1-oxooctan-2-yl)amino)-1,5-dioxo-pentan-2-yl)carbamoyl)-L-glutamate (**58**)



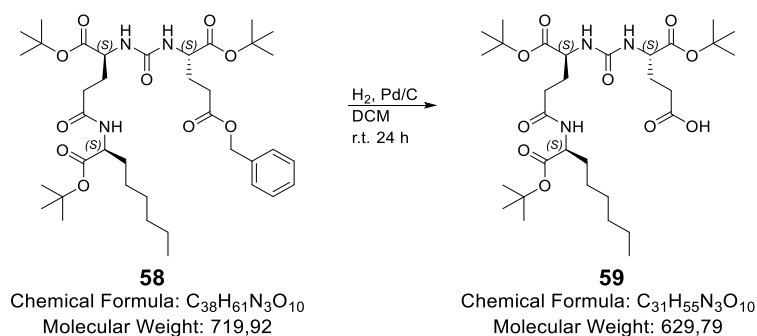
Compound **58** was synthesized in analogy to a previously published procedure by Bergmeier et al.<sup>[296]</sup> with some minor modifications. Glassware and reagents were handled under air- and moisture-free conditions (GP12). Lyophilized educt **57** (crude product, ~ 81.8 mg, 0.12 mmol, 1.00 eq.) was dissolved in 2 mL dry DCM and the first portion of

## MATERIALS AND METHODS

*O*-*tert*-butyl-*N,N'*-diisopropylisourea (**39**) (40.1  $\mu$ L, 0.18 mmol, 1.50 eq.) was added. The reaction mixture was stirred under reflux ( $\sim 42$   $^{\circ}$ C) and argon atmosphere for 22 h. A second portion of **39** (200  $\mu$ L, 0.90 mmol, 7.49 eq.) was added and also DCM, in order to keep the solvent amount constantly between 2 and 3 mL. After stirring for further 24 h at reflux temperature and under argon atmosphere, the reaction was terminated by diluting the suspension with DCM. Solid by-products were removed by filtration and the organic layer was washed once with H<sub>2</sub>O. The aqueous phase was extracted twice with DCM. The combined organic phases were transferred into a round bottom flask and the solvent removed under reduced pressure. Purification by preparative RP-HPLC (70 - 90% B in 20 min, Method C, 5 mL/min) provided 41.4 mg (48%) of compound **58** as a colorless solid.

RP-HPLC (10 - 90% B in 15 min, Method A, 1 mL/min):  $t_R = 19.2$  min;  $k = 11.8$ . Calculated monoisotopic mass (C<sub>38</sub>H<sub>61</sub>N<sub>3</sub>O<sub>10</sub>): 719.44, found:  $m/z = 720.6$  [M(**58**)+H]<sup>+</sup>, 742.6 [M(**58**)+Na]<sup>+</sup>, 758.6 [M(**58**)+K]<sup>+</sup>.

(5*S*, 10*S*, 14*S*)-10,14-bis(*tert*-butoxycarbonyl)-5-hexyl-2,2-dimethyl-4,7,12-trioxo-3-oxa-6,11,13-triazaheptadecan-17-oic acid (**59**)

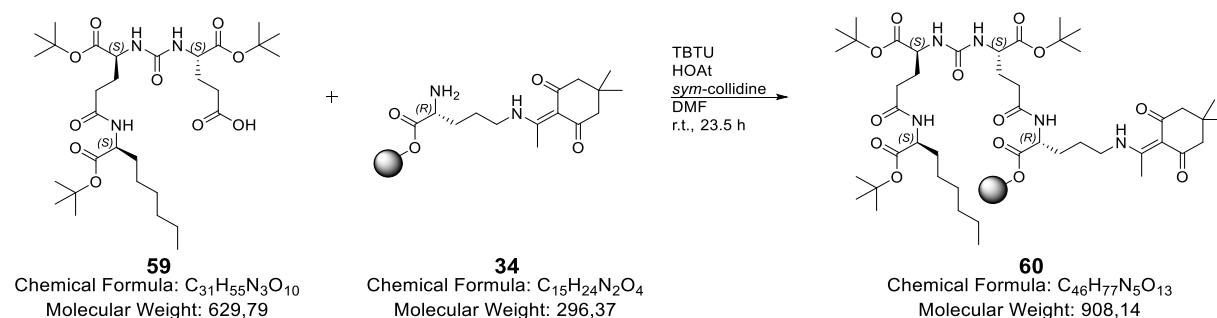


Compound **58** (41.4 mg, 57.5  $\mu$ mol, 1.00 eq.) was dissolved in 6 mL DCM and the solution was flushed five minutes with argon to remove dissolved oxygen. 6.12 mg of palladium on carbon (10% wt) (corresponds to 0.61 mg palladium, 5.75  $\mu$ mol, 0.10 eq.) were added and the flask was sealed with a rubber septum. Remaining air was displaced with argon and subsequently replaced by hydrogen gas. The mixture was stirred under hydrogen atmosphere at room temperature for 24 h. Palladium on carbon was filtered off, and the solvent was evaporated *in vacuo*. This afforded 35.5 mg (98.1%) of compound **59** as a colorless clear oil, which was used in the next step without further purification.

RP-HPLC (10 - 90% B in 15 min, Method A, 1 mL/min):  $t_R = 15.8$  min;  $k = 9.5$ . Calculated monoisotopic mass (C<sub>31</sub>H<sub>55</sub>N<sub>3</sub>O<sub>10</sub>): 629.39, found:  $m/z = 630.5$  [M(**59**)+H]<sup>+</sup>, 652.5 [M(**59**)+Na]<sup>+</sup>.

## MATERIALS AND METHODS

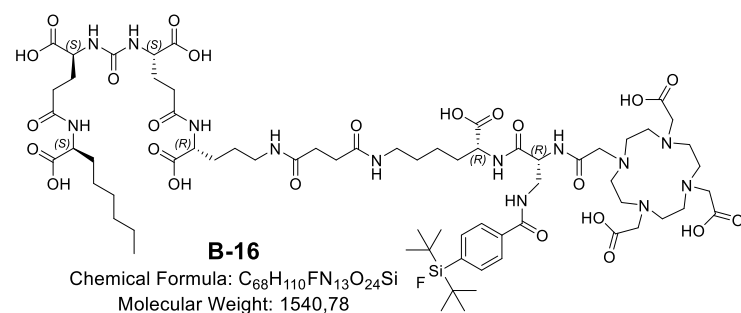
### *L*-Glu(*L*-2-Aoc-OtBu)-OtBu-carbonyl-*L*-Glu[D-Orn(Dde)-2-CT]-OtBu (**60**)



According to GP3, fragment **59** (35.5 mg, 56.4  $\mu$ mol, 1.00 eq.) was coupled to resin-bound H-D-Orn(Dde) (**34**) (81.2  $\mu$ mol 1.44 eq.), with TBTU (36.2 mg, 0.11 mmol, 2.00 eq.) and HOAt (15.0 mg, 0.11 mmol, 2.00 eq.) as coupling reagents and *sym*-collidine (67.7  $\mu$ L, 0.51 mmol, 9.00 eq.) as base. After shaking for 23.5 h at room temperature, formation of product **60** could be confirmed (GP8), as only one major peak with the expected *m/z*-ratio of 908.4 occurred.

RP-HPLC (40 - 95% B in 15 min, Method A, 1 mL/min):  $t_R$  = 12.7 min;  $k$  = 7.5. Calculated monoisotopic mass (C<sub>46</sub>H<sub>77</sub>N<sub>5</sub>O<sub>13</sub>): 907.55, found:  $m/z$  = 454.8 [M(**60**)+2H]<sup>2+</sup>, 908.4 [M(**60**)+H]<sup>+</sup>.

### Proinhibitor **B-16**



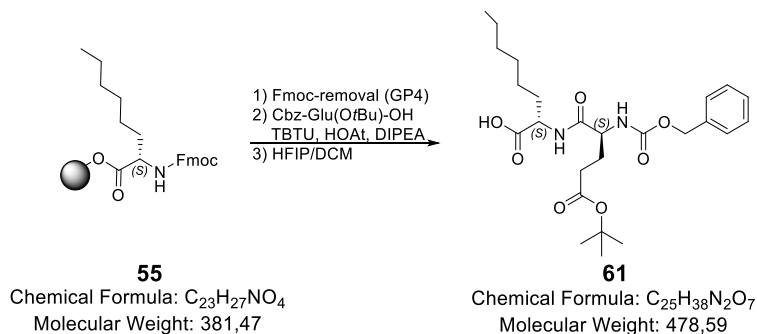
Further reactions on resin-bound compound **60** (81.5  $\mu$ mol, 1.00 eq.) were performed according to standard Fmoc-SPPS on 2-CT resin, applying the above-mentioned methods (GP3 - GP8). For chelator attachment, DOTA-NHS (67.8 mg,

89.6  $\mu$ mol, 1.10 eq.) and DIPEA (118  $\mu$ L, 0.69 mmol, 8.47 eq.) were each dissolved in DMF. First, DIPEA in DMF was added to the resin for preactivation. After five minutes, DOTA-NHS in DMF was added and incubated with the resin-bound amine for 23.2 h. An adequate conversion (RP-HPLC/MS analysis after GP7) was achieved and the peptide was cleaved off the resin with TFA/TIPS/DCM (GP9) and purified afterwards by preparative RP-HPLC (40 - 70% B in 20 min, Method B, 5 mL/min). Subsequent lyophilization afforded 20.0 mg (16.0% yield, chemical purity > 99%) of pure product **B-16** as a colorless powder.

RP-HPLC (10 - 90% B in 15 min, Method A, 1 mL/min):  $t_R$  = 9.44 min;  $k$  = 5.5. Calculated monoisotopic mass (C<sub>68</sub>H<sub>110</sub>FN<sub>13</sub>O<sub>24</sub>Si): 1539.75, found:  $m/z$  = 770.5 [M(**B-16**)+2H]<sup>2+</sup>, 1539.9 [M(**B-16**)+H]<sup>+</sup>, 1924.9 [M<sub>5</sub>(**B-16**)+4H]<sup>4+</sup>.

## MATERIALS AND METHODS

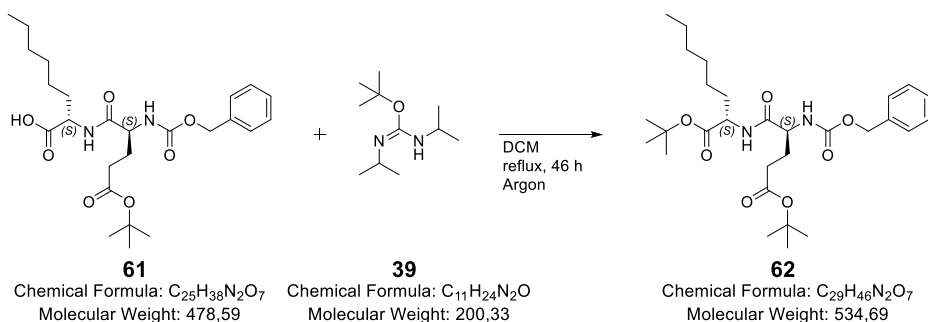
### (S)-2-((S)-2-(((benzyloxy)carbonyl)amino)-5-(tert-butoxy)-5-oxopentanamido)octanoic acid (**61**)



Fmoc-L-2-Amino-octanoic acid was coupled to 2-CTC resin according to GP2. Further reactions on resin-bound compound **55** (load: 0.59 mmol/g, 0.63 mmol, 1.00 eq., n = 3) were performed according to standard Fmoc-SPPS on 2-CT resin, applying the above-mentioned methods (GP3 & GP4). In brief, the Fmoc protective group was removed (GP4) and Cbz-L-Glu(OtBu)-OH (321 mg, 0.95 mmol, 1.50 eq.) was coupled (GP3) over a period of 2 h, using TBTU (405 mg, 1.26 mmol, 2.00 eq.), HOAt (171 mg, 1.26 mmol, 2.00 eq.) and DIPEA (582  $\mu$ L, 3.42 mmol, 5.43 eq.). Some resin beads were taken and treated with TFA according to GP7. RP-HPLC/MS analysis revealed nearly complete conversion to product **61**. The protected dipeptide was cleaved off the resin by incubation with HFIP/DCM (GP11). Purification of the crude product by flash chromatography (40 - 90% B in 10 min, Method D, 12 mL/min) provided 649 mg (72.0%) of compound **61** as a colorless, viscous oil.

RP-HPLC (10 - 90% B in 15 min, Method A, 1 mL/min):  $t_R = 14.8$  min;  $k = 8.9$ . Calculated monoisotopic mass (C<sub>25</sub>H<sub>38</sub>N<sub>2</sub>O<sub>7</sub>): 478.27, found:  $m/z = 422.8$  [M(**61**)-tBu+H]<sup>+</sup>, 478.8 [M(**61**)+H]<sup>+</sup>, 500.7 [M(**61**)+Na]<sup>+</sup>, 956.8 [M<sub>2</sub>(**61**)+H]<sup>+</sup>, 978.8 [M<sub>2</sub>(**61**)+Na]<sup>+</sup>, 994.7 [M<sub>2</sub>(**61**)+K]<sup>+</sup>.

### Tert-butyl (S)-2-((S)-2-(((benzyloxy)carbonyl)amino)-5-(tert-butoxy)-5-oxopentanamido)octanoate (**62**)



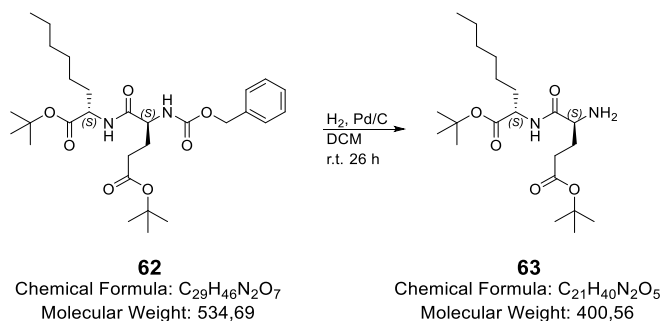
Compound **62** was synthesized in analogy to a previously published procedure by Bergmeier *et al.*<sup>[296]</sup> with some minor modifications. Glassware and reagents were handled under air- and moisture-free conditions (GP12). Lyophilized educt **61** (649 mg, 1.36 mmol, 1.00 eq.) was dissolved in 2 mL dry DCM and the first portion of O-*tert*-butyl-*N,N'*-diisopropylisourea (**39**) (454  $\mu$ L, 2.04 mmol, 1.50 eq.) was added. The reaction mixture was stirred under reflux (~ 42 °C) and argon atmosphere for 22 h. A second portion of **39** (454  $\mu$ L, 2.04 mmol, 1.50 eq.) was added and also

## MATERIALS AND METHODS

DCM, in order to keep the solvent amount constantly between 2 and 3 mL. After stirring for further 24 h at reflux temperature and under argon atmosphere, the reaction was terminated by diluting the suspension with DCM. Solid by-products were removed by filtration and the organic layer once washed with H<sub>2</sub>O. The aqueous phase was extracted twice with DCM. The combined organic phases were transferred into a round bottom flask and the solvent removed under reduced pressure. Purification by flash chromatography (40 - 90% B in 10 min, Method D, 12 mL/min) provided 481 mg (66.2%) of compound **62** as a colorless solid.

RP-HPLC (10 - 90% B in 15 min, Method A, 1 mL/min):  $t_R = 16.7$  min;  $k = 10.1$ . Calculated monoisotopic mass (C<sub>29</sub>H<sub>46</sub>N<sub>2</sub>O<sub>7</sub>): 534.33, found:  $m/z = 423.0$  [M(**62**)-2*t*Bu+H]<sup>+</sup>, 479.1 [M(**62**)-*t*Bu+H]<sup>+</sup>, 535.2 [M(**62**)+H]<sup>+</sup>, 557.0 [M(**62**)+Na]<sup>+</sup>, 579.2 [M(**62**)+K]<sup>+</sup>.

### *Tert-butyl (S)-2-((S)-2-amino-5-(tert-butoxy)-5-oxopentanamido)octanoate (63)*

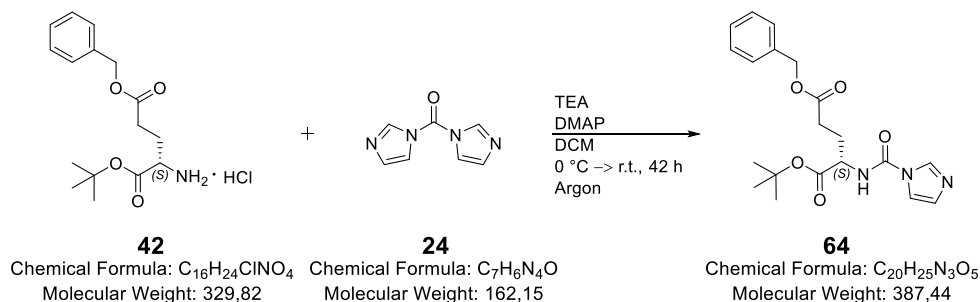


Compound **62** (481 mg, 0.89 mmol, 1.00 eq.) was dissolved in 10 mL DCM and the solution was flushed 5 minutes with argon to remove dissolved oxygen. 94.2 mg of palladium on carbon (10% wt) (corresponds to 9.42 mg palladium, 89.0 μmol, 0.10 eq.) were added and the flask was sealed with a rubber septum. Remaining air was displaced with argon and subsequently replaced by hydrogen gas. The mixture was stirred under hydrogen atmosphere at room temperature for 26 h. Palladium on carbon was filtered off, and the solvent was evaporated *in vacuo*. This afforded 162 mg (45.3%) of compound **63** as a slightly brown viscous oil, which was used in the next step without further purification.

RP-HPLC (40 - 95% B in 15 min, Method A, 1 mL/min):  $t_R = 7.07$  min;  $k = 3.7$ . Calculated monoisotopic mass (C<sub>21</sub>H<sub>40</sub>N<sub>2</sub>O<sub>5</sub>): 400.29, found:  $m/z = 401.0$  [M(**63**)+H]<sup>+</sup>, 422.9 [M(**63**)+Na]<sup>+</sup>, 438.9 [M(**63**)+K]<sup>+</sup>, 801.0 [M<sub>2</sub>(**63**)+H]<sup>+</sup>, 822.9 [M<sub>2</sub>(**63**)+Na]<sup>+</sup>.

## MATERIALS AND METHODS

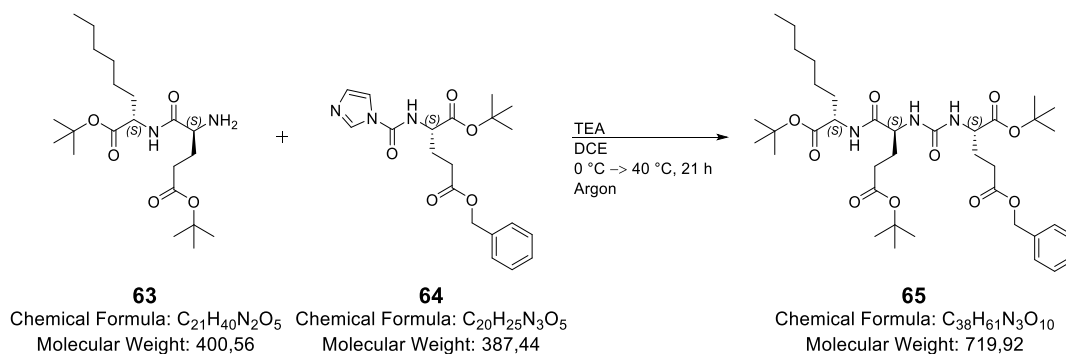
### 5-Benzyl 1-(tert-butyl) (1H-imidazole-1-carbonyl)-L-glutamate (**64**)



Compound **42** (396 mg, 1.20 mmol, 1.00 eq.) was dissolved in 10 mL DCE and cooled to 0 °C. Triethylamine (416  $\mu$ L, 3.00 mmol, 2.50 eq.), DMAP on polystyrene (3.00 mmol/g, 16.0 mg, 48.0  $\mu$ mol, 0.04 eq.) and 1,1'-carbonyldiimidazole (**24**) (214 mg, 1.32 mmol, 1.10 eq.) were added and the mixture was stirred for further 5 min at 0 °C. Afterwards, it was warmed to room temperature and stirred for 42 h under argon atmosphere. DMAP was filtered off and the solution was washed once with saturated NaHCO<sub>3</sub>, brine and H<sub>2</sub>O. The combined organic phases were dried over Na<sub>2</sub>SO<sub>4</sub>, filtered and the solvent was removed under reduced pressure. The obtained crude product (439 mg, 94.5%) was analyzed via RP-HPLC/MS and revealed almost exclusively product **64**, which was used in the next step without further purification.

RP-HPLC (10 - 90% B in 15 min, Method A, 1 mL/min):  $t_R$  = 10.1 min;  $k$  = 5.7. Calculated monoisotopic mass (C<sub>20</sub>H<sub>25</sub>N<sub>3</sub>O<sub>5</sub>): 387.18, found:  $m/z$  = 388.2 [M(**64**)+H]<sup>+</sup>.

### 5-Benzyl 1-(tert-butyl) (((S)-5-(tert-butoxy)-1-(((S)-1-(tert-butoxy)-1-oxooctan-2-yl)amino)-1,5-dioxopentan-2-yl)carbamoyl)-L-glutamate (**65**)



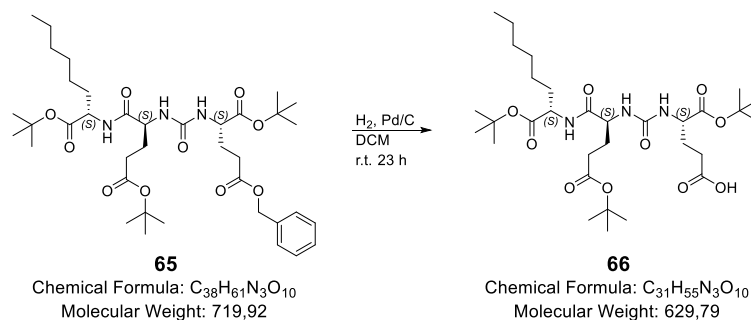
Compound **65** was synthesized in analogy to a previously published procedure by Weineisen *et al.*<sup>[199]</sup> with some minor modifications. The H-L-Glu(OtBu)-L-2-Aoc-OtBu dipeptide **63** (162 mg, 0.40 mmol, 1.10 eq.) was dissolved in 10 mL DCE and compound **64** (141 mg, 0.36 mmol, 1.00 eq.) was added. At 0 °C, triethylamine (139  $\mu$ L, 1.00 mmol, 2.78 eq.) was added and the mixture was stirred for further five minutes at 0 °C. The solution was warmed to 40 °C and stirred for 21 h under argon atmosphere. The reaction mixture was washed once with H<sub>2</sub>O and brine. The combined aqueous phases were extracted once with DCM. The entire organic layer was dried over Na<sub>2</sub>SO<sub>4</sub>, filtered and the solvent removed *in vacuo*. Purification of the crude product by

## MATERIALS AND METHODS

preparative RP-HPLC (45 - 90% B in 20 min, Method B, 5 mL/min) afforded 128 mg (49%) of compound **65** as a colorless clear viscous oil.

RP-HPLC (40 - 95% B in 15 min, Method A, 1 mL/min):  $t_R = 17.5$  min;  $k = 10.7$ . Calculated monoisotopic mass ( $C_{38}H_{61}N_3O_{10}$ ): 719.44, found:  $m/z = 720.0$  [ $M(65)+H$ ] $^+$ , 742.0 [ $M(65)+MeCN+H$ ] $^+$ .

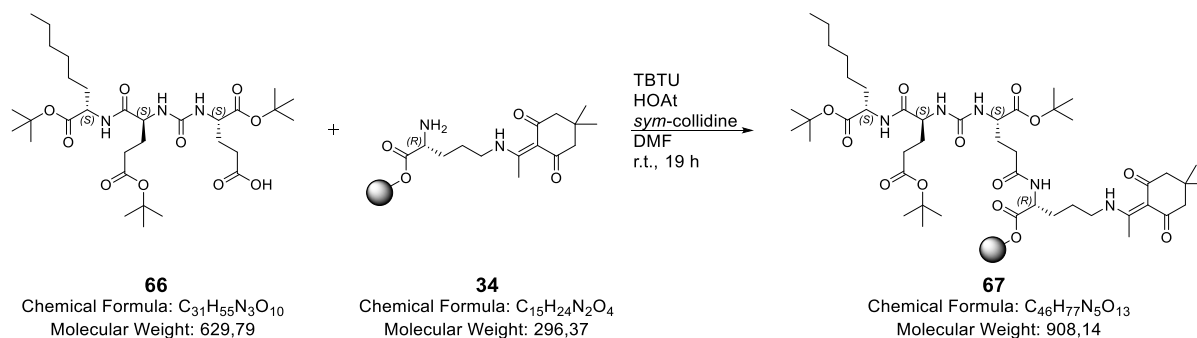
(5*S*,8*S*,12*S*)-8-(3-(*tert*-butoxy)-3-oxopropyl)-12-(*tert*-butoxycarbonyl)-5-hexyl-2,2-dimethyl-4,7,10-trioxo-3-oxa-6,9,11-triazapentadecan-15-oic acid (**66**)



Compound **65** (128 mg, 0.18 mmol, 1.00 eq.) was dissolved in 6 mL DCM and the solution was flushed 5 minutes with argon to remove dissolved oxygen. 19.2 mg of palladium on carbon (10% wt) (corresponds to 1.92 mg palladium, 18.0  $\mu$ mol, 0.10 eq.) were added and the flask was sealed with a rubber septum. Remaining air was displaced with argon and subsequently replaced by hydrogen gas. The mixture was stirred under hydrogen atmosphere at room temperature for 23 h. Palladium on carbon was filtered off, and the solvent was evaporated *in vacuo*. This afforded 102 mg (89.9%) of compound **66** as a colorless solid, which was used in the next step without further purification.

RP-HPLC (40 - 95% B in 15 min, Method A, 1 mL/min):  $t_R = 13.1$  min;  $k = 7.7$ . Calculated monoisotopic mass ( $C_{31}H_{55}N_3O_{10}$ ): 629.39, found:  $m/z = 630.0$  [ $M(66)+H$ ] $^+$ , 651.9 [ $M(66)+Na$ ] $^+$ , 667.9 [ $M(66)+K$ ] $^+$ .

*L*-Glu(*Ot*Bu)-(L-2-Aoc-*Ot*Bu)-carbonyl-*L*-Glu[D-Orn(Dde)-2-CT]-*Ot*Bu (**67**)



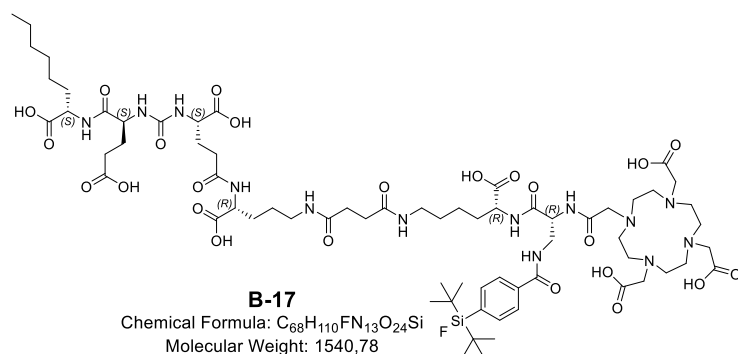
According to GP3, fragment **66** (102 mg, 0.16 mmol, 1.00 eq.) was coupled to resin-bound H-D-Orn(Dde) (**34**) (0.23 mmol 1.44 eq.), with TBTU (104 mg, 0.32 mmol, 2.00 eq.) and HOAt

## MATERIALS AND METHODS

(44.0 mg, 0.32 mmol, 2.00 eq.) as coupling reagents and *sym*-collidine (191  $\mu$ L, 1.44 mmol, 9.00 eq.) as base. After shaking for 19 h at room temperature, formation of product **67** could be confirmed (GP8), as only one major peak with the expected *m/z*-ratio of 908.0 occurred.

RP-HPLC (40 – 95% B in 15 min, Method A, 1 mL/min):  $t_R$  = 13.7 min;  $k$  = 8.1. Calculated monoisotopic mass ( $C_{46}H_{77}N_5O_{13}$ ): 907.55, found:  $m/z$  = 908.0  $[M(\mathbf{67})+H]^+$ , 1814.9  $[M_2(\mathbf{67})+H]^+$ .

### Proinhibitor **B-17**

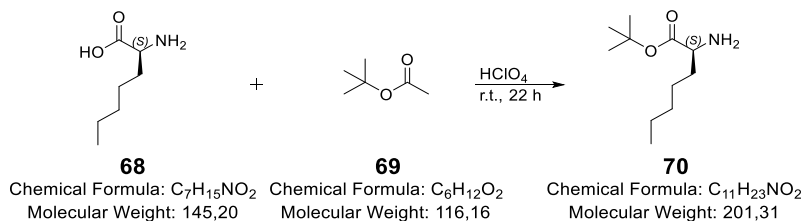


Further reactions on resin-bound compound **67** (0.23 mmol, 1.00 eq.) were performed according to standard Fmoc-SPPS on 2-CT resin, applying the above-mentioned methods (GP3 - GP8). For chelator attachment, DOTA-NHS (175 mg, 0.23 mmol, 1.00 eq.) and DIPEA

(324  $\mu$ L, 1.91 mmol, 8.30 eq.) were each dissolved in DMF. First, DIPEA in DMF was added to the resin for preactivation. After five minutes, DOTA-NHS in DMF was added and incubated with the resin-bound amine for 16 h. An adequate conversion (RP-HPLC/MS analysis after GP7) was reached and the peptide was cleaved off the resin with TFA/TIPS/DCM (GP9) and purified afterwards by preparative RP-HPLC (40 - 65% B in 20 min, Method B, 5 mL/min). Subsequent lyophilization afforded 16.6 mg (4.68% yield, chemical purity > 99%) of pure product **B-17** as a colorless powder.

RP-HPLC (10 - 90% B in 15 min, Method A, 1 mL/min):  $t_R$  = 9.15 min;  $k$  = 5.1. Calculated monoisotopic mass ( $C_{68}H_{110}FN_{13}O_{24}Si$ ): 1539.75, found:  $m/z$  = 770.5  $[M(\mathbf{B-17})+2H]^{2+}$ , 1539.9  $[M(\mathbf{B-17})+H]^+$ .

### *Tert*-butyl (*S*)-2-aminoheptanoate (**70**)

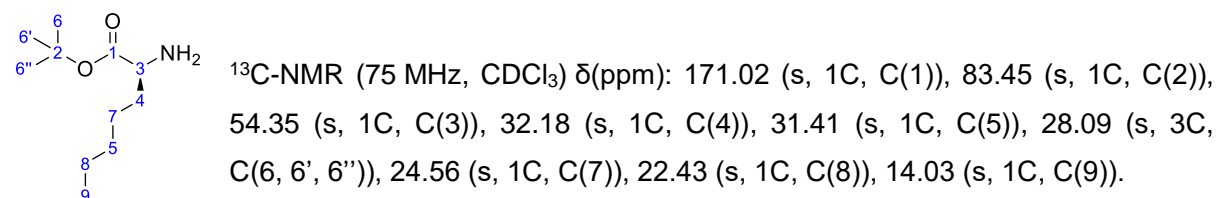
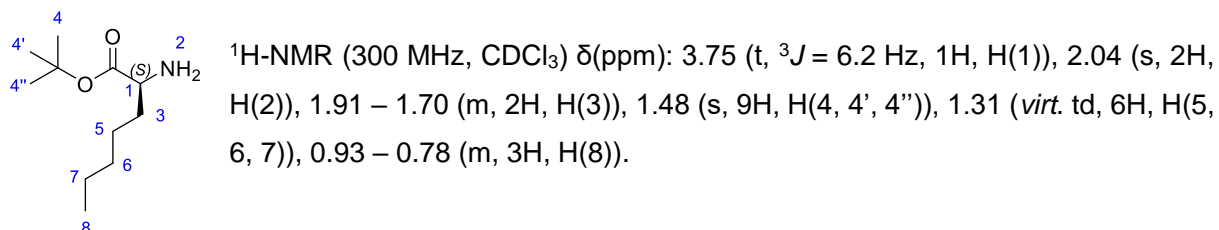


Compound **70** was synthesized in analogy to a previously published procedure by Hyun *et al.*<sup>[298]</sup> with some minor modifications. (*S*)-2-Aminoheptanoic acid (**68**) (300 mg, 2.07 mmol, 1.00 eq.) was dissolved in 7.13 mL of *tert*-butyl acetate (**69**) and 70% (v/v) perchloric acid (aq.) (384  $\mu$ L, 4.74 mmol, 2.29 eq.) was added slowly. The reaction mixture was stirred for 22 h at room temperature.  $H_2O$  and some drops of 0.3 M HCl were added for quenching. The pH value of the

## MATERIALS AND METHODS

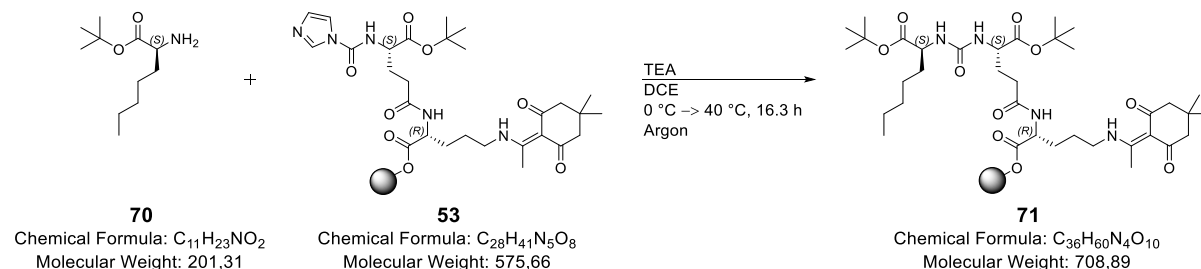
aqueous phase was adjusted to 9 with 10% (w/v) Na<sub>2</sub>CO<sub>3</sub> (aq.) and extracted three times with DCM. The combined organic phases were dried over Na<sub>2</sub>SO<sub>4</sub>, filtered and the solvent was removed under reduced pressure. Purification by column chromatography (DCM/MeOH/acetone = 5/1/1) yielded 446 mg (> 99%) of pure product **70** as a slightly yellow viscous oil.

$t_R$  (RP-HPLC): not detectable at 220/254 nm. Calculated monoisotopic mass (C<sub>11</sub>H<sub>23</sub>NO<sub>2</sub>): 201.17, found:  $m/z$  = 202.0 [M(**70**)+H]<sup>+</sup>, 243.0 [M(**70**)+MeCN+H]<sup>+</sup>.  $R_f$ -value: 0.76 (DCM/MeOH/acetone = 5/1/1).



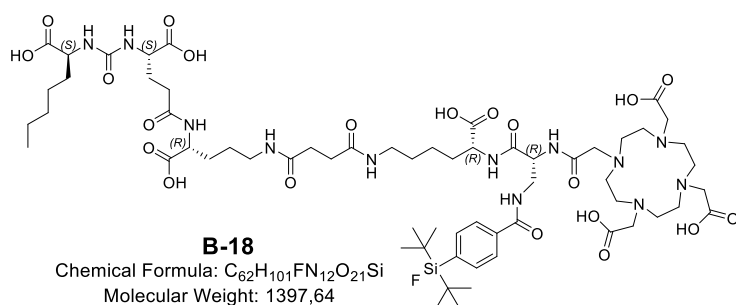
**70**

### L-2-Aha-OtBu-carbonyl-L-Glu[D-Orn(Dde)-2-CT]-OtBu (**71**)



Compound **53** (0.24 mmol, 1.00 eq.) was transferred into a round bottom flask and suspended in 2.50 mL DCE. At 0 °C, triethylamine (83.2 μL, 0.60 mmol, 2.50 eq.) and *tert*-butyl (S)-2-aminoheptanoate (**70**) (60.9 mg, 0.30 mmol, 1.25 eq.) were added and the mixture was stirred for further 5 min at 0 °C. Afterwards, it was warmed to 40 °C and stirred for 16.3 h under argon atmosphere. The resin was washed with DCM (4x), some resin beads were taken and treated with HFIP/DCM (1/4) according to GP8. RP-HPLC/MS analysis revealed nearly complete conversion to product **71**.

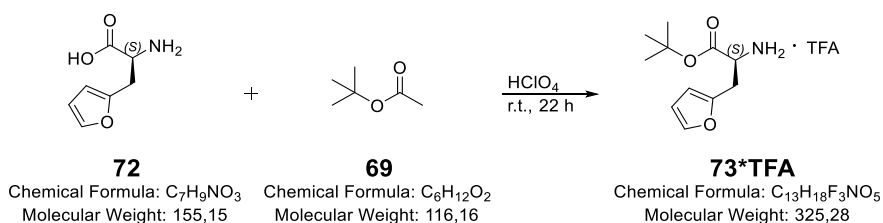
RP-HPLC (10 - 90% B in 15 min, Method A, 1 mL/min):  $t_R$  = 14.2 min;  $k$  = 8.5. Calculated monoisotopic mass (C<sub>36</sub>H<sub>60</sub>N<sub>4</sub>O<sub>10</sub>): 708.43, found:  $m/z$  = 709.1 [M(**71**)+H]<sup>+</sup>, 731.1 [M(**71**)+Na]<sup>+</sup>.

L-2-Aminoheptanoic acid derivative **B-18**


Further reactions on resin-bound compound **71** (0.24 mmol, 2.00 eq.) were performed according to standard Fmoc-SPPS on 2-CT resin, applying the above-mentioned methods (GP3 - GP8). For chelator attachment, DOTA-NHS (91.4 mg,

0.12 mmol, 1.00 eq.) and DIPEA (286  $\mu$ L, 1.68 mmol, 14.0 eq.) were each dissolved in DMF. First, DIPEA in DMF was added to the resin for preactivation. After five minutes, DOTA-NHS in DMF was added and incubated with the resin-bound amine for 70.5 h. An adequate conversion (RP-HPLC/MS analysis after GP7) was reached and the peptide was cleaved off the resin with TFA/TIPS/DCM (GP9) and purified afterwards by preparative RP-HPLC (30 - 80% B in 20 min, Method B, 5 mL/min and 25 - 70% B in 15 min, Method B, 1 mL/min). Subsequent lyophilization afforded 3.17 mg (1.89% yield, chemical purity 95.5%) of pure product **B-18** as a colorless powder.

RP-HPLC (10 - 90% B in 15 min, Method A, 1 mL/min):  $t_R = 11.8$  min;  $k = 6.9$ . Calculated monoisotopic mass ( $C_{62}H_{101}FN_{12}O_{21}Si$ ): 1396.70, found:  $m/z = 699.4$  [ $M(\mathbf{B-18})+2H$ ] $^{2+}$ , 1398.9 [ $M(\mathbf{B-18})+H$ ] $^{+}$ .

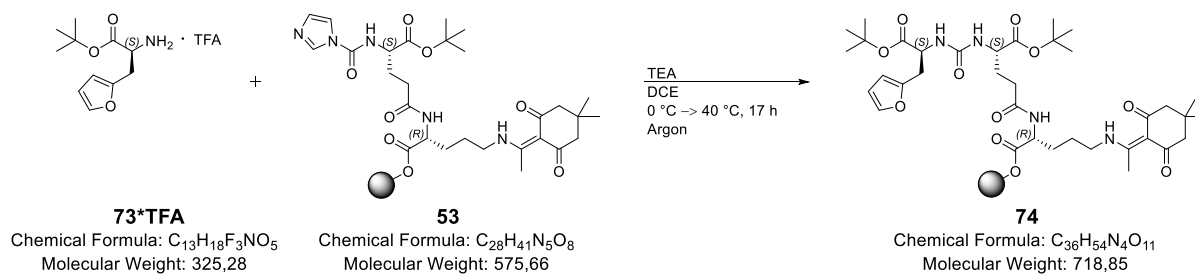
 Tert-butyl (S)-2-amino-3-(furan-2-yl)propanoate (**73\*TFA**)


Compound **73** was synthesized in analogy to a previously published procedure by Hyun *et al.*<sup>[298]</sup> with some minor modifications. 3-(2-Furyl)-L-alanine (**72**) (300 mg, 2.93 mmol, 1.00 eq.) was dissolved in 6.65 mL of tert-butyl acetate (**69**) and 70% (v/v) perchloric acid (aq.) (359  $\mu$ L, 4.42 mmol, 2.29 eq.) was added slowly. The reaction mixture was stirred for 22 h at room temperature.  $H_2O$  and some drops of 0.3 M HCl were added for quenching. The pH value of the aqueous phase was adjusted to 9 with 10% (w/v)  $Na_2CO_3$  (aq.) and extracted three times with DCM. The combined organic phases were dried over  $Na_2SO_4$ , filtered and the solvent was removed under reduced pressure. Purification by column chromatography (DCM/MeOH/acetone = 5/1/1) and preparative RP-HPLC (30 - 75% B in 20 min, Method B, 9 mL/min) yielded 65.5 mg (10.4%) of pure product **73\*TFA** as a colorless solid.

## MATERIALS AND METHODS

RP-HPLC (10 - 90% B in 15 min, Method A, 1 mL/min) for **73(w/o TFA)**:  $t_R = 6.93$  min;  $k = 3.6$ . Calculated monoisotopic mass for **73(w/o TFA)** ( $C_{11}H_{17}NO_3$ ): 211.12, found:  $m/z = 212.1$   $[M(73)+H]^+$ , 253.1  $[M(73)+MeCN+H]^+$ .  $R_f$ -value: 0.69 (DCM/MeOH/acetone = 5/1/1).

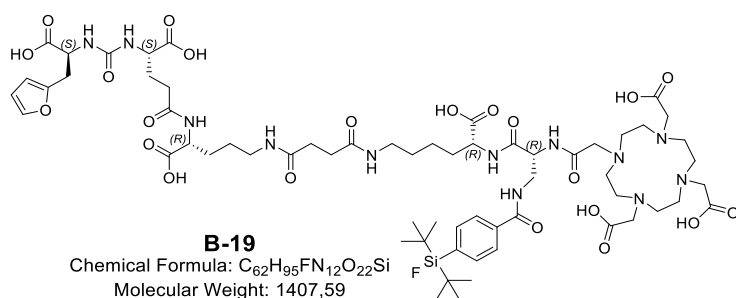
### 3-(2-Furyl)-L-alanine-OtBu-carbonyl-L-Glu[D-Orn(Dde)-2-CT]-OtBu (**74**)



Compound **53** (0.29 mmol, 1.45 eq.) was transferred into a round bottom flask and dissolved in 8.00 mL DCE. At 0 °C, triethylamine (69.8  $\mu$ L, 0.50 mmol, 2.50 eq.) and **73**\*TFA (65.5 mg, 0.20 mmol, 1.00 eq.) were added and the mixture was stirred for further 5 min at 0 °C. Afterwards, it was warmed to 40 °C and stirred for 17 h under argon atmosphere. The resin was washed with DCM (4 $\times$ ), some resin beads were taken and treated with HFIP/DCM (1/4) according to GP8. RP-HPLC/MS analysis revealed nearly complete conversion to product **74**.

RP-HPLC (10 - 90% B in 15 min, Method A, 1 mL/min):  $t_R = 12.4$  min;  $k = 7.3$ . Calculated monoisotopic mass ( $C_{36}H_{54}N_4O_{11}$ ): 718.38, found:  $m/z = 718.8$   $[M(74)+H]^+$ , 740.7  $[M(74)+Na]^+$ , 756.8  $[M(74)+K]^+$ .

### Furyl derivative **B-19**

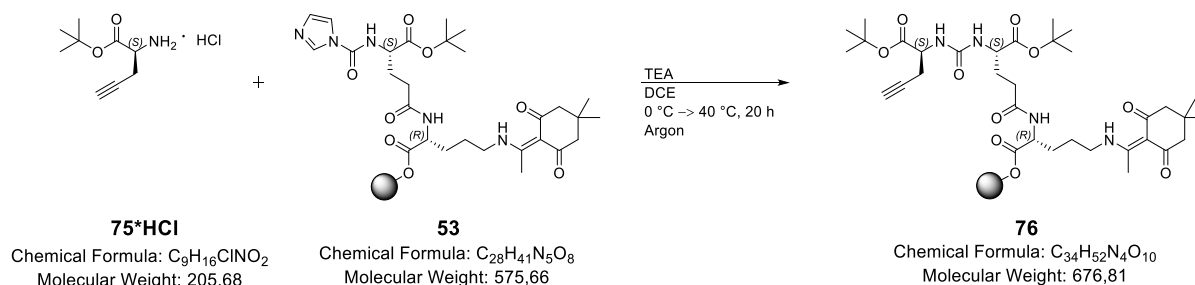


Further reactions on resin-bound compound **74** (0.29 mmol, 2.00 eq.) were performed according to standard Fmoc-SPPS on 2-CT resin, applying the above-mentioned methods (GP3 - GP8). For chelator attachment, DOTA-NHS (110 mg, 0.15 mmol, 1.00 eq.) and DIPEA (345  $\mu$ L, 2.03 mmol, 13.5 eq.) were each dissolved in DMF. First, DIPEA in DMF was added to the resin for preactivation. After five minutes, DOTA-NHS in DMF was added and incubated with the resin-bound amine for 13 h. An adequate conversion (RP-HPLC/MS analysis after GP7) was reached and the peptide was cleaved off the resin with TFA/TIPS/DCM (GP9) and purified afterwards by preparative RP-HPLC (35 - 80% B in 20 min, Method B, 5 mL/min). Subsequent lyophilization afforded 8.72 mg (4.13% yield, chemical purity > 99%) of pure product **B-19** as a colorless powder.

## MATERIALS AND METHODS

RP-HPLC (10 - 90% B in 15 min, Method A, 1 mL/min):  $t_R = 11.3$  min;  $k = 6.5$ . Calculated monoisotopic mass ( $C_{62}H_{95}FN_{12}O_{22}Si$ ): 1406.64, found:  $m/z = 703.8$  [ $M(\mathbf{B-19})+2H$ ] $^{2+}$ , 1406.6 [ $M(\mathbf{B-19})+H$ ] $^+$ .

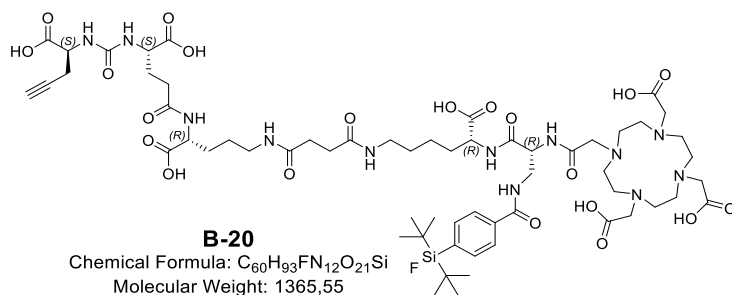
### (2S)-2-Amino-4-pentynoate-OtBu-carbonyl-L-Glu[D-Orn(Dde)-2-CT]-OtBu (**76**)



Compound **53** (0.24 mmol, 1.00 eq.) was transferred into a round bottom flask and dissolved in 2.18 mL DCE. At 0 °C, triethylamine (83.2  $\mu$ L, 0.60 mmol, 2.50 eq.) and *tert*-butyl (2S)-2-amino-4-pentynoate (**75**)\*HCl (59.6 mg, 0.29 mmol, 1.20 eq.) were added and the mixture was stirred for further 5 min at 0 °C. Afterwards, it was warmed to 40 °C and stirred for 20 h under argon atmosphere. The resin was washed with DCM (4x), some resin beads were taken and treated with HFIP/DCM (1/4) according to GP8. RP-HPLC/MS analysis revealed nearly complete conversion to product **76**.

RP-HPLC (40 - 95% B in 15 min, Method A, 1 mL/min):  $t_R = 6.05$  min;  $k = 3.0$ . Calculated monoisotopic mass ( $C_{34}H_{52}N_4O_{10}$ ): 676.37, found:  $m/z = 677.0$  [ $M(\mathbf{76})+H$ ] $^+$ , 699.0 [ $M(\mathbf{76})+Na$ ] $^+$ .

### Alkyne derivative **B-20**



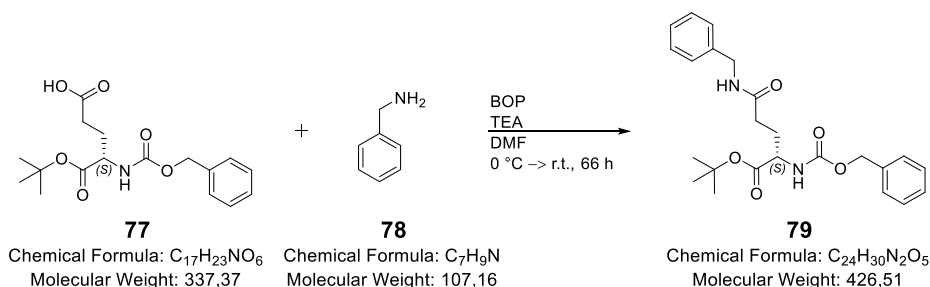
Further reactions on resin-bound compound **76** (0.24 mmol, 2.00 eq.) were performed according to standard Fmoc-SPPS on 2-CT resin, applying the above-mentioned methods (GP3 - GP8). For chelator attachment, DOTA-NHS (91.4 mg,

0.12 mmol, 1.00 eq.) and DIPEA (286  $\mu$ L, 1.68 mmol, 14.0 eq.) were each dissolved in DMF. First, DIPEA in DMF was added to the resin for preactivation. After five minutes, DOTA-NHS in DMF was added and incubated with the resin-bound amine for 71 h. An adequate conversion (RP-HPLC/MS analysis after GP7) was reached and the peptide was cleaved off the resin with TFA/TIPS/DCM (GP9) and purified afterwards by preparative RP-HPLC (30 - 80% B in 20 min, Method B, 5 mL/min). Subsequent lyophilization afforded 10.9 mg (6.65% yield, chemical purity 98.5%) of pure product **B-20** as a colorless powder.

## MATERIALS AND METHODS

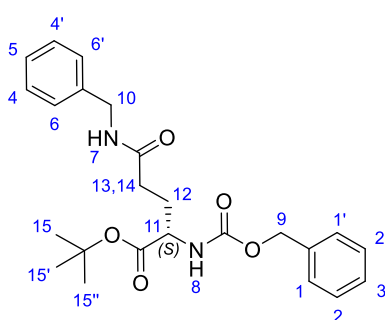
RP-HPLC (10 - 90% B in 15 min, Method A, 1 mL/min):  $t_R = 11.1$  min;  $k = 6.4$ . Calculated monoisotopic mass ( $C_{60}H_{93}FN_{12}O_{21}Si$ ): 1364.63, found:  $m/z = 682.7$  [ $M(\mathbf{B-20})+2H$ ] $^{2+}$ , 1364.4 [ $M(\mathbf{B-20})+H$ ] $^+$ .

### *Tert-butyl N<sup>5</sup>-benzyl-N<sup>2</sup>-((benzyloxy)carbonyl)-L-glutamate (79)*

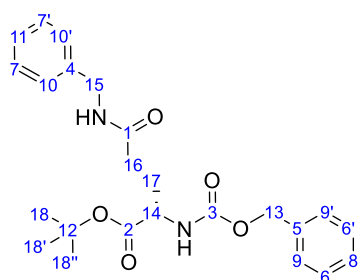


Compound **79** was synthesized in analogy to a previously published procedure by Kozikowski *et al.*<sup>[222]</sup> Benzyl amine (**78**) (305  $\mu\text{L}$ , 2.80 mmol, 1.40 eq.) and BOP (1.06 g, 2.40 mmol, 1.20 eq.) were added to a solution of *N*-Cbz-L-Glu-O*t*Bu (**77**) (675 mg, 2.00 mmol, 1.00 eq.) in 18.0 mL DMF. The resulting solution was cooled to 0 °C and triethylamine (638  $\mu\text{L}$ , 4.60 mmol, 2.30 eq.) was added. After stirring for 66 h at room temperature the reaction mixture was poured into ice-cold water (100 mL) and extracted four times with EtOAc. The organic layer was washed successively with 1 M HCl,  $H_2O$ , saturated  $NaHCO_3$  and brine. The organic phase was dried over  $Na_2SO_4$ , filtered and the solvent was removed *in vacuo*. Purification by column chromatography (EtOAc/*n*-hexane = 1/1) yielded 876 mg (2.05 mmol, > 99%) of *N*-Cbz-L-Gln(Bn)-O*t*Bu (**79**) as a colorless solid.

$t_R$  (RP-HPLC): not determined.  $m/z$ : not determined.  $R_f$ -value: 0.54 (EtOAc/*n*-hexane = 1/1).



$^1\text{H-NMR}$  (400 MHz,  $CDCl_3$ )  $\delta$ (ppm): 7.38 – 7.26 (m, 10H, H(1, 1', 2, 2', 3, 4, 4', 5, 6, 6')), 6.27 (s, 1H, H(7)), 5.56 (d,  $^3J = 8.1$  Hz, 1H, H(8)), 5.08 (s, 2H, H(9)), 4.42 (*virt. t.*, 2H, H(10)), 4.23 (td,  $^3J = 8.8, 3.8$  Hz, 1H, H(11)), 2.26 (*virt. ddt.*, 3H, H(12, 13)), 2.02 – 1.86 (m, 1H, H(14)), 1.45 (s, 9H, H(15, 15', 15'')).

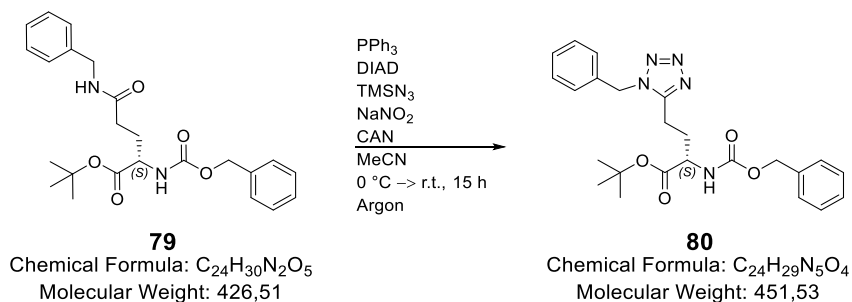


**79**

$^{13}\text{C-NMR}$  (101 MHz,  $CDCl_3$ )  $\delta$ (ppm): 171.92 (s, 1C, C(1)), 171.15 (s, 1C, C(2)), 156.51 (s, 1C, C(3)), 138.37 (s, 1C, C(4)), 136.37 (s, 1C, C(5)), 128.82 (s, 2C, C(6, 6')), 128.65 (s, 2C, C(7, 7')), 128.33 (s, 1C, C(8)), 128.26 (s, 2C, C(9, 9')), 127.95 (s, 2C, C(10, 10')), 127.61 (s, 1C, C(11)), 82.68 (s, 1C, C(12)), 67.16 (s, 1C, C(13)), 54.13 (s, 1C, C(14)), 43.84 (s, 1C, C(15)), 32.72 (s, 1C, C(16)), 29.42 (s, 1C, C(17)), 28.11 (s, 3C, C(18, 18', 18'')).

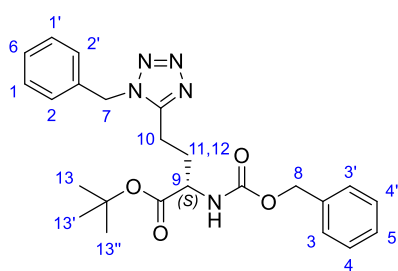
## MATERIALS AND METHODS

### *Tert-butyl (S)-4-(1-benzyl-1H-tetrazol-5-yl)-2-(((benzyloxy)carbonyl)amino)butanoate (80)*

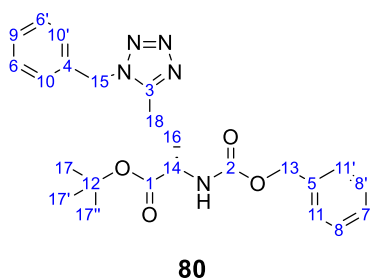


Compound **80** was synthesized in analogy to a previously published procedure by Kozikowski *et al.*<sup>[222]</sup> Diisopropyl azodicarboxylate (530  $\mu$ L, 2.70 mmol, 1.35 eq.) was added to a solution of PPh<sub>3</sub> (683 mg, 2.60 mmol, 1.30 eq.) and *N*-Cbz-L-Gln(Bn)-OtBu (**79**) (853 mg, 2.00 mmol, 1.00 eq.) in 10 mL ice-cold, anhydrous MeCN over two minutes. Trimethylsilyl azide (372  $\mu$ L, 2.80 mmol, 1.40 eq.) was added over five minutes, and the solution was allowed to stir for 15 h at room temperature. Afterwards, the solution was cooled to 0 °C and 726  $\mu$ L of a 3 M NaNO<sub>2</sub> solution (aq.) (152 mg, 2.20 mmol, 1.10 eq.) was added. The mixture was allowed to stir for 30 min at room temperature and 3.30 mL of cerium(IV) ammonium nitrate (1.21 g, 2.20 mmol, 1.10 eq.) in H<sub>2</sub>O was added. The solution was stirred for further 20 min and subsequently poured into ice-cold H<sub>2</sub>O. The mixture was extracted three times with DCM and the combined organic phases were washed once with water, then dried over Na<sub>2</sub>SO<sub>4</sub>, filtered and the solvent removed *in vacuo*. Purification by column chromatography (EtOAc/*n*-hexane = 1/2) yielded 222 mg (24.6%) of product **80** as a colorless solid.

RP-HPLC (10 - 90% B in 15 min, Method A, 1 mL/min):  $t_R$  = 14.5 min;  $k$  = 8.7. Calculated monoisotopic mass (C<sub>24</sub>H<sub>29</sub>N<sub>5</sub>O<sub>4</sub>): 451.22, found:  $m/z$  = 395.7 [M(**80**)-tBu+H]<sup>+</sup>, 451.7 [M(**80**)+H]<sup>+</sup>.  $R_F$ -value: 0.28 (EtOAc/*n*-hexane = 1/2).



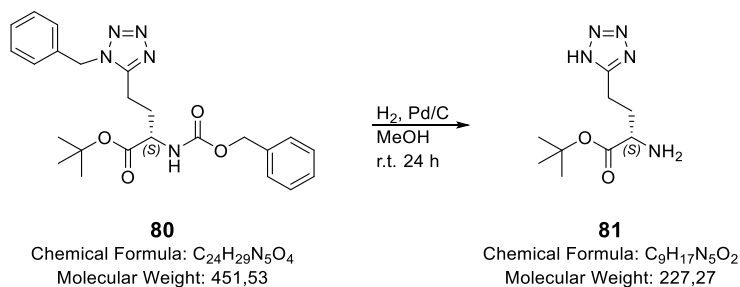
<sup>1</sup>H-NMR (400 MHz, CDCl<sub>3</sub>)  $\delta$ (ppm): 7.43 – 7.28 (m, 8H, H(1, 1', 2, 2', 3, 3', 4, 4')), 7.14 (*virt.* dd, 2H, H(5, 6)), 5.56 – 5.30 (m, 2H, H(7)), 5.24 – 4.99 (m, 2H, H(8)), 4.26 (td, <sup>3</sup>J = 8.2, 4.4 Hz, 1H, H(9)), 2.75 (*virt.* tq, 2H, H(10)), 2.34 (*virt.* dq, 1H, H(11)), 2.01 (*virt.* dddd, 1H, H(12)), 1.42 (s, 9H, H(13, 13', 13'')).



<sup>13</sup>C-NMR (101 MHz, CDCl<sub>3</sub>)  $\delta$ (ppm): 170.51 (s, 1C, C(1)), 156.19 (s, 1C, C(2)), 154.26 (s, 1C, C(3)), 136.31 (s, 1C, C(4)), 133.33 (s, 1C, C(5)), 129.40 (s, 2C, C(6, 6')), 129.11 (s, 1C, C(7)), 128.73 (s, 2C, C(8, 8')), 128.45 (s, 1C, C(9)), 128.30 (s, 2C, C(10, 10')), 127.67 (s, 2C, C(11, 11')), 83.11 (s, 1C, C(12)), 67.23 (s, 1C, C(13)), 53.93 (s, 1C, C(14)), 50.90 (s, 1C, C(15)), 30.29 (s, 1C, C(16)), 28.06 (s, 3C, C(17, 17', 17'')), 19.98 (s, 1C, C(18)).

## MATERIALS AND METHODS

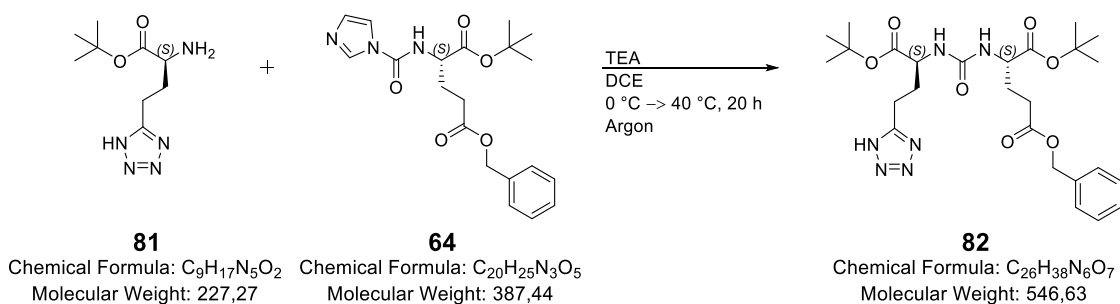
### *Tert-butyl (S)-2-amino-4-(1H-tetrazol-5-yl)butanoate (81)*



Compound **80** (120 mg, 0.27 mmol, 1.00 eq.) was dissolved in 15.0 mL MeOH and the solution was flushed 5 minutes with argon to remove dissolved oxygen. 12.0 mg of palladium on carbon (10% wt) (corresponds to 1.20 mg palladium, 11.3  $\mu$ mol, 0.04 eq.) were added and the flask was sealed with a rubber septum. Remaining air was displaced with argon and subsequently replaced by hydrogen gas. The mixture was stirred under hydrogen atmosphere at room temperature for 23 h. Palladium on carbon was filtered off, and the solvent was evaporated *in vacuo*. This afforded a mixture of product **81** (minor portion) and reactant **80** with free  $\alpha$ -amine, still bearing the Bn-protective group at the tetrazole moiety (major portion). However, as a certain conversion to product **81** could be observed by RP-HPLC/MS analysis and the *N*-Cbz-protective group was cleaved off efficiently, the crude product was used in the next step without further purification.

RP-HPLC (10 - 90% B in 15 min, Method A, 1 mL/min):  $t_R = 4.60$  min;  $k = 2.1$ . Calculated monoisotopic mass (C<sub>9</sub>H<sub>17</sub>N<sub>5</sub>O<sub>2</sub>): 227.14, found:  $m/z = 228.0$  [M(**81**)+H]<sup>+</sup>, 268.7 [M(**81**)+MeCN+H]<sup>+</sup>.

### *5-Benzyl 1-(tert-butyl) (((S)-1-(tert-butoxy)-1-oxo-4-(1H-tetrazol-5-yl)butan-2-yl)carbamoyl)-L-glutamate (82)*



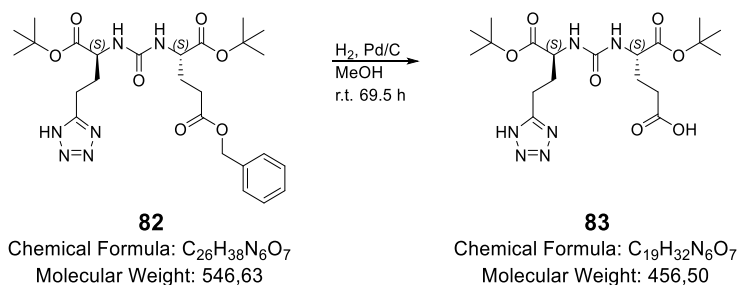
Compound **82** was synthesized in analogy to a previously published procedure by Weineisen *et al.*<sup>[199]</sup> with some minor modifications. *Tert*-butyl (*S*)-2-amino-4-(1*H*-tetrazol-5-yl)butanoate (**81**) (~ 100 mg crude product, ~ 266  $\mu$ mol, 1.20 eq.) was dissolved in 2.00 mL DCE and compound **64** (86.0 mg, 222  $\mu$ mol, 1.00 eq.) was added. At 0 °C, triethylamine (76.9  $\mu$ L, 555  $\mu$ mol, 2.50 eq.) was added and the mixture was stirred for further five minutes at 0 °C. The solution was warmed to 40 °C and stirred for 20 h under argon atmosphere. The solvent was removed *in vacuo* and the crude product was purified via flash chromatography (10 - 90% B in

## MATERIALS AND METHODS

15 min, Method D, 12 mL/min), which afforded 39.6 mg (32.7%) of compound **82** as a colorless solid.

RP-HPLC (30 - 90% B in 15 min, Method A, 1 mL/min):  $t_R = 11.3$  min;  $k = 6.5$ . Calculated monoisotopic mass ( $C_{26}H_{38}N_6O_7$ ): 546.28, found:  $m/z = 490.4$  [ $M(\mathbf{82})\text{-}t\text{Bu}+\text{H}$ ] $^+$ , 546.7 [ $M(\mathbf{82})+\text{H}$ ] $^+$ , 568.8 [ $M(\mathbf{82})+\text{Na}$ ] $^+$ .

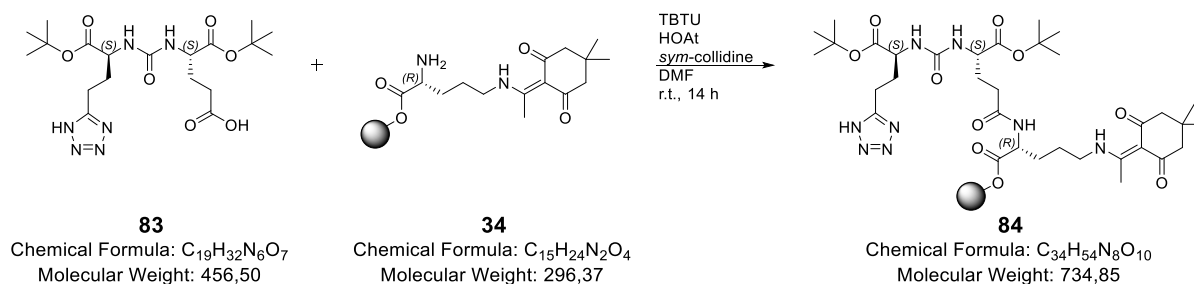
*(S)*-5-(*tert*-butoxy)-4-(3-((*S*)-1-(*tert*-butoxy)-1-oxo-4-(1*H*-tetrazol-5-yl)butan-2-yl)ureido)-5-oxopentanoic acid (**83**)



Compound **82** (17.0 mg, 31.2  $\mu\text{mol}$ , 1.00 eq.) was dissolved in 6.00 mL MeOH and the solution was flushed 5 minutes with argon to remove dissolved oxygen. 3.30 mg of palladium on carbon (10% wt) (corresponds to 330  $\mu\text{g}$  palladium, 3.12  $\mu\text{mol}$ , 0.10 eq.) were added and the flask was sealed with a rubber septum. Remaining air was displaced with argon and subsequently replaced by hydrogen gas. The mixture was stirred under hydrogen atmosphere at room temperature for 69.5 h. Palladium on carbon was filtered off, and the solvent was evaporated *in vacuo*. This afforded 44.0 mg of crude product as a colorless oil, with some minor by-products and remaining reactant **82**. As the main component could be identified as product **83** by RP-HPLC/MS analysis, the crude product was used in the next step without further purification.

RP-HPLC (10 - 90% B in 15 min, Method A, 1 mL/min):  $t_R = 8.94$  min;  $k = 5.0$ . Calculated monoisotopic mass ( $C_{19}H_{32}N_6O_7$ ): 456.23, found:  $m/z = 345.9$  [ $M(\mathbf{83})\text{-}2t\text{Bu}+\text{H}$ ] $^+$ , 456.7 [ $M(\mathbf{83})+\text{H}$ ] $^+$ , 478.7 [ $M(\mathbf{83})+\text{Na}$ ] $^+$ , 912.5 [ $M_2(\mathbf{83})+\text{H}$ ] $^+$ , 934.7 [ $M_2(\mathbf{83})+\text{Na}$ ] $^+$ , 950.3 [ $M_2(\mathbf{83})+\text{K}$ ] $^+$ .

*(S)*-2-Amino-4-(1*H*-tetrazol-5-yl)butanoic acid-*O**t*Bu-carbonyl-*L*-Glu[*D*-Orn(*Dde*)-2-*CT*]-*O**t*Bu (**84**)



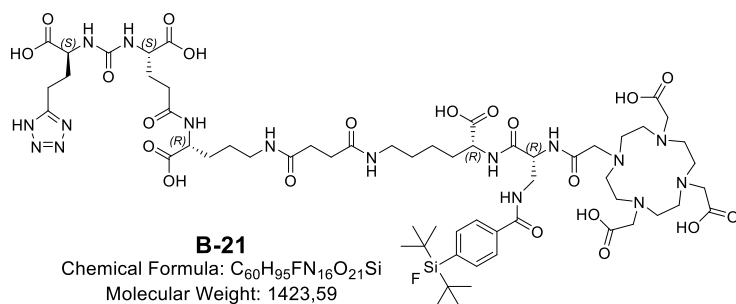
According to GP3, fragment **83** (28.5 mg, ~ 62.4  $\mu\text{mol}$ , 1.00 eq.) was coupled to resin-bound H-*D*-Orn(*Dde*) (**34**) (89.0  $\mu\text{mol}$  1.43 eq.) with TBTU (40.1 mg, 125  $\mu\text{mol}$ , 2.00 eq.) and HOAt

## MATERIALS AND METHODS

(17.0 mg, 125  $\mu\text{mol}$ , 2.00 eq.) as coupling reagents and *sym*-collidine (74.5  $\mu\text{L}$ , 562  $\mu\text{mol}$ , 9.00 eq.) as base. After shaking for 14 h at room temperature, formation of product **84** could be confirmed (GP8), as only one major peak with the expected  $m/z$ -ratio of 734.9 occurred.

RP-HPLC (10 - 90% B in 15 min, Method A, 1 mL/min):  $t_R = 9.91$  min;  $k = 5.6$ . Calculated monoisotopic mass ( $\text{C}_{34}\text{H}_{54}\text{N}_8\text{O}_{10}$ ): 734.40, found:  $m/z = 734.9$  [ $\text{M}(\mathbf{84})+\text{H}$ ] $^+$ .

### Tetrazole derivative **B-21**



Further reactions on resin-bound compound **84** (89.0  $\mu\text{mol}$ , 2.00 eq.) were performed according to standard Fmoc-SPPS on 2-CT resin, applying the above-mentioned methods (GP3 - GP8). For chelator attachment, DOTA-NHS (33.9 mg,

44.5  $\mu\text{mol}$ , 1.00 eq.) and DIPEA (106  $\mu\text{L}$ , 0.62 mmol, 14.0 eq.) were each dissolved in DMF. First, DIPEA in DMF was added to the resin for preactivation. After five minutes, DOTA-NHS in DMF was added and incubated with the resin-bound amine for 15 h. As only low conversion (RP-HPLC/MS analysis after GP8) was reached, further DOTA-NHS (33.9 mg, 44.5  $\mu\text{mol}$ , 1.00 eq.) and DIPEA (106  $\mu\text{L}$ , 0.62 mmol, 14.0 eq.) was added and again incubated for 71 h. Again, no increased conversion could be observed and hence, HOAt (24.2 mg, 0.18 mmol, 2.00 eq.) and DIPEA (212  $\mu\text{L}$ , 1.24 mmol, 28.0 eq.) were added to the reaction mixture. RP-HPLC/MS analysis after 20 h revealed no further significant increase of product signal and hence, the peptide was cleaved off the resin with TFA/TIPS/DCM (GP9) and purified afterwards by preparative RP-HPLC (25 - 80% B in 20 min, Method B, 5 mL/min and 25 - 70% B in 15 min, Method B, 1 mL/min). Subsequent lyophilization afforded 3.55 mg (5.60% yield, chemical purity > 99%) of pure product **B-21** as a colorless powder.

RP-HPLC (10 - 90% B in 15 min, Method A, 1 mL/min):  $t_R = 10.8$  min;  $k = 6.2$ . Calculated monoisotopic mass ( $\text{C}_{60}\text{H}_{95}\text{FN}_{16}\text{O}_{21}\text{Si}$ ): 1422.66, found:  $m/z = 711.6$  [ $\text{M}(\mathbf{B-21})+2\text{H}$ ] $^{2+}$ , 1422.5 [ $\text{M}(\mathbf{B-21})+\text{H}$ ] $^+$ .

### 3.2.3. Cold metal complexation

For  $^{nat}\text{Ga}$ - and  $^{nat}\text{Lu}$ -complexation reactions, previously published procedures were applied with minor modifications.<sup>[140, 199]</sup>

#### General procedures for $^{nat}\text{Ga}$ -complexation (GP13 & GP14)

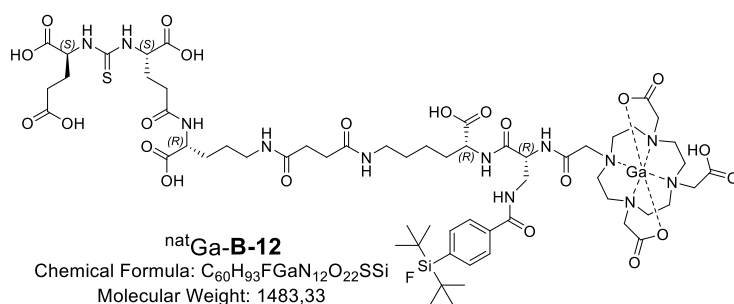
**GP13:** DOTA-conjugated peptide (4.70 mM in *t*BuOH, 1.00 eq.) was added to  $\text{Ga}(\text{NO}_3)_3 \cdot 6 \text{H}_2\text{O}$  (49.2 mM in  $\text{H}_2\text{O}$ , 3.50 eq.). The mixture was stirred for 30 min at 75 °C and afterwards filtered through single use syringe filters (Sartorius Minisart®) to remove  $\text{Ga}(\text{OH})_3$  precipitate.<sup>[299-301]</sup> The  $^{nat}\text{Ga}$ -complexed peptide was obtained after RP-HPLC purification and lyophilization.

**GP14:** DOTA-conjugated peptide (11.0 mM in HEPES buffer (2.7 M, pH = 3), 1.00 eq.) was added to  $\text{Ga}(\text{NO}_3)_3 \cdot 6 \text{H}_2\text{O}$  (33.0 mM in HEPES buffer (2.7 M, pH = 3), 3.50 eq.). The mixture was stirred for 30 min at 75 °C and afterwards filtered through single use syringe filters (Sartorius Minisart®) to remove  $\text{Ga}(\text{OH})_3$  precipitate. The  $^{nat}\text{Ga}$ -complexed peptide was obtained after RP-HPLC purification and lyophilization.

#### General procedure for $^{nat}\text{Lu}$ -complexation (GP15)

100  $\mu\text{L}$  of the precursor (2.00 mM in DMSO, 0.20  $\mu\text{mol}$ , 1.00 eq.) were added to 60.0  $\mu\text{L}$  of  $\text{LuCl}_3$  (20 mM in Tracepur®- $\text{H}_2\text{O}$ , 1.20  $\mu\text{mol}$ , 6.00 eq.) and 40.0  $\mu\text{L}$  Tracepur®- $\text{H}_2\text{O}$ . The reaction mixture was heated for 25 to 30 min at 95 °C. Occasionally, reaction temperatures were adjusted (70 °C for  $^{nat}\text{Lu-B-13}$  and  $^{nat}\text{Lu-B-15}$ ) to maintain high chemical purity. The resulting solution, now 1.00 mM (0.50 mM for  $^{nat}\text{Lu-B-15}$ ), was directly used as stock solution for affinity determinations.

#### $^{nat}\text{Ga}$ -Thioureate **B-12**

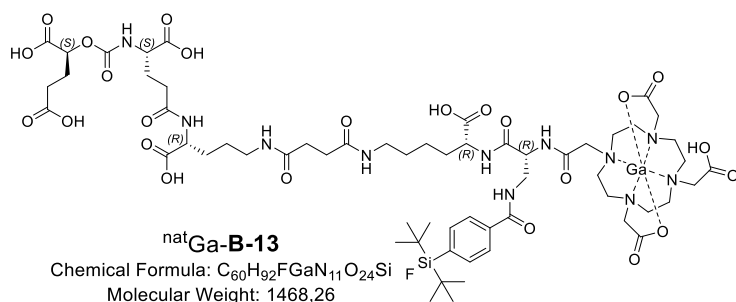


The  $^{nat}\text{Ga}$ -complexed peptide (GP13) was purified by RP-HPLC (30 - 50% B in 20 min, Method B, 5 mL/min) and afforded 70.0  $\mu\text{g}$  (3.35%) of pure product  $^{nat}\text{Ga-B-12}$  as a colorless powder after lyophilization.

RP-HPLC (10 - 90% B in 15 min, Method A, 1 mL/min):  $t_R = 8.65$  min;  $k = 4.7$ . Calculated monoisotopic mass ( $\text{C}_{60}\text{H}_{93}\text{FGaN}_{12}\text{O}_{22}\text{SSi}$ ): 1481.53, found:  $m/z = 742.5$  [ $\text{M}(^{nat}\text{Ga-B-12})+2\text{H}$ ] $^{2+}$ , 1483.0 [ $\text{M}(^{nat}\text{Ga-B-12})+\text{H}$ ] $^+$ , 1503.6 [ $\text{M}(^{nat}\text{Ga-B-12})+\text{Na}$ ] $^+$ .

## MATERIALS AND METHODS

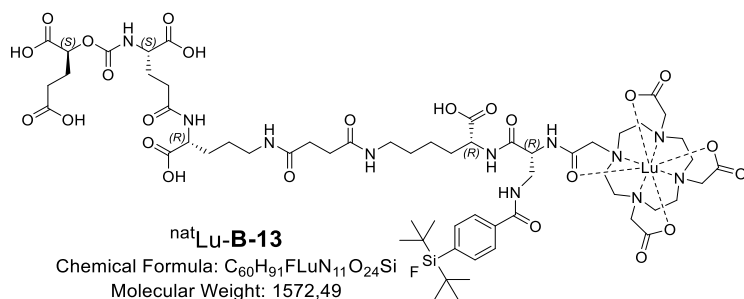
### <sup>nat</sup>Ga-Carbamate **B-13**



The <sup>nat</sup>Ga-complexed peptide (GP14) was purified by RP-HPLC (25 - 45% B in 15 min, Method A, 1 mL/min) and afforded 1.64 mg (26.5%) of pure product <sup>nat</sup>Ga-B-13 as a colorless powder after lyophilization.

RP-HPLC (25 - 45% B in 15 min, Method A, 1 mL/min):  $t_R = 12.0$  min;  $k = 7.0$ . Calculated monoisotopic mass (C<sub>60</sub>H<sub>92</sub>FGaN<sub>11</sub>O<sub>24</sub>Si): 1466.53, found:  $m/z = 734.9$  [M(<sup>nat</sup>Ga-B-13)+2H]<sup>2+</sup>, 1468.0 [M(<sup>nat</sup>Ga-B-13)+H]<sup>+</sup>, 1835.8 [M<sub>5</sub>(<sup>nat</sup>Ga-B-13)+4H]<sup>4+</sup>, 1957.3 [M<sub>4</sub>(<sup>nat</sup>Ga-B-13)+3H]<sup>3+</sup>.

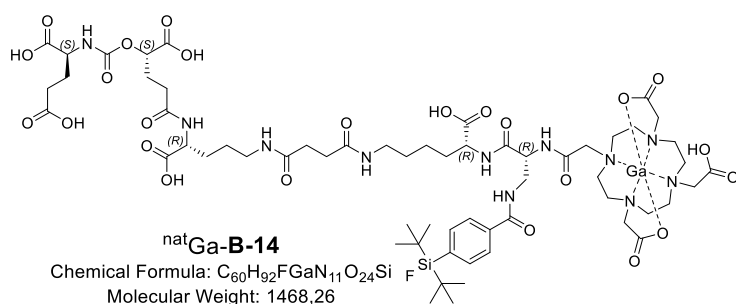
### <sup>nat</sup>Lu-Carbamate **B-13**



<sup>nat</sup>Lu-B-13 (GP15) was obtained in 92.3% chemical purity (> 99% yield) as determined by RP-HPLC.

RP-HPLC (10 - 90% B in 15 min, Method A, 1 mL/min):  $t_R = 8.48$  min;  $k = 4.7$ . Calculated monoisotopic mass (C<sub>60</sub>H<sub>91</sub>FLuN<sub>11</sub>O<sub>24</sub>Si): 1571.54, found:  $m/z = 787.1$  [M(<sup>nat</sup>Lu-B-13)+2H]<sup>2+</sup>, 1573.2 [M(<sup>nat</sup>Lu-B-13)+H]<sup>+</sup>, 1598.0 [M(<sup>nat</sup>Lu-B-13)+Na]<sup>+</sup>.

### <sup>nat</sup>Ga-Carbamate **B-14**

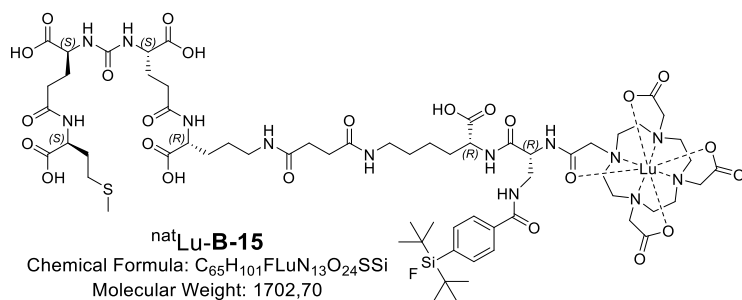


The <sup>nat</sup>Ga-complexed peptide (GP14) was purified by RP-HPLC (20 - 60% B in 15 min, Method A, 1 mL/min) and afforded 0.53 mg (15.7%) of pure product <sup>nat</sup>Ga-B-14 as a colorless powder after lyophilization.

RP-HPLC (10 - 90% B in 15 min, Method A, 1 mL/min):  $t_R = 8.46$  min;  $k = 4.6$ . Calculated monoisotopic mass (C<sub>60</sub>H<sub>92</sub>FGaN<sub>11</sub>O<sub>24</sub>Si): 1466.53, found:  $m/z = 734.3$  [M(<sup>nat</sup>Ga-B-14)+2H]<sup>2+</sup>, 1468.2 [M(<sup>nat</sup>Ga-B-14)+H]<sup>+</sup>, 1835.5 [M<sub>5</sub>(<sup>nat</sup>Ga-B-14)+4H]<sup>4+</sup>, 1957.4 [M<sub>4</sub>(<sup>nat</sup>Ga-B-14)+3H]<sup>3+</sup>.

## MATERIALS AND METHODS

### *nat*Lu-Proinhibitor **B-15**

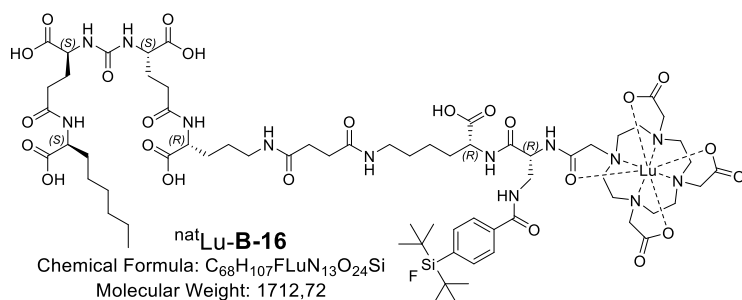


mass (C<sub>65</sub>H<sub>101</sub>FLuN<sub>13</sub>O<sub>24</sub>SSi): 1701.60, found:  $m/z = 851.3$  [M(<sup>nat</sup>Lu-B-15)+2H]<sup>2+</sup>, 1701.8 [M(<sup>nat</sup>Lu-B-15)+H]<sup>+</sup>.

<sup>nat</sup>Lu-B-15 (GP15) was obtained in > 99% chemical purity (> 99% yield) as determined by RP-HPLC.

RP-HPLC (10 - 90% B in 15 min, Method A, 1 mL/min):  $t_R = 8.62$  min;  $k = 4.7$ . Calculated monoisotopic

### *nat*Lu-Proinhibitor **B-16**

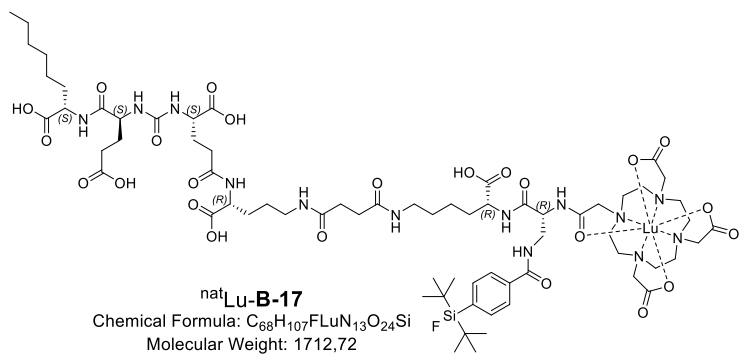


mass (C<sub>68</sub>H<sub>107</sub>FLuN<sub>13</sub>O<sub>24</sub>Si): 1711.67, found:  $m/z = 856.4$  [M(<sup>nat</sup>Lu-B-16)+2H]<sup>2+</sup>, 1711.6 [M(<sup>nat</sup>Lu-B-16)+H]<sup>+</sup>.

<sup>nat</sup>Lu-B-16 (GP15) was obtained in > 99% chemical purity (> 99% yield) as determined by RP-HPLC.

RP-HPLC (10 - 90% B in 15 min, Method A, 1 mL/min):  $t_R = 9.48$  min;  $k = 5.3$ . Calculated monoisotopic

### *nat*Lu-Proinhibitor **B-17**



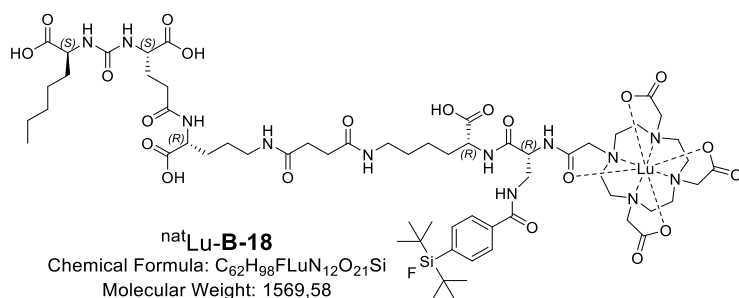
1711.67, found:  $m/z = 856.1$  [M(<sup>nat</sup>Lu-B-17)+2H]<sup>2+</sup>, 1711.1 [M(<sup>nat</sup>Lu-B-17)+H]<sup>+</sup>.

<sup>nat</sup>Lu-B-17 (GP15) was obtained in > 99% chemical purity (> 99% yield) as determined by RP-HPLC.

RP-HPLC (10 - 90% B in 15 min, Method A, 1 mL/min):  $t_R = 9.29$  min;  $k = 5.2$ . Calculated monoisotopic mass (C<sub>68</sub>H<sub>107</sub>FLuN<sub>13</sub>O<sub>24</sub>Si):

## MATERIALS AND METHODS

### *nat*Lu-L-2-Aminoheptanoic acid derivative **B-18**

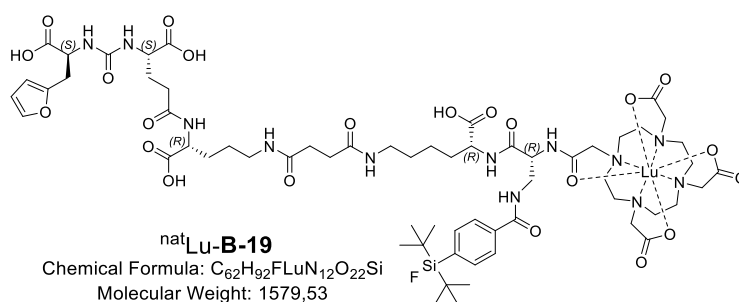


mass (C<sub>62</sub>H<sub>98</sub>FLuN<sub>12</sub>O<sub>21</sub>Si): 1568.61, found:  $m/z = 784.5 [M(^{nat}\text{Lu-B-18})+2H]^{2+}$ ,  
1568.0 [M(<sup>nat</sup>Lu-B-18)+H]<sup>+</sup>.

<sup>nat</sup>Lu-B-18 (GP15) was obtained in 94.9% chemical purity (> 99% yield) as determined by RP-HPLC.

RP-HPLC (10 - 90% B in 15 min, Method A, 1 mL/min):  $t_R = 11.7$  min;  $k = 6.8$ . Calculated monoisotopic

### *nat*Lu-Furyl derivative **B-19**

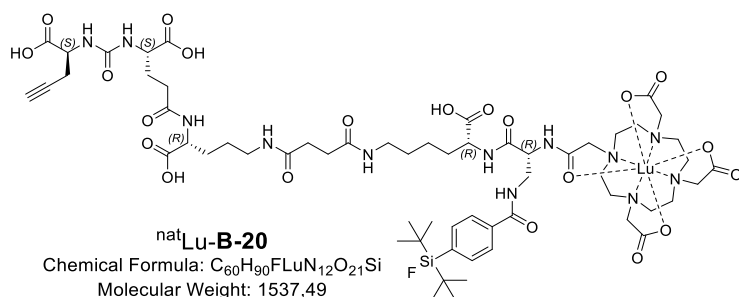


mass (C<sub>62</sub>H<sub>92</sub>FLuN<sub>12</sub>O<sub>22</sub>Si): 1578.56, found:  $m/z = 789.7 [M(^{nat}\text{Lu-B-19})+2H]^{2+}$ ,  
1579.3 [M(<sup>nat</sup>Lu-B-19)+H]<sup>+</sup>.

<sup>nat</sup>Lu-B-19 (GP15) was obtained in 98.1% chemical purity (> 99% yield) as determined by RP-HPLC.

RP-HPLC (10 - 90% B in 15 min, Method A, 1 mL/min):  $t_R = 11.2$  min;  $k = 6.5$ . Calculated monoisotopic

### *nat*Lu-Alkyne derivative **B-20**



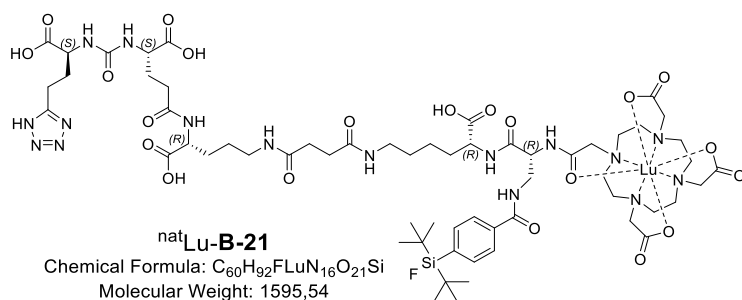
mass (C<sub>60</sub>H<sub>90</sub>FLuN<sub>12</sub>O<sub>21</sub>Si): 1536.55, found:  $m/z = 769.6 [M(^{nat}\text{Lu-B-20})+2H]^{2+}$ ,  
1538.4 [M(<sup>nat</sup>Lu-B-20)+H]<sup>+</sup>.

<sup>nat</sup>Lu-B-20 (GP15) was obtained in 99.1% chemical purity (> 99% yield) as determined by RP-HPLC.

RP-HPLC (10 - 90% B in 15 min, Method A, 1 mL/min):  $t_R = 10.9$  min;  $k = 6.3$ . Calculated monoisotopic

## MATERIALS AND METHODS

### <sup>nat</sup>Lu-Tetrazole derivative **B-21**



<sup>nat</sup>Lu-**B-21** (GP15) was obtained in 92.9% chemical purity (> 99% yield) as determined by RP-HPLC.

RP-HPLC (10 - 90% B in 15 min, Method A, 1 mL/min):  $t_R = 10.6$  min;  $k = 6.1$ . Calculated monoisotopic

mass (C<sub>60</sub>H<sub>92</sub>FLuN<sub>16</sub>O<sub>21</sub>Si): 1594.58, found:  $m/z = 797.5$  [M(<sup>nat</sup>Lu-**B-21**)+2H]<sup>2+</sup>, 816.6 [M(<sup>nat</sup>Lu-**B-21**)+K+H]<sup>2+</sup>, 1595.0 [M(<sup>nat</sup>Lu-**B-21**)+H]<sup>+</sup>.

Reaction conditions, chemical purities and yields of the <sup>nat</sup>Ga- and <sup>nat</sup>Lu-rhPSMA ligands described above are summarized in *Table 4*.

**Table 4:** Reaction conditions, chemical purity and yield of the investigated <sup>nat</sup>Ga- and <sup>nat</sup>Lu-rhPSMA ligands.

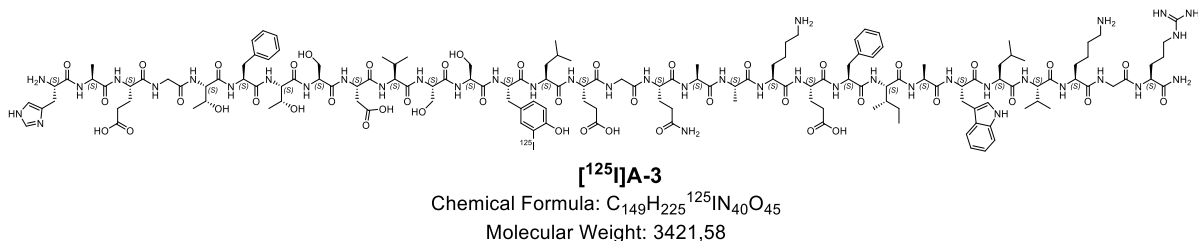
PSMA (pro)inhibitor	Reaction conditions	Chemical purity	Yield <sup>a</sup>
<sup>nat</sup> Ga- <b>B-12</b>	75 °C, 30 min	93.0%	3.35%
<sup>nat</sup> Ga- <b>B-13</b>	75 °C, 30 min	97.2%	26.5%
<sup>nat</sup> Lu- <b>B-13</b>	70 °C, 25 min	92.3%	> 99%
<sup>nat</sup> Ga- <b>B-14</b>	75 °C, 30 min	97.6%	15.7%
<sup>nat</sup> Lu- <b>B-15</b>	70 °C, 30 min	> 99%	> 99%
<sup>nat</sup> Lu- <b>B-16</b>	95 °C, 25 min	> 99%	> 99%
<sup>nat</sup> Lu- <b>B-17</b>	95 °C, 25 min	> 99%	> 99%
<sup>nat</sup> Lu- <b>B-18</b>	95 °C, 25 min	94.9%	> 99%
<sup>nat</sup> Lu- <b>B-19</b>	95 °C, 25 min	98.1%	> 99%
<sup>nat</sup> Lu- <b>B-20</b>	95 °C, 25 min	99.1%	> 99%
<sup>nat</sup> Lu- <b>B-21</b>	95 °C, 25 min	92.9%	> 99%

<sup>a</sup>calculated relative to the uncomplexed precursor. Number of experiments is n = 1.

### 3.3. Radiolabeling

#### 3.3.1. <sup>125</sup>I-labeling

##### [<sup>125</sup>I]Tyr(3-I)<sup>19</sup>-Glucagon-like peptide 1 ([<sup>125</sup>I]A-3)



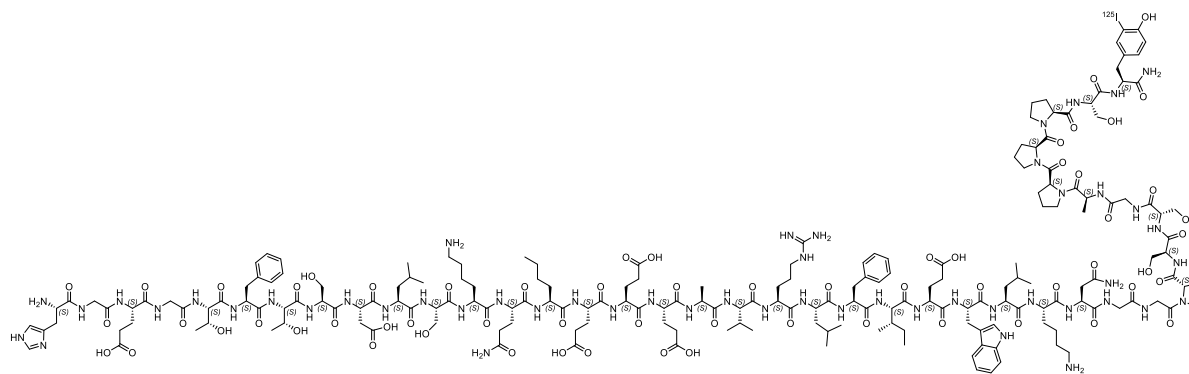
<sup>125</sup>I-Labeled GLP-1 was prepared via the iodogen method<sup>[302]</sup>, with some minor modifications. The precursor GLP-1 (~ 0.1 mg, 30.3 nmol, 121 eq.) was dissolved in 20 μL H<sub>2</sub>O and 280 μL TRIS buffer (25 mM TRIS HCl, 0.04 M NaCl, pH = 7.5). The solution was transferred to a vial, which has been precoated<sup>1</sup> with 150 μg Iodogen (1,3,4,6-tetrachloro-3α,6α-diphenylglycouril, Thermo Fisher Scientific, Darmstadt, Germany) (347 nmol, 1388 eq.). Afterwards, 15 ± 5 MBq [<sup>125</sup>I]NaI (74 MBq/nmol, 3.7 GBq/mL in 40 mM NaOH, Hartmann Analytic, Braunschweig, Germany) (5.00 μL, 250 pmol, 1.00 eq.) were added, the reaction solution was incubated for 15 min at r.t. and purified by radio-RP-HPLC (33 - 40% B in 20 min, Method A, 1 mL/min) to afford 6.26 MBq (34.2% RCY, 49% RCP) of product [<sup>125</sup>I]A-3. Immediately after purification, radiolysis-induced by-products occurred to different extents depending on added reagents and radiolysis inhibitors (see section 4.1.1).

RP-HPLC (33 - 40% B in 20 min, Method A, 1 mL/min):  $t_R = 8.20$  min;  $k = 4.5$ ;  $t_R$  (cold standard) = 8.10 min (33 - 40% B in 20 min, Method A, 1 mL/min).

<sup>1</sup> Precoating was performed according to the method described by Salacinski *et al.* and the vials were stored at -20 °C.<sup>[302]</sup>

## MATERIALS AND METHODS

### [Nle<sup>14</sup>, [<sup>125</sup>I]Tyr(3-I)<sup>40</sup>]Exendin-4 (**A-17**)



#### **A-17**

Chemical Formula: C<sub>194</sub>H<sub>292</sub><sup>125</sup>I<sub>N</sub><sub>51</sub>O<sub>62</sub>

Molecular Weight: 4455,67

<sup>125</sup>I-labeled exendin-4 was prepared via the Iodogen method<sup>[302]</sup>, with some minor modifications. The precursor (Nle<sup>14</sup>, Tyr<sup>40</sup>)exendin-4 (150 µg, 30.6 nmol, 122 eq.) was dissolved in 20 µL DMSO and 280 µL TRIS buffer (25 mM TRIS HCl, 0.04 M NaCl, pH = 7.5). The solution was transferred to a vial, which has been precoated<sup>1</sup> with 15.0 µg Iodogen (34.7 nmol, 139 eq.). Afterwards, 15 ± 5 MBq [<sup>125</sup>I]NaI (74 MBq/nmol, 3.7 GBq/mL in 40 mM NaOH, Hartmann Analytic, Braunschweig, Germany) (5.00 µL, 250 pmol, 1.00 eq.) were added, the reaction solution was incubated for 15 min at r.t. and 150 µL thereof were purified by radio-RP-HPLC (0% B (2 min) → 0 - 37.5% B (3 min) → 37.5% B (35 min) → 38% B (10 min), Method A, 1 mL/min) to afford 3.15 MBq (48.8% RCY, > 99% RCP) of product **A-17**. The radioligand was stored in the HPLC solvent (stock solution) at -80 °C until further use. Prior to the *in vitro* experiments, the radioligand was dissolved in HBSS (with or w/o 1% BSA) to achieve a final concentration of 0.41 nM in the respective assays. The radioligand stock solution was used to a maximum of 14 days to ensure a RCP of > 92% (Table 5) and replaced by freshly prepared radioligand afterwards.

RP-HPLC (20 - 70% 15 min, Method A, 1 mL/min):  $t_R = 9.00$  min;  $k = 5.0$ ;  $t_R$  (cold standard) = 8.90 min (20 - 70% 15 min, Method A, 1 mL/min).

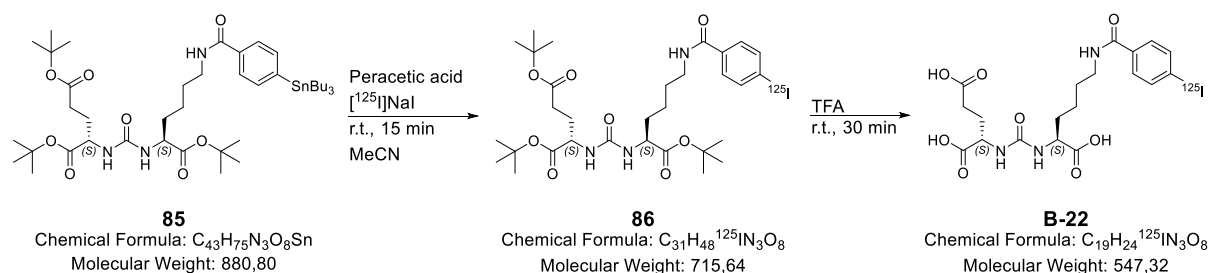
**Table 5:** Stability study of reference radioligand [Nle<sup>14</sup>, [<sup>125</sup>I]Tyr(3-I)<sup>40</sup>]Exendin-4 (**A-17**).

Days after radioiodination	RCP of [Nle <sup>14</sup> , [ <sup>125</sup> I]Tyr(3-I) <sup>40</sup> ]Exendin-4 ( <b>A-17</b> ) <sup>a</sup>
0	≥ 95% (n = 4)
4	95%
9	95%
16	92%
20	82%
24	82%
29	78%
36	78%

<sup>a</sup>n = 1, unless otherwise stated.

## MATERIALS AND METHODS

### (((S)-1-Carboxy-5-(4-(Iodo-<sup>125</sup>I)benzamido)pentyl)carbamoyl)-L-glutamic acid ([[<sup>125</sup>I]I-BA)KuE) (**B-22**)



The reference ligand for *in vitro* studies ([[<sup>125</sup>I]I-BA)KuE (**B-22**) was prepared according to a previously published procedure by Weineisen *et al.*<sup>[199]</sup> Peracetic acid was prepared by mixing 130  $\mu$ L hydrogen peroxide (30%) with 50  $\mu$ L acetic acid. After an incubation period of two hours, 20  $\mu$ L of the peracetic acid solution and [<sup>125</sup>I]NaI (5.00  $\mu$ L, 250 pmol, 1.00 eq.) were added to a solution of approximately 0.10 mg of stannylated precursor **85** (110 nmol, 440 eq.) in 30.0  $\mu$ L MeCN/acetic acid (2/1) and incubated at room temperature for 15 minutes. The reaction mixture was diluted with 10 mL water and loaded onto a C18 Sep Pak Plus cartridge (360 mg, Waters GmbH, Eschborn, Germany), which was initially preconditioned with 10 mL MeOH and washed with 10 mL H<sub>2</sub>O. The loaded cartridge was washed with 10 mL H<sub>2</sub>O and the product was eluted with 1.50 mL MeOH/EtOH (1/1). The solvent was removed by careful heating to 70 °C and under a stream of nitrogen. The *tert*-butyl protective groups were removed by incubation of product **86** with 400  $\mu$ L TFA for 45 minutes. After evaporation of TFA under N<sub>2</sub>, the residue was diluted in 400  $\mu$ L MeCN/H<sub>2</sub>O (2/8) and product **B-22** was isolated by radio-RP-HPLC (20 - 40% B in 20 min, Method A, 1 mL/min) to afford 7.97 MBq (38.9% RCY, > 99% RCP). The radioligand was stored in the HPLC solvent (stock solution) at 8 °C until further use. Prior to the *in vitro* experiments, the radioligand was dissolved either in HBSS (1% BSA) (affinity) or DMEM-F12 (5% BSA) (internalization) to achieve a final concentration of 0.20 nM in the respective assays. The radioligand stock solution was used to a maximum of four weeks and replaced by freshly prepared radioligand afterwards.

RP-HPLC (10 - 90% B in 15 min, Method A, 1 mL/min):  $t_R$  = 8.50 min;  $k$  = 4.7;  $t_R$  (cold standard) = 8.40 min (10 - 90% B in 15 min, Method A, 1 mL/min).

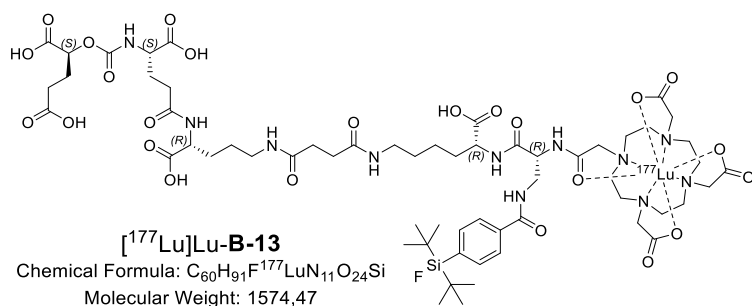
### 3.3.2. $^{177}\text{Lu}$ -labeling

For  $^{177}\text{Lu}$ -labeling, previously published procedures were applied with minor modifications.<sup>[136, 303]</sup> Radiochemical yields (RCY) are given decay corrected (d.c.) to the start of synthesis.

#### General procedure for $^{177}\text{Lu}$ -complexation (GP16)

5.00  $\mu\text{L}$  of the precursor (0.20 mM in DMSO, 1.00 nmol, 1.00 eq.) were added to 10.0  $\mu\text{L}$  of 1 M NaOAc buffer (aq.) (pH = 5.5). Subsequently, 14.0 to 63.5 MBq  $^{177}\text{LuCl}_3$  ( $A_s > 3000$  GBq/mg, 740 MBq/mL, 0.04 M HCl, ITG, Garching, Germany) were added and the mixture was filled up to 100  $\mu\text{L}$  with 0.04 M HCl (in Tracepur<sup>®</sup>-H<sub>2</sub>O). 10.0  $\mu\text{L}$  of 0.1 M sodium ascorbate (aq.) (in Tracepur<sup>®</sup>-H<sub>2</sub>O) were added and the reaction mixture was heated for 25 min at 95 °C. Occasionally, reaction temperatures were adjusted (70 °C for  $^{nat}\text{Lu}$ -**B-13** and 80 °C for  $^{nat}\text{Lu}$ -**B-15**) to maintain high chemical purity. In case of incomplete complexation, removal of free  $^{177}\text{Lu}^{3+}$  via HLB cartridge (30 mg) was required. Therefore, the cartridge was preconditioned with EtOH (10 mL) and PBS (10 mL), the reaction solution was diluted in 5 - 10 mL PBS and loaded onto the cartridge. After washing the cartridge with 5 mL PBS, the radioligand was eluted with 200  $\mu\text{L}$  EtOH/PBS (1/1).

#### $^{177}\text{Lu}$ Lu-Carbamate **B-13**

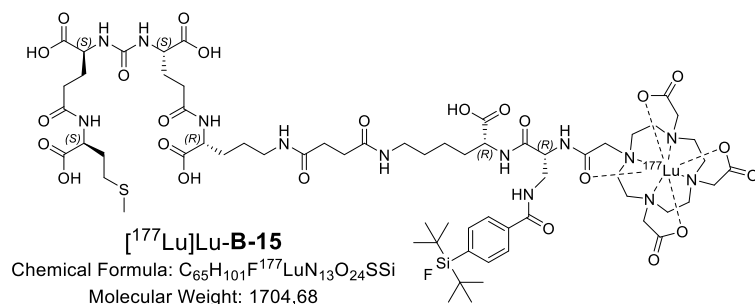


$^{177}\text{Lu}$ Lu-**B-13** (GP16) was obtained in  $69.7 \pm 18.2\%$  ( $n = 6$ ) isolated RCY. The apparent molar activities ( $A_m$ ) were 12.5 to 21.9 GBq/ $\mu\text{mol}$  at the end of synthesis. RCP as determined by radio-RP-HPLC and radio-TLC

was  $96.9 \pm 2.1\%$ .

RP-HPLC (10 - 90% B in 15 min, Method A, 1 mL/min):  $t_R = 9.59$  min;  $k = 5.4$ ;  $t_R$  (cold standard) = 9.49 min (10 - 90% B in 15 min, Method A, 1 mL/min).

#### $^{177}\text{Lu}$ Lu-Proinhibitor **B-15**



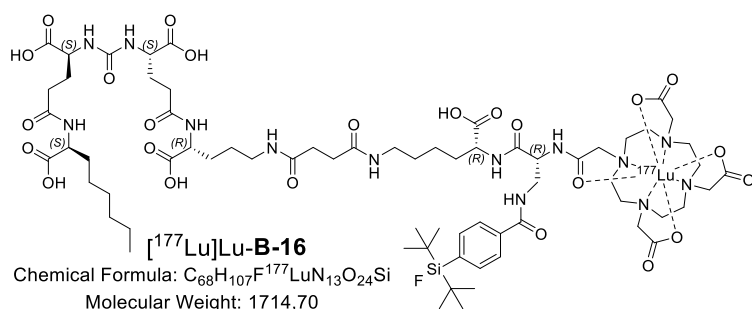
$^{177}\text{Lu}$ Lu-**B-15** (GP16) was purified by radio-RP-HPLC, which afforded the final product in  $44.0 \pm 7.6\%$  ( $n = 4$ ) isolated RCY. Exact apparent  $A_m$  of products, which were purified by radio-RP-HPLC could not be determined as the

## MATERIALS AND METHODS

amount of cold precursor within the product fraction could only be estimated. In these cases, the amount of substance was roughly calculated by the percentage of product, determined by radio-RP-HPLC. This afforded apparent  $A_m$  of approximately 4.64 to 14.5 GBq/ $\mu$ mol. RCP as determined by radio-RP-HPLC and radio-TLC was  $89.3 \pm 1.9\%$ . Higher RCPs could not be achieved, as right after purification, quality control revealed up to 13% of oxidized by-product again.

RP-HPLC (10 - 90% B in 15 min, Method A, 1 mL/min):  $t_R = 10.1$  min;  $k = 5.7$ ;  $t_R$  (cold standard) = 10.0 min (10 - 90% B in 15 min, Method A, 1 mL/min).

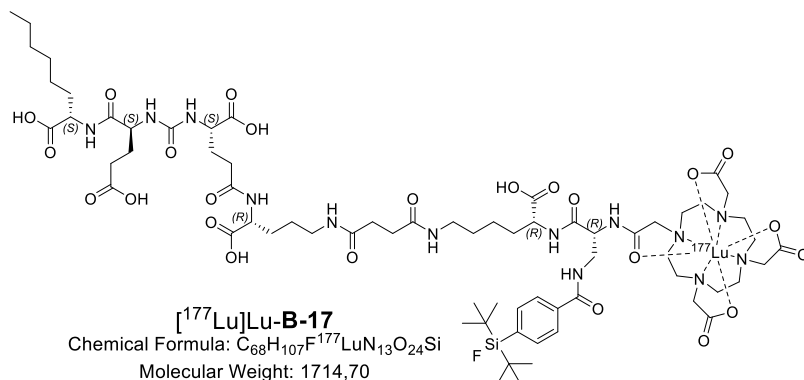
### [<sup>177</sup>Lu]Lu-Proinhibitor B-16



[<sup>177</sup>Lu]Lu-B-16 (GP16) was obtained in  $81.4 \pm 6.9\%$  ( $n = 2$ ) isolated RCY. The apparent  $A_m$  were 24.1 and 24.8 GBq/ $\mu$ mol at the end of synthesis. RCP as determined by radio-RP-HPLC and radio-TLC was  $98.2 \pm 0.1\%$ .

RP-HPLC (10 - 90% B in 15 min, Method A, 1 mL/min):  $t_R = 11.1$  min;  $k = 6.4$ ;  $t_R$  (cold standard) = 11.0 min (10 - 90% B in 15 min, Method A, 1 mL/min).

### [<sup>177</sup>Lu]Lu-Proinhibitor B-17

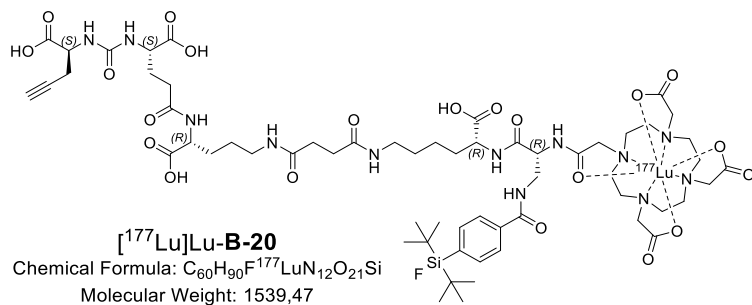


[<sup>177</sup>Lu]Lu-B-17 (GP16) was obtained in  $> 99\%$  ( $n = 1$ ) isolated RCY. The apparent  $A_m$  was 27.4 GBq/ $\mu$ mol at the end of synthesis. RCP as determined by radio-RP-HPLC and radio-TLC was 94.7%.

RP-HPLC (10 - 90% B in 15 min, Method A, 1 mL/min):  $t_R = 11.0$  min;  $k = 6.3$ ;  $t_R$  (cold standard) = 10.9 min (10 - 90% B in 15 min, Method A, 1 mL/min).

## MATERIALS AND METHODS

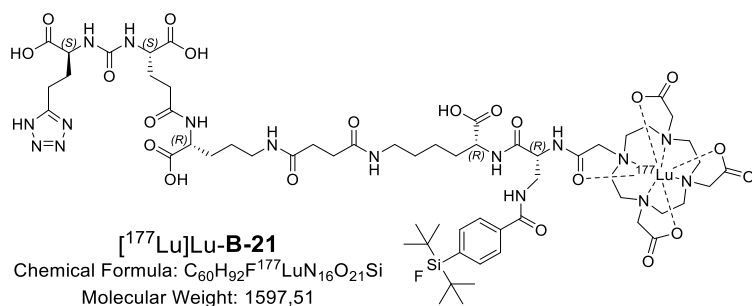
### [<sup>177</sup>Lu]Lu-Alkyne derivative **B-20**



[<sup>177</sup>Lu]Lu-**B-20** (GP16) was obtained in 70.3 or > 99% (n = 3) isolated RCY. The apparent A<sub>m</sub> were 26.3 to 62.0 GBq/μmol at the end of synthesis. RCP as determined by radio-RP-HPLC and radio-TLC was 93.6 ± 2.5%.

RP-HPLC (10 - 90% B in 15 min, Method A, 1 mL/min): t<sub>R</sub> = 10.3 min; k = 5.9; t<sub>R</sub> (cold standard) = 10.2 min (10 - 90% B in 15 min, Method A, 1 mL/min).

### [<sup>177</sup>Lu]Lu-Tetrazole derivative **B-21**



[<sup>177</sup>Lu]Lu-**B-21** (GP16) was obtained in > 99% (n = 4) isolated RCY. The apparent A<sub>m</sub> ranged from 42.2 to 63.5 GBq/μmol at the end of synthesis. RCP as determined by radio-RP-HPLC and radio-TLC was 97.2 ± 1.2%.

RP-HPLC (10 - 90% B in 15 min, Method A, 1 mL/min): t<sub>R</sub> = 10.0 min; k = 5.7; t<sub>R</sub> (cold standard) = 9.90 min (10 - 90% B in 15 min, Method A, 1 mL/min).

Reaction conditions, radiochemical yields, apparent molar activities, used activities and radiochemical purities of the [<sup>177</sup>Lu]Lu-rhPSMA ligands described above are summarized in *Table 6*.

## MATERIALS AND METHODS

**Table 6:** Reaction conditions, RCY, apparent  $A_m$ , used activities and RCP of the investigated [ $^{177}\text{Lu}$ ]Lu-rhPSMA ligands.

<b>PSMA (pro)inhibitor</b>	<b>Reaction conditions</b>	<b>RCY<sup>a</sup></b>	<b>apparent <math>A_m</math> [GBq/<math>\mu\text{mol}</math>]</b>	<b>used activities [MBq]</b>	<b>RCP</b>	<b>No. of experi- ments</b>
[ $^{177}\text{Lu}$ ]Lu-B-13	70 °C, 25 min	69.7 $\pm$ 18.2%	12.5 - 21.9	22.3 - 62.2	96.9 $\pm$ 2.1%	6
[ $^{177}\text{Lu}$ ]Lu-B-15	80 °C, 25 min	44.0 $\pm$ 7.6%	4.64 - 14.5	14.0 - 35.9	89.3 $\pm$ 1.9%	4
[ $^{177}\text{Lu}$ ]Lu-B-16	95 °C, 25 min	81.4 $\pm$ 6.9%	24.1 & 24.8	28.0 & 32.5	98.2 $\pm$ 0.1%	2
[ $^{177}\text{Lu}$ ]Lu-B-17	95 °C, 25 min	> 99%	27.4	27.4	94.7%	1
[ $^{177}\text{Lu}$ ]Lu-B-20	95 °C, 25 min	70.3 to > 99%	26.3 - 62.0	37.5 - 62.0	93.6 $\pm$ 2.5%	3
[ $^{177}\text{Lu}$ ]Lu-B-21	95 °C, 25 min	> 99%	42.2 - 63.5	42.2 - 63.5	97.2 $\pm$ 1.2%	4

<sup>a</sup>decay corrected to the start of synthesis. Data for isolated RCY and RCP are expressed as mean  $\pm$  SD.

### 3.4. *In vitro* experiments

#### 3.4.1. Cell culture

INS-1E cells, expressing the rat GLP-1 receptor<sup>[304]</sup> were kindly provided by Dr. Günter Päth (Universitätsklinikum Freiburg, Freiburg, Germany) and cultivated in RPMI 1640 medium (11.1 mM D-glucose, 2.00 mM L-glutamine; REF-number: 21875-034; Fisher Scientific GmbH, Schwerte, Germany) supplemented with 10% fetal bovine serum (Merck KgaA, Darmstadt, Germany), 50  $\mu$ M  $\beta$ -mercaptoethanol, 10 mM HEPES (both from Fisher Scientific GmbH, Schwerte, Germany) and 1 mM sodium pyruvate (Merck KgaA, Darmstadt, Germany). Cells were kept at 37 °C in a humidified 5% CO<sub>2</sub> atmosphere.

HEK293 and HEK293-hGLP-1R cells (HEK293 cells stably transfected with the human GLP-1 receptor)<sup>[305]</sup> were kindly provided by Prof. Dr. Timothy Kieffer (University of British Columbia, Vancouver, Canada). Cells were cultivated in high glucose DMEM (25.0 mM D-glucose, 3.97 mM GlutaMAX; REF-number: 61965-026; Fisher Scientific GmbH, Schwerte, Germany) supplemented with 10% fetal bovine serum and 1 mM sodium pyruvate. Medium for stably transfected HEK293-hGLP-1R cells was constantly supplemented with 1 mg/mL Geneticin (G-418 Biochrom, Merck KgaA, Darmstadt, Germany) as selection antibiotic. Both cell lines were kept at 37 °C in a humidified 5% CO<sub>2</sub> atmosphere.

PSMA positive LNCaP cells (300265; Cell Lines Service, Eppelheim, Germany) were cultivated in DMEM/Ham's F-12 (1/1) (17.5 mM D-glucose, 2.50 mM GlutaMAX; REF-number: 31331-028; Fisher Scientific GmbH, Schwerte, Germany) supplemented with 10% fetal bovine serum and kept at 37 °C in a humidified 5% CO<sub>2</sub> atmosphere.

One day ( $24 \pm 2$  h) prior to all *in vitro* experiments, the cultivated cells were harvested using a mixture of trypsin/ethylenediaminetetraacetic acid (0.05%/0.02%) in PBS (Merck KgaA, Darmstadt, Germany) and centrifuged at 1 300 rpm (ca. 190  $\times$  g) for 3 min at room temperature (Heraeus Megafuge 16, Thermo Fisher Scientific, Darmstadt, Germany). After centrifugation, the supernatant was disposed and the cell pellet was resuspended in culture medium. Cells were counted with a Neubauer hemocytometer (Paul Marienfeld GmbH & Co. KG, Lauda-Königshofen, Germany) and seeded in 24-well plates.

Radioligand uptake studies with INS-1E, HEK293 and HEK293-hGLP-1R were performed by transferring different amounts of cells ( $1 \times 10^5$  -  $2 \times 10^6$  cells/mL per well) into 24-well plates (Greiner Bio-One, Kremsmünster, Austria). The optimal amount of cell-bound radioligand (% of added dose) was determined at different temperatures (4 °C or r.t.), different time points (1 h, 1.5 h, 2 h, 6 h or 12 h), in different media (HBSS (1% BSA) or culture medium) and with different concentrations of the radioligand [Nle<sup>14</sup>, [<sup>125</sup>I]Tyr(3-I)<sup>40</sup>]exendin-4 (0.41 nM, 0.75 nM or 0.82 nM).

## MATERIALS AND METHODS

IC<sub>50</sub> values of GLP-1R or PSMA ligands were determined by transferring 1.50 × 10<sup>5</sup> cells/mL per well into 24-well plates, whereas internalization (PSMA ligands only) was assessed by transferring 1.25 × 10<sup>5</sup> cells/mL per well into poly-L-lysine (PLL)-coated 24-well plates.

Chemical purities of peptides evaluated in *in vitro* studies were > 95% for GLP-1R ligands (except for **A-10** and **A-15**) and > 92% for PSMA ligands as determined by RP-HPLC.

### 3.4.2. Affinity determinations (IC<sub>50</sub>)

For GLP-1R affinity (IC<sub>50</sub>) determinations, the culture medium was removed and the cells were washed with 500 µL of HBSS (Merck KgaA, Darmstadt, Germany), containing 1% BSA (Merck KgaA, Darmstadt, Germany). Afterwards, 200 µL of HBSS (1% BSA) were added to each well and equilibrated on ice (4 °C) for 15 min. 25 µL/well of either HBSS (1% BSA) (= control) or of solutions, containing the respective unlabeled ligand in increasing concentrations (10<sup>-10</sup> - 10<sup>-4</sup> M in HBSS) were added, followed by the addition of 25 µL of [Nle<sup>14</sup>, [<sup>125</sup>I]Tyr(3-I)<sup>40</sup>]exendin-4 in HBSS (1% BSA) to each well. Experiments were carried out in triplicates for each concentration. The final concentrations of unlabeled ligand ranged from 10<sup>-11</sup> - 10<sup>-5</sup> M and the final radioligand concentration was 0.41 nM in all binding assays. The cells were incubated for two hours at 4 °C. Incubation was terminated by removal of the incubation medium. The cells were washed with 250 µL of HBSS (1% BSA) and the wash medium was combined with the respective supernatant. This fraction represents the amount of free radioligand. The cells were lysed by addition of 250 µL of 1 M aqueous NaOH. After 20 min, the lysate of each well was transferred to the respective vial as well as 250 µL of 1 M NaOH used for rinsing the well. Quantification of the amount of free and bound activity was performed in a γ-counter. The corresponding IC<sub>50</sub> values were calculated using the GraphPad PRISM7 software. IC<sub>50</sub> values of GLP-1 were determined in parallel on the same day to ensure assay validity. Only IC<sub>50</sub> values of the new compounds, for which the affinity of the corresponding GLP-1 control experiment was in a range of 23.2 ± 12.2 nM (n = 11), were considered.

For PSMA affinity (IC<sub>50</sub>) determinations, the culture medium was removed and the cells were washed with 500 µL of HBSS (1% BSA). Afterwards, 200 µL of HBSS (1% BSA) were added to each well and equilibrated on ice (4 °C) for 15 min. 25 µL/well of either HBSS (1% BSA) (= control) or of solutions, containing the respective unlabeled ligand in increasing concentrations (10<sup>-10</sup> - 10<sup>-4</sup> M in HBSS) were added, followed by the addition of 25 µL of ([<sup>125</sup>I]I-BA)KuE in HBSS (1% BSA) to each well. Experiments were carried out in triplicates for each concentration. The final concentrations of unlabeled ligand ranged from 10<sup>-11</sup> - 10<sup>-5</sup> M and the final radioligand concentration was 0.20 nM in all binding assays. The cells were incubated for one hour at 4 °C. Incubation was terminated by removal of the incubation medium. The cells were washed with 250 µL of HBSS (1% BSA) and the wash medium was combined with the respective supernatant.

## MATERIALS AND METHODS

This fraction represents the amount of free radioligand. The cells were lysed by addition of 250  $\mu$ L of 1 M aqueous NaOH. After 20 min, the lysate of each well was transferred to the respective vial as well as 250  $\mu$ L of 1 M NaOH used for rinsing the well. Quantification of the amount of free and bound activity was performed in a  $\gamma$ -counter. The corresponding  $IC_{50}$  values were calculated using the GraphPad PRISM7 software.  $IC_{50}$  values of ( $^{nat}I$ -BA)KuE were determined in parallel on the same day to ensure assay validity. Only  $IC_{50}$  values, for which the affinity of the corresponding ( $^{nat}I$ -BA)KuE control experiment was in a range of  $3.95 \pm 1.35$  nM ( $n = 6$ ) were considered, except for compounds **B-2** to **B-11** for which the affinity of ( $^{nat}I$ -BA)KuE was in a range of  $21.7 \pm 7.9$  nM ( $n = 3$ ).

### 3.4.3. Stability studies of PSMA substrate mimetics

Similar to PSMA affinity ( $IC_{50}$ ) determinations, the culture medium was removed and the cells were washed with 500  $\mu$ L of HBSS. Afterwards, 225  $\mu$ L of HBSS were added to each well and equilibrated on ice (4  $^{\circ}C$ ) for 15 min. 25  $\mu$ L/well of solutions, containing the respective unlabeled ligand in a  $10^{-3}$  M concentration (**B-8** to **B-11** dissolved in  $H_2O$ ) were added. Experiments were carried out in triplicates for each concentration. The final concentrations of the ligands were  $10^{-4}$  M. The cells were incubated for one hour at 4  $^{\circ}C$ . Afterwards, the supernatant was transferred to a ultra centrifugal filter unit (VWR International GmbH, Darmstadt, Germany) equipped with a 30 kDa filter and centrifuged at 12 000 rpm ( $\sim 14\ 000 \times g$ ). The filtrate was frozed, lyophilized and dissolved in a mixture of  $H_2O/MeCN$  (1/1) prior to RP-HPLC analysis.

### 3.4.4. Internalization studies

The culture medium was removed and the cells were washed with 500  $\mu$ L of DMEM-F12 containing 5% BSA. Afterwards, 200  $\mu$ L of DMEM-F12 (5% BSA) were added to each well and left to equilibrate at 37  $^{\circ}C$  for 15 min. 25  $\mu$ L of DMEM-F12 (5% BSA) were added to each well, followed by the addition of 25  $\mu$ L of the respective  $^{177}Lu$ -labeled ligand (10.0 nM in DMEM-F12 (5% BSA)). For blocking PSMA-specific binding and uptake, 25  $\mu$ L of 2-PMPA (100  $\mu$ M in DMEM (5%BSA)) instead of DMEM-F12 (5% BSA) were added prior to radiotracer addition. The same procedure was conducted with ( $[^{125}I]$ -BA)KuE (2.0 nM in DMEM-F12 (5% BSA)) which served as the reference. Each experiment (control and blockade) was performed in triplicate. The final concentration of the  $^{177}Lu$ -labeled ligand was 1.0 nM and that of ( $[^{125}I]$ -BA)KuE was 0.2 nM in all internalization assays. The cells were incubated for one hour at 37  $^{\circ}C$ . Incubation was terminated by placing the plate on ice (4  $^{\circ}C$ , 1 min) and removal of the incubation medium. The cells were washed with 250  $\mu$ L of ice-cold PBS and the wash medium was combined with the respective supernatant. This fraction represents the amount of free radioligand. 250  $\mu$ L of ice-cold 2-PMPA (10  $\mu$ M in PBS) were added and the cells were incubated for 10 min at 4  $^{\circ}C$ . Afterwards, the cells were rinsed again with 250  $\mu$ L of ice-cold PBS and the wash medium was combined with the

## MATERIALS AND METHODS

respective supernatant. This fraction represents the amount of cell surface-bound ligand. In the last step, the cells were lysed by addition of 250  $\mu\text{L}$  of 1 M aqueous NaOH. After 20 min, the lysate of each well was transferred to the respective vial as well as 250  $\mu\text{L}$  of 1 M NaOH used for rinsing the well. This fraction represents the amount of internalized radioligand. Quantification of the amount of free, cell surface-bound and internalized activity was performed in a  $\gamma$ -counter. The corresponding internalization values were corrected for nonspecific binding and normalized to the specific binding observed for the reference ( $[^{125}\text{I}]\text{-BA}$ )KuE.

### 3.4.5. Lipophilicity

The  $\log D_{7.4}$  values were determined, using the shake-flask method as previously described.<sup>[140]</sup> The radiolabeled tracer (0.5 - 1 MBq, 20  $\mu\text{L}$ ) was dissolved in 1 mL of a 1/1 mixture (v/v) of PBS (pH 7.4) and *n*-octanol in a reaction vial ( $n = 6$ ). After vigorous mixing of the suspension for 3 min at r.t., the vial was centrifuged at 9 000 rpm (ca. 7 700  $\times g$ ) for 5 min at room temperature (Heraeus Biofuge 15, Thermo Fisher Scientific, Darmstadt, Germany) and 150  $\mu\text{L}$  aliquots of both layers were measured in a  $\gamma$ -counter.

### 3.5. *In vivo* experiments

All animal experiments were conducted in accordance with general animal welfare regulations in Germany (German animal protection act, as amended on 18.05.2018, Art. 141 G v. 29.3.2017 I 626, approval no. 55.2-1-54-2532-71-13) and the institutional guidelines for the care and use of animals. To establish tumor xenografts, LNCaP cells (approximately  $10^7$  cells) were suspended in 200  $\mu$ L of a 1/1 mixture (v/v) of DMEM F-12 and Matrigel (BD Biosciences, Heidelberg, Germany) and inoculated subcutaneously onto the right shoulder of 6 - 8 weeks old CB17-SCID mice (Charles River Laboratories, Sulzfeld, Germany). Mice were used for experiments when tumor size reached 5 - 10 mm in diameter (3 - 6 weeks after inoculation). Radiochemical purities of  $^{177}\text{Lu}$ -labeled peptides evaluated in *in vivo* studies were  $96.1 \pm 2.8\%$  ( $n = 9$ ) as determined by radio-RP-HPLC, with the exception of [ $^{177}\text{Lu}$ ]Lu-**B-15** (87% RCP).

#### 3.5.1. Biodistribution studies

Approximately 2 - 10 MBq (0.20 nmol) of the  $^{177}\text{Lu}$ -labeled PSMA inhibitors were injected into the tail vein of LNCaP tumor xenograft-bearing male SCID CB17/lcr-Prkdc<sup>scid</sup>/lcrIcoCrl mice ( $n = 3$  to 5). They were sacrificed by  $\text{CO}_2$  asphyxiation and cervical dislocation either 1 h or 24 h *post injectionem* (p.i.) ( $n = 3$  for [ $^{177}\text{Lu}$ ]Lu-**B-15**, -**B-16** & -**B-17** (proinhibitor compounds),  $n = 4$  for [ $^{177}\text{Lu}$ ]Lu-**B-20** (alkyne),  $n = 5$  for [ $^{177}\text{Lu}$ ]Lu-**B-13** (carbamate) and  $n = 5$  for [ $^{177}\text{Lu}$ ]Lu-**B-21** (tetrazole)). Selected organs were removed, weighed and organ activities measured in a  $\gamma$ -counter. *In vivo* data of investigated PSMA inhibitors are given in *Table 7* to *10*.

## MATERIALS AND METHODS

**Table 7:** Biodistribution of [<sup>177</sup>Lu]Lu-rhPSMA-10 ([<sup>177</sup>Lu]Lu-B-1) and related derivatives with modified inhibitor motifs at 24 h p.i. in male LNCaP tumor xenograft-bearing CB17-SCID mice. Data are expressed as a percentage of the injected dose per gram (% ID/g), mean ± standard deviation (n = 2 for [<sup>177</sup>Lu]Lu-B-15\*; n = 3 for [<sup>177</sup>Lu]Lu-B-16 and [<sup>177</sup>Lu]Lu-B-17; n = 4 for [<sup>177</sup>Lu]Lu-B-20; n = 5 for [<sup>177</sup>Lu]Lu-B-21, [<sup>177</sup>Lu]Lu-B-13 and [<sup>177</sup>Lu]Lu-B-21. \*Ingestion of radioactively contaminated animal feed led to putative high activities in stomach and intestine, therefore excluding all values of mouse 3).

Organ	[ <sup>177</sup> Lu]Lu-B-1 ([ <sup>177</sup> Lu]Lu-rhPSMA-10)	[ <sup>177</sup> Lu]Lu-B-13 (carbamate)	[ <sup>177</sup> Lu]Lu-B-15 (proinhibitor I)	[ <sup>177</sup> Lu]Lu-B-16 (proinhibitor II)	[ <sup>177</sup> Lu]Lu-B-17 (proinhibitor III)	[ <sup>177</sup> Lu]Lu-B-20 (alkyne)	[ <sup>177</sup> Lu]Lu-B-21 (tetrazole)
Blood	0.00 ± 0.00	0.00 ± 0.00	0.00 ± 0.00	0.00 ± 0.00	0.01 ± 0.00	0.01 ± 0.01	0.00 ± 0.00
Heart	0.02 ± 0.00	0.02 ± 0.01	0.01 ± 0.00	0.03 ± 0.01	0.03 ± 0.01	0.01 ± 0.00	0.02 ± 0.00
Lung	0.03 ± 0.00	0.03 ± 0.01	0.33 ± 0.30	0.10 ± 0.08	0.04 ± 0.01	0.03 ± 0.03	0.05 ± 0.02
Liver	0.18 ± 0.06	0.13 ± 0.05	0.05 ± 0.00	0.14 ± 0.02	0.17 ± 0.05	0.09 ± 0.04	0.18 ± 0.04
Spleen	0.17 ± 0.03	0.09 ± 0.01	0.05 ± 0.01	0.11 ± 0.03	0.08 ± 0.02	0.04 ± 0.00	0.11 ± 0.03
Pancreas	0.01 ± 0.00	0.02 ± 0.01	0.01 ± 0.00	0.03 ± 0.01	0.02 ± 0.00	0.01 ± 0.01	0.02 ± 0.00
Stomach	0.06 ± 0.01	0.06 ± 0.04	0.14 ± 0.07	0.05 ± 0.01	0.04 ± 0.01	0.12 ± 0.11	0.12 ± 0.11
Intestine	0.11 ± 0.05	0.12 ± 0.06	0.55 ± 0.04	0.18 ± 0.06	0.10 ± 0.05	0.32 ± 0.29	0.52 ± 0.68
Kidneys	1.97 ± 0.78	0.31 ± 0.05	0.48 ± 0.02	2.36 ± 0.39	2.04 ± 0.75	1.29 ± 0.28	3.23 ± 0.77
Adrenals	0.06 ± 0.04	0.04 ± 0.01	0.00 ± 0.00	0.04 ± 0.00	0.03 ± 0.01	0.02 ± 0.02	0.17 ± 0.19
Muscle	0.00 ± 0.00	0.01 ± 0.01	0.00 ± 0.00	0.02 ± 0.00	0.01 ± 0.00	0.00 ± 0.00	0.02 ± 0.01
Bone	0.02 ± 0.01	0.02 ± 0.01	0.00 ± 0.00	0.02 ± 0.01	0.04 ± 0.01	0.03 ± 0.01	0.18 ± 0.04
Tumor	9.82 ± 0.30	1.20 ± 0.55	0.09 ± 0.02	0.33 ± 0.11	0.14 ± 0.05	0.10 ± 0.03	0.68 ± 0.16
Submandibular gland	0.04 ± 0.01	0.03 ± 0.01	0.02 ± 0.01	0.07 ± 0.01	0.05 ± 0.02	0.02 ± 0.00	0.04 ± 0.01
Parotid gland	0.04 ± 0.01	0.04 ± 0.02	0.02 ± 0.00	0.09 ± 0.03	0.06 ± 0.01	0.02 ± 0.00	0.06 ± 0.02

## MATERIALS AND METHODS

**Table 8:** Biodistribution of [<sup>177</sup>Lu]Lu-rhPSMA-10 ([<sup>177</sup>Lu]Lu-B-1), [<sup>177</sup>Lu]Lu-rhPSMA-7.3 and related derivatives with modified inhibitor motifs at 1 h p.i. in male LNCaP tumor xenograft-bearing CB17-SCID mice. Data are expressed as a percentage of the injected dose per gram (% ID/g), mean ± standard deviation (n = 4 for [<sup>177</sup>Lu]Lu-rhPSMA-7.3 and n = 5 for [<sup>177</sup>Lu]Lu-B-1, [<sup>177</sup>Lu]Lu-B-13 and [<sup>177</sup>Lu]Lu-B-21).

Organ	[ <sup>177</sup> Lu]Lu-B-1 <sup>a</sup> ([ <sup>177</sup> Lu]Lu-rhPSMA-10)	[ <sup>177</sup> Lu]Lu-rhPSMA-7.3 <sup>b</sup>	[ <sup>177</sup> Lu]Lu-B-13 (carbamate)	[ <sup>177</sup> Lu]Lu-B-21 (tetrazole)
<b>Blood</b>	0.48 ± 0.15	0.63 ± 0.21	0.97 ± 0.18	1.09 ± 0.30
<b>Heart</b>	0.42 ± 0.15	0.78 ± 0.37	0.36 ± 0.04	0.41 ± 0.04
<b>Lung</b>	0.80 ± 0.16	1.37 ± 0.24	2.88 ± 2.96	1.23 ± 0.27
<b>Liver</b>	0.40 ± 0.13	0.66 ± 0.09	0.87 ± 0.28	0.74 ± 0.17
<b>Spleen</b>	10.7 ± 2.9	33.3 ± 8.6	2.51 ± 0.95	1.04 ± 0.15
<b>Pancreas</b>	0.31 ± 0.12	0.66 ± 0.25	0.25 ± 0.06	0.33 ± 0.11
<b>Stomach</b>	0.26 ± 0.08	0.55 ± 0.24	0.30 ± 0.09	1.55 ± 1.67
<b>Intestine</b>	0.28 ± 0.10	0.32 ± 0.09	0.36 ± 0.17	0.67 ± 0.21
<b>Kidneys</b>	173 ± 56	208 ± 31	61.8 ± 25.9	33.2 ± 3.8
<b>Adrenals</b>	1.30 ± 0.37	n.d.	1.46 ± 0.70	0.61 ± 0.42
<b>Muscle</b>	0.36 ± 0.10	0.26 ± 0.08	0.13 ± 0.04	0.15 ± 0.03
<b>Bone</b>	0.37 ± 0.24	0.45 ± 0.17	0.18 ± 0.02	0.47 ± 0.44
<b>Tumor</b>	12.2 ± 1.8	12.4 ± 1.4	5.31 ± 0.94	3.40 ± 0.63
<b>Submandibular gland</b>	n.d.	1.44 ± 0.25	0.37 ± 0.08	0.40 ± 0.05
<b>Parotid gland</b>	n.d.	n.d.	0.62 ± 0.20	0.56 ± 0.08

<sup>a</sup>Values for [<sup>177</sup>Lu]Lu-rhPSMA-10 ([<sup>177</sup>Lu]Lu-B-1) at 1 h p.i. were taken from patent WO002019020831A1.<sup>[289]</sup>

<sup>b</sup>Values for [<sup>177</sup>Lu]Lu-rhPSMA-7.3 (= [<sup>177</sup>Lu]Lu-B-1 with (S)-DOTAGA chelator instead of DOTA) at 1 h p.i. were taken from Yusufi *et al.*<sup>[290]</sup>

## MATERIALS AND METHODS

**Table 9:** Tumor-to-tissue ratios of [<sup>177</sup>Lu]Lu-rhPSMA-10 ([<sup>177</sup>Lu]Lu-B-1) and related derivatives with modified inhibitor motifs at 24 h p.i. in male LNCaP tumor xenograft-bearing CB17-SCID mice. Data are expressed as mean ratios ± standard deviation (n = 4 for [<sup>177</sup>Lu]Lu-B-20; n = 5 for [<sup>177</sup>Lu]Lu-B-1, [<sup>177</sup>Lu]Lu-B-13 and [<sup>177</sup>Lu]Lu-B-21).

Ratio Tumor-to-	[ <sup>177</sup> Lu]Lu-B-1 ([ <sup>177</sup> Lu]Lu-rhPSMA-10)	[ <sup>177</sup> Lu]Lu-B-13 (carbamate)	[ <sup>177</sup> Lu]Lu-B-20 (alkyne)	[ <sup>177</sup> Lu]Lu-B-21 (tetrazole)
<b>blood</b>	11498 ± 1953	947 ± 652	26.8 ± 16.9	227 ± 50
<b>kidney</b>	5.66 ± 1.99	3.80 ± 1.36	0.08 ± 0.01	0.22 ± 0.06
<b>muscle</b>	2441 ± 373	127 ± 92	27.7 ± 10.9	55.9 ± 24.3
<b>liver</b>	57.5 ± 13.1	8.94 ± 2.94	1.46 ± 0.88	3.74 ± 0.50
<b>submandibular gland</b>	275 ± 49	34.5 ± 9.2	6.11 ± 1.78	16.9 ± 2.2
<b>parotid gland</b>	250 ± 64	31.8 ± 9.3	6.38 ± 3.06	12.2 ± 1.7

**Table 10:** Tumor-to-tissue ratios of [<sup>177</sup>Lu]Lu-B-1, [<sup>177</sup>Lu]Lu-rhPSMA-7.3 and related derivatives with modified inhibitor motifs at 1 h p.i. in male LNCaP tumor xenograft-bearing CB17-SCID mice. Data are expressed as mean ratios ± standard deviation (n = 3 for [<sup>177</sup>Lu]Lu-rhPSMA-7.3 and n = 5 for [<sup>177</sup>Lu]Lu-B-1, [<sup>177</sup>Lu]Lu-B-13 and [<sup>177</sup>Lu]Lu-B-21).

Ratio Tumor-to-	[ <sup>177</sup> Lu]Lu-B-1 <sup>a</sup> ([ <sup>177</sup> Lu]Lu-rhPSMA-10)	[ <sup>177</sup> Lu]Lu-rhPSMA-7.3 <sup>b</sup>	[ <sup>177</sup> Lu]Lu-B-13 (carbamate)	[ <sup>177</sup> Lu]Lu-B-21 (tetrazole)
<b>blood</b>	25.4 ± 8.8	18.3 ± 2.8	5.57 ± 1.18	3.46 ± 1.62
<b>kidney</b>	0.07 ± 0.02	0.06 ± 0.01	0.09 ± 0.03	0.10 ± 0.03
<b>muscle</b>	33.8 ± 10.7	44.3 ± 5.1	44.1 ± 9.0	24.9 ± 10.2
<b>liver</b>	30.5 ± 10.9	18.7 ± 3.4	6.61 ± 2.19	5.00 ± 2.11
<b>submandibular gland</b>	n.d.	7.91 ± 0.87	14.7 ± 3.5	8.74 ± 2.52
<b>parotid gland</b>	n.d.	n.d.	9.09 ± 3.13	6.20 ± 1.74

<sup>a</sup>Values for [<sup>177</sup>Lu]Lu-rhPSMA-10 ([<sup>177</sup>Lu]Lu-B-1) at 1 h p.i. were taken from patent WO002019020831A1.<sup>[289]</sup>

<sup>b</sup>Values for [<sup>177</sup>Lu]Lu-rhPSMA-7.3 (= [<sup>177</sup>Lu]Lu-B-1 with (S)-DOTAGA chelator instead of DOTA) at 1 h p.i. were taken from Yusufi *et al.*<sup>[290]</sup>

### 3.5.2. Metabolite analysis

[<sup>177</sup>Lu]Lu-**B-21** (9.64 MBq) was injected into the tail vein of a LNCaP tumor xenograft-bearing SCID CB17/lcr-Prkdc<sup>scid</sup>/lcrIcoCrl mouse. The animal was sacrificed 1 h p.i. and subjected to the standard procedure for biodistribution studies. In addition, urine was taken from all mice that were investigated in this experiment (8.4 - 9.0 MBq) and pooled (n = 5). Relevant dissected organs (tumor, kidneys, liver) and body fluids (blood and urine) were collected, homogenized if necessary and subjected to mechanochemical as well as solid phase extraction (SPE). Tissue extracts were analyzed by radio-RP-HPLC at a predefined gradient (25 - 40% MeCN (0.1% TFA) in 20 min), for which the retention time (18.3 min) of the intact cold standard (<sup>nat</sup>Lu-**B-21**) was previously determined and hence, served as a reference (*Figure 35*). The radioactivity detector was placed downstream of the UV-detector causing for a slight time delay of the radioactivity signals.

#### *Mechanochemical extraction of dissected organs (tumor, kidneys, liver)*

Four 2 mL Protein LoBind tubes (Eppendorf AG, Hamburg, Germany) were equipped with steel and ceramic beads from Lysis Tubes W (analytikjena, Jena, Germany) for kidneys, tumor and liver (bisected). 1 mL of radioimmunoprecipitation assay (RIPA) buffer containing 2.00 µmol of 2-PMPA was added to each tube and the organs were homogenized with a MM-400 ball mill (Retsch GmbH, Haan, Germany) at 30 Hz for 20 min. Afterwards, the homogenates were transferred to Protein LoBind tubes free from steel and ceramic beads and centrifuged (15 200 rpm, 25 830 × g, 10 min, 21 °C) The first supernatants were stored, and the precipitates were again subjected to mechanochemical extraction with 1 mL RIPA buffer (2.00 µmol 2-PMPA) at 30 Hz for 20 min. After centrifugation (15 200 rpm, 25 830 × g, 10 min, 21 °C), also the second supernatants were kept for SPE.

#### *Work-up procedure for body fluids (blood and urine)*

After cardiac puncture, 1 mL Tracepur<sup>®</sup>-H<sub>2</sub>O was directly added to the collected blood sample and centrifuged twice (13 000 rpm, ca. 16 000 × g, 5 min) to separate the plasma from the blood cells. The precipitate was dissolved in 500 µL Tracepur<sup>®</sup>-H<sub>2</sub>O and again centrifuged (13 000 rpm, ca. 16 000 × g, 5 min), together with the first supernatant. Both supernatants were kept for SPE. Pooled urine samples were centrifuged (13 000 rpm, ca. 16 000 × g, 5 min) and the supernatant was directly analyzed via radio-RP-HPLC.

#### *Solid phase extraction of organs and body fluids*

For solid phase extraction, the supernatants were loaded onto Strata-X cartridges (33 µm Polymeric Reversed Phase, 200 mg, Phenomenex, Aschaffenburg, Germany), which were initially preconditioned with 5 mL MeOH and 5 mL H<sub>2</sub>O. In total, ten cartridges were loaded with supernatants of the respective organs and blood (2× tumor, 2× kidneys, 4× liver, 2× blood). The cartridges were washed with 1 mL Tracepur<sup>®</sup>-H<sub>2</sub>O and dried prior to elution. For each cartridge,

## MATERIALS AND METHODS

750  $\mu\text{L}$  of MeCN/H<sub>2</sub>O (6/4, 0.1% TFA) were used for elution and extracts of related organs/blood were combined. Further H<sub>2</sub>O was added to obtain the starting gradient and the extracts were analyzed via radio-RP-HPLC (25 - 40% B in 20 min, Method A). The extraction efficiencies were calculated before and after SPE and the results are given in *Table 11*.

**Table 11:** Extraction efficiencies of [<sup>177</sup>Lu]Lu-B-21 from liver, tumor, kidneys and blood using a MM-400 ball mill. The percentage of activity after sample extraction and after SPE purification was quantified, decay corrected and the overall extracted activity was calculated.

Organs and body fluids	efficiency [% extracted radioactivity]		
	sample extraction	SPE purification	overall
<b>liver</b>	96.1	67.2	64.5
<b>tumor</b>	97.3	76.1	74.0
<b>kidneys</b>	96.0	74.8	71.8
<b>blood</b>	94.8	78.9	74.8

### 3.5.3. $\mu\text{SPECT/CT}$ imaging

Imaging experiments were conducted using a MILabs VECTor<sup>4</sup> small-animal SPECT/PET/OI/CT. The resulting data were analyzed by the associated PMOD (version 4.0) software. SCID CB17/lcr-Prkdc<sup>scid</sup>/lcrIcoCrl mice were anaesthetized with isoflurane and the <sup>177</sup>Lu-labeled rhPSMA compounds were injected via the tail vein. Mice were euthanized 1 h or 24 h p.i. by CO<sub>2</sub> asphyxiation and cervical dislocation and blood samples for later biodistribution or metabolite analysis were taken by cardiac puncture before image acquisition. Static images were acquired with 45 min acquisition time using the HE-GP-RM collimator and a step-wise multi-planar bed movement. All images were reconstructed using the MILabs-Rec software (version 10.02) and a pixel-based Similarity-Regulated Ordered Subsets Expectation Maximization (SROSEM) algorithm with a window-based scatter correction (20% below and 20% above the photopeak, respectively). Voxel size CT: 80  $\mu\text{m}$ , voxel size SPECT: 0.8 mm, 1.6 mm (FWHM) Gaussian blurring post processing filter, with calibration factor in kBq/mL and decay correction, no attenuation correction.

## IV. RESULTS AND DISCUSSION

### 4.1. GLP-1 receptor ligand development

This GLP-1R ligand development focused on the identification of high-affinity small peptide ligands (< 30 amino acids<sup>[306]</sup>) that could serve as basic structures for radiometallation or might be directly labeled via <sup>18</sup>F-<sup>19</sup>F isotopic exchange (SiFA approach). Such modifications were supposed to reduce non-target tissue uptake in patients, especially in the kidneys. For this purpose, a novel cell-based assay for screening of GLP-1R-targeting compounds should be developed and implemented.

#### 4.1.1. Reference ligand identification and optimization of <sup>125</sup>I-labeling

Due to its known high affinity towards its cognate receptor and the use of its radioiodinated form ([<sup>125</sup>I]Tyr(3-I)<sup>19</sup>-GLP-1) in numerous previous studies<sup>[40, 45, 52, 106, 307]</sup>, the natural ligand GLP-1R was initially chosen as reference ligand.

Linear syntheses of GLP-1 and Tyr(3-I)<sup>19</sup>-GLP-1, which served as cold standard to confirm the identity of [<sup>125</sup>I]Tyr(3-I)<sup>19</sup>-GLP-1 ([<sup>125</sup>I]**A-3**) during radio-RP-HPLC reaction controls, were accomplished on Rink amide ChemMatrix<sup>®</sup> resin. Moreover, the latter one was used as a probe for defining gradients suitable for separation of [<sup>125</sup>I]**A-3** and its unlabeled precursor GLP-1 (**A-2**). Radiosynthesis of [<sup>125</sup>I]**A-3** was conducted by the Iodogen method<sup>[302]</sup>, but the resulting product was readily decomposed via radiolysis, since by-products (9 - 51%) were already detectable right after radio-RP-HPLC purification. Consequently, inhibition of radiolysis was pursued by different attempts including addition of radiolysis inhibitors (sodium ascorbate/ gentisic acid/ L-methionine) during or after radiosynthesis, or by using a radiolysis inhibitor (ethanol) directly as part of the radio-RP-HPLC solvent (solvent A =  $\frac{1}{3}$  EtOH +  $\frac{2}{3}$  H<sub>2</sub>O) + 0.1% TFA, solvent B = MeCN + 0.1% TFA).<sup>[308]</sup> Additionally, different ranges of pH<sup>[309]</sup> (1-2 up to 9-10) as well as different solvents for storage (HPLC solvent or pure EtOH, both with or without radiolysis inhibitors) were investigated on their effect to attenuate decomposition of [<sup>125</sup>I]Tyr(3-I)<sup>19</sup>-GLP-1.

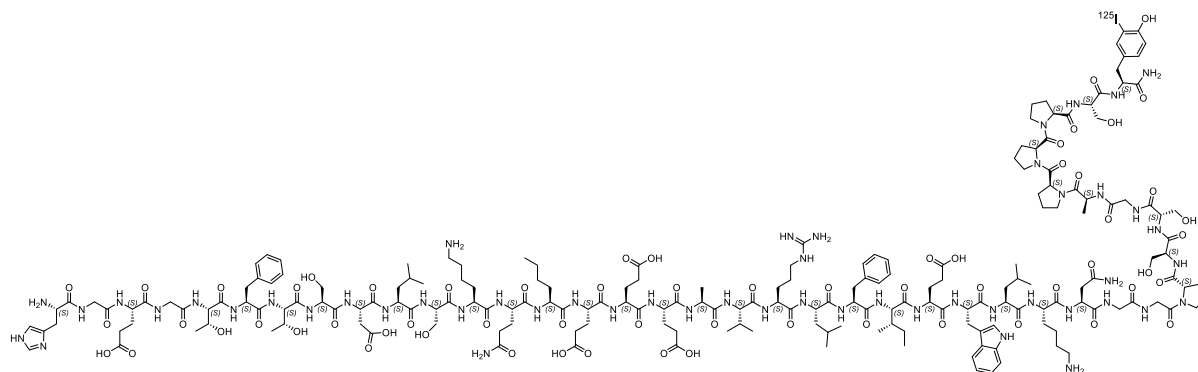
Unfortunately, despite dedicated efforts, synthesis of the <sup>125</sup>I-labeled GLP-1 derivative resulted in only low RCY (always ≤ 34%, n = 4) and exhibited only insufficient stability (≤ 53% RCP at 20.6 ± 1.8 h). Consequently, the attempts to establish [<sup>125</sup>I]Tyr(3-I)<sup>19</sup>-GLP-1 as reference ligand for cell-based competitive binding assays were abandoned.

Instead, the use of exendin-4 was pursued as radiolabeled derivatives thereof were proven to enable insulinoma imaging with high sensitivity and selectivity, emphasizing its suitability as radiolabeled reference ligand. Particularly, the introduction of L-norleucine as a non-oxidizable

## RESULTS AND DISCUSSION

isosteric surrogate for L-methionine at position 14, that led to metabolic stable radioligands with improved binding capabilities and similar biodistribution patterns<sup>[105]</sup>, could also be beneficial for the radiolytic stability of the <sup>125</sup>I-labeled reference compound.

Radioiodination was performed on the C-terminal tyrosine residue of [Nle<sup>14</sup>, Tyr<sup>40</sup>]exendin-4, as modifications at this ultimate position did not affect receptor binding significantly in previous studies.<sup>[95, 105, 118]</sup>



A-17

**Figure 18:** Molecular structure of the radiolabeled reference ligand [Nle<sup>14</sup>, [<sup>125</sup>I]Tyr(3-I)<sup>40</sup>]exendin-4 (A-17).

In analogy to [<sup>125</sup>I]Tyr(3-I)<sup>19</sup>-GLP-1, radiosynthesis was performed by the Iodogen method. Slight modifications of this procedure (DMSO instead of H<sub>2</sub>O to dissolve the peptide and 15.0 µg Iodogen instead of 150 µg Iodogen) led to 45.6 ± 15% RCY (n = 4). In addition, the resulting product [Nle<sup>14</sup>, [<sup>125</sup>I]Tyr(3-I)<sup>40</sup>]exendin-4 was found to be sufficiently stable for at least 16 days (RCP ≥ 92%). As detected by radio-RP-HPLC, several radiolysis-induced contaminations were found to be formed over time, resulting in a RCP of ≤ 78% at 29 days after radiosynthesis. Consequently, cell-based assays with [Nle<sup>14</sup>, [<sup>125</sup>I]Tyr(3-I)<sup>40</sup>]exendin-4 as radioligand were conducted within a time frame of 14 days to ensure a RCP > 92%. Competitive binding experiments were only considered if the respective IC<sub>50</sub> of GLP-1 laid within the range predefined for affinity determinations (23.2 ± 12.2 nM, n = 11). DMSO as a radiolysis inhibitor was not added to the radioligand stock solution, since an amount of 10% (v/v) did not lead to a significant increase in radiochemical stability over the observed period (36 days). Higher amounts were not tested due to the risk of cell toxic effects during *in vitro* experiments.

#### 4.1.2. Development and implementation of a cell-based assay for screening of GLP-1R-targeting compounds

[Nle<sup>14</sup>, [<sup>125</sup>I]Tyr(3-I)<sup>40</sup>]Exendin-4 (**A-17**) was first evaluated in 2017 by Lämpchen *et al.* in *in vitro* and *in vivo* studies, and showed a  $K_d$  value of  $4.1 \pm 1.1$  nM in GLP-1R positive INS-1E cells.<sup>[118]</sup> Therefore, the development of a competitive binding assay started with the incubation of **A-17** with INS-1E and HEK293-hGLP-1R cells under varying conditions as well as with HEK293 cells (original cell line used for transfection), which served as a negative control due to absent GLP-1R expression.

With **A-17**, a high affinity radioligand was produced, that complies also further essential criteria like high selectivity and high molar activity (74 MBq/nmol). High affinity allows to study ligand binding at a low concentration, which will reduce nonspecific binding and hence, result in a higher ratio of specific-to-nonspecific binding. In addition, high affinity ligands generally exhibit slow rates of offset, advantageous for the separation of bound from free ligand, where it is important to ensure that the washing steps do not cause significant dissociation. Moreover, by its high molar activity, very small quantities of bound ligand can be accurately measured.<sup>[310]</sup>

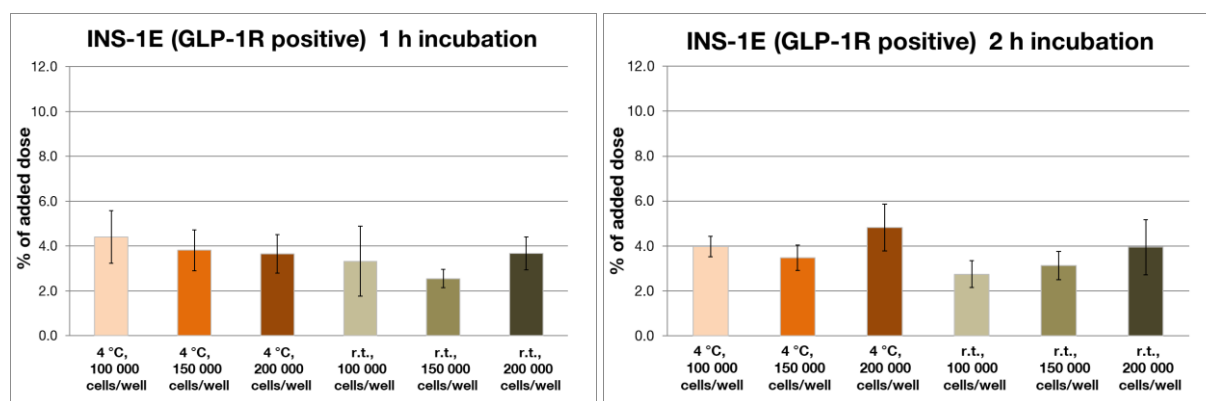
Further key factors in the development of reliable competition experiments are the radioligand concentration, receptor concentration, incubation time and temperature as well as the assay volume, which regulates the amount of radioligand relative to the number of binding sites in the assay. Especially, the latter three aspects in combination with the affinity of the radioligand represent crucial parameters for the development of a competitive assay under equilibrium conditions. Thereby, association of a radioligand to its cognate receptor and dissociation of the resulting ligand-receptor complex are reversible processes that occur concomitantly until equilibrium has been reached.<sup>[310, 311]</sup>

For practical reasons, some parameters were defined in advance. First, the assay volume was kept constantly at 250  $\mu$ L and experiments were conducted with isotonic HBSS (1% BSA) unless otherwise noted. Second, the amount of radioligand was initially set to a constant value of 100 000 cpm/well, which resulted in a final radioligand concentration of 0.41 nM/well unless otherwise noted. Third, the amount of bound radioligand should reach a value of 10 - 20% to give a satisfying ratio of specific-to-nonspecific binding. Higher values were tried to avoid, since radioligand depletion might occur during affinity studies (at 4 °C or r.t.) and interfere with equilibrium conditions.<sup>[310]</sup> In contrast, the receptor concentration (= cells/well), incubation time, incubation temperature and occasionally, the incubation medium and radioligand concentration were varied, as depicted in *Figures 19 to 24*.

## RESULTS AND DISCUSSION

### 4.1.2.1. Radioligand binding studies on INS-1E cells

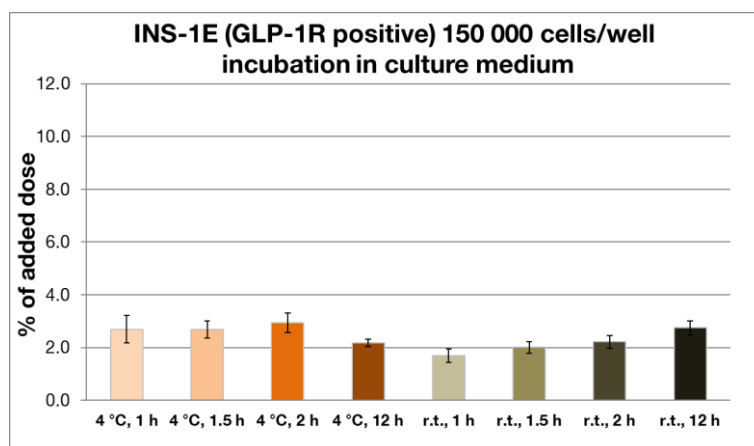
Initially, different amounts of INS-1E cells (100 000, 150 000 or 200 000 cells/well) were incubated with [Nle<sup>14</sup>, [<sup>125</sup>I]Tyr(3-I)<sup>40</sup>]exendin-4 at different temperatures (4 °C or r.t., *Figure 19*). Receptor-mediated internalization was suppressed at 4 °C<sup>[312]</sup> but also no raise of radioligand uptake could be detected at room temperature, indicating that either no internalization occurred at this temperature or the rate of externalization equals the rate of internalization. Moreover, the slight decline of bound activity at room temperature might indicate for a change of the rates of onset and offset, that accelerates diffusion of the radioligand from the GLP-1R.<sup>[310]</sup> Also a change in receptor expression might be conceivable, as this effect was observed at both time points 1 h and 2 h.



**Figure 19:** Incubation of INS-1E cells with [Nle<sup>14</sup>, [<sup>125</sup>I]Tyr(3-I)<sup>40</sup>]exendin-4 (0.41 nM) in 250 µL HBSS (1% BSA) at different temperatures (4 °C or r.t.) and different amount of cells (100 000, 150 000 or 200 000 cells/well). In addition, experiments (n = 6) were terminated after different time points (1 h, left or 2 h, right).

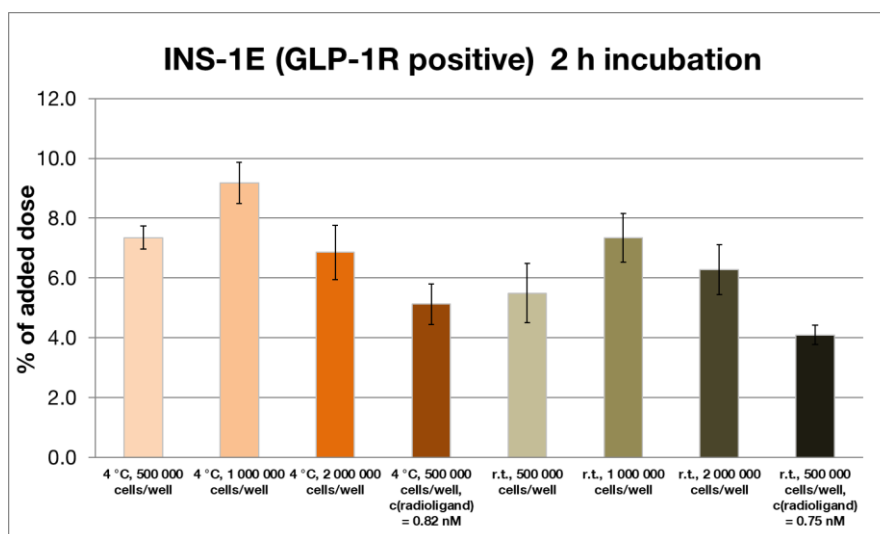
The maximum value for radioligand binding reached only 4.8% of added dose after 2 h at 4 °C in this study (200 000 cells/well), leading to a further experiment in which the incubation medium was changed from HBSS (1% BSA) to culture medium (*Figure 20*). Since different temperatures and incubation periods were investigated, the cell amount was kept constant at 150 000 cells/well. This value was chosen, as it represents an average of the binding values from the first INS-1E experiment, also covering the values obtained for 100 000 and 200 000 cells/well.

## RESULTS AND DISCUSSION



**Figure 20:** Incubation of INS-1E cells with [Nle<sup>14</sup>, [<sup>125</sup>I]Tyr(3-I)<sup>40</sup>]exendin-4 (0.41 nM) in 250  $\mu$ L culture medium (RPMI 1640 with 10% fetal bovine serum, 50  $\mu$ M  $\beta$ -mercaptoethanol, 1 mM sodium pyruvate and 10 mM HEPES) at different temperatures (4 °C or r.t.) and a constant number of 150 000 cells/well. Experiments (n = 6) were terminated after different time points (1 h, 1.5 h, 2 h or 12 h).

Additives within the culture medium were suspected to be essential for high receptor expression, but an increase in radioligand uptake could not be achieved. Instead, radioligand uptake was further decreased to a maximum value of 2.9% of added dose (4 °C, 2 h) by incubation in culture medium. Nonspecific binding of the radioligand to fetal bovine serum or other medium components most likely resulted in an overall lower amount of free **A-17** accessible to the cell surface and the receptors.<sup>[310]</sup> Hence, for further binding experiments the number of cells was increased but the incubation medium was again changed back to HBSS (1% BSA). Since the highest overall uptake values were obtained after 2 h of incubation in the first and second INS-1E experiment, this period was kept constant for the following third experiment. Aside from variation of the cell number, the influence of the temperature and also of the radioligand concentration was investigated (*Figure 21*).



**Figure 21:** Incubation of INS-1E cells with different amounts of [Nle<sup>14</sup>, [<sup>125</sup>I]Tyr(3-I)<sup>40</sup>]exendin-4 (0.41 nM, 0.75 nM or 0.82 nM) in 250  $\mu$ L (c(radioligand) = 0.41 nM/0.82 nM) or 275  $\mu$ L (c(radioligand) = 0.75 nM) HBSS (1% BSA) at different temperatures (4 °C or r.t.) and different amounts of cells (500 000, 1 000 000 or 2 000 000 cells/well). All experiments (n = 6) were terminated after an incubation period of 2 h.

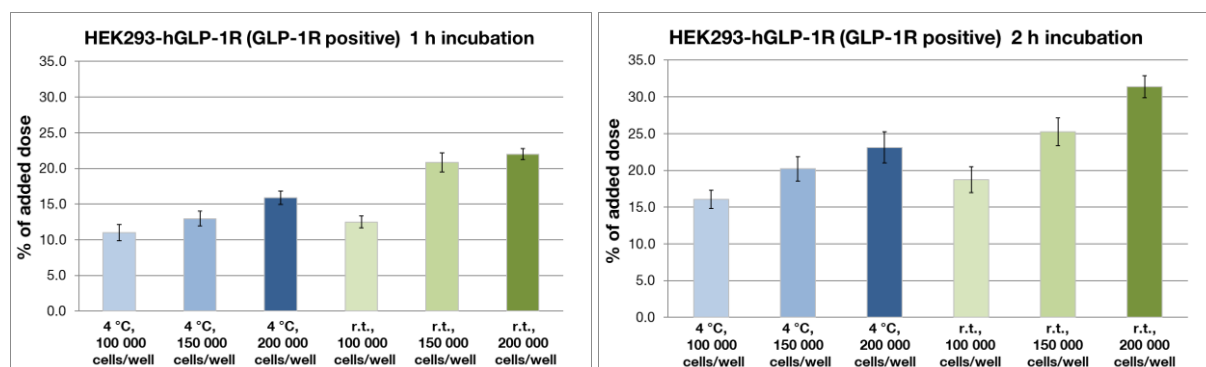
## RESULTS AND DISCUSSION

Increased amounts of cells (i.e. receptors) indeed led to a higher amount of bound radioligand, with a maximum amount of 9.2% of added dose (4 °C, 1 000 000 cells/well). Contrary to the high amount of cells used in the assay of Lappchen *et al.* ( $1.8 \times 10^6$  cells/well)<sup>[118]</sup>, the optimal cell number for this INS-1E cell-based assay was found to be  $\sim 1.0 \times 10^6$  cells/well at 4 °C and at room temperature. A further increase in cells/well as well as raise of the radioligand concentration to 0.75 nM or 0.82 nM did not result in any improvement.

### 4.1.2.2. Radioligand binding studies on HEK293-hGLP-1R and HEK293 cells

Similar to the binding experiments with INS-1E cells, HEK293-hGLP-1R cells were investigated to determine whether comparable or even superior results in radioligand binding could be achieved with this cell line. Particularly due to the expression of human GLP-1R (INS-1E: expression of rat GLP-1R) and the high receptor density, the transfected cell line was supposed to be advantageous over INS-1E for the development of a valid cell-based assay. For negative control, binding experiments were also performed with the HEK293 cell line, which was originally used for stable GLP-1R transfection.

In analogy to the first INS-1E experiment, different amounts of HEK293-hGLP-1R cells (100 000, 150 000 or 200 000 cells/well) were incubated with [Nle<sup>14</sup>, [<sup>125</sup>I]Tyr(3-I)<sup>40</sup>]exendin-4 at different temperatures (4 °C or r.t., *Figure 22*). Receptor-mediated internalization was suppressed at 4 °C but elevated radioactivity accumulation at room temperature indicated receptor-mediated internalization. From that it was deduced that competitive binding studies should not be conducted at room temperature, as the obtained values would lead to misinterpretation of the results, particularly when ligands with different internalization propensities are evaluated.

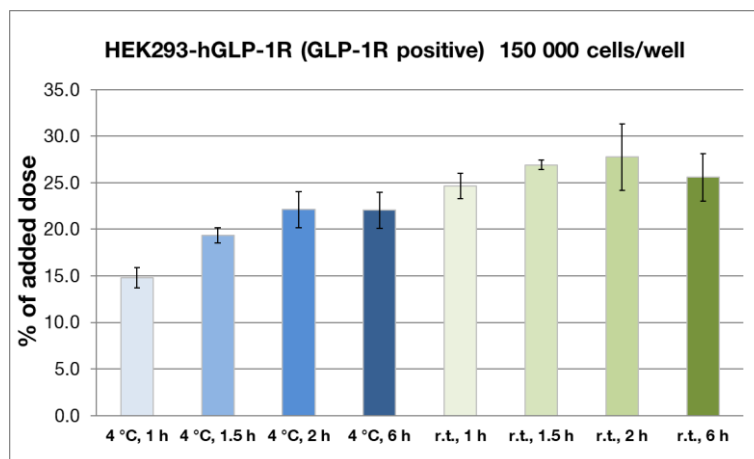


**Figure 22:** Incubation of HEK293-hGLP-1R cells with [Nle<sup>14</sup>, [<sup>125</sup>I]Tyr(3-I)<sup>40</sup>]exendin-4 (0.41 nM) in 250  $\mu$ L HBSS (1% BSA) at different temperatures (4 °C or r.t.) and different amount of cells (100 000, 150 000 or 200 000 cells/well). Experiments (n = 6) were terminated after different time points (1 h, left or 2 h, right).

The maximum value for radioligand binding by far exceeded the maximum value obtained for INS-1E cells (9.2%, 4 °C, 2 h, 1 000 000 cells/well) and reached 31% of added dose with 200 000 cells/well after 2 h of incubation at room temperature. Beyond that, the binding experiment

## RESULTS AND DISCUSSION

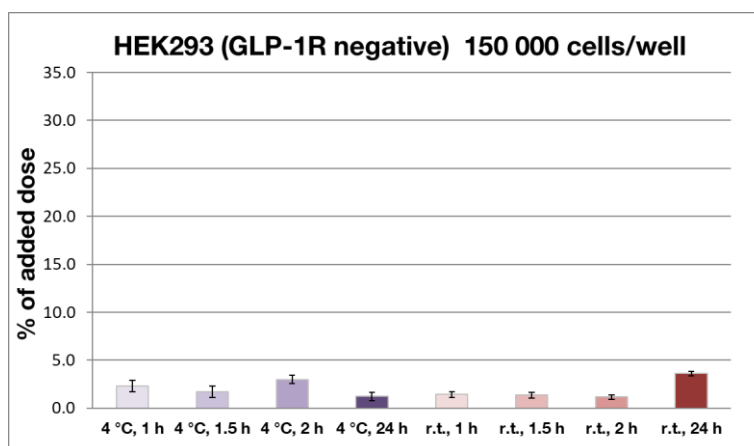
conducted with 150 000 cells/well at 4 °C and terminated after 2 h provided an expedient binding value of 20% of added dose. As a result, no further studies with increasing cells/well as for INS-1E cells were conducted, since the resulting values were expected to exceed the 20% threshold, leading to an increased risk of radioligand depletion.<sup>[310]</sup> Instead, further experiments to determine the optimal incubation period were pursued (*Figure 23*). Therefore, an amount of 150 000 cells/well was kept constant for maintaining the binding of [Nle<sup>14</sup>, [<sup>125</sup>I]Tyr(3-I)<sup>40</sup>]exendin-4 in a range of 20% of added dose.



**Figure 23:** Incubation of HEK293-hGLP-1R cells with [Nle<sup>14</sup>, [<sup>125</sup>I]Tyr(3-I)<sup>40</sup>]exendin-4 (0.41 nM) in 250  $\mu$ L HBSS (1% BSA) at different temperatures (4 °C or r.t.) and a constant number of 150 000 cells/well. Experiments (n = 6) were terminated after different time points (1 h, 1.5 h, 2 h or 6 h).

Equilibrium conditions were reached after 2 h when incubated at 4 °C, since a plateau in radioligand binding between the 2 h and 6 h time point was attained. Radioligand binding at different time points was also investigated at room temperature to verify the increased activity accumulation at this temperature in multiple independent experiments, thereby substantiating the theory of receptor-mediated internalization. At room temperature, equilibrium was already attained after 1.5 h but as mentioned above, competitive binding assays were planned to be conducted at 4 °C to avoid the generation of misleading results. Hence, an incubation period of 2 h at 4 °C with 150 000 cells/well was supposed to provide the most reliable results for GLP-1R-targeting ligands. An analogous experiment was conducted with HEK293 cells, which served as a negative control (*Figure 24*). This cell line was used for stable transfection with GLP-1R and was supposed to show only low radioligand binding, mainly induced by nonspecific and non-GLP-1R-mediated interactions of the radioligand with the cell surface. Actually, radioligand binding did not exceed 3.6% of added dose (r.t., 24 h, 150 000 cells/well), thus emphasizing that activity accumulation on stably transfected HEK293-hGLP-1R cells is primarily GLP-1R-mediated.

## RESULTS AND DISCUSSION



**Figure 24:** Incubation of HEK293 cells with [Nle<sup>14</sup>, [<sup>125</sup>I]Tyr(3-I)<sup>40</sup>]exendin-4 (0.41 nM) in 250 µL HBSS (1% BSA) at different temperatures (4 °C or r.t.) and a constant number of 150 000 cells/well. Experiments (n = 6) were terminated after different time points (1 h, 1.5 h, 2 h or 24 h).

For internalization studies (37 °C) a maximum value of 10% of added dose was set, in order to avoid radioligand-induced GLP-1 receptor desensitization (= reduction of membrane-bound receptors via agonist binding).<sup>[310]</sup> However, development of internalization assays using either INS-1E or HEK293-hGLP-1R cells should be pursued only if suitable small peptide candidates with high affinity were obtained.

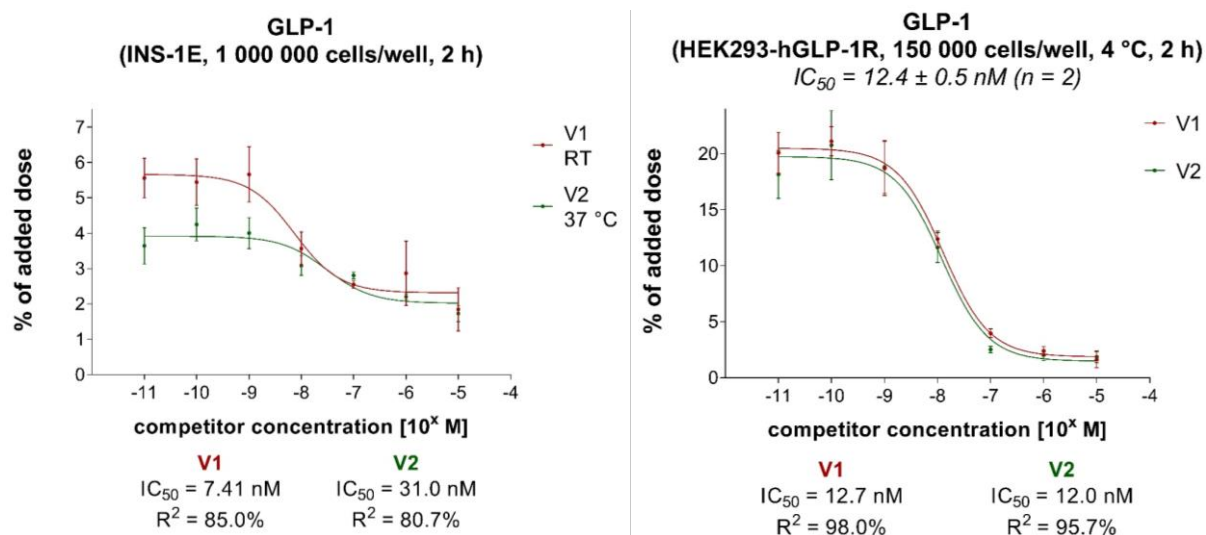
### 4.1.2.3. Competitive binding experiments

Since all experiments on INS-1E cells revealed values below 20% of added dose with no assay condition to be clearly preferred, initial competitive binding studies were conducted with different amounts of cells (150 000 cells/well, 500 000 cells/well and 1 000 000 cells/well) and also at different temperatures (4 °C, r.t., 37 °C). Only the incubation period was set to 2 h, as the highest overall uptake values were obtained at this time point (second and third INS-1E experiment) and no further increase in radioligand binding could be observed at 12 h (second INS-1E experiment). For initial competitive binding experiments, the natural ligand GLP-1 was used, providing assay concentrations of 10<sup>-5</sup> - 10<sup>-11</sup> M. Cell counts ranging from 150 000 to 500 000 cells/well (4 °C, 2 h) revealed no detectable IC<sub>50</sub> values. With 1 000 000 cells/well affinity towards INS-1E cells was detectable (*Figure 25*), but with low maximal cell binding (4 - 6% of added dose at 10<sup>-11</sup> M GLP-1) leading to low specific-to-nonspecific binding ratios.

By contrast, first competitive binding studies on HEK293-hGLP-1R cells revealed a high specific-to-nonspecific binding ratio resulting from a remarkably high level of maximal radioligand binding (~ 20% of added dose at 10<sup>-11</sup> M). A reliable IC<sub>50</sub> value of 12.4 ± 0.5 nM (n = 2) (R<sup>2</sup> ≥ 95.7%) for GLP-1 was obtained, which confirmed high affinity of the endogenous ligand towards human GLP-1R and hence, the validity of the assay (*Figure 25*). Co-incubation with GLP-1 for assessment of nonspecific binding (~ 2% of added dose) was favored, since displacing of the

## RESULTS AND DISCUSSION

radioligand **A-17** with the chemically analogous cold standard [Nle<sup>14</sup>, Tyr(3-I)<sup>40</sup>]exendin-4 would have led to displacement at all binding sites, also at those responsible for nonspecific accumulation of **A-17**.



**Figure 25:** Results after initial competitive binding experiments obtained by co-incubation of GLP-1 ( $10^{-5}$  -  $10^{-11}$  M) with the radioligand [Nle<sup>14</sup>, [<sup>125</sup>I]Tyr(3-I)<sup>40</sup>]exendin-4 (0.41 nM) in 250  $\mu$ L HBSS (1% BSA) on INS-1E cells (left) or HEK293-hGLP-1R cells (right).

From these results it was deduced, that reliable and valid IC<sub>50</sub> data could be obtained by incubation with HEK293-hGLP-1R cells rather than with INS-1E cells. Hence, the latter were not used for further competitive binding assays and only the HEK293-hGLP-1R cell model was implemented. Co-incubation of the cold standard with the radioligand [Nle<sup>14</sup>, [<sup>125</sup>I]Tyr(3-I)<sup>40</sup>]exendin-4 revealed an IC<sub>50</sub> value of  $7.63 \pm 2.78$  nM (n = 6) for [Nle<sup>14</sup>, Tyr(3-I)<sup>40</sup>]exendin-4. Thus, high affinity of the radioligand towards HEK293-hGLP-1R cells under these assay conditions was proven and affirmed its use in competitive binding experiments (IC<sub>50</sub>). As no change in radioligand concentration was found to be necessary neither for radioligand binding studies nor for IC<sub>50</sub> studies, the activity was kept constant leading to a final ligand concentration of 0.41 nM/well in all conducted competitive binding assays.

### 4.1.3. Synthesis and *in vitro* evaluation of small peptides targeting the GLP-1 receptor

Initially, **A-1**-similar undecapeptides with a SiFA moiety were prepared, followed by further modified and occasionally more GLP-1-similar peptides. Due to limited synthetic access to the (2'-Et, 4'-OMe)BIP unit of lead peptide **A-1**, preparation and *in vitro* evaluation of derivatives **A-4** to **A-16** were conducted prior to **A-1**, wherefore its IC<sub>50</sub> value was considered in retrospect, but could not be used as a reference during GLP-1R ligand development. For this reason, all IC<sub>50</sub> values of the following compounds were mainly compared to those obtained for GLP-1 (**A-2**) [Nle<sup>14</sup>, Tyr(3-I)<sup>40</sup>]exendin-4 ([<sup>nat</sup>I]**A-17**) and [Nle<sup>14</sup>, Tyr<sup>40</sup>]exendin-4. Anyway, comparison to these peptides was supposed to provide a valid assessment of the novel designed GLP-1R-targeting peptides, since GLP-1 and exendin-4 both represent high-affinity GLP-1R ligands known from the literature. By contrast, the affinity of **A-1** has not been determined yet to our knowledge.

#### 4.1.3.1. SiFA-tagged undecapeptides

Based on the assumption, that bulky hydrophobic residues are tolerated by the GLP-1R at position 10 and 11 (structure of **A-1**, section 2.1), (2'-Et, 4'-OMe)-BIP at position 10 was substituted by a SiFA moiety with concomitant variation of the  $\alpha$ -quaternary amino acid at position 6 (*Table 12*). Both variants were synthesized to evaluate the effect of SiFA at position 10 and hence, their suitability as small peptide agents directly usable for <sup>18</sup>F-labeling.

Simultaneously, variations at position 6 were investigated to examine whether differences in EC<sub>50</sub> were transferable to the *in vitro* affinity assay used within the course of this thesis. Initial SAR studies conducted by Mapelli *et al.* revealed a factor of 3.2 between the non-fluorinated and fluorinated compounds (named 20 and 21 in *Figure 26*). It was assumed that literature data of EC<sub>50</sub> determinations cannot be simply adopted for IC<sub>50</sub> determination, due to differences in assay conditions. Hence, the ratio between the ( $\alpha$ -Me)Phe and ( $\alpha$ -Me)-(2-F)-Phe peptide might have been altered also due to the newly introduced SiFA substituent at position 10. Therefore, it was important to specify which  $\alpha$ -quaternary amino acid would be preferred at position 6 and should be incorporated in future SiFA-bearing GLP-1R ligands.

## RESULTS AND DISCUSSION

**Table 2.** 11-mer GLP-1R Agonists: Positions 2 and 6 SAR

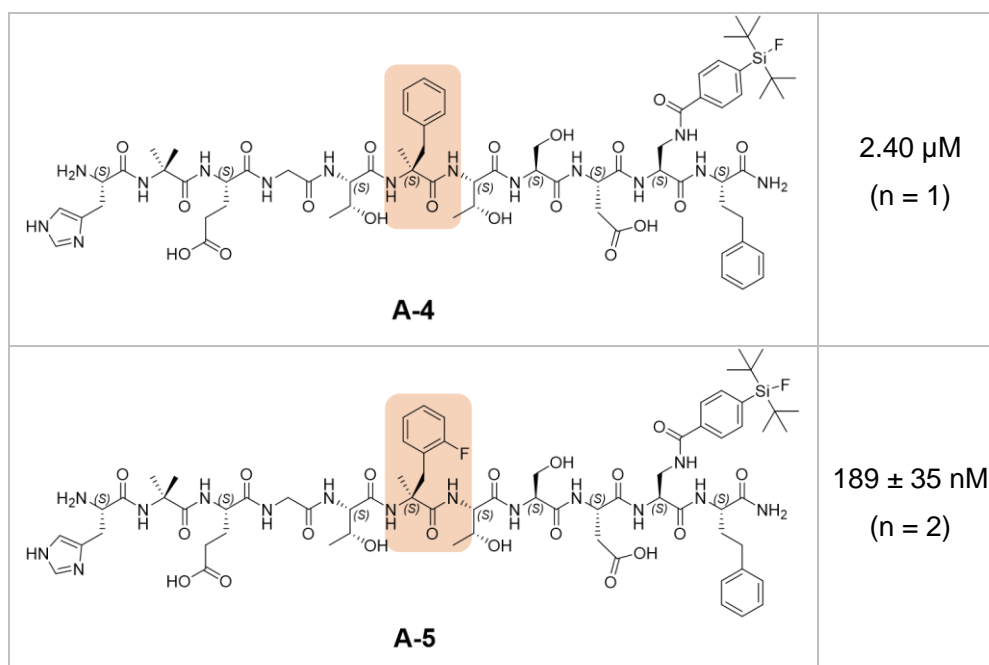
peptide no.	Xaa2	Xaa6	hGLP-1R cAMP EC <sub>50</sub> (nM)
19	Ala	(L)- $\alpha$ -Me-Phe	2.4 $\pm$ 2.8
20	Aib	(L)- $\alpha$ -Me-Phe	0.28
21	Aib	(L)- $\alpha$ -Me-(2-F)-Phe	0.087 $\pm$ 0.04
22	Aib	(L)- $\alpha$ -Me-(2,6-di-F)-Phe	0.093 $\pm$ 0.07

Factor: 3.2

**Figure 26:** Representative results of SAR studies conducted by Mapelli *et al.* EC<sub>50</sub> values are displayed in the rightmost column and indicate favorable properties for the ( $\alpha$ -Me)-(2-F)-Phe residue (~ 3.2-fold lower EC<sub>50</sub> than for ( $\alpha$ -Me)Phe). Ligands were developed in an attempt to further induce helical structure by  $\alpha$ -methylamino acids in the 11-mer peptides.<sup>[111]</sup> Figure 26 was adapted from reference [111] and slightly modified.

In general, a positive trend towards **A-5** could be determined (IC<sub>50</sub> = 189  $\pm$  35 nM, n = 2) indicating more favorable properties for undecapeptides with ( $\alpha$ -Me)-(2-F)-Phe instead of ( $\alpha$ -Me)Phe as  $\alpha$ -quaternary amino acid at position 6 (Table 12). A factor of ~ 13 was obtained for the IC<sub>50</sub> ratio **A-4/A-5** and thus confirmed the results obtained by Mapelli *et al.* to some extent, despite the higher factor determined within this study.

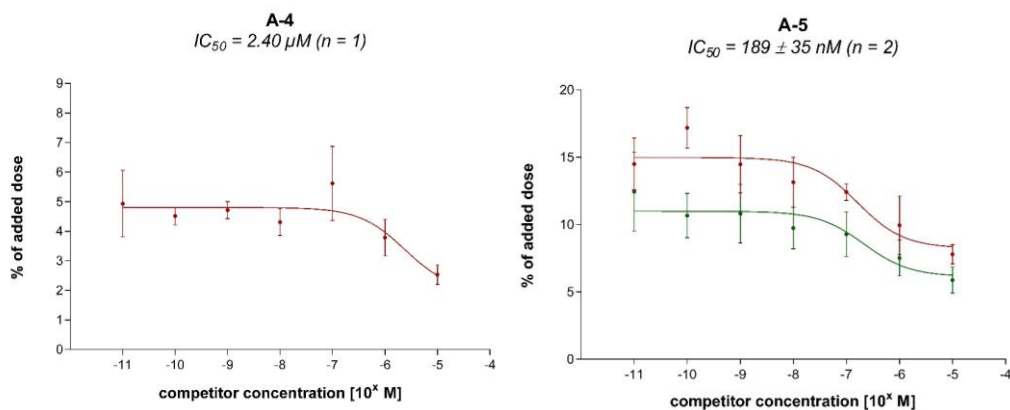
**Table 12:** Structural formulas and IC<sub>50</sub> data of peptides **A-4** and **A-5**. Varying  $\alpha$ -quaternary amino acids at position 6 are highlighted in red.



Initial competitive binding experiments with bovine serum albumin (BSA) in the incubation buffer gave no detectable affinity neither for **A-4** nor for **A-5**. Due to the presence of the lipophilic SiFA moiety<sup>[313]</sup>, experiments were repeated in assay buffer (HBSS) without BSA. Thereby, lipophilicity-induced nonspecific adhesion and retention by BSA should be avoided.<sup>[314]</sup> The curves

## RESULTS AND DISCUSSION

of displacement indicated  $IC_{50}$  values of  $2.40 \mu\text{M}$  ( $n = 1$ ) for **A-4** and  $189 \pm 35 \text{ nM}$  ( $n = 2$ ) for **A-5**, though still high unspecific binding could be observed (maximal radioligand displacement 61 - 69% of maximal radioligand binding, *Figure 27*).



**Figure 27:** Sigmoidal dose-response curves for compounds **A-4** and **A-5** in 250  $\mu\text{L}$  HBSS using HEK293-hGLP-1R cells (150 000 cells/well, 4  $^{\circ}\text{C}$ , 2 h) and  $[\text{Nle}^{14}, [^{125}\text{I}]\text{Tyr}(3\text{-I})^{40}]\text{exendin-4}$  (0.41 nM) as radioligand.

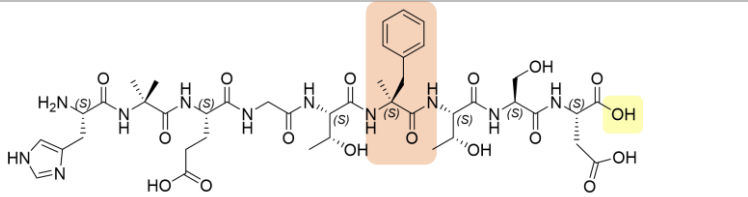
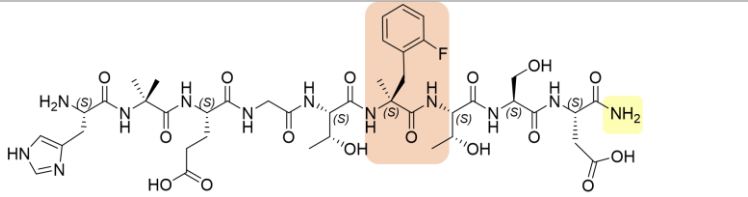
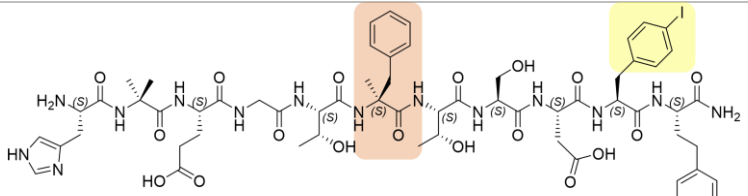
However, both peptides revealed only low ability to displace radioligand **A-17** from HEK293-hGLP-1R cells and notably surpassed  $IC_{50}$  values of GLP-1 ( $23.2 \pm 12.2 \text{ nM}$ ,  $n = 11$ ) and  $[\text{Nle}^{14}, \text{Tyr}(3\text{-I})^{40}]\text{exendin-4}$  ( $7.63 \pm 2.78 \text{ nM}$ ,  $n = 6$ ). Hence, further undecapeptides containing a sterically demanding C-terminal dipeptide (L-Dap(SiFA) $^{10}$ -L-homoPhe $^{11}$ -NH $_2$ ) were not synthesized. From these initial results it could not be deduced that undecapeptides with bulky substituents at the C-terminus would generally provide positive results, i.e. high affinity ligands. Therefore, the focus was shifted to examine if bulky substituents are mandatory or even harmful for receptor binding.

### 4.1.3.2. Peptides without C-terminal bulky substituents

The N-terminal fragments of **A-4** and **A-5**, represented by **A-6** and **A-7** respectively, were investigated but exhibited no detectable affinity (*Table 13*). Even introduction of an amidated C-terminus in **A-7** installed for mimicking resemblance to a true peptide bond, did not result in any benefit. Likewise, substitution of the L-Dap(SiFA) moiety of **A-4** by a simple L-Phe(4-I) residue (**A-8**) eliminated any detectable affinity. Obviously, this hydrophobic residue cannot compensate for the sterically demanding SiFA-moiety as in **A-4** ( $IC_{50} = 2.40 \mu\text{M}$ ). Consequently, the C-terminal dipeptide of lead peptide **A-1** or at least a hydrophobic bulky substituent at position 10 seems to be indispensable for radioligand displacement within the  $10^{-11}$  to  $10^{-5} \text{ M}$  range.

## RESULTS AND DISCUSSION

**Table 13:** Structural formulas and IC<sub>50</sub> data of *N*-terminal fragments of peptides **A-4** and **A-5**, represented by **A-6** and **A-7**, respectively and Phe(4-I)-derivatized **A-4**. Varying  $\alpha$ -quaternary amino acids at position 6 are highlighted in red, further structural differences are highlighted in yellow.

 <p style="text-align: center;"><b>A-6</b></p>	<p>no detectable affinity (n = 1)</p>
 <p style="text-align: center;"><b>A-7</b></p>	<p>no detectable affinity (n = 2)</p>
 <p style="text-align: center;"><b>A-8</b></p>	<p>no detectable affinity (n = 2)</p>

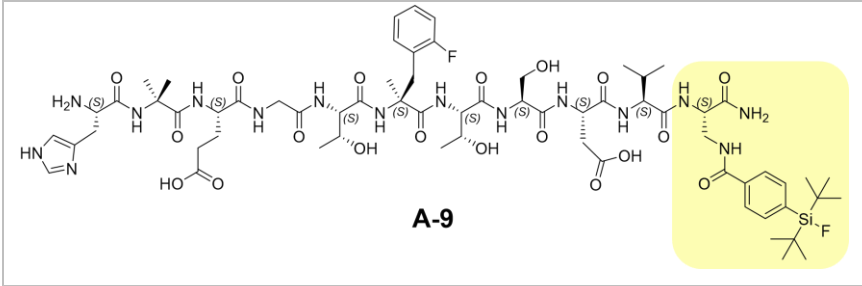
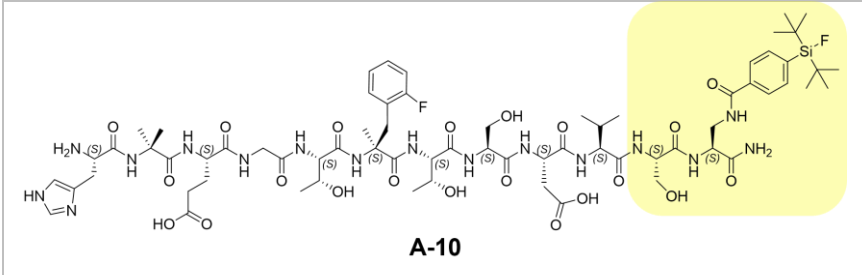
Since a certain tolerance, and especially for undecapeptides, a mandatory need for bulky substituents emerged, SiFA-bearing **A-1**-similar peptides were further investigated, however, with structures closer related to the endogenous ligand GLP-1. Thereby, an increased affinity should be reached since the peptides investigated so far revealed IC<sub>50</sub> values not below 189 ± 35 nM (n = 2) and therefore were not able to compete with high affinity GLP-1R-targeting peptides like GLP-1 (23.2 ± 12.2 nM) and [Nle<sup>14</sup>, Tyr(3-I)<sup>40</sup>]exendin-4 (7.63 ± 2.78 nM).

### 4.1.3.3. SiFA-tagged chimeras of **A-1** and GLP-1

Expanding the structural range, peptides with different chain lengths (11 - 15 amino acids) were synthesized and GLP-1-inherent amino acids were placed at the appropriate positions. Introduction of a SiFA moiety at position 11 was not tolerated, as no affinity was detected for peptide **A-9**. In order to avoid detrimental effects of the SiFA unit on ligand receptor interactions of the crucial *N*-terminal nonapeptide, repositioning towards the *C*-terminus was pursued. However, shifting the SiFA fragment to position 12 (**A-10**) revealed no positive effect (*Table 14*).

## RESULTS AND DISCUSSION

**Table 14:** Structural formulas and IC<sub>50</sub> data of SiFA-bearing small peptides **A-9** and **A-10**. Structural differences are highlighted in yellow.

 <p style="text-align: center;"><b>A-9</b></p>	<p>no detectable affinity (n = 2)</p>
 <p style="text-align: center;"><b>A-10</b></p>	<p>no detectable affinity (n = 1)</p>

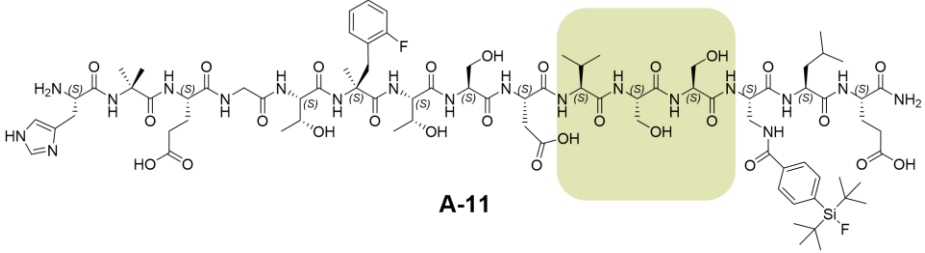
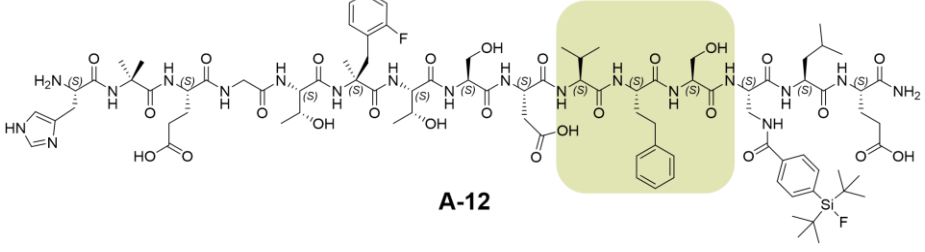
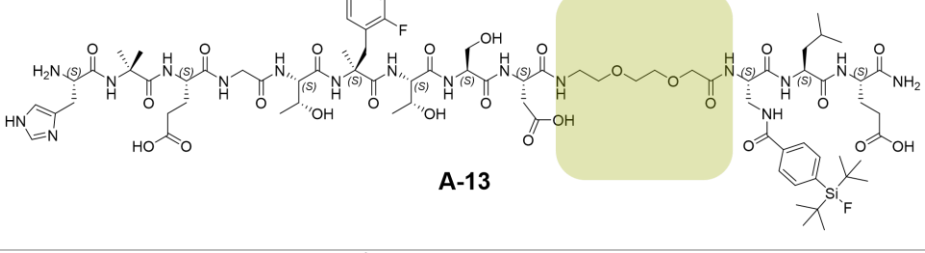
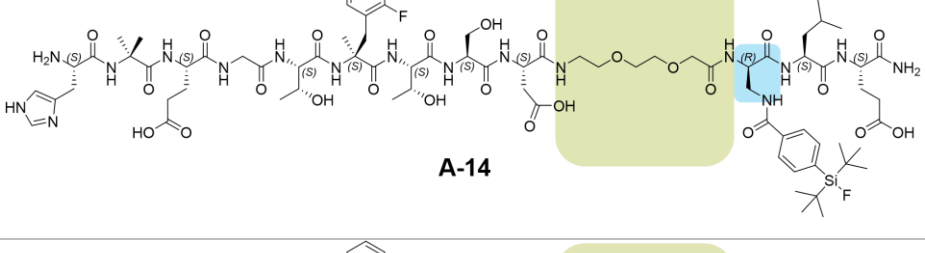
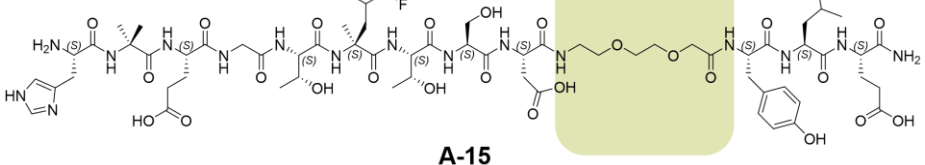
By contrast, compounds with SiFA at position 13 like in **A-11**, **A-12** and **A-13** displayed affinities in the micromolar range ( $2.95 \pm 0.31 \mu\text{M}$  to  $348 \pm 117 \mu\text{M}$ , *Table 15*). Indeed, an aromatic tyrosine residue can be found at this position in endogenous GLP-1, indicating a certain tolerance for this structural modification. It is important to note, that further variations from original GLP-1 residues between Asp<sup>9</sup> and Dap(SiFA)<sup>13</sup> seem to be not well tolerated in those peptides, although no crucial role for receptor binding and activation could be ascribed by previous SAR studies.<sup>[40, 45]</sup> Substitution of L-Ser<sup>11</sup> by a L-homoPhe residue as realized in peptide **A-1**, resulted in a ~ 2.4-fold decline in affinity ( $2.95 \pm 0.31 \mu\text{M}$  for **A-11** vs.  $7.12 \pm 2.47 \mu\text{M}$  for **A-12**). Consequently, L-homoPhe at position 11 might be advantageous for receptor-ligand-interactions in undecapeptides like **A-1**, but obstructive if incorporated at the same position in extended peptides like **A-12**.

Furthermore, affinity also remarkably decreased by introduction of a short hydrophilic poly(ethylene oxide)-similar linker (O2Oc), which was installed in peptides **A-13**, **A-14** and **A-15** (*Table 15*). First, this linker fragment was supposed to compensate to a certain extent for the overall lipophilic character of the SiFA unit and was therefore introduced adjacent to the SiFA moiety in **A-13** and **A-14**.<sup>[315]</sup> Second, the general effect of a higher O2Oc-based flexibility<sup>[316]</sup> was investigated by *in vitro* evaluation of the SiFA-free analog **A-15**. Whereas peptide **A-13** showed low but still detectable affinity ( $348 \pm 117 \mu\text{M}$ ), no radioligand displacement was observed for its D-stereoisomer **A-14**. Also **A-15** failed to displace radioligand **A-17** within the measured concentration range. These results indicate that the natural L-configuration at position 13 might be preferred and that a SiFA moiety potentially provides more favorable results in comparison to the original tyrosine residue, at least for truncated pentadecapeptides. Moreover, a certain rigidity introduced by the original GLP-1 residues Val<sup>10</sup>, Ser<sup>11</sup> and Ser<sup>12</sup> seems to be indispensable, since pentadecapeptides **A-11** and **A-12** still showed higher affinities ( $2.95 \pm 0.31 \mu\text{M}$  and  $7.12 \pm 2.47 \mu\text{M}$ ) compared to the more flexible O2Oc-modified analog **A-13** ( $348 \pm 117 \mu\text{M}$ ).

## RESULTS AND DISCUSSION

Pentadecapeptides **A-11**, **A-12**, **A-13**, **A-14** and **A-15** were synthesized until Glu<sup>15</sup> (Glu<sup>21</sup> in GLP-1 counting method) for positioning a hydrophilic, anionic residue in close spatial proximity to the SiFA unit for partial compensation of the rather hydrophobic character.

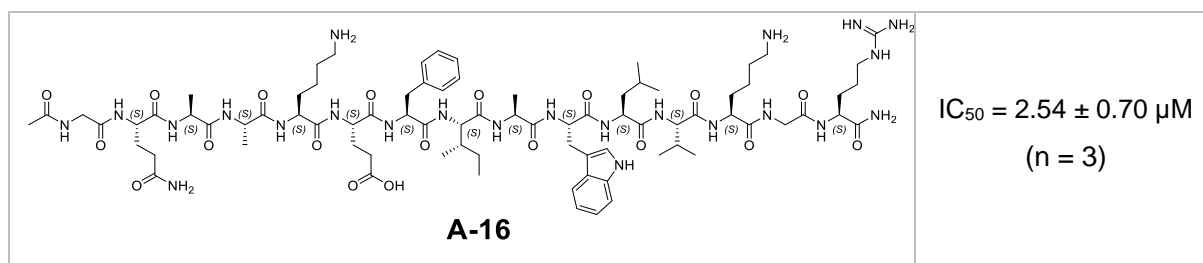
**Table 15:** Structural formulas and IC<sub>50</sub> data of SiFA-bearing small peptides **A-11** to **A-14** as well as of tyrosine derivative **A-15**. Structural differences between position 9 and 13 are highlighted in green. The altered stereoconfiguration in **A-14** is highlighted in blue.

 <p style="text-align: center;"><b>A-11</b></p>	<p>IC<sub>50</sub> = 2.95 ± 0.31 μM (n = 2)</p>
 <p style="text-align: center;"><b>A-12</b></p>	<p>IC<sub>50</sub> = 7.12 ± 2.47 μM (n = 2)</p>
 <p style="text-align: center;"><b>A-13</b></p>	<p>IC<sub>50</sub> = 348 ± 117 μM (n = 2)</p>
 <p style="text-align: center;"><b>A-14</b></p>	<p>no detectable affinity (n = 2)</p>
 <p style="text-align: center;"><b>A-15</b></p>	<p>no detectable affinity (n = 2)</p>

#### 4.1.3.4. C-terminal pentadecapeptide of GLP-1

The importance of the C-terminal fragment of GLP-1 for receptor binding and selectivity was already proven by several studies (section 1.1.1 and 1.1.2).<sup>[32, 33, 52, 112]</sup> Based on these findings and the rather poor results obtained so far with N-terminal fragments of GLP-1 and derivatives thereof, a potential usability of the 15-residue C-terminal fragment of GLP-1 was investigated. Interestingly the isolated, acetylated C-terminal half of GLP-1 (**A-16**) exhibited a low but noticeable affinity ( $2.54 \pm 0.70 \mu\text{M}$ , Table 16). However, expedient optimizations of this pentadecapeptide would be necessary to obtain a basic structure that tolerates modifications like chelator or SiFA attachment whilst keeping high affinity towards GLP-1R. For now, the  $\text{IC}_{50}$  of **A-16** exceeds the  $\text{IC}_{50}$  of GLP-1 by a factor of 109.

**Table 16:** Structural formula and  $\text{IC}_{50}$  data of the C-terminal half of GLP-1 (**A-16**).



Critical data analysis. In general, DIPEA was used for coupling of Fmoc-L-Dap(Dde)-OH in all peptides except for **A-11** and **A-12** (*sym*-collidine). During the course of another project, carried out in parallel, the synthesis of PSMA inhibitors on 2-CT resin revealed susceptibility of Fmoc-D-Dap(Dde)-OH to racemization when DIPEA was used as a base.<sup>[232]</sup> Hence, it could not be excluded that for GLP-1R-addressing SiFA peptides racemization has occurred, despite no observable peak splitting. Comparable to the PSMA derivatives (unwanted D- to L-transformation), up to 40% might have been converted from L- into the D-enantiomer in extreme cases. However, a rough assessment of the peptides by the measured  $\text{IC}_{50}$  would have been still possible despite such a high percentage of unwanted by-product. Even assuming that D-enantiomers would generally exhibit absolutely no binding affinity, these values would have laid at least in the same order of magnitude as described below (*worst case analysis*).

For peptides **A-10** and **A-15** chemical purity only reached 68% and 75% respectively, due to by-products hardly separable during preparative RP-HPLC. Furthermore, peptide **A-15** showed a split product peak with identical *m/z*-ratios at 8.62 min (38% peak area) and 8.76 min (62% peak area). Since no Fmoc-L-/D-Dap(Dde)-OH in combination with DIPEA was used in the synthesis of **A-15**, it was assumed that no racemization but rather different protonation states or conformations of the peptide caused peak splitting. Hence, affinity studies were performed yet for a first assessment of the  $\text{IC}_{50}$  of both peptides.

## RESULTS AND DISCUSSION

A conservative *worst case analysis* for **A-15** revealed an affinity ~ 3.4-fold lower if only 29% (38% of 75%) of pure product would have been present in the substance used for dilution series. For a theoretical affinity of 100 nM (or 1.00  $\mu$ M) that would have led to a measured affinity of ~ 340 nM (or 3.40  $\mu$ M). However, since both peptides **A-10** and **A-15** showed no detectable  $IC_{50}$ , and no radioligand displacement was observable even at a  $10^{-5}$  M concentration, further purification steps were not pursued.

It has to be noted that during the synthesis of compound **A-13**, racemization was detected after the coupling of Fmoc-L-Dap(Dde)-OH and resulted in an enantiomeric ratio (*er*) of ~ 3/7 for **A-13/A-14**. Peptides **A-13** and **A-14** were isolated by collecting the respective fractions separately ( $t_R = 6.81$  min for **A-13** and  $t_R = 9.39$  min for **A-14**, 80 - 100% Method B, 1 mL/min) via semi-preparative HPLC. Based on the following affinity determinations, peptide **A-13** was assumed to represent the stereoisomer comprising L-Dap(SiFA)<sup>13</sup>, since the natural ligand GLP-1 is assembled exclusively of L-amino acids. Further endeavors to determine the exact enantiomeric identity of compounds **A-13** and **A-14** were not undertaken, since even the favored enantiomer had a very low affinity ( $348 \pm 117$   $\mu$ M). For all other compounds, no racemization was observed.

In total, these approaches did not lead to high affinity GLP-1R ligands, wherefore no internalization or other *in vitro* and *in vivo* experiments were conducted due to the poor  $IC_{50}$  data generated by these compounds. Instead, synthesis of lead peptide **A-1** was pursued to determine its affinity and general usability as basic structure for further radiolabeled **A-1**-based diagnostics/therapeutics. Thereby, the value of (2'-Et, 4'-OMe)BIP at position 10 should be examined and whether it represents the crucial residue for the design of high affinity undecapeptides.

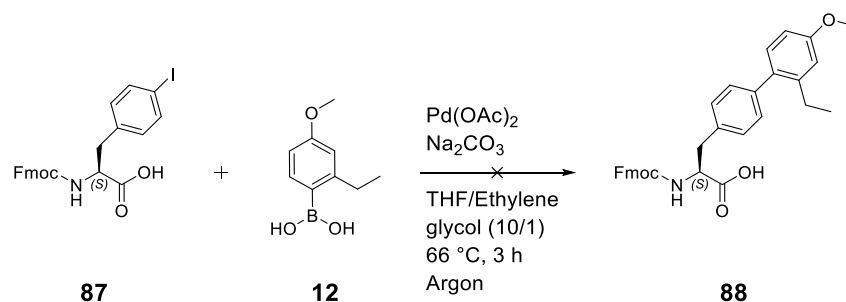
### 4.1.3.5. Lead peptide A-1

In the following section, the synthesis of lead peptide **A-1** will be discussed first and results obtained from affinity experiments will be presented afterwards. In particular, the preparation of the biphenylalanine residue (2'-Et, 4'-OMe)BIP of the C-terminal dipeptide represents an essential step for which additional synthetic efforts in form of Suzuki-Miyaura cross-coupling<sup>[317]</sup> reactions were required. In order to preserve the prescribed L-configuration of the biphenylalanine fragment, only cross-coupling conditions were chosen which were described to meet this requirement explicitly. Initial attempts for (2'-Et, 4'-OMe)BIP synthesis focused on enabling the linear synthesis of **A-1** on Rink amide ChemMatrix<sup>®</sup> resin. However, synthesis of lead peptide **A-1** could be only accomplished by fragment coupling in solution as depicted in *Scheme 5*.

Apart from already published protocols for on-resin synthesis of lead peptide **A-1**<sup>[111, 114]</sup>, an early approach intended the preparation of Fmoc-(2'-Et, 4'-OMe)BIP-OH as an amino acid building block potentially usable for Fmoc-based SPPS (*Scheme 1*). Thus, possible on-resin Suzuki-Miyaura reaction-based disadvantages (e.g. degradation of the resin or resin-bound product by high

## RESULTS AND DISCUSSION

temperature & basic conditions; laborious/incomplete Pd-catalyst removal post reaction from solid phase support) should be circumvented. Therefore, reaction conditions close to those published by Maity *et al.*<sup>[318]</sup> were chosen by which the Fmoc protective group as well as the stereoconfiguration should be preserved. According to this procedure, the most effective reagents which provided the highest yields were used. Only originally used PdCl<sub>2</sub> was replaced by Pd(OAc)<sub>2</sub> due to practical availability. This modification was considered as well tolerable, since both Pd(II)-catalysts can be used interchangeably for Suzuki-Miyaura cross-coupling reactions.<sup>[319]</sup>

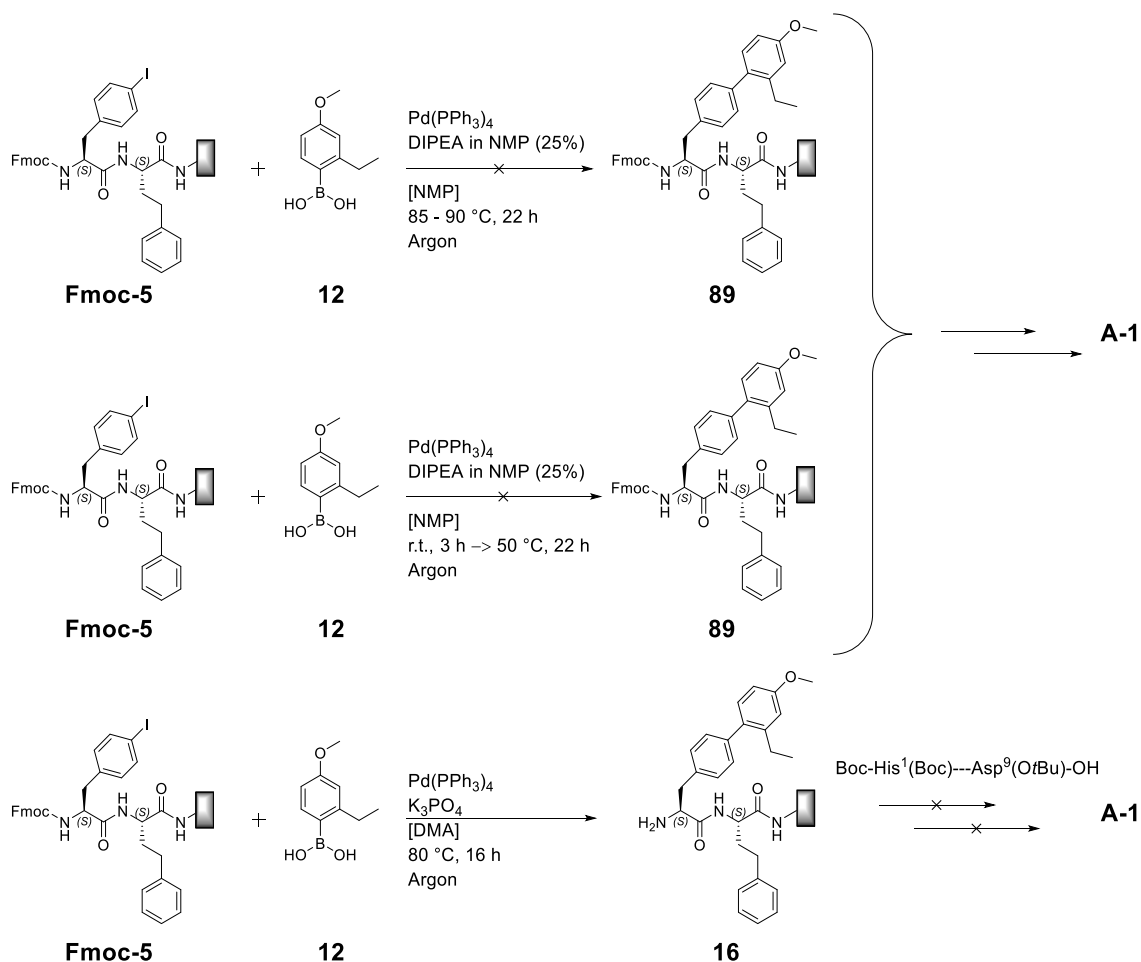


**Scheme 1:** First attempt for solution phase synthesis of Fmoc-(2'-Et, 4'-OMe)BIP-OH (**88**), potentially usable as an amino acid building block in Fmoc-based SPPS for preparation of **A-1** on Rink amide ChemMatrix<sup>®</sup> resin.<sup>[318]</sup>

No product formation (**88**) ( $m/z \approx 521$ ) could be observed after 3 h at 66 °C. Moreover, reactant Fmoc-Phe(4-I)-OH (**87**) was not detectable anymore. Instead, mainly two unidentifiable compounds ( $m/z = 341.1$  & 291.8, respectively) remained. Hence, reactions with extended reaction time were not conducted and due to this unfruitful attempt in solution, synthesis of **A-1** based on reaction protocols that include on-resin Suzuki-Miyaura cross-coupling reactions, was further pursued.

Despite several attempts to realize on-resin synthesis as described by Mapelli *et al.*<sup>[111]</sup>, **A-1** could not be obtained by a linear reaction protocol (*Scheme 2*, first row). Suzuki-Miyaura cross-coupling on Fmoc-**5** only led to non-identifiable products. Since Fmoc instead of Boc was used as *N*-terminal protective group, the rather harsh conditions (85 - 90 °C) might have caused liberation of the free amino terminus and even further degradation of the dipeptide, as no product and not even the Fmoc-free by-product could be identified after a reaction period of 22 h. In order to avoid temperature-induced decomposition, the reaction was conducted at 50 °C but led to no detectable conversion after 17.5 h. Instead, only reactant Fmoc-**5** remained (*Scheme 2*, second row). An alternative procedure, described by Haque *et al.*<sup>[114]</sup> afforded product **16** ( $m/z = 460.2$ ) but further coupling reactions, also with fragment Boc-His<sup>1</sup>(Boc)---Asp<sup>9</sup>(OtBu)-OH did not result in any detectable conversion (*Scheme 2*, bottom row). Despite this failure in convergent synthesis of **A-1** on solid-phase support, an effective reaction protocol for synthesis of biphenyl residue (2'-Et, 4'-OMe)BIP could be established by this approach (compound **16**). Therefore, all following Suzuki-Miyaura cross-coupling reactions on resin were performed according to this procedure and slightly adjusted in case of insufficient conversion (e.g. 80 °C → 90 °C, *Scheme 4*)

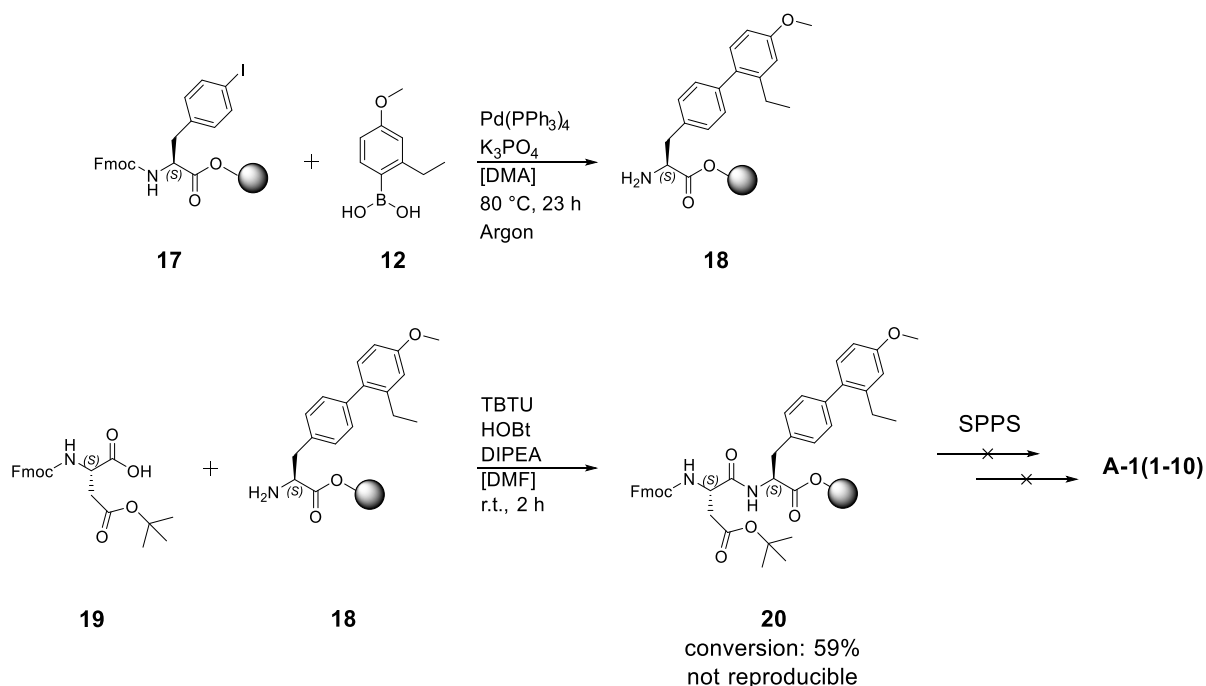
## RESULTS AND DISCUSSION



**Scheme 2:** Attempts for linear (first two rows) and convergent (third row) synthesis of **A-1** on Rink amide ChemMatrix<sup>®</sup> resin.

In order to exclude solid support-based unreactivity, (2'-Et, 4'-OMe)BIP was planned to be synthesized on 2-CT resin. In case of a positive result, the respective *N*-terminal decapeptide should be finalized on 2-CT resin and coupled to *C*-terminal H-L-homoPhe-RACM. Indeed, the reaction conditions were well tolerated by the resin, and formation of H-(2'-Et, 4'-OMe)BIP (**18**) could be confirmed by RP-HPLC/MS analysis (*Scheme 3*). However, further coupling reactions on the already Fmoc-deprotected amino acid **18** were of minor success or not reproducible when scaled up (from 19.0  $\mu\text{mol}$  to 42.0  $\mu\text{mol}$ ) (*Scheme 3*), similar to the unfruitful reactions on Rink amide ChemMatrix<sup>®</sup> resin.

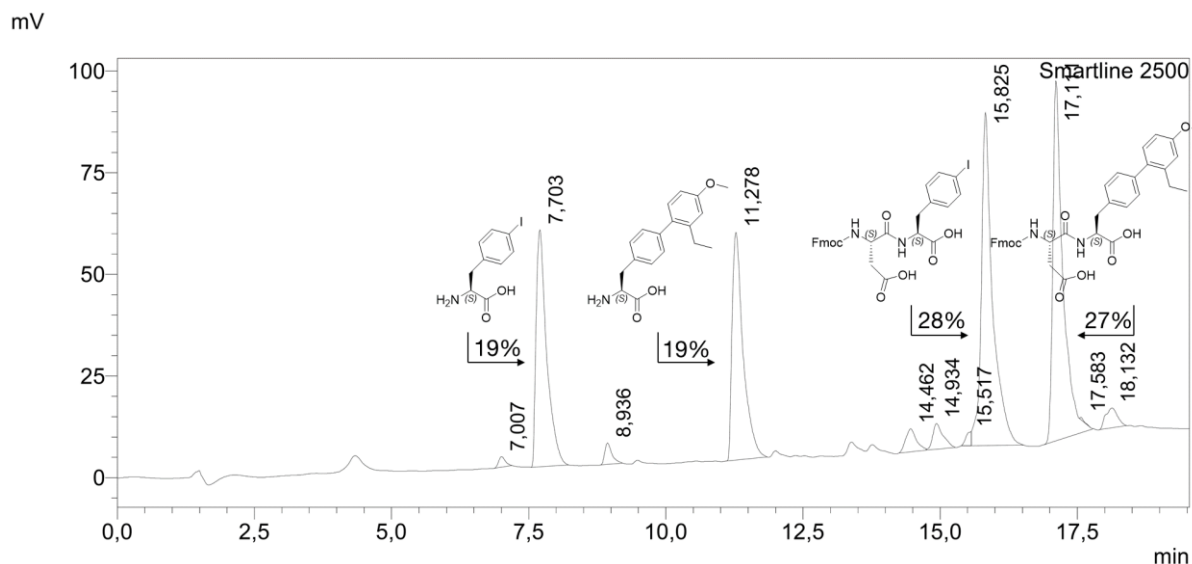
## RESULTS AND DISCUSSION



**Scheme 3:** Synthetic route for **18** (above) and first attempt for synthesis of an **A-1** fragment (1-10) on 2-CT resin, based on compound **18** (below).

In a first approach Fmoc-L-Asp(*t*Bu)-OH was successfully coupled (19.0  $\mu\text{mol}$  scale), as determined by RP-HPLC/MS (27% total proportion, 59% conversion, *Figure 28*). However, several attempts to promote further conversion of residual **18** did not lead to any significant change of the ratio **18/20** (max. 62% conversion). Neither increasing equivalents of Fmoc-L-Asp(*t*Bu)-OH and base (DIPEA) nor changing the coupling reagent combination from TBTU/HOBt to HATU/HOAt, COMU/EDC $\cdot$ HCl or PyBOP/HOAt led to any detectable improvement. Besides, also experiments that aimed at coupling with the more reactive, *in situ* formed acid chloride Fmoc-L-Asp(*t*Bu)-Cl failed to reach a higher conversion. When scaled up to 42.0  $\mu\text{mol}$ , reactions conducted analogously to previous experiments did not lead to any measurable conversion and even the use of the activated form Fmoc-L-Asp(O*t*Bu)-Pfp was unsuccessful.

## RESULTS AND DISCUSSION



**Figure 28:** HPLC-chromatogram (20 - 80% B in 15 min, Method A, 1 mL/min, GP7) after coupling of Fmoc-L-Asp(OtBu)-OH to 2-CT resin with bound **17**(-Fmoc) and **18**. Conversion of **18** to **20** amounted to 59% and the total proportion of **20** ( $t_R$  [**20**-tBu]  $\approx$  17.1 min) was 27%.

Despite a yet improvable conversion, the Fmoc-protective group of **20** (19.0  $\mu$ mol scale) was removed and the protected *N*-terminal fragment (1-8) Boc-L-His-Aib-L-Glu(OtBu)-Gly-L-Thr(tBu)-L-( $\alpha$ -Me)-(2-F)-Phe-L-Thr(tBu)-L-Ser(tBu)-OH\*TFA was added. However, this approach of fragment coupling did not lead to the intended decapeptide Boc-L-His-Aib-L-Glu(OtBu)-Gly-L-Thr(tBu)-L-( $\alpha$ -Me)-(2-F)-Phe-L-Thr(tBu)-L-Ser(tBu)-L-Asp(OtBu)-(2'-Et, 4'-OMe)BIP-OH. Instead, only **17**(-Fmoc) and **18** could be identified. Moreover, the Fmoc-free forms of the two dipeptides present in *Figure 28* ( $t_R \approx$  15.8 and 17.1 min) were now undetectable. Either the *m/z*-ratios of the respective HPLC fractions were misinterpreted (= false identity) or coupling conditions led to decomposition of both dipeptides.

On the 42.0  $\mu$ mol scale, coupling of Fmoc-Gly-OH was performed in a separate attempt in order to check for a potential Fmoc-L-Asp(OtBu)-OH-related non-reactivity. Therefore, the resin was treated with 20% piperidine in DMF (v/v) to remove any residual/not detectable *N*-terminal protective groups and then incubated with the amino acid (3.00 eq.), coupling reagents TBTU/HOAt (3.00 eq.) and DIPEA (18.0 eq.) (r.t., 46 h). Again, no conversion to the desired Fmoc-Gly-functionalized product could be detected by RP-HPLC/MS.

The non-reactivity of RACM resin-bound dipeptide **16** as well as 2-CT resin-bound **18** and Fmoc-free **20** led to the assumptions that:

- 1) the bulky (2'-Et, 4'-OMe)-BIP-residue might impair on-resin peptide chain elongation or
- 2) Suzuki-Miyaura cross-coupling reaction conditions or reagents might have caused deactivation of the (dipeptide's) *N*-terminus, not detectable by mass spectrometry.

## RESULTS AND DISCUSSION

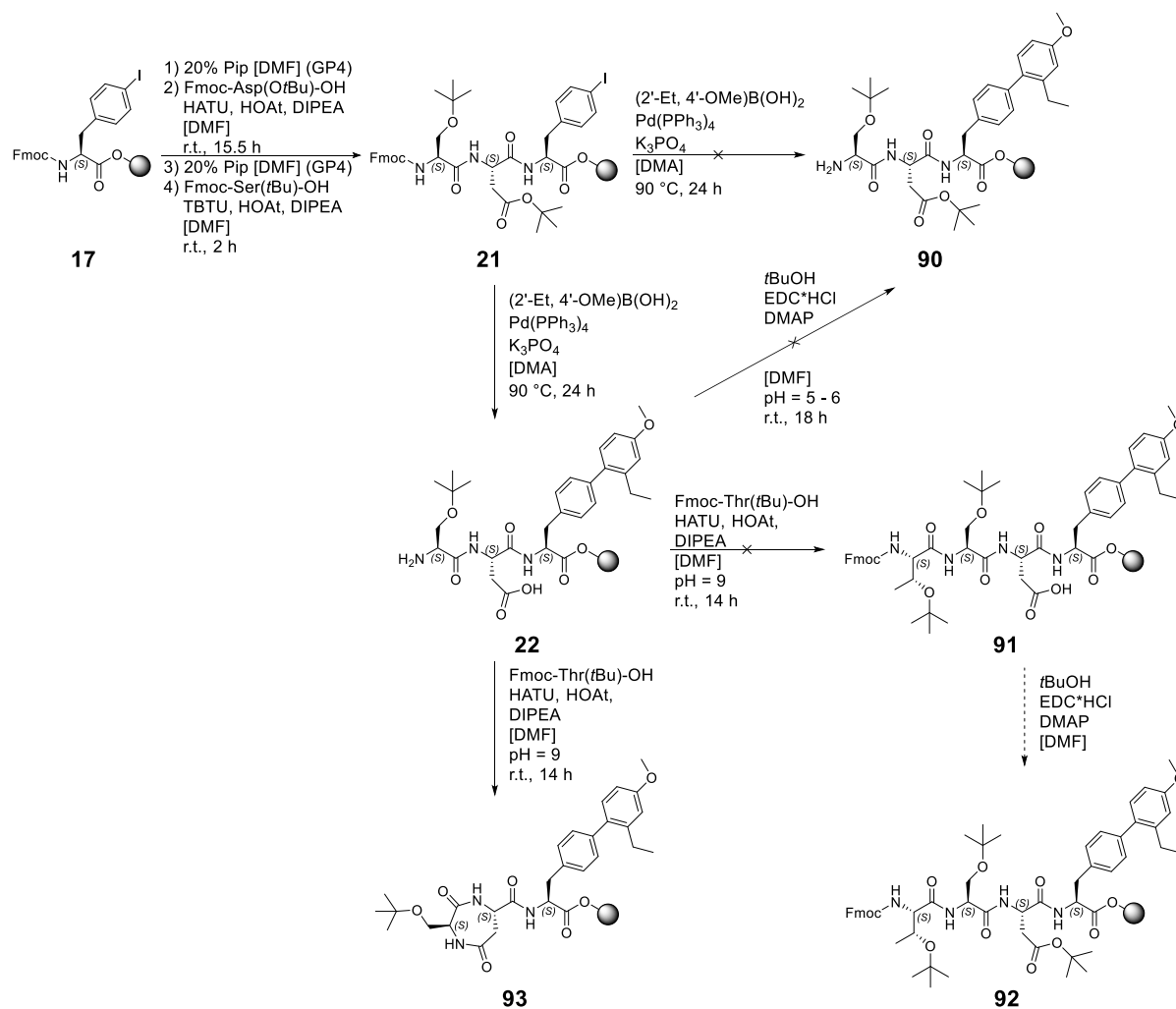
To examine the first theory, the peptide was elongated by two *N*-terminal residues prior to the cross-coupling reaction on 2-CT resin. However, Suzuki-Miyaura reaction conditions mainly yielded **22** (*Scheme 4*). The *m/z*-ratio of product **90** could not be detected and led to the assumption that the *t*Bu-ester protective group of aspartate probably was cleaved off under the rather harsh reaction conditions (80 °C, aq. K<sub>3</sub>PO<sub>4</sub>, pH = 13 at t = 0), whereas the *t*Bu-ether protective group of serine still remained intact.<sup>[320]</sup>

Restoration of the missing *t*Bu-protective group at the aspartate was not pursued in first place, since simultaneous inactivation of the free *N*-terminus was expected by intramolecular cyclization via *t*Bu-ester formation reagents like EDC\*HCl and DMAP.<sup>[320, 321]</sup> Therefore, **22** was incubated with Fmoc-Thr(*t*Bu)-OH (5.00 eq.), coupling reagents (5.00 eq. HATU & HOAt) and base (18.0 eq. DIPEA) for 14 h at room temperature (*Scheme 4*). It was speculated that intermolecular peptide chain elongation might be preferred over intramolecular heptacyclic ring formation, due to the high amount of amino acid equivalents. If successful, *t*Bu-ester restoration on compound **91** was planned and would have led to product **92** without the risk of intramolecular cyclization.

However, no fraction of the acquired HPLC Chromatogram revealed a *m/z*-ratio of the expected product **91**. Instead, only intramolecular cyclization occurred and yielded **93** as the main identifiable component. Consequently, the strategy was changed now focusing on restoration of L-Asp(O*t*Bu) prior to any amino acid coupling.

Selective alkylation at the aspartate residue was tried to accomplish by *t*BuOH, EDC\*HCl and DMAP at a pH value of 5 - 6 to avoid again intramolecular cyclization. Therefore, the pH value of the reaction was adjusted by addition of HCl in dioxane to keep the serine *N*-terminus (pK<sub>a</sub> = 9 - 10) protonated/inactive and the aspartyl side chain carboxylate (pK<sub>a</sub> = 3.87) in its deprotonated form.<sup>[322]</sup> No formation of product **90** could be detected after this attempt, ascribed either to potential inactivation of DMAP or EDC\*HCl at this pH or residual H<sub>2</sub>O in the reaction solution. Selective alkylation via *tert*-butyl acetate and 70% (v/v) perchloric acid (aq.) as performed for the synthesis of PSMA ligands **B-18** and **B-19** (section 4.2.2.1) was not performed. The rather strong acidic conditions were presumed to cause cleavage of the tripeptide from the resin and irreversible cleavage of the *t*Bu-protective group from serine.

## RESULTS AND DISCUSSION

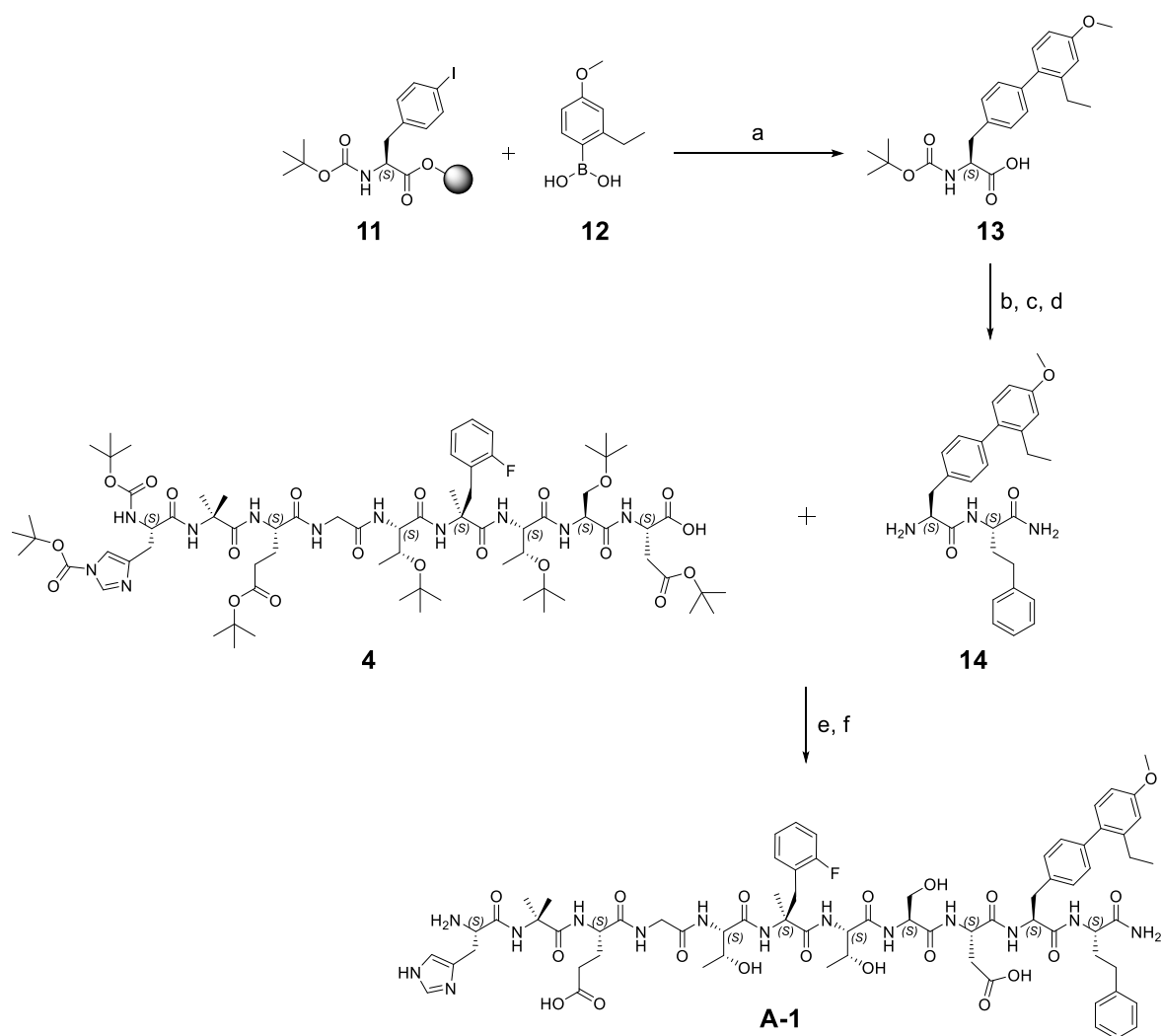


**Scheme 4:** Planned synthetic routes for **90** and **92** based on Suzuki-Miyaura cross-coupling on tripeptide **21** and actually obtained synthesis products **22** and **93**.

In sum, Suzuki-Miyaura cross-coupling on tripeptide **21** led to formation of the intended (2'-Et, 4'-OMe)BIP, however, reaction conditions were not compatible with the adjacent aspartate. Consequently, further experiments based on this tripeptide approach were abandoned and the focus was switched on a strategy to prevent deactivation of the *N*-terminus after cross-coupling, as stated in the second theory (see above).

Therefore, synthesis of **13** with a cross-coupling resistant Boc-protective group at the *N*-terminus was initiated (*Scheme 5*), based on the previously successful on-resin synthesis of **18** (*Scheme 3*).

## RESULTS AND DISCUSSION



**Scheme 5:** Synthetic route for the preparation of lead peptide **A-1**. a) Pd(PPh<sub>3</sub>)<sub>4</sub>, K<sub>3</sub>PO<sub>4</sub> [DMA], 80 °C, 22 h, argon; b) H-L-homoPhe-RACM, PyBOP, HOAt, DIPEA [DMF/DCM], r.t., 24 h; c) TFA/TIPS/H<sub>2</sub>O; d) tetraalkylammonium carbonate [THF], r.t., 2 h; e) HOAt, DIC [DMF/DCM], r.t., 19 h; f) TFA/TIPS/H<sub>2</sub>O. Detailed synthesis procedures are given in MATERIALS AND METHODS (chapter III).

On-resin Suzuki-Miyaura cross-coupling using compounds **11** and **12** provided the (2'-Et, 4'-OMe)BIP fragment **13** still functionalized with a cross-coupling resistant Boc-protective group at the *N*-terminus. Cleavage of **13** from the resin by HFIP/DCM (1/4) was not mandatory, since a major part was already cleaved from the 2-CT resin by the cross-coupling conditions. Boc-protected **13** was coupled to RACM resin-bound H-L-homoPhe and subsequent cleavage with TFA/TIPS/H<sub>2</sub>O (95/2.5/2.5) revealed dipeptide **14**. Fragment coupling of purified **4** and **14** provided lead peptide **A-1**\*2TFA as colorless powder (2.05 mg, 16.1% referred to **14**) after removal of all acid-labile protective groups and RP-HPLC purification (Scheme 5). This strategy involved three RP-HPLC purification steps in total, after synthesis of **13**, **14** and **A-1**.

In previous studies, GLP-1R binding affinities of **A-1** and related derivatives either remained undefined, or were not compared to established ligands, such as GLP-1 or exendin-4.<sup>[111, 113-116]</sup>

## RESULTS AND DISCUSSION

Therefore, the affinity of this GLP-1 mimetic was determined and revealed a rather unfavorable  $IC_{50}$  value of  $669 \pm 242$  nM ( $n = 5$ ), which was not expected due to the very close  $EC_{50}$  of **A-1** to endogenous GLP-1 ( $EC_{50}(\mathbf{A-1}) = 31$  pM,  $EC_{50}(\text{GLP-1}) = 34$  pM), as determined by Mapelli *et al.* and Haque *et al.*<sup>[111, 113]</sup> Compared to the  $IC_{50}$  data obtained for the known high affinity ligands GLP-1 ( $23.2 \pm 12.2$  nM), [Nle<sup>14</sup>, Tyr(3-I)<sup>40</sup>]exendin-4 ( $7.63 \pm 2.78$  nM) and [Nle<sup>14</sup>, Tyr<sup>40</sup>]exendin-4 ( $9.87 \pm 1.82$  nM), **A-1** notably exceed those values (~ 29 to 88-fold).

For direct comparison,  $IC_{50}$  data of all previously analyzed compounds as well as of **A-1**, GLP-1 (**A-2**), [Nle<sup>14</sup>, Tyr<sup>40</sup>]exendin-4 and [Nle<sup>14</sup>, Tyr(3-I)<sup>40</sup>]exendin-4 ([<sup>nat</sup>I]**A-17**) are displayed in *Table 17*. Due to different *in vitro* displacement behaviors initially observed for **A-4** and **A-5**, SiFA-tagged peptides were investigated in assays supplemented with (w/) and without (w/o) BSA to determine optimum binding conditions.

**Table 17:**  $IC_{50}$  data of SiFA-tagged undecapeptides (**A-4** and **A-5**), peptides without C-terminal bulky substituents (**A-6**, **A-7** and **A-8**), SiFA-tagged chimeras of **A-1** and GLP-1 (**A-9** to **A-14**), tyrosine derivative **A-15** as well as the C-terminal pentadecapeptide of GLP-1 (**A-16**) developed for targeting the GLP-1 receptor.  $IC_{50}$  values of reference ligands **A-1**, GLP-1 (**A-2**), [Nle<sup>14</sup>, Tyr<sup>40</sup>]exendin-4 and [Nle<sup>14</sup>, Tyr(3-I)<sup>40</sup>]exendin-4 ([<sup>nat</sup>I]**A-17**) are also listed.

Peptide	$IC_{50} \pm SD$	No. of experiments	Peptide	$IC_{50} \pm SD$	No. of experiments
<b>A-1</b>	$669 \pm 242$ nM	5 (w/ BSA <sup>a</sup> )	<b>A-11</b>	$2.95 \pm 0.31$ $\mu$ M	2 (w/ BSA)
<b>A-2</b> (GLP-1)	$23.2 \pm 12.2$ nM $65.0$ nM	11 (w/ BSA) 1 (w/o BSA)	<b>A-12</b>	$7.12 \pm 2.47$ $\mu$ M	2 (w/ BSA)
<b>A-4</b>	$2.40$ $\mu$ M	1 (w/o BSA)	<b>A-13</b>	$348 \pm 117$ $\mu$ M	2 (w/ BSA)
<b>A-5</b>	$189 \pm 35$ nM	2 (w/o BSA)	<b>A-14</b>	not detectable	2 (w/ and w/o BSA)
<b>A-6</b>	not detectable	1 (w/ BSA)	<b>A-15</b>	not detectable	2 (w/ and w/o BSA)
<b>A-7</b>	not detectable	2 (w/ and w/o BSA)	<b>A-16</b>	$2.54 \pm 0.70$ $\mu$ M	3 (w/ BSA)
<b>A-8</b>	not detectable	2 (w/ and w/o BSA)	[ <sup>nat</sup> I] <b>A-17</b> ([Nle <sup>14</sup> , Tyr(3-I) <sup>40</sup> ]exendin-4)	$7.63 \pm 2.78$ nM	6 (w/ BSA)
<b>A-9</b>	not detectable	2 (w/ and w/o BSA)	[Nle <sup>14</sup> , Tyr <sup>40</sup> ]exendin-4	$9.87 \pm 1.82$ nM	3 (w/ BSA)
<b>A-10</b>	not detectable	1 (w/ BSA)			

SD, standard deviation; assay conditions are indicated in brackets after the No. of experiments.

<sup>a</sup>'w/ BSA' indicates supplementation with 1% BSA, whereas 'w/o BSA' indicates no supplementation with BSA.

## RESULTS AND DISCUSSION

Among all GLP-1R-targeting ligands, only **A-5** provided distinctly lower  $IC_{50}$  values ( $189 \pm 35$  nM,  $n = 2$ ) than lead peptide **A-1** ( $669 \pm 242$  nM,  $n = 5$ ). Although this suggests a higher GLP-1R affinity for **A-5**, nonspecific binding of this SiFA-bearing compound was notably high as displayed by the respective dose-response curves (*Figure 27*). In addition, later competitive binding experiments revealed unexpectedly high values for **A-5** ( $1.14 \pm 0.08$   $\mu$ M,  $n = 2$ ) indicating either peptide decomposition or SiFA-mediated nonspecific binding of the peptide to storage tubes (increasing loss of substance over time by adhesion). Introduction of charged amino acid residues (positive and/or negative) or other lipophilicity-reducing auxiliaries in close spatial proximity to the SiFA moiety might compensate for lipophilicity-induced unspecific binding of **A-5**.<sup>[313, 314]</sup> Accordingly, competitive binding studies with these ligands may provide more reliable  $IC_{50}$  values. Nevertheless, for the design of GLP-1R-addressing small peptides with affinities in the range of GLP-1 and exendin-3/4, substantial optimizations were presumed to be required.

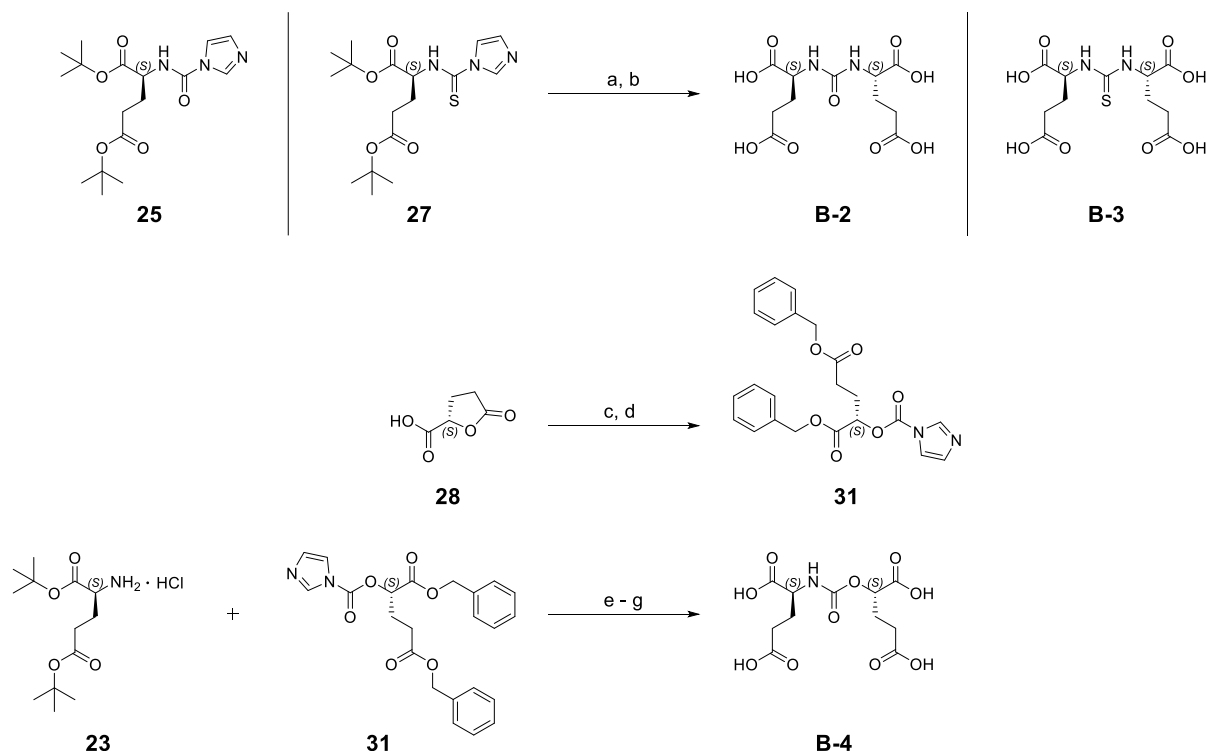
All in all, the rather poor results obtained for short-chained GLP-1 receptor ligands unveiled a huge discrepancy between the high potency of these ligands known from the literature and their actual low affinities, determined in HEK293-hGLP-1R cell-based assays. Especially **A-1** was supposed to possess a high affinity towards GLP-1R positive cells due to its inherent low  $EC_{50}$  of 31 pM determined by Haque *et al.*<sup>[113]</sup> However, **A-1** lost its potential as a basic structure for novel promising small peptide GLP-1R agonists, since affinity studies revealed an unfavorable  $IC_{50}$  of  $669 \pm 242$  nM ( $n = 5$ ). As no further structures of small peptides were found on the basis of which high affinity GLP-1R ligands could be developed, a prompt generation of those ligands suitable for radiolabeling was presumed to be unlikely within the time frame of this PhD thesis. It also remains questionable if small peptide approaches would generally provide high-affinity ligands, since previous SAR studies suggested that non-contiguous residues within the *N*- and *C*-terminus of GLP-1 and also in between were essential for high affinity and potency (section 1.1.2).<sup>[52, 53]</sup> As a consequence, yet synthesized SiFA-bearing ligands were not subjected to radiofluorination and no further GLP-1R ligands (e.g. suitable for chelator attachment) were synthesized and evaluated in *in vitro* or *in vivo* studies.

## 4.2. PSMA ligand development

### 4.2.1. Preliminary studies on isolated PSMA inhibitor motifs and PSMA substrate mimetics

#### 4.2.1.1. Investigations on isolated PSMA inhibitor motifs with modifications within the central Zn<sup>2+</sup>-binding unit

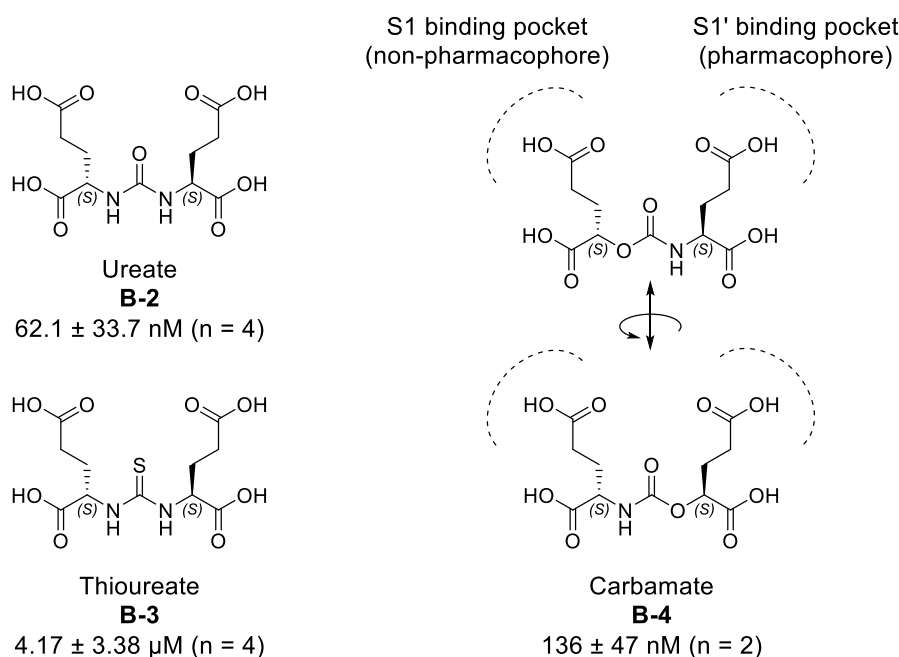
For this first preliminary study, the established EuE binding motif **B-2** as well as the corresponding thioureate **B-3** and carbamate **B-4** were synthesized. Whereas **B-2** and **B-3** could be readily obtained after three steps by previously published and slightly modified procedures<sup>[199, 223]</sup>, a more laborious protocol was required for carbamate **B-4** (Scheme 6). Due to absent commercial availability, the carbamate oxygen-bearing fragment dibenzyl (S)-2-hydroxypentanedioate had to be synthesized in advance. Starting from enantiopure (S)-5-oxotetrahydrofuran-2-carboxylic acid (**28**), further synthesis steps focused on conditions to ensure and maintain L-configuration of the final PSMA binding motif. Additionally, selective introduction of protective groups at the  $\alpha$ - and  $\gamma$ -carboxylate of (S)-2-hydroxypentanedioic acid was pursued, with concomitant liberation of the secondary alcohol of the benzyl diester.<sup>[291, 292]</sup>



**Scheme 6:** Simplified synthetic routes for the preparation of ureate **B-2**, thioureate **B-3** (first row) and carbamate **B-4** (second and third row). a) H-Glu(OtBu)-OtBu<sup>+</sup>HCl (**23**), TEA [DCM], 0 °C → r.t., 19 - 24 h; b) TFA/DCM (1/1), r.t., 22 - 34 h; c) Bn-OH, CSA, [toluene], reflux, 24 h, argon; d) CDI [DCM], r.t., 20.5 h, argon; e) TEA [DCE], 45 °C, 94 h → 40 °C, 27 h, argon; f) H<sub>2</sub>, Pd/C [MeOH/EtOH], r.t., 22 h; g) TFA/DCM (1/1), r.t. 2 h. Detailed synthesis procedures are given in MATERIALS AND METHODS (chapter III).

## RESULTS AND DISCUSSION

For this class of compounds, HPLC-linked UV/Vis-detection was not easily possible due to lacking functional groups able to absorb significantly at 220 nm.<sup>[323, 324]</sup> Carbonyl groups (together with -OH or -NH as auxochromes) representing the only absorbing moieties within **B-2**, **B-3** and **B-4** exhibit lower extinction coefficients than aromatic ring systems for example, and were therefore only detectable by injection of higher amounts of substance. In addition, their presumed ability to occupy different protonation states, even in HPLC-solvent supplemented with 0.1% TFA, occasionally resulted in broad HPLC signals instead of sharp peaks during RP-HPLC purification. In following *in vitro* LNCaP-cell based assays, purified thioureate **B-3** and carbamate **B-4** were compared to the classical ureate-based PSMA binding motif **B-2** (Figure 29).



**Figure 29:** Structures and affinities of isolated PSMA inhibitor EuE (**B-2**) and modified inhibitor compounds thioureate **B-3** and carbamate **B-4**. Possible varying orientations of carbamate **B-4** within the PSMA binding pocket are depicted on the right.

The  $IC_{50}$  values indicated a clear preference for the established EuE binding motif ( $IC_{50}(\mathbf{B-2}) = 62.1 \pm 33.7$  nM) and revealed a certain intolerance of the binuclear catalytic site of PSMA towards thioureate **B-3** ( $IC_{50}(\mathbf{B-3}) = 4.17 \pm 3.38$   $\mu$ M). Carbamate **B-4** was found to exhibit moderate affinity towards PSMA ( $IC_{50}(\mathbf{B-4}) = 136 \pm 47$  nM), suggesting a potential applicability in rhPSMA ligands. Since **B-4** was built up symmetrically, placement of the carbamate oxygen could proceed either towards the pharmacophore S1' subpocket or towards the non-pharmacophore S1 subpocket. Therefore, the moderate affinity detected for **B-4** was presumed to result from an average value generated by a 'high affinity orientation' and a 'low affinity orientation' (Figure 29). Recently published results on carbamate analogs of DCIBzL (= (I-BA)KuE or **B-5**) by Yang *et al.* additionally support this theory.<sup>[293]</sup>

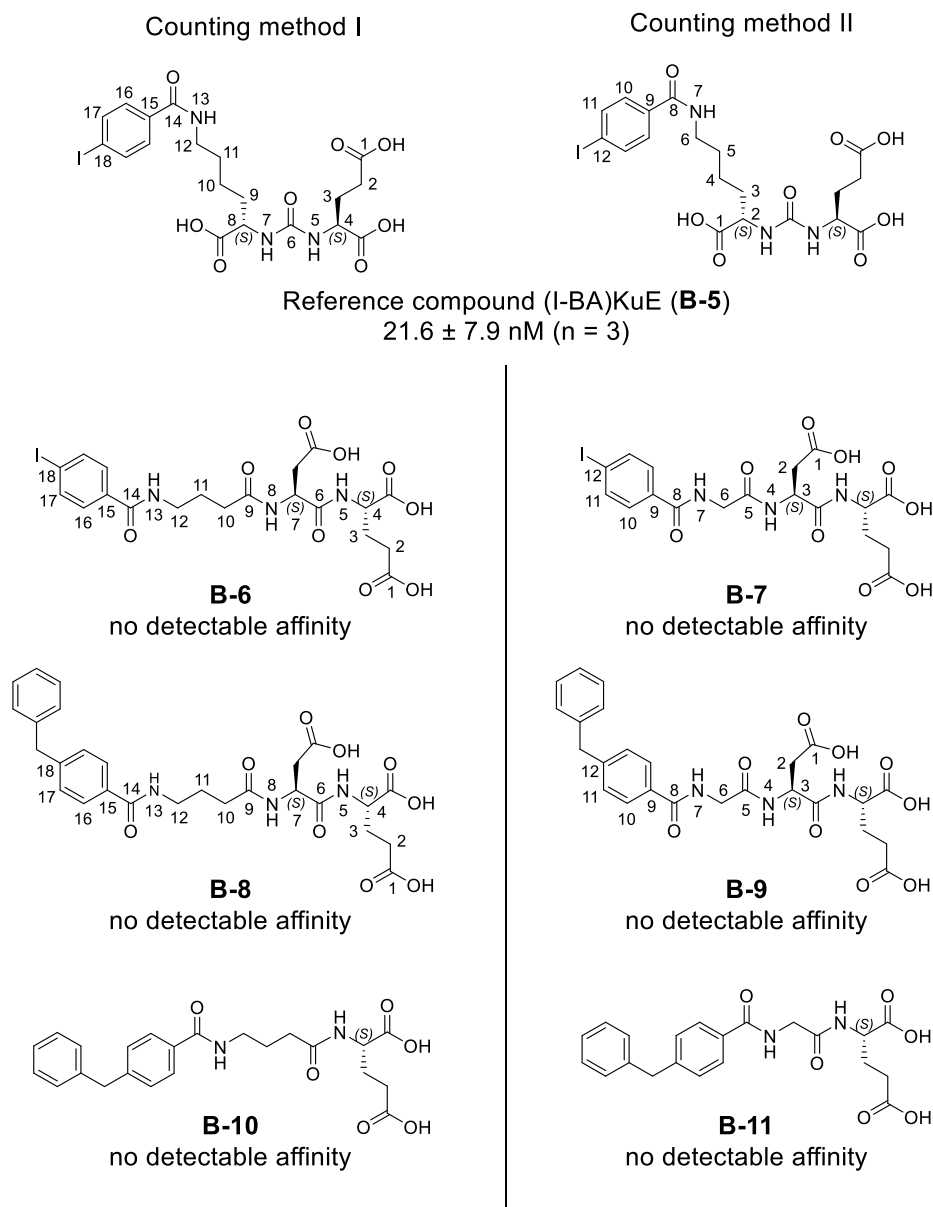
## RESULTS AND DISCUSSION

It has to be noted, that urea-based PSMA binding motif EuE (**B-2**) exhibited a lower affinity compared to the KuE-based reference (I-BA)KuE (**B-5**;  $IC_{50}(\mathbf{B-5}) = 21.7 \pm 7.9$  nM,  $n = 3$ ). This finding can be attributed to missing components able to interact with distinct residues within the entrance funnel of the enzyme. Specific aromatic or lipophilic residues in a well-defined distance to the central ureate are apparently essential for permanent interaction with important binding sites like the S1 accessory hydrophobic pocket or arene-binding site.<sup>[167]</sup> As a result, all binding motifs were planned to be implemented into the structures of mature rhPSMA ligands, regardless of their differences in affinities revealed by these preliminary studies (section 4.2.2). Thereby, it should be investigated if and to which extent attachment of a linker fragment, SiFA moiety and chelator would improve PSMA binding affinity. Furthermore, the 'preferred' arrangement of the carbamate should be determined by implementation in structures in which orientation towards the S1 or S1' pocket is inherently predefined. In case of identification of one or more high affinity ligands, evaluations concerning their ability to reduce unwanted salivary gland uptake in mice should be conducted.

### 4.2.1.2. Preliminary studies on PSMA substrate mimetics

Besides the investigation of possible modification sites within the inhibitor motif, a different approach for ligand design, based on the natural PSMA substrate NAAG was pursued. Therefore, NAAG-similar compounds with bulky hydrophobic residues, attached for addressing the S1 accessory hydrophobic pocket and pre-defining ligand orientation within the active site, were synthesized and evaluated *in vitro* (Figure 30). Thereby, an optimal orientation of the respective ligands was striven by keeping the distances between the C-terminal  $\gamma$ -carboxylate and the *para*-iodophenyl residue, based on the already established (I-BA)KuE scaffold (counting method I, **B-6** & **B-8**). Based on the potential interaction of the P1- $\alpha$ -carboxylate with the positively charged guanidinium groups of Arg<sup>463</sup>, Arg<sup>543</sup> and Arg<sup>536</sup> (arginine patch), an alternative preferred orientation of the *para*-iodophenyl residue might be conceivable (counting method II, **B-7** & **B-9**).<sup>[166]</sup> In order to investigate whether aspartyl residues within the ligands are mandatory, **B-10** and **B-11** were synthesized and evaluated.

## RESULTS AND DISCUSSION



**Figure 30:** Synthesized NAAG-similar compounds with bulky hydrophobic residues, attached for addressing the S1 accessory pocket and pre-defining ligand orientation within the active site. Structures and *in vitro* results of **B-6** and **B-8**, following counting method I, as well as of **B-10** are depicted in the left column. Structures and *in vitro* results of **B-7** and **B-9**, following counting method II, as well as of **B-11** are depicted in the right column.

The first attempts for synthesis of **B-6** and **B-7**, unintentionally provided diphenylmethane derivatives **B-8** and **B-9** after Pd-catalyzed hydrogenolysis of the benzyl protective group of the C-terminal glutamate. The toluene-Pd(II)-H complex, generated by the intended benzyl ester cleavage<sup>[325]</sup> most likely underwent a process similar to a palladium-catalyzed cross-coupling reaction together with *in situ* produced R-[metal(II)]-I, under base- and ligand-free conditions as described by Jadhav *et al.*<sup>[326]</sup> Pd(II) might represent metal(II), since Pd(0) is able to readily insert into the phenyl-iodine bond (oxidative addition)<sup>[327]</sup>, also if immobilized on solid support.<sup>[326]</sup> Alternatively, metal(II) might have been generated from trace metal impurities (Al, Cu, Fe, Zn, etc.)

## RESULTS AND DISCUSSION

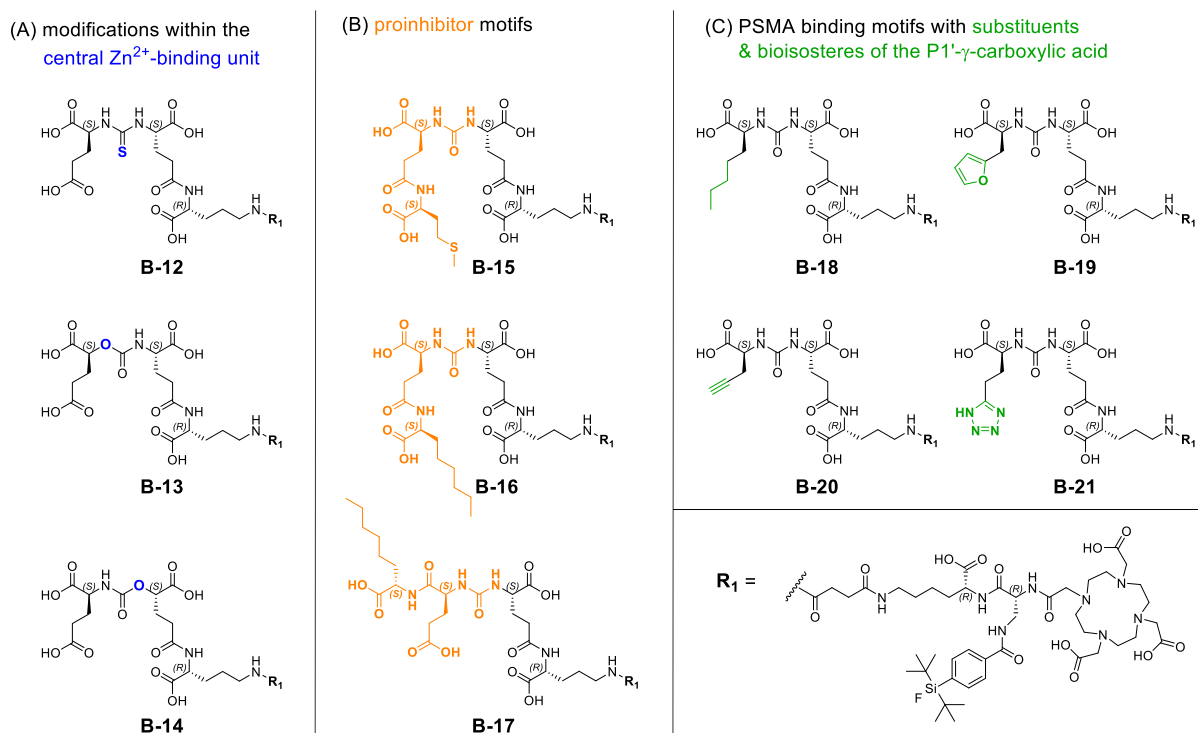
that possibly diffused out of the glassware or were already present within the purified reactant, solvent (MeOH) or palladium on carbon.<sup>[328]</sup> Therefore, only *t*Bu-protected amino acids were now used for synthesis of iodinated compounds **B-6** and **B-7**, in order to avoid Pd-catalyzed hydrogenation steps and hence, cross-reactivities and product degradation.

Nevertheless, the performance of **B-8** and **B-9** in *in vitro* assays for IC<sub>50</sub> determination was also investigated, due to an intact PSMA binding moiety and a potential beneficial effect of the hydrophobic bisphenyl fragment at this position (enhanced interaction with the arene-binding site during ligand accommodation and/or enhanced interaction with residues of the S1 accessory hydrophobic pocket). **B-10** and **B-11** were obtained via omission of the penultimate aspartyl residue and the unintended Pd-catalyzed cross-coupling reaction as described above and investigated to determine if an aspartyl residue is inevitably needed for effective ligand binding.

In contrast to reference ligand (I-BA)KuE (**B-5**) (IC<sub>50</sub> = 21.6 ± 7.9 nM, n = 3), no PSMA substrate mimetic displayed any measureable affinity within the chosen range (10<sup>-11</sup> - 10<sup>-5</sup> M, extension to 10<sup>-15</sup> - 10<sup>-5</sup> M for **B-8**). Test experiments for **B-8**, in which BSA as an additive in assay buffer (HBSS) was omitted, did not lead to any improvement. Hence, an increased binding propensity of **B-8** to bovine serum albumin could be excluded as potential reason for non-observable radioligand displacement. Likewise, no benefit from BSA-free conditions was expected for all other substrate mimetics as well as for **B-10** and **B-11**. Examination of possible substrate degradation under the prevalent assay conditions was conducted with a UV/Vis-detectable ligand concentration (10<sup>-4</sup> M final ligand concentration). RP-HPLC analysis after the experiment revealed no degradation of **B-8**, **B-9**, **B-10** or **B-11**, which in turn implied, that lacking ability for radioligand displacement indeed resulted from absent PSMA affinity of these ligands. Based on these results, a non-PSMA-binding character was also ascribed to **B-6** and **B-7**. In order to exclude cross-contamination and cell passage number effects (e.g. gene expression, phenotype variation)<sup>[329, 330]</sup>, *in vitro* experiments of **B-6** and **B-7** were repeated with new, authenticated LNCaP cells, which again revealed no detectable affinity. Consequently, syntheses of the iodinated analogs of **B-10** and **B-11** were not pursued. In general, this substrate mimetics approach had to be further adjusted for implementation in mature rhPSMA ligands, wherefore proinhibitors were introduced. Synthesis, *in vitro* and *in vivo* evaluation of these derivatives as well as of other compounds with masked PSMA inhibitor fragments is further discussed in the following section.

#### 4.2.2. Synthesis, *in vitro* and *in vivo* evaluation of radiohybrid PSMA ligands with modifications at the inhibitor part

PSMA ligands with modified binding motifs (Figure 31) were synthesized according to known or modified organic chemical synthesis procedures. On-resin synthesis of binding motifs was established and adjusted in individual cases (section 4.2.2.1). Elongation steps were performed according to standard solid phase peptide synthesis protocols for rhPSMA derivatives and optimizations concerning (radio)metal complexation reactions were performed if necessary (section 4.2.2.2). The following sections cover the syntheses of compounds **B-12** to **B-21** (Figure 31), highlighting special synthetical aspects, improvements to already described procedures as well as methods for preservation of the mandatory L-configuration of the PSMA binding motif during inhibitor modification.<sup>[160, 238]</sup> Moreover, routes for optimization of DOTA-chelator attachment are described. The results obtained for the final ligands in *in vitro* and *in vivo* studies are presented afterwards.



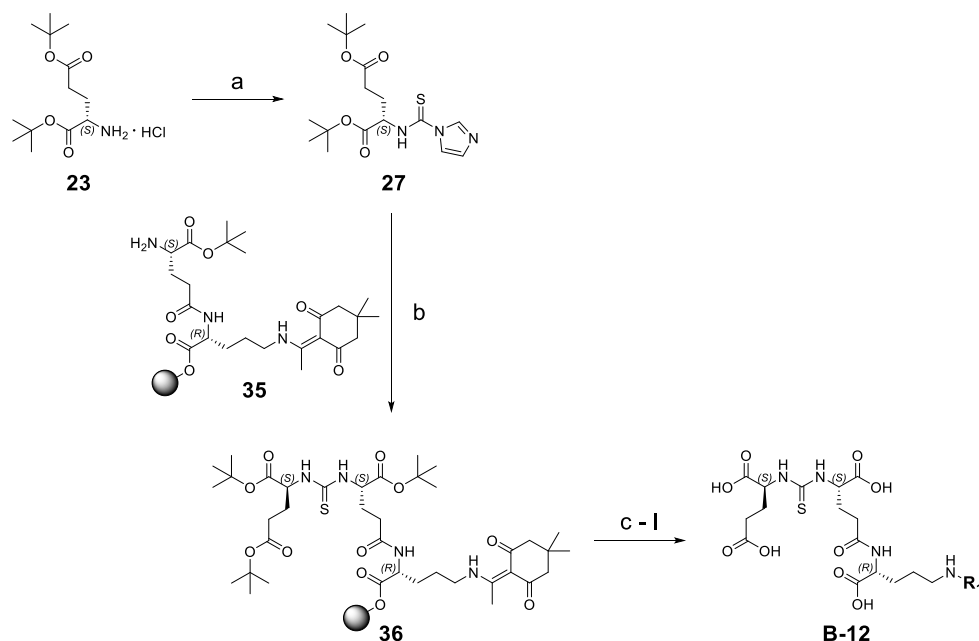
**Figure 31:** Detailed structures of the modified PSMA inhibitors investigated within the course of this PhD thesis, with (A) thiourea **B-12**, carbamates **B-13** and **B-14** (B) proinhibitors **B-15**, **B-16** and **B-17** and (C) L-2-aminoheptanoic acid (L-aha, **B-18**), furyl (**B-19**), alkyne (**B-20**) and tetrazole (**B-21**) derivatives. All compounds are depicted in their free chelator form and represent PSMA ligands comprising modifications within the central  $Zn^{2+}$ -binding unit (A), proinhibitor motifs (B) and substituents & bioisosteres of the P1'- $\gamma$ -carboxylic acid (C).

#### 4.2.2.1. Synthesis

##### **Synthesis of PSMA binding motifs comprising modifications within the central Zn<sup>2+</sup>-binding unit: thioureate **B-12**, carbamate **B-13** and carbamate **B-14****

**Thioureate B-12.** Introduction of a thioureate functionality (**B-12**) was easily achieved via a slight modification of the standard procedure for KuE motifs<sup>[223]</sup>, using 1,1'-thiocarbonyldiimidazole instead of 1,1'-carbonyldiimidazole (CDI) (*Scheme 7*). The binding motif was synthesized by incubation of **27** with H-Glu[D-Orn(Dde)-2-CT]-OtBu (**35**). This on-resin assembly was first established for thioureate **B-12** and simplified the reaction process significantly. In contrast to L-Lys-urea-L-Glu binding motifs<sup>[331]</sup>, PSMA inhibitor motifs based on L-Glu-urea-L-Glu were synthesized exclusively in solution in previously published approaches.<sup>[140, 332-334]</sup> This included at least one purification step and afterwards, removal of an orthogonal protective group at P1-position, in order to liberate a free carboxylic acid, which could be coupled to a resin-bound amine. Both time- and substance-consuming steps could be avoided by this on-resin method. Hence, this strategy served as a basis for the synthesis of further modified rhPSMA peptides within this PhD thesis (proinhibitor **B-15**, L-2-aminoheptanoic acid derivative **B-18**, furyl derivative **B-19** and alkyne derivative **B-20**). Moreover, it might serve as a general procedure for the preparation of L-Glu-urea-L-Glu binding motifs. After purification by RP-HPLC, **B-12** was directly complexed with <sup>nat</sup>Ga<sup>3+</sup> and evaluated solely in *in vitro* studies, wherefore the purity of **B-12** in its free chelator form was not determined.

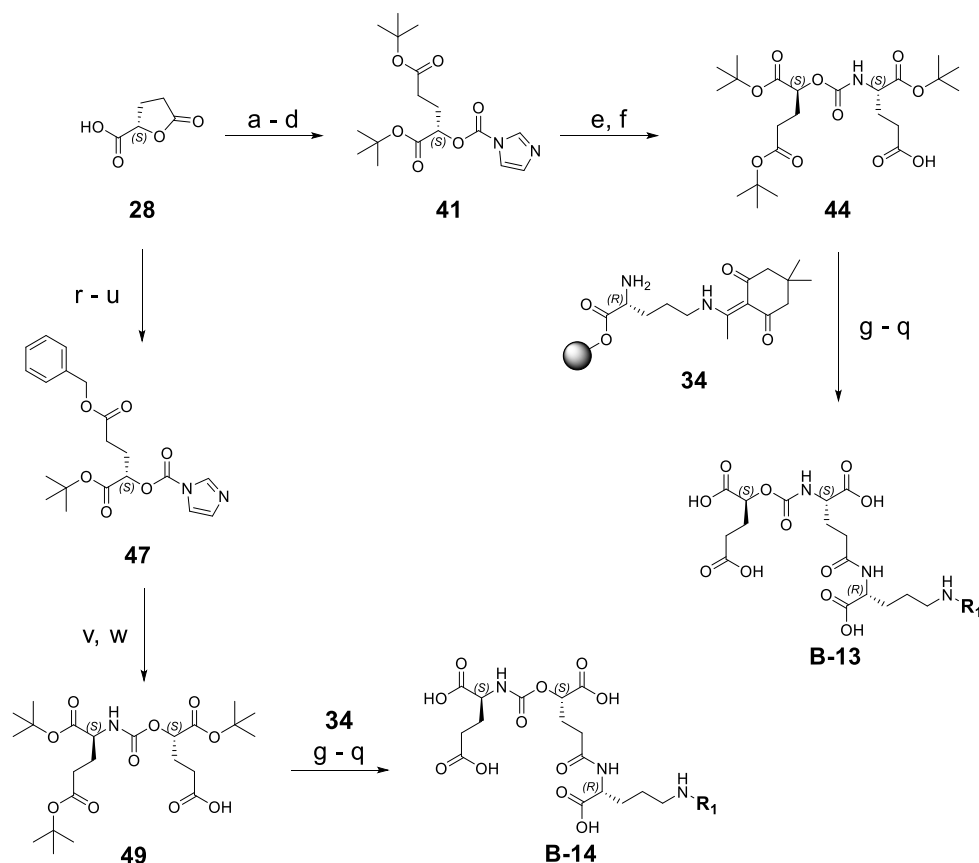
## RESULTS AND DISCUSSION



**Scheme 7:** Synthetic route for the preparation of thioureate **B-12**. a) 1,1'-thiocarbonyldiimidazole, TEA, DMAP [DCM], 0 °C → r.t., 24 h; b) TEA [DCE], 0 °C → 40 °C, 18 h, argon; c) 2% hydrazine [DMF]; d) succinic anhydride, DIPEA [DMF]; e) Fmoc-D-Lys-OtBu\*HCl, TBTU, HOAt, DIPEA [DMF]; f) 20% piperidine [DMF]; g) Fmoc-D-Dap(Dde)-OH, TBTU, HOAt, *sym*-collidine [DMF]; h) imidazole, NH<sub>2</sub>OH\*HCl [NMP/DMF]; i) SiFA-BA, TBTU, HOAt, *sym*-collidine [DMF]; j) 20% piperidine [DMF]; k) DOTA\*6 H<sub>2</sub>O, TBTU, HOAt, *sym*-collidine [DMF/DMSO]; l) TFA/TIPS/H<sub>2</sub>O. Detailed synthesis procedures are given in MATERIALS AND METHODS (chapter III).

**Carbamates B-13 and B-14.** In line with preliminary studies on isolated PSMA inhibitor motifs, synthetical accessibility of carbamates **B-13** and **B-14** was clearly more demanding compared to thioureate **B-12** (Scheme 8). Syntheses of the PSMA binding moieties of both carbamates (**44** and **49**) were performed completely by a solution phase strategy. All synthesis steps towards precursor molecules **41** and **47**, starting from enantiopure (*S*)-5-oxotetrahydrofuran-2-carboxylic acid, focused on conditions to ensure L-configuration of the entire PSMA binding motif.<sup>[199, 293-297]</sup> Thereby, new strategies for di-*tert*-butyl-protected derivative **41** as well as for orthogonal protected derivative **47** had to be developed as described below (*Special aspects of the synthesis of carbamates B-13 and B-14*). Introduction of different protective groups (*tert*-butyl or benzyl) at the  $\gamma$ -carboxylate of compounds **41** and **47** was of utmost importance. These steps, already conducted at an early stage of synthesis, were crucial for determination of carbamate orientation. Carbamate **B-13** was obtained in a chemical purity of > 98% (13.8% yield) after RP-HPLC purification and complexed with <sup>nat</sup>Ga<sup>3+</sup>, <sup>nat</sup>Lu<sup>3+</sup> and [<sup>177</sup>Lu]Lu<sup>3+</sup> for *in vitro* and *in vivo* studies. Carbamate **B-14** was directly complexed with <sup>nat</sup>Ga<sup>3+</sup> and evaluated solely in *in vitro* studies, wherefore the purity of **B-14** in its free chelator form was not determined.

## RESULTS AND DISCUSSION



**Scheme 8:** Synthetic routes for the preparation of carbamate **B-13** and **B-14**. a) *t*BuOH, EDC<sup>\*</sup>HCl, DMAP (on polystyrene), [DCM], 0 °C → r.t., 17 h, argon; b) KOH<sub>(aq)</sub> (1 M), 0 °C → r.t., 1 h; c) *O-tert-butyl-N,N'*-diisopropylisourea [DCM], reflux, 96 h, argon; d) CDI [DCM], r.t., 20 h, argon; e) H-L-Glu(OBzl)-O*t*Bu<sup>\*</sup>HCl, TEA [DCE], 0 °C → 45 °C, 41 h → 55 °C, 70.5 h, argon; f) H<sub>2</sub>, Pd/C [DCM], r.t., 18 h; g) TBTU, HOAt, *sym*-collidine (for **B-13**)/DIPEA (for **B-14**) [DMF], r.t., 65 - 85 h; h) 2% hydrazine [DMF]; i) succinic anhydride, DIPEA [DMF]; j) Fmoc-D-Lys-O*t*Bu<sup>\*</sup>HCl, TBTU, HOAt, DIPEA [DMF]; k) 20% piperidine [DMF]; l) Fmoc-D-Dap(Dde)-OH, TBTU, HOAt, *sym*-collidine [DMF]; m) imidazole, NH<sub>2</sub>OH<sup>\*</sup>HCl [NMP/DMF]; n) SiFA-BA, TBTU, HOAt, *sym*-collidine [DMF]; o) 20% piperidine [DMF]; p) DOTA-NHS, DIPEA [DMF] (for **B-13**)/DOTA<sup>\*</sup>6 H<sub>2</sub>O, TBTU, HOAt, *sym*-collidine [DMF/DMSO] (for **B-14**); q) TFA/TIPS/DCM. r) *t*BuOH, EDC<sup>\*</sup>HCl, DMAP (on polystyrene), [DCM], 0 °C → r.t., 17 h, argon; s) KOH<sub>(aq)</sub> (1 M), 0 °C → r.t., 1 h; t) Na<sub>2</sub>CO<sub>3(aq)</sub> (10%), [MeOH/H<sub>2</sub>O], benzyl bromide [DMSO], r.t., 4.5 h, argon; u) CDI [DCM], r.t., 21 h, argon; v) H-L-Glu(O*t*Bu)-O*t*Bu<sup>\*</sup>HCl, TEA [DCE], 0 °C → 45 °C, 96 h → 40 °C, 27 h, argon; w) H<sub>2</sub>, Pd/C [DCM], r.t., 24 h; Detailed synthesis procedures are given in MATERIALS AND METHODS (chapter III).

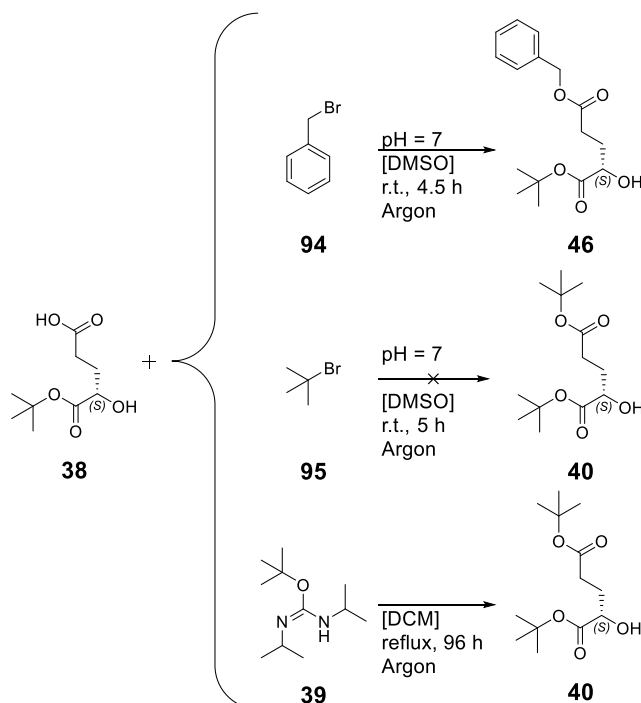
**Special aspects of the synthesis of carbamates B-13 and B-14.** A well-defined strategy for protective group installation had to be set in advance for the binding motifs of carbamate **B-13** and **B-14**. For **B-13**, a new strategy for the preparation of di-*tert*-butyl-protected pentanedioate derivative **41** was developed. The dibenzyl-protected carbamate fragment **31**, previously developed for preliminary studies on isolated PSMA inhibitor motifs (section 4.2.1.1) could not be used. By its application, methods for benzyl ester cleavage would have been inevitably needed after peptide completion. However, unwanted hydrogenation of the aromatic SiFA unit by Pd-catalyzed hydrogenolysis, hardly detectable by RP-HPLC/MS analysis should be avoided.

## RESULTS AND DISCUSSION

Furthermore, other palladium-induced side reactions as described for the synthesis of PSMA peptide mimetics (section 4.2.1.2) could not be excluded. Moreover, the amount of peptide degradation possibly caused by Pd-free benzyl ester cleavage (e.g. nucleophilic substitution, reduction, basic hydrolysis)<sup>[320]</sup> was difficult to assess in advance but deemed too risky at this late stage of synthesis. Therefore, *tert*-butyl esters were chosen as protective groups for the P1'- $\alpha$ - and - $\gamma$ -carboxylate as well as for the P1- $\alpha$ -carboxylate. Only the P1- $\gamma$ -carboxylic acid was planned to be functionalized as benzyl ester, since removal of this orthogonal protective group after inhibitor motif assembly would then provide one single free carboxylic acid, by which compound **44** could be selectively attached to H-D-Orn(Dde)-2-CT (**34**).

Also for carbamate **B-14** dibenzyl-protected compound **31** couldn't be used, due to orthogonal protective groups, required for placement of the carbamate oxygen at P1 position. Therefore, a benzyl protective group was introduced selectively at the  $\gamma$ -carboxylate of (*S*)-5-(*tert*-butoxy)-4-hydroxy-5-oxopentanoic acid (**38**) (Scheme 9).

Analogously, *tert*-butyl bromide (**95**) was used in a first attempt to synthesize the respective P1' analog **40**, planned as a building block for **B-13**. Since no conversion was observed, a more time consuming (~ 96 h) and complex procedure under air- and moisture free conditions was introduced, using *O-tert*-butyl-*N,N'*-diisopropylisourea (**39**) as alkylation reagent. Importantly, simultaneous alkylation of the free secondary hydroxy group in both attempts was prevented, applying these selective alkylation procedures.<sup>[295-297]</sup>



**Scheme 9.** Simplified synthetic routes for the preparation of compounds **46** and **40**, serving as precursor molecules for carbamate **B-14** and carbamate **B-13**, respectively. Starting from (*S*)-5-(*tert*-butoxy)-4-hydroxy-5-oxopentanoic acid (**38**), the concept for synthesis of **46** (first row)<sup>[297]</sup> could not be directly transferred to the synthesis of the *tert*-butyl analog **40** (second row). Instead, *O-tert*-butyl-*N,N'*-diisopropylisourea (**39**) had to be used as alkylation reagent (third row).<sup>[296]</sup>

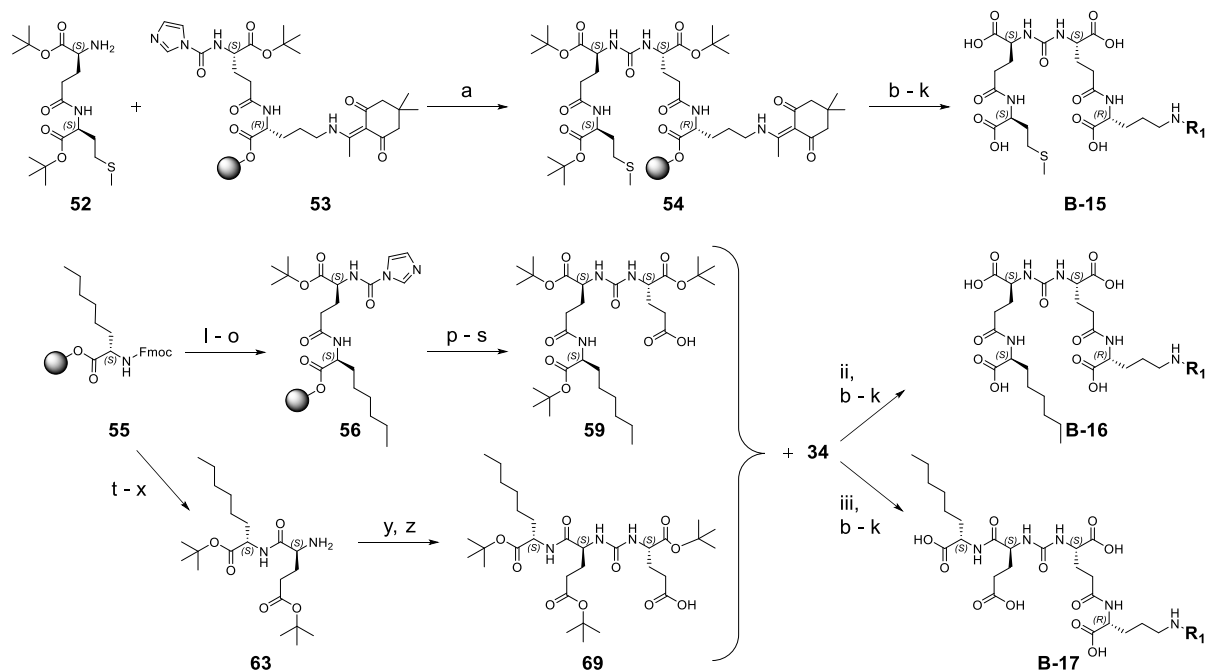
## RESULTS AND DISCUSSION

As described more precisely in the following subsection for proinhibitors **B-15**, **B-16** and **B-17**, on-resin assembly of the binding motifs was not always straightforward and led to chemically inert dimerization products. Hence, this strategy was avoided for carbamate **B-13** and **B-14**, since solution phase synthesis already showed slow reaction rates (45 °C, 41 h → 55 °C, 70.5 h for preparation of **44**(OBzl) and 45 °C, 96 h → 40 °C, 27 h for preparation of **49**(OBzl)).

Stability of both carbamate-based inhibitor units towards the conditions used for Dde-removal from ornithin, was examined by treatment of a small resin portion with 2% hydrazine monohydrate in DMF according to GP5. Thereby, only the expected cleavage of Dde from ornithine was observed and no degradation of the inhibitor motif by hydrazide formation or reductive side reactions could be detected by RP-HPLC/MS.<sup>[335, 336]</sup> Hence, these carbamate conjugates were proven to be stable towards 2% hydrazine monohydrate in DMF and the respective ligands could be finalized on 2-CT resin.

**Synthesis of proinhibitors B-15, B-16 & B-17**

Synthesis procedures for all proinhibitor binding motifs had to be adjusted due to unreactive starting material or unwanted dimerization reactions (*Scheme 10*). Therefore, binding motifs were either introduced by on-resin synthesis (**B-15**) or by separate synthesis of the proinhibitor unit in a mixed solid/solution phase approach (**B-16** and **B-17**).



**Scheme 10:** Synthetic routes for the preparation of proinhibitor **B-15**, **B-16** and **B-17**. a) TEA [DCE], 0 °C → 40 °C, 16 h, argon; b) 2% hydrazine [DMF]; c) succinic anhydride, DIPEA [DMF]; d) Fmoc-D-Lys-OtBu\*HCl, TBTU, HOAt, DIPEA; e) 20% piperidine [DMF]; f) Fmoc-D-Dap(Dde)-OH, TBTU, HOAt, *sym*-collidine [DMF]; g) imidazole, NH<sub>2</sub>OH\*HCl [NMP/DMF]; h) SiFA-BA, TBTU, HOAt, *sym*-collidine [DMF]; i) 20% piperidine [DMF]; j) DOTA-NHS, DIPEA [DMF]; k) TFA/TIPS/DCM (+ dithiothreitol for **B-15** only); l) 20% piperidine [DMF]; m) Fmoc-L-Glu-OtBu, TBTU, HOAt, DIPEA [DMF]; n) 20% piperidine [DMF]; o) CDI, TEA [DCE], 0 °C → 40 °C, 14 h, argon; p) H-L-Glu(OBzl)-OtBu\*HCl, TEA [DCE], 0 °C → 40 °C, 4.3 h, argon; q) HFIP/DCM (1/4); r) *O*-*tert*-butyl-*N,N'*-diisopropyl-isourea [DCM], reflux, 46 h, argon; s) H<sub>2</sub>, Pd/C [DCM], r.t., 24 h; t) 20% piperidine [DMF]; u) Cbz-L-Glu(OtBu)-OH, TBTU, HOAt, DIPEA (GP3); v) HFIP/DCM (1/4); w) *O*-*tert*-butyl-*N,N'*-diisopropyl-isourea [DCM], reflux, 46 h, argon; x) H<sub>2</sub>, Pd/C [DCM], r.t., 26 h; y) (1*H*-imidazole-1-carbonyl)-L-Glu(OBzl)-OtBu, TEA [DCE], 0 °C → 40 °C, 21 h, argon; z) H<sub>2</sub>, Pd/C [DCM], r.t., 23 h; ii) TBTU, HOAt, *sym*-collidine [DMF], r.t., 23.5 h; iii) TBTU, HOAt, *sym*-collidine [DMF], r.t., 19 h; Detailed synthesis procedures are given in MATERIALS AND METHODS (chapter III).

**Proinhibitor B-15.** Dipeptide H-L-Glu(L-Met-OtBu)-OtBu (**52**) was generated in solution and coupling to resin-bound compound **53** provided the tris-*t*Bu-protected binding motif **54**, which afforded product **B-15** after on-resin elongation. Functionalization of **35** (H-L-Glu[D-Orn(Dde)-2-CT]-OtBu) to yield its carbonylimidazole derivative **53** was required, as conversion of dipeptide **52** with CDI was not successful. Dimerization as a competing reaction was more favored and hence, only the urea-conjugated dimer of **52** could be isolated after this attempt.

## RESULTS AND DISCUSSION

Notably, carbonylimidazole functionalization of resin-bound peptide **35** worked properly in this approach, as a certain distance to the resin anchor (2-chlorotrityl group) was preserved. By contrast, carbonylimidazole attachment did not work at the first 2-CT resin-bound amino acid, provided that it was coupled to the resin by its  $\alpha$ -carboxylate. After purification by RP-HPLC, **B-15** was obtained in a chemical purity of 98.0% (0.08% yield) and complexed with  $^{\text{nat}}\text{Lu}^{3+}$  and  $[^{177}\text{Lu}]\text{Lu}^{3+}$  for *in vitro* and *in vivo* studies. Synthesis of proinhibitor **B-15** was particularly impeded by oxidation of methionine, which resulted in the low overall yield after RP-HPLC purification (0.08%). Moreover, oxidation tendency remained at  $^{177}\text{Lu}$ -labeling and also during radio-RP-HPLC purification, which impaired preparation of products with RCP higher than 90%, even at lower temperatures (70 - 80°C).

*Proinhibitor B-16.* Synthesis of the binding motif of proinhibitor **B-16** (**59**) was accomplished via a mixed solid/solution phase strategy, starting with resin-bound Fmoc-L-2-aminooctanoic acid (Fmoc-L-2-Aoc-OH) (**55**). After multiple steps, compound **59** was prepared, suitable for coupling to compound **34**. Subsequent on-resin elongation afforded proinhibitor **B-16**, which was obtained in a chemical purity of > 99% (16.0% yield) after RP-HPLC purification. **B-16** was complexed with  $^{\text{nat}}\text{Lu}^{3+}$  and  $[^{177}\text{Lu}]\text{Lu}^{3+}$  for *in vitro* and *in vivo* studies.

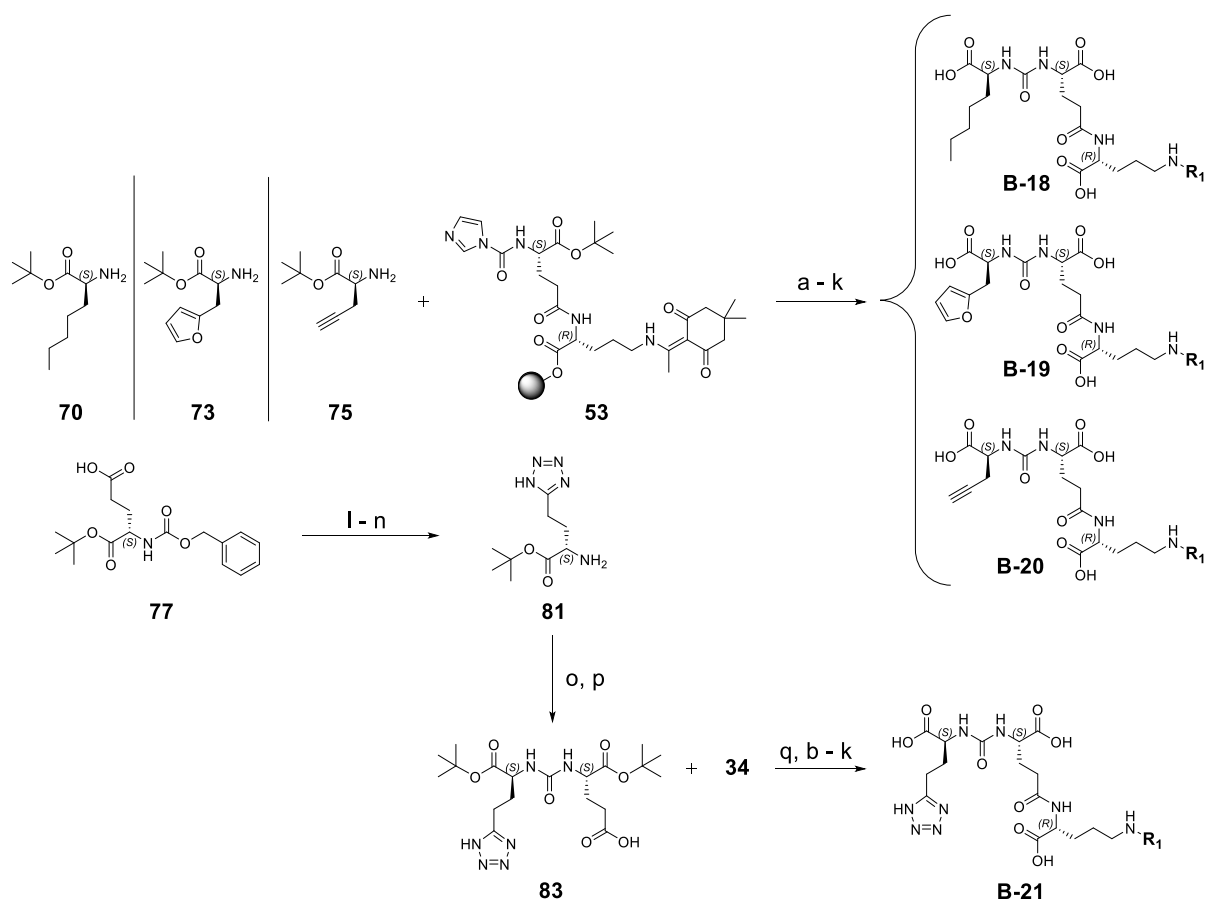
*Proinhibitor B-17.* Dipeptide H-L-Glu(OtBu)-L-2-Aoc-OtBu (**63**) was generated by coupling of Cbz-L-Glu(OtBu)-OH to resin-bound H-L-2-Aoc, cleavage from the resin and alkylation of the C-terminal carboxyl group with *O-tert-butyl-N,N'*-diisopropylisourea (**39**). In order to avoid dimerization of **63**, also here on-resin coupling to compound **53** was pursued (according to **B-15**) but could not be realized. As opposed to the procedure for proinhibitor **B-15**, the starting dipeptide **63** did not react and only on-resin urea-conjugated dimerization of peptide **53** was detected. Therefore, the strategy was changed to solution phase synthesis to obtain tris-*t*Bu-protected binding motif **69**. Coupling to **34** and subsequent on-resin elongation afforded product **B-17** in > 99% chemical purity (4.68% yield) after RP-HPLC purification. Proinhibitor **B-17** was complexed with  $^{\text{nat}}\text{Lu}^{3+}$  and  $[^{177}\text{Lu}]\text{Lu}^{3+}$  for *in vitro* and *in vivo* studies.

### **Synthesis of PSMA binding motifs with substituents & bioisosteres of the P1'- $\gamma$ -carboxylic acid: L-2-aminoheptanoic acid (L-2-aha) (B-18), furyl (B-19), alkyne (B-20) and tetrazole (B-21) derivatives**

Introduction of the carboxylic acid substituents **70**, **73** and **75** was realized by on-resin coupling to compound **53** (Scheme 11). For compound **70** and **73**, prior attachment of a *t*Bu protective group via *tert*-butyl acetate was necessary.<sup>[298]</sup> This strategy was used to assure esterification of the carboxylic acid moiety only. *O-tert-butyl-N,N'*-diisopropylisourea could not be used in this case, as its usage would have led to simultaneous alkylation of the free primary amine.<sup>[295]</sup> Synthesis of the tetrazole bioisostere was successfully accomplished following a multi-step procedure described by Kozikowski *et al.*<sup>[222]</sup> For the tetrazole unit, which is one of the most commonly used carboxylic acid

## RESULTS AND DISCUSSION

bioisosteres in modern drug design, it is important to highlight its close resemblance to the carboxylic acid group concerning the planar geometry and acidity.<sup>[337, 338]</sup> However, the increased lipophilicity of tetrazoles, which has been reported to be almost 10 times higher compared to their carboxylic acid counterpart, has to be considered.<sup>[338]</sup>



**Scheme 11:** Synthetic routes for the preparation of L-2-aminoheptanoic acid (L-2-aha) (**B-18**), furyl (**B-19**), alkyne (**B-20**) and tetrazole derivative (**B-21**). a) TEA [DCE], 0 °C → 40 °C, 16.3 - 20 h, argon; b) 2% hydrazine [DMF]; c) succinic anhydride, DIPEA [DMF]; d) Fmoc-D-Lys-OtBu\*HCl, TBTU, HOAt, DIPEA [DMF]; e) 20% piperidine [DMF]; f) Fmoc-D-Dap(Dde)-OH, TBTU, HOAt, *sym*-collidine [DMF]; g) imidazole, NH<sub>2</sub>OH\*HCl [NMP/DMF]; h) SiFA-BA, TBTU, HOAt, *sym*-collidine [DMF]; i) 20% piperidine [DMF]; j) DOTA-NHS, DIPEA [DMF]; k) TFA/TIPS/DCM; l) benzyl amine, BOP, TEA [DMF], 0 °C → r.t., 66 h; m) PPh<sub>3</sub>, DIAD, TMSN<sub>3</sub> [MeCN], 0 °C → r.t., 15 h, argon → NaNO<sub>2</sub>(aq), r.t., 30 min CAN(aq), r.t., 20 min; n) H<sub>2</sub>, Pd/C [MeOH], r.t., 24 h; o) (1*H*-imidazole-1-carbonyl)-L-Glu(OBzl)-OtBu, TEA [DCE], 0 °C → 40 °C, 20 h, argon; p) H<sub>2</sub>, Pd/C [MeOH], r.t., 69.5 h; q) TBTU, HOAt, *sym*-collidine [DMF], r.t., 14 h; Detailed synthesis procedures are given in MATERIALS AND METHODS (chapter III).

*L*-2-Aminoheptanoic acid derivative **B-18**. Reactant **70** was generated in solution, using (S)-2-aminoheptanoic acid and *tert*-butyl acetate according to a previously published procedure by Hyun *et al.* with some minor modifications.<sup>[298]</sup> On-resin coupling of **70** to compound **53** provided an alkane-functionalized binding motif, which then afforded product **B-18** in 95.5% chemical purity

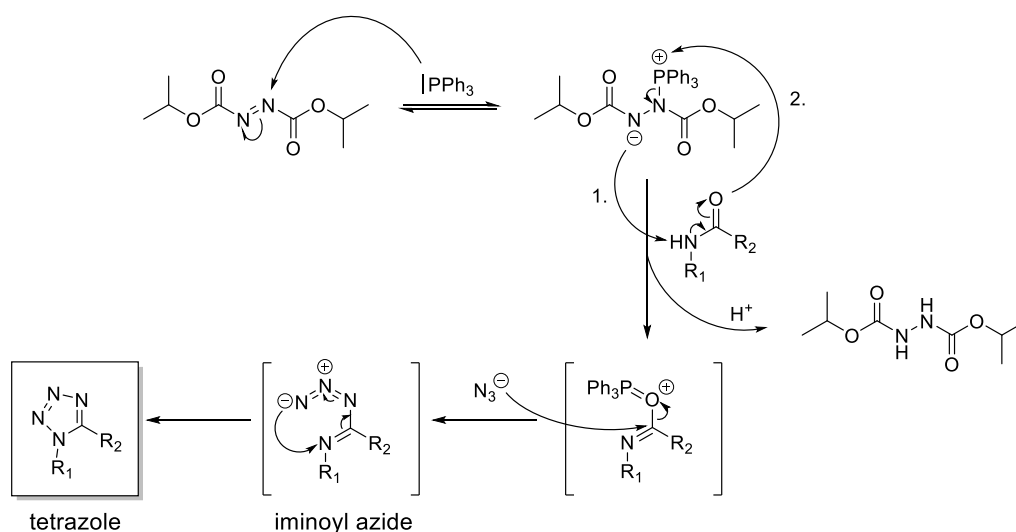
## RESULTS AND DISCUSSION

(0.95% yield) after RP-HPLC purification. L-2-Aminoheptanoic acid derivative **B-18** was complexed with  $^{nat}\text{Lu}^{3+}$  for *in vitro* studies.

**Furyl derivative B-19.** In analogy to reactant **70**, *tert*-butyl (S)-2-amino-3-(furan-2-yl)propanoate (**73**) was generated in solution using 3-(2-furyl)-alanine and *tert*-butyl acetate.<sup>[298]</sup> On-resin coupling of **73** to compound **53** provided a furyl-functionalized binding motif, which then afforded product **B-19** in > 99% chemical purity (2.14% yield) after RP-HPLC purification. Furyl derivative **B-19** was complexed with  $^{nat}\text{Lu}^{3+}$  for *in vitro* studies.

**Alkyne derivative B-20.** Reactant **75** was commercially available and used directly for on-resin coupling to compound **53**. Subsequent elongation afforded product **B-20** in 98.5% chemical purity (3.33% yield) after RP-HPLC purification. Alkyne derivative **B-20** was complexed with  $^{nat}\text{Lu}^{3+}$  and  $^{177}\text{Lu}^{3+}$  for *in vitro* and *in vivo* studies.

**Tetrazole derivative B-21.** Synthesis of tetrazole binding motif **83** was performed completely by a solution phase strategy. All synthesis steps, starting from enantiopure Cbz-L-Glu-O*t*Bu (**77**), focused on conditions to ensure and maintain L-configuration of the entire PSMA binding motif.<sup>[199, 222]</sup> Tetrazole ring formation was conducted by a Mitsunobu<sup>[339]</sup>-like reaction using triphenylphosphine (PPh<sub>3</sub>), diisopropyl azodicarboxylate (DIAD) and trimethylsilyl azide (TMSN<sub>3</sub>) as azide anion source. This reaction was originally developed in 1991 by Duncia *et al.* enabling direct conversion of an amide into a tetrazole in one step, involving tautomerization of the intermediately generated iminoyl azide (Scheme 12).<sup>[340]</sup> After coupling of binding motif **83** to resin-bound **34** and further elongation, product **B-21** was obtained in > 99% chemical purity (2.80% yield) after RP-HPLC purification. Tetrazole derivative **B-21** was complexed with  $^{nat}\text{Lu}^{3+}$  and  $^{177}\text{Lu}^{3+}$  for *in vitro* and *in vivo* studies.



**Scheme 12:** Proposed mechanism for tetrazole formation by one step conversion of an amide with PPh<sub>3</sub>, DIAD and TMSN<sub>3</sub> as reagents.<sup>[339, 340]</sup>

**Optimization of DOTA chelator attachment**

Apart from individual modifications within the PSMA inhibitor unit, adjustments have been made concerning the final step in ligand synthesis, i.e. chelator attachment. Initially, DOTA(*t*Bu)<sub>3</sub> was used for preparation of **B-12**, together with TBTU, HOAt and *sym*-collidine as coupling reagents, according to a previously published procedure by Wurzer *et al.*<sup>[140]</sup> Incomplete cleavage of the *tert*-butyl protective groups from the chelator by TFA/TIPS/H<sub>2</sub>O (95/2.5/2.5), even after an incubation time of 4 h at r.t., and poor separability of the by-products via RP-HPLC led to the use of DOTA\*6 H<sub>2</sub>O instead of DOTA(*t*Bu)<sub>3</sub>.<sup>[341]</sup> However, limited solubility of DOTA\*6 H<sub>2</sub>O in DMF afforded addition of DMSO, resulting in a solvent mixture of DMF/DMSO = 5/1 (v/v). Thioureate **B-12** (> 99% conversion) and carbamate **B-14** (42.5% conversion) could be readily obtained after 19.8 ± 0.4 h (n = 2). By contrast, low product formation was observed for carbamate **B-13**, for which an adequate conversion (44.0%) was observed only after repeated coupling cycles (3 in total) and an overall reaction time of 116.5 h (28.5 h: 17.2%; +20 h: 20.3%; +68 h: 44.0%). Instead, incubation of the fully protected precursor with DOTA-NHS and DIPEA revealed almost complete conversion already after 18 h (> 99%). Therefore, the commercially available reagent DOTA-NHS was used for subsequent syntheses of proinhibitors **B-15** to **B-17** as well as for peptides **B-18** to **B-21** (bearing P1'- $\gamma$ -carboxylate substituents and bioisosteres). This active ester is readily soluble in DMF and could be directly applied in combination with a base (DIPEA or *sym*-collidine) with no need of further coupling reagents like TBTU and HOAt. Despite poor reactivity of the tetrazole precursor (26.5% conversion after 3 coupling cycles with DOTA-NHS and DIPEA, 106 h in total), DOTA-functionalization of all other peptides worked properly with 95.8 ± 7.8% conversion (n = 6) within 13 to 71 h. Therefore, DOTA-NHS is recommended for future syntheses of rhPSMA ligands and in particular for those, which might have been modified with oxidation-labile moieties (e.g. methionine) comparable to proinhibitor **B-15**. Since coupling reagents were found to remarkably promote oxidation-induced peptide degradation, also at short incubation periods of 2 h, their omission might enable a higher overall yield of the respective peptide after cleavage from the resin and RP-HPLC purification.

**4.2.2.2. Cold complexation and radiolabeling**

Cold metal complexation with 3.5-molar excess of Ga(NO<sub>3</sub>)<sub>3</sub>\*6 H<sub>2</sub>O (75 °C, 30 min) or 6-fold molar excess of LuCl<sub>3</sub> (70 - 95 °C, 25 min) led to formation of the respective <sup>nat</sup>Ga/<sup>nat</sup>Lu-rhPSMA ligands. <sup>nat</sup>Ga-complexed compounds <sup>nat</sup>Ga-**B-12**, **-B-13** and **-B-14** were obtained in a chemical purity of ≥ 93% after purification by RP-HPLC (*Table 4*). <sup>nat</sup>Lu-Complexation mixtures of <sup>nat</sup>Lu-**B-13** as well as <sup>nat</sup>Lu-**B-15** to <sup>nat</sup>Lu-**B-21** (0.5 - 1.0 mM in DMSO/H<sub>2</sub>O = 1/1) were directly used as stock solutions for affinity determination, as chemical purity was always > 92% (n = 8).

Radiolabeling (<sup>177</sup>Lu) was performed using manual procedures yielding the products [<sup>177</sup>Lu]Lu-**B-13**, **-B-15**, **-B-16**, **-B-17**, **-B-20** and **-B-21** in radiochemical purities of 96.4 ± 2.2%

## RESULTS AND DISCUSSION

( $n = 16$ ) as determined by radio-RP-HPLC. Proinhibitor [ $^{177}\text{Lu}$ ]Lu-**B-15** represented the sole exception and was obtained in a decreased RCP of  $89.3 \pm 1.9\%$  ( $n = 4$ ). In case of incomplete complexation, removal of free [ $^{177}\text{Lu}$ ]Lu $^{3+}$  via SPE was performed. Moreover, in case of proinhibitor **B-15**, removal of radioactive by-products was conducted by preparative radio-RP-HPLC. Isolated radiochemical yields for all  $^{177}\text{Lu}$ -labeled compounds ranged from 33.4 to  $> 99\%$  with apparent molar activities between 4.64 and 63.5 GBq/ $\mu\text{mol}$  (Table 6).

In general, all derivatives containing modifications within the  $\text{Zn}^{2+}$ -binding unit showed enhanced formation of intramolecular condensation by-products during complexation.  $^{\text{nat}}\text{Ga}$ -labeling of thioureate **B-12** afforded the product ( $m/z = 1484$ ) in 3.35% yield and two intramolecular condensation by-products as the major portion ( $m/z = 1466$ ). In addition, significant amounts of intramolecular condensation by-products (17.9 - 19.3%) were generated during  $^{\text{nat}}\text{Lu}$ - and  $^{177}\text{Lu}$ -labeling of carbamate **B-13** at 95 °C (standard reaction temperature). Therefore, all  $^{\text{nat}}/^{177}\text{Lu}$ -complexation reactions of **B-13** were performed at 70 °C, as formation of unwanted by-products could be almost completely reduced. Since intramolecular condensation was not observed for the original L-Glu-urea-L-Glu compound  $^{\text{nat}}\text{Ga}/^{\text{nat}}\text{Lu}$ -**B-1**<sup>[140, 289]</sup>, modifications within the  $\text{Zn}^{2+}$ -binding moiety might facilitate the formation of cyclic anhydrides or pyroglutamic acid-like by-products, with the latter usually only being possible at temperatures  $> 140$  °C.<sup>[342, 343]</sup> Besides carbamate **B-13**, only proinhibitor **B-15** showed a similar thermal instability during  $^{\text{nat}}\text{Lu}$ - and  $^{177}\text{Lu}$ -labeling, mainly induced by oxidation of methionine. Therefore, the reaction temperatures were adjusted to 70 °C for  $^{\text{nat}}\text{Lu}$ -complexation and to 80 °C for  $^{177}\text{Lu}$ -labeling of **B-15**, respectively. Indeed, formation of unwanted by-products could be almost completely reduced for cold metal complexation, however, oxidation tendency for proinhibitor **B-15** remained during radiolabeling even at lower temperatures (70 - 80°C) and also during radio-RP-HPLC purification, which resulted in lower RCPs of  $89.3 \pm 1.9\%$ . A reaction temperature of 80 °C was chosen, as remaining free [ $^{177}\text{Lu}$ ]Lu $^{3+}$  could be reduced (27.8% at 70 °C to 12.9% at 80 °C) and oxidization of precursor **B-15** could be kept within 6.6 to 13%.

### 4.2.2.3. *In vitro* evaluation

#### **Results of affinity, internalization and lipophilicity measurements**

*PSMA affinity.* Binding to PSMA was determined using LNCaP human prostate cancer cells in a competitive binding assay with  $^{\text{nat}}\text{Ga}$ - or  $^{\text{nat}}\text{Lu}$ -complexes of compounds **B-12** to **B-21**. For comparison,  $\text{IC}_{50}$  values of  $^{\text{nat}}\text{Lu}$ -rhPSMA-10 ( $^{\text{nat}}\text{Lu}$ -**B-1**) ( $2.76 \pm 0.51$  nM) were determined, and also *in vitro* data of  $^{\text{nat}}\text{Lu}$ -rhPSMA-7.3 ( $5.73 \pm 2.23$  nM) are listed due to its later use in comparative biodistribution studies. The results show loss of affinity to a varying extent for all modifications except for carbamate  $^{\text{nat}}\text{Lu}$ -**B-13** (Table 18). Surprisingly, this derivative showed an equally high affinity ( $7.11 \pm 0.71$  nM) as compared to the reference  $^{\text{nat}}\text{Lu}$ -**B-1**. Additionally, tetrazole derivative  $^{\text{nat}}\text{Lu}$ -**B-21** exhibited high affinity ( $16.4 \pm 3.8$  nM) towards PSMA expressing LNCaP cells.

## RESULTS AND DISCUSSION

*Internalization.* LNCaP cells were also used to investigate internalization of the  $^{177}\text{Lu}$ -labeled compounds **B-1**, **B-13**, **B-15**, **B-16**, **B-17**, **B-20** and **B-21**. No internalization studies were performed on thioureate **B-12**, carbamate **B-14**, L-2-aminoheptanoic acid derivative **B-18** and furyl derivative **B-19**, as these candidates were excluded due to poor  $\text{IC}_{50}$  data. Normalized to the uptake of ( $^{125}\text{I}$ )-BA)KuE, the results in *Table 18* show internalization values of < 10% for almost all modified compounds. Only [ $^{177}\text{Lu}$ ]Lu-**B-13** exhibited a significant PSMA-mediated internalization ( $67.8 \pm 0.5\%$ ), although ~ 3-fold lower compared to [ $^{177}\text{Lu}$ ]Lu-**B-1** ( $177 \pm 15\%$ ).

*Lipophilicity.* In analogy to internalization studies, log D values were determined for  $^{177}\text{Lu}$ -labeled compounds **B-1**, **B-13**, **B-15**, **B-16**, **B-17**, **B-20** and **B-21** (*Table 18*). Within the proinhibitor subgroup, methionine-functionalized derivative **B-15** displayed the most hydrophilic character with a log D value of  $-2.89 \pm 0.18$ . Moreover, carbamate [ $^{177}\text{Lu}$ ]Lu-**B-13** represents the most hydrophilic compound of all modified rhPSMA inhibitors (log D =  $-3.40 \pm 0.45$ ), comparable to EuE-based derivatives [ $^{177}\text{Lu}$ ]Lu-**B-1** (log D =  $-3.78 \pm 0.01$ ) and [ $^{177}\text{Lu}$ ]Lu-rhPSMA-7.3 (log D =  $-3.14 \pm 0.13$ ).

## RESULTS AND DISCUSSION

**Table 18.** PSMA binding affinity (IC<sub>50</sub>), internalization (%) and lipophilicity (log D) of the investigated compounds.<sup>a</sup>

PSMA inhibitor	IC <sub>50</sub>	%Internalization compared to the reference <sup>b</sup>	log D
[ <sup>nat</sup> 177Lu]Lu-rhPSMA-7.3	5.73 ± 2.23 nM	1 h: 184 ± 12	-3.14 ± 0.13 <sup>c</sup>
[ <sup>nat</sup> 177Lu]Lu-B-1 <sup>d</sup>	2.76 ± 0.51 nM	1 h: 177 ± 15	-3.78 ± 0.01
<sup>nat</sup> Ga-B-12	> 3 μM (n = 2)	n.d.	n.d.
<sup>nat</sup> Ga-B-13	21.3 ± 1.7 nM	n.d.	n.d.
[ <sup>nat</sup> 177Lu]Lu-B-13	7.11 ± 0.71 nM	1 h: 67.8 ± 0.5	-3.40 ± 0.45
<sup>nat</sup> Ga-B-14	> 1 μM (n = 2)	n.d.	n.d.
[ <sup>nat</sup> 177Lu]Lu-B-15	26.5 ± 16.3 μM	0.5 h, 1 h, 2 h, 4 h: ≤ 0.17 ± 0.32	-2.89 ± 0.18
[ <sup>nat</sup> 177Lu]Lu-B-16	2.52 ± 1.17 μM	0.5 h, 1 h, 2 h, 4 h: ≤ 0.03 ± 0.03	-2.52 ± 0.22
[ <sup>nat</sup> 177Lu]Lu-B-17	6.30 ± 3.59 μM	0.5 h, 1 h, 2 h, 4 h: 0.00 ± 0.00	-2.37 ± 0.22
<sup>nat</sup> Lu-B-18	> 2 μM (n = 2)	n.d.	n.d.
<sup>nat</sup> Lu-B-19	> 440 nM (n = 2)	n.d.	n.d.
<sup>nat</sup> Lu-B-20	138 ± 53 nM	1 h: 1.17 ± 0.43	-2.83 ± 0.08
[ <sup>nat</sup> 177Lu]Lu-B-21	16.4 ± 3.8 nM	1 h: 9.86 ± 3.16	-2.91 ± 0.05

<sup>a</sup>Binding assays (IC<sub>50</sub>) were performed using LNCaP cells (150 000 cells/well) and ([<sup>125</sup>I]-BA)KuE (c = 0.2 nM) as radioligand. Cells were incubated in HBSS (1% BSA) at 4 °C for 1 h. <sup>b</sup>Internalization values were corrected for unspecific binding and normalized to the external reference ([<sup>125</sup>I]-BA)KuE (13.0 ± 2.5% internalization at 1 h (n = 21), c = 0.2 nM, 1.0 nM for <sup>177</sup>Lu-compounds; 37 °C, 1 h, 125 000 cells/well, PLL-coated plates). <sup>c</sup>log D value for [<sup>177</sup>Lu]Lu-rhPSMA-7.3 was kindly provided by Dr. A. Wurzer. <sup>d</sup>Data from Patent application EP21150122. Data for binding (IC<sub>50</sub>) and internalization are expressed as mean ± SD (n = 3) unless otherwise stated. Data are expressed as mean ± SD (n = 6) for log D.

## RESULTS AND DISCUSSION

### **Discussion of the *in vitro* results**

*Modifications within the central Zn<sup>2+</sup>-binding unit.* IC<sub>50</sub> and lipophilicity data of [<sup>nat/177</sup>Lu]Lu-**B-13** were very similar to those obtained for reference ligand [<sup>nat/177</sup>Lu]Lu-**B-1**, wherefore carbamate **B-13** was considered as an auspicious candidate for high tumor accumulation *in vivo* with potential reduction of salivary gland uptake.

The IC<sub>50</sub> data of carbamate **B-13** (7.11 ± 0.71 nM) and **B-14** (> 1 µM) confirm the presence of a 'high affinity' and 'low affinity orientation' as postulated for carbamate **B-2** in section 4.2.1.1. and were further corroborated by studies from Yang *et al.* and Barinka *et al.*<sup>[238, 293]</sup> Hence, these observations emphasize the necessity of a hydrogen bond donor at the (non-pharmacophore) P1 position and provide a certain flexibility within the pharmacophore S1' subpocket.

Implementation of thioureate **B-3** (4.17 ± 3.38 µM) into a mature rhPSMA ligand resulted in no benefit (> 3 µM) but revealed a direct transferability of results obtained from isolated PSMA inhibitors to mature compounds. Hence, ligand assessment in advance via isolated PSMA inhibitor motifs was proven to be possible at least for modifications within the central Zn<sup>2+</sup>-binding unit.

Since thioureate derivative **B-12** revealed sulfur to be less tolerated inside the binding pocket, it was assumed that thiourethane derivatives (= combination of carbamates **B-13** or **B-14** with thioureate) would also lead to poor results. In consequence, their synthesis was not further pursued. Interestingly, zinc(II)-sulfur interactions within the catalytic site are quite common for metalloprotease inhibitors.<sup>[344]</sup> For this reason, a different orientation of the thioureate residues (*anti*-conformation) or an altered hydrogen bonding to the C=S moiety possibly causes for a low-PSMA-binding character.<sup>[345, 346]</sup> Alternatively, it remains conceivable that the sulfur atom in L-Glu-thiourea-L-Glu derivatives is not optimally coordinated via both Zn<sup>2+</sup> ions inside the binuclear catalytic center of PSMA, due to its larger atomic and van der Waals radius.<sup>[347]</sup>

## RESULTS AND DISCUSSION

*Proinhibitors.* Competitive binding experiments revealed very low (micromolar) affinities towards PSMA for <sup>nat</sup>Lu-**B-15**, **-B-16** and **-B-17** ( $26.5 \pm 16.3 \mu\text{M}$ ,  $2.52 \pm 1.17 \mu\text{M}$  and  $6.30 \pm 3.59 \mu\text{M}$ , respectively). Due to these unfavorable IC<sub>50</sub> values at standard conditions (incubation at 4 °C for 1 h), internalization studies were conducted, in order to investigate possible substrate cleavage kinetics. Barinka *et al.* observed a substrate conversion of up to 20% after 0.5 h using stock solutions of purified recombinant human GCP II.<sup>[253]</sup> Later time points were considered in our LNCaP cell-based experiments for taking potential slower cleavage kinetics into account. Therefore, internalization at 37 °C was determined at several time points of 0.5 h, 1 h, 2 h and 4 h. Since no internalization could be detected at any time point for [<sup>177</sup>Lu]Lu-**B-15**, **-B-16** or **-B-17**, it was assumed that no proinhibitor cleavage occurred. Enzymatic activity of PSMA could not be assured under these *in vitro* conditions as they were significantly different to the originally conducted assays, which were optimized to reach maximum cleavage efficiency.<sup>[252, 253]</sup> Hence, *in vivo* studies were conducted, as we suggested that cleavage of the proinhibitor motifs might be strongly dependent on the tumor cells' microenvironment and might only occur under real-life conditions. However, poor results (tumor uptake < 0.50% ID/g at 24 h p.i.) were also obtained from these experiments (discussed in more detail in section 4.2.2.4).

Altogether, these findings led to the assumption, that proinhibitor cleavage did not occur in significant amounts within the observation times used for the *in vitro* and *in vivo* studies, probably due to the low affinity of these conjugates. For this reason, synthesis and evaluation of proinhibitor IV (= methionine at the α-carboxylate) was abandoned, as no positive results were expected.

*Substituents & bioisosteres of the P1'-γ-carboxylic acid.* As expected for the tetrazole moiety<sup>[338]</sup>, *in vitro* studies confirmed a slightly increased lipophilicity for [<sup>177</sup>Lu]Lu-**B-21** (~ 7.4-fold increase compared to [<sup>177</sup>Lu]Lu-**B-1**). Apart from a considerably low internalization ( $9.86 \pm 3.16\%$ ), *in vitro* data were found to be at least in the same order of magnitude as those of [<sup>nat/177</sup>Lu]Lu-**B-1**. Consequently, tetrazole derivative **B-21** was also proposed to exhibit high tumor accumulation *in vivo* with potential simultaneous reduction of salivary gland uptake.

For alkyne derivative **B-20**, weak internalization ( $1.17 \pm 0.43\%$ ) could be attributed to the medium affinity of <sup>nat</sup>Lu-**B-20** ( $138 \pm 53 \text{ nM}$ ). Nevertheless, **B-20** was subjected to biodistribution studies, in order to investigate whether higher tumor-to-salivary gland ratios could be achieved, although accompanied by a certain loss of tumor uptake. Furyl derivative **B-19** was expected to provide a similar binding affinity to the alkyne-modified ligand **B-20**, as published by Wang *et al.*<sup>[251]</sup> However, a more than 3-fold higher IC<sub>50</sub> value (> 440 nM) led to cessation of further *in vitro* and *in vivo* investigations. Also L-2-aminoheptanoic acid derivative **B-18** was not further evaluated as its affinity (> 2 μM) was considered as too low.

## RESULTS AND DISCUSSION

In sum, carbamate **B-13**, proinhibitors **B-15**, **B-16**, **B-17**, alkyne derivative **B-20** and tetrazole derivative **B-21** were subjected to *in vivo* evaluation. High IC<sub>50</sub> values led to cessation of further *in vitro* and *in vivo* investigations of thioureate **B-12**, carbamate **B-14**, L-2-aha derivative **B-18** and furyl derivative **B-19**.

### 4.2.2.4. *In vivo* evaluation

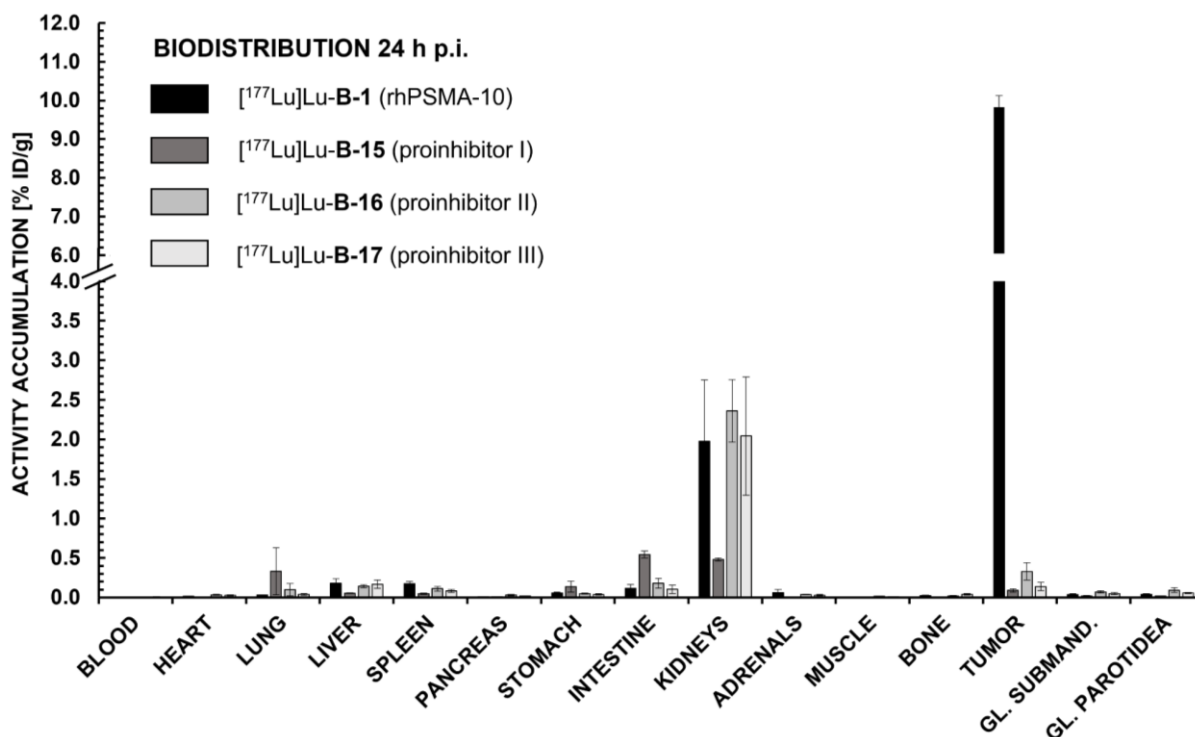
For biodistribution studies of PSMA ligands, the animal model established in our group for evaluation of therapeutic radioligands (i.e. biodistribution at 24 h p.i. in LNCaP tumor xenograft-bearing male CB17-SCID mice (n = 3 to 5)) was chosen. With the aim to improve PSMA-targeted RLT via reduction of unwanted activity accumulation in salivary glands, mainly the 24 h p.i. time point in mice was considered. As a general rule of thumb, activity distribution at ~ 7 days p.i. in humans (European average weight 70 kg) corresponds to the value obtained at 24 h p.i. in mice (average weight 20 g), due to their elevated metabolic rate.<sup>[348]</sup> Thus, at 24 h p.i. in mice, the wash-out from not-target organs with simultaneous persistent high tumor uptake should assure high tumor doses. Therefore, this experimental setup was also used for identification of differences in salivary gland uptake of PSMA-targeting radioligands.

However, data that confirm capability of this animal model to distinguish compounds with different salivary gland uptake at 24 h p.i. were absent at the beginning of the study. Due to certain species-dependent differences<sup>[287, 288]</sup>, a generally lower uptake in mouse salivary glands might lead to non-detectable differences between EuE- and non-EuE-based inhibitors. Therefore, biodistribution at 1 h p.i. should be examined with ligands that provide sufficiently high tumor uptake (i.e. **B-13** and **B-21**), in order to determine if tumor-to-salivary gland ratios at this early time point allow for a clearer distinction.

## RESULTS AND DISCUSSION

### Results of biodistribution experiments, metabolite studies and $\mu$ SPECT/CT studies

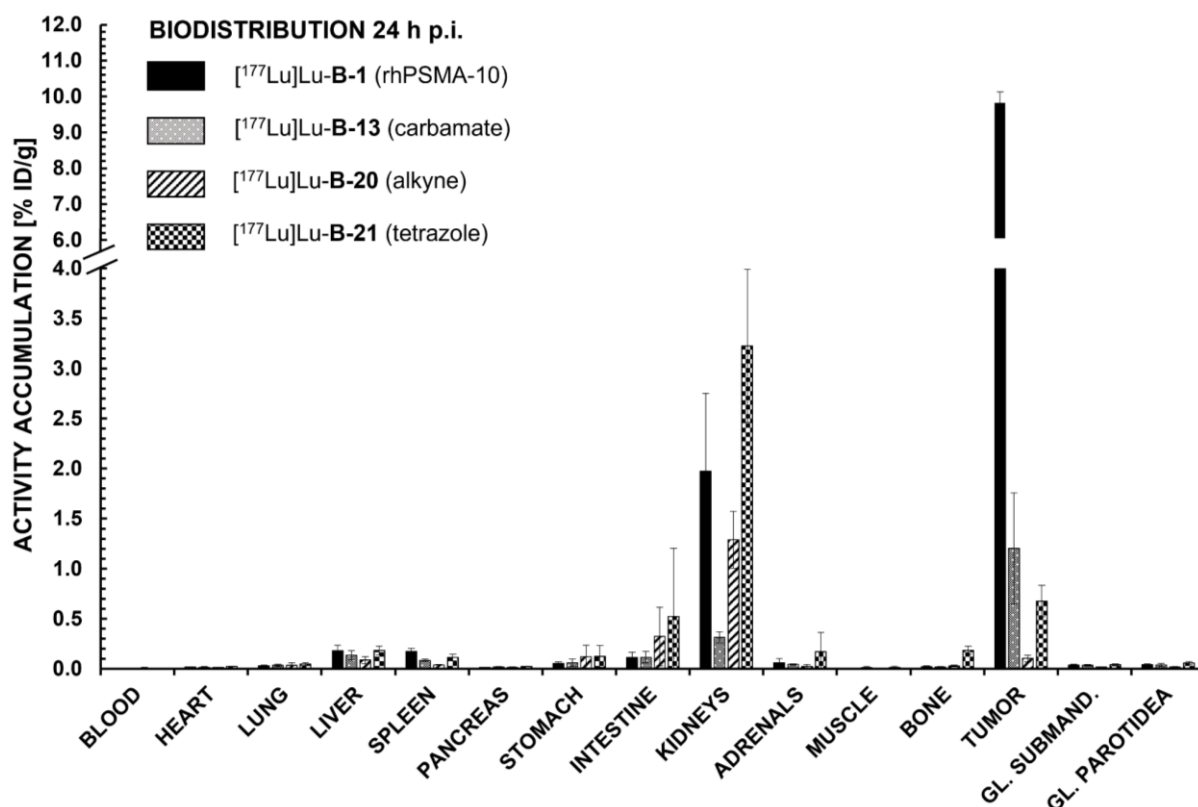
Proinhibitors **B-15**, **B-16** and **B-17**. Biodistribution data at 24 h p.i. revealed low tumor uptake for all ligands ( $< 0.50\%$  ID/g, Figure 32), reflecting the low internalization and unfavorable  $IC_{50}$  values observed in *in vitro* experiments.



**Figure 32:** Biodistribution data (% ID/g) of [<sup>177</sup>Lu]Lu-PSMA-10 ([<sup>177</sup>Lu]Lu-B-1), [<sup>177</sup>Lu]Lu-B-15, [<sup>177</sup>Lu]Lu-B-16 and [<sup>177</sup>Lu]Lu-B-17 in tumor xenograft-bearing CB17-SCID mice at 24 h p.i. (n = 2 for [<sup>177</sup>Lu]Lu-B-15<sup>†</sup>, n = 3 for [<sup>177</sup>Lu]Lu-B-16 and [<sup>177</sup>Lu]Lu-B-17 and n = 5 for [<sup>177</sup>Lu]Lu-rhPSMA-10 ([<sup>177</sup>Lu]Lu-B-1)). Submandibular and parotid glands were dissected separately and their values are depicted in the columns 'GL. SUBMAND.' and 'GL. PAROTIDEA', respectively. Data expressed as percentage of injected dose per gram (% ID/g), mean  $\pm$  SD. The exact values used for this bar diagram are given in MATERIALS AND METHODS (chapter III, section 3.5.1). <sup>†</sup>Ingestion of radioactively contaminated animal feed led to putative high activities in stomach and intestine, wherefore values of mouse 3 were excluded.

Carbamate **B-13**, alkyne **B-20** and tetrazole **B-21**. For further *in vivo* studies at 24 h p.i., derivatives with medium to high affinity were chosen (i.e. [<sup>177</sup>Lu]Lu-B-13, -B-20 and -B-21). For all modified peptides, a more than 8-fold lower tumor accumulation (0.10 to 1.20% ID/g) in comparison to the original compound [<sup>177</sup>Lu]Lu-B-1 (9.82  $\pm$  0.33% ID/g) could be observed with unchanging salivary gland uptake (between 0.02  $\pm$  0.00% ID/g and 0.09  $\pm$  0.03% ID/g) (Figure 33).

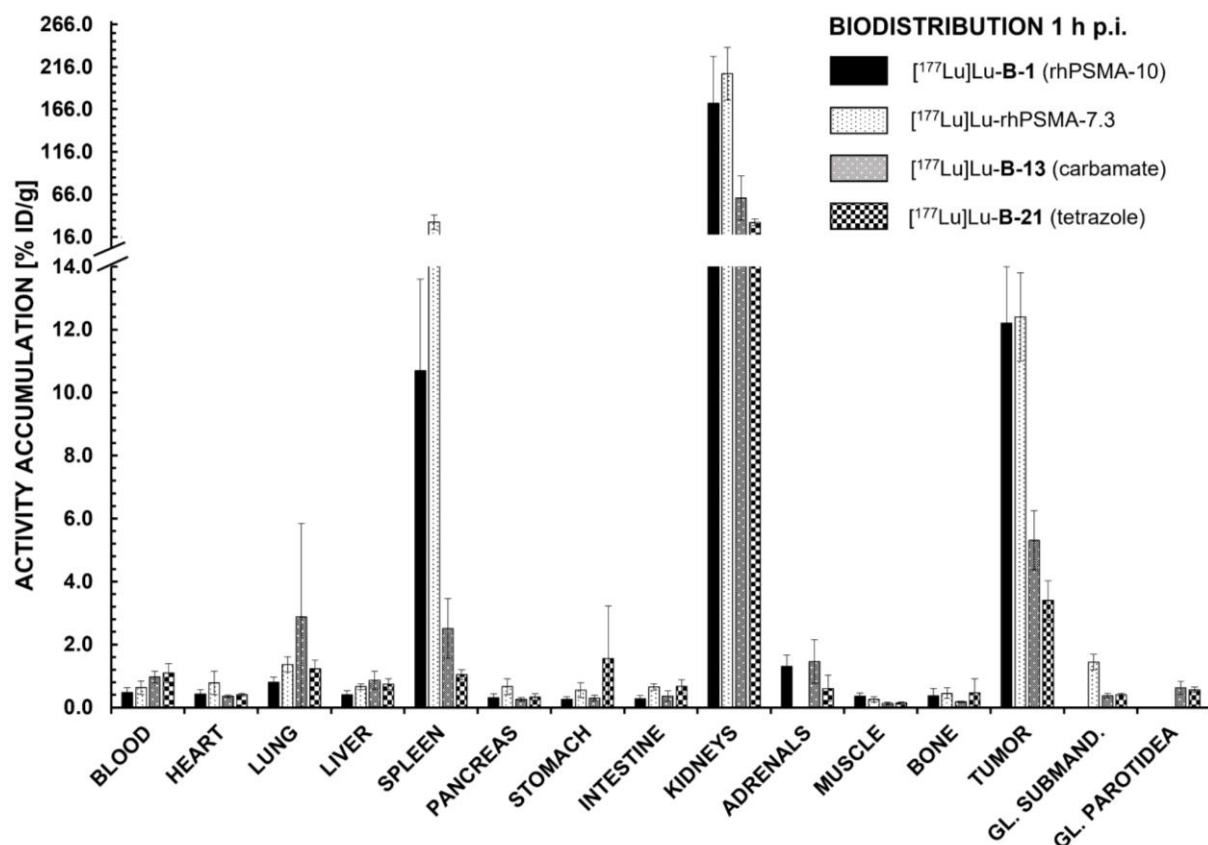
## RESULTS AND DISCUSSION



**Figure 33:** Biodistribution data (% ID/g) of [<sup>177</sup>Lu]Lu-rhPSMA-10 ([<sup>177</sup>Lu]Lu-B-1), [<sup>177</sup>Lu]Lu-B-13, [<sup>177</sup>Lu]Lu-B-20 and [<sup>177</sup>Lu]Lu-B-21 in tumor xenograft-bearing CB17-SCID mice at 24 h p.i. (n = 4 for [<sup>177</sup>Lu]Lu-B-20 and n = 5 for all other experiments). Submandibular and parotid glands were dissected separately and their values are depicted in the columns ,GL. SUBMAND.' and ,GL. PAROTIDEA', respectively. Data expressed as percentage of injected dose per gram (% ID/g), mean ± SD. The exact values used for this bar diagram are given in MATERIALS AND METHODS (chapter III, section 3.5.1).

Biodistribution of [<sup>177</sup>Lu]Lu-B-13 (carbamate) and -B-21 (tetrazole) was also analyzed at 1 h p.i. and compared to [<sup>177</sup>Lu]Lu-B-1 and its (S)-DOTAGA-modified analog [<sup>177</sup>Lu]Lu-rhPSMA-7.3, due to absent data for salivary gland uptake of [<sup>177</sup>Lu]Lu-B-1 at 1 h p.i. (Figure 34). The use of [<sup>177</sup>Lu]Lu-rhPSMA-7.3 as an additional reference ligand was supposed to serve as a reasonable option, since rhPSMA-10 and rhPSMA-7.3 only differ in the chelator (Figure 14 and Figure 17), wherefore the salivary gland uptake should remain unaffected. Although relative tumor uptake ratios were improved compared to the 24 h p.i. time point, tumor accumulation of [<sup>177</sup>Lu]Lu-B-13 ( $5.31 \pm 0.94\%$  ID/g) was already only about half of the uptake of [<sup>177</sup>Lu]Lu-B-1 ( $12.2 \pm 1.8\%$  ID/g). [<sup>177</sup>Lu]Lu-B-21 showed a 3.5-fold lower tumor uptake ( $3.40 \pm 0.63\%$  ID/g). Interestingly, at 1 h p.i. a clearer distinction was possible between EuE-based compound rhPSMA-7.3 and modified derivatives B-13 and B-21 concerning activity uptake in submandibular glands (parotid glands were not dissected for rhPSMA-7.3). [<sup>177</sup>Lu]Lu-B-13 ( $0.37 \pm 0.08\%$  ID/g) and [<sup>177</sup>Lu]Lu-B-21 ( $0.40 \pm 0.05\%$  ID/g) exhibited a ~4-fold lower submandibular gland uptake in comparison to [<sup>177</sup>Lu]Lu-rhPSMA-7.3 ( $1.44 \pm 0.25\%$  ID/g). The resulting differences in tumor-to-salivary gland values and their relevance are discussed below (*Tumor-to-salivary gland ratios*).

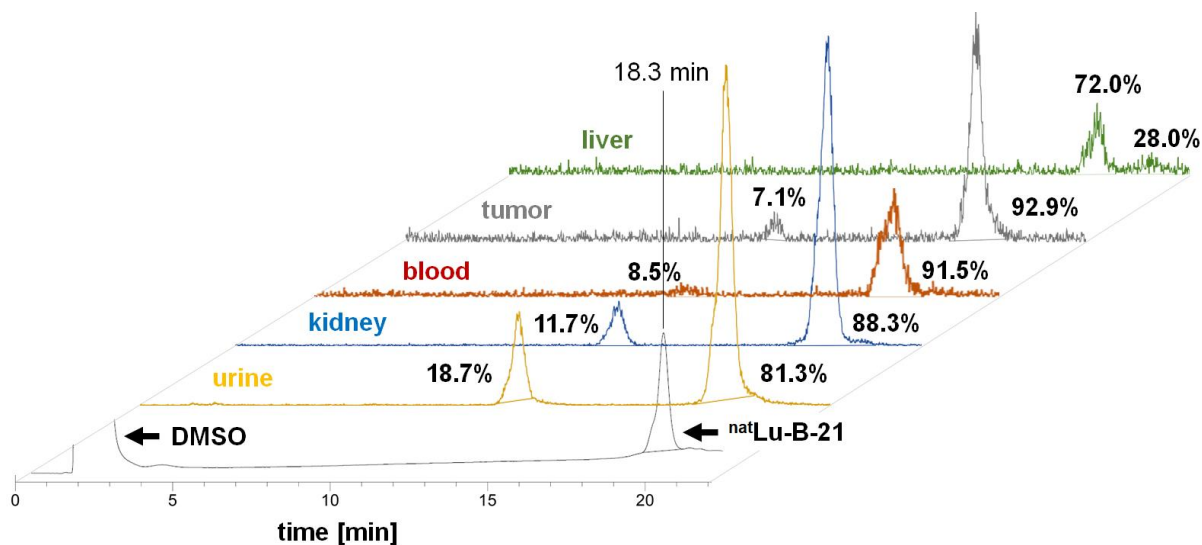
## RESULTS AND DISCUSSION



**Figure 34:** Biodistribution data (% ID/g) of [<sup>177</sup>Lu]Lu-rhPSMA-10 ([<sup>177</sup>Lu]Lu-B-1), [<sup>177</sup>Lu]Lu-rhPSMA-7.3, [<sup>177</sup>Lu]Lu-B-13 and [<sup>177</sup>Lu]Lu-B-21 in tumor xenograft-bearing CB17-SCID mice at 1 h p.i. (n = 4 for [<sup>177</sup>Lu]Lu-rhPSMA-7.3 and n = 5 for all other experiments). Submandibular and parotid glands were dissected separately and their values are depicted in the columns ,GL. SUBMAND.' and ,GL. PAROTIDEA', respectively. Not determined: Adrenal and parotid gland values for [<sup>177</sup>Lu]Lu-rhPSMA-7.3, submandibular and parotid gland values for [<sup>177</sup>Lu]Lu-B-1. Data expressed as percentage of injected dose per gram (% ID/g), mean ± SD. The exact values used for this bar diagram are given in MATERIALS AND METHODS (chapter III, section 3.5.1).

## RESULTS AND DISCUSSION

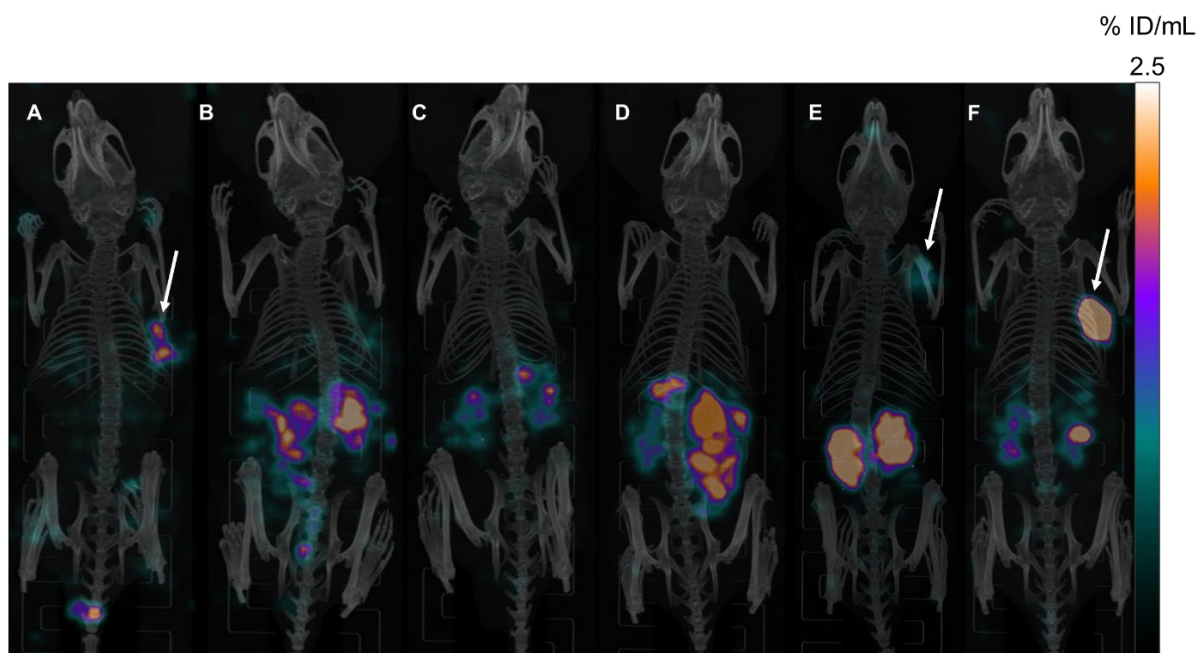
*Metabolite analysis.* [ $^{177}\text{Lu}$ ]Lu-B-21 (tetrazole) was analyzed according to its metabolic stability at 1 h p.i. As depicted in *Figure 35*, only one metabolite with higher hydrophilicity was detected in tumor, kidney, blood and urine. The maximum proportion of this metabolite did not exceed 18.7% (urine). This metabolite was not detectable in liver homogenate, instead a more lipophilic metabolite could be observed at  $t_R = 20.5$  min (28.0%).



**Figure 35:** Radio-RP-HPLC analyses of extracts from homogenized organs and body fluids of tumor-xenograft bearing CB17-SCID mice, 1 h p.i. of [ $^{177}\text{Lu}$ ]Lu-B-21 (9.64 MBq, gradient: 25 - 40% MeCN (0.1% TFA) in 20 min, flow rate: 1 mL/min). The radioactivity detector was placed downstream of the UV-detector causing for a slight time delay of the radioactivity signals compared to the intact cold standard ( $^{\text{nat}}\text{Lu-B-21}$ ), for which the retention time (18.3 min) was determined in advance. Detailed values for extraction efficiencies of homogenates and body fluids are given in MATERIALS AND METHODS (chapter III, section 3.5.2).

*$\mu\text{SPECT/CT}$  studies.* For visualization of the biodistribution data, maximum intensity projections (MIPs) of  $\mu\text{SPECT/CT}$  scans of LNCaP xenograft-bearing mice, acquired 24 h p.i. of [ $^{177}\text{Lu}$ ]Lu-B-13, [ $^{177}\text{Lu}$ ]Lu-B-16, [ $^{177}\text{Lu}$ ]Lu-B-17, [ $^{177}\text{Lu}$ ]Lu-B-20, [ $^{177}\text{Lu}$ ]Lu-B-21 and [ $^{177}\text{Lu}$ ]Lu-B-1 ([ $^{177}\text{Lu}$ ]Lu-rhPSMA-10) are depicted in *Figure 36*.

## RESULTS AND DISCUSSION



**Figure 36:** Maximum intensity projections (MIPs) of  $\mu$ SPECT/CT scans in LNCaP xenograft-bearing mice, acquired 24 h p.i. of (A) [ $^{177}\text{Lu}$ ]Lu-B-13 (carbamate) (3.2 MBq) (B) [ $^{177}\text{Lu}$ ]Lu-B-16 (proinhibitor II) (5.3 MBq) (C) [ $^{177}\text{Lu}$ ]Lu-B-17 (proinhibitor III) (4.5 MBq) (D) [ $^{177}\text{Lu}$ ]Lu-B-20 (alkyne) (9.7 MBq) (E) [ $^{177}\text{Lu}$ ]Lu-B-21 (tetrazole) (7.0 MBq) (F) [ $^{177}\text{Lu}$ ]Lu-rhPSMA-10 (B-1) (2.8 MBq). For clear comparison, all images were scaled to the same maximum uptake value (2.5% ID/mL). Arrows indicate apparent tumor uptake in (A), (E) and (F). No  $\mu$ SPECT/CT image is displayed for [ $^{177}\text{Lu}$ ]Lu-B-15 (proinhibitor I), as ingestion of radioactive animal feed led to putative high activities in stomach and intestine. Therefore, all values of this mouse (= mouse 3) from the respective biodistribution study and also its  $\mu$ SPECT/CT image were excluded. Static images were acquired *post mortem* ( $\text{CO}_2$  asphyxiation and cervical dislocation) and after cardiac puncture with an acquisition time of 45 min. Further biodistribution studies were performed after the scan and included in the calculation of % ID/g values provided by Figure 32 and Figure 33 and Table 7.

## RESULTS AND DISCUSSION

### **Discussion of the *in vivo* results**

*Proinhibitors B-15, B-16 and B-17.* With a maximum tumor accumulation of  $0.33 \pm 0.11\%$  ID/g for [ $^{177}\text{Lu}$ ]Lu-**B-16** (L-2-aoc at the  $\gamma$ -carboxylate) and a minimum tumor accumulation of  $0.09 \pm 0.02\%$  ID/g for [ $^{177}\text{Lu}$ ]Lu-**B-15** (L-methionine at the  $\gamma$ -carboxylate), all proinhibitors showed very low affinity to PSMA and thus - not unexpectedly - low tumor uptake (*Figure 32*). Consequently, no additional biodistribution studies at 1 h p.i. were conducted. Furthermore, non-target tissue uptake was similar to that of [ $^{177}\text{Lu}$ ]Lu-**B-1** or even higher, wherefore no tumor-to-tissue ratios were calculated. In summary, proinhibitor cleavage could not be observed in *in vitro* and *in vivo* experiments within the respective observation periods.

*Carbamate B-13, alkyne B-20 and tetrazole B-21.* Though  $\text{IC}_{50}$  and lipophilicity data of carbamate **B-13** were comparable to [ $^{177}\text{Lu}$ ]rhPSMA-10 ([ $^{177}\text{Lu}$ ]Lu-**B-1**), internalization was ~ 3-fold lower, which might explain decreased tumor accumulation at 24 h and 1 h p.i. (*Figure 33* and *Figure 34*). However, low internalization may not be the only reason for decreased tumor uptake. As observed for SST<sub>2</sub> antagonists, high tumor uptake can also be reached with a negligible capacity to internalize.<sup>[349]</sup> A two-fold lower tumor accumulation already 1 h p.i. ( $5.31 \pm 0.94\%$  ID/g) in combination with a rapid decline to  $1.20 \pm 0.55\%$  ID/g at 24 h p.i., led to the assumption that *in vivo* decomposition of the inhibitor motif might have generated a non-PSMA-binding ligand, resulting in fast renal excretion ( $0.31 \pm 0.05\%$  ID/g for [ $^{177}\text{Lu}$ ]Lu-**B-13** vs.  $1.97 \pm 0.87\%$  ID/g for [ $^{177}\text{Lu}$ ]Lu-**B-1**, 24 h p.i.). Enzymatic bioconversion processes by specific esterases could have led to this molecular degradation. Applications of carbamate-based prodrugs, liberating the biologically active substance by *in vivo* hydrolysis support this theory.<sup>[350]</sup> Metabolite studies at 1 h p.i. may confirm this assumption, however, further biodistribution studies of this low tumor-accumulating compound did not seem sensible for animal welfare reasons. Based on these findings, metabolite studies for tetrazole derivative [ $^{177}\text{Lu}$ ]Lu-**B-21** were planned to be conducted with animals already subjected to biodistribution studies at 1 h p.i. in order to avoid any additional *in vivo* experiments.

Almost negligible accumulation of alkyne derivative [ $^{177}\text{Lu}$ ]Lu-**B-20** in tumor tissue ( $0.10 \pm 0.03\%$  ID/g, 24 h p.i., *Figure 33*) as well as weak PSMA-mediated internalization ( $1.17 \pm 0.43\%$  compared to the reference) was attributed to the medium affinity of <sup>nat</sup>Lu-**B-20** ( $138 \pm 53$  nM). Consequently, no additional biodistribution studies at 1 h p.i. were conducted. PSMA-ligands with  $\text{IC}_{50}$  values  $> 20$  nM and very low internalization ( $< 5\%$ ) should be not considered for future *in vivo* studies, since no improvements for tumor-to-tissue ratios can be expected.

Similar to carbamate **B-13**, *in vivo* biokinetics of tetrazole derivative [ $^{177}\text{Lu}$ ]Lu-**B-21** did not benefit from its favorable  $\text{IC}_{50}$  value ( $16.4 \pm 3.8$  nM). Compared to [ $^{177}\text{Lu}$ ]Lu-**B-13**, even lower tumor uptake values were reached at 24 h p.i. ( $0.68 \pm 0.16\%$  ID/g, *Figure 33*) and 1 h p.i. ( $3.40 \pm 0.63\%$  ID/g, *Figure 34*). In order to determine if low tumor accumulation of [ $^{177}\text{Lu}$ ]Lu-**B-21** results from radioligand decomposition, metabolite studies were performed at 1 h p.i. (*Figure 35*). Since the

## RESULTS AND DISCUSSION

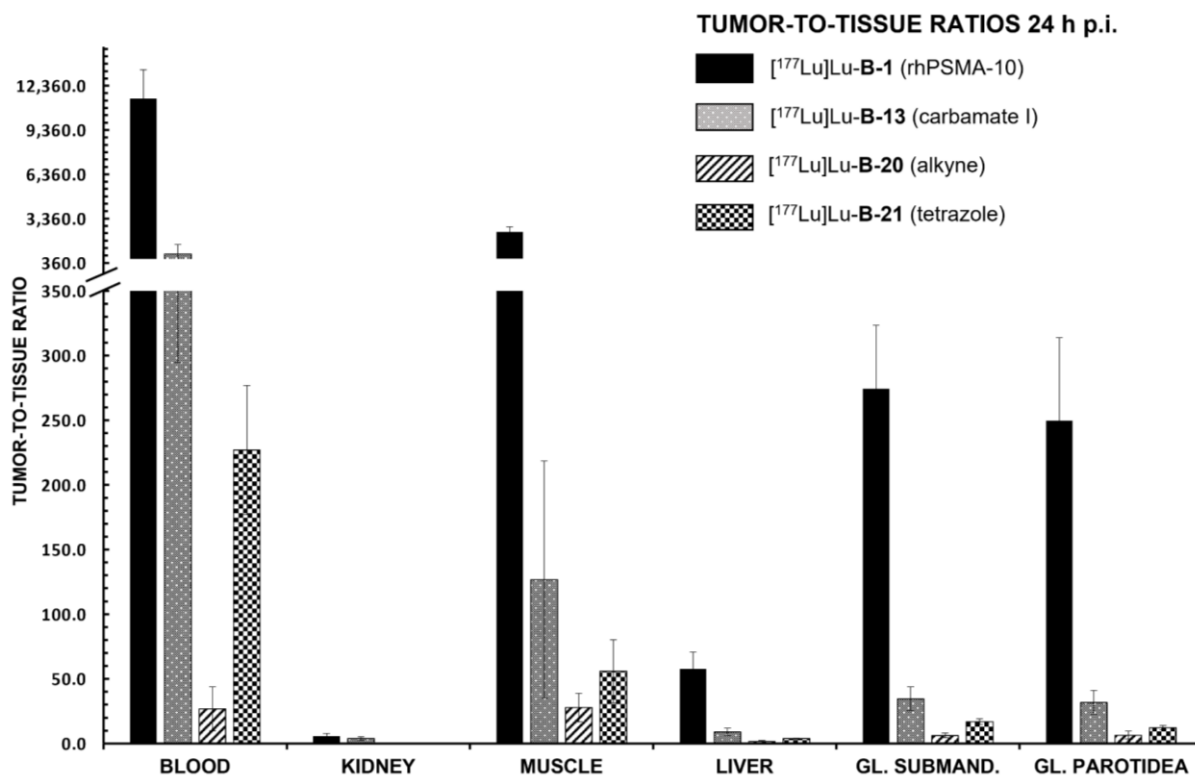
metabolite proportion was rather low in tumor tissue (7.1%) and circulating blood (8.5%), low retention of [<sup>177</sup>Lu]Lu-**B-21** within the LNCaP tumor xenograft cannot be assigned to severe metabolic instability. As a result, low internalization remains as the primary detrimental factor for low tumor accumulation of [<sup>177</sup>Lu]Lu-**B-21**. Therefore, poor *in vivo* performance of [<sup>177</sup>Lu]Lu-**B-21** was mainly attributed to a notably decreased internalization of the final ligand accompanied by a slightly reduced affinity.

Although not crucial for SST<sub>2</sub> ligands, internalization might actually play a more decisive role for tumor uptake of radiolabeled PSMA ligands than previously assumed. Varying internalization values of the high-affinity ligands [<sup>177</sup>Lu]Lu-**B-13/B-21** and [<sup>177</sup>Lu]Lu-rhPSMA-10/7.3 represent the main distinguishing feature *in vitro* and might therefore account for the huge differences in tumor accumulation.

Theoretically, a multitude of further substituents as P1'-γ-carboxylic acid bioisosteres might be conceivable. Based on the respective pK<sub>a</sub> values and/or plasma protein binding squaric acid derivatives, acyl sulfonamides, sulfonylureas, oxazolidine diones or cyclopentane-1,3-diones might serve as potential candidates.<sup>[351]</sup> Apparently, successful implementation also requires a carboxylic acid-like orientation within the binding pocket and an analogous allocation of negative charge. Thus, IC<sub>50</sub> data give a first indication whether further *in vitro* and *in vivo* investigations are rational. However, promising *in vitro* results are not sufficient to predict suitable *in vivo* characteristics, as demonstrated by carbamate **B-13** and tetrazole derivative **B-21**.

Tumor-to-salivary gland ratios. Tumor-to-submandibular and tumor-to-parotid gland values of [<sup>177</sup>Lu]Lu-**B-13** both decreased by a factor of 8 when compared to [<sup>177</sup>Lu]Lu-**B-1** (Figure 37). An even higher decrease (16 to 20 times lower) was observed for [<sup>177</sup>Lu]Lu-**B-21** (tetrazole) and the alkyne analog [<sup>177</sup>Lu]Lu-**B-20**, which exhibited the lowest tumor-to-salivary gland ratios (39 - 45 times lower than for [<sup>177</sup>Lu]Lu-**B-1**) (Figure 37). However, reduced tumor-to salivary gland values at 24 h p.i. in comparison to reference compound [<sup>177</sup>Lu]Lu-**B-1** were found to be mainly induced by the decreased tumor accumulation rather than by an altered salivary gland uptake (Table 7, Figure 32 and Figure 33). Salivary gland uptake values of EuE- and non-EuE-based ligands ranged between 0.02 ± 0.00% ID/g and 0.09 ± 0.03% ID/g and hence, revealed no major difference.

## RESULTS AND DISCUSSION

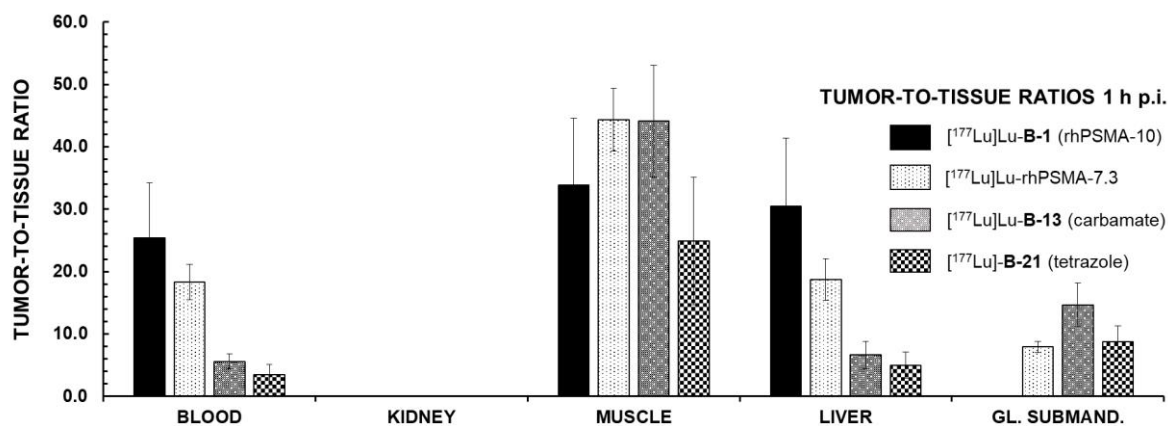


**Figure 37:** Tumor-to-tissue ratios of [<sup>177</sup>Lu]Lu-rhPSMA-10 ([<sup>177</sup>Lu]Lu-B-1), [<sup>177</sup>Lu]Lu-B-13, [<sup>177</sup>Lu]Lu-B-20 and [<sup>177</sup>Lu]Lu-B-21 in selected organs at 24 h p.i. (n = 4 for [<sup>177</sup>Lu]Lu-B-20 and n = 5 for all other experiments). The exact values calculated for this bar diagram are given in MATERIALS AND METHODS (chapter III, section 3.5.1).

Since no values for salivary glands (submandibularis and parotidea) were available for [<sup>177</sup>Lu]Lu-B-1 at the 1 h p.i. time point, carbamate **B-13** and tetrazole derivative **B-21** were compared with structurally strongly related [<sup>177</sup>Lu]Lu-rhPSMA-7.3 (= [<sup>177</sup>Lu]Lu-B-1 with a (S)-DOTAGA chelator instead of DOTA) for which at least submandibular gland values were available. These examinations revealed notably different results for modified peptides at 1 h p.i. (Figure 38). Interestingly, two-fold lower tumor-to-submandibularis and -parotidea ratios of [<sup>177</sup>Lu]Lu-B-13 and -B-21 were determined at 1 h p.i. ( $14.7 \pm 3.5$  and  $8.74 \pm 2.52$ , respectively) compared to their respective values at 24 h p.i. ( $34.5 \pm 9.2$  and  $16.9 \pm 2.2$ , respectively) (Table 9 and Table 10 in MATERIALS AND METHODS, section 3.5.1). However, at this early time point carbamate [<sup>177</sup>Lu]Lu-B-13 displayed an approximately two-fold higher tumor-to-submandibular gland value ( $14.7 \pm 3.5$ ) in comparison to EuE-based derivative [<sup>177</sup>Lu]Lu-rhPSMA-7.3 ( $7.91 \pm 0.87$ ). Moreover, tetrazole [<sup>177</sup>Lu]Lu-B-21 exhibited a similar tumor-to-submandibular gland ratio ( $8.74 \pm 2.52$ ), despite lower tumor-to-tissue ratios for all other investigated organs. This in turn indicates that differences in salivary gland uptake should not be assessed at the 24 h p.i. time point. Besides, also the 1 h p.i. time point in this animal model is only partly suited, despite initial positive results obtained for the distinction of EuE- and non-EuE-based inhibitors. All salivary gland uptake values were still located at the lower detection limit (between  $0.37 \pm 0.08\%$  ID/g and

## RESULTS AND DISCUSSION

$1.44 \pm 0.25\%$  ID/g), wherefore it is difficult to assess whether differences in salivary gland uptake result from varying molecular structures or from discrepancies in the experimental setup.



**Figure 38:** Tumor-to-tissue ratios of [<sup>177</sup>Lu]Lu-rhPSMA-10 ([<sup>177</sup>Lu]Lu-B-1), [<sup>177</sup>Lu]Lu-rhPSMA-7.3, [<sup>177</sup>Lu]Lu-B-13 and [<sup>177</sup>Lu]Lu-B-21 in selected organs at 1 h p.i. (n = 3 for [<sup>177</sup>Lu]Lu-rhPSMA-7.3 and n = 5 for all other experiments). To enable better comparability, available tumor-to-tissue values for [<sup>177</sup>Lu]Lu-B-1 were included besides those obtained for [<sup>177</sup>Lu]Lu-rhPSMA-7.3, [<sup>177</sup>Lu]Lu-B-13 and [<sup>177</sup>Lu]Lu-B-21. Tumor-to-parotid gland ratios are not shown in the drawing, as these values were not determined for both [<sup>177</sup>Lu]Lu-B-1 and [<sup>177</sup>Lu]Lu-rhPSMA-7.3. The exact values calculated for this bar diagram are given in MATERIALS AND METHODS (chapter III, section 3.5.1).

Critical assessment of the rationale for inhibitor modification. In a general context, PSMA ligands comprising modifications within the inhibitor motif (like in compounds **B-12** to **B-21**) might be overestimated if considered as the sole strategy for reduction of non-target tissue uptake in PCa patients. This theory was pursued, since pre-injection of monosodium glutamate was shown to significantly reduce activity accumulation in salivary glands of mice.<sup>[281]</sup> Transfer of this concept to PCa patients was recently examined in clinical trials (early Phase I study)<sup>[352]</sup>, but nevertheless, the exact mechanism of how monosodium glutamate affects non-target binding of radiolabeled PSMA inhibitors still remains unknown. Although small molecule/anion/glutamate transporter systems were proposed for non-target tissue accumulation, this effect could also originate from differences in physiological pH of healthy salivary gland parenchyma and poorly differentiated tumor tissue and/or tumor-associated stroma (Warburg effect).<sup>[353]</sup> Previous Western blot analyses have shown a variation of the PSMA protein within the salivary glands by 20 kDa (in total: 120 kDa; PSMA of LNCaP cell extracts: 100 kDa).<sup>[151]</sup> Additionally, genetic analyses revealed mRNA expression of PSMA in salivary glands.<sup>[150, 277]</sup> Posttranslational modified versions of PSMA (e.g. different glycosylation pattern, otherwise than on PCa) on the surface of salivary gland cells might serve as a reasonable concept for integrating all these contradictory findings.<sup>[142, 151]</sup> Binding of antibodies that are highly specific towards epitopes of PCa-related PSMA (intra- or extracellular) would not be possible in this case.<sup>[188, 211, 275, 278]</sup> By contrast, small molecule ligands would still be able to bind,

## RESULTS AND DISCUSSION

as their binding mechanism is probably not affected by posttranslational changes at the surface of the protein.

Furthermore, inconsistent *in vitro* results concerning the binding of PSMA-specific mAbs to salivary gland tissue are still present.<sup>[275, 354]</sup> This indicates that not enough fundamental research was performed yet to provide a clear statement of PSMA expression on salivary gland parenchyma.

In sum, none of the presented rhPSMA compounds with modified inhibitor unit exhibited favorable properties that would justify their use in RLT of PSMA positive PCa lesions. Only carbamate [<sup>177</sup>Lu]Lu-**B-13** exhibited a two-fold higher tumor-to-submandibular gland ratio at 1 h p.i., however accompanied by a two-fold decrease in tumor uptake. Therefore, the aim of generating a high affinity radioligand that enables targeting of PSMA positive tumor lesions with simultaneous reduction of salivary gland uptake could only be partially attained.

## V. SUMMARY AND CONCLUSION

For the design of GLP-1R ligands with improved pharmacokinetics, initial experiments focused on the preparation of a stable radioiodinated reference ligand. [Nle<sup>14</sup>, [<sup>125</sup>I]Tyr(3-I)<sup>40</sup>]Exendin-4 was identified as a suitable candidate (RCP  $\geq$  92% over at least 16 days) and used for the development of a HEK293-hGLP-1R cell-based competitive binding assay, successfully implemented for screening of GLP-1R-targeting compounds. In general, exendin-4 served as an important reference structure within this PhD thesis. Besides the use of radioiodinated exendin-4, the cold standard as well as the radioiodination precursor were used to evaluate the performance of the assay and for comparing IC<sub>50</sub> data of new derived agents not only to GLP-1, but also to a further known high affinity GLP-1R ligand, i.e. exendin-4. This additional evaluation was assumed to strengthen the overall assay validity and comparability of the results.

Short-chained peptides (9 to 15 amino acids), mainly derived from undecapeptide **A-1** and GLP-1 were synthesized on-resin or via fragment coupling in solution and evaluated after RP-HPLC purification. **A-1** could not be obtained by a linear reaction protocol as described in the literature, wherefore an alternative synthetic route was established. In particular, the preparation of the biphenylalanine residue (2'-Et, 4'-OMe)BIP of **A-1** required additional synthetical efforts in form of Suzuki-Miyaura cross-coupling reactions and non-reactivity after cross-coupling had to be overcome.

IC<sub>50</sub> values of undecapeptides **A-4** and **A-5** confirmed literature data for quaternary  $\alpha$ -amino acids at position 6, with ( $\alpha$ -Me)-(2-F)-Phe to be favored over ( $\alpha$ -Me)Phe. However, in sum, no compound was found to be able to compete with favorable *in vitro* characteristics of GLP-1 (23.2  $\pm$  12.2 nM), [Nle<sup>14</sup>, Tyr(3-I)<sup>40</sup>]exendin-4 (7.63  $\pm$  2.78 nM) and [Nle<sup>14</sup>, Tyr<sup>40</sup>]exendin-4 (9.87  $\pm$  1.82 nM). Particularly for lead peptide **A-1**, the expected high affinity could not be confirmed. Instead, this undecapeptide provided rather high IC<sub>50</sub> values of 669  $\pm$  242 nM. Therefore, the use of **A-1** as a basic scaffold for the design of further GLP-1R-targeting radioligands is not recommended, despite favorable EC<sub>50</sub> values provided by the literature.

Only SiFA-tagged peptide **A-5** showed IC<sub>50</sub> values (189  $\pm$  35 nM) that were lower than those of **A-1**, but still not in a range which allows for *in vivo* evaluation. For this purpose, substantial optimizations concerning lipophilicity and affinity need to be realized. Due to the poor IC<sub>50</sub> values obtained so far, no further *in vitro* and *in vivo* studies were performed with any of the ligands developed within this work. Accordingly, <sup>18</sup>F-labeling of the SiFA-modified precursors was not pursued. In consequence, radioligands targeting GLP-1R<sup>+</sup> tumor lesions with reduced kidney uptake and/or enhanced renal excretion could not be generated. In order to reach an improved tumor localization and enable TRT of malignant insulinomas as well as of other GLP-1R-overexpressing malignancies, further investigations on pharmacokinetically optimized peptides should be envisaged.

## SUMMARY AND CONCLUSION

For the design of PSMA ligands with improved pharmacokinetics, compounds with modifications at the central Zn<sup>2+</sup>-binding unit, proinhibitor motifs and derivatives with P1'- $\gamma$ -carboxylic acid substituents and bioisosteres were investigated. Syntheses of the binding motifs were conducted on-resin or via fragment coupling in solution and evaluated after RP-HPLC purification. All synthesis steps focused on conditions to ensure L-configuration of the entire PSMA binding motif. For carbamates **B-13** and **B-14**, introduction of different protective groups (*tert*-butyl or benzyl) at the  $\gamma$ -carboxylate of compounds **41** and **47** was of utmost importance. These steps, already conducted at an early stage of synthesis, were crucial for determination of carbamate orientation. Oxidation tendency of methionine-containing proinhibitor **B-15** not only resulted in low overall yields after RP-HPLC purification (0.08%), also the preparation of the <sup>177</sup>Lu-labeled product was impaired, resulting in RCPs of 89.3 ± 1.9%, even at lower temperatures (80°C).

No modified inhibitor structure was found to be able to compete with favorable *in vivo* characteristics of the EuE-based radiohybrid compound [<sup>177</sup>Lu]Lu-rhPSMA-10. Although two derivatives (**B-13** and **B-21**) were found to exhibit high affinities towards PSMA<sup>+</sup> LNCaP cells (IC<sub>50</sub> = 7.11 ± 0.71 nM and 16.4 ± 3.8 nM, respectively), the expected tumor uptake was not observed in both cases. Concerning carbamate **B-13**, low tumor uptake (5.31 ± 0.94% ID/g, 1 h p.i. and 1.20 ± 0.55% ID/g, 24 h p.i.) can be partially attributed to its less internalizing character. Additionally, the binding motif might have been subjected to *in vivo* degradation, which led to decreased tumor uptake and an enhanced overall excretion rate. Metabolite studies at 1 h p.i. may confirm this assumption, however, further biodistribution studies of this low tumor-accumulating compound did not seem sensible for animal welfare reasons. For tetrazole derivative [<sup>177</sup>Lu]Lu-**B-21**, examination of possible competing metabolites revealed only one compound in tumor, blood, kidneys and urine, which was detected to a maximum extent of 18.7% (urine) at 1 h p.i. This metabolite was not detectable in liver homogenate, instead a more lipophilic metabolite could be observed, which accounted for 28.0%. Since the metabolite proportion was rather low in tumor tissue (7.1%) and circulating blood (8.5%), low tumor accumulation already at 1 h p.i. (3.40 ± 0.63% ID/g) cannot be attributed to severe metabolic instability. Mainly the low internalizing character in combination with a lower affinity resulted in low tumor uptake of [<sup>177</sup>Lu]Lu-**B-21** at 1 h (3.40 ± 0.63% ID/g) and 24 h p.i. (0.68 ± 0.16% ID/g).

Lower tumor accumulation with unchanging salivary gland uptake finally revealed that no compound developed in this work could outperform [<sup>177</sup>Lu]Lu-rhPSMA-10 in terms of tumor-to-salivary gland ratios. Importantly, lower tumor-to-salivary gland ratios were mainly induced by lower tumor accumulation, since salivary gland uptake values in these mice were equally low for all investigated compounds at 24 h p.i. (between 0.02 ± 0.00% ID/g and 0.09 ± 0.03% ID/g). Hence, differences in salivary gland uptake in the established animal model appear to be not detectable at this examination time point.

## SUMMARY AND CONCLUSION

By contrast, at 1 h p.i. clearer distinctions between EuE- and non-EuE based inhibitors were possible concerning their salivary gland uptake and revealed carbamate [ $^{177}\text{Lu}$ ]Lu-**B-13** to exhibit a two-fold higher tumor-to-submandibular gland ratio compared to the EuE-based derivative [ $^{177}\text{Lu}$ ]Lu-rhPSMA-7.3. Despite this detectable difference, it has to be noted that salivary gland uptake at 1 h p.i. was still at a low level (between  $0.37 \pm 0.08\%$  ID/g and  $1.44 \pm 0.25\%$  ID/g). Therefore, it remains to be proven that early examination time points in this animal model generally allow for a clear identification of radiolabeled PSMA inhibitors with reduced salivary gland uptake in future studies.

## VI. REFERENCES

1. Schottelius, M. and H.-J. Wester, *Molecular imaging targeting peptide receptors*. Methods, 2009. **48**(2): p. 161-177.
2. Reubi, J.C., *Peptide receptors as molecular targets for cancer diagnosis and therapy*. Endocr. Rev., 2003. **24**(4): p. 389-427.
3. Lewis, J., A.D. Windhorst, and B.M. Zeglis, *Radiopharmaceutical chemistry*. 2019.
4. Giammarile, F., et al., *Non-FDG PET/CT in Diagnostic Oncology: a pictorial review*. European Journal of Hybrid Imaging, 2019. **3**(1): p. 20.
5. *Technetium-99m Radiopharmaceuticals: Status and Trends*. 2010, Vienna: INTERNATIONAL ATOMIC ENERGY AGENCY.
6. Chen, K. and X. Chen, *Design and development of molecular imaging probes*. Current topics in medicinal chemistry, 2010. **10**(12): p. 1227-1236.
7. Lee, S., J. Xie, and X. Chen, *Peptide-Based Probes for Targeted Molecular Imaging*. Biochemistry, 2010. **49**(7): p. 1364-1376.
8. <https://clinicaltrials.gov/>. Accessed on May 1st, 2021.
9. Kręćisz, P., et al., *Radiolabeled Peptides and Antibodies in Medicine*. Bioconjugate Chemistry, 2021. **32**(1): p. 25-42.
10. Henrich, U. and M. Benešová, *[(68)Ga]Ga-DOTA-TOC: The First FDA-Approved (68)Ga-Radiopharmaceutical for PET Imaging*. Pharmaceuticals (Basel, Switzerland), 2020. **13**(3): p. 38.
11. Farolfi, A., et al., *Current and Emerging Clinical Applications of PSMA PET Diagnostic Imaging for Prostate Cancer*. Journal of Nuclear Medicine, 2021. **62**(5): p. 596-604.
12. Pant, K., et al., *Radiolabelled Polymeric Materials for Imaging and Treatment of Cancer: Quo Vadis?* Advanced Healthcare Materials, 2017. **6**(6): p. 1601115.
13. Kijewski, M.F., *Chapter 32 - Positron Emission Tomography (PET) and Single-Photon Emission Computed Tomography (SPECT) Physics*, in *Handbook of Neuro-Oncology Neuroimaging (Second Edition)*, H.B. Newton, Editor. 2016, Academic Press: San Diego. p. 353-358.
14. Cherry, S.R., J.A. Sorenson, and M.E. Phelps, *chapter 17 - Single Photon Emission Computed Tomography*, in *Physics in Nuclear Medicine (Fourth Edition)*, S.R. Cherry, J.A. Sorenson, and M.E. Phelps, Editors. 2012, W.B. Saunders: Philadelphia. p. 279-306.
15. Cherry, S.R., J.A. Sorenson, and M.E. Phelps, *chapter 18 - Positron Emission Tomography*, in *Physics in Nuclear Medicine (Fourth Edition)*, S.R. Cherry, J.A. Sorenson, and M.E. Phelps, Editors. 2012, W.B. Saunders: Philadelphia. p. 307-343.
16. Soudabeh, M., *Front-end Data Processing of New Positron Emission Tomography Demonstrator*, in *Faculty council of Computing and Electrical Engineering 2014*, Tampere University of Technology: Finland.
17. Wängler, C., et al., *Silicon-[18F]Fluorine Radiochemistry: Basics, Applications and Challenges*. Applied Sciences, 2012. **2**(2): p. 277-302.
18. Turkington, T.G., *Introduction to PET Instrumentation*. Journal of Nuclear Medicine Technology, 2001. **29**(1): p. 4-11.

## REFERENCES

19. Kratochwil, C., et al., *<sup>213</sup>Bi-DOTATOC receptor-targeted alpha-radionuclide therapy induces remission in neuroendocrine tumours refractory to beta radiation: a first-in-human experience.* European Journal of Nuclear Medicine and Molecular Imaging, 2014. **41**(11): p. 2106-2119.
20. O'Keefe, D.S., et al., *A Perspective on the Evolving Story of PSMA Biology, PSMA-Based Imaging, and Endoradiotherapeutic Strategies.* Journal of Nuclear Medicine, 2018. **59**(7): p. 1007-1013.
21. Jones, W., et al., *PSMA Theranostics: Review of the Current Status of PSMA-Targeted Imaging and Radioligand Therapy.* Cancers, 2020. **12**(6): p. 1367.
22. Körner, M., et al., *Glucagon-like peptide-1 receptor overexpression in cancer and its impact on clinical applications.* Frontiers in Endocrinology, 2012. **3**(158).
23. Jazayeri, A., et al., *Crystal structure of the GLP-1 receptor bound to a peptide agonist.* Nature (London, U. K.), 2017. **546**(7657): p. 254-258.
24. Körner, M., et al., *GLP-1 Receptor Expression in Human Tumors and Human Normal Tissues: Potential for In Vivo Targeting.* Journal of Nuclear Medicine, 2007. **48**(5): p. 736-743.
25. Tornehave, D., et al., *Expression of the GLP-1 receptor in mouse, rat, and human pancreas.* J Histochem Cytochem, 2008. **56**(9): p. 841-51.
26. Wei, Y. and S. Mojsov, *Tissue-specific expression of the human receptor for glucagon-like peptide-I: brain, heart and pancreatic forms have the same deduced amino acid sequences.* FEBS Lett, 1995. **358**(3): p. 219-24.
27. Runge, S., et al., *Crystal Structure of the Ligand-bound Glucagon-like Peptide-1 Receptor Extracellular Domain.* Journal of Biological Chemistry, 2008. **283**(17): p. 11340-11347.
28. Mayo, K.E., et al., *International Union of Pharmacology. XXXV. The glucagon receptor family.* Pharmacol Rev, 2003. **55**(1): p. 167-94.
29. Graaf, C.d., et al., *Glucagon-Like Peptide-1 and Its Class B G Protein–Coupled Receptors: A Long March to Therapeutic Successes.* Pharmacological Reviews, 2016. **68**(4): p. 954-1013.
30. Moon, M.J., et al., *Ligand Binding Pocket Formed by Evolutionarily Conserved Residues in the Glucagon-like Peptide-1 (GLP-1) Receptor Core Domain.* J. Biol. Chem., 2015. **290**(9): p. 5696-5706.
31. Wilmen, A., et al., *Five Out of Six Tryptophan Residues in the N-Terminal Extracellular Domain of the Rat GLP-1 Receptor Are Essential for its Ability to Bind GLP-1.* Peptides, 1997. **18**(2): p. 301-305.
32. Hoare, S.R.J., *Mechanisms of peptide and nonpeptide ligand binding to Class B G-protein-coupled receptors.* Drug Discovery Today, 2005. **10**(6): p. 417-427.
33. Wu, F., et al., *Full-length human GLP-1 receptor structure without orthosteric ligands.* Nature Communications, 2020. **11**(1): p. 1272.
34. Hareter, A., et al., *The positive charge of the imidazole side chain of histidine7 is crucial for GLP-1 action.* Endocr. J. (Tokyo), 1997. **44**(5): p. 701-705.
35. Gilman, A.G., *G PROTEINS: TRANSDUCERS OF RECEPTOR-GENERATED SIGNALS.* Annual Review of Biochemistry, 1987. **56**(1): p. 615-649.

## REFERENCES

36. Gurevich, V.V. and E.V. Gurevich, *GPCR Signaling Regulation: The Role of GRKs and Arrestins*. *Frontiers in Pharmacology*, 2019. **10**(125).
37. Zhang, Y., et al., *Cryo-EM structure of the activated GLP-1 receptor in complex with a G protein*. *Nature (London, U. K.)*, 2017. **546**(7657): p. 248-253.
38. Ashcroft, F.M., *ATP-sensitive potassium channelopathies: focus on insulin secretion*. *The Journal of clinical investigation*, 2005. **115**(8): p. 2047-2058.
39. Holst, J.J., *The physiology of glucagon-like peptide 1*. *Physiol. Rev.*, 2007. **87**(4): p. 1409-1439.
40. Gallwitz, B., et al., *Structure/Activity Characterization of Glucagon-Like Peptide-1*. *European Journal of Biochemistry*, 1994. **225**(3): p. 1151-1156.
41. Kieffer, T.J. and J. Francis Habener, *The Glucagon-Like Peptides*. *Endocrine Reviews*, 1999. **20**(6): p. 876-913.
42. Dhanvantari, S., N.G. Seidah, and P.L. Brubaker, *Role of prohormone convertases in the tissue-specific processing of proglucagon*. *Mol Endocrinol*, 1996. **10**(4): p. 342-55.
43. Drucker, D.J., *The biology of incretin hormones*. *Cell Metab.*, 2006. **3**(3): p. 153-165.
44. Ørskov, C., et al., *Tissue and Plasma Concentrations of Amidated and Glycine-Extended Glucagon-Like Peptide I in Humans*. *Diabetes*, 1994. **43**(4): p. 535-539.
45. Adelhorst, K., et al., *Structure-activity studies of glucagon-like peptide-1*. *Journal of Biological Chemistry*, 1994. **269**(9): p. 6275-6278.
46. Manandhar, B. and J.-M. Ahn, *Glucagon-like Peptide-1 (GLP-1) Analogs: Recent Advances, New Possibilities, and Therapeutic Implications*. *Journal of Medicinal Chemistry*, 2015. **58**(3): p. 1020-1037.
47. Mentlein, R., B. Gallwitz, and W.E. Schmidt, *Dipeptidyl-peptidase IV hydrolyzes gastric inhibitory polypeptide, glucagon-like peptide-1(7-36)amide, peptide histidine methionine and is responsible for their degradation in human serum*. *Eur. J. Biochem.*, 1993. **214**(3): p. 829-35.
48. Hupe-Sodmann, K., et al., *Characterisation of the processing by human neutral endopeptidase 24.11 of GLP-1(7-36) amide and comparison of the substrate specificity of the enzyme for other glucagon-like peptides*. *Regulatory Peptides*, 1995. **58**(3): p. 149-156.
49. Hupe-Sodmann, K., et al., *Endoproteolysis of Glucagon-like Peptide (GLP)-1(7-36) amide by Ectopeptidases in RINm5F Cells*. *Peptides*, 1997. **18**(5): p. 625-632.
50. Mentlein, R., *Mechanisms underlying the rapid degradation and elimination of the incretin hormones GLP-1 and GIP*. *Best Pract Res Clin Endocrinol Metab*, 2009. **23**(4): p. 443-52.
51. Sarrauste de Menthère, C., et al., *Structural requirements of the N-terminal region of GLP-1-[7-37]-NH<sub>2</sub> for receptor interaction and cAMP production*. *European Journal of Medicinal Chemistry*, 2004. **39**(6): p. 473-480.
52. Hjorth, S.A., et al., *Glucagon and glucagon-like peptide 1: selective receptor recognition via distinct peptide epitopes*. *J. Biol. Chem.*, 1994. **269**(48): p. 30121-4.
53. Parker, J.C., et al., *Structure-function analysis of a series of glucagon-like peptide-1 analogs*. *The Journal of Peptide Research*, 1998. **52**(5): p. 398-409.
54. Rajeev, S.P. and J. Wilding, *GLP-1 as a target for therapeutic intervention*. *Current Opinion in Pharmacology*, 2016. **31**(Supplement C): p. 44-49.

## REFERENCES

55. Herrmann, C., et al., *Glucagon-Like Peptide-1 and Glucose-Dependent Insulin-Releasing Polypeptide Plasma Levels in Response to Nutrients*. Digestion, 1995. **56**(2): p. 117-126.
56. Heller, R.S., T.J. Kieffer, and J.F. Habener, *Insulinotropic glucagon-like peptide I receptor expression in glucagon-producing alpha-cells of the rat endocrine pancreas*. Diabetes, 1997. **46**(5): p. 785-91.
57. Nauck, M.A., et al., *Glucagon-like peptide 1 inhibition of gastric emptying outweighs its insulinotropic effects in healthy humans*. American Journal of Physiology-Endocrinology and Metabolism, 1997. **273**(5): p. E981-E988.
58. Campbell, Jonathan E. and Daniel J. Drucker, *Pharmacology, Physiology, and Mechanisms of Incretin Hormone Action*. Cell Metabolism, 2013. **17**(6): p. 819-837.
59. Drucker, D.J. and M.A. Nauck, *The incretin system: glucagon-like peptide-1 receptor agonists and dipeptidyl peptidase-4 inhibitors in type 2 diabetes*. The Lancet, 2006. **368**(9548): p. 1696-1705.
60. Deacon, C.F., et al., *Dipeptidyl peptidase IV resistant analogues of glucagon-like peptide-1 which have extended metabolic stability and improved biological activity*. Diabetologia, 1998. **41**(3): p. 271-278.
61. Montrose-Rafizadeh, C., et al., *High Potency Antagonists of the Pancreatic Glucagon-like Peptide-1 Receptor*. Journal of Biological Chemistry, 1997. **272**(34): p. 21201-21206.
62. Plamboeck, A., et al., *Neutral endopeptidase 24.11 and dipeptidyl peptidase IV are both mediators of the degradation of glucagon-like peptide 1 in the anaesthetised pig*. Diabetologia, 2005. **48**(9): p. 1882-1890.
63. Deacon, C.F., et al., *Both Subcutaneously and Intravenously Administered Glucagon-Like Peptide I Are Rapidly Degraded From the NH<sub>2</sub>-Terminus in Type II Diabetic Patients and in Healthy Subjects*. Diabetes, 1995. **44**(9): p. 1126-1131.
64. Brown, E., D.J. Cuthbertson, and J.P. Wilding, *Newer GLP-1 receptor agonists and obesity-diabetes*. Peptides, 2018. **100**: p. 61-67.
65. Buteau, J., *GLP-1 receptor signaling: effects on pancreatic  $\beta$ -cell proliferation and survival*. Diabetes Metab., 2008. **34**(Suppl. 2): p. S73-S77.
66. Christ, E., et al., *Innovative imaging of insulinoma: the end of sampling? A review*. Endocrine-related cancer, 2020. **27**(4): p. R79-R92.
67. Jodal, A., R. Schibli, and M. Béhé, *Targets and probes for non-invasive imaging of  $\beta$ -cells*. European Journal of Nuclear Medicine and Molecular Imaging, 2017. **44**(4): p. 712-727.
68. Hubalewska-Dydejczyk, A., et al., *GLP-1 and exendin-4 for imaging endocrine pancreas. A review. Labelled glucagon-like peptide-1 analogues: past, present and future*. Q J Nucl Med Mol Imaging, 2015. **59**(Copyright (C) 2017 U.S. National Library of Medicine.): p. 152-60.
69. Jodal, A., et al., *A comparison of three 67/68Ga-labelled exendin-4 derivatives for  $\beta$ -cell imaging on the GLP-1 receptor: the influence of the conjugation site of NODAGA as chelator*. EJNMMI Research, 2014. **4**(1): p. 31.
70. Krenning, E.P., et al., *Localisation of endocrine-related tumours with radioiodinated analogue of somatostatin*. Lancet, 1989. **1**(8632): p. 242-4.

## REFERENCES

71. Reubi, J.C. and B. Waser, *Concomitant expression of several peptide receptors in neuroendocrine tumours: molecular basis for in vivo multireceptor tumour targeting*. European Journal of Nuclear Medicine and Molecular Imaging, 2003. **30**(5): p. 781-793.
72. Rayamajhi, S.J., et al., *Cross sectional and nuclear medicine imaging of pancreatic insulinomas*. Abdominal Radiology, 2017. **42**(2): p. 531-543.
73. Krenning, E.P., et al., *<sup>111</sup>In-octreotide scintigraphy in oncology*. Digestion, 1993. **54 Suppl 1**: p. 84-7.
74. Christ, E., et al., *Glucagon-like peptide-1 receptor imaging for localization of insulinomas*. J Clin Endocrinol Metab, 2009. **94**(11): p. 4398-405.
75. Gotthardt, M., et al., *Use of the incretin hormone glucagon-like peptide-1 (GLP-1) for the detection of insulinomas: initial experimental results*. European Journal of Nuclear Medicine and Molecular Imaging, 2002. **29**(5): p. 597-606.
76. Wicki, A., et al., *[Lys40(Ahx-DTPA-111In)NH2]-Exendin-4 Is a Highly Efficient Radiotherapeutic for Glucagon-Like Peptide-1 Receptor-Targeted Therapy for Insulinoma*. Clin. Cancer Res., 2007. **13**(12): p. 3696-3705.
77. Service, F.J., et al., *Functioning insulinoma--incidence, recurrence, and long-term survival of patients: a 60-year study*. Mayo Clin Proc, 1991. **66**(7): p. 711-9.
78. Rushakoff R, S.A.a.C.O. *Insulinoma and other Hypoglycemias*. Updated 2009 Jan 1.
79. Henquin, J.-C., et al., *Human Insulinomas Show Distinct Patterns of Insulin Secretion In Vitro*. Diabetes, 2015. **64**(10): p. 3543-3553.
80. Grant, C.S., *Insulinoma*. Best Practice & Research Clinical Gastroenterology, 2005. **19**(5): p. 783-798.
81. Gao, H., et al., *PET of Insulinoma Using <sup>18</sup>F-FBEM-EM3106B, a New GLP-1 Analogue*. Mol. Pharmaceutics, 2011. **8**(5): p. 1775-1782.
82. Körner, M., et al., *Somatostatin receptor subtype 2A immunohistochemistry using a new monoclonal antibody selects tumors suitable for in vivo somatostatin receptor targeting*. The American journal of surgical pathology, 2012. **36**(2): p. 242-252.
83. Chatziioannou, A., et al., *Imaging and localization of pancreatic insulinomas*. Clinical Imaging, 2001. **25**(4): p. 275-283.
84. Wild, D., et al., *Glucagon-Like Peptide-1 Versus Somatostatin Receptor Targeting Reveals 2 Distinct Forms of Malignant Insulinomas*. Journal of Nuclear Medicine, 2011. **52**(7): p. 1073-1078.
85. van Schaik, E., et al., *Improved Control of Severe Hypoglycemia in Patients with Malignant Insulinomas by Peptide Receptor Radionuclide Therapy*. The Journal of Clinical Endocrinology & Metabolism, 2011. **96**(11): p. 3381-3389.
86. Donow, C., et al., *Surgical pathology of gastrinoma. Site, size, multicentricity, association with multiple endocrine neoplasia type 1, and malignancy*. Cancer, 1991. **68**(6): p. 1329-1334.
87. Sbardella, E. and A.B. Grossman, *Pheochromocytoma: An approach to diagnosis*. Best Practice & Research Clinical Endocrinology & Metabolism, 2020. **34**(2): p. 101346.

## REFERENCES

88. Wild, D., et al., *[Lys40(Ahx-DTPA-111In)NH<sub>2</sub>]exendin-4, a very promising ligand for glucagon-like peptide-1 (GLP-1) receptor targeting*. J Nucl Med, 2006. **47**(12): p. 2025-33.
89. Jansen, T.J.P., et al., *Exendin-4 analogs in insulinoma theranostics*. Journal of labelled compounds & radiopharmaceuticals, 2019. **62**(10): p. 656-672.
90. Moon, M.J., et al., *Tyr1 and Ile7 of glucose-dependent insulinotropic polypeptide (GIP) confer differential ligand selectivity toward GIP and glucagon-like peptide-1 receptors*. Mol Cells, 2010. **30**(2): p. 149-54.
91. Eng, J., et al., *Isolation and characterization of exendin-4, an exendin-3 analogue, from Heloderma suspectum venom. Further evidence for an exendin receptor on dispersed acini from guinea pig pancreas*. Journal of Biological Chemistry, 1992. **267**(11): p. 7402-5.
92. Yap, M.K.K. and N. Misuan, *Exendin-4 from Heloderma suspectum venom: From discovery to its latest application as type II diabetes combatant*. Basic & Clinical Pharmacology & Toxicology, 2019. **124**(5): p. 513-527.
93. Parkes, D.G., et al., *Insulinotropic actions of exendin-4 and glucagon-like peptide-1 in vivo and in vitro*. Metabolism, 2001. **50**(5): p. 583-589.
94. Brom, M., et al., *Radiolabelled GLP-1 analogues for in vivo targeting of insulinomas*. Contrast Media Mol. Imaging, 2012. **7**(2): p. 160-166.
95. Joosten, L., et al., *Enhanced Specific Activity by Multichelation of Exendin-3 Leads To Improved Image Quality and In Vivo Beta Cell Imaging*. Mol. Pharmaceutics, 2018. **15**(2): p. 486-494.
96. Eng, J., et al., *Purification and structure of exendin-3, a new pancreatic secretagogue isolated from Heloderma horridum venom*. J Biol Chem, 1990. **265**(33): p. 20259-62.
97. Raufman, J.P., L. Singh, and J. Eng, *Exendin-3, a novel peptide from Heloderma horridum venom, interacts with vasoactive intestinal peptide receptors and a newly described receptor on dispersed acini from guinea pig pancreas. Description of exendin-3(9-39) amide, a specific exendin receptor antagonist*. J Biol Chem, 1991. **266**(5): p. 2897-902.
98. Wild, D., et al., *Glucagon-like peptide 1-receptor scans to localize occult insulinomas*. N. Engl. J. Med., 2008. **359**(7): p. 766-768.
99. Christ, E., et al., *Glucagon-like peptide-1 receptor imaging for the localisation of insulinomas: a prospective multicentre imaging study*. Lancet Diabetes Endocrinol., 2013. **1**(2): p. 115-122.
100. <https://clinicaltrials.gov/ct2/results?cond=Insulinoma&term=glp-1R&cntry=&state=&city=&dist=&Search=Search>. Accessed on June 12, 2021.
101. Sowa-Staszczak, A., et al., *Glucagon-like peptide-1 receptor imaging with [Lys40(Ahx-HYNIC-99mTc/EDDA)NH<sub>2</sub>]-exendin-4 for the detection of insulinoma*. Eur. J. Nucl. Med. Mol. Imaging, 2013. **40**(4): p. 524-531.
102. Antwi, K., et al., *Localization of hidden insulinomas with 68Ga-DOTA-exendin-4 PET/CT: a pilot study*. J. Nucl. Med., 2015. **56**(7): p. 1075-1078.
103. Luo, Y., et al., *Glucagon-Like Peptide-1 Receptor PET/CT with 68Ga-NOTA-Exendin-4 for Detecting Localized Insulinoma: A Prospective Cohort Study*. J Nucl Med, 2016. **57**(5): p. 715-20.

## REFERENCES

104. Antwi, K., et al., *Comparison of glucagon-like peptide-1 receptor (GLP-1R) PET/CT, SPECT/CT and 3T MRI for the localisation of occult insulinomas: evaluation of diagnostic accuracy in a prospective crossover imaging study*. *Eur J Nucl Med Mol Imaging*, 2018. **45**(13): p. 2318-2327.
105. Velikyan, I. and O. Eriksson, *Advances in GLP-1 receptor targeting radiolabeled agent development and prospective of theranostics*. *Theranostics*, 2020. **10**(1): p. 437-461.
106. Kiesewetter, D.O., et al., *<sup>18</sup>F-radiolabeled analogs of exendin-4 for PET imaging of GLP-1 in insulinoma*. *European Journal of Nuclear Medicine and Molecular Imaging*, 2012. **39**(3): p. 463-473.
107. Brand, C., et al., *In Vivo Imaging of GLP-1R with a Targeted Bimodal PET/Fluorescence Imaging Agent*. *Bioconjugate Chem.*, 2014. **25**(7): p. 1323-1330.
108. Donnelly, D., *The structure and function of the glucagon-like peptide-1 receptor and its ligands*. *British journal of pharmacology*, 2012. **166**(1): p. 27-41.
109. Willard, F.S., A.B. Bueno, and K.W. Sloop, *Small Molecule Drug Discovery at the Glucagon-Like Peptide-1 Receptor*. *Experimental Diabetes Research*, 2012. **2012**: p. 9.
110. Knudsen, L.B., et al., *Small-molecule agonists for the glucagon-like peptide 1 receptor*. *Proc. Natl. Acad. Sci. U. S. A.*, 2007. **104**(3): p. 937-942.
111. Mapelli, C., et al., *Eleven Amino Acid Glucagon-like Peptide-1 Receptor Agonists with Antidiabetic Activity*. *Journal of Medicinal Chemistry*, 2009. **52**(23): p. 7788-7799.
112. Underwood, C.R., et al., *Crystal Structure of Glucagon-like Peptide-1 in Complex with the Extracellular Domain of the Glucagon-like Peptide-1 Receptor*. *J. Biol. Chem.*, 2010. **285**(Copyright (C) 2017 American Chemical Society (ACS). All Rights Reserved.): p. 723-730.
113. Haque, T.S., et al., *Identification of potent 11mer Glucagon-Like Peptide-1 Receptor agonist peptides with novel C-terminal amino acids: Homohomophenylalanine analogs*. *Peptides*, 2010. **31**(5): p. 950-955.
114. Haque, T.S., et al., *Exploration of structure–activity relationships at the two C-terminal residues of potent 11mer Glucagon-Like Peptide-1 receptor agonist peptides via parallel synthesis*. *Peptides*, 2010. **31**(7): p. 1353-1360.
115. Hoang, H.N., et al., *Short Hydrophobic Peptides with Cyclic Constraints Are Potent Glucagon-like Peptide-1 Receptor (GLP-1R) Agonists*. *Journal of Medicinal Chemistry*, 2015. **58**(9): p. 4080-4085.
116. Swedberg, J.E., et al., *Cyclic alpha-conotoxin peptidomimetic chimeras as potent GLP-1R agonists*. *European Journal of Medicinal Chemistry*, 2015. **103**: p. 175-184.
117. Swedberg, J.E., et al., *Truncated Glucagon-like Peptide-1 and Exendin-4  $\alpha$ -Conotoxin p14a Peptide Chimeras Maintain Potency and  $\alpha$ -Helicity and Reveal Interactions Vital for cAMP Signaling in Vitro*. *Journal of Biological Chemistry*, 2016. **291**(30): p. 15778-15787.
118. Lappchen, T., et al., *Radioiodinated Exendin-4 Is Superior to the Radiometal-Labelled Glucagon-Like Peptide-1 Receptor Probes Overcoming Their High Kidney Uptake*. *PLoS One*, 2017. **12**(1): p. e0170435.
119. Luo, Y., et al., *<sup>68</sup>Ga-NOTA-exendin-4 PET/CT in detection of occult insulinoma and evaluation of physiological uptake*. *Eur J Nucl Med Mol Imaging*, 2015. **42**(3): p. 531-2.

## REFERENCES

120. Gotthardt, M., et al., *A new technique for in vivo imaging of specific GLP-1 binding sites: First results in small rodents*. *Regulatory Peptides*, 2006. **137**(3): p. 162-167.
121. Brom, M., et al., *68Ga-labelled exendin-3, a new agent for the detection of insulinomas with PET*. *European Journal of Nuclear Medicine and Molecular Imaging*, 2010. **37**(7): p. 1345-1355.
122. Vegt, E., et al., *Renal uptake of different radiolabelled peptides is mediated by megalin: SPECT and biodistribution studies in megalin-deficient mice*. *European Journal of Nuclear Medicine and Molecular Imaging*, 2011. **38**(4): p. 623-632.
123. Jodal, A., et al., *Evaluation of <sup>111</sup>In-Labelled Exendin-4 Derivatives Containing Different Meprin  $\beta$ -Specific Cleavable Linkers*. *PLOS ONE*, 2015. **10**(4): p. e0123443.
124. Gotthardt, M., et al., *Indication for Different Mechanisms of Kidney Uptake of Radiolabeled Peptides*. *Journal of Nuclear Medicine*, 2007. **48**(4): p. 596-601.
125. Kiesewetter, D.O., et al., *Evaluation of an [(18)F]AIF-NOTA Analog of Exendin-4 for Imaging of GLP-1 Receptor in Insulinoma*. *Theranostics*, 2012. **2**(10): p. 999-1009.
126. Rolleman, E.J., et al., *Safe and effective inhibition of renal uptake of radiolabelled octreotide by a combination of lysine and arginine*. *European Journal of Nuclear Medicine and Molecular Imaging*, 2003. **30**(1): p. 9-15.
127. Vegt, E., et al., *Albumin-derived peptides efficiently reduce renal uptake of radiolabelled peptides*. *European Journal of Nuclear Medicine and Molecular Imaging*, 2010. **37**(2): p. 226-234.
128. Yim, C.B., et al., *Synthesis and preclinical characterization of [64Cu]NODAGA-MAL-exendin-4 with a N $\epsilon$ -maleoyl-L-lysyl-glycine linkage*. *Nucl Med Biol*, 2013. **40**(8): p. 1006-12.
129. Zhang, M., et al., *Improving the Theranostic Potential of Exendin 4 by Reducing the Renal Radioactivity through Brush Border Membrane Enzyme-Mediated Degradation*. *Bioconjugate Chemistry*, 2019. **30**(6): p. 1745-1753.
130. Mikkola, K., et al., *Low kidney uptake of GLP-1R-targeting, beta cell-specific PET tracer, (18)F-labeled [Nle(14),Lys(40)]exendin-4 analog, shows promise for clinical imaging*. *EJNMMI Res*, 2016. **6**(1): p. 91.
131. Wu, Z., et al., *Development and evaluation of 18F-TTCO-Cys40-Exendin-4: a PET probe for imaging transplanted islets*. *J Nucl Med*, 2013. **54**(2): p. 244-51.
132. Yue, X., et al., *One-Pot Two-Step Radiosynthesis of a New 18F-Labeled Thiol Reactive Prosthetic Group and Its Conjugate for Insulinoma Imaging*. *Molecular Pharmaceutics*, 2014. **11**(11): p. 3875-3884.
133. Boerman, O.C. and M. Gotthardt, *18F-Labelled exendin to image GLP-1 receptor-expressing tissues: from niche to blockbuster?* *European journal of nuclear medicine and molecular imaging*, 2012. **39**(3): p. 461-462.
134. Xu, Q., et al., *Preliminary evaluation of [18F]AIF-NOTA-MAL-Cys39-exendin-4 in insulinoma with PET*. *J Drug Target*, 2015. **23**(9): p. 813-20.
135. Dialer, L.O., et al., *Radiosynthesis and evaluation of an 18F-labeled silicon containing exendin-4 peptide as a PET probe for imaging insulinoma*. *EJNMMI Radiopharmacy and Chemistry*, 2018. **3**(1): p. 1.

## REFERENCES

136. Weineisen, M., et al., *68Ga- and 177Lu-Labeled PSMA I&T: Optimization of a PSMA-Targeted Theranostic Concept and First Proof-of-Concept Human Studies*. J Nucl Med, 2015. **56**(8): p. 1169-76.
137. Ellero, C., et al., *Prophylactic use of anti-emetic medications reduced nausea and vomiting associated with exenatide treatment: a retrospective analysis of an open-label, parallel-group, single-dose study in healthy subjects*. Diabetic medicine : a journal of the British Diabetic Association, 2010. **27**(10): p. 1168-1173.
138. Wessmann, S.H., G. Henriksen, and H.J. Wester, *Cryptate mediated nucleophilic 18F-fluorination without azeotropic drying*. Nuklearmedizin, 2012. **51**(1): p. 1-8.
139. Jacobson, O., D.O. Kiesewetter, and X. Chen, *Fluorine-18 radiochemistry, labeling strategies and synthetic routes*. Bioconjugate chemistry, 2015. **26**(1): p. 1-18.
140. Wurzer, A., et al., *Radiohybrid Ligands: A Novel Tracer Concept Exemplified by 18F- or 68Ga-Labeled rhPSMA Inhibitors*. Journal of Nuclear Medicine, 2020. **61**(5): p. 735-742.
141. Ghosh, A. and W.D.W. Heston, *Tumor target prostate specific membrane antigen (PSMA) and its regulation in prostate cancer*. J. Cell. Biochem., 2004. **91**(3): p. 528-539.
142. Barinka, C., et al., *Glutamate Carboxypeptidase II in Diagnosis and Treatment of Neurologic Disorders and Prostate Cancer*. Current Medicinal Chemistry, 2012. **19**(6): p. 856-870.
143. Davis, M.I., et al., *Crystal structure of prostate-specific membrane antigen, a tumor marker and peptidase*. Proc. Natl. Acad. Sci. U. S. A., 2005. **102**(17): p. 5981-5986.
144. Chang, S.S., et al., *Five different anti-prostate-specific membrane antigen (PSMA) antibodies confirm PSMA expression in tumor-associated neovasculature*. Cancer Res, 1999. **59**(13): p. 3192-8.
145. Silver, D.A., et al., *Prostate-specific membrane antigen expression in normal and malignant human tissues*. Clin Cancer Res, 1997. **3**(Copyright (C) 2015 U.S. National Library of Medicine.): p. 81-5.
146. Sácha, P., et al., *Expression of glutamate carboxypeptidase II in human brain*. Neuroscience, 2007. **144**(4): p. 1361-72.
147. Berger, U.V., et al., *N-acetylated alpha-linked acidic dipeptidase is expressed by non-myelinating Schwann cells in the peripheral nervous system*. J Neurocytol, 1995. **24**(2): p. 99-109.
148. Byun, Y., et al., *Recent Development of Diagnostic and Therapeutic Agents Targeting Glutamate Carboxypeptidase II (GCP II), in Drug Design of Zinc-Enzyme Inhibitors*. 2009, John Wiley & Sons, Inc. p. 881-910.
149. Navratil, M., et al., *Structural and biochemical characterization of the folyl-poly-γ-L-glutamate hydrolyzing activity of human glutamate carboxypeptidase II*. FEBS J., 2014. **281**(14): p. 3228-3242.
150. Israeli, R.S., et al., *Expression of the Prostate-specific Membrane Antigen*. Cancer Research, 1994. **54**(7): p. 1807-1811.

## REFERENCES

151. Troyer, J.K., M.L. Beckett, and G.L. Wright Jr., *Detection and characterization of the prostate-specific membrane antigen (PSMA) in tissue extracts and body fluids*. International Journal of Cancer, 1995. **62**(5): p. 552-558.
152. Troyer, J.K., et al., *Biochemical characterization and mapping of the 7E11-C5.3 epitope of the prostate-specific membrane antigen*. Urologic Oncology: Seminars and Original Investigations, 1995. **1**(1): p. 29-37.
153. Rajasekaran, A.K., G. Anilkumar, and J.J. Christiansen, *Is prostate-specific membrane antigen a multifunctional protein?* Am. J. Physiol., 2005. **288**(5, Pt. 1): p. C975-C981.
154. Mesters, J.R., et al., *Structure of glutamate carboxypeptidase II, a drug target in neuronal damage and prostate cancer*. The EMBO Journal, 2006. **25**(6): p. 1375-1384.
155. Barinka, C., et al., *Identification of the N-glycosylation sites on glutamate carboxypeptidase II necessary for proteolytic activity*. Protein Science : A Publication of the Protein Society, 2004. **13**(6): p. 1627-1635.
156. Ghosh, A. and W.D.W. Heston, *Effect of carbohydrate moieties on the folate hydrolysis activity of the prostate specific membrane antigen*. The Prostate, 2003. **57**(2): p. 140-151.
157. Holmes, E.H., et al., *Analysis of glycosylation of prostate-specific membrane antigen derived from LNCaP cells, prostatic carcinoma tumors, and serum from prostate cancer patients*. The Prostate, 1996. **29**(S7): p. 25-29.
158. Schulke, N., et al., *The homodimer of prostate-specific membrane antigen is a functional target for cancer therapy*. Proc Natl Acad Sci U S A, 2003. **100**(22): p. 12590-5.
159. Barinka, C., et al., *Structural Insight into the Pharmacophore Pocket of Human Glutamate Carboxypeptidase II*. J. Med. Chem., 2007. **50**(14): p. 3267-3273.
160. Ferraris, D.V., K. Shukla, and T. Tsukamoto, *Structure-activity relationships of glutamate carboxypeptidase II (GCPII) inhibitors*. Curr. Med. Chem., 2012. **19**(9): p. 1282-1294.
161. Barinka, C., et al., *Structural Basis of Interactions between Human Glutamate Carboxypeptidase II and Its Substrate Analogs*. J. Mol. Biol., 2008. **376**(Copyright (C) 2016 American Chemical Society (ACS). All Rights Reserved.): p. 1438-1450.
162. Barinka, C., et al., *Interactions between Human Glutamate Carboxypeptidase II and Urea-Based Inhibitors: Structural Characterization*. Journal of Medicinal Chemistry, 2008. **51**(24): p. 7737-7743.
163. Pavlicek, J., J. Ptacek, and C. Barinka, *Glutamate carboxypeptidase II: an overview of structural studies and their importance for structure-based drug design and deciphering the reaction mechanism of the enzyme*. Curr. Med. Chem., 2012. **19**(9): p. 1300-1309.
164. Zhang, A.X., et al., *A Remote Arene-Binding Site on Prostate Specific Membrane Antigen Revealed by Antibody-Recruiting Small Molecules*. J. Am. Chem. Soc., 2010. **132**(36): p. 12711-12716.
165. Ganguly, T., et al., *A high-affinity [18 F]-labeled phosphoramidate peptidomimetic PSMA-targeted inhibitor for PET imaging of prostate cancer*. Nuclear Medicine and Biology, 2015. **42**(10): p. 780-787.

## REFERENCES

166. Nakajima, R., et al., *2-Amino adipic Acid-C(O)-Glutamate Based Prostate-Specific Membrane Antigen Ligands for Potential Use as Theranostics*. ACS Med. Chem. Lett., 2018. **9**(11): p. 1099-1104.
167. Kopka, K., et al., *Glu-Ureido-Based Inhibitors of Prostate-Specific Membrane Antigen: Lessons Learned During the Development of a Novel Class of Low-Molecular-Weight Theranostic Radiotracers*. J Nucl Med, 2017. **58**(Suppl 2): p. 17s-26s.
168. Carter, r.E., A.R. Feldman, and J.T. Coyle, *Prostate-specific membrane antigen is a hydrolase with substrate and pharmacologic characteristics of a neuropeptidase*. Proc. Natl. Acad. Sci. U. S. A., 1996. **93**(Copyright (C) 2015 American Chemical Society (ACS). All Rights Reserved.): p. 749-53.
169. Pinto, J.T., et al., *Prostate-specific membrane antigen: a novel folate hydrolase in human prostatic carcinoma cells*. Clin Cancer Res, 1996. **2**(9): p. 1445-51.
170. Evans, J.C., et al., *The therapeutic and diagnostic potential of the prostate specific membrane antigen/glutamate carboxypeptidase II (PSMA/GCPII) in cancer and neurological disease*. British Journal of Pharmacology, 2016. **173**(21): p. 3041-3079.
171. Rajasekaran, S.A., et al., *A Novel Cytoplasmic Tail MXXXL Motif Mediates the Internalization of Prostate-specific Membrane Antigen*. Molecular Biology of the Cell, 2003. **14**(12): p. 4835-4845.
172. Barwe, S.P., et al., *Preferential association of prostate cancer cells expressing prostate specific membrane antigen to bone marrow matrix*. Int. J. Oncol., 2007. **30**(4): p. 899-904.
173. Kaittani, C., et al., *Prostate-specific membrane antigen cleavage of vitamin B9 stimulates oncogenic signaling through metabotropic glutamate receptors*. The Journal of experimental medicine, 2018. **215**(1): p. 159-175.
174. Liu, H., et al., *Constitutive and Antibody-induced Internalization of Prostate-specific Membrane Antigen*. Cancer Research, 1998. **58**(18): p. 4055-4060.
175. Goodman, O.B., Jr., et al., *Interaction of prostate specific membrane antigen with clathrin and the adaptor protein complex-2*. Int J Oncol, 2007. **31**(5): p. 1199-203.
176. Anilkumar, G., et al., *Prostate-specific membrane antigen association with filamin A modulates its internalization and NAALADase activity*. Cancer Res, 2003. **63**(10): p. 2645-8.
177. Wright, G.L., Jr., et al., *Upregulation of prostate-specific membrane antigen after androgen-deprivation therapy*. Urology, 1996. **48**(2): p. 326-34.
178. Vaz, S., et al., *Influence of androgen deprivation therapy on PSMA expression and PSMA-ligand PET imaging of prostate cancer patients*. European Journal of Nuclear Medicine and Molecular Imaging, 2020. **47**(1): p. 9-15.
179. Eiber, M., et al., *Prostate-Specific Membrane Antigen Ligands for Imaging and Therapy*. Journal of Nuclear Medicine, 2017. **58**(Supplement 2): p. 67S-76S.
180. Bakht, M.K., et al., *Influence of Androgen Deprivation Therapy on the Uptake of PSMA-Targeted Agents: Emerging Opportunities and Challenges*. Nuclear Medicine and Molecular Imaging, 2017. **51**(3): p. 202-211.

## REFERENCES

181. Ghosh, A. and W.D.W. Heston, *Understanding Prostate-Specific Membrane Antigen and Its Implication in Prostate Cancer*, in *The Oncogenomics Handbook*, W.J. LaRochelle and R.A. Shimkets, Editors. 2005, Humana Press: Totowa, NJ. p. 597-615.
182. William K. Oh, M.H., Anthony V. D'Amico, et al., *Biology of Prostate Cancer*, in *Holland-Frei Cancer Medicine*, P.R. Kufe DW, Weichselbaum RR, et al., Editor. 2003, Hamilton (ON): BC Decker.
183. Ferlay, J., et al., *Estimating the global cancer incidence and mortality in 2018: GLOBOCAN sources and methods*. International Journal of Cancer, 2019. **144**(8): p. 1941-1953.
184. Ferlay, J., et al., *Cancer incidence and mortality worldwide: sources, methods and major patterns in GLOBOCAN 2012*. Int J Cancer, 2015. **136**(5): p. E359-86.
185. Denmeade, S.R. and J.T. Isaacs, *A history of prostate cancer treatment*. Nature Reviews Cancer, 2002. **2**(5): p. 389-396.
186. Gutman, A.B. and E.B. Gutman, *An "acid" phosphatase occurring in the serum of patients with metastasizing carcinoma of the prostate gland*. J. Clin. Invest., 1938. **17**: p. 473-8.
187. Papsidero, L.D., et al., *A prostate antigen in sera of prostatic cancer patients*. Cancer Res, 1980. **40**(7): p. 2428-32.
188. Horoszewicz, J.S., E. Kawinski, and G.P. Murphy, *Monoclonal antibodies to a new antigenic marker in epithelial prostatic cells and serum of prostatic cancer patients*. Anticancer Res, 1987. **7**(5B): p. 927-35.
189. Bouchelouche, K., P.L. Choyke, and J. Capala, *Prostate Specific Membrane Antigen—A Target for Imaging and Therapy with Radionuclides*. Discovery medicine, 2010. **9**(44): p. 55-61.
190. Cimadamore, A., et al., *New Prostate Cancer Targets for Diagnosis, Imaging, and Therapy: Focus on Prostate-Specific Membrane Antigen*. Front Oncol, 2018. **8**: p. 653.
191. Chang, S.S., *Overview of Prostate-Specific Membrane Antigen*. Reviews in Urology, 2004. **6**(Suppl 10): p. S13-S18.
192. Tewari, A.K., *Prostate Cancer: A Comprehensive Perspective*. 2013: Springer London.
193. Wieser, G., et al., *Positron emission tomography (PET) imaging of prostate cancer with a gastrin releasing peptide receptor antagonist - from mice to men*. Theranostics, 2014. **4**(4): p. 412-419.
194. Hricak, H., et al., *Imaging Prostate Cancer: A Multidisciplinary Perspective*. Radiology, 2007. **243**(1): p. 28-53.
195. Kiess, A.P., et al., *Prostate-specific membrane antigen as a target for cancer imaging and therapy*. Q J Nucl Med Mol Imaging, 2015. **59**(3): p. 241-68.
196. Picchio, M., et al., *The role of choline positron emission tomography/computed tomography in the management of patients with prostate-specific antigen progression after radical treatment of prostate cancer*. Eur Urol, 2011. **59**(1): p. 51-60.
197. Souvatzoglou, M., et al., *The Sensitivity of [11C]Choline PET/CT to Localize Prostate Cancer Depends on the Tumor Configuration*. Clinical Cancer Research, 2011. **17**(11): p. 3751-3759.
198. Picchio, M., et al., *PET-CT for treatment planning in prostate cancer*. Q J Nucl Med Mol Imaging, 2009. **53**(2): p. 245-68.

## REFERENCES

199. Weineisen, M., et al., *Synthesis and preclinical evaluation of DOTAGA-conjugated PSMA ligands for functional imaging and endoradiotherapy of prostate cancer*. EJNMMI Research, 2014. **4**(1): p. 63.
200. Ross, J.S., et al., *Correlation of Primary Tumor Prostate-Specific Membrane Antigen Expression with Disease Recurrence in Prostate Cancer*. Clinical Cancer Research, 2003. **9**(17): p. 6357-6362.
201. Chang, S.S., N.H. Bander, and W.D. Heston, *Monoclonal antibodies: will they become an integral part of the evaluation and treatment of prostate cancer--focus on prostate-specific membrane antigen? Curr Opin Urol*, 1999. **9**(5): p. 391-5.
202. Zhou, J., et al., *NAAG peptidase inhibitors and their potential for diagnosis and therapy*. Nat Rev Drug Discov, 2005. **4**(12): p. 1015-1026.
203. Akhtar, N.H., et al., *Prostate-specific membrane antigen-based therapeutics*. Adv Urol, 2012. **2012**: p. 973820.
204. Pan, M.-H., et al., *Biodistributions of (177)Lu- and (111)In- labeled 7E11 Antibodies to Prostate-Specific Membrane Antigen in Xenograft Model of Prostate Cancer and Potential Use of (111)In-7E11 as a Pretherapeutic Agent for (177)Lu-7E11 Radioimmunotherapy*. Molecular imaging and biology : MIB : the official publication of the Academy of Molecular Imaging, 2009. **11**(3): p. 159-166.
205. Liu, H., et al., *Monoclonal Antibodies to the Extracellular Domain of Prostate-specific Membrane Antigen Also React with Tumor Vascular Endothelium*. Cancer Research, 1997. **57**(17): p. 3629-3634.
206. Niaz, M.O., et al., *Review of Lutetium-177-labeled Anti-prostate-specific Membrane Antigen Monoclonal Antibody J591 for the Treatment of Metastatic Castration-resistant Prostate Cancer*. Cureus, 2020. **12**(2): p. e7107.
207. Rizvi, T., C. Deng, and P.K. Rehm, *Indium-111 Capromab Pendetide (ProstaScint(®)) Demonstrates Renal Cell Carcinoma and Aortocaval Nodal Metastases from Prostate Adenocarcinoma*. World J Nucl Med, 2015. **14**(3): p. 209-11.
208. Bickel, U., *Antibody delivery through the blood-brain barrier*. Advanced Drug Delivery Reviews, 1995. **15**(1-3): p. 53-72.
209. Barrett, J.A., et al., *First-in-Man Evaluation of 2 High-Affinity PSMA-Avid Small Molecules for Imaging Prostate Cancer*. Journal of Nuclear Medicine, 2013. **54**(3): p. 380-387.
210. Foss, C.A., et al., *Radiolabeled Small-Molecule Ligands for Prostate-Specific Membrane Antigen: In vivo Imaging in Experimental Models of Prostate Cancer*. Clin. Cancer Res., 2005. **11**(11): p. 4022-4028.
211. Bander, N.H., et al., *Phase I Trial of 177Lutetium-Labeled J591, a Monoclonal Antibody to Prostate-Specific Membrane Antigen, in Patients With Androgen-Independent Prostate Cancer*. Journal of Clinical Oncology, 2005. **23**(21): p. 4591-4601.
212. Herrmann, K., et al., *Biodistribution and radiation dosimetry for a probe targeting prostate-specific membrane antigen for imaging and therapy*. J. Nucl. Med., 2015. **56**(6): p. 855-861.

## REFERENCES

213. Schottelius, M., et al., (111)In]PSMA-I&T: expanding the spectrum of PSMA-I&T applications towards SPECT and radioguided surgery. *EJNMMI Res*, 2015. **5**(1): p. 68.
214. Jackson, P.F., et al., *Design, synthesis, and biological activity of a potent inhibitor of the neuropeptidase N-acetylated alpha-linked acidic dipeptidase*. *J Med Chem*, 1996. **39**(Copyright (C) 2015 U.S. National Library of Medicine.): p. 619-22.
215. Jackson, P.F., et al., *Design and Pharmacological Activity of Phosphinic Acid Based NAALADase Inhibitors*. *Journal of Medicinal Chemistry*, 2001. **44**(24): p. 4170-4175.
216. Machulkin, A.E., et al., *Small-molecule PSMA ligands. Current state, SAR and perspectives*. *Journal of Drug Targeting*, 2016: p. 1-15.
217. Majer, P., et al., *Synthesis and Biological Evaluation of Thiol-Based Inhibitors of Glutamate Carboxypeptidase II: Discovery of an Orally Active GCP II Inhibitor*. *Journal of Medicinal Chemistry*, 2003. **46**(10): p. 1989-1996.
218. Stoermer, D., et al., *Design, Synthesis, and Pharmacological Evaluation of Glutamate Carboxypeptidase II (GCP II) Inhibitors Based on Thioalkylbenzoic Acid Scaffolds*. *J. Med. Chem.*, 2012. **55**(Copyright (C) 2015 American Chemical Society (ACS). All Rights Reserved.): p. 5922-5932.
219. Stoermer, D., et al., *Synthesis and biological evaluation of hydroxamate-Based inhibitors of glutamate carboxypeptidase II*. *Bioorganic & Medicinal Chemistry Letters*, 2003. **13**(13): p. 2097-2100.
220. Blank, B.R., et al., *N-substituted glutamyl sulfonamides as inhibitors of glutamate carboxypeptidase II (GCP2)*. *Chem. Biol. Drug Des.*, 2011. **77**(4): p. 241-247.
221. Nan, F., et al., *Dual Function Glutamate-Related Ligands: Discovery of a Novel, Potent Inhibitor of Glutamate Carboxypeptidase II Possessing mGluR3 Agonist Activity*. *J. Med. Chem.*, 2000. **43**(5): p. 772-774.
222. Kozikowski, A.P., et al., *Synthesis of Urea-Based Inhibitors as Active Site Probes of Glutamate Carboxypeptidase II: Efficacy as Analgesic Agents*. *Journal of Medicinal Chemistry*, 2004. **47**(7): p. 1729-1738.
223. Maresca, K.P., et al., *A Series of Halogenated Heterodimeric Inhibitors of Prostate Specific Membrane Antigen (PSMA) as Radiolabeled Probes for Targeting Prostate Cancer*. *Journal of Medicinal Chemistry*, 2009. **52**(2): p. 347-357.
224. Hillier, S.M., et al., *Preclinical Evaluation of Novel Glutamate-Urea-Lysine Analogues That Target Prostate-Specific Membrane Antigen as Molecular Imaging Pharmaceuticals for Prostate Cancer*. *Cancer Research*, 2009. **69**(17): p. 6932-6940.
225. Mease, R.C., et al., *N-[N-[(S)-1,3-Dicarboxypropyl]Carbamoyl]-4-[18F]Fluorobenzyl-L-Cysteine, [18F]DCFBC: A New Imaging Probe for Prostate Cancer*. *Clin. Cancer Res.*, 2008. **14**(10): p. 3036-3043.
226. Chen, Y., et al., *Radiohalogenated Prostate-Specific Membrane Antigen (PSMA)-Based Ureas as Imaging Agents for Prostate Cancer*. *Journal of medicinal chemistry*, 2008. **51**(24): p. 7933-7943.

## REFERENCES

227. Zechmann, C.M., et al., *Radiation dosimetry and first therapy results with a <sup>124</sup>I/<sup>131</sup>I-labeled small molecule (MIP-1095) targeting PSMA for prostate cancer therapy*. Eur. J. Nucl. Med. Mol. Imaging, 2014. **41**(7): p. 1280-1292.
228. Hillier, S.M., et al., *<sup>99m</sup>Tc-Labeled Small-Molecule Inhibitors of Prostate-Specific Membrane Antigen for Molecular Imaging of Prostate Cancer*. Journal of Nuclear Medicine, 2013. **54**(8): p. 1369-1376.
229. Eder, M., et al., *<sup>68</sup>Ga-Complex Lipophilicity and the Targeting Property of a Urea-Based PSMA Inhibitor for PET Imaging*. Bioconjugate Chemistry, 2012. **23**(4): p. 688-697.
230. Giesel, F.L., et al., *<sup>18</sup>F-Labelled PSMA-1007 shows similarity in structure, biodistribution and tumour uptake to the theragnostic compound PSMA-617*. European Journal of Nuclear Medicine and Molecular Imaging, 2016. **43**(10): p. 1929-1930.
231. Kratochwil, C., et al., *<sup>225</sup>Ac-PSMA-617 for PSMA-Targeted  $\alpha$ -Radiation Therapy of Metastatic Castration-Resistant Prostate Cancer*. Journal of Nuclear Medicine, 2016. **57**(12): p. 1941-1944.
232. Wurzer, A., et al., *Preclinical comparison of four [<sup>18</sup>F, natGa]rhPSMA-7 isomers: influence of the stereoconfiguration on pharmacokinetics*. EJNMMI Research, 2020. **10**(1): p. 149.
233. Behr, S.C., et al., *Phase I Study of CTT1057, an <sup>18</sup>F-Labeled Imaging Agent with Phosphoramidate Core Targeting Prostate-Specific Membrane Antigen in Prostate Cancer*. Journal of Nuclear Medicine, 2019. **60**(7): p. 910-916.
234. Dannoon, S., et al., *Structure–Activity Relationship of <sup>18</sup>F-Labeled Phosphoramidate Peptidomimetic Prostate-Specific Membrane Antigen (PSMA)-Targeted Inhibitor Analogues for PET Imaging of Prostate Cancer*. Journal of Medicinal Chemistry, 2016. **59**(12): p. 5684-5694.
235. Novakova, Z., et al., *Design of composite inhibitors targeting glutamate carboxypeptidase II: the importance of effector functionalities*. FEBS J., 2016. **283**(1): p. 130-143.
236. Liu, T., et al., *Pseudoirreversible inhibition of prostate-specific membrane antigen by phosphoramidate peptidomimetics*. Biochemistry, 2008. **47**(48): p. 12658-60.
237. Tsukamoto, T., et al., *Enantiospecificity of Glutamate Carboxypeptidase II Inhibition*. Journal of Medicinal Chemistry, 2005. **48**(7): p. 2319-2324.
238. Barinka, C., et al., *Structural and computational basis for potent inhibition of glutamate carboxypeptidase II by carbamate-based inhibitors*. Bioorg. Med. Chem., 2019. **27**(2): p. 255-264.
239. <https://clinicaltrials.gov/ct2/results?cond=Prostate+Cancer&term=psma&cntry=&state=&city=&dist=&Search=Search>. Accessed on June 12, 2021.
240. Tateishi, U., *Prostate-specific membrane antigen (PSMA)–ligand positron emission tomography and radioligand therapy (RLT) of prostate cancer*. Japanese Journal of Clinical Oncology, 2020. **50**(4): p. 349-356.
241. Giesel, F.L., et al., *Intraindividual Comparison of <sup>18</sup>F-PSMA-1007 and <sup>18</sup>F-DCFPyL PET/CT in the Prospective Evaluation of Patients with Newly Diagnosed Prostate Carcinoma: A Pilot Study*. Journal of Nuclear Medicine, 2018. **59**(7): p. 1076-1080.

## REFERENCES

242. Afshar-Oromieh, A., et al., *The diagnostic value of PET/CT imaging with the (68)Ga-labelled PSMA ligand HBED-CC in the diagnosis of recurrent prostate cancer*. European journal of nuclear medicine and molecular imaging, 2015. **42**(2): p. 197-209.
243. Vallabhajosula, S., et al., *99mTc-Labeled Small-Molecule Inhibitors of Prostate-Specific Membrane Antigen: Pharmacokinetics and Biodistribution Studies in Healthy Subjects and Patients with Metastatic Prostate Cancer*. Journal of Nuclear Medicine, 2014. **55**(11): p. 1791-1798.
244. Robu, S., et al., *Preclinical Evaluation and First Patient Application of 99mTc-PSMA-I&S for SPECT Imaging and Radioguided Surgery in Prostate Cancer*. Journal of Nuclear Medicine, 2017. **58**(2): p. 235-242.
245. Zhou, Y., et al., *64Cu-based Radiopharmaceuticals in Molecular Imaging*. Technol. Cancer Res. Treat., 2019. **18**: p. 1533033819830758.
246. Eppard, E., et al., *Clinical Translation and First In-Human Use of [(44)Sc]Sc-PSMA-617 for PET Imaging of Metastasized Castrate-Resistant Prostate Cancer*. Theranostics, 2017. **7**(18): p. 4359-4369.
247. Wüstemann, T., et al., *Targeting prostate cancer: Prostate-specific membrane antigen based diagnosis and therapy*. Medicinal Research Reviews, 2019. **39**(1): p. 40-69.
248. Lawal, I.O., et al., *Prostate-specific membrane antigen-targeted endoradiotherapy in metastatic prostate cancer*. Curr Opin Urol, 2020. **30**(1): p. 98-105.
249. Schottelius, M., et al., *Synthesis and Preclinical Characterization of the PSMA-Targeted Hybrid Tracer PSMA-I&F for Nuclear and Fluorescence Imaging of Prostate Cancer*. Journal of Nuclear Medicine, 2019. **60**(1): p. 71-78.
250. Benešová, M., et al., *Preclinical Evaluation of a Tailor-Made DOTA-Conjugated PSMA Inhibitor with Optimized Linker Moiety for Imaging and Endoradiotherapy of Prostate Cancer*. Journal of Nuclear Medicine, 2015. **56**(6): p. 914-920.
251. Wang, H., et al., *Bioisosterism of urea-based GCPII inhibitors: Synthesis and structure–activity relationship studies*. Bioorganic & Medicinal Chemistry Letters, 2010. **20**(1): p. 392-397.
252. Plechanovova, A., et al., *Novel Substrate-Based Inhibitors of Human Glutamate Carboxypeptidase II with Enhanced Lipophilicity*. J. Med. Chem., 2011. **54**(21): p. 7535-7546.
253. Barinka, C., et al., *Substrate specificity, inhibition and enzymological analysis of recombinant human glutamate carboxypeptidase II*. J. Neurochem., 2002. **80**(3): p. 477-487.
254. Mhaka, A., et al., *Use of methotrexate-based peptide substrates to characterize the substrate specificity of prostate-specific membrane antigen (PSMA)*. Cancer Biol. Ther., 2004. **3**(6): p. 551-558.
255. Denmeade, S.R., et al., *Engineering a prostate-specific membrane antigen-activated tumor endothelial cell prodrug for cancer therapy*. Sci. Transl. Med., 2012. **4**(140): p. 140ra86, 13 pp.
256. Ristau, B.T., D.J. Bacich, and D.S. O'Keefe, *The prostate-specific membrane antigen: lessons and current clinical implications from 20 years of research*. Urol Oncol, 2014. **32**(3): p. 272-9.
257. Damber, J.E. and G. Aus, *Prostate cancer*. Lancet, 2008. **371**(9625): p. 1710-21.

## REFERENCES

258. Zhao, F., et al., *Sites of synchronous distant metastases and prognosis in prostate cancer patients with bone metastases at initial diagnosis: a population-based study of 16,643 patients*. *Clinical and translational medicine*, 2019. **8**(1): p. 30-30.
259. Tsao, C.-K. and W.K. Oh, *First-Line Treatment of Hormone-Sensitive Metastatic Prostate Cancer: Is There a Single Standard of Care?* *Journal of Clinical Oncology*, 2018. **36**(11): p. 1060-1061.
260. Kirby, M., C. Hirst, and E.D. Crawford, *Characterising the castration-resistant prostate cancer population: a systematic review*. *International Journal of Clinical Practice*, 2011. **65**(11): p. 1180-1192.
261. Zustovich, F. and R. Barsanti, *Targeted  $\alpha$  Therapies for the Treatment of Bone Metastases*. *International journal of molecular sciences*, 2017. **19**(1): p. 74.
262. Sartor, O. and D. Sharma, *Radium and other alpha emitters in prostate cancer*. *Transl Androl Urol*, 2018. **7**(3): p. 436-444.
263. Kulkarni, H.R., et al., *PSMA-Based Radioligand Therapy for Metastatic Castration-Resistant Prostate Cancer: The Bad Berka Experience Since 2013*. *Journal of Nuclear Medicine*, 2016. **57**(Supplement 3): p. 97S-104S.
264. Kulkarni, H., et al., *First clinical results with Lu-177 PSMA-TUM1 for the treatment of castrate-resistant metastatic prostate cancer*. *Journal of Nuclear Medicine*, 2014. **55**(supplement 1): p. 10-10.
265. Kratochwil, C., et al., *PSMA-Targeted Radionuclide Therapy of Metastatic Castration-Resistant Prostate Cancer with  $^{177}\text{Lu}$ -Labeled PSMA-617*. *Journal of Nuclear Medicine*, 2016. **57**(8): p. 1170-1176.
266. Rahbar, K., et al., *German Multicenter Study Investigating  $^{177}\text{Lu}$ -PSMA-617 Radioligand Therapy in Advanced Prostate Cancer Patients*. *Journal of Nuclear Medicine*, 2017. **58**(1): p. 85-90.
267. Chakravarty, R., et al., *Targeted  $\alpha$ -therapy of prostate cancer using radiolabeled PSMA inhibitors: a game changer in nuclear medicine*. *American journal of nuclear medicine and molecular imaging*, 2018. **8**(4): p. 247-267.
268. Morgenstern, A., et al., *An Overview of Targeted Alpha Therapy with  $^{225}\text{Ac}$  and  $^{213}\text{Bi}$* . *Current radiopharmaceuticals*, 2018. **11**(3): p. 200-208.
269. Sgouros, G., *Alpha-particles for targeted therapy*. *Advanced Drug Delivery Reviews*, 2008. **60**(12): p. 1402-1406.
270. Tönnemann, R., et al.,  *$^{177}\text{Lu}$ -PSMA-617 Salivary Gland Uptake Characterized by Quantitative In Vitro Autoradiography*. *Pharmaceuticals (Basel, Switzerland)*, 2019. **12**(1): p. 18.
271. Kratochwil, C., et al., *Targeted  $\alpha$ -Therapy of Metastatic Castration-Resistant Prostate Cancer with  $^{225}\text{Ac}$ -PSMA-617: Dosimetry Estimate and Empiric Dose Finding*. *Journal of Nuclear Medicine*, 2017. **58**(10): p. 1624-1631.
272. Hohberg, M., et al., *Lacrimal Glands May Represent Organs at Risk for Radionuclide Therapy of Prostate Cancer with  $^{177}\text{Lu}$ -PSMA-617*. *Molecular Imaging and Biology*, 2016. **18**(3): p. 437-445.

## REFERENCES

273. Oh, S.W., et al., *Quantitative and qualitative analysis of biodistribution and PET image quality of novel radiohybrid PSMA ligand, 18F- rhPSMA-7, in patients with prostate cancer*. Journal of Nuclear Medicine, 2019. **60**(supplement 1): p. 1557.
274. Kratochwil, C., et al., *Targeted  $\alpha$ -Therapy of Metastatic Castration-Resistant Prostate Cancer with 225Ac-PSMA-617: Swimmer-Plot Analysis Suggests Efficacy Regarding Duration of Tumor Control*. Journal of Nuclear Medicine, 2018. **59**(5): p. 795-802.
275. Rupp, N.J., et al., *First clinicopathologic evidence of a non-PSMA-related uptake mechanism for 68Ga-PSMA-11 in salivary glands*. J. Nucl. Med., 2019. **60**(9): p. 1270-1276.
276. van Kalmthout, L., et al., *First Experience With 177Lu-PSMA-617 Therapy for Advanced Prostate Cancer in the Netherlands*. Clinical Nuclear Medicine, 2019. **44**(6): p. 446-451.
277. O'Keefe, D.S., D.J. Bacich, and W.D.W. Heston, *Comparative analysis of prostate-specific membrane antigen (PSMA) versus a prostate-specific membrane antigen-like gene*. The Prostate, 2004. **58**(2): p. 200-210.
278. Lopes, A.D., et al., *Immunohistochemical and Pharmacokinetic Characterization of the Site-specific Immunoconjugate CYT-356 Derived from Antiprostate Monoclonal Antibody 7E11-C5*. Cancer Research, 1990. **50**(19): p. 6423-6429.
279. Maurer, T., et al., *Current use of PSMA-PET in prostate cancer management*. Nature Reviews Urology, 2016. **13**(4): p. 226-235.
280. Tagawa, S.T., et al., *Phase II Study of Lutetium-177-Labeled Anti-Prostate-Specific Membrane Antigen Monoclonal Antibody J591 for Metastatic Castration-Resistant Prostate Cancer*. Clinical Cancer Research, 2013. **19**(18): p. 5182-5191.
281. Rousseau, E., et al., *Monosodium Glutamate Reduces 68Ga-PSMA-11 Uptake in Salivary Glands and Kidneys in a Preclinical Prostate Cancer Model*. Journal of Nuclear Medicine, 2018. **59**(12): p. 1865-1868.
282. Baum, R.P., et al., *Injection of Botulinum Toxin for Preventing Salivary Gland Toxicity after PSMA Radioligand Therapy: an Empirical Proof of a Promising Concept*. Nuclear medicine and molecular imaging, 2018. **52**(1): p. 80-81.
283. van Kalmthout, L.W.M., et al., *Impact of external cooling with icepacks on (68)Ga-PSMA uptake in salivary glands*. EJNMMI research, 2018. **8**(1): p. 56-56.
284. Rathke, H., et al., *Initial clinical experience performing sialendoscopy for salivary gland protection in patients undergoing 225Ac-PSMA-617 RLT*. European Journal of Nuclear Medicine and Molecular Imaging, 2019. **46**(1): p. 139-147.
285. Yilmaz, B., et al., *Effect of External Cooling on 177Lu-PSMA Uptake by the Parotid Glands*. Journal of Nuclear Medicine, 2019. **60**(10): p. 1388-1393.
286. Patani, G.A. and E.J. LaVoie, *Bioisosterism: A Rational Approach in Drug Design*. Chemical Reviews, 1996. **96**(8): p. 3147-3176.
287. Knedlik, T., et al., *Mouse glutamate carboxypeptidase II (GCPII) has a similar enzyme activity and inhibition profile but a different tissue distribution to human GCPII*. FEBS Open Bio, 2017. **7**(9): p. 1362-1378.

## REFERENCES

288. Roy, J., et al., *Comparison of Prostate-Specific Membrane Antigen Expression Levels in Human Salivary Glands to Non-Human Primates and Rodents*. *Cancer Biotherapy and Radiopharmaceuticals*, 2020. **35**(4): p. 284-291.
289. Wurzer, A.J., H.-J. Wester, and M.J. Eiber, *Preparation of peptides as dual mode radiotracers and therapeutics*. 2019, Technische Universitaet Muenchen, Germany; Technische Universitaet Muenchen - Klinikum Rechts der Isar . p. 134pp.
290. Yusufi, N., et al., *Comparative preclinical biodistribution, dosimetry and endoradiotherapy in mCRPC using 19F/177Lu-rhPSMA-7.3 and 177Lu-PSMA I&T*. *Journal of Nuclear Medicine*, 2020: p. jnumed.120.254516.
291. Clark, J.S. and Y.-S. Wong, *Construction of the 11-oxabicyclo[6.2.1]undecane core of the cladiellins by a novel rearrangement reaction*. *Chemical Communications*, 2000(12): p. 1079-1080.
292. Ravid, U., R.M. Silverstein, and L.R. Smith, *Synthesis of the enantiomers of 4-substituted  $\gamma$ -lactones with known absolute configuration*. *Tetrahedron*, 1978. **34**(10): p. 1449-52.
293. Yang, X., et al., *[18F]Fluorobenzoyllysinepentanedioic Acid Carbamates: New Scaffolds for Positron Emission Tomography (PET) Imaging of Prostate-Specific Membrane Antigen (PSMA)*. *Journal of Medicinal Chemistry*, 2016. **59**(1): p. 206-218.
294. Zhang, D.-W., et al.,  *$\alpha$  N-O turn induced by fluorinated  $\alpha$ -aminoxy diamide: synthesis and conformational studies*. *Tetrahedron*, 2009. **65**(48): p. 9997-10001.
295. Mathias, L.J., *Esterification and alkylation reactions employing isoureas*. *Synthesis*, 1979(8): p. 561-76.
296. Bergmeier, S.C., A.A. Cobas, and H. Rapoport, *Chiroselective synthesis of (1S,3R)-1-amino-3-(hydroxymethyl)cyclopentane, precursor for carbocyclic nucleoside synthesis. Dieckmann cyclization with an  $\alpha$ -amino acid*. *J. Org. Chem.*, 1993. **58**(9): p. 2369-76.
297. Shin, I., et al., *Synthesis of Optically Active Phthaloyl *d*-Aminoxy Acids from *l*-Amino Acids or *l*-Hydroxy Acids as Building Blocks for the Preparation of Aminoxy Peptides*. *The Journal of Organic Chemistry*, 2000. **65**(22): p. 7667-7675.
298. Hyun, S.-H., et al., *Oriented Insertion of  $\phi$ 29 N-Hexahistidine-tagged gp10 Connector Protein Assemblies into C20BAS Bolalipid Membrane Vesicles*. *J. Am. Chem. Soc.*, 2010. **132**(48): p. 17053-17055.
299. Hacht, B., *Gallium(III) Ion Hydrolysis under Physiological Conditions*. *Bulletin of the Korean Chemical Society*, 2008. **29**(2): p. 372-376.
300. Green, M.A. and M.J. Welch, *Gallium radiopharmaceutical chemistry*. *International Journal of Radiation Applications and Instrumentation. Part B. Nuclear Medicine and Biology*, 1989. **16**(5): p. 435-448.
301. Wood, S.A. and I.M. Samson, *The aqueous geochemistry of gallium, germanium, indium and scandium*. *Ore Geology Reviews*, 2006. **28**(1): p. 57-102.
302. Salacinski, P.R.P., et al., *Iodination of proteins, glycoproteins, and peptides using a solid-phase oxidizing agent, 1,3,4,6-tetrachloro-3 $\alpha$ ,6 $\alpha$ -diphenyl glycoluril (iodogen)*. *Anal. Biochem.*, 1981. **117**(1): p. 136-46.

## REFERENCES

303. Sosabowski, J.K. and S.J. Mather, *Conjugation of DOTA-like chelating agents to peptides and radiolabeling with trivalent metallic isotopes*. Nat Protoc, 2006. **1**(2): p. 972-6.
304. Merglen, A., et al., *Glucose Sensitivity and Metabolism-Secretion Coupling Studied during Two-Year Continuous Culture in INS-1E Insulinoma Cells*. Endocrinology, 2004. **145**(2): p. 667-678.
305. Gromada, J., et al., *Stimulation of cloned human glucagon-like peptide 1 receptor expressed in HEK 293 cells induces cAMP-dependent activation of calcium-induced calcium release*. FEBS Letters, 1995. **373**(2): p. 182-186.
306. Liu, S. and D.S. Edwards, *99mTc-Labeled Small Peptides as Diagnostic Radiopharmaceuticals*. Chemical Reviews, 1999. **99**(9): p. 2235-2268.
307. Graziano, M.P., et al., *Cloning and Functional Expression of a Human Glucagon-like Peptide-1 Receptor*. Biochemical and Biophysical Research Communications, 1993. **196**(1): p. 141-146.
308. de Blois, E., *Radiochemical Aspects of Receptor Scintigraphy: labeling with radiometals, optimisation and radiochemical purity*. 2014, Erasmus University Rotterdam.
309. Le Caër, S., *Water Radiolysis: Influence of Oxide Surfaces on H<sub>2</sub> Production under Ionizing Radiation*. Water, 2011. **3**(1): p. 235-253.
310. Foreman, J.C. and T. Johansen, *Textbook of Receptor Pharmacology, Second Edition*. 2003: CRC Press LLC. 289 pp.
311. Hein, P., et al., *Receptor and Binding Studies*, in *Practical Methods in Cardiovascular Research*, S. Dhein, F.W. Mohr, and M. Delmar, Editors. 2005, Springer Berlin Heidelberg: Berlin, Heidelberg. p. 723-783.
312. McQueen, J. and P.F. Semple, *21 - Angiotensin Receptor Assay and Characterization*, in *Methods in Neurosciences*, P.M. Conn, Editor. 1991, Academic Press. p. 312-330.
313. Bernard-Gauthier, V., et al., *<sup>18</sup>F-Labeled Silicon-Based Fluoride Acceptors: Potential Opportunities for Novel Positron Emitting Radiopharmaceuticals*. BioMed Research International, 2014. **2014**: p. 454503.
314. Lexa, K.W., E. Dolgih, and M.P. Jacobson, *A structure-based model for predicting serum albumin binding*. PloS one, 2014. **9**(4): p. e93323-e93323.
315. Israelachvili, J., *The different faces of poly(ethylene glycol)*. Proceedings of the National Academy of Sciences of the United States of America, 1997. **94**(16): p. 8378-8379.
316. Dingels, C., *Expanding the scope of poly(ethylene glycol)s for bioconjugation to squaric acid-mediated PEGylation and pH-sensitivity*. 2015. p. No pp.
317. Miyaura, N., K. Yamada, and A. Suzuki, *A new stereospecific cross-coupling by the palladium-catalyzed reaction of 1-alkenylboranes with 1-alkenyl or 1-alkynyl halides*. Tetrahedron Letters, 1979. **20**(36): p. 3437-3440.
318. Maity, J., D. Honcharenko, and R. Strömberg, *Synthesis of fluorescent d-amino acids with 4-acetamidobiphenyl and 4-N,N-dimethylamino-1,8-naphthalimido containing side chains*. Tetrahedron Letters, 2015. **56**(33): p. 4780-4783.
319. Suzuki, A., *Recent advances in the cross-coupling reactions of organoboron derivatives with organic electrophiles, 1995-1998*. J. Organomet. Chem., 1999. **576**(1-2): p. 147-168.
320. Wuts, P.G.M., *Greene's Protective Groups in Organic Synthesis*. 2014: Wiley.

## REFERENCES

321. Davies, J.S., *The cyclization of peptides and depsipeptides*. J Pept Sci, 2003. **9**(8): p. 471-501.
322. Serjeant, E.P., and Boyd Dempsey., *Ionisation Constants of Organic Acids in Aqueous Solution*. 1979: Oxford: Pergamon Press.
323. Meyer, V.R., *Practice of High-Performance Liquid Chromatography. 6th Ed*. 1990: Otto Salle Verlag. 292 pp.
324. 1.3.1 *Einzelne chromophore Gruppen und ihre Wechselwirkung*, in *Spektroskopische Methoden in der organischen Chemie*, M. Hesse, H. Meier, and B. Zeeh, Editors. 2012, Georg Thieme Verlag: Stuttgart.
325. Soom, N.a.T., T., *Hydrogenation of Alkenes with NaBH<sub>4</sub>, CH<sub>3</sub>CO<sub>2</sub>H, Pd/C in the Presence of O- and N-Benzyl Functions*. International Journal of Organic Chemistry, 2016. **6**: p. 1 - 11.
326. Jadhav, S.N., et al., *Ligand-free Pd catalyzed cross-coupling reactions in an aqueous hydrotropic medium*. Green Chemistry, 2016. **18**(7): p. 1898-1911.
327. *Mechanistic Aspects of Metal-Catalyzed C-C- and C,X-Bond-Forming Reactions*, in *Metal-Catalyzed Cross-Coupling Reactions*. 2004. p. 1-40.
328. Thomé, I., A. Nijs, and C. Bolm, *Trace metal impurities in catalysis*. Chemical Society Reviews, 2012. **41**(3): p. 979-987.
329. Hughes, P., et al., *The costs of using unauthenticated, over-passaged cell lines: how much more data do we need?* BioTechniques, 2007. **43**(5): p. 575-586.
330. Esquenet, M., et al., *LNCaP prostatic adenocarcinoma cells derived from low and high passage numbers display divergent responses not only to androgens but also to retinoids*. The Journal of Steroid Biochemistry and Molecular Biology, 1997. **62**(5): p. 391-399.
331. Mosayebnia, M., et al., *Novel and Efficient Method for Solid Phase Synthesis of Urea-Containing Peptides Targeting Prostate Specific Membrane Antigen (PSMA) in Comparison with Current Methods*. Iranian journal of pharmaceutical research : IJPR, 2018. **17**(3): p. 917-926.
332. Robu, S., et al., *Synthesis and preclinical evaluation of novel (18)F-labeled Glu-urea-Glu-based PSMA inhibitors for prostate cancer imaging: a comparison with (18)F-DCFPyl and (18)F-PSMA-1007*. EJNMMI research, 2018. **8**(1): p. 30-30.
333. Lu, G., et al., *Synthesis and SAR of 99mTc/Re-labeled small molecule prostate specific membrane antigen inhibitors with novel polar chelates*. Bioorganic & Medicinal Chemistry Letters, 2013. **23**(5): p. 1557-1563.
334. Kularatne, S.A., et al., *Design, Synthesis, and Preclinical Evaluation of Prostate-Specific Membrane Antigen Targeted 99mTc-Radioimaging Agents*. Molecular Pharmaceutics, 2009. **6**(3): p. 790-800.
335. Smith, R.F., et al., *Reactions of hydrazines with esters and carboxylic acids*. The Journal of Organic Chemistry, 1968. **33**(2): p. 851-855.
336. Furst, A., R.C. Berlo, and S. Hooton, *Hydrazine as a Reducing Agent for Organic Compounds (Catalytic Hydrazine Reductions)*. Chemical Reviews, 1965. **65**(1): p. 51-68.
337. Ballatore, C., D.M. Huryn, and A.B. Smith, *Carboxylic Acid (Bio)Isosteres in Drug Design*. ChemMedChem, 2013. **8**(3): p. 385-395.

## REFERENCES

338. Herr, R.J., *5-Substituted-1H-tetrazoles as carboxylic acid isosteres: medicinal chemistry and synthetic methods*. Bioorganic & Medicinal Chemistry, 2002. **10**(11): p. 3379-3393.
339. Mitsunobu, O., *The Use of Diethyl Azodicarboxylate and Triphenylphosphine in Synthesis and Transformation of Natural Products*. Synthesis, 1981. **1981**(01): p. 1-28.
340. Duncia, J.V., M.E. Pierce, and J.B. Santella, III, *Three synthetic routes to a sterically hindered tetrazole. A new one-step mild conversion of an amide into a tetrazole*. J. Org. Chem., 1991. **56**(7): p. 2395-400.
341. Schottelius, M., M. Schwaiger, and H.-J. Wester, *Rapid and high-yield solution-phase synthesis of DOTA-Tyr3-octreotide and DOTA-Tyr3-octreotate using unprotected DOTA*. Tetrahedron Lett., 2003. **44**(11): p. 2393-2396.
342. Wu, H., et al., *Phase Transformations of Glutamic Acid and Its Decomposition Products*. Crystal Growth & Design, 2010. **10**(2): p. 988-994.
343. Agarwal, R., S.K. Burley, and S. Swaminathan, *A novel mode of dimerization via formation of a glutamate anhydride crosslink in a protein crystal structure*. Proteins: Structure, Function, and Bioinformatics, 2008. **71**(2): p. 1038-1041.
344. Rodriguez, C.E., et al., *Competitive inhibition of a glutamate carboxypeptidase by phosphoramidothionate derivatives of glutamic acid*. Bioorganic & Medicinal Chemistry Letters, 1999. **9**(10): p. 1415-1418.
345. Masunov, A. and J.J. Dannenberg, *Theoretical study of urea and thiourea. 2. Chains and ribbons*. J. Phys. Chem. B, 2000. **104**(4): p. 806-810.
346. Lenthall, J.T., et al., *Hydrogen bonding interactions with the thiocarbonyl  $\pi$ -system*. CrystEngComm, 2011. **13**(9): p. 3202-3212.
347. Batsanov, S.S., *Van der Waals Radii of Elements*. Inorganic Materials, 2001. **37**(9): p. 871-885.
348. Stabin, M.G., *Fundamentals of Nuclear Medicine Dosimetry*. 2008, New York, NY: Springer.
349. Dude, I., et al., *Evaluation of agonist and antagonist radioligands for somatostatin receptor imaging of breast cancer using positron emission tomography*. EJNMMI radiopharmacy and chemistry, 2017. **2**(1): p. 4-4.
350. Ghosh, A.K. and M. Brindisi, *Organic Carbamates in Drug Design and Medicinal Chemistry*. Journal of Medicinal Chemistry, 2015. **58**(7): p. 2895-2940.
351. Lassalas, P., et al., *Structure Property Relationships of Carboxylic Acid Isosteres*. Journal of medicinal chemistry, 2016. **59**(7): p. 3183-3203.
352. <https://clinicaltrials.gov/ct2/show/NCT04282824>, Accessed on June 12, 2021.
353. Vāvere, A.L., et al., *A Novel Technology for the Imaging of Acidic Prostate Tumors by Positron Emission Tomography*. Cancer Research, 2009. **69**(10): p. 4510-4516.
354. Wolf, P., et al., *Three conformational antibodies specific for different PSMA epitopes are promising diagnostic and therapeutic tools for prostate cancer*. The Prostate, 2010. **70**(5): p. 562-569.

## VII. APPENDIX

### 7.1. List of abbreviations

2-CT	2-chlorotrityl
2-CTC	2-chlorotrityl chloride
2-PMPA	2-(phosphonomethyl)pentanedioic acid
7-TMD	seven-transmembrane domain
AA	amino acid
$\alpha$ -Me	alpha-methyl
Ac	acetyl
AcOH	acetic acid
Ahx	aminohexanoic acid
Aib	$\alpha$ -aminoisobutyric acid
$A_m$	molar activity
ATF	activating transcription factor
ATP	adenosine 5'-triphosphate
Bcl-2/-xL	B-cell lymphoma-2/xL
BIP	4, 4'-biphenylalanine
Boc	<i>tert</i> -butyloxycarbonyl
BOP	(Benzotriazol-1-yloxy)tris(dimethylamino)phosphonium hexafluorophosphate
BSA	bovine serum albumin
cAMP	3', 5'-cyclic adenosine monophosphate
CAN	cerium(IV) ammonium nitrate
CCK <sub>2</sub>	cholecystokinin receptor 2
cDNA	complementary deoxynucleic acid
CHO cells	chinese hamster ovary cells
CNS	central nervous system
CREB	cAMP response element-binding protein
cryo-EM	cryogenic electron microscopy
CT	computed tomography
Dap	2,3-diaminopropionic acid
DCE	1,2-dichloroethane
DCHA	dicyclohexylammonium
DCM	dichloromethane
Dde	<i>N</i> -1-(4,4-dimethyl-2,6-dioxocyclohex-1-ylidene)ethylamine
DDTC	diethyldithiocarbamate
DIAD	diisopropyl azodicarboxylate

## APPENDIX

DIC	<i>N,N'</i> -diisopropylcarbodiimide
DIPEA	<i>N,N'</i> -diisopropylethylamine
DMA	dimethyl acetamide
DMAP	4-dimethylaminopyridine
DMEM	Dulbecco's modified Eagle medium
DMF	dimethylformamide
DMSO	dimethyl sulfoxide
DNA	deoxyribonucleic acid
DOPA	3,4-dihydroxyphenylalanine
DOTA	1,4,7,10-tetraazacyclododecane-1,4,7,10-tetraacetic acid
DOTA-GA	1,4,7,10-tetraazacyclododecane-1-glutaric anhydride-4,7,10-triacetic acid
dpm/mg	disintegrations per minute and per milligram
DPP IV	dipeptidyl peptidase IV
DTPA	diethylenetriaminepentaacetic acid
EC <sub>50</sub>	half maximal effective concentration
ECD	extracellular domain
EDC	<i>N</i> -(3-dimethylaminopropyl)- <i>N'</i> -ethylcarbodiimide
EDDA	ethylenediamine- <i>N,N'</i> -diacetic acid
EM	electron microscopy
EMA	European Medicines Agency
Epac	exchange protein activated by cAMP
eq.	equivalent(s)
er	enantiomeric ratio
ER	endoplasmic reticulum
Et <sub>2</sub> O	diethyl ether
EtOH	ethanol
EuE	L-glutamate-urea-L-glutamate
FDA	Food and Drug Administration
FDG	fluorodeoxyglucose
FLT	fluorothymidine
Fmoc	fluorenylmethoxycarbonyl
G <sub>αs</sub>	G <sub>s</sub> alpha subunit
GCGR	glucagon receptor
GDP	guanosine 5'-diphosphate
GEP-NET	gastroenteropancreatic neuroendocrine tumor
GHRHR	growth hormone-releasing hormone receptor
GIP	glucose-dependent insulinotropic polypeptide
GLP-1	glucagon-like peptide 1

## APPENDIX

GLP-1R	glucagon-like peptide 1 receptor
GLP-2	glucagon-like peptide 2
GLP-2R	glucagon-like peptide 2 receptor
GPCR	G protein-coupled receptor
G <sub>s</sub>	heterotrimeric G protein that stimulates cAMP-dependent pathway
GTP	guanosine 5'-triphosphate
HATU	<i>O</i> -(7-Azabenzotriazol-1-yl)- <i>N,N,N',N'</i> -tetramethyluronium hexafluorophosphat
HBSS	Hank's buffered salt solution
HEK293	human embryonic kidney 293 cells
HEPES	(4-(2-hydroxyethyl)-1-piperazineethanesulfonic acid)
HFIP	1,1,1,3,3,3-hexafluoro-2-propanol
hGLP-1R	human glucagon-like peptide 1 receptor
HOAt	1-hydroxy-7-azabenzotriazole
HOBt	1-hydroxybenzotriazole
HYNIC	hydrazinonicotinamide
IA/g	injected activity per gram
IC <sub>50</sub>	half maximal inhibitory concentration
ID/g	injected dose per gram
INS	insulinoma
K <sub>ATP</sub>	ATP-sensitive potassium channel
K <sub>i</sub>	inhibition constant
KuE	L-lysine-urea-L-glutamate
K <sub>V</sub>	voltage-gated potassium channel
LC-MS	liquid chromatography-mass spectrometry
MAL	maleimide
MAPK	mitogen-activated protein kinase
MeCN	acetonitrile
MEN I	multiple endocrine neoplasia type I
MeOH	methanol
MRI	magnetic resonance imaging
mRNA	messenger ribonucleic acid
NAAG	<i>N</i> -acetyl-L-aspartyl-L-glutamic acid
Nb35	nanobody 35
n.c.a.	no-carrier added
n.d.	not determined
NEDH	New England Deaconess Hospital
NEP 24.11	neutral endopeptidase 24.11
NET	neuroendocrine tumor

## APPENDIX

NMP	<i>N</i> -methyl-2-pyrrolidone
No.	Number
NOTA	1,4,7-triazacyclononane-1,4,7-triacetic acid
NTD	<i>N</i> -terminal domain
O2Oc	8-amino-3,6-dioxaoctanoic acid
PACAP	pituitary adenylate cyclase-activating polypeptide
PBS	phosphate-buffered saline
PC1/3	prohormone convertase 1/3
PC2	prohormone convertase 2
PET	positron emission tomography
p.i.	post injectionem
PI3K	phosphatidylinositol-3-kinase
PKA	protein kinase A
PPh <sub>3</sub>	triphenylphosphane
PRRT	peptide receptor radionuclide therapy
PSA	prostate-specific antigen
PSMA	prostate-specific membrane antigen
PyBOP	benzotriazol-1-yl-oxytripyrrolidinophosphonium hexafluorophosphate
RACM	Rink amide ChemMatrix®
Ras	Rat sarcoma G protein
RCP	radiochemical purity
RCY	radiochemical yield
Ref.	references
RIN	rat insulinoma
RLT	radioligand therapy
RP-HPLC	reversed-phase high-performance liquid chromatography
RPMI	Roswell Park Memorial Institute
r.t.	room temperature
SAR	structure-activity relationship
SCTR	secretin receptor
SD	standard deviation
SiFA	silicon-based fluoride acceptor
SiFA-BA	silicon-based fluoride acceptor-benzoic acid
SPECT	single-photon emission computed tomography
SPPS	solid-phase peptide synthesis
SST <sub>2</sub>	somatostatin receptor subtype 2
SUV	standardized uptake value
t <sub>1/2</sub>	half-life

## APPENDIX

TBTU	2-(1 <i>H</i> -benzotriazole-1-yl)-1,1,3,3-tetramethylamminium tetrafluoroborate
TFA	trifluoroacetic acid
TIPS	triisopropylsilane
TMD	transmembrane domain
TMSN <sub>3</sub>	trimethylsilyl azide
t <sub>R</sub>	retention time (reversed-phase high-performance liquid chromatography)
Trt	trityl
U-HPLC	ultra high-performance liquid chromatography
UK	United Kingdom
UV/Vis	ultraviolet/visible light
VIP	vasoactive intestinal polypeptide
VPAC <sub>1</sub>	vasoactive intestinal polypeptide receptor 1
w/	with
w/o	without

## 7.2. Publications and notes on the protection of copyright

Substantial parts of this work have been published, are covered by a patent application or were submitted to a peer-reviewed journal, with Veronika Barbara Felber listed as first and corresponding author (journal articles) or inventor (patent application).

### Peer-reviewed journal articles

- Veronika Barbara Felber, Manuel Amando Valentin, Hans-Jürgen Wester. Design of PSMA ligands with modifications at the inhibitor part: an approach to reduce the salivary gland uptake of radiolabeled PSMA inhibitors? *European Journal of Nuclear Medicine and Molecular Imaging – Radiopharmacy and Chemistry*, 2021. 6(1), 10. <https://doi.org/10.1186/s41181-021-00124-1>.
- Veronika Barbara Felber, Hans-Jürgen Wester. Small peptide-based GLP-1R ligands: an approach to reduce the kidney uptake of radiolabeled GLP-1R-targeting agents? *European Journal of Nuclear Medicine and Molecular Imaging – Radiopharmacy and Chemistry*, 2021. 6(1), 29. <https://doi.org/10.1186/s41181-021-00136-x>.

### Patent applications

- Veronika Barbara Felber, Manuel Amando Valentin, Hans-Jürgen Wester. Dual mode radiotracers and -therapeutics. EP21150122; 2021.

## 7.3. Funding

Parts of the research leading to these results has received funding from the Deutsche Forschungsgemeinschaft (DFG) under grant agreement no. SFB 824 project Z1.

## 7.4. Acknowledgements

I would firstly like to thank Prof. Dr. Hans-Jürgen Wester for his support and guidance throughout my graduate studies. I am grateful that I was given the opportunity to work on various research projects and that I received the accreditations for attending training courses and conferences. I have truly enjoyed the time I spent working in his laboratory.

I would also like to thank current and past members of the research group of Prof. Wester. Dr. Alexander Schmidt, Dr. Theresa Osl, Dr. Stephanie Robu, Dr. Andreas Poschenrieder and Monika Beschorner provided invaluable insight into the daily laboratory routine during the early phase of my research and I highly appreciate your numerous hints and advices. I learned a lot and I always tried to pass my knowledge on to my students and colleagues like you did.

## APPENDIX

Many thanks to Prof. Margret Schottelius and PD Dr. Johannes Notni for your efforts to help on tricky scientific issues.

I thank Dr. Roswitha Beck and Dr. Nicole Urtz-Urban for their assistance and guidance concerning animal studies and everything around. My independence in this area I owe to you, I guess.

I would like to give special thanks to Dr. Alexander Wurzer, Dr. Thomas Günther, Steffi Färber, Daniel Di Carlo, Markus Fahnauer, Sebastian Fischer, Jan-Philip Kunert, Matthias Konrad and Mara Parzinger for valuable suggestions throughout my research. From each of you I learned special tips and tricks and time that we spent in discussions (or gossip) was greatly appreciated. Regarding the metabolite experiment, I am very grateful for Sebastian's support.

Many thanks to Jana Herbst, Tanja Reichhart, Sandra Deiser and Nadine Holzleitner for joining our team and your support in so many cases. Your presence always kept me in a good mood!

Also the work of my students is highly appreciated, wherefore I would like to acknowledge Manuel Valentin, Franziska Schuderer, Stephanie Ferstl, Patricia Bratrach and Nghia Nguyen Trong for their efforts and enthusiasm regarding their research.

I would also like to thank Dr. Nahid Yusufi for kindly providing biodistribution data of [<sup>177</sup>Lu]Lu-rhPSMA-7.3.

Many thanks to Prof. Dr. Timothy Kieffer (University of British Columbia, Vancouver, Canada) for providing HEK293 and stably transfected HEK293-h-GLP-1R cells as well as to Dr. Günter Päth (University Hospital Freiburg, Freiburg, Germany) for providing INS-1E cells.

I thank Dr. Tobias Kapp, Dr. Florian Reichart and Dr. Andreas Räder from the research group of Prof. Dr. Horst Kessler for assisting in the acquisition of mass spectra at the chemistry department, providing lab space or chemicals, if reaction equipment or hydrogen gas was missing again.

I am truly grateful to Christine Winkler, Irmgard Kaul and the members of the Radiochemie München (Herbert, Gerhard, Andreas, Hansi, Steffi, Marie, Doris, ...) and their support in all technical and organizational issues.

Finally, I would like to thank my friends and my family for their infinite patience, their love and encouragement.